Dissertation zur Erlangung des Doktorgrades
der Fakultät für Chemie und Pharmazie
der Ludwig-Maximilians-Universität München

Massenspektrometrische Methoden zur Untersuchung enzymatisch modifizierter RNA

Felix Phil Hagelskamp

aus

Hamburg, Deutschland

2021

Erklärung

Diese Dissertation wurde im Sinne von § 7 der Promotionsordnung vom 28. November 2011 von Frau Prof. Dr. Stefanie Kaiser betreut.

Eidesstattliche Versicherung

Diese Dissertation wurde eigenständig und ohne unerlaubte Hilfe erarbeitet.

München,…10.12.2021… ….....

Felix Phil Hagelskamp

Dissertation eingereicht am: 18.10.2021

1. Gutachterin: Prof. Dr. Stefanie Kaiser
2. Gutachter: Prof. Dr. Thomas Carell

Mündliche Prüfung am: 03.12.2021

Danksagung

An erster Stelle möchte ich Frau Prof. Dr. Stefanie Kaiser danken. Seit meinem F-Praktikum in dem anfangs noch personell sehr kleinen Arbeitskreis wurde mir von deiner Seite viel geholfen und vertraut, sodass ich immer weiter in dem Bereich der RNA-Modifikationen forschen und mein Wissen vertiefen wollte. Das Thema und der Arbeitskreis haben mich - im positiven Sinne - nicht mehr losgelassen, was die angehängte Masterarbeit und spätestens die Promotion gezeigt haben. Dabei haben nicht nur deine intensive Betreuung, dein respektvoller Umgang, sondern auch deine Fähigkeit zur Motivation und deine menschliche Führungsweise beigetragen. Die Gruppenausflüge zur Wiesn, zum Grillen an der Isar, zum Laser-Tag, zum Wandern (in Zukunft vielleicht nicht mehr) und so viele weitere haben die Harmonie innerhalb der Gruppe gestärkt und sind mir persönlich in sehr guter Erinnerung geblieben. Ein großer Dank geht an dich, da du meine wissenschaftliche und persönliche Weiterentwicklung gefördert hast, als Beispiel ist die Konferenz am Weizmann Institut in Israel zu nennen, zu der du mich an deiner Stelle geschickt hast. Ich wünsche dir eine erfolgreiche Professur in Frankfurt mit einem personell und instrumentell wachsenden Team. Dieses wirst du – davon bin ich überzeugt - mit so viel Engagement und Menschlichkeit leiten und deshalb viele Grants einsammeln und unzählige Publikationen in deiner Laufbahn veröffentlichen.

Des Weiteren möchte ich Prof. Dr. Thomas Carell für die Anfertigung des Zweitgutachtens danken. Die Integration in den Arbeitskreis Carell und die großzügige Nutzung vieler Instrumente am Anfang liefen perfekt und ohne sie wären die ersten Experimente nicht zu realisieren gewesen. Auch außerhalb der Forschung wurden wir zu privaten Grillfeiern, der jährlichen gemeinsamen Weihnachtsfeier und weiteren Partys eingeladen.

Der Umgang untereinander im Arbeitskreis war legendär, immer lustig, unbeschreiblich kollegial und freundschaftlich! Ich bin so dankbar Teil dieses Teams gewesen zu sein und werde jeden Einzelnen von euch vermissen. Mit Yasemin „Wollen Sie hier jetzt vorbei?“ Yoluc, als Party-Queen, Wiesn-Proletin, Gossip-Tante und Speckhüftchen-Expertin hat es immer besonders viel Spaß gemacht, sich in Rage zu diskutieren und sich als Sitznachbarn zu ärgern. Dr. Matthias Heiß, deine hilfsbereite Art im Labor, deine Musikauswahl, deine „White Basils“ waren wunderbar und die Anleitungen zu noch-perfekteren Inkscape-Abbildungen sind gemerkt. Ob

Mozzarella gezupft oder geschnitten und wie ein Burgerpatty zubereitet werden soll, das waren immer die wichtigsten Fragen. Dem SpeedVac-Beauftragten Dr. Valentin Reichle danke ich für die Stimmung im und nach dem Labor auf Ballermann-Niveau und deine komischen 5-Minuten waren sehr auflockernd. Paria Asadi Atoi, es hat immer sehr viel Spaß gemacht, sich ein neues „Wort des Tages“ für dich auszudenken und ich hoffe, dass die ganzen Ausnahmen und Verwirrungen in der deutschen Sprache, die wir dir beigebracht haben, dich nicht daran hindern, „C2“-Sprecherin zu werden. Dr. Steffen Kaiser danke ich für die zahlreichen, aber auch sehr detaillierten Tipps zur Arbeit mit RNA und der IVT-Herstellung. „Möge die T7 mit dir sein!“. Dr. Kayla Borland, mit dir konnte ich nicht nur mein Englisch verbessern, sondern auch sehr gut im Oligo-MS Projekt zusammenarbeiten. Den „neuen“-Doktoranden Elite-Gregor Ammann, Nur Yesiltac, Max Berg und Hagen Wesseling wünsche ich eine erfolgreiche und abwechslungsreiche Arbeit. Ihr werdet Oligo-MS auf das nächste Level heben! Gregor hat dafür bestimmt schon ein kleines Computerprogramm selbst geschrieben. Bedanken möchte ich mich auch bei meinen Praktikanten, Yuhao Jiang und Max Zöschg, für ihre gelungene Arbeit und wünsche euch alles Gute für die Zukunft in der Forschung.

Mit Dr. Alex Schön (spielt nur mit drei Laufenden und hat kein Geld mehr im Wägeschälchen), Markus Hillmeier (spielt mehr Grün-Solos, als er grüne Pullover in der Woche trägt und das sind wirklich viele), Stefan Wiedemann (spielt jeden Mist, weil er ihn nicht wegschmeißen möchte) und Florian Schelter (spielt vom Mitspieler und Gegner gefürchtete, unorthodoxe Anspiele) war es immer schön Schafkopf zu spielen und die Halbe/Halbe-Tour nach Heidenheim sind mir im Gedächtnis geblieben. Bei Maren, Basti und JFS möchte ich mich für die sportliche Zeit beim Wandern und Badminton bedanken.

Zu guter Letzt danke ich euch, Sabine und Achim, dass ihr mich immer unterstützt habt, sowohl finanziell als auch mental und mir immer ein sicheres und geliebtes Gefühl gegeben habt. Ich konnte mich ohne Druck entwickeln. Ihr habt mir über Motivationslöcher geholfen und mich bestärkt, das zu tun, was ich wirklich will. Ohne euch hätte ich diese Arbeit nicht geschafft. Ganz besonderer Dank gilt dir, Elina! Danke für deine bedingungslose Liebe, die du mir gibst, dein Verständnis bei Problemen, die gemeinsamen Interessen und Reisen auf alle Kontinente. Ich hoffe, dass wir in der Zukunft noch viele gemeinsame, glückliche Erlebnisse miteinander teilen können.

Inhaltsverzeichnis

Publikationsliste

Publikationen, die während meiner Promotionszeit erstellt wurden:

- „Broadly applicable oligonucleotide mass spectrometry for the analysis of RNA writers and erasers *in vitro*", **F. Hagelskamp**[#], K. Borland[#], J. Ramos, A. G. Hendrick, D. Fu, S. Kellner, *Nucleic Acids Res*., **2020**, Apr 17; 48 (7): e41.
- „Analysis of the epitranscriptome with ion-pairing reagent free oligonucleotide mass spectrometry", **F. Hagelskamp**, S. Kellner, *Methods in Enzymology*, **2021**, 658: 111-135. RNA Modification Enzymes (7).
- „Cell culture NAIL-MS allows insight into human tRNA and rRNA modification dynamics *in vivo*", M. Heiß, **F. Hagelskamp**, V. Marchand, Y. Motorin, S. Kellner, *Nat. Comm*., **2021**, 12 (1); 389.
- „Identification and rescue of a tRNA wobble inosine deficiency causing intellectual disability disorder", J. Ramos, M. Proven, J. Halvardson, **F. Hagelskamp**, E. Kuchinskaya, B. Phelan, R. Bell, S. M. Kellner, L. Feuk, A. C. Thuresson, D. Fu, *RNA*, **2020**, Nov; 26 (11): 1654-1666.
- „Formation of tRNA Wobble Inosine in Humans Is Disrupted by a Millennia-Old Mutation Causing Intellectual Disability", J. Ramos, L. Han, Y. Li, **F. Hagelskamp**, S. M. Kellner, F. S. Alkuraya, E. M. Phizicky, D. Fu, *Mol Cell Biol*., **2019**, Sep 11; 39 (19): e00203-19.
- „Surpassing limits of static RNA modification analysis with dynamic NAIL-MS", V. F. Reichle, S. Kaiser, M. Heiß, **F. Hagelskamp**, K. Borland, S. Kellner; *Methods (San Diego, Calif.)*, **2019**, 156: 91-101.

Konferenzbeiträge:

- „Analytical tools to study RNA writers and erasers *in vitro*", GBM-Meeting der Studiengruppe RNA-Biochemie (Bonn, Deutschland, Oktober **2018**)
- „Ion pairing reagent free oligonucleotide mass spectrometry enables to quantify and study RNA writers and erasers *in vitro* in sequence context", 2nd Symposium on Nucleic Acid Modifications, RNA Modifications: Form, Function and Mechanism, 73rd Katzir Conference (Weizmann Institute of Science, Rehovot, Israel, Juni **2019**) mit Auszeichnung für den *3rd poster prize*

Weitere Publikation, die nicht im Hauptteil dieser Arbeit erscheint:

- „Strategies to avoid artifacts in mass spectrometry-based epitranscriptome analyses”, S. Kaiser, S. R. Byrne, **F. Hagelskamp**, P. C. Dedon, B. Cao, S. Kellner *et al.*, *Angew Chem Int Ed Engl*., **2021**, Aug 2. PMID: 34339593.

Abkürzungsverzeichnis

(D)MRM	*(dynamic) multiple reaction monitoring* (engl.)
° C	Grad Celcius
µg	Mikrogramm
µL	Microliter
µm	Micrometer
2-HG	2-Hydroxyglutarat
3D	3-dimensional
8-oxo-G	8-Oxoguanosin
A	Adenosin
Å	Ångström (Einheit)
ac^{4}C	N4-Acetylcytidin
Acm D	Actinomycin D
ADAT	*adenosindeaminase acting on tRNA* (engl.)
Akt	Aktivator
AlkB	*α-ketoglutarate-dependent dioxygenase AlkB* (engl.)
AlkBH	*homolog of α-ketoglutarate-dependent dioxygenase AlkB* (engl.)
Am	2´-O-Methyladenosin
Arg	Arginin
ASCC3	*activating signal cointegrator 1 complex subunit 3* (engl.)
Asp	Asparaginsäure
B&W	*binding & wash* (engl.)
BHT	Butylhydroxytoluol
bp	Basenpaar
bspw	beispielsweise
C	Cytidin
ca^{5}C	5-Carboxycytosin
CARD	*comparative analysis of RNA digests* (engl.)
CIP	*calf-intestinal-phosphatase* (engl.)
Cm	2´-O-Methylcytidin
CMCT	*N*-Cyclohexyl-*N'*-(2-morpholinoethyl)-carbodiimid-methyl-*p*-toluolsulfonat
Cys	Cystein
D	Dihydrouridin
d. h.	das heißt
DMEM	*Dulbecco´s Modified Eagle Medium* (engl.)
DMSO	Dimethylsulfoxid
DNA	*deoxyribonucleic acid* (engl.)
dNTP	Desoxyribonukleosid-5'-T*riphosphat*
DTT	Dithiothreitol
E. coli	*Escherichia coli* (lat.)
EDTA	Ethylendiamintetraacetat
EE	Enhancer-Element

engl.	englisch für
Enz	Enzym
eq	Äquivalent
ESI	Elektrosprayionisation
esiRNA	*Endoribonuclease-prepared siRNA* (engl.)
f^{5}C	5-Formylcytidin
FBS	*fetal bovine serum* (engl.)
FTO	*Fat mass and obesity-associated protein* (engl.)
G	Guanosin
Glu	Glutaminsäure
Gly	Glycin
Gm	2´-O-Methylguanosin
h	*hours* (engl.)
H. sapiens	*Homo sapiens* (lat.)
HEK	*Human embryonic kidney cells* (engl.)
HeLa	*Henrietta Lacks cells* (engl.)
HEPES	2-(4-(2-Hydroxyethyl)-1-piperazinyl)-ethansulfonsäure
HFIP	1,1,1,3,3,3-Hexafluor-2-propanol
His	Histidin
ho^{5}C	5-Hydroxycytidin
HPLC	*high performance liquid chromatography* (engl.)
HRMS	*high resolution mass spectrometry* (engl.)
I	Inosin
IDH	Isocitratdehydrogenase
ITS	*internal transcribed spacer* (engl.)
IVT	*in vitro* transkribiert
k^{2}C	2-Lysidin
KD	*knockdown* (engl.)
kDa	Kilo-Dalton
KP	Kernpromotor
Ktrl	Kontrolle
LC	*liquid chromatography* (engl.)
M	Molar
m/z	Masse-zu-Ladungs-Verhältnis
m^{1}A	1-Methyladenosin
m^{1}G	1-Methylguanosin
m^{22}G	N^2,N^2-Dimethylguanosin
m^{3}C	3-Methylcytidin
m^{5}C	5-Methylcytidin
m^{5}Cm	5,2´-O-Dimethylcytidin
m^{66}A	N^6,N^6-Dimethyladenosin
m^{6}A	N^6-Methyladenosin
m^{7}G	7-Methylguanosin
MALDI	Matrix–Assistierte Laser–Desorption–Ionisierung
METTL	*methyltransferase-like* (engl.)

min	Minute
Mio	Millionen
miRNA	*micro RNA* (engl.)
mL	Milliliter
mm	Millimeter
MMS	Methylmethansulfonat
mRNA	*messenger RNA* (engl.)
MS	Massenspektrometrie
N	Newton (Einheit)
n.s.	nicht signifikant
NAIL-MS	*nucleic acid isotope labeling coupled mass spectrometry* (engl.)
ng	Nanogramm
NMR	*nuclear magnetic resonance* (engl.)
NSUN2	NOP2/Sun RNA-Methyltransferase 2
nts	Nukleotide
ON	Oligonukleotid
P	Phosphoryliert
PBS	*phosphate-buffered saline* (engl.)
PCR	*polymerase chain reaction* (engl.)
PIC	Präinitiationskomplex
p-Wert	Signifikanzwert
Q	Queuosin
QQQ	Triplequadrupol
Rib.	Ribose
RNA	*ribonucleic acid* (engl.)
rNTP	Ribonukleosid-5'-Triphosphat
ROS	*reactive oxygen species* (engl.)
RP	*reverse phase* (engl.)
rpm	Umdrehungen pro Minute
rRNA	*ribosomal RNA* (engl.)
R_t	Retentionszeit
S	Svedberg (Einheit)
S. cerevisiae	*Saccharomyces cerevisiae* (lat.)
SAM	S-Adenosylmethionin
scr.	*scramble* (engl.)
SEC	*size exclusion chromatography* (engl.)
Ser	Serin
SILAC	*stable isotope labeling of amino acids in cell culture* (engl.)
SILIS	*stable isotope labeled internal standard* (engl.)
SILNAS	*stable isotope labeled ribonucleic acid as internal standard* (engl.)
siRNA	*small interfering RNA* (engl.)
snoRNA	*small nucleolar RNA* (engl.)
SPD	*snake venom phosphodiesterase* (engl.)
SSC	*saline sodium citrate* (engl.)

Std	Stunden
TBP	TATA-Box-Bindeprotein
TEA	Triethylamin
TF	Transkriptionsfaktor
THU	Tetrahydrouridin
ToF	*time of flight* (engl.)
TRIS	Tris(hydroxymethyl)aminomethan
TRMT	*tRNA-methyltransferase* (engl.)
tRNA	*transfer RNA* (engl.)
TS	Terminationssequenz
TSS	Transkriptionsstartseite
U	Uridin
U/µL	*enzymatic units per microliter* (engl.)
UBF	*upstream binding factor* (engl.)
UKE	*upstream control element* (engl.)
Um	2´-O-Methyluridin
UV	Ultraviolettstrahlung
Val	Valin
WTAP	*pre-mRNA-splicing regulator WTAP* (engl.)
x g	Mehrfaches der Erdbeschleunigung
yW	Wybutosin
z. B.	zum Beispiel
α-KG	α-Ketoglutarat
Ψ	Pseudouridin

Zusammenfassung

Die Dynamik von RNA-Modifikationen ist im Bereich der Epitranskriptom-Forschung von zentraler Bedeutung. Die Wichtigkeit von RNA-modifizierenden Enzymen, welche die RNA-Modifikationsdichte beeinflussen, wird insbesondere deutlich, wenn man die Verbindung zu neurologischen Erkrankungen, geistiger Einschränkung und vielen Krebsarten kennt. Eine Aminosäuremutation im ADAT2/3-Enzymkomplex sorgt für eine Verringerung des Inosingehalts mancher tRNA-Moleküle und ist molekulare Grundlage für die Ausbildung einer schweren geistigen Beeinträchtigung in betroffenen Patienten[1]. Ein weiteres Enzym NSUN2 methyliert mehrere Cytidine in der variablen Schleife einiger tRNA-Molekülen und seine durch einen Splicingfehler hervorgerufene Dysfunktion ist mit dem Dubowitz-Syndrom assoziiert[2]. Die Liste der RNA-Modifikation abhängigen Krankheiten ist lang und die molekularen Grundlagen bedürfen weiterer Erforschung.

Die Massenspektrometrie bietet bei der Detektion und Quantifizierung vieler RNA-Modifikationen vielversprechende Ansätze. Um das Level einer Modifikation nicht nur statisch zu bestimmen, habe ich maßgeblich bei der Entwicklung von NAIL-MS (engl. für *nucleic acid isotope labeling coupled mass spectrometry*) mitgewirkt. Mit dieser zur dynamischen Protein-Analyse SILAC (engl. für *stable isotope labeling of amino acids in cell culture*) analogen und innovativen Methode ist es möglich, zeitlich aufgelöst RNA in alte, post-methylierte und neue Nukleoside zu unterteilen und somit die dynamische Natur von RNA-Modifikationen besser zu erfassen. Nach gelungener Einführung dieser NAIL-MS-Methode in humaner Zellkultur, habe ich NAIL-MS dazu verwendet, das detaillierte Modifikationsprofil humaner Zellen mit AlkBH1, 3, 5-Enzymdefizienz zu ermitteln. Für AlkBH5, welches m^6A in mRNA oxidativ demethyliert, konnte ich zusammen mit meiner Kollegin Dr. Kayla Borland eine demethylierende Aktivität in den lebenden Zellen beobachten. Sowohl AlkBH3 als auch AlkBH1 sollen m^1A und m^3C in tRNA demethylieren. Allerdings konnte ich mittels NAIL-MS keine demethylierende Aktivität der beiden Enzyme in tRNA oder rRNA gegenüber den möglichen Substraten m^1A, m^3C, m^6A und m^5C *in vivo* feststellen. Im Gegensatz dazu, konnten *in vitro* einige dieser Modifikations-Demethylierungen, wie erwartet, bestätigt und weitergehend absolut quantifiziert werden. Somit ist es mir gelungen, die bestehende, auf *in vitro* Daten beruhende Literatur zu bestätigen. Allerdings scheinen die Enzyme keine demethylierende Aktivität in ungestressten humanen Zellen zu

haben. Die Komplexität humaner Zellen wird deshalb nicht nur bei der schwierigeren Wahl der Isotopenmarkierungsstrategie deutlich, sondern auch in der unerforschten Vielfalt an molekularen Adaptionsmechanismen, die für eine Kontrolle der RNA-Modifikationsdichte wichtig sind.

Die NAIL-MS-Pulse-Chase-Analytik ist neben der Beobachtung bestehender RNA-Modifikationen hilfreich bei der Zuordnung in co- oder post-transkriptionelle Modifikationsprozesse. Bisherige Ergebnisse der Arbeitsgruppe deuteten darauf hin, dass viele Modifikationen in rRNA und tRNA, aber auch m^6A in mRNA, nachträglich in die RNA eingebracht werden. Da m^6A-modifiziernde Enzyme ausschließlich im Zellkern lokalisiert sind und an naszenten mRNAs arbeiten, wollte ich das Phänomen der post-transkriptionellen Modifikation genauer untersuchen. Durch die Verwendung des RNA-Transkriptionsinhibitors Actinomycin D (Acm D) konnte die Analyse der enzymatischen Post-Methylierung von Transkriptionsprozessen abgegrenzt werden. Der Gehalt an post-methyliertem m^6A verringerte sich unter Acm D-Stress, was auf einen zeitlich limitierten Transkriptionsmechanismus in der Zelle hindeutet, in dem Hybrid-RNA aus unmarkierten und isotopenmarkierten Bausteinen aufgebaut wird. Meine Ergebnisse deuten darauf hin, dass NAIL-MS-Experimente eine zeitliche Limitation aufweisen, welche bei Experimentdesign bedacht werden müssen. Proteom- und Oligonukleotid-MS-Experimente werden hierzu weitere Erkenntnisse liefern.

Die herkömmliche Oligonukleotid-MS-Analytik, die aufgrund der Benutzung von Ionenpaarreagenzien von nur wenigen Arbeitskreisen und auf speziell für diesen Zweck angeschafften Massenspektrometern durchgeführt wird, kann nicht kompatibel mit der Nukleosid-MS-Analytik verknüpft werden. Um diese Hürde zu beseitigen, habe ich eine Oligonukleotid-LC-Methode etabliert, mit deren Hilfe sich ionenpaarreagenzfrei, MS-schonend und kontaminationsarm, RNAs sequenzspezifisch analysieren lassen. Modifikationen in enzymatisch-modifizierter *in vitro* transkribierter (IVT) tRNA können somit chromatographisch von unmodifizierter getrennt, sequenziell nachgewiesen und quantifiziert werden. Die Deaminierung von Adenosin zu Inosin in der Anticodonschleife der IVT $tRNA^{Val}_{AAC}$ konnte ich quantitativ und positionsgenau bestimmen. Die Methode basiert auf einem spezifischen RNase T1-Verdau, mit dem auch RNA-Modifikationen in nativer totaler tRNA kartiert werden können.

Zusammenfassend lässt sich sagen, dass sowohl mit der NAIL-MS als auch mit der Oligonukleotid-MS-Analytik das Wissen über RNA-Modifikationen, ihre Mechanismen und ihre Dynamik vergrößert wird und es für klinische Zwecke in der Behandlung von Krankheiten und zur Qualitätskontrolle einer wachsenden Zahl an RNA-basierten Medikamenten und Vakzinen genutzt werden kann.

Abstract

The dynamics of RNA modifications are important to the field of epitranscriptome research. The importance of RNA-modifying enzymes influencing RNA modification density becomes particularly clear when the link to neurological diseases, mental retardation and many cancer diseases is known. An amino acid mutation in the ADAT2/3 enzyme complex causes a reduction in the inosine content of some tRNA molecules and serves as molecular basis for the development of severe mental retardation in affected patients[1]. Another enzyme called NSUN2 methylates several cytidines in the variable loop of some tRNA molecules and its dysfunction caused by a splicing defect is associated with the Dubowitz syndrome[2]. The list of RNA modification-dependent diseases is long and the molecular basis requires further investigation.

Mass spectrometry offers promising approaches in the detection and quantification of many RNA modifications. In order to determine the level of a modification not only statically, I played a major role in the development of NAIL-MS (*nucleic acid isotope labeling coupled mass spectrometry*). With this innovative method, which is analogous to the dynamic protein analysis SILAC (*stable isotope labeling of amino acids in cell culture*), it is possible to subdivide RNA into old, post-methylated and new nucleosides in a temporally resolved manner and thus better capture the dynamic nature of RNA modifications. After successfully introducing this NAIL-MS method in human cell culture, I used NAIL-MS to determine the detailed modification profile of human cells with AlkBH1, 3, 5 enzyme deficiency. For AlkBH5, which oxidatively demethylates m^6A in mRNA, I was able to observe demethylation activity in the living cells together with my colleague Dr. Kayla Borland. Both AlkBH3 and AlkBH1 are reported to demethylate m^1A and m^3C in tRNA. However, using NAIL-MS, I could not detect any demethylation activity of both enzymes in tRNA or rRNA towards the possible substrates m^1A, m^3C, m^6A and m^5C *in vivo*. In contrast, some of these modification demethylations could be confirmed and further absolutely quantified *in vitro*, as expected. Thus, I have been able to confirm the existing literature based on *in vitro* data. However, the enzymes do not appear to have demethylating activity in unstressed human cells. The complexity of human cells is therefore not only evident in the more difficult choice of isotope labeling strategy, but also in the unexplored diversity of molecular adaptive mechanisms that are important for controlling RNA modification density.

In addition to observing existing RNA modifications, NAIL-MS pulse-chase analysis is helpful in assigning them to co- or post-transcriptional modification processes. Previous results of the our group indicated that many modifications in rRNA and tRNA, but also m^6A in mRNA, are subsequently introduced into the RNA. Since m^6A-modifying enzymes are exclusively localized in the nucleus and work on nascent mRNAs, I wanted to investigate the phenomenon of post-transcriptional modification in more detail. By using the RNA transcription inhibitor Actinomycin D (Acm D), the analysis of enzymatic post-methylation could be distinguished from transcription processes. The level of post-methylated m^6A decreased under Acm D stress, suggesting a time-limited transcription mechanism in the cell in which hybrid RNA is constructed from unlabeled and isotopically labeled building blocks. My results suggest that NAIL-MS experiments have a temporal limitation that needs to be considered in experimental planning. Proteome and oligonucleotide MS experiments will provide further insights into this.

Conventional oligonucleotide MS analysis, which is carried out by only a few working groups due to the use of ion-pairing reagents and on dedicated mass spectrometers, cannot be linked compatibly with nucleoside MS analysis. To remove this hurdle, I have established an oligonucleotide LC method that can be used to analyze RNAs in a sequence-specific manner without the need for ion-pairing reagents, in a way that is gentle on MS and low in contamination. Modifications in enzymatically modified *in vitro* transcribed (IVT) tRNA can thus be chromatographically separated from unmodified ones, sequentially detected and quantified. I was able to quantitatively and positionally determine the deamination of adenosine to inosine in the anticodon loop of IVT $tRNA^{Val}_{AAC}$. The method is based on a specific RNase T1 digestion, which can also be used to map RNA modifications in native total tRNA.

In summary, both NAIL-MS and oligonucleotide MS analytics increase the knowledge of RNA modifications, their mechanisms and their dynamics and can be used for clinical purposes in the treatment of diseases and for quality control of a growing number of RNA-based drugs and vaccines.

1. Einleitung und Theorie

1.1 Struktur und Synthese der RNA

1.1.1 RNA als Baustein des Lebens

Ribonukleinsäure oder kurz RNA ist ein Biopolymer, welches an verschiedensten Prozessen in der Zelle und somit des Lebens beteiligt ist. Eine herausragende Position nimmt die RNA in der Molekularbiologie ein. Im zentralen Dogma der Molekularbiologie, welches 1958 von Francis Crick postuliert[3] und 1970 ergänzt[4] wurde, verbindet sie die Transkription, die Umschreibung der genetischen Information aus DNA in RNA, mit der Translation, der Synthese von Proteinen in einer jeden Zelle. Des Weiteren besitzt die RNA vielfältige regulatorische Funktionen bis hin zur Selbstregulation und kann als Ribozym katalytisch aktiv sein. Die RNA ist aus den vier kanonischen Nukleobasen, Cytosin, Uracil, Guanin und Adenin, aufgebaut. Durch die definierte Abfolge dieser Basen entsteht ein Code. Die Nukleobasen werden über die N1 bei Pyrimidinen oder N9 bei Purinen mit der C1´-Position einer Riboseeinheit glykosidisch verknüpt. Die entstehenden Nukleoside Cytidin (C), Uridin (U), Guanosin (G) und Adenosin (A) sind über die C5´ und C3´-Position der benachbarten Ribose-Zuckerpucker miteinander kovalent über einen Phosphodiester verbunden (siehe Abbildung **1.1**).

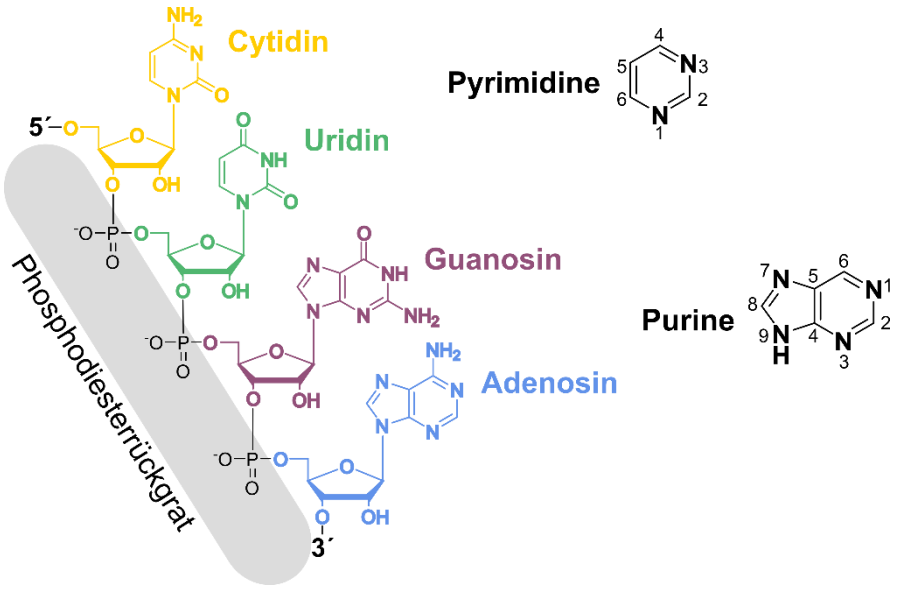

Abbildung 1.1: Aufbau der RNA. Das grauhinterlegte Phosphodiesterrückgrat verbindet die vier kanonischen Nukleotide der RNA, Cytidin (gelb), Uridin (grün), Guanosin (lila) und Adenosin (blau). Die Synthese der RNA findet von 5´-Ende zum 3´-Ende statt. In schwarz sind neben der RNA die beteiligten Heterozyklen und ihre Nummerierung abgebildet.

1.1.2 RNA-Spezies und ihre Synthese

Durch die definierte Aneinanderreihung der RNA-Nukleotide zu einer Primärsequenz entstehen unterschiedliche RNA-Spezies. Die messenger RNA (mRNA[5]) dient als kurzzeitiger Speicher der genetischen Information, enthält den Grundplan für die Proteinbiosynthese und ist eine codierende RNA-Spezies. Nicht-Protein-codierende Spezies sind ribosomale RNAs, welche als Ribosom den Ort der Proteinbiosynthese stellen. Die 28S rRNA ist aus circa 4700 Nukleotiden (nts) aufgebaut, die 18S rRNA aus ungefähr 1900, 5,8S rRNA 160 und 5S rRNA 120. Des Weiteren gibt es die 75 – 90 nts langen Transfer-RNAs (tRNAs), die als Adaptermoleküle mRNA lesen und die passenden Aminosäuren für das neu entstehende Protein liefern[6]. Kleine regulatorische RNAs, wie miRNA und siRNA, zählen auch zu den nicht-codierenden RNAs.

Alle RNAs in der Zelle werden von Polymerasen hergestellt. Die Polymerasen zählen als Enzyme zur Unterklasse der Nukleotidyltransferasen, da sie unter Bildung einer Phosphodiesterbindung ein Nukleotid zu dem bestehenden RNA-Strang hinzufügen (transferieren). Die RNA-Polymerasen teilen sich in DNA-abhängige RNA-Polymerasen, welche aus einem DNA-Templat (Gen) RNA synthetisieren/transkribieren können, und in RNA-abhängige RNA-Polymerasen auf. Hier sind die an der Polyadenylierung von mRNAs beteiligte Poly(A)-Polymerase[7] und Polynukleotidphosphorylase, die sowohl zum Auf- als auch zum Abbau des Poly(A)-Schwanzes der mRNA beiträgt[8], und die virale RNA-Polymerase genannt.

Der weitausgrößere Teil der DNA-abhängigen RNA-Polymerasen teilt sich wiederum in Einzelenzympolymerasen, wie der T7-Bakteriophagen Polymerase, und den multimeren Enzymkomplexen. Die nachfolgend erwähnten RNA-Polymerasen gehören zu den Enzymkomplex-Polymerasen.

Während in prokaryotischen Organismen eine einzige RNA-Polymerase das komplette Transkriptom, die Gesamtheit aller RNAs in einer Zelle, herstellt, benötigen Eukaryoten dafür mehrere RNA-Polymerasen. Diese sind nach ihrer Elutionszeit bei der erstmaligen chromatographischen Auftrennung aus Seeigeln durch Robert Roeder 1969 RNA-Polymerase I (zuständig für 28S, 18S und 5,8S rRNA-Synthese), II (zuständig für mRNAs und smallRNAs) und III (tRNA, 5S rRNA und weitere smallRNAs) genannt worden[9]. Pflanzen besitzen zudem zwei weitere RNA-Polymerasen IV und V, die siRNAs synthetisieren und somit zur Genregulation

beitragen[10, 11]. Die aus fünf Proteinuntereinheiten bestehende bakterielle RNA-Polymerase (2α,β,β´,ω) wird bei Anlagerung an den transkriptionsinitiierenden σ-Faktor funktionsfähig[12]. Diese fünf großen Proteinuntereinheiten sind in allen Bereichen des Lebens evolutionär konserviert. Zusätzlich zu diesen prokaryotisch orthologen Einheiten teilen die eukaryotischen RNA-Polymerasen einen gemeinsamen Kern an fünf weiteren Untereinheiten. Des Weiteren besitzen sie weitere nahe verwandte Proteineinheiten, die zu einem ähnlichen Aussehen der RNA-Polymerasen beitragen[13] [14] [15] [16]. In Abbildung **1.2** ist eine generelle Struktur mit funktionalen Bereichen der RNA-Polymerase abgebildet, die einer Krabbenschere ähnelt. Das obere und untere Ende der Schere interagieren mit dem doppelsträngigen DNA-Templat, welches an der unteren Seite der Schere bis zu der Wand entlangläuft. An der Wand befindet sich das katalytisch aktive Zentrum der RNA-Polymerase mit zwei divalenten Metallionen, einer aktivierenden Schleife und einer Brückenhelix. Der neue DNA/RNA-Hybridstrang wird senkrecht zum DNA-Doppelstrang nach oben gebogen. Beide Stränge werden von einer Klemme in Position gehalten. Der Stengel interagiert mit dem neu synthetisierten Strang. Ein Zusammenhaltsbereich sorgt für die Stabilität des gesamten multimeren Enzymkomplexes[17].

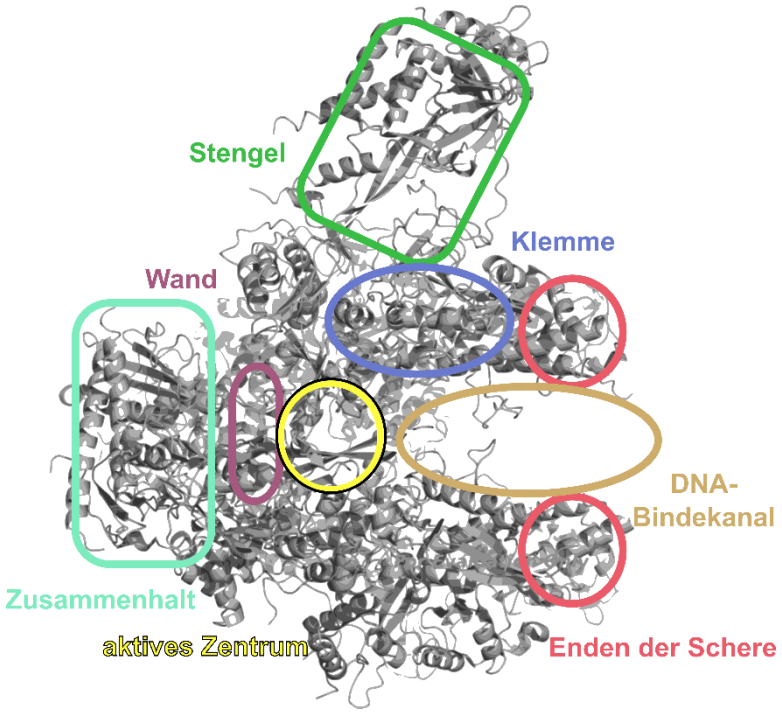

Abbildung 1.2: Generelle Struktur einer RNA-Polymerase. Die für die RNA-Synthese wichtigen Bereiche der Polymerase sind farblich umkreist und ihre genaue Funktion im Fließtext erläutert. Diese Abbildung wurde mit Hilfe der Kristallstruktur (PDB: 1Y1W) erstellt und von Werner et al. adaptiert[17].

Um eine erfolgreiche Transkription zu gewährleisten, benötigen die RNA-Polymerasen Transkriptionsfaktoren, wie den σ-Faktor (Prokaryoten) oder eine Vielzahl an unterschiedlichen Proteinen (Eukaryoten)[18] [19] [20]. Die konservierten Transkriptionsfaktoren, sowie die Polymerase-Untereinheiten sind in folgender Tabelle **1.1** dargestellt.

	Prokaryoten	Eukaryoten		
		RNA-Pol I	**RNA-Pol II**	**RNA-Pol III**
RNA-Pol Untereinheiten	β-Untereinheit	A190	RPB1	C160
	β´-Untereinheit	A135	RPB2	C128
	α-Untereinheit	AC40	RPB3	AC40
	α-Untereinheit	AC19	RPB11	AC19
	ω-Untereinheit	RPB6	RPB6	RPB6
		RPB5	RPB5	RPB5
		RPB8	RPB8	RPB8
		RPB10	RPB10	RPB10
		RPB12	RPB12	RPB12
		A14	RPB4	C17
		A43	RPB7	C25
		A12	RPB9	C11
Transkriptionsfaktoren	Rho			
	σ-Faktoren			
		A49	TFIIFα	C53
		A34,5	TFIIFβ	C37
			TFIIEα	C82
			TFIIEβ	C34
		TBP	TBP	TBP
			TFIIB	BRF1
			TFIIS	TFIIS
			SPT4	SPT4
	NusG		SPT5	SPT5

Tabelle 1.1: Evolutionär konservierte RNA-Polymerase-Untereinheiten und Transkriptionsfaktoren. Orthologe Untereinheiten und Transkriptionsfaktoren sind gelistet, wenn sie mindestens in einer weiteren Spezies vorkommen. Die Tabelle wurde nach der Adaption[17] vereinfacht.

Der Prozess der Transkription lässt sich bei jeder Polymerase in folgende drei Schritte unterteilen: der Initiation, der Elongation und der Termination. Genauer wird bei der Initiation die Bildung eines Präinitiationskomplexes (*engl.* PIC) bestehend aus der Polymerase, der Genpromotorsequenz und verschiedenen Transkriptionsfaktoren vorangetrieben. Bei der Elongation, also der Verlängerung des neuen

Nukleinsäurestranges, findet die Umschreibung der Gene in die korrespondierende RNA-Sequenz statt. Die Termination sorgt für einen Stopp der Transkription und die Loslösung der Polymerase von dem betroffenen Genabschnitt. Zur Transkription verschiedener RNA-Spezies müssen unterschiedliche Genabschnitte in der DNA von den Polymerasen angesteuert werden. Es fällt auf, dass die 18S, 5,8S und 28S rRNA auf einem Genabschnitt hintereinander –nur von sogenannten intern und extern transkribierten Trenn-DNA-Sequenzen unterbrochen- wiederholend vorkommen (siehe Abbildung **1.3**)[21]. Diese wiederholende Abfolge des rRNA-Gens sorgt für eine Vielzahl an Kopien der rRNA zur selben Zeit. Viele RNA-Polymerasen I können so zeitgleich rRNAs synthetisieren. Unter dem Elektronenmikroskop wird die sogenannte „Miller-Spreitung“ (nach O. L. Miller Jr.) sichtbar, da ein rDNA-Abschnitt Ausgangspunkt für mehrere Polymerasen ist, die neue Transkripte der rRNA herstellen [22]. Ein strangaufwärts befindliches Kontrollelement (UKE) und eine Kernpromotorsequenz bilden Regulationsmöglichkeiten für die Aktivität der Polymerase I.

Der mit 94 % größte Anteil aller Gene für RNA-Polymerasen wird von RNA-Polymerase II transkribiert[23], was mit der Vielzahl und Variabilität von Protein-codierenden mRNAs begründet werden kann. Die zugehörigen DNA-Sequenzen besitzen verschiedene Enhancerelemente Richtung 5´-Ende, die Transkriptionsfaktoren oder allgemein Aktivatoren binden können. Diese Bindung vermittelt unter anderem eine Umstrukturierung des Chromatins, sodass nicht durch Histone verpacktes Euchromatin die Erreichbarkeit für die Polymerase II garantiert. Die für mRNA-Gene charakteristische TATA-Sequenz[24] befindet sich 30 Nukleotide vor der Transkriptionsstartseite. Strangabwärts (zum 3´-Ende) markiert eine Polyadenylierungsseite (pA) das Ende des jeweiligen mRNA-Gens. Die Gensequenzen für die RNA-Polymerase III unterscheiden sich ihrer geringeren Länge, da die Transkripte eine Größe von 500 Nukleotiden nicht überschreiten. Für Synthese von 5S rRNA benötigt die RNA-Polymerase III die internen Kontrollregionen Box A und Box C sowie ein intermediär vorkommendes Element, für tRNAs die Box A und B.

Nach den sequenziellen Grundlagen soll im Folgenden auf den genauen Ablauf der Transkription durch die drei eukaryotischen RNA-Polymerasen, sowie die Prozessierung der RNA-Spezies-Transkripte eingegangen werden.

Die Transkription von rRNA durch RNA-Pol I beginnt mit dem Initiierungsschritt, in dem UBF (*engl*. für upstream binding factor) an das Kontrollelement bindet. Dieses rekrutiert nun im gebundenen Zustand TBP (*engl*. für TATA-Sequence binding protein), drei assoziierte Proteine (TAF 1A, C, D) und im Menschen das SL1-Protein [25] [26]. Der so entstandene Präinitiationskomplex lässt die RNA-Pol I nun zur Elongation übergehen, während die vorhandenen Transkriptionsfaktoren eine weitere RNA-Polymerase I an die Gensequenz leiten können. Die RNA-Pol I wird durch ein 1000 Basenpaare strangabwärts des 3´-Genendes gebundenes TTF1-Protein an der weiteren Ablesung des Stranges gestoppt und mittels weiterer Proteine von der Gensequenz gelöst[27]. Die Synthese und die Prozessierung von 28S, 18S und 5,8S rRNA erfolgt im Nukleolus. Die co-transkiptional modifizierte 45S prä-rRNA-Spezies wird zunächst durch Nukleasen an den 5´- und 3´-Enden getrimmt, d.h. die extern transkribierten Trenn-DNA-Sequenzen abgespalten. Nachfolgend wird die 41S prä-rRNA durch Entfernen der internen Trenn-DNA-Sequenzen in eine 20S prä-rRNA und eine 32S prä-rRNA umgewandelt. Dieser Schritt wird von Endo- und Exonucleasen ausgeführt und stellt kein Splicing dar. Während die 20S prä-rRNA zur 18S rRNA reift, faltet die 32S prä-rRNA sich intramolekular über Wasserstoffbrücken und reift zum 28S und 5,8S rRNA-Komplex. Die letzte rRNA, die 5S rRNA, wird von RNA-Pol III hergestellt und deswegen später in diesem Kapitel erwähnt.

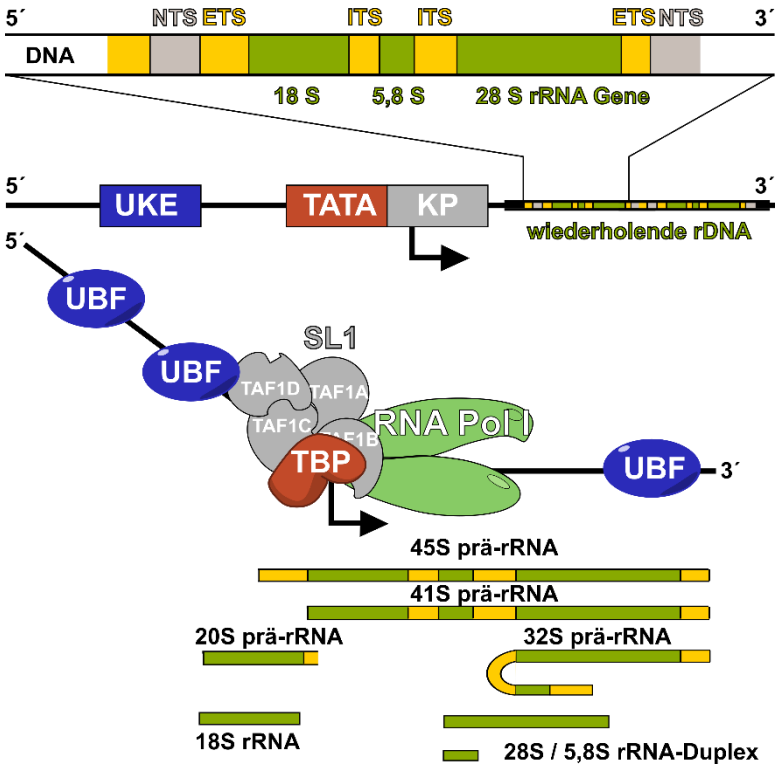

Abbildung 1.3: Synthese der rRNA durch RNA-Polymerase I mit Prozessierung. Die Gensequenz, die für die 3 rRNA-Spezies codiert, wird auch rDNA genannt und teilt sich in nicht-transkribierte (NTS), extern-transkribierte (ETS) und intern-transkribierte (ITS) Trenn-DNA-Sequenzen auf, die wiederholend zwischen den 18S, 5,8S und 28S-Genabschnitten liegen. Das strangaufwärts sitzende Kontrollelement (UKE) ist Bindestelle für Proteine (UBF). Um die Transkriptionsstartseite (mit Pfeil markiert) liegen der Kernpromoter (KP) und die TATA-Box. Die PIC-Formation, sowieso die prä-rRNA-Reifung sind im unteren Teil der Grafik dargestellt.

mRNAs und eine Vielzahl an kleinen, regulierenden RNAs entstehen durch die Transkription mit RNA-Pol II (Abbildung **1.4**). In der Größe variiende Zellen besitzen eine konstante Menge an mRNAs, dafür sorgen die transkriptionslimitierende RNA-Pol II und ein gegenläufiger Trend der mRNA-Stabilität[28]. Mit 44 Polypeptiden, welche als Initiationsfaktoren mitwirken, ist die Komplexitität am größten. Die Initiation startet durch die Bindung eines Aktivators an strangaufwärts befindlichen Enhancerelementen und mit der Rekrutierung von TFIIB und TBP (Untereinheit von TFIID) an der TATA-Box. TFIIE, TFIIF und TFIIH sorgen für die Öffnung der DNA und der RNA-Pol II-Klammer, den Zusammenhalt des PICs und die Phosphorylierung der carboxy-terminalen-Domäne der RNA-Pol II[29] [30]. Das Protein Mediator reguliert den Phoshorylierungstatus der Polymerase in Abhängigkeit von anwesenden, strangaufwärts gebundenen Aktivatoren oder Repressoren und ist auch mit den Transkriptionsfaktoren des PICs verbunden[31]. Die Elongation der RNA-Pol II startet mit einem Nukleotidadditionszyklus, bei dem das zur DNA komplementäre rNTP im aktiven Zentrum des Enzyms selektiert und insertiert wird[32]. Hierbei helfen zwei Metallionen, eines fest und eines flexibel, die durch negativgeladene Aminosäureseitenketten koordiniert werden. Über einen S_N2-Mechanismus attackiert die freie 3´-OH-Gruppe des zuvor eingebauten Nukleotids das α-Phosphat des zu insertierenden rNTPs. Die Freisetzung des Pyrophosphates fördert vielleicht die Öffnung des aktiven Zentrums. Bevor ein nächstes Nukleotid eingebaut werden kann, muss die RNA-Pol II translokiert und die Direktionalität festgelegt werden[33]. Das passiert mittels einer molekularen Ratsche, die von einer aktivierenden Schleife und einer Brückenhelix gebildet wird. Nur nach erfolgreicher Translokation kann ein neues rNTP eingebaut werden. Der Elongationkomplex ist durch die DNA/RNA-Hybridbildung sehr stabil, besitzt eine kleine Fehlereinbaurate und kann 30 – 50 nts pro Sekunde verknüpfen[34]. Nachdem die Polyadenylierungsseite (pA) auf dem Gen von der RNA-Pol II transkribiert wurde, durchläuft die Polymerase circa 1000 bp strangabwärts Terminationssequenzen, die das Transkript und die RNA-Pol II freisetzen[35]. Die schon

erwähnte RNA-abhängige Poly(A)-Polymerase hängt nun einen Poly(A)-Schwanz an das neu entstandene Transkript. Zeitgleich mit der Synthese der mRNA im Zellkern findet dort auch die Prozessierung statt. Sowohl das 5´-Capping[36], sowie das Splicing [37] als auch die Polyadenylierung[38] finden co-transkriptional statt. Auch die Nukleotide des neuen mRNA-Stranges werden noch im Zellkern modifiziert, bevor die mRNA durch die Kernpore in das Cytosol transportiert wird.

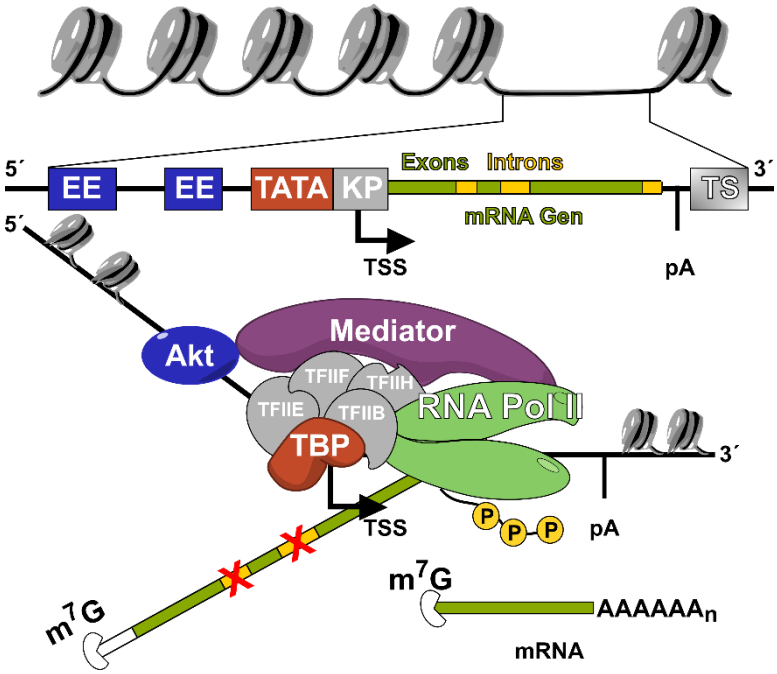

Abbildung 1.4: Synthese der mRNA durch RNA-Polymerase II mit Prozessierung. Die Gensequenz, die für mRNA codiert, ist in der Vergrößerung des Euchromatins abgebildet und teilt sich in Enhancerelemente (EE), Terminationssequenz (TS) und den um die Transkriptionsstartseite (TSS) liegenden Kernpromoter (KP) und die TATA-Box auf. Die PIC-Formation mit dem Protein Mediator und der phosphorylierten (P) carboxy-terminalen Domäne der Polymerase, sowie die prä-mRNA-Reifung sind im unteren Teil der Grafik dargestellt.

Sowohl cytosolische tRNAs (Abbildung **1.5 A**) als auch die 5S rRNA (Abbildung **1.5 B**) und weitere kleine, regulierende RNAs werden von der RNA-Polymerase III hergestellt. Auf mitochrondriale tRNA-Synthese wird im Folgenden nicht eingegangen. Für die Synthese von cytosolischen, eukaryotischen tRNAs formen die Kontrollregionen Box A und Box B eine zweigeteilte Bindestelle für den Transkriptionsfaktor TFIIIC auf der Gensequenz. Interessant ist, dass die Boxen A und B für die konservierten Bereiche der D-Schleifen und der TΨC-Schleifen in der tRNA codieren. Der PIC besteht für die Klasse-2-Gene, wie tRNA-Gene, aus TFIIIC und TFIIIB als Promotorbindungsfaktor[18]. Außerdem ist er deutlich stabiler als der Pol II-

PIC, was in robusterer Transkription und schnellerem Pol III-Recycling an die Promotersequenz resultiert[39]. Die tRNA-Transkription wird mit Erreichen einer Thymidin-reichen Gensequenz terminiert, da die komplementär synthetisierte Uridin-reiche Schleife eine Dissoziation der RNA-Pol III von der prä-tRNA auslöst. Die Prozessierung der tRNA besteht aus mehreren Schritten. Durch die Ribonuclease RNase P wird das 5´-Ende des Transkripts gekürzt[40] und danach durch weitere Exo- und Endonucleasen das 3´-Ende gestutzt[41]. Mit Hilfe einer Nukleotidyltransferase wird die charakteristische CCA-Sequenz an das neue 3´-Ende der prä-tRNA übertragen[42]. Einige prä-tRNAs haben Intronsequenzen in der Nähe des späteren Anticodons und werden durch eine Endonuclease herausgesplict[43]. Wichtig ist hierbei zu erwähnen, dass dieser Schritt unabhängig von Spliceosom ist. Während der Splicing-Schritt im Cytosol stattfindet, teilt sich die tRNA-Modifikations-Maschinerie in nuklear- und cytosolisch arbeitende Writer-Enzyme auf. Nur gekürzte und gesplicte tRNAs falten sich zur korrekten 3D-L-Struktur und somit stellt dieser Prozess eine Qualitätskontrolle sicher.

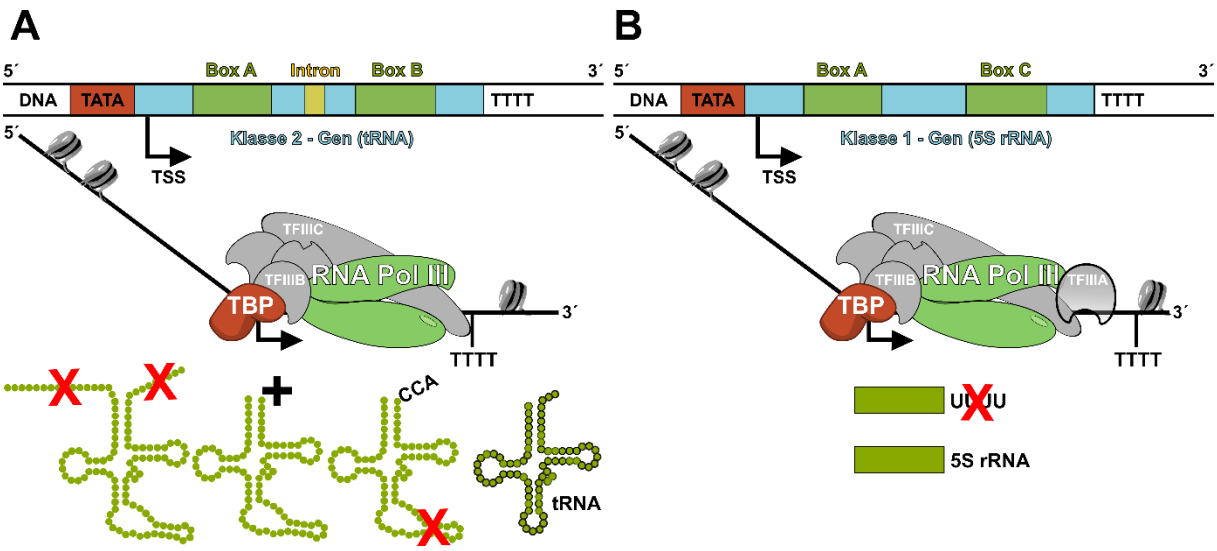

Abbildung 1.5: Synthese der tRNA und 5S rRNA durch RNA-Polymerase III mit Prozessierung. Die Gensequenz, die für tRNA codiert, ist in **A** abgebildet. Die PIC-Formation, sowieso die prä-tRNA-Reifung mit Verkürzung, CCA-Addition und Intronsplicing sind im unteren Teil der Grafik dargestellt. **B** zeigt die 5S rRNA-Synthese mit dem spezifischen Transkriptionsfaktor TFIIIA und die Verkürzung am 3´-Ende der prä-rRNA stellt die einzige Prozessierung dar.

Für die Synthese der 5S rRNA-Spezies werden die Klasse-1-Gene transkribiert. Dafür bindet ein sequenzspezifischer Transkriptionsfaktor TFIIIA, der nicht an der tRNA-Transkription beteiligt ist, an die C-Box und rekrutiert das Protein TFIIIC[44]. Während die Termination identisch zur tRNA-Transkription abläuft, besitzt die 5S rRNA keine 5´-

Sequenz, die gekürzt werden muss, sodass das finale 5S rRNA-Transkript ein 5´-Triphosphat besitzt.

1.1.3 Inhibition der RNA-Synthese

Die Entdeckung der drei eukaryotischen Polymerasen und das Fehlen einer universellen Polymerase (wie in Prokaryoten) durch Roeder wurde durch die selektive Inhibierung der RNA-Polymerasen auf α-Amanitin im Jahr 1970 bestätigt[45] [46]. Im Verlauf dieses Kapitel werden sowohl α-Amanitin als auch weitere RNA-Synthese-Inhibitoren und ihr detaillierter Wirkmechanismus vorgestellt. α-Amanitin ist ein aus acht Aminosäuren bestehendes bizyklisches Peptid und als Giftstoff in einer Gattung von Pilzen vorkommend. Es bindet Wasserstoffbrücken mit der Brückenhelix der RNA-Polymerase II, Bestandteil der „molekularen Ratsche“ aus. Genauer binden das Hydroxyprolin und das Dihydroxyleucin des α-Amanitins Glutaminseitenketten der Brückenhelix[47]. So wird die Translokation, die für die Elongation der RNA-Polymerase II essentiell ist, gestört[33] und die Syntheserate auf wenige Nukleotide pro Minute herabgesetzt[48]. Nur die RNA-Polymerase II wird durch α-Amanitin inhibiert. Es kommt zu einem Stopp der mRNA-Synthese und nachfolgend zum Zelltod durch Proteinbiosynthesestopp.

Ein selektiver Inhibitor der prokaryotischen RNA-Polymerase ist das Rifampicin, ein makrocyclisches Lactam, das durch die Selektivität antibiotisch wirkt[49]. Es bindet hauptsächlich über van der Waals-Bindungen an hydrophobe Seitenketten der β-Untereinheit der Polymerase. In der Bindungsregion gibt es nur eine geringe sequenzielle Übereinstimmung im Vergleich zu eukaryotischen Organismen, die aufgrund dessen eine Resistenz gegenüber Rifampicin besitzen[50]. Tief im DNA/RNA-Kanal blockiert es sterisch die Elongation des neuen RNA-Transkripts, wenn dieses eine Größe von 2 – 3 nts erreicht hat[51].

Eine weitere Klasse der RNA-Inhibitoren stellen die Nukleosid- oder Nukleobasenanaloga dar. Die Antimetabolite Cordycepin (3´-Desoxyadenosin) und 6-Mercaptopurin ähneln in ihrer chemischen Struktur dem Adenosin bzw. dem Purin. Cordycepin inhibiert die Nukleinsäuresynthese[52], indem es in der Zelle phosphoryliert und dann fälschlicherweise anstelle des Adenosintriphosphates in die RNA eingebaut wird. Aufgrund des Fehlens der 3´-Hydroxylgruppe kann keine Elongation der Transkription stattfinden[53]. Auch die Prozessierung der mRNA, die Polyadenylierung wird inhibiert[54]. 6-Mercaptopurin wirkt sowohl bei der Neusynthese als auch beim

Aufbau von Purinnukleosiden aus Purinen durch seine thiolierten Inosin- und Guanosinmetabolite mittels Feedbackloop inhibierend[55]. In Nukleinsäuren eingebaut, ist das 6-Thioguanosin zytotoxisch, da es DNA-Strangbrüche hervorruft[56].

Als letzter Inhibitor soll der Mechanismus des Actinomycin D besprochen werden, der im experimentellen Teil dieser Arbeit verwendet wurde. Actinomycin D besteht strukturell aus zwei zyklischen Peptiden, die an einen Phenoxazinring gekoppelt sind (Abbildung **1.6 B**). In der kleinen Furche der DNA-Doppelhelix interkaliert der Phenoxazinring zwischen zwei GC-Basenpaare, die zusätzlich mit jeweils einem der zyklischen Peptide interagieren (Abbildung **1.6 A**)[57] [58].

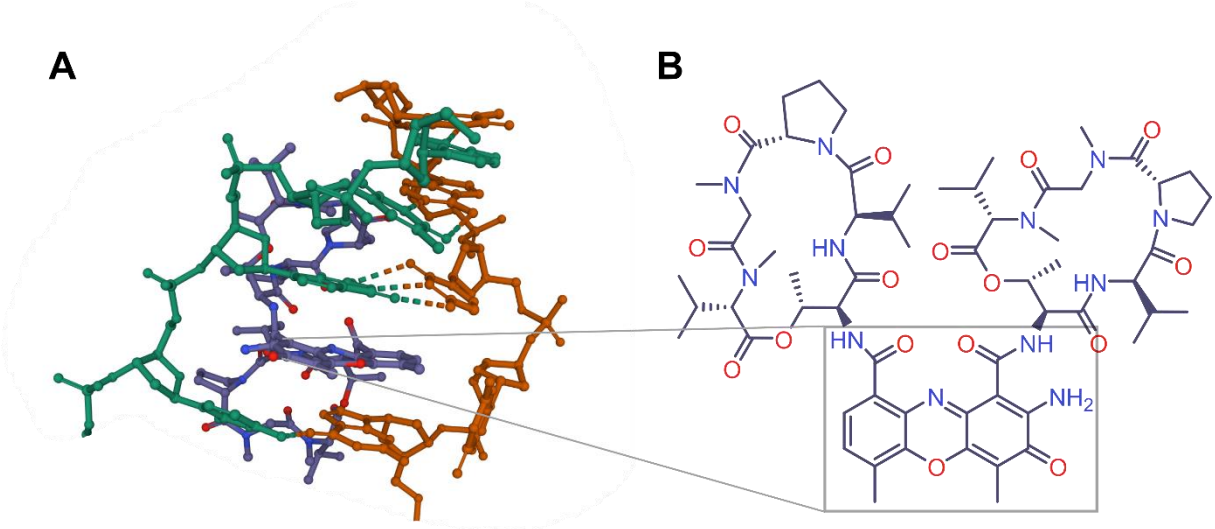

Abbildung 1.6: Interkalation des Actinomycin D in die DNA-Doppelhelix. In **A** ist die DNA in dunkelgrün und orange angefärbt. Das violette Actinomycin D-Molekül besitzt rot- und blaumarkierte Atome für Sauerstoff- und Stickstoffpositionen. Die Kristallstruktur kann unter der Protein Database Nummer 4HIV angesehen werden[58]. Die chemische Strukturformel in besserer Übersicht ist in **B** dargestellt.

Der sehr stabile Interkalationskomplex sorgt dafür, dass die Doppelhelix von Topoisomerasen und RNA-Polymerasen nicht mehr geöffnet werden kann[59] und die Transkription unterbleibt[60]. Actinomycin D hemmt verschiedene RNA-Spezies konzentrationsabhängig. rRNA-Spezies von RNA-Polymerase I werden bei geringeren Konzentrationen als mRNA (RNA-Pol II) und als tRNA (RNA-Pol III) gehemmt. Zwei Effekte liegen dieser Beobachtung zu Grunde. Erstens, je länger das RNA-Transkript, desto länger ist die DNA-Gensequenz und desto wahrscheinlicher ist es, dass ein Actinomycin D-Molekül in der Gensequenz interkaliert. Zweitens, rRNA hat - bedingt durch die Architektur des Genabschnittes - nur sehr wenige Transkriptionsstartseiten,

an denen die Ribosomen andocken können. Je weniger Andockstellen, desto weniger Actinomycin D-Moleküle reichen aus, um die ribosomale Transkription zu inhibieren[61].

1.2 RNA-Modifikationen und ihre Dynamik

1.2.1 Überblick über RNA-Modifikationen

RNA als Baustein des Lebens besteht nicht nur aus den vier kanonischen Nukleosiden C, U, G und A, sondern enthält bis zu 163 RNA-Modifikationen (Stand: 2017)[62], die eine zweite Ebene an Information eröffnen. Analog zur Epigenetik wird dieses durch Entdeckung neuer RNA-Modifikationen, sowie der Entschlüsselung von regulatorischen Prozessen, an denen die Modifikationen beteiligt sind, wachsende Forschungsgebiet Epitranskriptomik genannt. RNA-Modifikationen sind universell in allen Domänen des Lebens und in vielen RNA-Spezies vorkommend. Methylierungen an der Nukleobase (m = methyl wird **vor** dem Buchstaben des kanonischen Nukleosids geschrieben) oder an der 2´-Hydroxygruppe der Riboseeinheit (m = methyl wird **nach** dem Buchstaben des kanonischen Nukleosids geschrieben) sind die abundantesten chemischen Modifizierungen. Die häufigste RNA-Modifikation ist das Pseudouridin (siehe Abbildung **1.7**), welches als erste RNA-Modifikation detektiert wurde[63]. Hierbei handelt es sich um ein Konsitutionsisomer des kanonischen Uridins, welches durch das Enzym Pseudouridinsynthase durch glykosidischen Bindungsbruch, 180°-Drehung und Knüpfung einer C-C-Bindung aus Uridin hergestellt wird[64].

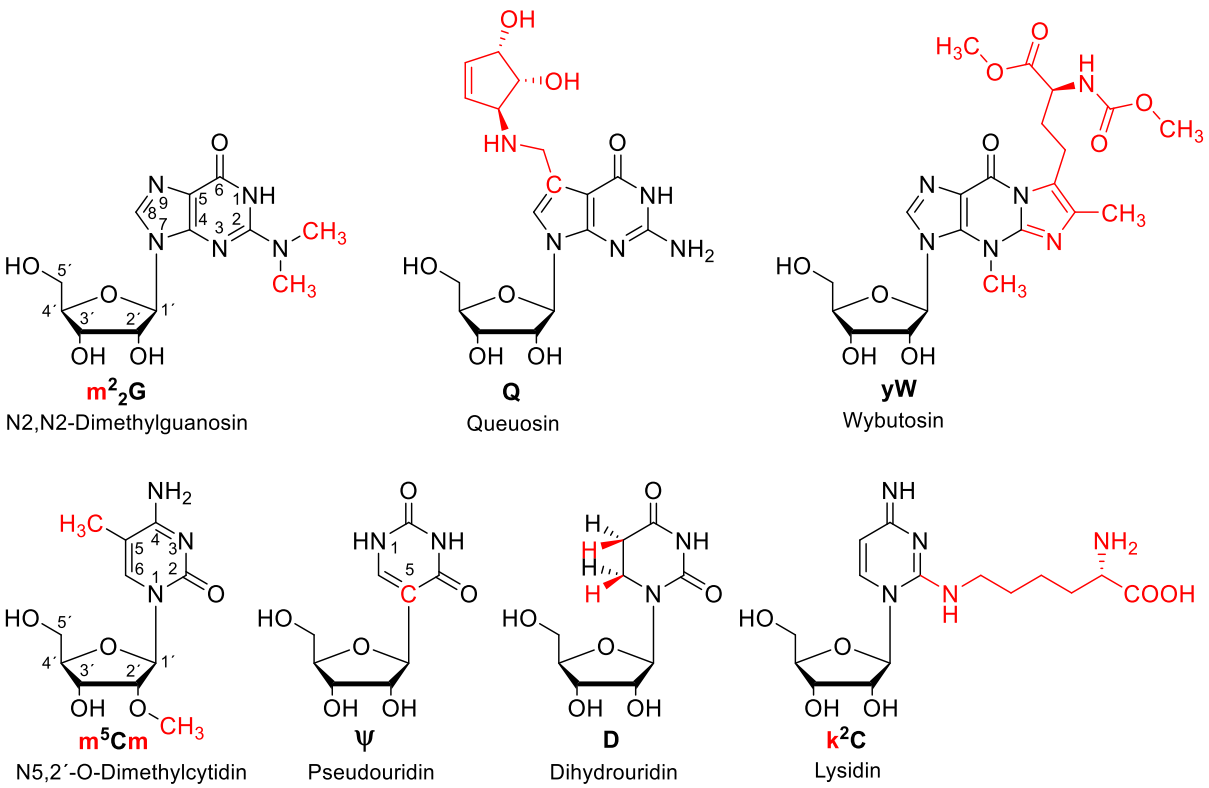

Abbildung 1.7: chemische Vielfalt der RNA-Modifikationen. In der oberen Spalte sind ausgewählte Purinnukleotide abgebildet. Die Nummerierung der Ringatom- und Zuckerpositionen ist anhand des $m^2{}_2G$ gezeigt. Analog befinden sich in der unteren Spalte die modifizierten Pyrimidinnukleotide, wobei zusätzlich zur Nummerierung am Beispiel des m^5Cm die spezielle Nummerierung des Pseudouridins abgebildet ist. Die modifizierten Positionen oder Reste sind rot markiert.

Die kanonischen RNA-Nukleoside können jedoch nicht nur an beliebigen Ringpositionen der Nukleobasen methyliert, sondern auch thioliert, acetyliert, deaminiert oder sogar mit Aminosäuren dekoriert werden. Diese Modifizierungen treten fast nur in der am meisten modifizierten RNA-Spezies, der tRNA, auf, in der 10 – 20 % aller Nukleotide chemisch derivatisiert vorliegen[65]. Darüber hinaus können RNA-Nukleoside mit komplexen chemischen Strukturen funktionalisiert werden, sodass beispielsweise ein Zugang zu Queuosin und Wybutosin möglich ist (Abbildung **1.7**).

1.2.2 Zellstress und Einfluss auf RNA-Modifikationen

Im Folgenden soll darauf eingegangen werden, wie die RNA-Modifikationen entstehen und wie sich das Modifikationsprofil beeinflussen lässt. Hierbei muss zwischen zwei verschiedenen Entstehungsprozessen unterschieden werden: den ungewollten Schädigungen oder den enzymatisch kontrollierten Modifizierungen.

Ungewollte Schädigungen der Nukleinsäuren haben einen vielfältigen Ursprung. So kann energiereiche UV-Strahlung bewirken, dass in der Zelle Pyrimidinhydrate oder Uridincyclobutandimere entstehen[66] [67]. Virale Infektionen[68], pflanzliche Inhaltsstoffe[69] [70] und physische sowie psychische Effekte[71] haben ebenfalls einen Einfluss auf den RNA-Modifikationsstatus. Auf molekularer Ebene werden Nukleobasen durch reaktive Sauerstoffspezies (ROS) oxidativ geschädigt, hier sind die in Abbildung **1.8** gezeigten 8-Oxo-Guanin (8-oxo-G) und 5-Hydroxy-Cytosin (ho^5C) zu nennen. Das mutagene Potenzial des 8-Oxo-Guanins lässt sich strukturell wie folgt erklären: Der Sauerstoff an Position C8 der Base behindert sich sterisch mit der Phosphatgruppe an Position C5´ des Zuckerpuckers. Um dem entgegenzuwirken, nimmt das Guanosin eine *syn*-Konformation ein und paart als Hoogsteenbasenpaar mit Adenosin anstelle von Cytidin, mit dem es normalerweise in der *anti*-Konformation ein Watson-Crick-Basenpaar bildet[72]. 8-Oxo-G als Oxidationsschaden ist in einzelsträngigen Nukleinsäuren abundanter und dort wiederum 5-mal häufiger in mRNA als in rRNA und tRNA vorkommend, weil die Duplexbildung, die Tertiärstruktur

und die Bindung an Proteine eine Attacke der ROS erschweren[73]. 5-Hyroxy-Cytosin entsteht durch Dehydratisierung der C6-Position eines Glycol-Intermediates[74]. Die höhere Elektronegativität des C5-Substituenten führt zwar nicht zu einer kompletten Abkehr der C:G-Watson-Crick-Paarung, aber ermöglicht eine wahrscheinlichere Basenpaarung mit einem Adenosin[75].

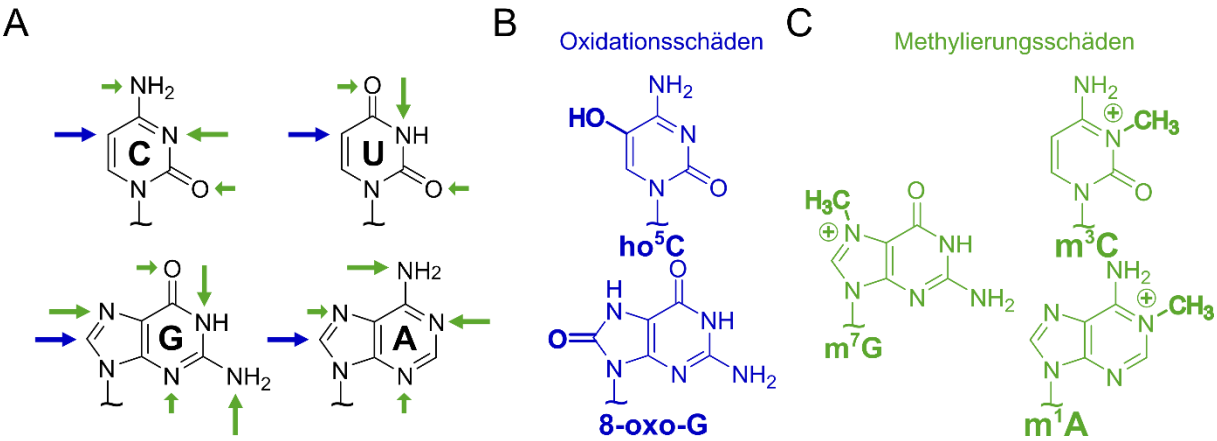

Abbildung 1.8: Konsequenzen der Oxidierung und Methylierung auf RNA-Nukleobasen. In **A** sind die vier kanonischen Nukleobasen und die Neigung bestimmter Positionen zur Oxidation (blauer Pfeil) sowie zur Alkylierung (grüner Pfeil; je größer, desto wahrscheinlicher ist eine Alkylierung an der Stelle) verdeutlicht[76]. **B** und **C** zeigen die chemischen Strukturen der häufigsten Oxidations- bzw. Methylierungsschäden in der RNA.

Neben diesen in der Abbildung **1.8** blau-markierten bevorzugten Oxidationspositionen besitzen Nukleobasen durch ihre Heteroatome weitere favorisierte Alkylierungsstellen, die zur besseren Unterscheidung grünmarkiert vorliegen. Methylierungsreagenzien, wie Methylmethansulfonat (MMS), bilden meistens die Hauptprodukte m^7G, m^3C und m^1A in der RNA. Durch Methylierungsreagenzien geschädigte RNA weist ungewollte strukturelle Änderungen auf, die die Watson-Crick-Basenpaarung behindern oder sogar komplett verhindern können und somit die Translation beeinflussen. Die häufigste Schädigung m^7G behindert zwar nicht die Basenpaarung, jedoch die Bindung von Proteinen an Nukleinsäuren[77] und beschleunigt auch die Depurinierung des Nukleotides[78].

1.2.3 Dynamik I: Writer-Enzyme

Die Zelle kann das Modifikationsprofil auch selbst mit Hilfe von Enzymen regulieren. Enzyme, die am Einbau der Modifikationen in Nukleinsäuren beteiligt sind, werden als „Writer“-Enzyme deklariert. In diesem Abschnitt werden vier dieser „Writer“ mit ihren

korrespondierenden RNA-Modifikationen und ihren bei Fehlregulation assoziierten Krankheiten vorgestellt.

Der heterodimere Enzymkomplex METTL3/14 inkorporiert die RNA-Modifikation m^6A in mRNA, wobei METTL3 die Methylierung der mRNA mit Hilfe des Cofaktors S-Adenosylmethionin (SAM) durchführt und METTL14 als struktureller Gerüstgeber dient[79]. Der Komplex assoziiert mit der Proteinuntereinheit WTAP, die diesen zum Kern der Zelle rekrutiert, wo die m^6A-Methylierung co-transkriptional abläuft[80] [81]. Zur vollen Methylierungsaktivität fehlt das Protein KIAA1429, welches durch Cross-Link und Proteom-MS-Studien entdeckt wurde[82]. m^6A die am häufigsten in mRNA vorkommende interne Modifikation, die in Introns und am 3´-Ende der mRNA stärker vertreten ist. Sequenziell zeichnen sich die möglichen m^6A-Methylierungsstellen durch ein RRACH-Motif aus[83]. Eingebautes m^6A verändert die Faltung der RNA[84], beeinflusst das Splicing[85] und beschleunigt allgemein die Prozessierung der prä-mRNA[86]. Zudem fördert es die Translation[87], beschleunigt den Transport von mRNA innerhalb der Zelle[88], UV-Reperaturmechanismus[89] und den Abbau von mRNAs[90]. Eine direkte Verbindung des m^6A zu Krankheiten gibt es nicht, jedoch fördert ein mutiertes oder ausgeschaltetes METTL3-Enzym Lungenkrebs[87] und akute myeloische Leukämie[91].

Ein anderes Writer-Enzym ist METTL6, das für m^3C in tRNA zuständig ist. Hierbei ist die Methylierungsaktivität nur auf spezifische tRNA-Serin-Akzeptoren und dort auf das Cytidin an Position 32 in der Anticodonschleife beschränkt[92]. METTL6, das im Nukleus und im Cytosol vorliegt, kann alleine kein m^3C generieren, sondern benötigt für die Methylierung an Position 32 die Seryl-tRNA-Synthase als Partner. Zusätzlich ist sowohl die Sequenz des Anticodonarms, als auch die Sequenz des langen variablen Arms des Serin-tRNA-Akzeptors wichtig, um eine Methylierung zu ermöglichen. Gerade die letztgenannte Eigenschaft erklärt, warum nur Serin- nicht aber Threonin-tRNA-Akzeptoren, die einen kürzen variablen Arm besitzen, Substrat für METTL6 sein können[93]. Durch Knockout-Studien in Mäusen wurde METTL6 nicht nur als m^3C-Methyltransferase bestätigt, sondern auch als Onkogen identifiziert. Es wurden Defekte in Zellwachstum und ein Beeinträchtigung der Pluripotenz nachgewiesen[94]. Eine Korrelation von METTL6 mit Brustkrebs und Lungenkrebs sind weitere Belege für ein Onkogen[95] [96].

Ein anderes Enzym, das auch tRNA als Substrat besitzt, aber eine andere RNA-Modifikation generiert, ist das TRMT1. Es dimethyliert ein Guanosin-Nukleotid an Position 26 zu $m^{22}G$ in tRNA. Wenn G_{26} dimethyliert in der tRNA vorliegt, kann es durch die Sterik keine dritte Wasserstoffbrücke zu einem Watson-Crick-gepaarten Cytidin mehr ausbilden. Gleichzeitig ist in der tRNA-Maturierung aber genau dieser Effekt grundlegend für eine korrekte, dreidimensionale Faltung des tRNA-Moleküls[97]. Das Writer-Enzym TRMT1 ist ein 659 Aminosäuren beinhaltendes Polypeptid mit einer SAM-basierten Methyltransferaseregion und einem Kern- sowie Mitochrondriumlokalisierungssequenz, die benötigt werden, damit TRMT1 die mitochrondrialen tRNA sowie 10 kern-transkribierende tRNA dimethylieren kann. Fehlendes TRMT1 in den Zellen mündet in einer verringerten Translationsrate und einer gesteigerten Sensitivität gegenüber oxidierenden ROS-Spezies[98]. TRMT1-Varianten, bei denen einzelne Aminosäuren mutiert sind, führen in den betroffenen Patienten zu geistiger Behinderung, Mikrozephalie und Epilepsie[99] [100] [101].

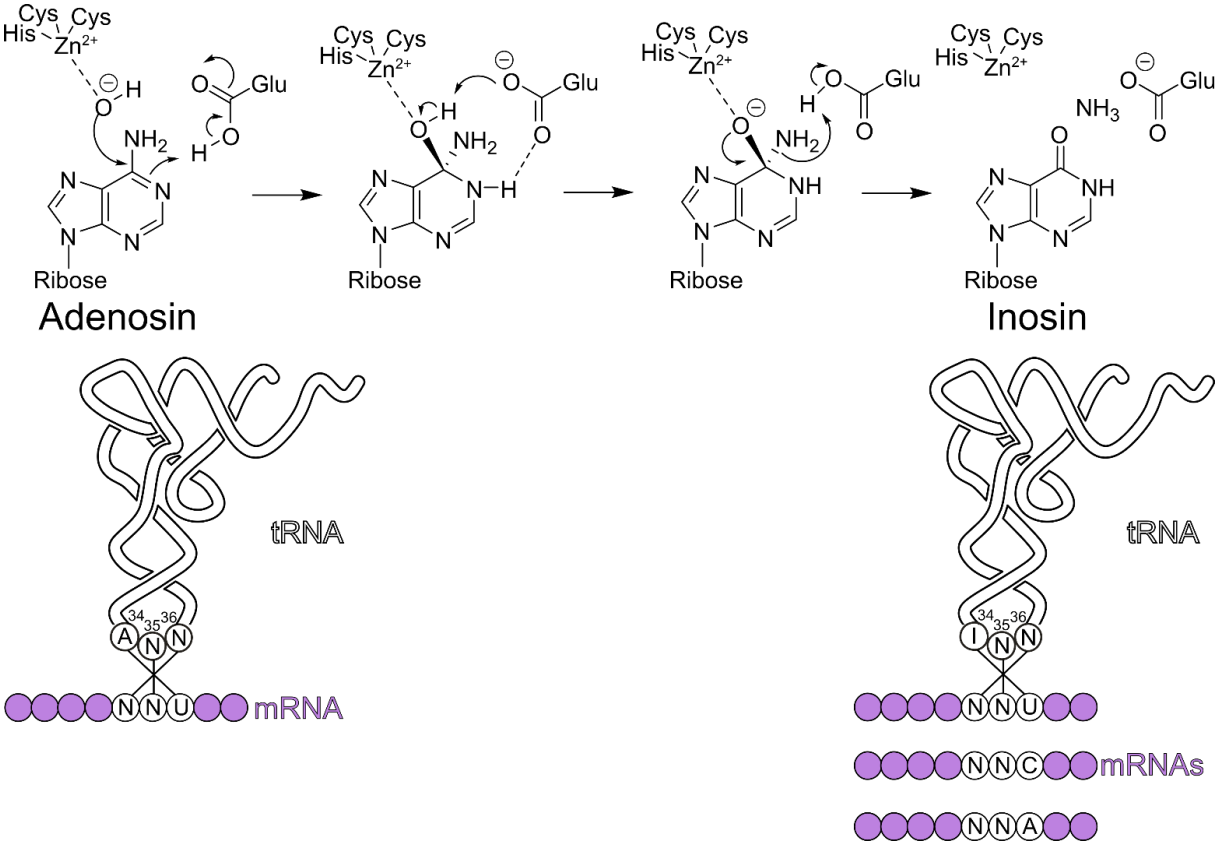

Abbildung 1.9: Deaminierung von Adenosin zu Inosin. Die schrittweise ablaufende Deaminierung ist mit Strukturformeln abgebildet. Die Histidin- (His), Cystein- (Cys) und Glutaminsäurereste (Glu) des ADAT2-Enzyms, sowie das Zinkion und das Wassermolekül sind ohne den strukturellen Kontext des Enzyms dargestellt. Die Auswirkung auf die Codon-Anticodonpaarung mit Adenosin oder Inosin sind unter den jeweiligen Basen schematisch gezeigt (adaptiert von[102]).

Als letztes tRNA-modifizierendes Writer-Enzym soll der heterodimere ADAT2/3-Komplex vorgestellt werden. Er deaminiert das Adenosin an Position 34 der tRNA, der sogenannten Wobble-Position, zu Inosin. Dieser Prozess, der in 8 verschiedenen tRNA-Isoakzeptoren höherer Eukaryoten abläuft, wird auch als A-zu-I-Editierung beschrieben[103]. Da Inosin anstelle von Adenosin nicht nur mit Uridin-enthaltenen-Codons der mRNA paaren kann, sondern auch Cytidin- und Adenosin-Codons lesen kann, findet eine Erweiterung der Decodiereigenschaften der tRNA statt, die Crick zu der Aufstellung der Wobble-Hypothese bewegt hat[104] [105] (Abbildung **1.9**). Die Aktivität des heterodimeren Enzymkomplexes ist essentiell für die Überlebensfähigkeit einer jeden Zelle, sodass das A-zu-I-Editieren als grundlegend für die Decodierung des genetischen Codes angesehen werden kann. Die Untereinheiten des ADAT2/3 teilen sich wie folgt auf: ADAT2 besitzt das katalytisch-aktive Zentrum, welches aus 2 Zinkfinger-Bindesequenzen besteht und über ein Glutamat- sowie Lysinreste die Deaminierungschemie (Abbildung **1.9**) durchführt. ADAT3 hingegen besitzt kein aktives Zentrum mehr, weil der wichtige Glutamatrest durch einen unpolaren Alaninrest evolutionär ersetzt wurde[106]. Ähnlich wie METTL14 dient ADAT3 als struktureller Gerüstgeber. Die N-terminale Domäne des ADAT3 erkennt die tRNA 3D-Struktur und nach Bindung der zu deaminierenden tRNA präsentiert sie die Anticodonschleife dem katalytisch aktiven Zentrum des ADAT2-Proteins[107]. Die Deaminierung der Postion 34 der tRNAs passiert bei der prä-tRNA-Prozessierung im Zellkern. Dies wurde durch farbstoffmarkierte ADAT2/3-Komplexe mittels Mikroskopie nachgewiesen[108]. Mutierte ADAT2/3-Varianten führen in den betroffen Patienten zu der Ausbildung einer geistigen Behinderung[1]. Neben der hier zitierten Literatur konnte dieses durch weitere im Resultateteil unter „Writer-Enzyme“ erwähnte Literatur bestätigt werden.

1.2.4 Dynamik II: Eraser-Enzyme

Nachdem Enzyme vorgestellt wurden, die Modifikationen in die RNA inkorporieren, soll es im folgenden Abschnitt, um Enzyme gehen, die RNA-Modifikationen entfernen. Solche Enzyme werden „Eraser“-Enzyme genannt und sind ein Beweis für die Dynamik der RNA-Modifikationsgehalts, also des Epitranskriptoms. Bakterielles AlkB wurde im Zusammenhang mit der Sensitivität der Zelle gegenüber methylierenden Reagenzien, wie Methylmethansulfonat (MMS), entdeckt[109]. Es wurde vermutet, dass es als Reperaturenzym für Zellstress dient und die geschädigten Nukleobasen

umwandelt, um die Zelle lebensfähig zu halten[110]. Erst die Zuteilung des AlkBs in die Enzymklasse der α-Ketoglutarat-Fe(II)-abhängigen Dioxygenasen verlieh dem AlkB die wissenschaftliche Aufmerksamkeit[111] und ein genauer Mechanismus der oxidativen Decarboxylierung von Methylierungsschäden konnte postuliert werden. Die reduktive Aktivierung eines Sauerstoffmoleküls ist hierbei an die Decarboxylierung des α-Ketoglutarats zu Succinat gekoppelt. Der Fe(II)-Ion im aktiven Zentrum des AlkB koordiniert mit zwei Histidin- und einem Aspartatrest des Enzyms. Bei Bindung des α-Ketoglutarats und des Sauerstoffs entsteht ein Fe(IV)-Oxo-Komplex, der in der Lage ist, die Methylgruppe einer Nukleobase (in Abbildung **1.10**: Die N1-Methylgruppe eines Adenins) zu hydroxylieren. Unter Freisetzung eines Formaldehyd-Moleküls wird die kanonische Nukleobase, hier Adenin, zurückgewonnen[112].

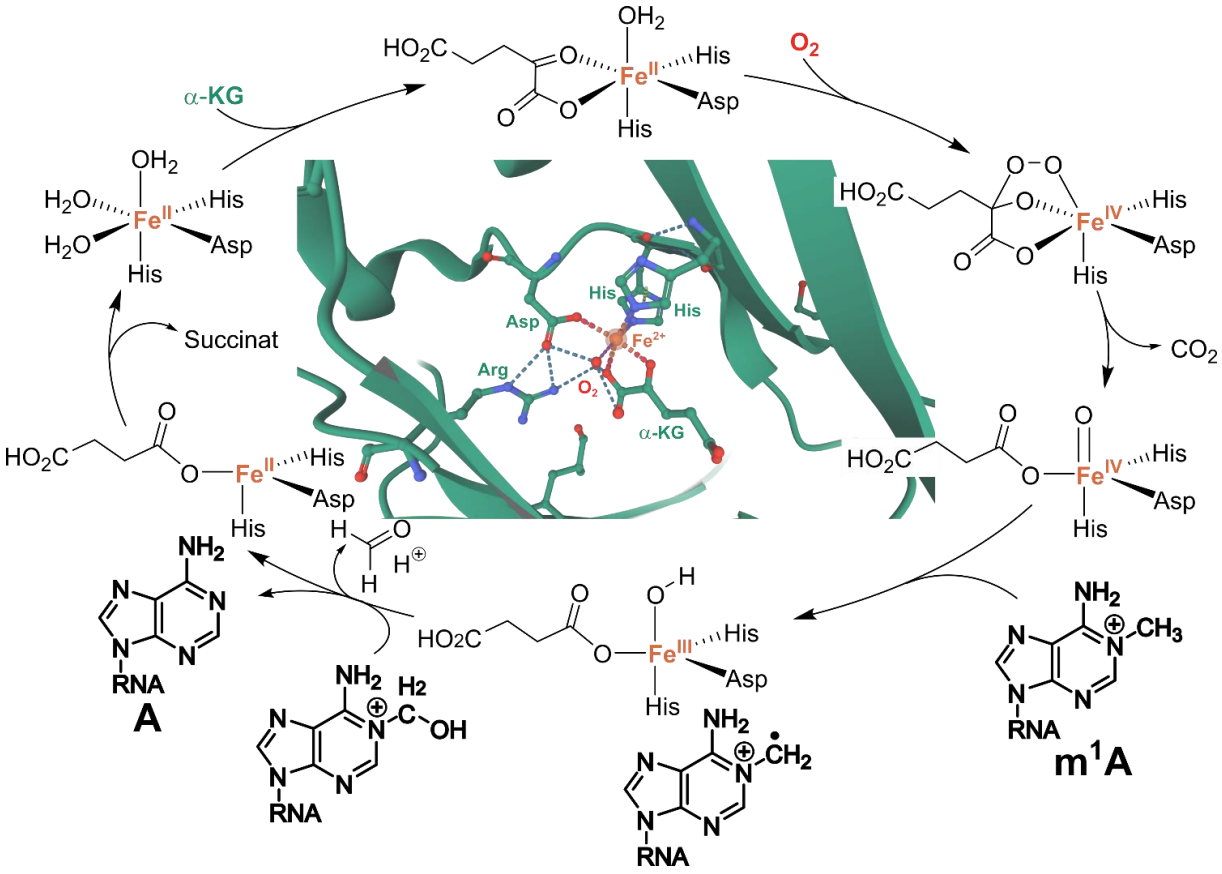

Abbildung 1.10: aktive Demethylierung der RNA-Modifikation m^{1}A durch die AlkB-Enzymfamilie. Die schrittweise ablaufende Demethylierung ist mit fettmarkierten Strukturformeln abgebildet. Der Reaktionszyklus des Eisenkomplex im katalytischen Zentrum ist sowohl strukturell-mechanistisch als auch kristallografisch gezeigt. Die Histidin- (His), Aspartat- (Cys) und Argininreste (Arg) sind abgekürzt und das Eisenion ist orange gefärbt. Für die Darstellung des Enzyms wurde die PDB 2IUW-Kristallstruktur bearbeitet[113]. Der Reaktionszyklus wurde von[112] adaptiert.

Nachdem die Aktivität des bakteriellen AlkB-Proteins an den Substraten m^1dA und m^3dC in einzelsträngiger DNA herausgefunden wurde[114] [115], konnten danach auch zwei humane Homologe des AlkB-Proteins identifiziert werden, AlkBH2 und AlkBH3[116], und ein Beweis für die Existenz eines Reperaturmechanismus für Alkylierungsschäden in Menschen geliefert werden[117]. Es fiel dabei auf, dass AlkB und AlkBH3 eine Präferenz für einzelsträngige DNA, aber auch RNA haben und AlkBH2 vorwiegend Schädigungen in Duplex-Nukleinsäuren repariert. Insgesamt gibt es 9 humane AlkB-Homologe, AlkBH1-8 und FTO, welche für einen Großteil der aktiven Demodifizierung in Menschen sorgen. Sie alle eint das Vorhandensein der katalytischen Domäne, welche eine Bindestelle für Fe(II) und α-KG enthält. Während sich z.B. AlkBH7 evolutionär früher separat entwickelt hat, zeigt die evolutionäre Nähe des AlkBH1, 3 und 5 sich an weiteren strukturellen Gemeinsamkeiten und der Fähigkeit Nukleinsäuren als Substrate zu erkennen und zu demethylieren. Im weiteren Teil dieses Kapitels soll auf diese AlkBH-Enzyme genauer eingegangen werden, da nur sie im Resultateteil dieser Arbeit erscheinen.

AlkBH1 ist eine DNA, mRNA und tRNA Demethylase in Säugetierzellen[118] [119] [120]. Sie ist sowohl im Kern als auch in den Mitochrondrien lokalisiert[121]. AlkBH1 hat einen großen Einfluss auf die Initiation der mitochondrialen Proteinsynthese, da es in mitochondrialer tRNA f^5C an Postiton 34 generiert[122] [123]. Auch an cytosolischer tRNA wirkt es als m^1A-Demethylase in der stressinduzierter Spaltung von tRNA in tRNA-Fragmente mit[124]. Die Modifikationen m^3C und m^6A sind weitere bekannte Substrate für das AlkBH1-Enzym[125] [126].

Ein weiteres in dieser Arbeit analysiertes Homolog ist AlkBH3, welches einzelsträngige DNA, tRNA und mRNA als Substrat präferiert[116] [127] [128]. In der DNA repariert es Alkylierungsschäden des Thymidins[129]. Der Prozess der DNA-Reparatur wird von der ASCC3, einer Helikase, unterstützt, die das AlkBH3 zu dem geschädigten Einzelstrang dirigiert[130]. ASCC3 ist zudem an der Qualitätskontrolle der ribosomalen Transkription von mRNA beteiligt und kann zwischen MMS-gestressten, aberranten und nativen mRNA Modifikationen unterscheiden, sodass AlkBH3 bevorzugt schadhaftes m^1A und m^3C in mRNA repariert[131]. Neben m^1A und m^3C in mRNA sind diese RNA-Modifikationen auch Hauptziel in tRNA und ihre Demethylierung fördert die Krebszellproliferation, sowie die Migration und Proteinsynthese dieser[132]. Wie schon das AlkBH3 sorgt es für eine m^1A-Demethylierung der tRNA und diese ist dann sensitiver gegenüber Angiogenin, das tRNA in tRNA-Fragmente spaltet[133]. *In vitro*

wurde zudem eine Fähigkeit zur Oxidation des m^5C in tRNA zu f^5C und ca^5C festgestellt[134].

AlkBH5 ist der Eraser für m^6A-Modifikationen in mRNA und in anderen langen nicht-kodierenden RNA-Spezies[135]. AlkBH5 arbeitet vor allem im Zellkern an einzelsträngiger DNA und RNA[136]. Es greift in den nuklearen Export von mRNA und den RNA-Metabolismus ein. Es ist in einer Vielzahl von Krebsarten, sowie der Spermatogenese und Fruchtbarkeit involviert[137]. Es demethyliert nicht nur m^6A, sondern auch $m^{66}A$, welches in ribosomaler RNA endogen ist[138].

Als hier letzter vorgestellter „Eraser“ ist das AlkBH7 nur in Mitochondrium und nicht im Zellkern vorkommend. Da es evolutionär weiter entfernt zu dem AlkBH1, 3 und 5 ist, war die Substratauswahl für AlkBH7 zunächst unbekannt[139]. Es wurde angenommen, dass es eine Rolle in Demethylierungsprozessen von Proteinen spielt[140]. Kürzlich wurde jedoch die mitochondriale prä-tRNA als Substrat für AlkBH7 entdeckt und gezeigt, dass AlkBH7 in dieser RNA-Spezies $m^{22}G$ und m^1A demethylieren kann[141].

Eine zusammenfassende Ansicht der Literatur über ausgewählte RNA-Modifikationen und ihrer AlkB und AlkBH-Demethylierungspartner ist in Tabelle **1.2** dargestellt. Abschließend lässt sich sagen, dass eine Fehlregulation oder die Inaktivität von AlkBH-Enzymen mit diversen Krankheiten korreliert.

	m^1A	m^3C	m^5C	m^1G	m^6A
	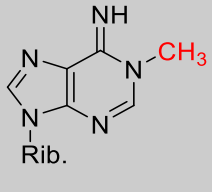		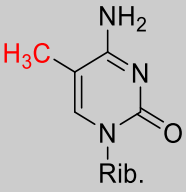	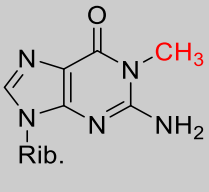	
AlkB	[117] [127] [142] [143]	[117] [127] [142] [144]		[145] [144]	
AlkBH1	[146] [126] [124]	[118] [125]	[126] [122] [123]		[126]
AlkBH3	[128] [116] [147] [117] [127] [133]	[116] [147] [117] [127] [133]			[132]
AlkBH5					[135] [136] [137] [138]
AlkBH7	[141]				

Tabelle 1.2: Übersicht über ausgewählte RNA-Demethylierungsziele von AlkB und AlkBH-Enzymen.

1.3 Detektion von RNA und RNA-Modifikationen

1.3.1 Überblick über Detektionsmethoden

Nachdem die Synthese von RNA, RNA-Modifikationen und die Dynamik des Epitranskriptoms vorgestellt wurde, steht in dem letzten Abschnitt die Detektion von RNA-Modifikationen im Fokus.

Als grundlegende Methode, um RNA-Modifikationen zu detektieren, wurden in der zweiten Hälfte des letzten Jahrhunderts alkalische Hydrolysate der RNA mittels Dünnschichtchromatografie aufgetrennt und radiographisch die ^{32}Phosphor-markierten kanonischen, aber auch modifizierten Nukleotide nachgewiesen[148] [149].

Mit der Zeit haben sich weitere Detektionsmethoden etabliert, wie etwa die RNA-Sequenzierung. Die Sequenzinformation der RNA bleibt erhalten, jedoch sind strukturell ähnliche RNA-Modifikationen ununterscheidbar. Die Reverse-Transkriptase (RT)-basierte Sequenzierung[150] kann zwar die exakte Position einer Modifikation feststellen, da sie an dieser Position gestoppt wird und ein verkürztes Transkript liefert, über die chemische Identität der Modifikation kann aber keine Aussage getroffen werden. Ein RT-Stopp kann bei einigen Modifikationen direkt erfolgen[151], andere RNA-Modifikationen müssen im Gegensatz dazu zunächst chemisch modifiziert werden, um das Enzym zu stoppen[152]. Hier sind exemplarisch die CMCT-Markierung für die Modifikation Ψ [153] und die Cyanoethylierung für Inosin erwähnt[154] [155]. Um die RNA-Sequenz in größerem Durchsatz und in Nukleotidauflösung zu analysieren, wurden *Next-Generation*- oder *Third-Generation-Sequencing*-Methoden entwickelt.

Kernspinresonanz(NMR)-Methoden können hingegen Informationen über den strukturellen Einfluss von RNA-Modifikationen geben. Nachdem isolierte NMR-Signale tRNA-Modifikationen zugeordnet[156] und viele verschiedene Modifikationen in tRNA-Molekülen durch das spezifische Auftreten neuer Signale kategorisiert werden konnten[157], gelang es im Zusammenspiel von NMR und der Aufnahme von UV-Schmelzkurven den Einfluss einer bestimmten Modifikation auf die tRNA-Struktur und Stabilität zu bestimmen[158]. Deuteriumaustausch-NMR konnte Aufschluss über die Dynamik und die Flexibilitätsänderung zwischen einem nativen und einem unmodifizierten tRNA-Molekül geben[159]. Mit ^{15}N *in vitro* transkribierter tRNA und NMR ist es sogar möglich, in einem Zellextrakt die Maturierung und den zeitlichen Einbau verschiedener Modifikationen in ein spezifisches tRNA-Molekül zu beobachten[160].

Eine die Nachteile der Sequenzierung kompensierende Methode ist die Massenspektrometrie (MS) von RNA-Molekülen und Modifikationen. Mit ihr lässt sich die Masse und Identität einer RNA oder Modifikation eindeutig bestimmen. Zwei Ionisationsmethoden haben sich für RNA als geeignet erwiesen: MALDI (*engl.* matrix assisted laser desorption/ionization) und ESI (*engl*. electrospray ionization)[161] [162]. Mit MALDI-MS ist es möglich RNA bis zu 150 kDa zu ionisieren[163], daher wird es häufig zur Analyse von Oligonukleotiden verwendet. Die Ionisierung bei MALDI-MS überträgt meistens eine Ladung, somit wird der Analyt instabil[164]. Später lassen sich die Spektren aufgrund einfacherer Massenzuordnung jedoch leichter auswerten. MALDI wird meistens mit einem hochauflösenden TOF-Detektor (*engl*. time of flight) gekoppelt. ESI-MS ist kostengünstiger als MALDI, schonender für die Analyten und besitzt den Vorteil einer modularen Kopplung mit einer vorgeschalteten RP(*engl*. reverse phase)-HPLC, auf der sich kleine Analyten, wie Nukleoside, chromatographisch trennen lassen und somit die Auswertung nicht komplexer werden lassen[165] [166]. Bei LC-ESI-MS wird meist ein niedrig-auflösendes Triple-Quadrupol-Massenspektrometer (QQQ) verwendet. Seine hohe Sensitivität, sowie die Regulierung verschiedener Spannungen sind ideal geeignet, um mehrere Nukleoside und Isotopologe gleichzeitig und mit abgestimmter Fragmentierung und massenspezifischer Filterung nachzuweisen[167].

1.3.2 Isotopenmarkierung von Biomolekülen

Eine Isotopenmarkierung bietet die Möglichkeit Mechanismen von molekularen Prozessen zu erforschen und kann gleichzeitig hilfreich sein, um molekulare Dynamiken *in vivo* mittels Massenspektrometrie relativ, aber auch absolut zu quantifizieren. Calvin klärte den Ablauf des nach ihm benannten Ribulosebisphosphatzyklus durch die Zugabe von stabilem isotopenmarkierten $^{14}CO_2$ und $NaH^{14}CO_3$[168].

Zusammen mit Massenspektrometrie findet die Isotopenmarkierung von Aminosäuren im Bereich der Proteomics als SILAC-Methode (*engl*. stable isotope labeled amino acids in cell culture) eine breite Anwendung[169]. Hierbei wurde die deuterierte Aminosäure D_3-Leucin dem Zellkulturmedium beigesetzt, um bei der anschließenden Proteinbiosynthese stabil isotopenmarkierte Proteine zu erhalten. Ein Teil der Zellen wurde weiterhin in Medium mit unmarkiertem Leucin kultiviert. Trotz nachfolgender Vereinigung der Zellextrakte aus unterschiedlichen Bedingungen lassen sich die einzelnen verdauten Proteine durch ihre Markierung zuordnen und es kann eine

Quantifizierung der Proteinlevel vorgenommen werden[169]. Diese Technik wurde mit der Verwendung von ^{13}C-markiertem Arginin und Lysin optimiert[170].

Nicht nur in dem Forschungsfeld der Proteom-MS, sondern auch bei der Analyse von Nukleinsäuren finden sich zahlreiche Beispiele für die Verwendung von Isotopenmarkierungen.

So konnte die Dynamik und der Mechanismus der oxidativen Decarboxylierungsprodukte von m^5C in DNA in Mäusestammzellen erforscht werden[171]. Zur Analyse von Oligonukleotiden wurde die CARD-Methode (*engl*. comparative analysis of RNA digests), sowie die optimierte SIL(*engl.* stable isotope labeled)-CARD-Methode entwickelt. Nach Kultivierung zweier Bakterienstämme und ihrer tRNA wird bei der CARD-Methode die tRNA mit RNase T1 entweder in $H_2{}^{16}O$ oder $H_2{}^{18}O$-Lösung verdaut und die generierten Oligonukleotide per MS analysiert, um Abweichungen zwischen den Bakterienstämmen und ihrem Modifikationsprofil festzustellen[172]. SIL-CARD nutzt hingegen den Einbau von ^{13}C und ^{15}N-markierten Nukleosidtriphosphaten in ein *in vitro* transkribiertes RNA-Referenzmolekül, welches mit dem zu analysierenden RNA-Molekül zu Oligonukleotiden verdaut und mittels MS quantifiziert werden kann[173].

Die Verwendung von ^{15}N-markiertem Nährmedium für Bakterien führte zu der Quantifizierung des 16S rRNA-Modifikationsprofils[174] und wurde nachfolgend durch Ausweitung der Markierungsstrategie mit ^{15}N-Ammoniumsulfat, D_3-Methionin und 5,6-D-Uracil optimiert, um 29 der 36 RNA-Modifikationen in bakterieller 16S und 23S rRNA zu quantifizieren[175]. Um die eben erwähnten RNA-Modifikationen auch absolut zu quantifizieren, wurde die SILNAS-Methode (*engl*. stable isotope labeled ribonucleic acid as internal standard) entwickelt. Mit Hilfe der Herstellung einer $^{13}C_{10}$-Guanosin *in vitro* transkribierten internen Kontroll-RNA konnten alle 122 Modifikationsstellen in ribosomaler RNA von Bakterien identifiziert und die dynamischen Modifikationsprozesse verfolgt werden[176].

Um Modifikationen in weiteren RNA-Spezies und in einer Vielzahl von Organismen absolut quantifizieren zu können, ist ein SILNAS oder allgemeiner ein stabil isotopenmarkierter interner Standard (*engl*.: stable isotope labeled internal standard, SILIS) essentiell. Zum einem kann dieser laborintensiv synthetisch herstellt werden, was beispielhaft für einige DNA-Modifikationen, tRNA-Modifikationen und 5´-mRNA-Kappenstrukturen gelungen ist[177] [178], dann deckt der interne Standard jedoch nicht

alle Variationen der Modifikationen ab. Zum anderen kann der Standard biosynthetisch aus den passenden Modellorganismen durch Zugabe von isotopenmarkierten Nährstoffen gewonnen werden und enthält dann alle in dem Organismus vorkommenden Modifikationen[179] [180].

Die Massenspektrometrie ist nicht per se quantitativ, weil das Ansprechverhalten des Detektors, die Ionensuppresion, sowie die Ionisierungseffizienz und weitere Faktoren vom jeweiligen Analyten abhängig sind. Die Isotopenmarkierung bietet in der Massenspektrometrie den Vorteil, dass alle Isotopologe einer Modifikation eines RNA-Fragments durch ihre physikochemischen Eigenschaften ein identisches Retentionsverhalten auf der HPLC-Säule vor dem Massenspektrometer besitzen, sich aber in diesem aufgrund ihrer unterschiedlichen Masse zuordnen lassen. Somit ist eine quantitative Analyse möglich.

1.3.3 Top-Down-MS

Abhängig von der Vorbereitung der RNA-Proben kann die MS-Analytik in drei Bereiche unterteilt werden: Top-Down-MS, Oligonukleotid-MS und Nukleosid-MS. Die nachfolgende Abbildung **1.11** stellt die Unterschiede zwischen diesen drei MS-Ansätzen schematisch dar.

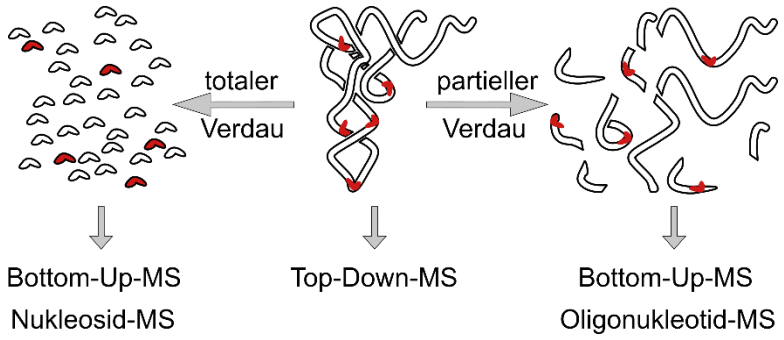

Abbildung 1.11: Schematischer Vergleich der MS-Methoden in der RNA-Modifikationsanalytik. Während bei den Bottom-Up-Ansätzen Verdauschritte in der Probenvorbereitung essentiell sind, ist in der Top-Down-Analytik keine Hydrolyse der RNA (hier: tRNA mit rotmarkierten Modifikationen) notwendig.

In der Top-Down-MS wird enzymatisch nicht hydrolysierte RNA ionisiert, die totale Masse analysiert, sodass die Sequenzinformation und genaue Position von RNA-Modifikationen nicht verloren geht.

McLuckey und Limbach konnten die Masse von Oligonukleotiden, tRNA Isoakzeptoren und 5S rRNA bestimmen und potentielle Modifikationsstellen identifizieren[181] [182].

Breuker und Kollegen gelang es eine 61 Nukleotid-lange RNA zu ionisieren und über Fragmentierung Modifikationen positionsgenau zuzuordnen[183] [184]. Ein gutes Maß für die Qualität einer Top-Down-MS-Methode ist die Sequenzabdeckung, die durch Fragmentierung und Generierung von Ionenserien überlappend verifiziert werden kann. Es konnte eine 39 Nukleotide lange RNA zu 100 % detektiert werden, d.h. jede der 37 Phosphodiesterbindungen in diesem Molekül wurde mindestens einmal gespalten und die beiden sich ergänzenden Teilfragmente konnten per MS detektiert werden[185]. Ein Vorteil des Top-Down-Ansatzes ist, dass laborintensive Verdauschritte vermieden werden und dass die Sequenzinformation der RNA vollständig erhalten bleibt. Dass hierfür reine RNA benötigt wird (also keine Zellextrakte), da sonst die Datenanalyse zu komplex wird, ist hingegen als Nachteil anzusehen. Des Weiteren benötigt diese Art der MS teure Instrumente, anspruchsvolle Software und die Unterscheidung von masse-identischen RNA-Modifikationen, wie m^1A von m^6A, aber auch Ψ von U, gestaltet sich sehr schwierig.

1.3.4 Bottom-Up-MS I: Oligonukleotid-MS

Oligonukleotid-MS basiert auf dem partiellen Verdau von RNA und der Rekonstruktion der gesamten Sequenz durch Identifizierung von Fragmenten, in denen Modifikationen teilweise im Kontext vorhanden sein können. Die Oligonukleotide können zuvor über HPLC chromatographisch separiert werden und einzeln in kleinere Einheiten oder Nukleoside fragmentiert werden (MS/MS). Dieses von McCloskey eingeführte Verfahren[186] ist in der Lage das komplette Modifikationsprofil von mRNA, einer Mixtur von vielen tRNA-Isoakzeptoren, rRNA und snoRNA zu detektieren.

Ein erster wichtiger Schritt im Gegensatz zu Top-Down-MS ist die Verwendung von sequenz-spezifischen RNasen, damit die RNA in leichter ionisierbare 5 – 15 lange Oligonukleotide gestückelt wird. Meistens werden unterschiedliche RNasen, wie RNase T1, RNase Colicin E5 oder RNase MazF, gemeinsam zum Verdau der zu analysierenden RNA eingesetzt, um eine höhere Sequenzabdeckung zu erreichen. Die Abbildung **1.12** zeigt eine $tRNA^{Val}_{AAC}$-Sequenz, die durch verschiedene RNasen unterschiedlich oft und somit in verschieden große Oligonukleotide geschnitten wurde. Hierbei ist zu erwähnen, dass unspezifischere RNasen, wie RNase A oder RNase U2, die nach jedem Pyrimidin- bzw. Purinnukleotid schneiden, zu kurze Fragmente generieren, die dann nicht mehr einzigartig der Sequenz zugeordnet werden können. Beim Verdau von totaler bakterieller tRNA ist es gelungen mit RNase T1, Cusativin und MC1 eine Abdeckung der Sequenz von 85 % zu erreichen[187]. Es zeigte sich

jedoch, dass die Unterscheidung von detektierten massegleichen Modifikationen innerhalb des Oligonukleotides nicht möglich war. Der Aufnahme von MS/MS-Spektren und der anschließenden Softwareanalyse kommen für die Identifizierung und Lokalisierung einer Modifikation deswegen eine Schlüsselrolle zu.

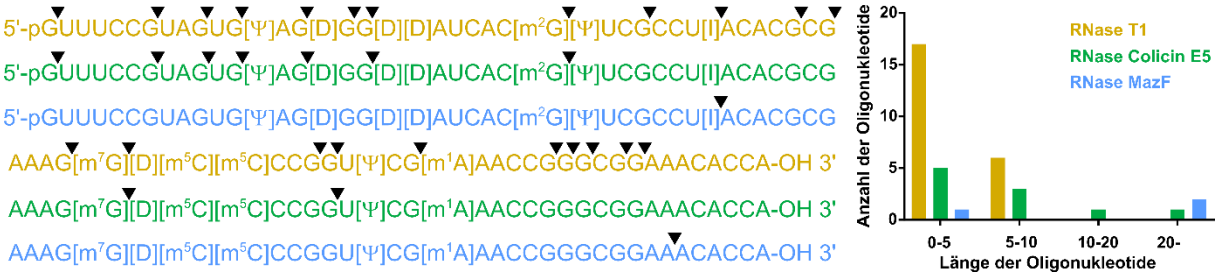

Abbildung 1.12: *In silico* Verdau des nativen tRNA$^{Val}_{AAC}$-Moleküls aus *H. sapiens* durch verschiedene RNasen. Die tRNA-Sequenz mit den nativen Modifikationen ist zur besseren Darstellung zweigeteilt und dreimal repetitiv gezeigt, um die unterschiedlichen RNase-Schnittstellen (markiert als schwarze Dreiecke über der Sequenz) anzuzeigen. Eine Kategorisierung der entstandenen Oligonukleotide ist im Balkendiagramm rechts gezeigt.

Durch Programme, wie RNAModMapper (RAMM) und NucleicAcidSearchEngine (NASE), ist es gelungen Modifikationen aus wenigen Nanogramm einer Mischung von RNA-Spezies in der Sequenz zu kartieren[188] [189]. Eine passende Isotopenmarkierungsstrategie kann die Modifikationszuordnung unterstützen. So konnten die masse-gleichen Modifikationen U und Ψ unterschieden und die Ψ-Modifikationsstellen in rRNA und snoRNA verifiziert werden[175] [190]. Die Fähigkeit des Oligonukleotid-MS-Ansatzes zur Sequenzbestätigung wurde durch die Analyse einer 3000 Nukleotide langen mRNA mit 70 % Sequenzabdeckung und durch die Detektion 34 von 35 tRNA Molekülen in einem tRNA-Gemisch nachgewiesen[191] [192].

Je komplexer das RNA-Gemisch, desto größer ist die Wahrscheinlichkeit co-eluierender Fragmente und die Anzahl an zu detektierenden Oligonukleotiden in der MS, gerade auch vor dem Hintergrund verschiedener Häufigkeit einzelner Fragmente. Um die Probenkomplexität zu verringern und die Detektion zu erleichtern, sind laborintensive Probenvorbereitungsschritte oder orthogonale LC/LC-Ansätze nötig. Die Auftrennung von Oligonukleotiden wurde so mit der 2D-LC-Technik verbessert [193] [194].

Zur Chromatographie für Oligonukleotid-MS wird zumeist eine RP-Säule (*engl*. reverse phase) genutzt. Aufgrund der Hydrophilie des negativ geladenen

Phosphodiesterrückgrats der Oligonukleotide, wird das Material der Säule jedoch mit Ionenpaarreagenzien modifiziert, um als Pseudo-Ionenaustauschsäule für eine bessere Retention der RNA-Fragmente zu sorgen. Als Ionenpaarreagenzien, auch Modifier genannt, eignen sich Triethylamin (TEA) oder Hexafluorisopropanol (HFIP), die mit ihren Alkylresten mit dem unpolaren Säulenmaterial interagieren, aber gleichzeitig auch polare oder ionische Gruppen besitzen, die mit der negativ RNA wechselwirken[195] [196]. Mit Ionenpaarreagenz wird zwar die Sensitivität der Oligonukleotide bei der Elektrosprayionisierung verbessert[197], es führt auf der anderen Seite jedoch dazu, dass das Massenspektrometer für nachfolgende Messungen kontaminiert wird und eine Ionensuppresion stattfinden kann, wenn im positiven Ionisierungsmodus gemessen wird, was in der Proteomics oder der Nukleosidanalyse meist Standard ist.

Um das Problem der Ionenpaarreagenznutzung zu umgehen und die Kompatibilität mit anderen Analysemethoden auf demselben Massenspektrometer zu gewährleisten, müssen andere Chromatographien entwickelt werden.

Eine Lösung ist die Verwendung von HILIC-Säulen (*engl*. hydrophilic interaction liquid chromatography), die mit wässrigem Ammoniumacetatpuffer und Acetonitril als Laufmittel ohne Ionenpaarreagenzzusatz auskommen[198]. Das Massenspektrometer wird hierbei im negativen Ionisierungsmodus betrieben.

Eine weitere Lösung für eine ionenpaarreagenzfreie Chromatographie, die RP-basiert ist, wurde als Teil dieser Arbeit entwickelt. Die Kompatibilität ist zusätzlich durch die Verwendung des Instruments im positiven Ionisierungsmodus gegeben.

1.3.5 Bottom-Up-MS II: Nukleosid-MS

Die Nukleosid-MS ist die Analyse total hydrolysierter RNA ohne Sequenzinformation, aber mit der präzisesten Bestimmung aller Modifikationen unabhängig von ihrer Abundanz.

Die RNA von Interesse wird durch einen Enzymmix bestehend aus Nuklease, Phosphodiesterase und alkalischer Phosphatase, der von Crain entwickelt wurde, verdaut[199]. Der totale Verdau besitzt neben dem Sequenzinformationsverlust weitere Nachteile. Zum Bespiel kann kontaminierte RNA nach dem Verdau den Modifikationsgehalt der RNA von Interesse verfälschen. Es können MS-Artefakte durch die Wahl des Verdauprotokoll entstehen, die es zu identifizieren gilt[200] [201]. Die

Fähigkeit mancher Nukleasen RNA und vor allem RNA-Modifikationen zu hydrolysieren kann begrenzt sein[202]. Die Nukleosid-MS benötigt zur effizienten Trennung der Modifikationen – wie die Oligonukleotid-MS – eine vorausgehende Chromatographie. Meist wird hier eine RP-HPLC verwendet, die zu einer Separation von einer Vielzahl an RNA-Modifikationen in 12 Minuten Laufzeit fähig ist[166].

Als Massenspektrometer der Wahl ist der Triple-Quadrupol (QQQ) im positiven Ionisierungsmodus, da dieser durch die doppelte Selektion des Nukleosids, der Nukleobase und einer internen Fragmentierung Signale mit einem niedrigen Signal-zu-Rausch-Verhältnis auch von sehr wenig vorkommenden RNA-Modifikationen sensitiv detektiert. Der positive Ionisierungsmodus hilft, dass Nukleobasen protoniert werden. Dies wird durch die Abwesenheit des negativ geladenen Phosphodiesterrückgrats begünstigt.

Da Massenspektrometrie nicht quantitativ ist, müssen interne Standards der Probe hinzugefügt werden, um mit der Messung eine quantitative Aussage zu erhalten. Als Goldstandard hat sich der SILIS, der im Kapitel „Isotopenmarkierung von Biomolekülen“ bereits vorgestellt wurde, etabliert. Er ist nötig, um Abweichungen zwischen den einzelnen Messungen zu nivellieren. Diese können in der Messzeit des Instrumentes, in der Sauberkeit des Geräts, der Laufmittelkomposition und dem Salzgehalt der Probe begründet sein. Mit einem biosynthetischen SILIS können bis zu 26 verschiedene RNA-Modifikationen in den verschiedensten Organismen quantifiziert werden[203].

Mit Hilfe der Isotopenmarkierung von RNA können nicht nur statische RNA-Modifikationslevel analysiert werden, es ist sogar möglich, die Dynamik der RNA-Modifikationen zu erfassen. Unser Labor entwickelte mit NAIL-MS (*engl*. für nucleic acid isotope labeling coupled mass spectrometry) eine zu SILAC analoge Technik, um auch in der Epitranskriptomik die Dynamik bessern abbilden zu können. In sogenannten Pulse-Chase-Experimenten können durch Mediumwechsel verschiedene Isotopenmarkierungen der RNA und ihrer Nukleoside erreicht werden. Es lassen sich mit Hilfe von NAIL-MS die Prozesse RNA-Abbau von RNA-Modifizierung und von RNA-Demodifizierung unterscheiden und zeitaufgelöst darstellen. Grundlegend hierfür ist eine auf den zu untersuchenden Organismus abgestimmte Isotopenmarkierungsstrategie mit optimalerweise 100 % Isotopenmarkierungseffizienz. Diese wurde bereits von unserem Labor für *E. coli* und

S. cerevisiae vorgestellt[204] [180]. Neben der Entdeckung der neuen RNA-Modifikation ms^2C in Bakterien[143] gelang es durch NAIL-MS auch die stressabhängige Dynamik der RNA-Modifikationen in Bakterien[205], sowie die Dynamik von rRNA- und tRNA-Modifikationen in Hefe unter Stressbedingungen aufzuklären[206]. Um die Dynamik des Epitranskriptoms in höheren eukaryotischen Organismen zu entschlüsseln, müssen weitere Schritte, die auch Teil dieser Arbeit sind, unternommen werden.

2. Ziel der Arbeit

Die massenspektrometrischen Methoden zur Analyse des Epitranskriptoms erheben meist nur statische Level der RNA-Modifikationen. Die Dynamik von RNA-Modifikationen ist mit neurologischen Erkrankungen, Krebs und geistiger Behinderung assoziiert. Um einen Fortschritt in der Diagnostik dieser Krankheiten zu erlangen, benötigt die Wissenschaft eine MS-Methode, die diese Schwächen kompensiert und die dynamischen und molekularen Prozesse des RNA-Modifikationsprofils in menschlichen Zellen auflösen kann. Ein großer Fortschritt gelang mit der Entwicklung der Technik NAIL-MS (*engl.* Nucleic Acid Isotope Labeling coupled Mass Spectrometry) und ihrer Etablierung in Modellorganismen wie *E. coli* und *S. cerevisiae*.

Ein Ziel meiner Arbeit soll in der Etablierung von NAIL-MS in humaner Zellkultur liegen, sowie in der zeitaufgelösten Untersuchung des Modifikationsprofils unterschiedlichster RNA-Spezies unter dem Einfluss von RNA-modifizierenden Enzymen.

Grundlegend für NAIL-MS ist eine erfolgreiche, effiziente Isotopenmarkierungsstrategie, d.h. die Auswahl geeigneter Isotopologe, die von der Zelle aufgenommen und durch die Biosynthese in neu hergestellten Nukleosiden inkorporiert werden. Während in Bakterien und Hefen die Aufnahme und der Einbau von Isotopologen einfacher zu realisieren ist, stellt die Komplexität des Zellkulturmediums eine Hürde für die Etablierung in humaner Zellkultur dar.

NAIL-MS beinhaltet einen Mediumaustauschschritt. Dieser bietet die Möglichkeit zur detaillierten Aufklärung RNA-abhängiger Prozesse und zu ihrer Differenzierung in: 1. Verdünnungseffekte alter RNAs durch die Entstehung neuer, isotopenmarkierter RNA-Moleküle und Modifikationen, 2. Degradation alter RNAs oder 3. aktiven Modifizierung bzw. Demodifizierungsprozesse durch Writer und Eraserenzyme. Gerade der letzte Punkt gewinnt in der Forschung mehr und mehr an Interesse. Die AlkBH-Enzymfamilie und ihr Einfluss auf das RNA-Modifikationsprofil sind deshalb Teil dieser Arbeit. Die Auswirkungen mehrerer humaner AlkB-Homologe auf RNA-Spezies sollen zunächst *in vitro* getestet werden, um Demethylierungsziele in RNAs zu bestätigen. In einem nächsten Schritt soll die RNA-Modifikationsdynamik *in vivo* in humaner Zellkultur erforscht werden.

Ein weiteres Ziel dieser Arbeit ist die Analyse von RNA-Modifizierungsprozessen durch Writer, in diesem Fall der Enzymkomplex ADAT2/3, im Sequenzkontext. Genetische

Mutationen des ADAT2/3-Gens, die zu einem verminderten Gehalt an Inosin in tRNA führen, sind in Patienten mit geistigen Beeinträchtigungen vorkommend. Um den wichtigen Prozess der A-zu-I-Editierung von tRNA-Molekülen nicht nur quantitativ mittels Nukleosid-MS und SILIS zu verfolgen, sondern auch den Ort der enzymatischen Aktivität in der Sequenz exakt zu bestimmen, ist es wichtig einen Oligonukleotid-MS-Ansatz zu wählen.

Die Entwicklung einer MS-schonenden, ionenpaarreagenzfreien Chromatographie hat Priorität, damit Oligonukleotid-MS kompatibel auf demselben Massenspektrometer neben der Nukleosid-Analytik durchgeführt werden kann. Nach Validierungsexperimenten mit isotopenmarkierten IVTs soll durch einen selektiven RNase T1-Verdau die Position des Editierungsprozesses bestimmt werden und darüber hinaus eine Grundlage für das Lokalisieren von RNA-Modifikationen im Sequenzkontext diverser RNAs geschaffen werden.

3. Ergebnisse und Diskussion

3.1 Einfluss des Enzymkomplexes ADAT2/3 auf Inosin in tRNA in mental retardierten Patienten (Writer-Enzyme)

Gemeinsamer Prolog

Eine wichtige posttranskriptionelle tRNA-Modifikation ist Inosin. Das Inosin entsteht durch hydrolytische Deaminierung von Adenosin und befindet sich in 8 humanen tRNA Isoakzeptoren an Position 34 in der Anticodonschleife. Hier bestimmt es die Paarung, erweitert die Paarungsmöglichkeiten mit dem Codon der mRNA, beeinflusst Translation und Proteinexpression. Enzyme, die diese A-zu-I-Deaminierung durchführen, sind in Bakterien, Hefen und komplexeren Eukaryoten vorkommend. In Menschen sorgen dafür die Homologe ADAT2 und ADAT3. Sie bilden einen heterodimeren Komplex, der für die Deaminaseaktivität essentiell ist. Eine einzige Mutation in dem humanen ADAT3-Gen ist dafür verantwortlich, dass es, wenn die Mutation homozygot ist, zu geistiger Behinderung, und neurologischen Störungen bei den betroffenen Patienten kommt. Die aus der genetischen Mutation folgende Valin-zu-Methionin-Missense-Mutation (V144M) des humanen ADAT3-Proteins stört die Oberflächenstruktur, bildet Proteinaggregate und führt so zu einer reduzierten Deaminaseaktivität und einem niedrigeren Inosingehalt in der tRNA. Dies wurde durch Kultivierung von Patienten-derivatisierten Lymphoblastzelllinien und der Analyse der RNA mittels Massenspektrometrie und Sequenzierung sowie weiterer Protein-basierter Forschung herausgefunden (*Mol Cell Biol*., **2019**). In einer weiteren Studie wurde eine neuartige Genvariante von ADAT3 in drei geistig behinderten Geschwistern charakterisiert. Die aus den Patienten derivatisierten Fibroblast-Zelllinien zeigen durch das A196V/Q274*-mutierte ADAT3-Protein ein reduziertes Inosinlevel in der tRNA. Durch Überexpression der katalytischen Domäne des ADAT2-Proteins in den Zellen wurde die Deaminaseaktivität sogar wiederhergestellt (*RNA*, **2020**).

„Formation of tRNA Wobble Inosine in Humans Is Disrupted by a Millennia-Old Mutation Causing Intellectual Disability", J. Ramos, L. Han, Y. Li, **F. Hagelskamp**, S. M. Kellner, F. S. Alkuraya, E. M. Phizicky, D. Fu, *Mol Cell Biol*., **2019**, Sep 11; 39 (19): e00203-19.

Autorenbeitrag: Die Aufreinigung der tRNA, die massenspektrometrische Messung und anschließende Quantifizierung der tRNA-Modifikationen der Lymphoblast-Zelllinien wurde von mir durchgeführt.

„Identification and rescue of a tRNA wobble inosine deficiency causing intellectual disability disorder", J. Ramos, M. Proven, J. Halvardson, **F. Hagelskamp**, E. Kuchinskaya, B. Phelan, R. Bell, S. M. Kellner, L. Feuk, A. C. Thuresson, D. Fu, *RNA*, **2020**, Nov; 26 (11): 1654-1666.

Autorenbeitrag: Die Aufreinigung der tRNA, die massenspektrometrische Messung und anschließende Quantifizierung der tRNA-Modifikationen der verschiedenen Fibroblast-Zelllinien wurde von mir durchgeführt.

AMERICAN SOCIETY FOR MICROBIOLOGY | Molecular and Cellular Biology®

RESEARCH ARTICLE

Formation of tRNA Wobble Inosine in Humans Is Disrupted by a Millennia-Old Mutation Causing Intellectual Disability

Jillian Ramos,[a,b] Lu Han,[b,c] Yan Li,[a,b] Felix Hagelskamp,[d] Stefanie M. Kellner,[d] Fowzan S. Alkuraya,[e,f] Eric M. Phizicky,[b,c] Dragony Fu[a,b]

[a]Department of Biology, University of Rochester, Rochester, New York, USA
[b]Center for RNA Biology, University of Rochester and University of Rochester Medical Center, Rochester, New York, USA
[c]Department of Biochemistry and Biophysics, University of Rochester Medical Center, Rochester, New York, USA
[d]Department of Chemistry, Ludwig Maximilians Universität München, Munich, Germany
[e]Department of Genetics, King Faisal Specialist Hospital and Research Center, Riyadh, Saudi Arabia
[f]Department of Anatomy and Cell Biology, College of Medicine, Alfaisal University, Riyadh, Saudi Arabia

ABSTRACT The formation of inosine at the wobble position of eukaryotic tRNAs is an essential modification catalyzed by the ADAT2/ADAT3 complex. In humans, a valine-to-methionine mutation (V144M) in ADAT3 that originated ~1,600 years ago is the most common cause of autosomal recessive intellectual disability (ID) in Arabia. While the mutation is predicted to affect protein structure, the molecular and cellular effects of the V144M mutation are unknown. Here, we show that cell lines derived from ID-affected individuals expressing only ADAT3-V144M exhibit decreased wobble inosine in certain tRNAs. Moreover, extracts from the same cell lines of ID-affected individuals display a severe reduction in tRNA deaminase activity. While ADAT3-V144M maintains interactions with ADAT2, the purified ADAT2/3-V144M complexes exhibit defects in activity. Notably, ADAT3-V144M exhibits an increased propensity to form aggregates associated with cytoplasmic chaperonins that can be suppressed by ADAT2 overexpression. These results identify a key role for ADAT2-dependent folding of ADAT3 in wobble inosine modification and indicate that proper formation of an active ADAT2/3 complex is crucial for proper neurodevelopment.

KEYWORDS RNA editing, adenosine deaminase, inosine, intellectual disability, molecular genetics, neurodevelopment, tRNA, tRNA modification

The hydrolytic deamination of adenosine (A) to inosine (I) at the wobble position of tRNA is an essential posttranscriptional tRNA modification in bacteria and eukaryotes (1, 2). Since inosine can pair with U, C, or A, a single tRNA isoacceptor containing the inosine modification at the wobble anticodon position can recognize up to three different codons containing a different nucleotide base at the third position. Thus, the degeneracy provided by the wobble inosine modification is necessary for the translation of C- or A-ending codons in organisms that lack a cognate G_{34}- or U_{34}-containing anticodon tRNA isoacceptor by expanding the reading capacity of tRNA isoacceptors (3). Moreover, it has been shown that highly translated genes in eukaryotic organisms, including humans, are correlated with an enrichment in wobble inosine tRNA-dependent codons, suggesting a critical role for tRNA inosine modification in maintaining proper levels of protein expression (4, 5).

In *Escherichia coli*, A-to-I conversion at the wobble position is present in a single tRNA (tRNA-Arg-ACG) and is catalyzed by the homodimeric complex TadA adenosine deaminase (1). In the yeast *Saccharomyces cerevisiae*, wobble inosine modification occurs in seven different tRNAs and is catalyzed by a heterodimeric enzyme complex consisting of the Tad2p and Tad3p subunits (2, 6). Tad2p is the catalytic subunit and

Citation Ramos J, Han L, Li Y, Hagelskamp F, Kellner SM, Alkuraya FS, Phizicky EM, Fu D. 2019. Formation of tRNA wobble inosine in humans is disrupted by a millennia-old mutation causing intellectual disability. Mol Cell Biol 39:e00203-19. https://doi.org/10.1128/MCB.00203-19.

Address correspondence to Dragony Fu, Dragonyfu@rochester.edu.

Received 23 May 2019
Returned for modification 11 June 2019
Accepted 27 June 2019
Accepted manuscript posted online 1 July 2019
Published 11 September 2019

contains a prototypical deaminase motif homologous to cytidine/deoxycytidine deaminases, including a conserved glutamic acid residue within the active site that is necessary for proton shuttling in the hydrolytic deamination reaction (7, 8). Tad3p also contains a canonical deaminase motif but lacks the conserved catalytic glutamate in the active site. However, Tad2p is inactive without Tad3p, indicating that formation of a heterodimeric Tad2p/Tad3p complex is required for adenosine deaminase activity (2). Functional homologs of *S. cerevisiae* Tad2p and Tad3p have been identified in all eukaryotes to date, including the human homologs ADAT2 and ADAT3 (9–12).

Exome sequencing and autozygosity mapping have identified a single c.382G>A mutation in the human *ADAT3* gene that is causative for autosomal recessive intellectual disability (ID) in multiple families of Saudi Arabian descent (13–15). All reported individuals homozygous for the V144M mutation exhibit cognitive deficits indicative of a neurodevelopmental disorder, with the majority displaying strabismus and growth delay. Additional clinical features of individuals homozygous for the ADAT3-V144M mutation include microcephaly, epilepsy, and occasional brain abnormalities such as white matter atrophy and arachnoid cysts. Subsequent large-scale sequencing has identified this ancient founder mutation to be one of the most common causes of autosomal recessive intellectual disability in patients from Saudi Arabia, with a carrier frequency of ~1% (16–18). However, the mechanistic cause of ADAT3-associated pathogenesis remains unclear.

The human *ADAT3* gene expresses two mRNA transcripts encoding ADAT3 proteins that differ only by the addition of 16 amino acid residues to the amino terminus of the longer ADAT3 isoform. Based upon the longer ADAT3 isoform, the ID-causing G>A transition results in a valine-to-methionine missense mutation at residue 144 (V144M). The mutated valine residue is conserved from yeast to humans and is predicted to perturb the surface structure of the ADAT3 protein (13). However, it is unknown how the V144M mutation affects ADAT3 function and whether this would affect tRNA inosine modification levels in ID-affected individuals who are homozygous for the autosomal recessive mutation. This would be important to test given the increasing awareness of tRNA modification in the etiology of other forms of Mendelian ID (19–30).

Here, we demonstrate that cells isolated from ID-affected individuals homozygous for the ADAT3-V144M mutation contain diminished levels of wobble inosine in several tRNA isoacceptors. Moreover, we find that extracts from these cells exhibit a drastic decrease in adenosine deaminase activity. While the ADAT3-V144M variant can form complexes with its heterodimeric partner ADAT2, ADAT2/3-V144M complexes exhibit greatly reduced enzymatic activity and an increased propensity to self-associate. Using subcellular localization studies combined with proteomics, we find that overexpressed ADAT3-V144M exhibits aberrant aggregation into cytoplasmic foci accompanied by targeting by the heat shock protein 60 (HSP60) and TRiC/CCT chaperonin complexes. Notably, the aggregation phenotype of ADAT3-V144M along with its association with chaperonins can be suppressed by coexpression with ADAT2. Altogether, these results uncover a potential molecular basis for ADAT3-associated neurodevelopmental disorders in the form of diminished inosine modifications at the wobble position of tRNA caused by ADAT3 misfolding and impaired enzymatic activity.

RESULTS

Individuals homozygous for the ADAT3-V144M mutation exhibit decreased wobble inosine modification in tRNAs. To examine the molecular effects of the V144M mutation in the human population, we generated lymphoblastoid cell lines (LCLs) from two unrelated human patients harboring homozygous V144M missense mutations in the *ADAT3* gene (referred to as V144M-LCLs, generated from patient 1 [P1] and P2) (Fig. 1A and B). P1 is a 6-year-old female with severe ID, short stature, microcephaly, strabismus, deafness, and a history of global developmental delay (13, 16). She is part of a consanguineous family with three similarly affected siblings (Fig. 1A). P2 is a 24-year-old male with features similar to those of P1, including severe ID, microcephaly, and developmental deficits as a child. P2 is also part of a consan-

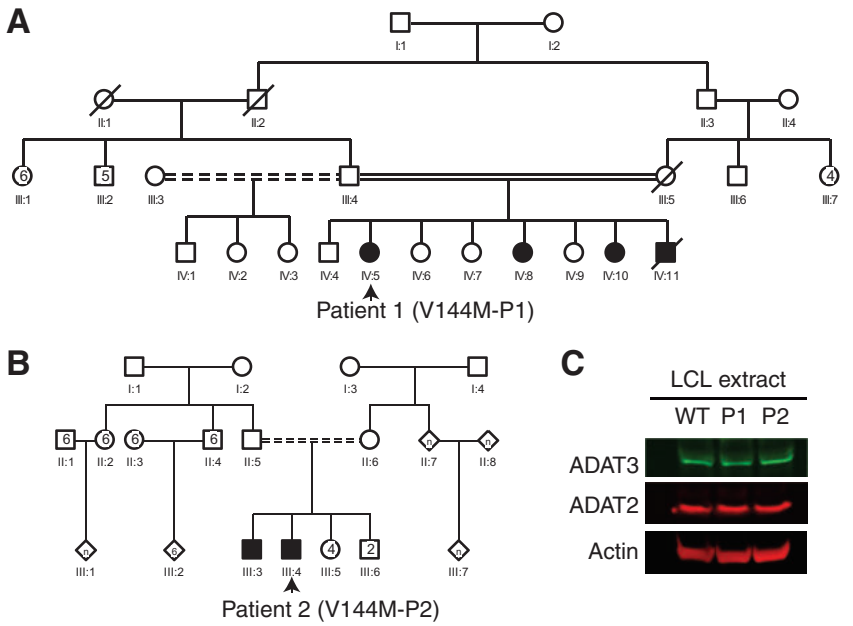

FIG 1 Individuals homozygous for the ADAT3-V144M mutation exhibit similar levels of ADAT3 expression. (A and B) Pedigrees of patient 1 (P1) and P2 containing homozygous V144M missense mutations in the ADAT3 gene. Male family members are denoted by squares, females are denoted by circles, individuals of unknown sex are denoted by diamonds, deceased individuals are denoted by slashes, ID-affected individuals with homozygous V144M mutations are denoted by shading, and consanguinity is denoted by double solid or shaded lines. (C) Immunoblot for the indicated proteins of extracts from LCLs donated from a wild-type (WT) individual and P1 and P2 harboring homozygous V144M mutations.

guineous family with a similarly affected brother (Fig. 1B) (14). LCLs generated from both ID-affected individuals with homozygous V144M mutations were compared to control lymphoblasts from an ethnically matched, healthy, unrelated individual (WT1-LCLs).

We first examined the levels of ADAT3 protein in LCLs to determine if the expression or stability of ADAT3 was affected by the V144M mutation. Based upon immunoblotting of whole-cell lysates, no major change in the endogenous levels of ADAT3 was detected between wild-type LCLs (WT-LCLs) and V144M-LCLs (Fig. 1C). Moreover, the levels of the ADAT3 heterodimeric binding subunit, ADAT2, were also similar between WT- and V144M-LCLs (Fig. 1C). The comparable steady-state levels of wild-type ADAT3 and the V144M variant suggest that the V144M mutation could be impacting ADAT3 function without affecting protein accumulation.

We next monitored the levels of tRNA modifications in WT- versus V144M-LCLs using liquid chromatography-mass spectrometry (LC-MS) of nucleosides from digested total tRNA (31). For these analyses, we also performed a comparison against a completely different LCL procured from a healthy individual of a similar age but a different ethnic background (WT2-LCLs). Among 13 tRNA modifications tested, we found that the inosine modification differed the greatest between WT- and V144M-LCLs, with V144M LCLs exhibiting a substantial decrease in tRNA inosine levels (Fig. 2A). Using absolute quantification by LC-MS with calibration standards, we found that the abundance of inosine was reduced by ~30% in the tRNAs of both V144M-LCLs compared to either WT-LCL (Fig. 2B). While we detected a significant decrease in the levels of inosine in the tRNA of V144M-LCLs ($P < 0.05$), no significant change was detected in the levels of any other tested modification ($P > 0.1$). These results provide the first evidence that the ADAT3-V144M mutation and its associated molecular defects have an impact on the levels of tRNA wobble inosine modification *in vivo*.

Focusing on a specific tRNA, we next investigated the wobble inosine status of tRNA-Val-AAC isolated from the V144M-LCLs of ID-affected individuals. Since inosine is

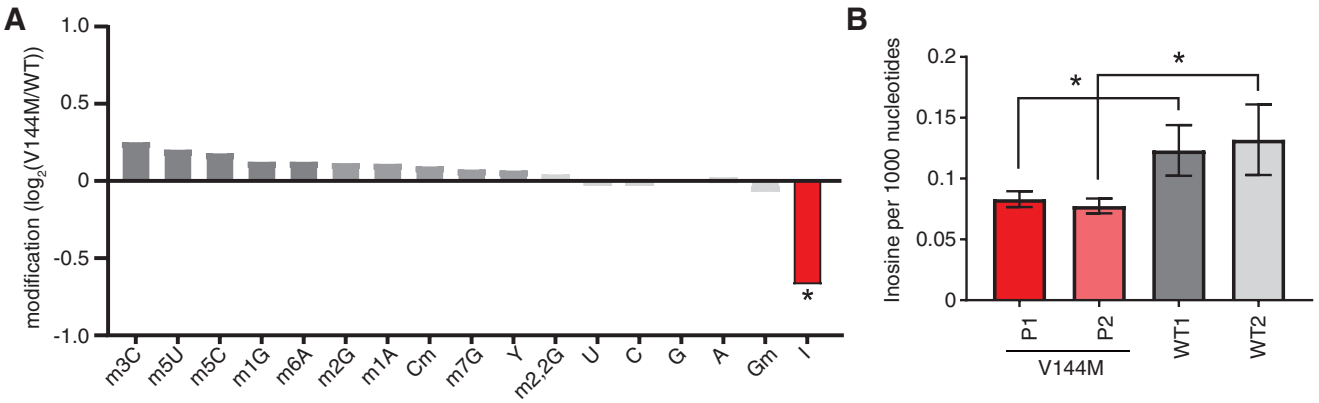

FIG 2 ID-affected individuals expressing only the ADAT3-V144M variant exhibit decreased wobble inosine modification in tRNA isoacceptors. (A) Comparison of tRNA modification levels between V144M- and WT-LCLs. Nucleosides from digested tRNA samples were analyzed by LC-MS. The *y* axis represents the $\log_2$ fold change in the levels of the indicated tRNA modifications between the two patients harboring homozygous V144M mutations described in the legend of Fig. 1A and two WT individuals. (B) Inosine modification levels in total tRNA from LCLs of two WT individuals and P1 and P2 harboring homozygous V144M mutations. Inosine levels were measured by absolute quantification to calculate the number of inosines per 1,000 nucleotides. The means and error bars represent measurements from 3 independent RNA samples from each cell line. *, $P < 0.05$.

read as G by reverse transcriptases (32–34), the formation of inosine at the wobble position of tRNA-Val-AAC can be directly detected by sequencing of amplified cDNA obtained by reverse transcription (RT) of cellular tRNA. In WT-LCLs, the majority of wobble adenosines in tRNA-Val-AAC were converted to inosine, as evidenced by the presence of a predominant "G" peak at position 34 (Fig. 3A). Notably, the level of wobble inosine modification in tRNA-Val-AAC was greatly reduced in both V144M-LCLs, with the majority of the peak signal at the wobble position being the unmodified "A" (Fig. 3A).

Based upon the inosine modification defect in tRNA-Val-AAC, we also investigated whether additional tRNAs containing inosine at the wobble position were affected by the ADAT3-V144M mutation. Due to technical challenges in RT-PCR sequencing analysis caused by the diverse number of tRNA isodecoder variants encoded by mammalian genomes, we investigated the modification status of human tRNAs using poisoned primer extension assays with a ddCTP terminator, to distinguish I_{34} (terminated with ddCTP) from A_{34}, terminated at the next guanosine (Fig. 3B to E). Using this assay, we observed a reduced frequency of I_{34} modification in tRNA-Ile-AAU, from nearly 100% to ~70% for P1 and 75% for P2 (Fig. 3B and C). For tRNA-Val-AAC and tRNA-Leu-AAG, we also observed a reduction in I_{34} in the tRNAs from both patients (Fig. 3D and E). Although accurate quantification of deamination for tRNA-Val-AAC and tRNA-Leu-AAG was not possible because of the high background signal in the primer extensions, the reduced I_{34} signal and consequent increase in readthrough products up to G_{30} were indicative of reduced inosine modification. These studies uncover a wobble inosine hypomodification defect for particular tRNAs in the cells of individuals who are homozygous for the ADAT3-V144M mutation. Moreover, while the ADAT3-V144M mutation reduces the deamination of multiple tRNAs, the effect is incomplete and not necessarily to the same extent in all affected tRNAs.

Human patient cells with homozygous ADAT3-V144M mutations exhibit perturbations in cellular tRNA adenosine deaminase activity. We next investigated whether the V144M mutation affects adenosine deaminase activity in the cells of ID-affected individuals expressing only the ADAT3-V144M variant. We performed an *in vitro* adenosine deaminase activity assay using whole-cell extracts prepared from the human LCLs described above. This was made possible since previous studies have shown that the activity of the ADAT2/3 enzyme complex is the only known cellular activity that catalyzes wobble inosine formation in tRNA (6). To detect inosine formation, we used an adenosine deaminase assay based upon the separation of digested RNA nucleoside products by thin-layer chromatography (TLC) (35, 36). For this assay, *in*

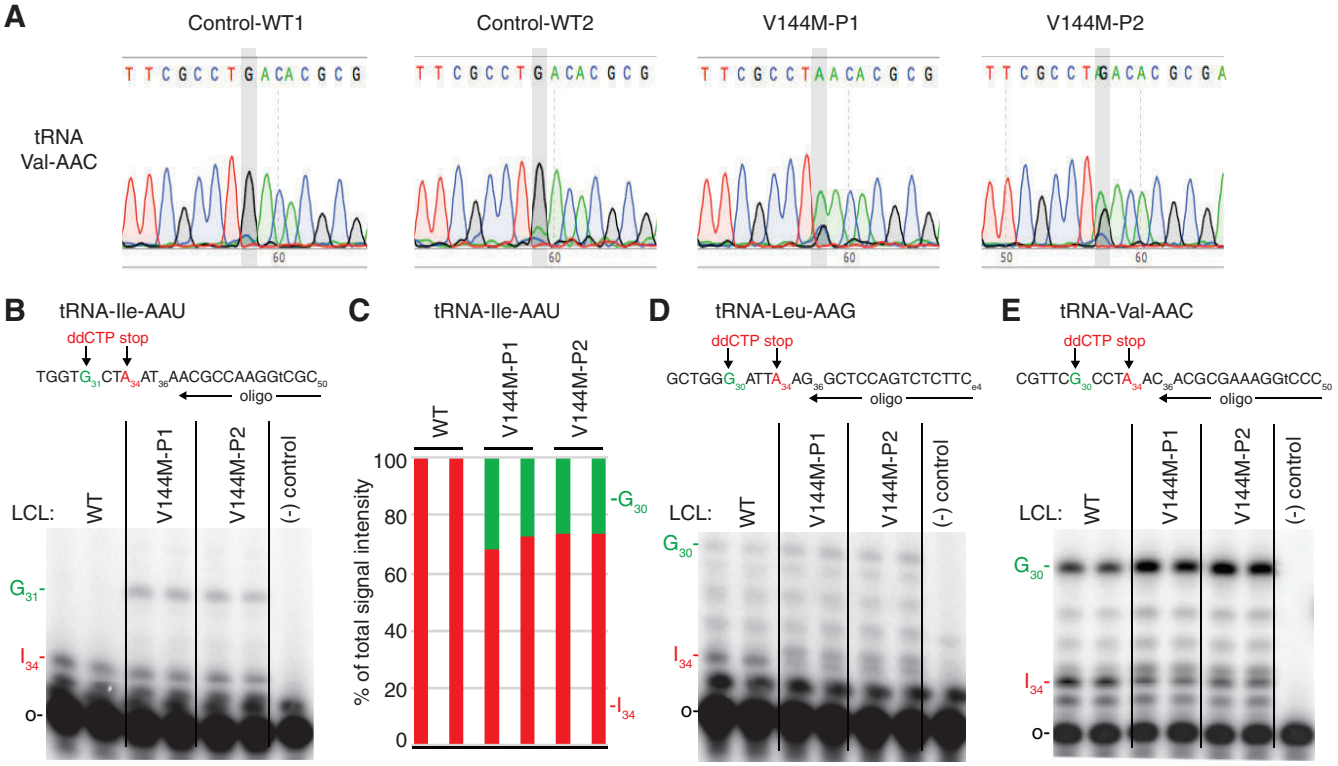

FIG 3 ID-affected individuals expressing only the ADAT3-V144M mutant exhibit a reduction in wobble inosine modification in tRNA isoacceptors. (A) Sequencing chromatogram analysis of RT-PCR products amplified from endogenous tRNA-Val-AAC isolated from LCLs of the indicated individuals. The wobble adenosine/inosine position is highlighted in gray. Inosine is read out as G. (B, D, and E) V144M-LCLs exhibit decreased inosine modification in tRNA-Ile-AAU, -Val-AAC, and -Leu-AAG. Primer extension analysis was performed with the indicated oligonucleotide probes against inosine-containing tRNAs in the presence of ddCTP. "G_n" denotes a readthrough product indicative of decreased inosine modification at position 34. "I_{34}" represents the stop position if inosine is present. "o" represents the labeled oligonucleotide used for primer extension. (−) control represents a primer extension reaction without the addition of reverse transcriptase. (C) Quantification of primer extension for tRNA-Ile-AAU. The RT stop signal due to inosine modification and the G_{31} readthrough product are plotted as a fraction of the total signal intensity for both bands.

vitro-transcribed tRNA substrates were internally radiolabeled at adenosine residues using [α-^{32}P]ATP and incubated with the whole-cell extract from either the wild-type or V144M individuals, and the RNAs were digested to nucleoside monophosphates with P1 nuclease followed by TLC separation to detect IMP formation. As the substrate, we used human tRNA-Val-AAC, since it has been shown to be a target of ADAT2/3-catalyzed deamination *in vitro* and *in vivo* (12).

While no detectable IMP was detected in tRNA preincubated with buffer alone (Fig. 4A, lane 1), we could readily detect the formation of IMP in tRNA-Val-AAC after preincubation with whole-cell extracts prepared from WT-LCLs (Fig. 4A, lanes 2 to 4). In addition to IMP, we also detected a faster-migrating adenosine modification that is consistent with the formation of 1-methyladenosine (m1A) (Fig. 4A) (37). Since human tRNA-Val-AAC has m1A at position 58 (38), the formation of m1A is likely due to endogenous TRMT6/TRMT61 complexes present in cellular extracts (39). The formation of m1A provides an internal control for cellular adenosine deaminase activity since it is catalyzed by two different enzyme complexes. Using a time course to monitor product formation, we detected similar levels of m1A formation between WT- and V144M-LCL extracts (Fig. 4B). In contrast, we found that V144M-LCL extracts exhibited a substantially lower rate of inosine formation in mature tRNA-Val (Fig. 4A and C). Thus, the V144M mutation appears to impair adenosine deaminase activity of endogenous ADAT2/3 complexes and uncovers a severe modification defect associated with the ADAT3-V144M variant in human individuals. Importantly, these findings suggest that individuals expressing only the ADAT3-V144M variant are likely to be compromised but not completely abolished in adenosine deaminase activity on wobble inosine-containing tRNA substrates *in vivo*.

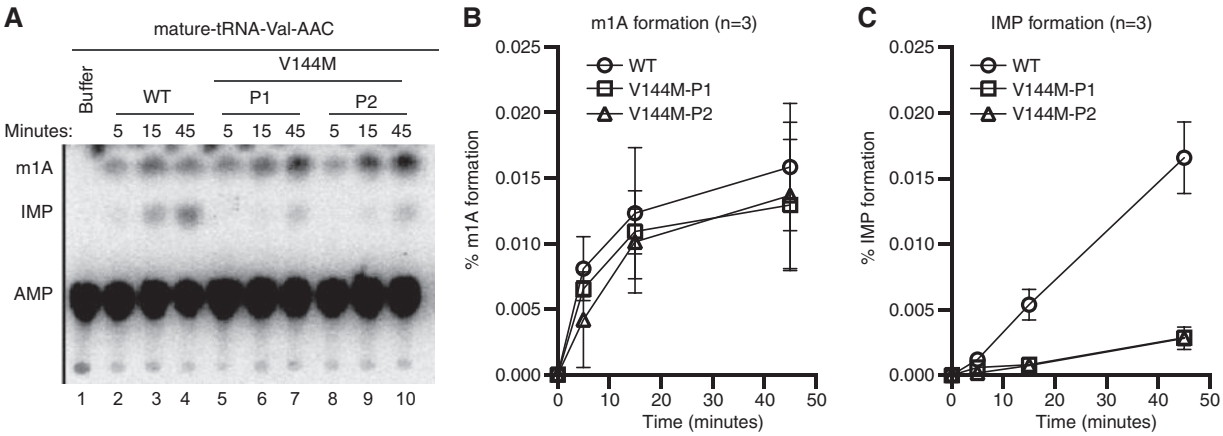

FIG 4 Individuals homozygous for the ADAT3-V144M mutation exhibit defects in adenosine deaminase activity. (A) Representative time course assay of adenosine deaminase activity using human cellular extracts and mature tRNA-Val-AAC from 5 to 45 min. (B and C) Quantification of m1A or IMP formation as a function of time for the indicated cellular extracts prepared from human LCLs. Percent m1A or IMP formation represents either the m1A/AMP+m1A+IMP or the IMP/AMP+m1A+IMP signal ($n = 3$).

Purified ADAT2/3 complexes assembled with ADAT3-V144M exhibit defects in adenosine deaminase activity. Eukaryotic ADAT3 interacts with the catalytic subunit ADAT2 to form an active adenosine deaminase complex. We first attempted to characterize the interaction of ADAT2 with ADAT3 using immunoprecipitation (IP) with the same antibody used for detection of endogenous ADAT3. In both cellular extracts prepared from wild-type individuals, we were able to enrich for ADAT3 on antibody-coated beads (Fig. 5A, compare lanes 1 and 2 versus lanes 5 and 6). Unexpectedly, ADAT3 was undetectable in the IPs from extracts prepared from either ADAT3-V144M patient (Fig. 5A, lanes 7 and 8). The lack of IP for ADAT3-V144M was not due to decreased levels of starting material since similar levels of ADAT3 were present in the input extracts of either WT- or V144M-LCLs (Fig. 5A, lanes 1 to 4). The lack of ADAT3 recovery from V144M-LCL extracts was also observed using an independent preparation of cellular extract (J. Ramos and D. Fu, unpublished data). Since the polyclonal antibody was generated against full-length human ADAT3, the altered IP characteristics suggest that ADAT3-V144M adopts a different structure and/or interaction than ADAT3-WT, which reduces its antigenicity under native conditions. Another possibility is that the location of the V144M mutation represents the primary antigenic determinant for this polyclonal antibody.

Since the endogenous ADAT3-V144M variant was resistant to immunoprecipitation, we developed a purification system based upon the expression of tagged ADAT3 variants in HEK 293T human embryonic cells. To analyze the interaction between ADAT3-V144M and ADAT2, we coexpressed green fluorescent protein (GFP)-tagged ADAT3-WT or -V144M with ADAT2 tagged with the Twin-Strep-tag in HEK 293T human embryonic kidney cells. The Strep-tag allows for one-step affinity purification of Strep-tagged proteins on Strep-Tactin resin under native conditions followed by gentle elution with biotin to preserve any protein-protein interactions (40). After purification of Strep-ADAT2 on Strep-Tactin resin, we found that comparable levels of GFP-ADAT3-WT and GFP-ADAT3-V144M interacted with ADAT2 (Fig. 5B). These results indicate that ADAT3-V144M can still form a complex with ADAT2.

To validate the interaction between ADAT2 and ADAT3-V144M, we used a reciprocal approach in which we purified ADAT3 and examined the amount of copurifying ADAT2. For these assays, we transiently expressed either ADAT3-WT or -V144M fused to a carboxy-terminal Strep-tag for purification and elution of ADAT2/3. Since ADAT2 levels have been shown to be limiting for the formation of ADAT2/3 complexes in human cells (15), we coexpressed His-tagged ADAT2 with either ADAT3-Strep-WT or ADAT3-Strep-V144M to facilitate the detection of any associated ADAT2. After purification on Strep-Tactin resin, bound ADAT3 complexes were eluted with biotin and analyzed by

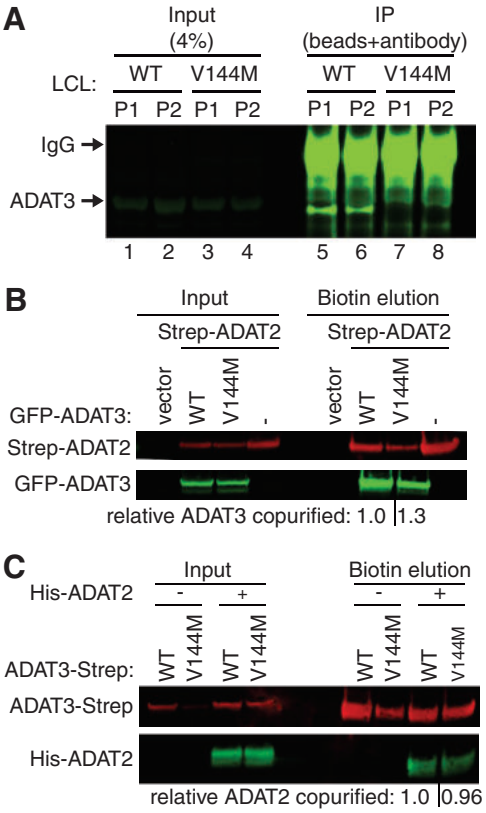

FIG 5 Purified ADAT2/3 complexes assembled with ADAT3-V144M exhibit defects in adenosine deaminase activity. (A) Immunoprecipitation (IP) of endogenous ADAT3. The input represents 4% of the starting extract used for IP. Arrows denote migration of ADAT3 and IgG. (B) ADAT3-V144M retains interaction with ADAT2. Shown are immunoblots for the indicated proteins from the input (5%) or biotin elutions of Strep-Tactin affinity purifications (10%) from HEK 293T cells transfected to express the Strep-tag alone (vector) or Strep-tagged ADAT2 with either GFP-ADAT3-WT or -V144M. "relative ADAT3 copurified" represents the ratio of the GFP-ADAT3 signal present in the eluted fraction normalized to the Strep-ADAT2 signal relative to ADAT3-WT. (C) ADAT3-WT and ADAT3-V144M copurify with similar levels of ADAT2. Shown are immunoblots for the indicated proteins from the input (5%) or biotin elutions from Strep-Tactin affinity purifications (20%) from HEK 293T cells transfected to express ADAT3-Strep-WT or ADAT3-Strep-V144M without or with His-ADAT2. "relative ADAT2 copurified" represents the ratio of the His-ADAT2 signal present in the eluted fraction normalized to the ADAT3-Strep signal relative to ADAT3-WT. Experiments for panels A through C were repeated three times, with comparable results.

immunoblotting. Using this approach, we detected the copurification of His-ADAT2 with either ADAT3-WT or ADAT3-V144M, consistent with the assembly of an ADAT2/3 complex from the expressed proteins (Fig. 5C). We detected comparable levels of His-ADAT2 that copurified with ADAT3-WT and -V144M, corroborating our finding that the ADAT3-V144M mutant maintains a similar interaction with ADAT2.

We next employed the TLC-based IMP detection assay described above to investigate whether the V144M mutation affects adenosine deaminase activity of purified ADAT2/3 complexes on *in vitro*-transcribed tRNA (Fig. 6A). ADAT2/3 complexes were purified using a strategy identical to the one described above, using Strep-tagged versions of either ADAT3-WT or -V144M coexpressed in the presence of His-tagged ADAT2. The purified complexes were analyzed by immunoblotting for ADAT2 and ADAT3 to ensure that equivalent amounts of complexes were used for enzymatic assays (Fig. 6B). Using a time course to monitor inosine formation, we found that purified ADAT2/3 complexes assembled with ADAT3-WT exhibited robust adenosine deaminase activity on mature tRNA-Val-AAC, as evidenced by the formation of inosine (Fig. 6C lanes 2 to 4). Compared to ADAT2/3-WT complexes, purified ADAT2/3-V144M complexes were significantly diminished in adenosine deaminase activity on mature tRNA-Val-AAC (Fig. 6C and D). The activity defect detected with purified ADAT2/3 complexes

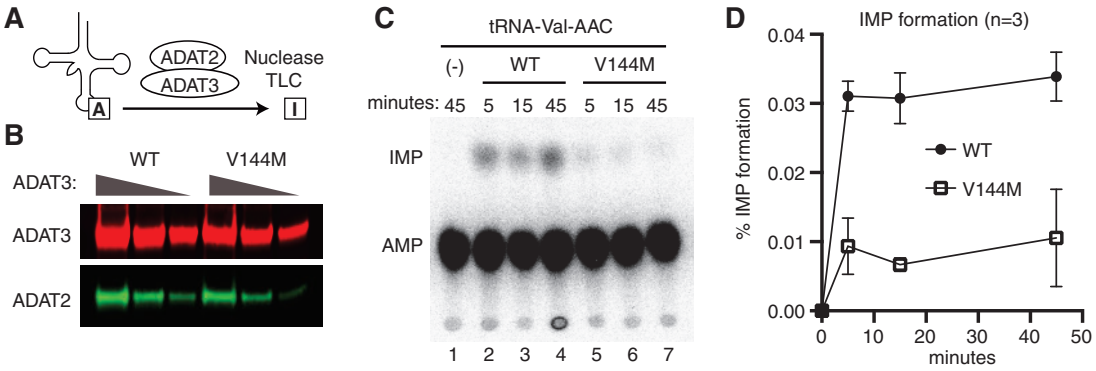

FIG 6 Purified ADAT2/3 complexes assembled with ADAT3-V144M exhibit defects in adenosine deaminase activity. (A) Schematic of the adenosine deaminase assay for inosine formation using *in vitro*-transcribed tRNA-Val-AAC. After incubation with ADAT2/3, labeled tRNA was digested with P1 nuclease, followed by separation of adenosine (A) from inosine (I) by thin-layer chromatography (TLC). (B) Immunoblot of purified ADAT2/3 complexes with 2-fold dilution series. The blot was probed for ADAT3-Strep and His-ADAT2. (C) Representative phosphorimager scan of TLC-separated nucleoside products from tRNAs incubated with buffer (−) or ADAT2/3 for the indicated times. The migration of IMP and AMP is indicated. (D) Quantification of IMP formation as a function of time for the indicated ADAT2/3 enzymes. Percent IMP formation represents the IMP/AMP plus IMP signal ($n = 3$).

assembled with ADAT3-V144M is consistent with the diminished adenosine deaminase activity of extracts prepared from V144M patient cells as described above. These findings reveal that while ADAT3-V144M can still associate with ADAT2 in human cells, the variant ADAT2/3-V144M complexes exhibit defects in adenosine deaminase activity.

ADAT3-V144M exhibits an increased propensity to self-associate. Using the tagged-ADAT3 system, we next investigated the biochemical properties of ADAT3 complexes using blue native polyacrylamide gel electrophoresis (BN-PAGE), which has been used previously to characterize protein complexes (41, 42). After fractionation of human cell extracts by BN-PAGE and blot transfer, total protein staining revealed approximately equal loading and transfer of proteins from 66 to 1,236 kDa (Fig. 7A). To ensure that protein complexes were maintained during electrophoresis, we probed against the TCP1 subunit of the TRiC/CCT chaperonin complex, which is known to migrate as a high-molecular-weight complex on BN-PAGE gels (43). We detected the TRiC/CCT chaperonin complex migrating at ~800 kDa, which is the expected molecular weight of the complex (Fig. 7A). Endogenous ADAT3 in HEK 293T cells was undetectable in human cell extracts by BN-PAGE immunoblotting, possibly due to masking of the epitope when ADAT3 is in complex with ADAT2 (Fig. 7A, vector). However, transiently expressed GFP-ADAT3-WT was detectable by BN-PAGE, with the majority of the signal concentrated in two bands migrating between the 100- and 250-kDa size markers (Fig. 7A, arrow and arrowhead). Based upon the molecular weight of ADAT3, the migration pattern of ADAT3-WT is consistent with ADAT3 homodimers or heterodimers with ADAT2. There is also the possibility that the upper band is an ADAT3 tetramer (Fig. 7A, arrowhead), which is a common property of cytidine and adenosine deaminases, including *Escherichia coli* TadA (44–46). ADAT3-V144M was also detectable by BN-PAGE as two bands migrating at molecular weights similar to those of the complexes detected in the ADAT3-WT sample although at lower levels than the WT (Fig. 7A, arrow and arrowhead). Notably, the ADAT3-V144M lane also contained high-molecular-weight complexes that exhibited an apparent molecular weight ranging from 400 to 1,000 kDa (Fig. 7A, bracket).

The high-molecular-weight complexes observed with ADAT3-V144M but not ADAT3-WT suggest that ADAT3-V144M has an increased propensity to self-associate or interact with additional proteins besides ADAT2. To test for self-oligomerization, we monitored the interaction of differentially tagged versions of wild-type ADAT3 with wild-type ADAT3 or of mutant ADAT3-V144M with mutant ADAT3-V144M. For these assays, we expressed either a WT version of GFP-ADAT3 with a WT form of ADAT3-Strep or a V144M mutant version of GFP-ADAT3 with the V144M mutant

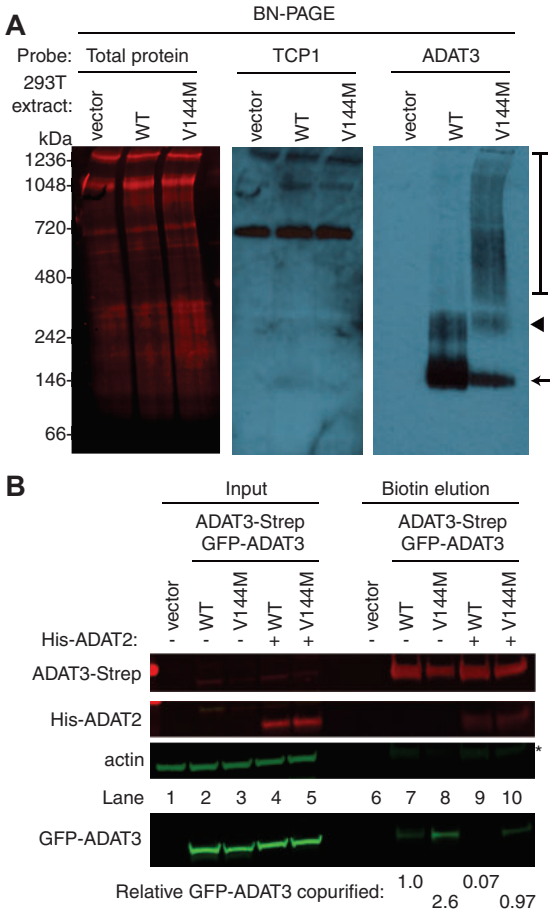

FIG 7 ADAT3-V144M exhibits an increased propensity to form higher-molecular-weight complexes indicative of aggregation. (A) Blue native polyacrylamide gel electrophoresis (BN-PAGE) analysis of ADAT3-GFP. Extracts prepared from HEK 293T cells expressing either ADAT3-WT or -V144M were separated on 3 to 12% BN-PAGE gels, followed by immunoblotting and probing with the indicated antibodies. The arrow and arrowhead point to predominant bands found in the WT and V144M extracts, while the bracket encompasses the high-molecular-weight signal detected in the ADAT3-V144M lane. Total protein indicates staining of the same blot to show loading of extracts. (B) Increased self-association of ADAT3-V144M. Shown are immunoblots for the indicated proteins from the input (5%) or biotin elutions from Strep-Tactin affinity purifications (20%) from HEK 293T cells transfected to express ADAT3-Strep-WT with GFP-ADAT3-WT or ADAT3-Strep-V144M with GFP-ADAT3-V144M in the absence or presence of ADAT2 coexpression. * represents the ADAT3-Strep signal from previous probing. The percentage of ADAT3 copurified represents the ratio of the GFP-ADAT3 signal present in the eluted fraction normalized to the Strep-ADAT3 signal relative to ADAT3-WT. Experiments for panels A and B were repeated three times.

form of ADAT3-Strep (Fig. 7B, lanes 2 to 5) (40). We detected a low level of GFP-ADAT3-WT copurifying with ADAT3-Strep-WT, suggesting that ADAT3 could already be susceptible to aggregation, even in the wild-type state (Fig. 7B, lane 7). Notably, we found that purification of ADAT3-Strep-V144M led to an increase in the amount of copurifying GFP-ADAT3-V144M compared to ADAT3-WT with itself (Fig. 7B, compare lanes 7 and 8). Moreover, we found that coexpression of His-ADAT2 could suppress the self-oligomerization of ADAT3-WT with another ADAT3-WT while partially reducing the self-association of the ADAT3-V144M variant (Fig. 7B, lanes 9 and 10). We also note that purification of either ADAT3-WT or -V144M led to similar levels of copurifying ADAT2 (Fig. 7B, lanes 9 and 10), consistent with our findings described above showing that ADAT3-V144M maintains interactions with ADAT2. These results provide evidence that the V144M mutation causes a change in the ADAT3 conformation that increases the propensity of ADAT3 to misfold and self-associate if not properly assembled with ADAT2. Moreover, the ability of ADAT2

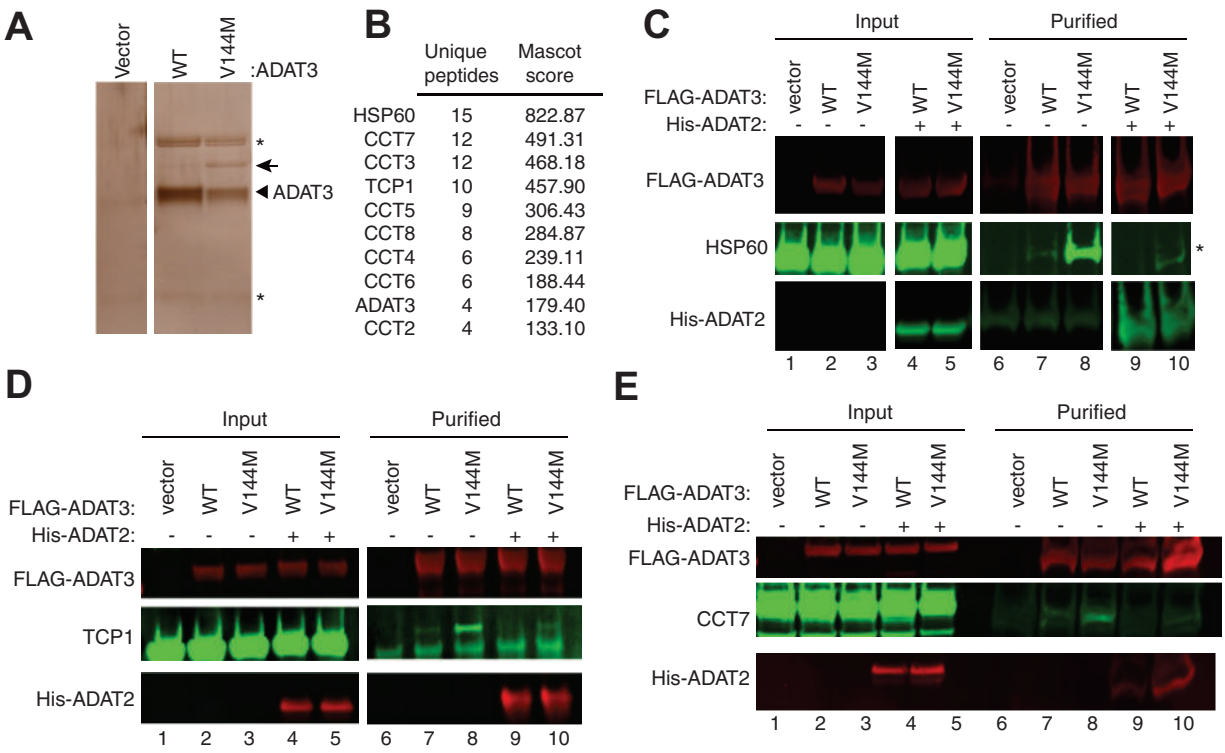

FIG 8 ADAT3-V144M is bound by the HSP60 and TRiC chaperonins. (A) Silver staining of eluted FLAG affinity purifications from HEK 293T cells expressing the FLAG tag alone (vector), FLAG-ADAT3-WT, or FLAG-ADAT3-V144M. The arrowhead represents FLAG-ADAT3, and the arrow represents a protein that specifically copurifies with ADAT3-V144M. (B) Chaperonin proteins identified by LC-MS proteomics specifically in ADAT3-V144M purifications. ADAT3 peptides are included for comparison. The number of unique peptides and Mascot score associated with each protein are noted. (C to E) Immunoblots for the indicated proteins from the input (5%) or FLAG affinity purifications (100%) from HEK 293T cells transfected to express FLAG-ADAT3-WT or -V144M without or with His-ADAT2. Purified samples represent SDS heat elutions of purified proteins retained on anti-FLAG antibody resin. IP immunoblots were repeated three times, with comparable results. * in panels A and C represents heavy and light chains of the anti-FLAG antibody used for affinity purification.

to prevent self-association of either ADAT3-WT or -V144M suggests a role for stoichiometric levels of ADAT2 and ADAT3 in promoting proper folding of ADAT3.

ADAT3-V144M is targeted by the cytoplasmic HSP60 and TRiC chaperonin complexes. The altered biochemical properties of ADAT3-V144M suggest that the V144M mutation causes an altered protein conformation with an increased proclivity to self-associate or interact with additional proteins. We thus investigated whether ADAT3-V144M exhibited differential protein interactions compared to ADAT3-WT. For protein interaction analysis, we expressed either the WT or V144M versions of ADAT3 as fusion proteins with the FLAG epitope tag in HEK 293T human cells. While the Strep-tag was used as described above to allow for native elution of ADAT2/3 complexes using biotin, the FLAG tag was used for these studies since it allowed for more efficient purification of protein complexes, as we have shown previously (47, 48). Following immunoprecipitation, the purified samples were analyzed by SDS-PAGE and silver staining to identify ADAT3-interacting proteins. While no observable bands were found in a control purification of cells transfected with the vector alone, we could detect the purification of FLAG-ADAT3-WT or -V144M (Fig. 8A, arrowhead) along with an additional band at ~60 kDa specifically enriched with the ADAT3-V144M purification (Fig. 8A, arrow). Analysis of the entire eluted samples from control and ADAT3 purifications by LC-MS validated the successful recovery of ADAT3-WT or ADAT3-V144M from cellular extracts (Fig. 8B; see also Table S1 in the supplemental material). Notably, LC-MS analysis also revealed the copurification of heat shock protein 60 (HSP60) and all eight subunits of the TCP1 ring complex (TRiC; also known CCT) with ADAT3-V144M but not ADAT3-WT (Fig. 8B and Table S1). HSP60 and TRiC subunits were identified among the top 20 best-scoring matches in the ADAT3-V144M purification. The HSP60 protein

forms a homooligomeric chaperonin complex consisting of a double-heptameric ring that associates with misfolded proteins in the cytoplasm and mitochondria to provide an environment for protein refolding (37, 49–51). Similar to HSP60, TRiC is a major eukaryotic cytoplasmic chaperonin that is responsible for the correct folding of endogenous client proteins that are prone to misfolding (38, 50). The interaction of chaperonin complexes with ADAT3-V144M is consistent with a change in protein conformation and misfolding induced by the V144M mutation. We also note that peptides matching ADAT2 were not identified in the purifications of either ADAT3-WT or -V144M when purified without coexpression of ADAT2. The lack of copurification of ADAT2 with overexpressed ADAT3 agrees with previous findings that the levels of endogenous ADAT2 are limiting for the formation of an ADAT2/3 complex (12).

To verify and characterize the interaction between HSP60 and ADAT3-V144M, we performed co-IP experiments followed by immunoblotting. For a subset of these assays, we coexpressed His-tagged ADAT2 with either WT or V144M versions of FLAG-ADAT3 to investigate whether ADAT2 influences HSP60 interactions as described above. While a low level of HSP60 copurified with ADAT3-WT, we detected a significantly increased amount of HSP60 associated with ADAT3-V144M (Fig. 8C, lanes 7 and 8). Interestingly, the interaction between HSP60 and ADAT3-V144M could be greatly suppressed by coexpression with ADAT2 (Fig. 8C, lanes 9 and 10). The reduction in HSP60 association with ADAT3 by ADAT2 coexpression again demonstrates that assembly of ADAT2 with ADAT3 is likely to prevent misfolding and subsequent targeting by chaperonin complexes. Of note, similar levels of ADAT2 copurified with both ADAT3-WT and -V144M (Fig. 8C, lanes 9 and 10), further corroborating the results described above showing that the V144M mutation does not compromise the interaction between ADAT2 and ADAT3.

Using an analogous co-IP approach, we also found that the TRiC complex subunits TCP1 and CCT7 exhibited a significantly increased association with ADAT3-V144M compared to wild-type ADAT3 (Fig. 8D and E, compare lanes 7 and 8). Similar to the ADAT3 interaction with HSP60, we also found that coexpression of ADAT2 could suppress the association between the TRiC complex and ADAT3-WT while significantly reducing the amount of TRiC associated with ADAT3-V144M (Fig. 8D and E, compare lanes 7 and 8 to lanes 9 and 10). The targeting of either ADAT3-WT or -V144M by cellular chaperonin complexes suggests that ADAT3-WT is prone to misfolding, with the V144M mutation further exacerbating the misfolding phenotype. Furthermore, these studies provide additional evidence that ADAT2 facilitates the proper folding of ADAT3.

ADAT3-V144M displays an aberrant subcellular localization that is suppressed by ADAT2 coexpression. The studies described above suggest that the ADAT3-V144M mutation perturbs the folding and/or activity of the ADAT2/3 complex on particular tRNA substrates, thereby leading to reduced levels of wobble inosine modifications. Since wobble inosine modification has been proposed to occur in the nucleus and cytoplasm of eukaryotes (11, 12, 39), we next monitored whether the subcellular localization of endogenous ADAT3 was altered by the V144M mutation. We first tested patient LCLs via immunofluorescence microscopy. While we could detect a weak fluorescence signal within WT- and V144M-LCLs, the diffuse signal combined with the spherical morphology of LCLs precluded any definitive conclusion on the subcellular localization of either ADAT3-WT or -V144M (Ramos and Fu, unpublished).

Due to the difficulty in visualizing ADAT3 in LCLs, the localization of ADAT3 was determined by microscopy of HeLa human cervical carcinoma cells transiently expressing ADAT3 fusion proteins with green fluorescent protein at the amino terminus (GFP-ADAT3). Whereas GFP alone displayed uniform accumulation in both the cytoplasm and nucleus of HeLa cells (Fig. 9A), the majority of cells expressing GFP-ADAT3-WT exhibited a diffuse cytoplasmic localization outlining the nucleus, with only a small percentage of transfected cells exhibiting a GFP-ADAT3 signal in the nucleus (Fig. 9A and B). The absence of nuclear localization for GFP-ADAT3-WT is likely due to the limiting amounts of the endogenous ADAT2 subunit that is required for the nuclear import of ADAT3 (12). In contrast, the ADAT3-V144M variant exhibited a distinct localization pattern with distribution in both the cytoplasm and nucleus rather than the

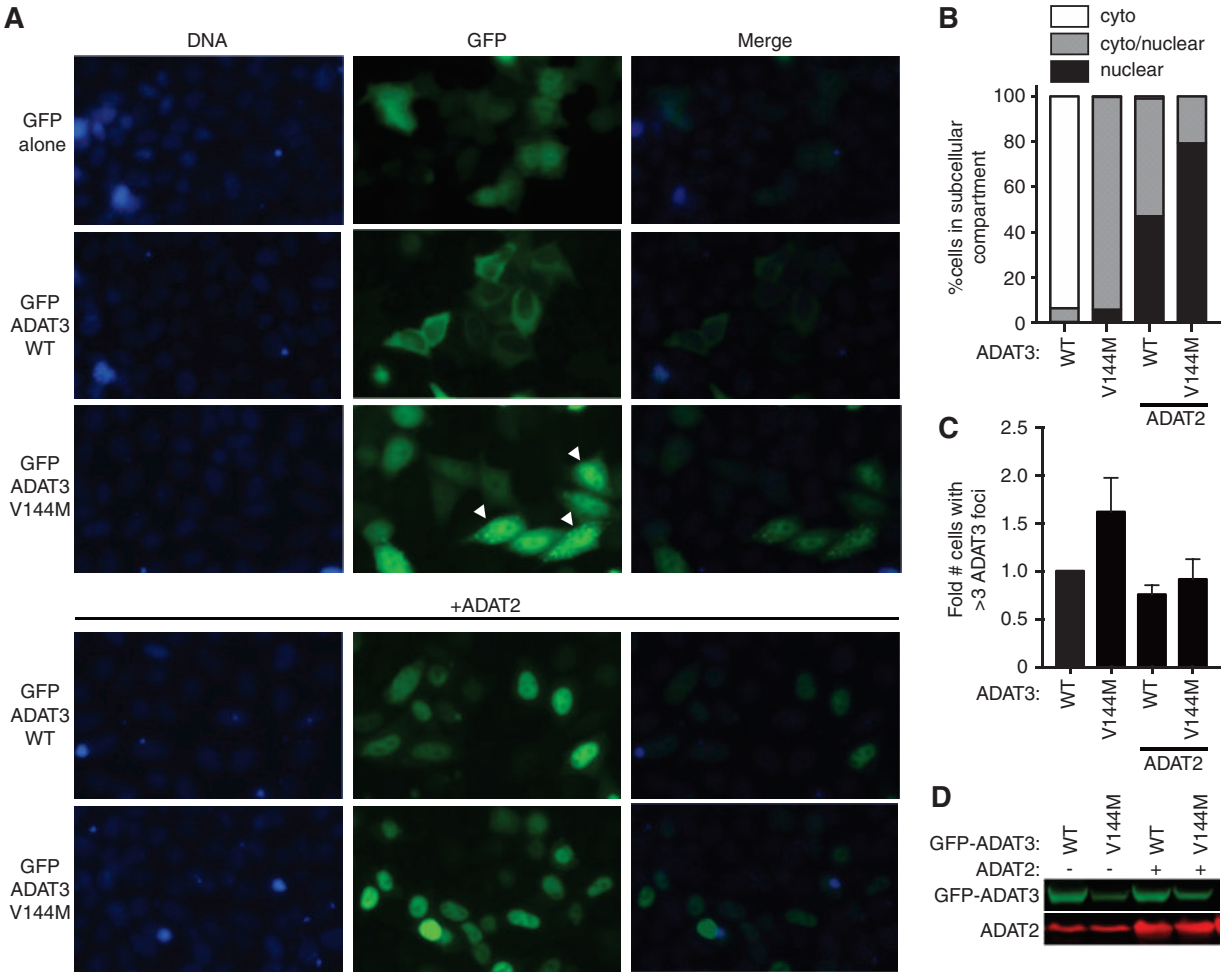

FIG 9 ADAT3-V144M displays an aberrant nucleocytoplasmic localization and increased susceptibility to form cytoplasmic aggregates. (A) Fluorescence microscopy images of GFP alone and GFP-tagged ADAT3-WT and -V144M expressed in HeLa cervical carcinoma cells. The bottom two rows exhibit cells cotransfected with untagged ADAT2. Nuclear DNA was stained with Hoechst stain, with merged images shown on the right. Arrowheads represent cells with >3 cytoplasmic foci of GFP-ADAT3. (B) Fraction of cells exhibiting GFP-ADAT3 that was either primarily cytoplasmic (cyto), similarly distributed between the cytoplasm and nucleus (cyto/nuclear), or primarily nuclear. (C) Fold change in the number of cells that exhibited more than three cytoplasmic foci of GFP-ADAT3. The fold change is expressed relative to ADAT3-WT without ADAT2 coexpression where 7% of cells exhibited more than three cytoplasmic foci. Experiments for panels B and C were repeated three times, with a minimum of 580 cells counted per experiment. (D) Immunoblot of GFP-ADAT3 expression without or with transient expression of ADAT2.

primarily cytoplasmic localization of ADAT3-WT (Fig. 9A and B). In addition to aberrant nuclear localization, we detected an increased population of GFP-positive cells that exhibited discrete, cytoplasmic foci when transfected with the ADAT3-V144M variant (Fig. 9A and C). The accumulation of ADAT3-V144M into distinct cytoplasmic foci is consistent with the increased propensity of ADAT3-V144M to self-associate into large multimeric complexes as described above. Moreover, the steady-state levels of the GFP-ADAT3-V144M variant were lower than those of ADAT3-WT, suggesting that the aberrant subcellular localization pattern of ADAT3-V144M was not simply due to greater expression (Fig. 9D).

In contrast to the cytoplasmic localization of transiently expressed GFP-ADAT3-WT alone, the coexpression of ADAT2 with ADAT3-WT led to GFP-ADAT3-WT being localized to the nucleus, with only a minor proportion of the signal remaining in the cytoplasm (Fig. 9A and B), consistent with the observation that ADAT2 dimerization with ADAT3 is required for nuclear import of the ADAT2/3 complex (12). Similarly, we found that coexpression of ADAT2 with ADAT3-V144M could also induce the translocation of GFP-ADAT3-V144M into the nucleus (Fig. 9A and B). The ability of ADAT2 coexpression to induce the translocation of GFP-ADAT3-V144M into the nucleus indi-

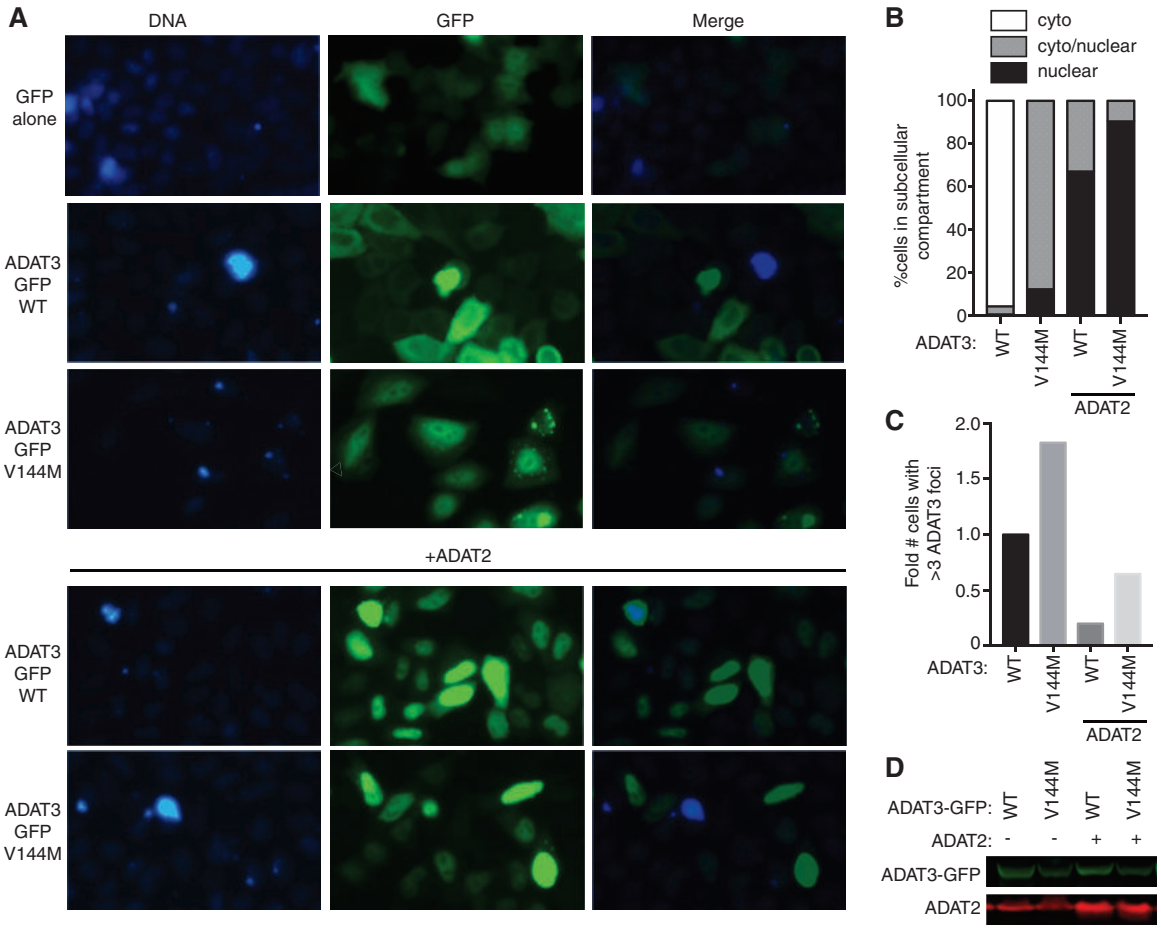

FIG 10 ADAT3-V144M displays an aberrant nucleocytoplasmic localization and increased susceptibility to form cytoplasmic aggregates also when tagged at the C terminus with GFP (ADAT3-GFP). (A) Fluorescence microscopy images of GFP alone and GFP-tagged ADAT3-WT and -V144M expressed in HeLa cervical carcinoma cells. Nuclear DNA was stained with Hoechst stain, with merged images shown on the right. (B) Fraction of cells exhibiting ADAT3-GFP that was either primarily cytoplasmic, similarly distributed between the cytoplasm and nucleus, or primarily nuclear. (C) Fold change in the number of cells that exhibited more than three cytoplasmic foci of GFP-ADAT3. For panels B and C, a minimum of 615 cells were counted per experiment. (D) Immunoblot of ADAT3-GFP expression without or with ADAT2 coexpression.

cates that ADAT3-V144M can still interact with ADAT2. However, while a slight, diffuse signal of GFP-ADAT3-WT remained in the cytoplasm even with ADAT2 coexpression, the ADAT3-V144M variant displayed much greater nuclear accumulation in the majority of cells. Remarkably, coexpression of ADAT2 with the ADAT3-V144M variant also reduced the percentage of cells with cytoplasmic GFP-ADAT3 foci to nearly wild-type levels (Fig. 9C).

We also found that carboxy-terminally GFP-tagged ADAT3-V144M exhibited the same aberrant nucleocytoplasmic localization pattern and increased formation of cytoplasmic foci observed with N-terminal GFP-ADAT3-V144M (Fig. 10A to C). Similar to the results observed with N-terminally GFP-tagged ADAT3-V144M, ADAT2 coexpression could also suppress the increased levels of foci associated with carboxy-terminally GFP-tagged ADAT3-V144M (Fig. 10C and D). Altogether, these results uncover an aberrant subcellular localization pattern for ADAT3-V144M characterized by a perturbed nucleocytoplasmic distribution and increased formation of cytoplasmic foci that can be ameliorated by coexpression with ADAT2. The increased propensity to self-oligomerize, interaction with cytoplasmic chaperones, and formation of aberrant cytoplasmic foci exhibited by ADAT3-V144M provide evidence for a protein folding defect induced by the V144M mutation that reduces enzymatic activity and wobble inosine levels in the tRNAs of ID-affected human individuals.

DISCUSSION

The molecular consequences of the ID-causing ADAT3-V144M mutation have previously been unknown. Here, we show that the ADAT3-V144M mutant accumulates to similar steady-state levels as ADAT3-WT and maintains an interaction with the ADAT2 subunit. However, the V144M mutation compromises the adenosine deaminase activity of ADAT2/3 complexes, increases the propensity of ADAT3 to oligomerize, and alters the subcellular localization properties of ADAT3. While the V144M mutation is a relatively minor change since valine and methionine represent amino acid residues with hydrophobic side chains, our studies uncover severe molecular defects associated with ADAT3-V144M that are likely to underlie the reduced wobble inosine levels detected in the tRNAs of ID-affected individuals with ADAT3-V144M mutations.

The changes in protein structure caused by the ADAT3-V144M mutation may alter the substrate recognition site of the ADAT2/3 complex, thereby affecting the binding or catalysis step of certain tRNA substrates. Intriguingly, studies with *Trypanosoma brucei* homologs of Tad2p/Tad3p have revealed a role for ADAT3 in substrate tRNA binding and coordination of a single zinc ion (36, 52). Moreover, we find that the ADAT3-V144M mutation has differential effects on wobble inosine levels, with certain tRNAs exhibiting a substantial decrease in tRNA modification and others displaying only a minor change. This differential effect could be due to the recognition mechanism of human ADAT2/3, which targets tRNA anticodon loops for inosine modification based upon their structural context rather than simply their sequence alone (53). Thus, ADAT2/3 complexes could have different specific activities on distinct tRNAs due to the additional structural features that affect protein-RNA binding and positioning in the active site. Further refinement using RNA binding assays and kinetics will provide insight into the specific effect of the V144M mutation on ADAT2/3 enzymatic activity that influences inosine modification levels *in vivo*.

The association of ADAT3-WT with cytoplasmic chaperonins suggests that endogenous ADAT3 could be prone to misfolding during translation or after release from the ribosome if not assembled with ADAT2. Consistent with our results, others have found that expression of soluble eukaryotic ADAT3 in *E. coli* requires coexpression of ADAT2 (10, 54). The increased tendency of ADAT3-V144M to form cytoplasmic foci suggests that the V144M mutation could further aggravate misfolding. Of note, structural studies have shown that methionine differs from other hydrophobic residues in that it can form noncovalent interactions with aromatic-containing residues such as tryptophan, tyrosine, or phenylalanine (55, 56). In addition, molecular modeling simulation experiments have identified that approximately one-third of solved protein structures contain a methionine-aromatic residue interaction (57). Thus, the replacement of a valine with methionine in the N-terminal extension of ADAT3 could lead to a nonspecific interaction with aromatic residues of another ADAT3 protein, leading to aggregation. Intriguingly, the perturbed nuclear localization and aggregation into discrete cytoplasmic foci exhibited by the ADAT3-V144M variant are reminiscent of other RNA binding proteins known to misfold and homooligomerize in neurological disorders, such as TDP-43 and TLS/FUS (58–62).

To gain insight into the potential structural effects of the V144M mutation that could account for our results, we used *in silico* comparison of ADAT3 against the known structures of tRNA adenosine deaminases (46, 63–65). Based upon template-based tertiary structure prediction (66), ADAT3 is predicted to fold into two distinct domains coinciding with the N-terminal extension and the C-terminal deaminase motif, as previously predicted (2, 63) (Fig. 11A and B). Valine 144 lies within the N-terminal extension at the end of a three-stranded beta sheet immediately before a tight turn caused by the adjacent proline at position 145. Notably, we find that replacing the valine with methionine leads to a clash in van der Waals radii with a threonine residue (T151) of the neighboring helix after the turn (Fig. 11C and D). Thus, the valine-to-methionine mutation could alter the proper folding of ADAT3.

Due to the intricate dynamics of tRNA processing (67–69), alterations in ADAT3

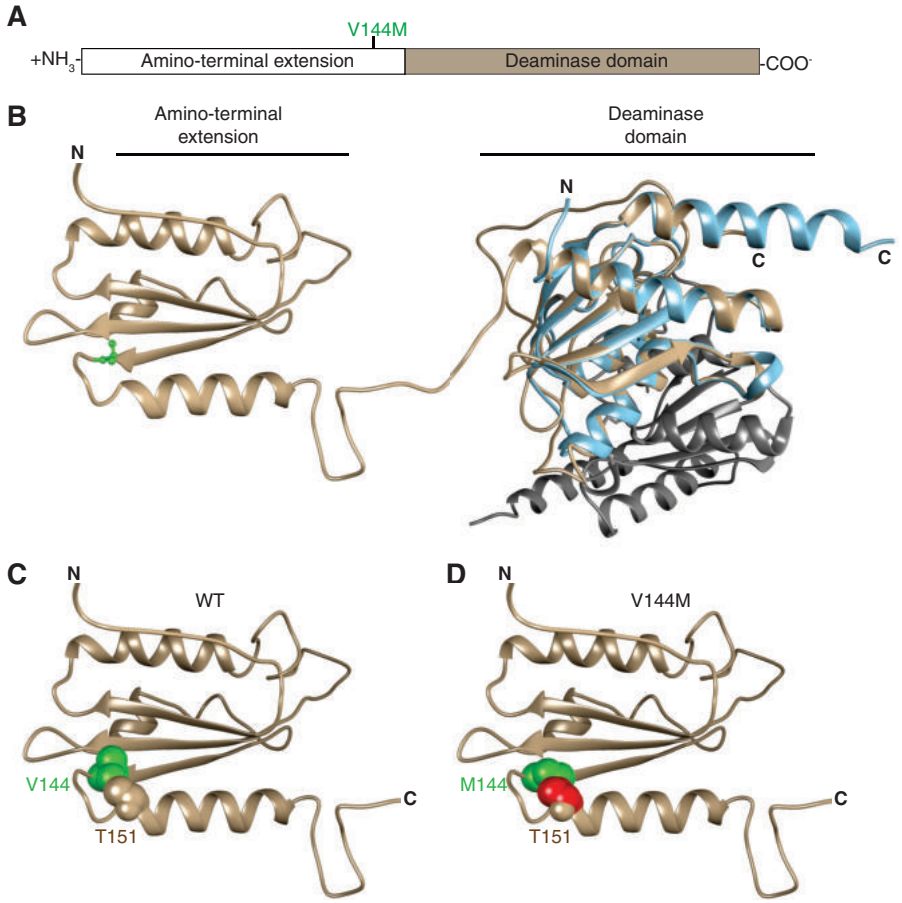

FIG 11 Predicted structure of ADAT3 and potential effects of the V144M mutation. (A) Schematic of ADAT3 with the location of the V144M mutation. (B) Based upon template-based tertiary structure prediction, ADAT3 is predicted to fold into two domains consisting of the amino-terminal extension and the deaminase domain. Valine 144 is highlighted in green in ball-and-stick form. The structure of the homodimeric *E. coli* TadA (PDB code 1Z3A) is aligned with the predicted C-terminal domain of ADAT3. Each monomer of TadA is shown in light blue and gray, respectively. (C) Amino-terminal extension of ADAT3, with the side chain of valine 144 shown in green in space-filling form. The side chain of threonine 151 is also shown in space-filling form in the same color as in the ribbon sequence. (D) Amino-terminal extension of ADAT3, with the V144M mutation shown in green. Atoms in the side chain of threonine 151 that clash with the methionine 144 side chain are shown in red.

nucleocytoplasmic localization by the V144M mutation provide another possible contributor to the decreased levels of wobble inosine tRNA modification in ID-affected individuals. The increased propensity of overexpressed ADAT3-V144M to localize to the nucleus suggests that there could be a relative decrease in the amount of cytoplasmic ADAT3 in ID-affected individuals with homozygous ADAT3-V144M mutations. The cytoplasmic population of ADAT3 assembled with ADAT2 could play a role in modifying tRNAs that have been exported without prior wobble inosine modification by nuclear ADAT2/3. Thus, the disruption of the nucleocytoplasmic ratio by the V144M mutation combined with the activity defect of ADAT2/3-V144M complexes could lead to the reduction in wobble inosine modification levels observed in the tRNAs of individuals homozygous for the ADAT3-V144M mutation. In addition, newly exported tRNAs lacking inosine could undergo retrograde transport back into the nucleus to be modified by nuclear ADAT2/3 (70, 71). Retrograde transport could play a critical role in providing at least enough tRNA wobble inosine modification for sufficient translation to sustain cell viability.

Based upon these findings, we hypothesize that a certain level of wobble inosine modification in particular tRNAs is necessary for the expression of cellular mRNAs that

are critical for proper cellular physiology and human development. Consistent with this prediction, studies in the yeast *Schizosaccharomyces pombe* and the plant *Arabidopsis thaliana* have shown that a decrease in tRNA wobble inosine modifications leads to temperature sensitivity, cell cycle arrest, and growth retardation (9, 11). Moreover, genome-wide studies predict numerous highly expressed genes that are dependent upon ADAT2/3-catalyzed wobble inosine modification for translation (72). Thus, the V144M mutation could alter the cellular proteome in multiple tissues, with particularly acute effects in the brain on neural growth and differentiation.

MATERIALS AND METHODS

Human subjects. Evaluation of affected members by a board-certified clinical geneticist included obtaining medical and family histories, clinical examination, neuroimaging, and clinical laboratory investigations. After obtaining written informed consent for enrollment in an institutional review board (IRB)-approved project (KFSHRC RAC number 2070023), venous blood was collected into EDTA and sodium heparin tubes for DNA extraction and establishment of lymphoblastoid cell lines (patients 11DG1699 and 09DG0640 and control subject 15DG0421), respectively. All studies abide by the principles of the Declaration of Helsinki.

Plasmids. The open reading frame for ADAT2 was PCR amplified from cDNA clone RC212395 (Origene) and cloned into pcDNA3.1 (Thermo Fisher) for expression as an untagged protein or as an N-terminal fusion protein with either the 6×His tag or Twin-Strep-tag (40). The open reading frame for human ADAT3 was PCR amplified from cDNA plasmid HsCD00326376 (PlasmID Repository, Harvard Medical School) and cloned into either pcDNA3.1-Strep-C, pcDNA3.1-3×FLAG-SBP, pcDNA3.1-N-EGFP, or pcDNA3.1-EGFP-C (73). The ADAT3-V144M variant was generated by Gibson mutagenesis and verified by Sanger sequencing.

Cell culture. HeLa S3 human cervical carcinoma and HEK 293T human embryonic kidney cell lines were cultured in Dulbecco's minimal essential medium (DMEM) containing 10% fetal bovine serum (FBS), 2 mM L-alanyl-L-glutamine (GlutaMAX; Gibco), and 1% penicillin-streptomycin. Human lymphoblastoid cell lines were cultured in RPMI 1640 medium containing 15% fetal bovine serum, 2 mM L-alanyl-L-glutamine (GlutaMAX; Gibco), and 1% penicillin-streptomycin.

Microscopy. HeLa cells were plated at 2.5×10^5 cells on a 6-well plate. Cells were transfected 1 day after plating with a total of 2.5 μg of DNA using Lipofectamine 3000. Cells were imaged at 48 h posttransfection on an Evos fluorescence microscopy imaging system (Thermo Fisher) for quantification of foci. For DNA staining, cells were washed twice with phosphate-buffered saline (PBS), incubated for 30 min at 37°C with PBS containing 10% FBS and 1 μM Hoechst stain, and then imaged. For quantification of cytoplasmic foci, 5 images of each well were taken, and the GFP-positive cells along with the cells containing more than 3 foci were counted in each of the 5 frames. The experiment was performed three times on N-terminally GFP-tagged ADAT3 with a minimum of 580 cells counted per experiment and independently verified by analysis in a blind manner. For C-terminally GFP-tagged ADAT3, the experiment was performed twice with independent verification. For quantification of nuclear ADAT3, data from each of the three experiments with N-terminally GFP-tagged ADAT3 were quantified using a minimum of 580 cells counted per experiment.

For visualization of ADAT3 in lymphoblastoid cells, 5×10^6 cells were DNA stained with Hoechst stain for 30 min at 37°C. Cells were washed twice with PBS, fixed with 4% formaldehyde (15 min), permeabilized with 0.3% Triton X-100 (10 min), and blocked in 5% bovine serum albumin (BSA)–PBS, followed by probing with primary anti-ADAT3 antibody (catalog number H00113179-B01P; Abnova). Primary antibody was used at a dilution of 1:500 and left overnight, with shaking at 4°C. After washing with PBS containing 0.15% Tween 20, the secondary antibody (Alexa Fluor 633-conjugated goat anti-mouse IgG at 1:200; Invitrogen) was incubated for 1 h at 25°C. After washing with PBS with 0.15% Tween 20, coverslips were mounted onto glass microscope slides with Aqua-Poly/Mount (catalog number 18606-20; Polysciences, Inc.) and left to dry overnight. All cells for visualization of ADAT3 using the commercial mouse ADAT3 antibody were imaged on a Leica SP5 confocal microscope.

Protein purification and analysis. Transient transfection and cellular extract production were performed as previously described (47). In brief, 2.5×10^6 HEK 293T cells were transiently transfected by calcium phosphate DNA precipitation with 10 to 20 μg of plasmid DNA, followed by preparation of the lysate by hypotonic freeze-thaw lysis at 48 h posttransfection. For anti-FLAG purification, the whole-cell extract from transiently transfected cell lines (1 mg of total protein) was rotated with 20 μl of anti-DYK DDDDK magnetic beads (TaKaRa BioUSA, Clontech, or Syd Labs) for 2 h at 4°C in lysis buffer (20 mM HEPES [pH 7.9], 2 mM $MgCl_2$, 0.2 mM EGTA, 10% glycerol, 1 mM dithiothreitol [DTT], 0.1 mM phenylmethylsulfonyl fluoride [PMSF], 0.1% NP-40) with 200 mM NaCl. Resin was washed three times using the same buffer, followed by RNA extraction or protein analysis. Strep-tagged proteins were purified using MagSTREP "type 3" XT beads (5% suspension; IBA Lifesciences) under conditions similar to those for anti-FLAG purifications and eluted with desthiobiotin.

Protein identification was performed by the URMC Mass Spectrometry Resource Laboratory. Briefly, protein samples were reduced, alkylated, and digested in solution with trypsin, followed by purification and desalting on an analytical C_{18} column tip. Peptide samples were analyzed by high-performance liquid chromatography (HPLC) coupled with electrospray ionization on a Q Exactive Plus hybrid quadrupole-orbitrap mass spectrometer (Thermo Fisher). Protein identification through tandem mass spectral correlation was performed using SEQUEST and Mascot.

Cellular extracts and purified protein samples were fractionated on NuPAGE Bis-Tris polyacrylamide gels (Thermo Scientific), followed by transfer to an Immobilon FL polyvinylidene difluoride (PVDF) membrane (Millipore) for immunoblotting. For analysis of LCL extracts, 5×10^6 lymphoblast cells were harvested, and proteins were extracted using radioisotope immunoprecipitation assay (RIPA) buffer (50 mM Tris HCl [pH 7.5], 1% NP-40, 0.5% sodium deoxycholate, 0.1% SDS, 150 mM NaCl, 2 mM EDTA). Antibodies against the following proteins were used: the FLAG epitope tag (catalog number A2220; Sigma), the 6×His tag (catalog number MA1-21315; Thermo Fisher), GFP (catalog number sc-9996; Santa Cruz Biotechnology), Strep-tag II (catalog number NC9261069; Thermo Fisher), ADAT3 (catalog number ab192987; Abcam), ADAT3 (catalog number H00113179-B01P; Abnova), ADAT2 (catalog number ab135429; Abcam), HSP60 (catalog number A302-845A; Bethyl Labs), CCT1 (catalog number sc-53454; Santa Cruz Biotechnologies), CCT7 (catalog number A304-730A-M; Bethyl Labs), and actin (catalog number MAB1501; EMD Millipore). Primary antibodies were detected using IRDye 800CW goat anti-mouse IgG (catalog number SA5-35521; Thermo Fisher), anti-rabbit IgG (catalog number SA5-35571; Thermo Fisher), or anti-rat IgG (catalog number 925-32219; Li-Cor Biosciences) or using IRDye 680RD goat anti-mouse IgG (catalog number 926-68070; Li-Cor Biosciences) or anti-rabbit IgG (catalog number 925-68071; Li-Cor Biosciences). Immunoblots were scanned using direct infrared fluorescence via the Odyssey system (Li-Cor Biosciences).

Adenosine deaminase assays. Internally radiolabeled tRNA substrates were prepared by T7 *in vitro* transcription of DNA templates generated by PCR amplification. Oligonucleotides containing the T7 promoter upstream of tRNA sequences were PCR amplified using Herculase II DNA polymerase or *Taq* DNA polymerase (New England Biolabs), followed by agarose gel purification of PCR amplification products. *In vitro* transcription was performed using Optizyme T7 RNA polymerase (Fisher Scientific) with 10 mM (each) UTP, CTP, and GTP; 1 mM ATP; and 250 μCi of [α-^{32}P]ATP (800 Ci/mmol; 10 mCi/ml). *In vitro* transcription reaction mixtures were incubated at 37°C for 2 h, followed by DNase treatment and purification using RNA Clean and Concentrator columns (Zymo Research). Full-length tRNA transcripts were verified on a 15% polyacrylamide-urea gel stained with SYBR gold nucleic acid stain (Thermo Fisher). Before conducting enzymatic assays, all tRNA substrates were refolded by thermal denaturation at 95°C for 2 min in buffer containing final concentrations of 5 mM Tris (pH 7.5) and 0.16 mM EDTA, quick chilling on ice for 2 min, and refolding at 37°C in the presence of HEPES (pH 7.5), $MgCl_2$, and NaCl.

For adenosine deaminase assays, ~12 ng of the refolded tRNA substrate was incubated with either the lymphoblastoid extract or Strep-tag-purified ADAT3. Reaction mixtures were incubated at 37°C for 5, 15, and 45 min, and RNA was purified using RNA Clean and Concentrator columns. The tRNA was eluted in 10 μl of water and subjected to nuclease P1 digestion overnight in a total volume of 13 μl with 0.125 U of P1 in 250 mM ammonium acetate (pH 5.35). Half of the P1 nuclease-treated samples were spotted onto Polygram polyester cellulose MN 300 plates (Macherey-Nagel) run in solvent B (0.1 M sodium phosphate buffer [pH 6.8]–NH_4 sulfate–*n*-propanol [100:60:2, vol/wt/vol]). Phosphorimaging was conducted on a Bio-Rad personal molecular imager, followed by analysis using NIH ImageJ software.

RNA analysis. RNA extraction was performed on 10×10^6 human lymphoblastoid cells using TRIzol LS reagent (Thermo Fisher). For RT-PCR, total RNA (~1.25 μg) was reverse transcribed for tRNA-Val-AAC using the Superscript IV enzyme followed by the QIAquick PCR purification kit. cDNA was then PCR amplified using Herculase II DNA polymerase (Agilent Genomics). The PCR product was gel extracted and analyzed by Sanger sequencing (ACGT, Inc.). The following primers were used: Val RT primer (TGTTTCC GCCTGGTTTTG), Val PCR primer F (GAACTAAGCTTGTTCAGAGTTCTACAGTCCGGACTACAAAGACCATGAC GGTGATTATAAAGATCATGACATGTTTCCGTAGTGTAGTGGTTATCAC), and Val PCR primer R (CACTTGTTTC CGCCTGGTTTTGATCCAGGGACC).

For primer extension assays to monitor inosine modification status, oligonucleotides were 5′-end labeled and purified as previously described (74). In a 5-μl annealing reaction mixture, 0.25 to 1 pmol of labeled primers was annealed to 0.6 μg of bulk RNA by incubation for 3 min at 95°C, followed by slow cooling and incubation for 30 min at 50°C to 55°C. The annealing product was then extended using 64 U Superscript III (Invitrogen) in a 10-μl reaction mixture containing 1× first-strand buffer, 2 mM ddCTP, 0.5 mM each of the other deoxynucleoside triphosphates (dNTPs), and 10 mM $MgCl_2$ at 50°C to 55°C for 1 h. Reactions were stopped by the addition of 2× RNA loading dye containing 98% formamide, 10 mM EDTA, 1 mg/ml bromophenol blue, and 1 mg/ml xylene cyanol and resolved on a 7 M urea–15% polyacrylamide gel, and the dried gel was imaged on a Typhoon phosphorimager and quantified as described previously (75). The primers for human tRNAs are as follows (lowercase letters refer to positions in the oligonucleotide probe that are not conserved among all tRNA sequences of a certain isoacceptor): Val(AAC)[50-36] (GGGaCCTTTCGCGTG), Ile(AAT)[50-36] (GCGaCCTTGGCGTTA), and Leu(AAG)[50-36] (GAA GAGACTGGAGCC).

Phosphorimager analysis. Phosphorimager scans were quantified using the Image Quant Fiji ImageJ processing package (76). For quantification of data from adenosine deaminase assays, the ratio of IMP/AMP pixel intensities was calculated using the peak signals from histogram plots of TLC images. Image quantification was performed using low-exposure scans that had peak signal intensities within the linear response range of the phosphorimager (data not shown).

For primer extension analysis of tRNA-Ile-AAU, peak signals from histogram plots of individual gel lanes were quantified based upon the area under the curve after adjustment to the background signal in an empty lane (data not shown). The percent signal intensity of each peak corresponding to an RT pause or stop was expressed relative to the total signal intensity of all quantifiable peaks between inosine and the guanosine stop.

TABLE 1 Mass spectrometry parameters of all analyzed nucleosides

Compound[a]	Precursor ion (*m/z*)	Product ion (*m/z*)	Ret[b] time (min)	Δ ret time (min)	Fragmentor voltage (V)	Collision energy (eV)	Cell accelerator voltage (V)	Polarity
A	268	136	5.1	1	110	21	5	Positive
A SILIS	278	141	5.1	1	110	21	5	Positive
C	244	112	2	1	175	13	5	Positive
C SILIS	253	116	2	1	175	13	5	Positive
Cm	258	112	3.7	1	180	9	5	Positive
Cm SILIS	270	116	3.7	1	180	9	5	Positive
G	284	152	4	1	95	17	5	Positive
G SILIS	294	157	4	1	95	17	5	Positive
Gm	298	152	4.8	1	100	9	5	Positive
Gm SILIS	311	157	4.8	1	100	9	5	Positive
I	269	137	3.8	1	100	9	5	Positive
I SILIS	279	142	3.8	1	100	9	5	Positive
m1A	282	150	3.5	1	110	21	5	Positive
m1A SILIS	295	158	3.5	1	110	21	5	Positive
m1G	298	166	4.7	1	105	13	5	Positive
m1G SILIS	311	174	4.7	1	105	13	5	Positive
m22G	312	180	5.5	1	105	13	5	Positive
m22G SILIS	328	191	5.5	1	105	13	5	Positive
m2G	298	166	4.9	1	95	17	5	Positive
m2G SILIS	311	174	4.9	1	95	17	5	Positive
m5C	258	126	3.5	1	185	13	5	Positive
m5C SILIS	270	133	3.5	1	185	13	5	Positive
m5U	259	127	4	1	95	9	5	Positive
m5U SILIS	271	134	4	1	95	9	5	Positive
m6A	282	150	6.4	1	125	17	5	Positive
m6A SILIS	295	158	6.4	1	125	17	5	Positive
m7G	299	167	3.6	1	105	14	5	Positive
m7G SILIS	311	174	3.6	1	105	14	5	Positive
U	245	113	2.7	1	95	5	5	Positive
U SILIS	254	117	2.7	1	95	5	5	Positive
Y	245	209	1.6	1	90	5	5	Positive
Y SILIS	254	218	1.6	1	90	5	5	Positive

[a]SILIS, stable isotope-labeled internal standards; Cm, 2′-*O*-methylcytidine; Gm, 2′-*O*-methylguanosine; I, inosine; m1A, 1-methyladenosine; m1G, 1-methylguanosine; m22G, N^2,N^2-dimethylguanosine; m5C, 5-methylcytosine; m5U, 5-methyluridine; m6A, N^6-methyladenosine; m7G, N^7-methyladenosine.
[b]Ret, retention.

Blue native PAGE. Protein extracts was prepared by resuspending transfected HEK 293T cells with lysis buffer (20 mM HEPES [pH 7.9], 2 mM $MgCl_2$, 0.2 mM EGTA, 10% glycerol, 1 mM DTT, 0.1 mM PMSF) supplemented with 0.05% digitonin. Cells were incubated on ice for 5 min, followed by a 30-min centrifugation at 20,000 × *g* at 4°C. The supernatants representing soluble protein extracts were analyzed by blue native PAGE (BN-PAGE) according to the manufacturer's protocol (Thermo Fisher). Briefly, samples were mixed with G-250 sample loading buffer and loaded onto 3 to 12% or 4 to 16% Novex Bis-Tris gels. Electrophoresis was performed at 150 V at 25°C until the dye front reached the bottom of the gel. Proteins were transferred and immunoblotted as described above, with the transfer time increased to 3 h.

LC-MS analysis. Total RNA was fractionated on an AdvanceBio column (300-Å pore size, 2.7-μm particle size, 7.8 by 300 mm; Agilent, Waldbronn, Germany) at 40°C using isocratic elution with 100 mM ammonium acetate at pH 7 as the mobile phase. The tRNA was collected in 1 ml 0.1 M NH_4 acetate (NH_4OAc) and vaporized by a SpeedVac until less than 50 μl remained in the vial. The tRNA fraction was ethanol precipitated, and tRNA pellets were resolved in 50 μl MilliQ water. Total tRNA (~200 ng) was processed and analyzed by LC-MS as previously described (47, 77). The signal from each modified nucleoside was normalized to the levels of canonical nucleosides (1,000 nucleotides [nt]) for quantification. LC-MS measurements of modified nucleosides were carried out on three biological replicates, followed by statistical analysis based upon unpaired Student's *t* test.

For absolute quantification of inosine, calibration solutions of inosine and the canonical nucleosides cytidine, uridine, guanosine, and adenosine were prepared with their respective synthetic standards (Sigma-Aldrich) and mixed to starting concentrations of 1 pmol/μl for the modified nucleoside and 100 pmol/μl for the canonical nucleosides. The resulting solution was diluted 1:1, and both dilutions were serially diluted 1:10 to a final concentration of 50 amol/μl for the modified nucleoside and 5 fmol/μl for the canonical nucleosides. A 1/10 volume of 10× yeast stable isotope-labeled internal standards (SILIS) was added to each calibration solution. Ten microliters of each calibration solution was subjected to LC-MS analysis before sample analysis using the same method as the one used for the samples.

The limit of detection (defined as a SILIS/nucleoside (S/N) ratio of >3) and limit of quantification (defined as an S/N ratio of >10) of inosine were 5 fmol. The MS peak areas of the modified nucleoside and canonicals were divided by the MS peak area of the corresponding SILIS and plotted over the

amount of injected material. The slope of the linear regression resulted in the relative response factors and was used to determine the amount of inosine in the analyzed samples. In a last step, the amounts of modified nucleoside (in picomoles) were divided by the sum of canonicals to receive the modification percentage per 1,000 canonical nucleosides. Mass spectrometry parameters are shown in Table 1.

SUPPLEMENTAL MATERIAL

Supplemental material for this article may be found at https://doi.org/10.1128/MCB.00203-19.

SUPPLEMENTAL FILE 1, XLSX file, 0.1 MB.

ACKNOWLEDGMENTS

We thank Mais Hashem for her assistance as a clinical research coordinator; Tarfa Alshiddi, Rana Alomar, and Eman Alobaid from the tissue culture core facility at KFSHRC; Joshua Dewe, Morgan Thomalla, and Michael Haft for preliminary studies; Kyle Swovick, Chen Chen, and Ben Phelan for quantification of foci; Daxiang Na for microscopy assistance; Mitch O'Connell for assistance on gel filtration studies; Kevin Welle and the URMC Mass Spectrometry Resource Lab for proteomics; and the Ghaemmaghami Lab for microscopy resources and discussion. We also thank the participating human subjects for donating their blood samples for research.

This work was supported by the Saudi Human Genome Program, King Salman Center for Disability Research, and King Abdulaziz City for Science and Technology grant 08-MED497-20 to F.S.A.; National Institutes of Health grant GM052347 to E.M.P.; and a University of Rochester Furth Fund award and National Science Foundation career award 1552126 to D.F.

We declare that we have no conflict of interest.

REFERENCES

1. Wolf J, Gerber AP, Keller W. 2002. tadA, an essential tRNA-specific adenosine deaminase from Escherichia coli. EMBO J 21:3841–3851. https://doi.org/10.1093/emboj/cdf362.
2. Gerber AP, Keller W. 1999. An adenosine deaminase that generates inosine at the wobble position of tRNAs. Science 286:1146–1149. https://doi.org/10.1126/science.286.5442.1146.
3. Grosjean H, de Crecy-Lagard V, Marck C. 2010. Deciphering synonymous codons in the three domains of life: co-evolution with specific tRNA modification enzymes. FEBS Lett 584:252–264. https://doi.org/10.1016/j.febslet.2009.11.052.
4. Rafels-Ybern A, Attolini CS, Ribas de Pouplana L. 2015. Distribution of ADAT-dependent codons in the human transcriptome. Int J Mol Sci 16:17303–17314. https://doi.org/10.3390/ijms160817303.
5. Novoa EM, Pavon-Eternod M, Pan T, Ribas de Pouplana L. 2012. A role for tRNA modifications in genome structure and codon usage. Cell 149:202–213. https://doi.org/10.1016/j.cell.2012.01.050.
6. Auxilien S, Crain PF, Trewyn RW, Grosjean H. 1996. Mechanism, specificity and general properties of the yeast enzyme catalysing the formation of inosine 34 in the anticodon of transfer RNA. J Mol Biol 262:437–458. https://doi.org/10.1006/jmbi.1996.0527.
7. Betts L, Xiang S, Short SA, Wolfenden R, Carter CW, Jr. 1994. Cytidine deaminase. The 2.3 A crystal structure of an enzyme: transition-state analog complex. J Mol Biol 235:635–656. https://doi.org/10.1006/jmbi.1994.1018.
8. Ko TP, Lin JJ, Hu CY, Hsu YH, Wang AH, Liaw SH. 2003. Crystal structure of yeast cytosine deaminase. Insights into enzyme mechanism and evolution. J Biol Chem 278:19111–19117. https://doi.org/10.1074/jbc.M300874200.
9. Tsutsumi S, Sugiura R, Ma Y, Tokuoka H, Ohta K, Ohte R, Noma A, Suzuki T, Kuno T. 2007. Wobble inosine tRNA modification is essential to cell cycle progression in G(1)/S and G(2)/M transitions in fission yeast. J Biol Chem 282:33459–33465. https://doi.org/10.1074/jbc.M706869200.
10. Rubio MA, Pastar I, Gaston KW, Ragone FL, Janzen CJ, Cross GA, Papavasiliou FN, Alfonzo JD. 2007. An adenosine-to-inosine tRNA-editing enzyme that can perform C-to-U deamination of DNA. Proc Natl Acad Sci U S A 104:7821–7826. https://doi.org/10.1073/pnas.0702394104.
11. Zhou W, Karcher D, Bock R. 2014. Identification of enzymes for adenosine-to-inosine editing and discovery of cytidine-to-uridine editing in nucleus-encoded transfer RNAs of Arabidopsis. Plant Physiol 166:1985–1997. https://doi.org/10.1104/pp.114.250498.
12. Torres AG, Piñeyro D, Rodríguez-Escribà M, Camacho N, Reina O, Saint-Léger A, Filonava L, Batlle E, Ribas de Pouplana L. 2015. Inosine modifications in human tRNAs are incorporated at the precursor tRNA level. Nucleic Acids Res 43:5145–5157. https://doi.org/10.1093/nar/gkv277.
13. Alazami AM, Hijazi H, Al-Dosari MS, Shaheen R, Hashem A, Aldahmesh MA, Mohamed JY, Kentab A, Salih MA, Awaji A, Masoodi TA, Alkuraya FS. 2013. Mutation in ADAT3, encoding adenosine deaminase acting on transfer RNA, causes intellectual disability and strabismus. J Med Genet 50:425–430. https://doi.org/10.1136/jmedgenet-2012-101378.
14. El-Hattab AW, Saleh MA, Hashem A, Al-Owain M, Asmari AA, Rabei H, Abdelraouf H, Hashem M, Alazami AM, Patel N, Shaheen R, Faqeih EA, Alkuraya FS. 2016. ADAT3-related intellectual disability: further delineation of the phenotype. Am J Med Genet A 170A:1142–1147. https://doi.org/10.1002/ajmg.a.37578.
15. Sharkia R, Zalan A, Jabareen-Masri A, Zahalka H, Mahajnah M. 6 October 2018. A new case confirming and expanding the phenotype spectrum of ADAT3-related intellectual disability syndrome. Eur J Med Genet https://doi.org/10.1016/j.ejmg.2018.10.001.
16. Anazi S, Maddirevula S, Faqeih E, Alsedairy H, Alzahrani F, Shamseldin HE, Patel N, Hashem M, Ibrahim N, Abdulwahab F, Ewida N, Alsaif HS, Al Sharif H, Alamoudi W, Kentab A, Bashiri FA, Alnaser M, AlWadei AH, Alfadhel M, Eyaid W, Hashem A, Al Asmari A, Saleh MM, AlSaman A, Alhasan KA, Alsughayir M, Al Shammari M, Mahmoud A, Al-Hassnan ZN, Al-Husain M, Osama Khalil R, Abd El Meguid N, Masri A, Ali R, Ben-Omran T, El Fishway P, Hashish A, Ercan Sencicek A, State M, Alazami AM, Salih MA, Altassan N, Arold ST, Abouelhoda M, Wakil SM, Monies D, Shaheen R, Alkuraya FS. 2017. Clinical genomics expands the morbid genome of intellectual disability and offers a high diagnostic yield. Mol Psychiatry 22:615–624. https://doi.org/10.1038/mp.2016.113.
17. Monies D, Abouelhoda M, AlSayed M, Alhassnan Z, Alotaibi M, Kayyali H, Al-Owain M, Shah A, Rahbeeni Z, Al-Muhaizea MA, Alzaidan HI, Cupler E, Bohlega S, Faqeih E, Faden M, Alyounes B, Jaroudi D, Goljan E, Elbardisy H, Akilan A, Albar R, Aldhalaan H, Gulab S, Chedrawi A, Al Saud BK, Kurdi W, Makhseed N, Alqasim T, El Khashab HY, Al-Mousa H, Alhashem A, Kanaan I, Algoufi T, Alsaleem K, Basha TA, Al-Murshedi F, Khan S, Al-Kindy A, Alnemer M, Al-Hajjar S, Alyamani S, Aldhekri H, Al-Mehaidib

A, Arnaout R, Dabbagh O, Shagrani M, Broering D, Tulbah M, Alqassmi A, Almugbel M, et al. 2017. The landscape of genetic diseases in Saudi Arabia based on the first 1000 diagnostic panels and exomes. Hum Genet 136:921–939. https://doi.org/10.1007/s00439-017-1821-8.
18. Abouelhoda M, Sobahy T, El-Kalioby M, Patel N, Shamseldin H, Monies D, Al-Tassan N, Ramzan K, Imtiaz F, Shaheen R, Alkuraya FS. 2016. Clinical genomics can facilitate countrywide estimation of autosomal recessive disease burden. Genet Med 18:1244–1249. https://doi.org/10.1038/gim.2016.37.
19. Khan M, Rafiq M, Noor A, Hussain S, Flores J, Rupp V, Vincent A, Malli R, Ali G, Khan F, Ishak G, Doherty D, Weksberg R, Ayub M, Windpassinger C, Ibrahim S, Frye M, Ansar M, Vincent J. 2012. Mutation in NSUN2, which encodes an RNA methyltransferase, causes autosomal-recessive intellectual disability. Am J Hum Genet 90:856–863. https://doi.org/10.1016/j.ajhg.2012.03.023.
20. Blanco S, Dietmann S, Flores JV, Hussain S, Kutter C, Humphreys P, Lukk M, Lombard P, Treps L, Popis M, Kellner S, Holter SM, Garrett L, Wurst W, Becker L, Klopstock T, Fuchs H, Gailus-Durner V, Hrabe de Angelis M, Karadottir RT, Helm M, Ule J, Gleeson JG, Odom DT, Frye M. 2014. Aberrant methylation of tRNAs links cellular stress to neurodevelopmental disorders. EMBO J 33:2020–2039. https://doi.org/10.15252/embj.201489282.
21. Shaheen R, Abdel-Salam GM, Guy MP, Alomar R, Abdel-Hamid MS, Afifi HH, Ismail SI, Emam BA, Phizicky EM, Alkuraya FS. 2015. Mutation in WDR4 impairs tRNA m(7)G46 methylation and causes a distinct form of microcephalic primordial dwarfism. Genome Biol 16:210. https://doi.org/10.1186/s13059-015-0779-x.
22. Shaheen R, Han L, Faqeih E, Ewida N, Alobeid E, Phizicky EM, Alkuraya FS. 2016. A homozygous truncating mutation in PUS3 expands the role of tRNA modification in normal cognition. Hum Genet 135:707–713. https://doi.org/10.1007/s00439-016-1665-7.
23. Najmabadi H, Hu H, Garshasbi M, Zemojtel T, Abedini S, Chen W, Hosseini M, Behjati F, Haas S, Jamali P, Zecha A, Mohseni M, Püttmann L, Vahid L, Jensen C, Moheb L, Bienek M, Larti F, Mueller I, Weissmann R, Darvish H, Wrogemann K, Hadavi V, Lipkowitz B, Esmaeeli-Nieh S, Wieczorek D, Kariminejad R, Firouzabadi S, Cohen M, Fattahi Z, Rost I, Mojahedi F, Hertzberg C, Dehghan A, Rajab A, Banavandi M, Hoffer J, Falah M, Musante L, Kalscheuer V, Ullmann R, Kuss A, Tzschach A, Kahrizi K, Ropers H. 2011. Deep sequencing reveals 50 novel genes for recessive cognitive disorders. Nature 478:57–63. https://doi.org/10.1038/nature10423.
24. Guy MP, Shaw M, Weiner CL, Hobson L, Stark Z, Rose K, Kalscheuer VM, Gecz J, Phizicky EM. 2015. Defects in tRNA anticodon loop 2′-O-methylation are implicated in nonsyndromic X-linked intellectual disability due to mutations in FTSJ1. Hum Mutat 36:1176–1187. https://doi.org/10.1002/humu.22897.
25. Freude K, Hoffmann K, Jensen LR, Delatycki MB, des Portes V, Moser B, Hamel B, van Bokhoven H, Moraine C, Fryns JP, Chelly J, Gecz J, Lenzner S, Kalscheuer VM, Ropers HH. 2004. Mutations in the FTSJ1 gene coding for a novel S-adenosylmethionine-binding protein cause nonsyndromic X-linked mental retardation. Am J Hum Genet 75:305–309. https://doi.org/10.1086/422507.
26. Davarniya B, Hu H, Kahrizi K, Musante L, Fattahi Z, Hosseini M, Maqsoud F, Farajollahi R, Wienker TF, Ropers HH, Najmabadi H. 2015. The role of a novel TRMT1 gene mutation and rare GRM1 gene defect in intellectual disability in two Azeri families. PLoS One 10:e0129631. https://doi.org/10.1371/journal.pone.0129631.
27. Abbasi-Moheb L, Mertel S, Gonsior M, Nouri-Vahid L, Kahrizi K, Cirak S, Wieczorek D, Motazacker M, Esmaeeli-Nieh S, Cremer K, Weißmann R, Tzschach A, Garshasbi M, Abedini S, Najmabadi H, Ropers H, Sigrist S, Kuss A. 2012. Mutations in NSUN2 cause autosomal-recessive intellectual disability. Am J Hum Genet 90:847–855. https://doi.org/10.1016/j.ajhg.2012.03.021.
28. Musante L, Ropers H. 2014. Genetics of recessive cognitive disorders. Trends Genet 30:32–39. https://doi.org/10.1016/j.tig.2013.09.008.
29. Shaheen R, Tasak M, Maddirevula S, Abdel-Salam GMH, Sayed ISM, Alazami AM, Al-Sheddi T, Alobeid E, Phizicky EM, Alkuraya FS. 2019. PUS7 mutations impair pseudouridylation in humans and cause intellectual disability and microcephaly. Hum Genet 138:231–239. https://doi.org/10.1007/s00439-019-01980-3.
30. de Brouwer APM, Abou Jamra R, Kortel N, Soyris C, Polla DL, Safra M, Zisso A, Powell CA, Rebelo-Guiomar P, Dinges N, Morin V, Stock M, Hussain M, Shahzad M, Riazuddin S, Ahmed ZM, Pfundt R, Schwarz F, de Boer L, Reis A, Grozeva D, Raymond FL, Riazuddin S, Koolen DA, Minczuk M, Roignant JY, van Bokhoven H, Schwartz S. 2018. Variants in PUS7 cause intellectual disability with speech delay, microcephaly, short stature, and aggressive behavior. Am J Hum Genet 103:1045–1052. https://doi.org/10.1016/j.ajhg.2018.10.026.
31. Su D, Chan CT, Gu C, Lim KS, Chionh YH, McBee ME, Russell BS, Babu IR, Begley TJ, Dedon PC. 2014. Quantitative analysis of ribonucleoside modifications in tRNA by HPLC-coupled mass spectrometry. Nat Protoc 9:828–841. https://doi.org/10.1038/nprot.2014.047.
32. Motorin Y, Muller S, Behm-Ansmant I, Branlant C. 2007. Identification of modified residues in RNAs by reverse transcription-based methods. Methods Enzymol 425:21–53. https://doi.org/10.1016/S0076-6879(07)25002-5.
33. Suzuki T, Ueda H, Okada S, Sakurai M. 2015. Transcriptome-wide identification of adenosine-to-inosine editing using the ICE-seq method. Nat Protoc 10:715–732. https://doi.org/10.1038/nprot.2015.037.
34. Kawahara Y. 2012. Quantification of adenosine-to-inosine editing of microRNAs using a conventional method. Nat Protoc 7:1426–1437. https://doi.org/10.1038/nprot.2012.073.
35. Grosjean H, Keith G, Droogmans L. 2004. Detection and quantification of modified nucleotides in RNA using thin-layer chromatography. Methods Mol Biol 265:357–391. https://doi.org/10.1385/1-59259-775-0:357.
36. Ragone FL, Spears JL, Wohlgamuth-Benedum JM, Kreel N, Papavasiliou FN, Alfonzo JD. 2011. The C-terminal end of the Trypanosoma brucei editing deaminase plays a critical role in tRNA binding. RNA 17:1296–1306. https://doi.org/10.1261/rna.2748211.
37. Saibil H. 2013. Chaperone machines for protein folding, unfolding and disaggregation. Nat Rev Mol Cell Biol 14:630–642. https://doi.org/10.1038/nrm3658.
38. Dalton KM, Frydman J, Pande VS. 2015. The dynamic conformational cycle of the group I chaperonin C-termini revealed via molecular dynamics simulation. PLoS One 10:e0117724. https://doi.org/10.1371/journal.pone.0117724.
39. Haumont E, Fournier M, de Henau S, Grosjean H. 1984. Enzymatic conversion of adenosine to inosine in the wobble position of yeast tRNAAsp: the dependence on the anticodon sequence. Nucleic Acids Res 12:2705–2715. https://doi.org/10.1093/nar/12.6.2705.
40. Schmidt TG, Batz L, Bonet L, Carl U, Holzapfel G, Kiem K, Matulewicz K, Niermeier D, Schuchardt I, Stanar K. 2013. Development of the Twin-Strep-tag and its application for purification of recombinant proteins from cell culture supernatants. Protein Expr Purif 92:54–61. https://doi.org/10.1016/j.pep.2013.08.021.
41. Wittig I, Braun HP, Schagger H. 2006. Blue native PAGE. Nat Protoc 1:418–428. https://doi.org/10.1038/nprot.2006.62.
42. Braz VA, Howard KJ. 2009. Separation of protein oligomers by blue native gel electrophoresis. Anal Biochem 388:170–172. https://doi.org/10.1016/j.ab.2009.02.019.
43. Noormohammadi A, Khodakarami A, Gutierrez-Garcia R, Lee HJ, Koyuncu S, Konig T, Schindler C, Saez I, Fatima A, Dieterich C, Vilchez D. 2016. Somatic increase of CCT8 mimics proteostasis of human pluripotent stem cells and extends C. elegans lifespan. Nat Commun 7:13649. https://doi.org/10.1038/ncomms13649.
44. Johansson E, Mejlhede N, Neuhard J, Larsen S. 2002. Crystal structure of the tetrameric cytidine deaminase from Bacillus subtilis at 2.0 A resolution. Biochemistry 41:2563–2570. https://doi.org/10.1021/bi011849a.
45. Xie K, Sowden MP, Dance GS, Torelli AT, Smith HC, Wedekind JE. 2004. The structure of a yeast RNA-editing deaminase provides insight into the fold and function of activation-induced deaminase and APOBEC-1. Proc Natl Acad Sci U S A 101:8114–8119. https://doi.org/10.1073/pnas.0400493101.
46. Kim J, Malashkevich V, Roday S, Lisbin M, Schramm VL, Almo SC. 2006. Structural and kinetic characterization of Escherichia coli TadA, the wobble-specific tRNA deaminase. Biochemistry 45:6407–6416. https://doi.org/10.1021/bi0522394.
47. Dewe JM, Fuller BL, Lentini JM, Kellner SM, Fu D. 2017. TRMT1-catalyzed tRNA modifications are required for redox homeostasis to ensure proper cellular proliferation and oxidative stress survival. Mol Cell Biol 37:e00214-17. https://doi.org/10.1128/MCB.00214-17.
48. Gu C, Ramos J, Begley U, Dedon PC, Fu D, Begley TJ. 2018. Phosphorylation of human TRM9L integrates multiple stress-signaling pathways for tumor growth suppression. Sci Adv 4:eaas9184. https://doi.org/10.1126/sciadv.aas9184.
49. Skjærven L, Cuellar J, Martinez A, Valpuesta JM. 2015. Dynamics, flexibility, and allostery in molecular chaperonins. FEBS Lett 589:2522–2532. https://doi.org/10.1016/j.febslet.2015.06.019.

50. Gruber R, Horovitz A. 2016. Allosteric mechanisms in chaperonin machines. Chem Rev 116:6588–6606. https://doi.org/10.1021/acs.chemrev.5b00556.
51. Vilasi S, Carrotta R, Mangione MR, Campanella C, Librizzi F, Randazzo L, Martorana V, Marino Gammazza A, Ortore MG, Vilasi A, Pocsfalvi G, Burgio G, Corona D, Palumbo Piccionello A, Zummo G, Bulone D, Conway de Macario E, Macario AJ, San Biagio PL, Cappello F. 2014. Human Hsp60 with its mitochondrial import signal occurs in solution as heptamers and tetradecamers remarkably stable over a wide range of concentrations. PLoS One 9:e97657. https://doi.org/10.1371/journal.pone.0097657.
52. Spears JL, Rubio MA, Gaston KW, Wywial E, Strikoudis A, Bujnicki JM, Papavasiliou FN, Alfonzo JD. 2011. A single zinc ion is sufficient for an active Trypanosoma brucei tRNA editing deaminase. J Biol Chem 286:20366–20374. https://doi.org/10.1074/jbc.M111.243568.
53. Saint-Leger A, Bello C, Dans PD, Torres AG, Novoa EM, Camacho N, Orozco M, Kondrashov FA, Ribas de Pouplana L. 2016. Saturation of recognition elements blocks evolution of new tRNA identities. Sci Adv 2:e1501860. https://doi.org/10.1126/sciadv.1501860.
54. Delker RK, Zhou Y, Strikoudis A, Stebbins CE, Papavasiliou FN. 2013. Solubility-based genetic screen identifies RING finger protein 126 as an E3 ligase for activation-induced cytidine deaminase. Proc Natl Acad Sci U S A 110:1029–1034. https://doi.org/10.1073/pnas.1214538110.
55. Zauhar RJ, Colbert CL, Morgan RS, Welsh WJ. 2000. Evidence for a strong sulfur-aromatic interaction derived from crystallographic data. Biopolymers 53:233–248. https://doi.org/10.1002/(SICI)1097-0282(200003)53:3<233::AID-BIP3>3.3.CO;2-W.
56. Reid K, Lindley P, Thornton J. 1985. Sulphur-aromatic interactions in proteins. FEBS Lett 190:209–213. https://doi.org/10.1016/0014-5793(85)81285-0.
57. Valley CC, Cembran A, Perlmutter JD, Lewis AK, Labello NP, Gao J, Sachs JN. 2012. The methionine-aromatic motif plays a unique role in stabilizing protein structure. J Biol Chem 287:34979–34991. https://doi.org/10.1074/jbc.M112.374504.
58. Cookson MR. 2017. RNA-binding proteins implicated in neurodegenerative diseases. Wiley Interdiscip Rev RNA 8:e1397. https://doi.org/10.1002/wrna.1397.
59. Van Deerlin VM, Leverenz JB, Bekris LM, Bird TD, Yuan W, Elman LB, Clay D, Wood EM, Chen-Plotkin AS, Martinez-Lage M, Steinbart E, McCluskey L, Grossman M, Neumann M, Wu IL, Yang WS, Kalb R, Galasko DR, Montine TJ, Trojanowski JQ, Lee VM, Schellenberg GD, Yu CE. 2008. TARDBP mutations in amyotrophic lateral sclerosis with TDP-43 neuropathology: a genetic and histopathological analysis. Lancet Neurol 7:409–416. https://doi.org/10.1016/S1474-4422(08)70071-1.
60. Woerner AC, Frottin F, Hornburg D, Feng LR, Meissner F, Patra M, Tatzelt J, Mann M, Winklhofer KF, Hartl FU, Hipp MS. 2016. Cytoplasmic protein aggregates interfere with nucleocytoplasmic transport of protein and RNA. Science 351:173–176. https://doi.org/10.1126/science.aad2033.
61. Farrawell NE, Lambert-Smith IA, Warraich ST, Blair IP, Saunders DN, Hatters DM, Yerbury JJ. 2015. Distinct partitioning of ALS associated TDP-43, FUS and SOD1 mutants into cellular inclusions. Sci Rep 5:13416. https://doi.org/10.1038/srep13416.
62. Conlon EG, Manley JL. 2017. RNA-binding proteins in neurodegeneration: mechanisms in aggregate. Genes Dev 31:1509–1528. https://doi.org/10.1101/gad.304055.117.
63. Elias Y, Huang RH. 2005. Biochemical and structural studies of A-to-I editing by tRNA:A34 deaminases at the wobble position of transfer RNA. Biochemistry 44:12057–12065. https://doi.org/10.1021/bi050499f.
64. Losey HC, Ruthenburg AJ, Verdine GL. 2006. Crystal structure of Staphylococcus aureus tRNA adenosine deaminase TadA in complex with RNA. Nat Struct Mol Biol 13:153–159. https://doi.org/10.1038/nsmb1047.
65. Kuratani M, Ishii R, Bessho Y, Fukunaga R, Sengoku T, Shirouzu M, Sekine S, Yokoyama S. 2005. Crystal structure of tRNA adenosine deaminase (TadA) from Aquifex aeolicus. J Biol Chem 280:16002–16008. https://doi.org/10.1074/jbc.M414541200.
66. Kallberg M, Wang H, Wang S, Peng J, Wang Z, Lu H, Xu J. 2012. Template-based protein structure modeling using the RaptorX Web server. Nat Protoc 7:1511–1522. https://doi.org/10.1038/nprot.2012.085.
67. Kessler AC, Silveira d'Almeida G, Alfonzo JD. 2018. The role of intracellular compartmentalization on tRNA processing and modification. RNA Biol 15:554–566. https://doi.org/10.1080/15476286.2017.1371402.
68. Blewett NH, Maraia RJ. 2018. La involvement in tRNA and other RNA processing events including differences among yeast and other eukaryotes. Biochim Biophys Acta 1861:361–372. https://doi.org/10.1016/j.bbagrm.2018.01.013.
69. Chatterjee K, Nostramo RT, Wan Y, Hopper AK. 2018. tRNA dynamics between the nucleus, cytoplasm and mitochondrial surface: location, location, location. Biochim Biophys Acta 1861:373–386. https://doi.org/10.1016/j.bbagrm.2017.11.007.
70. Shaheen HH, Horetsky RL, Kimball SR, Murthi A, Jefferson LS, Hopper AK. 2007. Retrograde nuclear accumulation of cytoplasmic tRNA in rat hepatoma cells in response to amino acid deprivation. Proc Natl Acad Sci U S A 104:8845–8850. https://doi.org/10.1073/pnas.0700765104.
71. Kessler AC, Kulkarni SS, Paulines MJ, Rubio MAT, Limbach PA, Paris Z, Alfonzo JD. 2018. Retrograde nuclear transport from the cytoplasm is required for tRNA(Tyr) maturation in T. brucei. RNA Biol 15:528–536. https://doi.org/10.1080/15476286.2017.1377878.
72. Rafels-Ybern A, Torres AG, Grau-Bove X, Ruiz-Trillo I, Ribas de Pouplana L. 2018. Codon adaptation to tRNAs with inosine modification at position 34 is widespread among eukaryotes and present in two bacterial phyla. RNA Biol 15:500–507. https://doi.org/10.1080/15476286.2017.1358348.
73. Fu D, Brophy JA, Chan CT, Atmore KA, Begley U, Paules RS, Dedon PC, Begley TJ, Samson LD. 2010. Human AlkB homolog ABH8 is a tRNA methyltransferase required for wobble uridine modification and DNA damage survival. Mol Cell Biol 30:2449–2459. https://doi.org/10.1128/MCB.01604-09.
74. D'Silva S, Haider SJ, Phizicky EM. 2011. A domain of the actin binding protein Abp140 is the yeast methyltransferase responsible for 3-methylcytidine modification in the tRNA anti-codon loop. RNA 17:1100–1110. https://doi.org/10.1261/rna.2652611.
75. Jackman JE, Montange RK, Malik HS, Phizicky EM. 2003. Identification of the yeast gene encoding the tRNA m1G methyltransferase responsible for modification at position 9. RNA 9:574–585. https://doi.org/10.1261/rna.5070303.
76. Schindelin J, Arganda-Carreras I, Frise E, Kaynig V, Longair M, Pietzsch T, Preibisch S, Rueden C, Saalfeld S, Schmid B, Tinevez JY, White DJ, Hartenstein V, Eliceiri K, Tomancak P, Cardona A. 2012. Fiji: an open-source platform for biological-image analysis. Nat Methods 9:676–682. https://doi.org/10.1038/nmeth.2019.
77. Heiss M, Reichle VF, Kellner S. 2017. Observing the fate of tRNA and its modifications by nucleic acid isotope labeling mass spectrometry: NAIL-MS. RNA Biol 14:1260–1268. https://doi.org/10.1080/15476286.2017.1325063.

Identification and rescue of a tRNA wobble inosine deficiency causing intellectual disability disorder

JILLIAN RAMOS,[1] MELISSA PROVEN,[1] JONATAN HALVARDSON,[2] FELIX HAGELSKAMP,[3] EKATERINA KUCHINSKAYA,[4] BENJAMIN PHELAN,[1] RYAN BELL,[1] STEFANIE M. KELLNER,[3] LARS FEUK,[2] ANN-CHARLOTTE THURESSON,[2] and DRAGONY FU[1]

[1]Department of Biology, Center for RNA Biology, University of Rochester, Rochester, New York 14627, USA
[2]Department of Immunology, Genetics and Pathology, Science for Life Laboratory, Uppsala University, 751 08 Uppsala, Sweden
[3]LMU Munich, Department of Chemistry, 81377 Munich, Germany
[4]Department of Clinical Genetics, and Department of Clinical Medicine, Linköping University, 581 83 Linköping, Sweden

ABSTRACT

The deamination of adenosine to inosine at the wobble position of tRNA is an essential post-transcriptional RNA modification required for wobble decoding in bacteria and eukaryotes. In humans, the wobble inosine modification is catalyzed by the heterodimeric ADAT2/3 complex. Here, we describe novel pathogenic ADAT3 variants impairing adenosine deaminase activity through a distinct mechanism that can be corrected through expression of the heterodimeric ADAT2 subunit. The variants were identified in a family in which all three siblings exhibit intellectual disability linked to biallelic variants in the *ADAT3* locus. The biallelic ADAT3 variants result in a missense variant converting alanine to valine at a conserved residue or the introduction of a premature stop codon in the deaminase domain. Fibroblast cells derived from two ID-affected individuals exhibit a reduction in tRNA wobble inosine levels and severely diminished adenosine tRNA deaminase activity. Notably, the ADAT3 variants exhibit impaired interaction with the ADAT2 subunit and alterations in ADAT2-dependent nuclear localization. Based upon these findings, we find that tRNA adenosine deaminase activity and wobble inosine modification can be rescued in patient cells by overexpression of the ADAT2 catalytic subunit. These results uncover a key role for the inactive ADAT3 deaminase domain in proper assembly with ADAT2 and demonstrate that ADAT2/3 nuclear import is required for maintaining proper levels of the wobble inosine modification in tRNA.

Keywords: tRNA modification; inosine; ADAT3; adenosine deaminase; intellectual disability

INTRODUCTION

The human *Adenosine Deaminase Acting on tRNA 3* (*ADAT3*) gene encodes a tRNA modification protein that has been linked to an autosomal-recessive form of ID (Alazami et al. 2013; El-Hattab et al. 2016; Salehi Chaleshtori et al. 2018; Sharkia et al. 2019; Thomas et al. 2019). Human ADAT3 forms an essential enzyme complex with its heterodimeric partner ADAT2 to catalyze the deamination of adenosine to inosine at the wobble position on a subset of tRNAs (Torres et al. 2015; Ramos et al. 2019). The presence of inosine at the wobble position is conserved in bacteria and eukaryotes (Gerber and Keller 1999; Wolf et al. 2002; Tsutsumi et al. 2007; Ragone et al. 2011; Zhou et al. 2014). The wobble inosine modification plays an essential function in organisms by expanding the decoding capacity of a tRNA thereby allowing a single wobble inosine-containing tRNA to decode -C, -A, and -U ending codons (Unger and Takemura 1973).

In *E. coli*, only tRNA-Arg-ACG is modified at the wobble position with inosine by the homodimeric TadA complex (Wolf et al. 2002). In contrast, eukaryotes contain multiple tRNA isoacceptors that are deaminated by the ADAT2/3 complex to yield inosine, including eight tRNA isoacceptors in human cells (Torres et al. 2015). This expansion of wobble inosine-containing tRNAs in eukaryotes is hypothesized to have occurred with the increased usage of specific codons in eukarya (Rafels-Ybern et al. 2017, 2019). In all cases, the inosine modification is essential for life in order to decode specific -C and -A ending codons as the

Corresponding authors: ann-charlotte.thuresson@igp.uu.se, dragonyfu@rochester.edu
Article is online at http://www.rnajournal.org/cgi/doi/10.1261/rna.076380.120.

genome does not encode a cognate tRNA to decode every codon (Rafels-Ybern et al. 2019).

A single base pair variant in the human *ADAT3* gene is the most common cause of autosomal recessive ID in Saudi Arabia, with a carrier frequency of 1% (MIM #615302) (Alazami et al. 2013; El-Hattab et al. 2016; Sharkia et al. 2019). The ID-associated *ADAT3* variant leads to a missense mutation altering valine at position 144 of ADAT3 to methionine (NM_138422.3, c.430 G > A, p.V144M). We have previously shown that individuals who are homozygous for the ADAT3–V144M variant exhibit a severe decrease in inosine modification on tRNAs (Ramos et al. 2019). Additionally, the ADAT3–V144M variant can still associate with ADAT2 but forms an adenosine deaminase complex that is greatly impaired in enzymatic activity.

Besides the *ADAT3* c.430 G > A (p.V144M) variant, only two other *ADAT3* variants have been reported in the human population that are associated with intellectual disability. These reports include an Iranian 6-yr-old girl homozygous for the *ADAT3* c.99_106dupGAGCCCGG, p.(Glu36Glyfs*44) (Salehi Chaleshtori et al. 2018) and two siblings of European descent carrying the compound heterozygous variants *ADAT3* c.587C > T, (p.Ala196Val) and c.586_587delinsTT, (p.Ala196Leu) (Thomas et al. 2019). However, the molecular and cellular effects of these *ADAT3* variants have not been characterized to any extent.

Here, we identify two novel compound heterozygous variants in *ADAT3* in three siblings presenting with intellectual disability, absent speech, seizures, and strabismus. Similar to patients with the ADAT3–V144M variant, we find that these children exhibit severe deficiency in wobble inosine modification. Notably, we identify a unique form of ADAT3 etiology in which ADAT2–ADAT3 interaction is perturbed leading to alterations in enzymatic activity and subcellular localization. Strikingly, we find that overexpression of the ADAT2 catalytic subunit can recover tRNA adenosine deaminase activity and wobble inosine modification in patient cells. Altogether, these results uncover a distinct form of ADAT3-associated ID that can be rescued through expression of the heterodimeric ADAT2 partner protein, thereby presenting a possible avenue for correcting diminished wobble inosine modification in patient cells.

RESULTS

Identification of compound variants in *ADAT3* linked to neurodevelopmental disorder

Through clinical referral for individuals with neurodevelopmental disorders, we identified a family consisting of nonconsanguineous parents and three children, one boy and two girls of ages 13, 9, and 4, respectively (Fig. 1A,B). Exome sequencing performed on the children (II:1, II:2, and II:3) revealed two novel variants of uncertain significance in the *Adenosine Deaminase Acting on tRNA 3* (*ADAT3*) gene (Fig. 1C). Follow-up Sanger sequencing validated the presence of the compound heterozygous variants in all three children (Supplemental Fig. 1). The children were compound heterozygous for a paternally inherited c.587C > T p.[A196V] variant and a maternally inherited c.820C > T p.[Q274*] variant (Fig. 1C, *ADAT3* [NM_138422.3]). No individuals have previously been reported to contain both variants. Both the single amino acid substitution and the frameshift variant occur at highly conserved residues in the conserved deaminase domain of ADAT3 (Fig. 1D; Supplemental Fig. 2A). The c.587C > T p.[A196V] missense variant is predicted to have a deleterious effect by multiple computational tools (SIFT, PolyPhen-2, MutationTaster), and there are seven heterozygous carriers in the gnomAD database (v2.1.1; allele frequency: 8.976×10^{-5}). The truncating variant, c.820C > T p.[Q274*], has been observed in two heterozygous carriers in gnomAD (allele frequency: 8.933×10^{-6}). RT-PCR of *ADAT3* mRNA from blood samples revealed expression of both allelic variants in the two older siblings while the third child has not been tested (Supplemental Fig. 2B).

All three siblings present with severe ID, absent speech, absence seizures (onset at 3 yr of age) and sleep disturbances. Moreover, the siblings exhibit short stature, intermittent strabismus and deeply set eyes. The ear lobes are short and superior helix squared. They also have a notched alae nasea, low hanging columella, a short and deep philtrum, prominent teeth and tapering fingers (Fig. 1A). Comparison to previously characterized individuals with ID linked to ADAT3 revealed a common set of features that included both cognitive and dysmorphic characteristics (Supplemental Table 1; Supplemental Information).

To determine the impact of the compound *ADAT3* variants, skin fibroblasts were harvested from both parents and the two eldest children. Samples were not collected from the third child due to the young age. Based upon immunoblotting of whole-cell lysates from skin fibroblasts, the children (II:1 and II:2; A196V/Q274*) exhibited a slight, but significant decrease in ADAT3 protein levels compared to the father (I:1-WT/A196V) (Fig. 1E,F, ADAT3). Since we did not observe a truncated ADAT3 protein product in the mother or children, the decrease in ADAT3 protein levels is consistent with reduced levels of full-length ADAT3 caused by the ADAT3–Q274* allele. A decrease in protein stability of the ADAT3–A196V protein and/or global protein synthesis could also contribute to the reduced ADAT3 levels in the children. Interestingly, we also detected a slight decrease in ADAT2 protein levels in the children (Fig. 1E,F, ADAT2). The decrease in ADAT2 levels suggests that ADAT2 stability could be linked to ADAT3 protein levels or a perturbation in cellular protein translation.

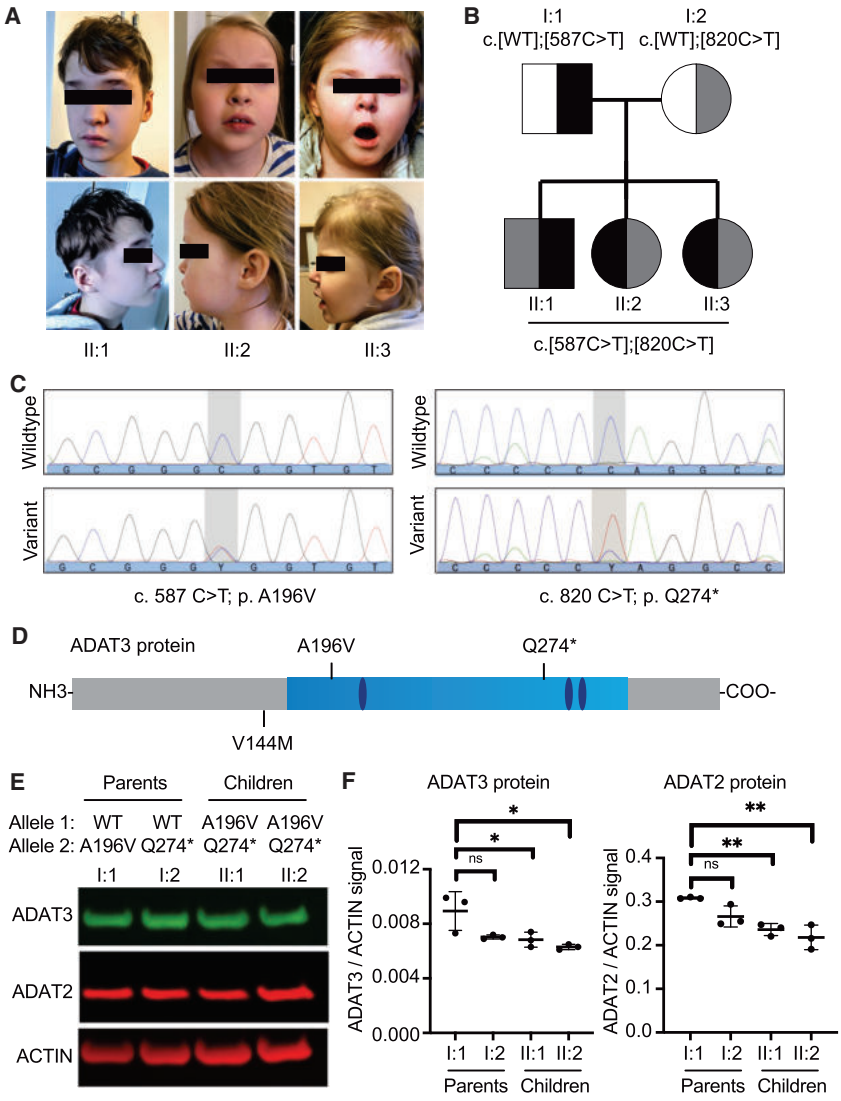

FIGURE 1. Biallelic heterozygous variants in *ADAT3* linked to intellectual disability. (*A*) Front and side views of each child at ages 12.5, 8.5, and 3.5 yr, respectively. (*B*) Pedigree of affected family. All three children have intellectual disability. (*C*) Whole exome sequencing identified two heterozygous variants of *ADAT3* in the children. The father is a heterozygous carrier of the c.587C > T variant, the mother is a heterozygous carrier of the c.820C > T variant. (*D*) Location of changes in the ADAT3 protein caused by biallelic variants identified here or a previously reported founder variant in *ADAT3*. The cytidine and deoxycytidylate deaminase zinc-binding region is shown in light blue and the zinc chelating residues in dark blue. (*E*) Immunoblot of the indicated proteins from fibroblast cellular lysates obtained from the parents (I:1, I:2) and children (II:1, II:2) of the ID-affected family shown in Figure 1. (*F*) Quantification of ADAT3 and ADAT2 levels after normalization to actin. $N = 3$. *Ordinary One-Way Anova—ADAT3/ACTIN:* I:2 ns = 0.06, II:1* = 0.04, II:2 * = 0.01. *Ordinary One-Way Anova—ADAT2/ACTIN:* I:2 ns = 0.11, II:1** = 0.009, II:2 ** = 0.002.

Individuals harboring the compound ADAT3 variants exhibit decreased wobble inosine modification in tRNA

We next investigated whether the ADAT3 variants impacted inosine modification status on endogenous tRNA substrates. The levels of inosine tRNA modification between the fibroblast cell lines was compared using liquid chromatography-mass spectrometry (LC-MS) as previously described (Ramos et al. 2019). After normalization to an average tRNA, we found that the fibroblasts from each child exhibited a ~50% reduction in inosine levels compared to the parental fibroblasts (Fig. 2A, inosine/tRNA). As comparison, no significant change in the ratio of the abundant m1A modification was detected between the four individuals (Fig. 2A, m1A/tRNA).

As additional verification for reduced wobble inosine modification, we monitored wobble inosine status in specific tRNAs using RT-PCR sequencing. Since inosine is a guanosine (G) analog, the presence of inosine can be detected by sequencing of cDNA products generated by RT-PCR of cellular tRNA (Motorin et al. 2007; Kawahara 2012; Wulff et al. 2017). Using this strategy, we measured the wobble inosine status of tRNA-Val-AAC and tRNA-Pro-AGG in the fibroblast cell lines. We also sequenced additional inosine-containing tRNA isoacceptors but the high sequence similarity between isodecoder variants prevented clear interpretation as previously noted by our laboratory and others (Torres et al. 2018; Ramos et al. 2019).

Fibroblasts prepared from both parental family members exhibited nearly complete adenosine to inosine modification at the wobble position on tRNA-Val-AAC, as shown by the presence of a G peak and the absence of an A peak (Fig. 2B, Valine-AAC, parents I:1 and I:2). In contrast, fibroblasts prepared from the two affected offspring individuals exhibited a reduction in inosine modification as revealed by the A peak signal being greater than the G peak (Fig. 2B, Valine-AAC, children II:1 and II:2). The presence of the C peak is due to tRNA-Val-CAC, which is nearly identical to tRNA-Val-AAC and is recognized by the same oligos used for RT-PCR amplification (Wulff et al. 2017). We also detected a similar decrease in inosine modification when examining the sequencing chromatograms of tRNA-Pro-AGG. While the A peak is

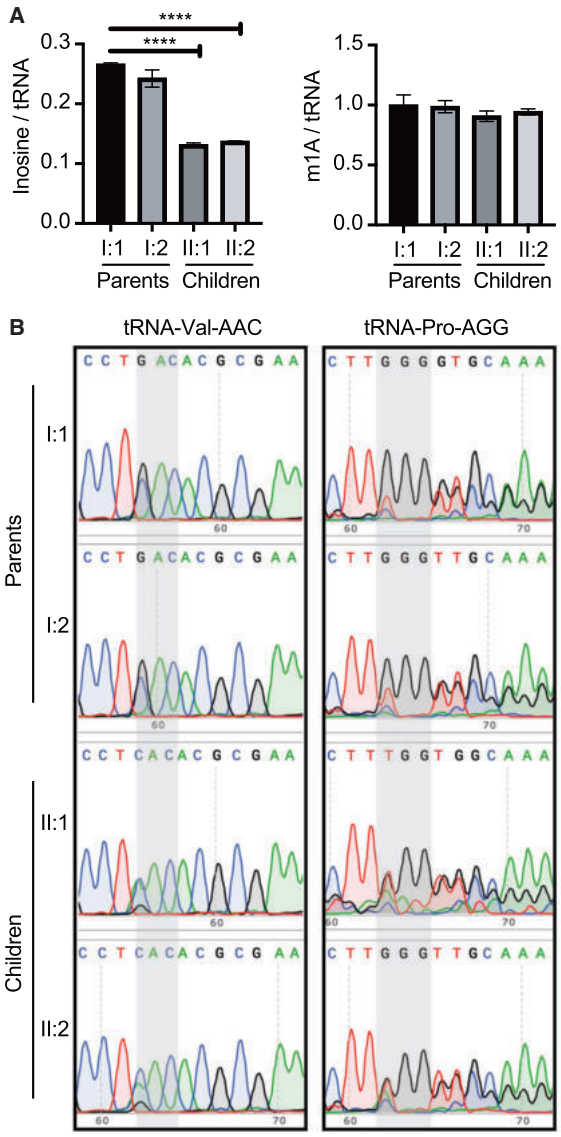

FIGURE 2. Reduced wobble inosine modification in the affected children harboring biallelic *ADAT3* variants. (*A*) LC-MS analysis of nucleosides prepared from small RNAs from fibroblasts of the indicated individuals. Inosine signal is normalized to an average tRNA molecule. Unpaired *t*-test (****) $P = <0.0001$. (*B*) RT-PCR sequencing analysis of the indicated tRNAs prepared from fibroblast cells harvested from the parents and children. Both children exhibit reduced wobble inosine signal compared to heterozygous parents. Gray highlights the anticodon loop. Inosine is read as G, while a tRNA that is unmodified will contain an A.

absent from the chromatograms of the two parental heterozygous controls, the two affected individuals with ID exhibited a detectable A peak (Fig. 2B, tRNA-Proline-AGG). Altogether, these results demonstrate that fibroblast cells harboring biallelic variants of *ADAT3* exhibit reduced inosine modification in at least two different tRNA isoacceptors. Moreover, the reduced inosine modification in the tRNA of patient fibroblast cells suggest that additional wobble inosine-containing tRNAs are likely to be impacted by the biallelic ADAT3 variants.

Reduced tRNA adenosine deaminase activity in patient fibroblasts harboring compound ADAT3 variants

We next measured the levels of tRNA adenosine deaminase activity between the fibroblast cell lines to elucidate the cause for the reduced wobble inosine modification in the children. We performed an adenosine deaminase activity assay using whole cell lysates extracted from fibroblasts and in vitro transcribed tRNA substrates internally radiolabeled at adenosine nucleotides. As model substrates, we used tRNA-Pro-AGG and tRNA-Thr-AGU, which are known to contain the inosine modification at position 34 (Rafels-Ybern et al. 2015; Torres et al. 2015). Moreover, these tRNA substrates are known to contain the m1A modification, which can be used an internal control as noted below. After incubation of radiolabeled tRNA with the cellular lysates, the tRNA was digested to nucleoside monophosphates and separated using thin-layer chromatography (TLC) to monitor inosine formation based upon the detection of inosine monophosphate (IMP) (Grosjean et al. 2004). As an internal control, adenosine deaminase activity was normalized against the formation of 1-methyladenosine (m1A) in the tRNA substrates, which is catalyzed by the separate TRMT6/TRMT61 complex in cellular extracts (Guy and Phizicky 2014).

Using this assay, no detectable formation of inosine or m1A was observed when either tRNA substrate was incubated with buffer alone (Fig. 3A,B, lane 1, Buffer). In lanes where tRNA had been incubated with cell lysates derived from parental fibroblasts, we detected the formation of IMP along with 1-methyladenosine (m1A) (Fig. 3A,B, lanes 2 and 3, I:1 and I:2, parents). In contrast, only a background level of inosine formation was detected in cell extracts derived from the children with the compound ADAT3 variants (Fig. 3A,B, lanes 4 and 5, II:1 and II:2, children). Quantification of IMP formation revealed a significant reduction in adenosine deaminase activity from cellular extracts prepared from the children compared to the parents (Fig. 3C,D, % IMP formation). In contrast, the level of m1A formation on the same tRNA substrates was not significantly different between extracts derived from cells of the parents or children (Fig. 3C,D, % m1A formation). These results indicate that fibroblasts harboring the biallelic ADAT3 variants exhibit defects in catalyzing inosine formation on tRNA substrates, consistent with reduced inosine modification in their tRNAs.

ID-associated ADAT3 variants exhibit defects in ADAT2 interaction

Both the A196V missense variant and Q274* truncation lie within the conserved noncatalytic deaminase domain of

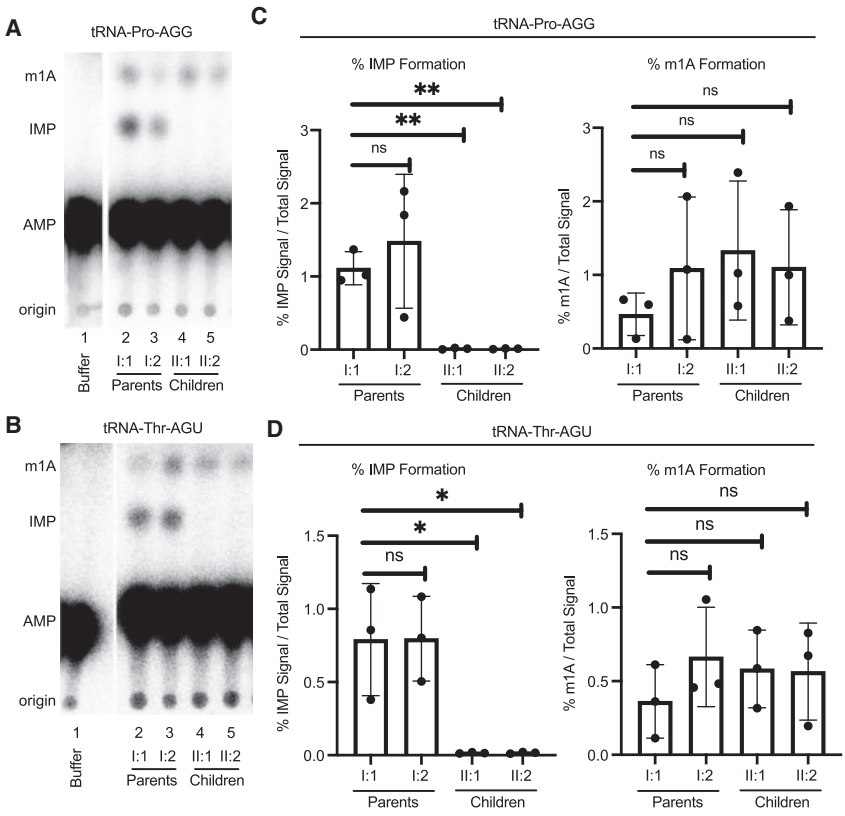

FIGURE 3. Individuals with the biallelic ADAT3 variants exhibit reduced adenosine deaminase activity. (*A*) Representative TLC plate of IMP formation after whole-cell extracts were incubated with in vitro transcribed tRNA-Pro-AGG. (*B*) Representative TLC plate of IMP formation after whole-cell extracts were incubated with in vitro transcribed tRNA-Thr-AGU. (*C*) Quantification of %IMP formation/total radioactive signal on tRNA-Proline-AGG. Unpaired *t*-test: ns = 0.53, (**) $P = 0.001$. Quantification of %m1A formation in the two samples harvested from the affected siblings indicate the extracts are active. Unpaired *t*-test: I:2 ns = 0.34, II:1 ns = 0.20, II:2 ns = 0.25. (*D*) Quantification of %IMP formation/total radioactive signal on tRNA-Threonine-AGU. Unpaired *t*-test: ns = 0.98, (*) $P = 0.024$. The formation of m1A in the two samples harvested from the affected siblings indicate the extracts are active. Unpaired *t*-test: I:2 ns = 0.28, II:1 ns = 0.35, II:2 ns = 0.44. Each point is one biological replicate. Three biological replicates were performed. The column on the graph represents the mean and the error bar represents the standard deviation of the three replicates.

ADAT3. Moreover, the Q274* variant would truncate nearly half the entire deaminase domain. Previous studies have shown that bacterial TadA forms a homodimer through an interface within the deaminase domain that includes the A196 residue (Kim et al. 2006). The ADAT2 subunit is predicted to heterodimerize with ADAT3 to form an active adenosine deaminase complex using a similar interaction as the bacterial TadA dimer (Elias and Huang 2005; Spears et al. 2011). Thus, we investigated whether the compound ADAT3 variants impact heterodimerization with the ADAT2 subunit. To assay subunit interactions, we expressed ADAT3 variants fused to a Twin-Strep Tag along with His-tagged ADAT2 in 293T human embryonic cells (Fig. 4A, lanes 2 through 4). The Strep-tag allows for purification of proteins under native conditions using streptactin-conjugated resin, allowing for maintenance of protein–protein interactions (Schmidt et al. 2013). To accurately determine the amount of copurifying ADAT2 and ensure the signal was within the linear range of detection, we loaded increasing amounts of the purified ADAT2/3 complexes for quantification (Fig. 4A, lanes 6 through 14). Notably, we detected a reduced amount of ADAT2 that copurified with ADAT3–A196V than with ADAT3–WT (Fig. 4A, compare ADAT2 in lanes 6–8 to lanes 9–11). Quantification of the blots revealed a ~50% reduction in copurifying ADAT2 with ADAT3–A196V compared to ADAT3–WT (Fig. 4B). The ADAT3–Q274* variant exhibited greatly reduced copurification of His-ADAT2 (Fig. 4A, Q274*, lanes 12–14 and Fig. 4B). These results indicate that the A196V variant impairs the interaction of ADAT3 with ADAT2 while the truncation of the ADAT3 carboxyl terminus greatly diminishes interaction with ADAT2.

In addition to monitoring the interaction between ADAT2 and ADAT3, we also tested whether expression of the ADAT3 variants could cause dominant negative effects on ADAT2 levels or wobble inosine modification. The ADAT3 variants were overexpressed in 293T cells using the same procedure as above (Fig. 4C). Based upon three independent replicates of each transfection, we detected no major change in ADAT2 levels between cells transfected with vector alone versus the ADAT3 constructs (Fig. 4D). RT-PCR analysis of wobble inosine modification in tRNA-Val-AAC or Pro-AGG revealed no detectable increase in unmodified wobble adenosine in cells expressing ADAT3–WT, A196V, or Q274* compared to control cells (Fig. 4E). These results suggest that the newly identified ADAT3 variants do not act in a dominant negative fashion to affect ADAT2 protein levels or wobble inosine modification. The lack of a dominant negative effect is also consistent with the lack of unmodified wobble adenosine in cells isolated from either parent who express the variant allele.

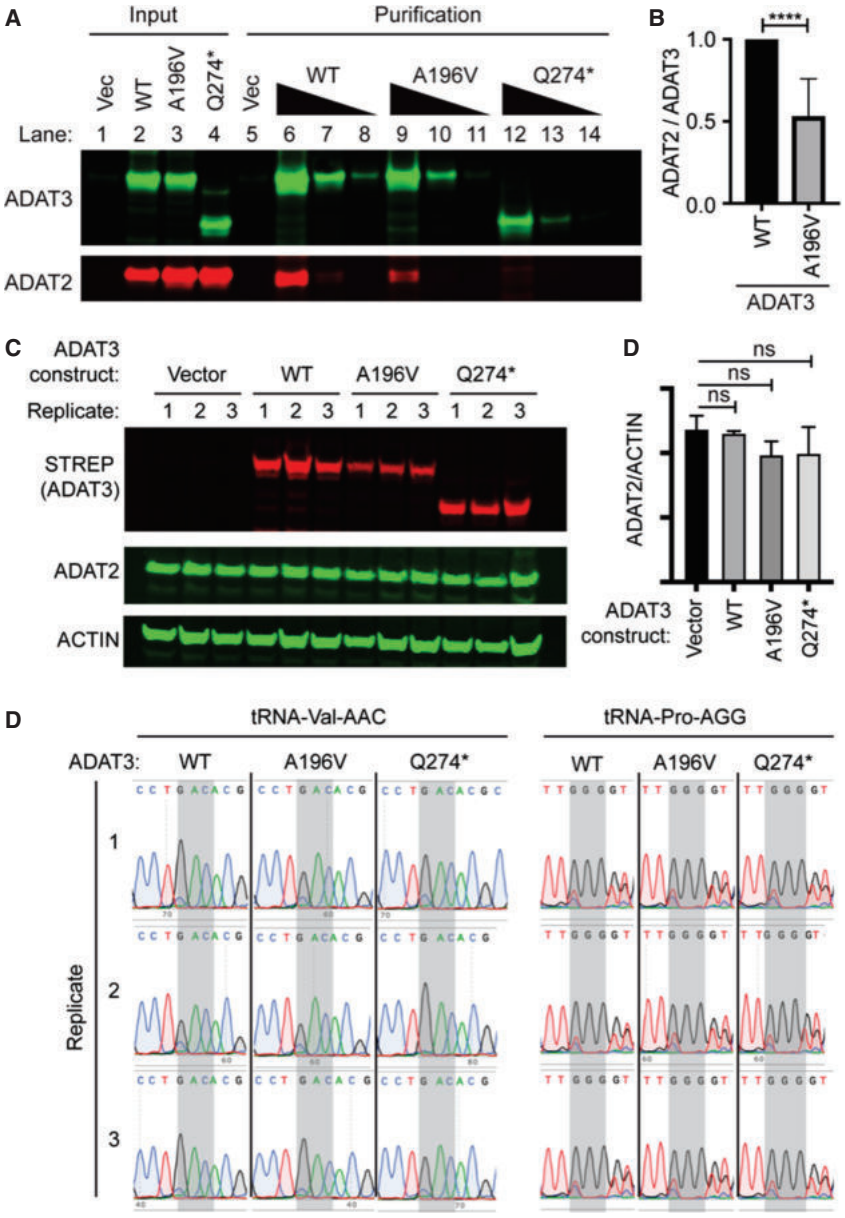

FIGURE 4. ADAT3 variants exhibit decreased ADAT2 interaction without detectable impact on endogenous ADAT2 expression or wobble inosine levels: (*A*) Representative ADAT3-Strep purifications with copurifying HIS-ADAT2. Input represents 5% of the starting extract while purifications represent threefold dilutions of the final eluted samples. (*B*) Quantification of ADAT3-STREP copurification. $N = 7$ purifications. Unpaired *t*-test (****) $P = <0.0001$. (*C*) Immunoblot of cellular extracts from 293T cells transfected with the indicated constructs in triplicate and probed against the STREP tag for ADAT3 expression, ADAT2, and ACTIN. (*D*) Quantification of ADAT2 signal relative to ACTIN signal. (*E*) RT-PCR sequencing chromatograms of tRNA-Val-AAC and tRNA-Pro-AGG harvested from cells transfected with the indicated constructs in triplicate.

ADAT3–A196V and Q274* exhibit alterations in subcellular localization

The interaction of ADAT2 with ADAT3 is required for translocation of ADAT3 into the nucleus (Torres et al. 2015). Since the newly identified ADAT3 variants in this study exhibit weakened or disrupted interaction with ADAT2, we investigated whether the ADAT3 variants also exhibited perturbations in subcellular localization. We used green fluorescent protein (GFP) tagging to visualize ADAT3 localization due to the low levels of endogenous ADAT3, which precludes accurate determination of cellular localization by microscopy (data not shown). We fused the ADAT3–WT, A196V, and Q274* variants to an amino-terminal GFP tag which were expressed in HeLa human cervical cells by transient transfection. We then monitored and binned GFP–ADAT3 localization into three categories: primarily cytoplasmic, ubiquitous distribution between the cytoplasm and nucleus, or primarily nuclear (see Materials and Methods for quantification parameters).

After transient transfection with the ADAT3–WT plasmid, we found that the majority of HeLa cells exhibited cytoplasmic distribution of GFP–ADAT3–WT (Fig. 5A, quantified in 5B, column 1). Similarly, the majority of cells expressing either GFP–ADAT3–A196V or the Q274* variants exhibited primarily cytoplasmic GFP signal (Fig. 5A, quantified in 4B, columns 2 and 3). As shown previously (Torres et al. 2015; Ramos et al. 2019), coexpression of ADAT2 with GFP–ADAT3–WT promotes the translocation of ADAT3 into the nucleus resulting in the majority of cells displaying GFP–ADAT3 localization in the nucleus compared to GFP–ADAT3 expression without ADAT2 (Fig. 5A,B, compare column 1 to column 4). ADAT2 coexpression could also promote the partial localization of GFP–ADAT3–A196V into the nucleus as noted by the increase in percentage of cells with ubiquitous or nuclear GFP localization (Fig. 5A,B, compare columns 2 and 5). However, in contrast to GFP–ADAT3–WT, the majority of cells expressing GFP–ADAT3–A196V with ADAT2 exhibited a ubiquitous distribution rather than being primarily nuclear (Fig. 5A,B, compare columns 4 and 5). The GFP–ADAT3–Q274* variant remained

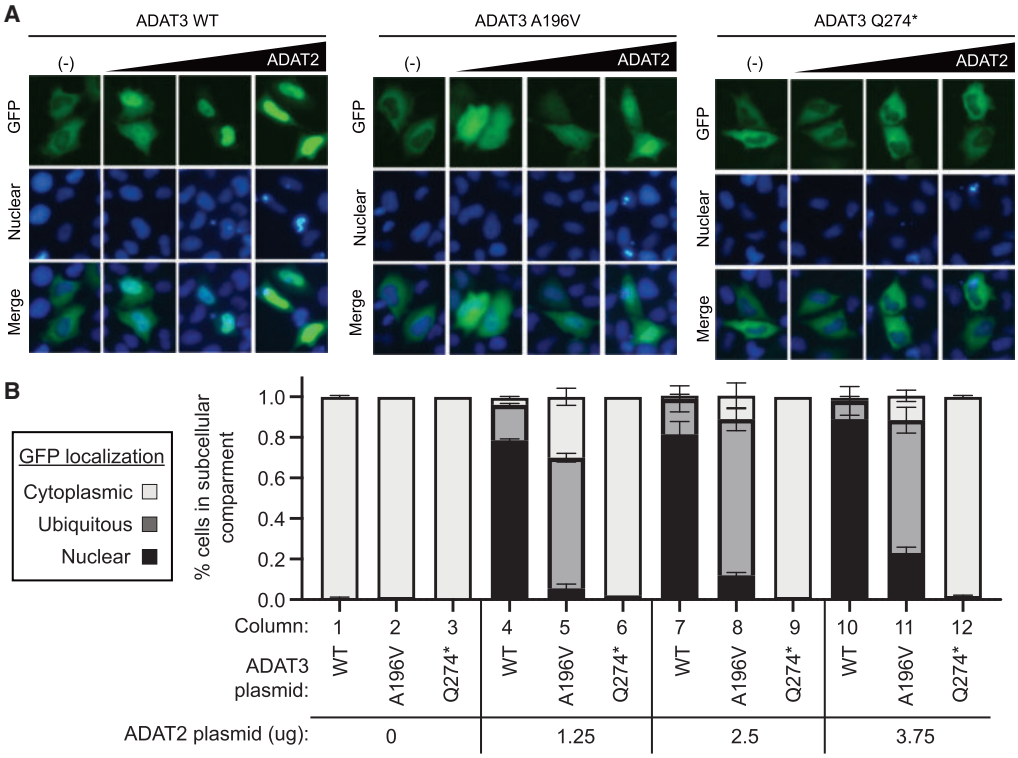

FIGURE 5. ADAT3 variants exhibit perturbations in ADAT2-dependent subcellular localization which can be rescued through overexpression of ADAT2. (*A*) Localization of GFP–ADAT3–WT and variants, without and with coexpression of ADAT2 in HeLa human cells. (*B*) Quantification of ADAT3–WT and ADAT3–A196V without or with coexpression of ADAT2. Localization was binned into three groups, primarily cytoplasmic, ubiquitous, and primarily nuclear. The amount of ADAT2 plasmid that was cotransfected with ADAT3 plasmid is indicated. Error bars represent standard deviation.

primarily in the cytoplasm without or with ADAT2 coexpression (Fig. 5A,B, compare columns 3 and 6). The decreased nuclear localization of ADAT3–A196V and ADAT3–Q274* in the presence of ADAT2 is consistent with the reduced interaction between ADAT3–A196V with ADAT2 and the near lack of interaction between ADAT3–Q274* with ADAT2 as shown above (Fig. 4A). Moreover, these results suggest that the reduced inosine modification in patients with the compound ADAT3 variants could be due to perturbations in enzymatic activity as well as subcellular localization caused by defects in ADAT2 interaction.

Since ADAT2 is limiting for formation of the ADAT2/3 heterodimer and subsequent nuclear translocation, we hypothesized that overexpression of ADAT2 could potentially rescue the localization defect of the ADAT3–A196V variant caused by its reduced interaction with ADAT2. To test this hypothesis, we performed transient transfection of GFP–ADAT3–WT and the GFP–ADAT3 variants along with increasing amounts of plasmid expressing ADAT2. Increasing the amount of ADAT2 plasmid that was cotransfected with ADAT3–WT had no major change in the percentage of cells with nuclear localization, suggesting that the lowest amount of ADAT2 plasmid resulted in the stoichiometric expression of ADAT2 with ADAT3–WT (Fig. 5B, compare column 4 to columns 7 and 10). As noted above, only ∼5% of cells transfected with GFP–ADAT3–A196V and the lowest amount of ADAT2 plasmid exhibited nuclear localization of ADAT3 (Fig. 5B, column 5). Intriguingly, increasing the amount of ADAT2 expression was sufficient to elevate the percentage of cells with primarily nuclear localization of GFP–ADAT3–A196V to ∼23%, and shifted the remaining cytoplasmic portion from 30% to 12% (Fig. 5B, compare column 5 to columns 8 and 11). In contrast, increasing the amount of ADAT2 expression had no effect on ADAT3–Q274* localization (Fig. 5B, compare column 6 to columns 9 and 12). These results suggest that increasing the cellular concentration of ADAT2 can promote interaction with ADAT3–A196V to induce increased nuclear translocation of ADAT3 while ADAT3–Q274* is completely abrogated in interaction with ADAT2.

ADAT2 overexpression in patient fibroblasts restores tRNA adenosine deaminase activity and wobble inosine modification

The heterodimeric ADAT2/3 complex has been shown to catalyze inosine formation on nuclear pre-tRNAs,

consistent with the localization of the ADAT2/3 complex in the nucleus (Torres et al. 2015). The rescue of ADAT3–A196V nuclear localization via increased expression of ADAT2 suggests that overexpression of ADAT2 could promote the association between ADAT3–A196V and ADAT2 to increase the levels of ADAT2/3 complexes in the nucleus. Encouraged by the above results, we tested whether overexpression of ADAT2 in patient fibroblasts is sufficient to restore wild-type levels of enzymatic activity and consequently, wobble inosine modification.

For stable recombinant protein expression in fibroblasts, we generated lentiviral expression constructs expressing either GFP as a negative control or untagged ADAT2 (Fig. 6A). After stable integration of the vectors into parental or patient fibroblasts, we monitored protein expression via immunoblot (Fig. 6B). Using this system, recombinant ADAT2 was overexpressed by 5 to 10 times above endogenous levels of ADAT2 in the stable fibroblast cell lines compared to control cell lines expressing only GFP (Fig. 6C).

We next determined whether overexpression of ADAT2 could impact the levels of adenosine deaminase activity in cellular extracts. Using the in vitro adenosine deaminase activity assay described above, we monitored IMP formation with tRNA-Pro-AGG and tRNA-Thr-AGU, using whole-cell extracts overexpressing either GFP or ADAT2. As observed above, the fibroblasts harvested from the parental cell lines exhibited both IMP and m1A formation while fibroblasts from the individuals with the biallelic ADAT3 variants displayed no detectable IMP formation at the amount of extract used in the assay (Fig. 6D,E, compare lanes 1 and 2 to lanes 3 and 4). In contrast, extracts prepared from patient fibroblasts overexpressing ADAT2 exhibited readily detectable adenosine deaminase on either tRNA-Pro-AGG or tRNA-Thr-AGU (Fig. 6D,E, compare lanes 3 and 4 to lanes 7 and 8). While the level of adenosine deaminase activity in the patient fibroblasts overexpressing ADAT2 was still reduced relative to extracts prepared from the parental fibroblasts, there was significantly higher activity compared to the control patient fibroblasts expressing just GFP alone (Fig. 6F,G). These results indicate that overexpression of ADAT2 is sufficient to restore adenosine

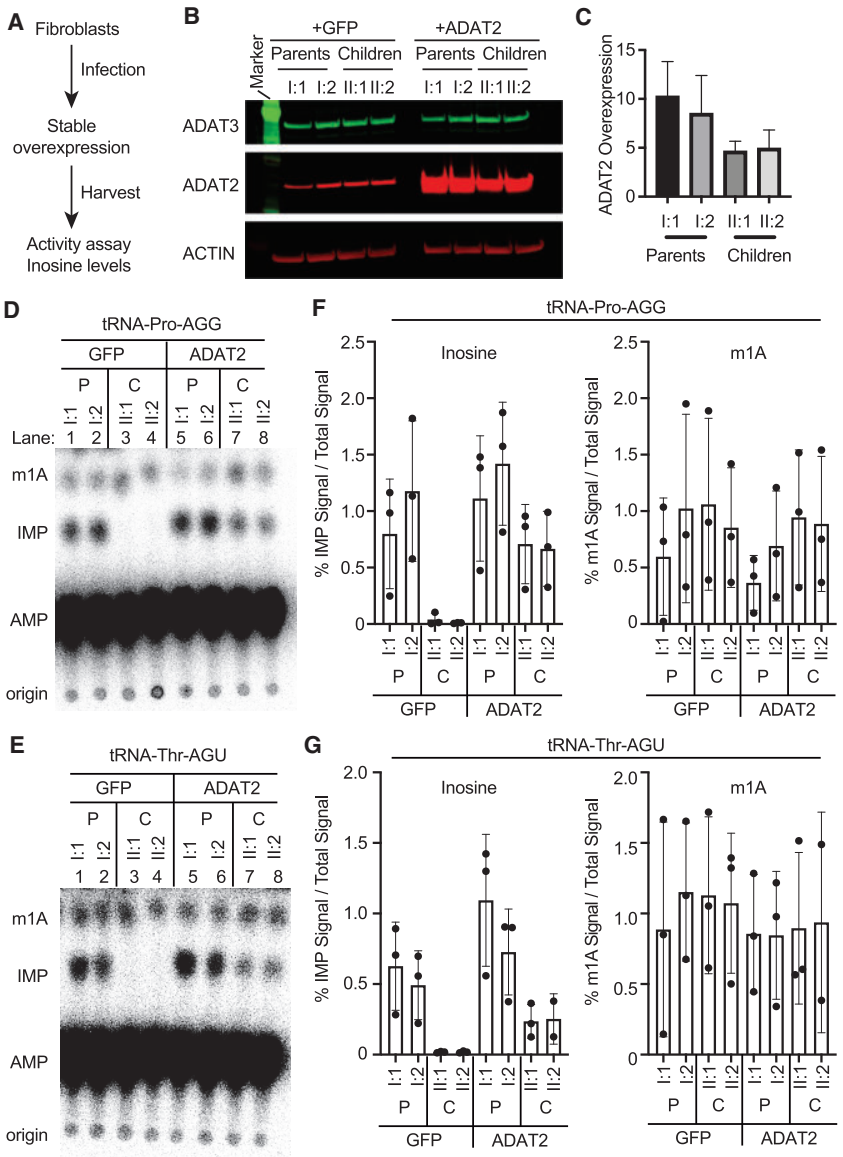

FIGURE 6. Overexpression of ADAT2 restores adenosine deaminase activity in fibroblasts harboring biallelic ADAT3 variants. (*A*) ADAT2 overexpression strategy using lentiviral infection of human fibroblast cell lines. (*B*) Immunoblot of the indicated fibroblast cell lines infected with either control virus expressing GFP or untagged ADAT2. (*C*) Quantification of ADAT2 overexpression. $N = 3$. Error bar represents standard deviation. (*D*) TLC plate of IMP formation after whole-cell extracts were incubated with internally radiolabeled in vitro transcribed tRNA-Pro-AGG. (*E*) TLC plate of IMP formation after whole-cell extracts were incubated with internally radiolabeled in vitro transcribed tRNA-Thr-AGU. (*F,G*) Quantification of IMP product formation in tRNA-Pro-AGG and tRNA-Thr-AGU. The first graph is IMP formation over total radioactive signal. The *right* graphs are m1A formation over total radioactive signal. Each point is one biological replicate. Three biological replicates were performed. The bar on the graph represents the mean and the error bar represents the standard deviation of the three replicates.

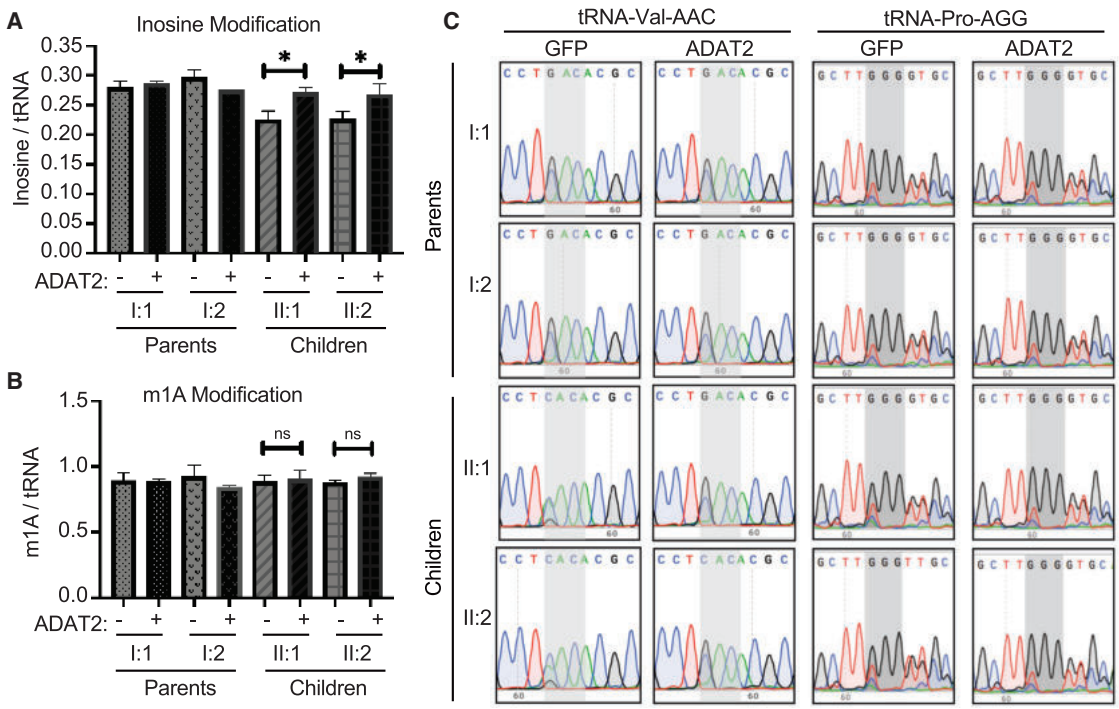

FIGURE 7. Overexpression of the ADAT2 subunit can rescue wobble inosine modification in patient fibroblasts from individuals harboring biallelic ADAT3 variants. (*A*) LC-MS analysis of digested nucleosides from small RNAs of the indicated fibroblast cell lines. Inosine and m1A levels per tRNA molecule were calculated. Unpaired *t*-test II:1 (*) $P = 0.01$, II:2 (*) $P = 0.03$. (*B*) m1A modification does not change with overexpression of ADAT2. Unpaired *t*-test II:1 ns = 0.7, II:2 ns = 0.1. (*C*) Sequencing of substrates tRNA-Val-AAC and tRNA-Pro-AGG. Gray shading highlights anticodon. +GFP are fibroblasts overexpressing GFP and +ADAT2 are fibroblasts overexpressing ADAT2. In fibroblast cells expressing GFP, inosine is reduced on the children, as seen by increased green peak over black peak. Fibroblasts overexpressing ADAT2 restore inosine formation on these two substrates, as seen by lack of green peak in II:1 and II:2 +ADAT2.

deaminase activity in patient fibroblasts harboring the compound heterozygous ADAT3 variants.

The restoration of adenosine deaminase activity in patient fibroblasts via ADAT2 overexpression suggests the possibility that inosine modification levels could also be rescued. To compare wobble inosine modification levels, we performed LC-MS on nucleosides from digested small RNAs extracted from the fibroblast cells overexpressing GFP or ADAT2. Quantification of inosine showed a significant restoration of inosine in the patient cells overexpressing ADAT2 (Fig. 7A, compare II:1 and II:2 without or with overexpression of ADAT2). In contrast, ADAT2 overexpression had no significant effect on m1A levels in any of the cell lines (Fig. 7B). As further validation for rescue of wobble inosine modification in patient fibroblasts, we monitored wobble inosine formation using RT-PCR sequencing of tRNA-Val-AAC and Pro-AGG. In parental fibroblasts expressing GFP alone, we detected a predominant G peak for the inosine modification at the wobble position of tRNA-Val-AAC and Pro-AGG that was not detectably altered by ADAT2 overexpression (Fig. 7C, Parents I:1 and I:2). In contrast, the patient cells containing the biallelic ADAT3 variants infected with GFP alone exhibited reduced inosine in tRNA-Val-AAC and Pro-AGG as detected by the predominant A peak (Fig. 7C, GFP, Children II:1 and II:2). Strikingly, overexpression of ADAT2 in the patient fibroblasts resulted in the restoration of wobble inosine in both tRNA-Val-AAC and tRNA-Pro-AGG (Fig. 7C, ADAT2, II:1 and II:2, children). These results demonstrate the potential to rescue the essential inosine modification in patient cells with ADAT3 variants through the overexpression of the ADAT2 heterodimeric binding partner.

DISCUSSION

In this study, we identify and characterize novel compound heterozygous variants in *ADAT3* that underscore the key role of wobble inosine modification in proper neurodevelopment. Three affected siblings carry a paternally inherited missense variant (c.587C > T; p.[Ala196Val]) and a maternally inherited truncated variant (c.820C > T; p.[Gln274*]). The three siblings in our study share many of the features previously described for *ADAT3* deficiency (Supplemental Table 1). In addition to ID, other commonly reported features include hypotonia, short stature, feeding difficulties, strabismus and microcephaly. In almost all cases absent or limited speech and motor delay were also

described. Microcephaly has also been identified in a subset of previously described cases associated with ADAT3 variants and was only observed in the youngest sister of this family, consistent with this sporadic occurrence.

All characterized patient cells with either the previously described ADAT3–V144M variant or the compound heterozygous variants exhibit reduced wobble-inosine tRNA modification. This observation supports the idea that reduced wobble inosine may be the major underlying cause of ID in patients with pathogenic *ADAT3* variants. Considering the essential requirement for wobble inosine modification for decoding of certain codons, it is not surprising that reduced inosine modification could have severe impact on neurodevelopment. Interestingly, a recent study has found that human embryonic stem cells optimize translation of codons that are dependent upon tRNAs containing the wobble inosine modifications (Bornelov et al. 2019). Moreover, the study found that inosine levels are highest in human pluripotent embryonic stem cells before differentiation. Future studies using ribosome profiling of patient cells would yield further insight into the mRNAs and the developmental pathways that are impacted by reduced wobble inosine modification.

The A196V and Q274* variants we report here differ from the previously characterized V144M variant in that the amino acid residue alterations lie within the conserved adenosine deaminase domain. The molecular and cellular phenotypes of the ADAT3 variants described in this study also differ from the biochemical defects observed with the previously described ADAT3–V144M variant. In that case, the V144M substitution alters ADAT3 protein folding without any detectable change in ADAT2 interaction or ADAT2-dependent nuclear localization (Ramos et al. 2019). In contrast, we found here that ADAT3–A196V and Q274* exhibit decreased or severely reduced interaction with ADAT2 and perturbations in ADAT2-dependent nuclear localization. While alanine and valine are both hydrophobic, the additional two methyl groups in valine could clash with residues in ADAT2 along the interaction interface. Thus, the alanine-to-valine substitution could alter the proper folding of the ADAT3 interaction interface with ADAT2. In turn, the reduced ADAT2 interaction would result in a decreased population of ADAT3 which is shuttled into the nucleus to catalyze inosine modification in pre-tRNAs destined for the cytoplasm.

Notably, we could suppress the nuclear localization defect exhibited by the ADAT3–A196V variant by increasing the expression of ADAT2. Interestingly, a previous study has identified a point mutation in the fission yeast *Schizosaccharomyces pombe* (*S. pombe*) homolog of ADAT3, Tad3p, which also impairs interaction with the ADAT2 homolog, Tad2p (Tsutsumi et al. 2007). Like the ADAT3–A196V variant described here, the Tad3p point mutation converts serine 275 in Tad3p to asparagine (S275N) in the adenosine deaminase domain. Similar to our findings, *S. pombe* cells expressing only Tad3-S275N exhibit reduced wobble inosine modification that can be rescued by Tad2p overexpression. The rescue of wobble inosine modification levels in *S. pombe* and in human cells presented here could be due to increased ADAT2 concentrations which shifts the equilibrium toward formation of the heterodimer.

Intellectual disability represents a neurodevelopmental disorder characterized by early onset cognitive impairments and limitations in adaptive behavior that can be caused by environmental or genetic factors (Patel et al. 2018; Bhaumik and Alexander 2020). In addition to ADAT3, whole exome sequencing has identified numerous variants in tRNA modification enzymes as the cause of neurodevelopmental disorders such as ID (Torres et al. 2014; Pereira et al. 2018; Ramos and Fu 2019). These studies highlight the emerging role of tRNA modification in proper gene expression and brain development (Angelova et al. 2018; Tuorto and Parlato 2019).

The findings presented here suggest a potential therapeutic strategy for ADAT3-associated intellectual disability disorders based on the overexpression of ADAT2 to rescue inosine tRNA modifications. Similarly, coexpression of ADAT2 to stoichiometric levels reduced the misfolding properties of the previously characterized ADAT3–V144M variant associated with ID (Ramos et al. 2019). However, many challenges and questions remain before this presents a viable option for therapy. For example, it remains unknown where and when wobble inosine modification is required for proper neurodevelopment. Based upon the increased dependency of stem cells on inosine modification, the requirement for proper wobble inosine modification levels could be very early in development or differentiation (Bornelov et al. 2019). Moreover, the requirement for the wobble inosine modification to decode a subset of codons suggests that certain proteins could be more significantly impacted by reduced wobble inosine levels in humans. However, it is unknown which mRNA transcripts are dependent upon wobble inosine for proper translation in human cells and whether ADAT2 overexpression is sufficient to rescue perturbations in translation. Finally, the overexpression of ADAT2 could cause nonspecific deamination of additional RNA substrates leading to off-target effects. Despite these hurdles, our studies provide the first insight into a potential strategy for modulating inosine levels in cells harboring ADAT3 variants.

MATERIALS AND METHODS

Cell lines

Human primary epithelial skin fibroblasts were cultured in Eagle's Minimum Essential Media (EMEM) (ATCC) containing 15% fetal bovine serum and 1% Penicillin/Streptomycin. Cells were grown at 37°C, 5% Oxygen, and 5% CO_2. HeLa S3 human cervical

carcinoma and 293T human embryonic kidney cell lines were cultured in Dulbecco's Minimal Essential Medium (DMEM) containing 10% fetal bovine serum, 2 mM L-alanyl-L-glutamine (GlutaMax, Gibco) and 1% Penicillin/Streptomycin. Cells were grown at 37°C, 20% Oxygen, and 5% CO_2.

Sequencing of tRNAs

Sequencing of tRNAs was performed identically to Ramos et al. (2019). RNA extraction was performed on 1×10^6 human fibroblast cell lines using TRIzol LS reagent (Thermo Fisher). For RT-PCR, total RNA (~1.25 µg) was reverse transcribed for tRNA-Val-AAC and Pro-AGG using Superscript IV enzyme followed by the QIAquick PCR purification kit. cDNA was then PCR amplified using Herculase II DNA polymerase (Agilent Genomics). The PCR product was gel extracted and analyzed by Sanger sequencing (ACGT, Inc). The following primers were used:

Val RT primer: TGTTTCCGCCTGGTTTTG

Val PCR primer F: GAACTAAGCTTGTTCAGAGTTCTACAG TCCGGACTACAAAGACCATGACGGTGATTATAAAGATCAT GACATGTTTCCGTAGTGTAGTGGTTATCAC

Val PCR primer R: CACT TGTTTCCGCCTGGTTTTGATCCA GGGACC

Pro RT primer: GGGCTCGTCCGGGATTT

Pro PCR primer F: GTTCAGAGTTCTACAGTCCGGACTAC AAAGACCATGACGGTGATTATAAAGATCATGACATGGCTC GTTGGTCTAGGGGTA

Pro PCR primer R: GGGCTCGTCCGGGATTT

Mass spectrometry of nucleosides

In the first step, the total RNA was fractionated on an AdvanceBio SEC column (300 A pore size, 2.7 µm particle size, 7.8 by 300 mm; Agilent) at 40°C using isocratic elution with 0.1 M NH4OAc buffer at pH 7 to separate the total tRNA fraction from larger RNA species. The tRNA was collected in 1 mL and lyophilized in the SpeedVac, until 50 µL remained in the vial. By adding 5 µL ammonium acetate (5 M) and 125 µL ice-cold and pure ethanol (100%), the tRNA was incubated overnight and precipitated by centrifugation (12,000*g*, 4°C, 30 min.). The tRNA pellets were resolved in 30 µL MilliQ water and their concentrations were measured using an IMPLEN nano-photometer (Implen). A maximum of 500 ng tRNA was processed and analyzed by LC-MS using an MRM method as previously described (Heiss et al. 2017; Ramos et al. 2019). The level of each modified nucleoside (I, m1A) was normalized to an average tRNA. The amount of injected tRNA was calculated by the detected amount of C in pmol and the average content of C in an average tRNA.

Transient transfection

Transient transfection and cellular extract production were performed as previously described (Dewe et al. 2017). In brief, 2.5 $\times 10^6$ 293T HEK cells were transiently transfected by calcium phosphate DNA precipitation with 10–20 µg of plasmid DNA followed by preparation of lysate by hypotonic freeze-thaw lysis 48 h post-transfection. For purification, whole cell extract from transiently transfected cells cell lines (1 mg of total protein) was rotated for 2 h at 4°C in lysis buffer (20 mM HEPES at pH 7.9, 2 mM $MgCl_2$, 0.2 mM EGTA, 10% glycerol, 1 mM DTT, 0.1 mM PMSF, 0.1% NP-40) with 200 mM NaCl. Resin was washed three times using the same buffer followed by protein analysis. Strep-tagged proteins were purified using MagSTREP "type3" XT beads, 5% suspension (IBA Lifesciences) and eluted with desthiobiotin.

Western blotting

Western blots were performed as previously described (Ramos et al. 2019). Briefly, cellular extracts and purified protein samples were fractionated on NuPAGE Bis-Tris polyacrylamide gels (Thermo Scientific) followed by transfer to Immobilon FL PVDF membrane (Millipore) for immunoblotting. For analysis of skin fibroblasts, 1×10^6 cells were harvested and proteins were extracted using radioisotope immunoprecipitation assay (RIPA) buffer (50 mM TrisHCl, pH 7.5, 1% NP-40, 0.5% sodium deoxycholate, 0.1% SDS, 150 mM NaCl, 2 mM EDTA). Antibodies were against the following proteins : 6xHis tag (MA1-21315, Thermo Fisher), GFP (sc-9996, Santa Cruz Biotechnology), Strep-tag II-tag (NC9261069, Thermo Fisher), ADAT3 (Abcam, ab192987), ADAT3 (H00113179-B01P, Abnova), ADAT2 (ab135429, Abcam), and actin (CST). Primary antibodies were detected using IRDye 800CW Goat anti-Mouse IgG (SA5-35521, Thermofisher) or Rabbit (SA5-35571, Thermofisher) or Rat (925-32219, LI-COR Biosciences), or IRDye 680RD Goat anti-Mouse IgG (926-68070, LI-COR Biosciences) or Rabbit (925-68071). Immunoblots were scanned using direct infrared fluorescence via the Odyssey System (LI-COR Biosciences).

Overexpression of ADAT2

The open reading frame of ADAT2 was PCR amplified with restriction overhangs and cloned into PLJM vector (Addgene: 19219). The vector was then cotransfected with packaging plasmids (psPAX2 and pMD2.G) into 293T cells for lentivirus production. The fibroblast cell lines were subsequently infected with the lentivirus in the presence of polybrene followed by stable clone selection using 100 µg/mL puromycin

Enzymatic assays

Enzymatic assays were performed as previously described (Ramos et al. 2019). Internally radiolabeled tRNA substrates were prepared by T7 in vitro transcription of DNA templates generated by PCR amplification. Oligonucleotides containing the T7 promoter upstream of tRNA sequences were PCR amplified using Herculase II DNA polymerase or Taq DNA Polymerase (New England Biolabs) followed by agarose gel purification of PCR amplification products. In vitro transcription was performed using Optizyme T7 RNA polymerase (Fisher Scientific) with 10 mM each of UTP, CTP, and GTP, 1 mM of ATP, and 250 µCi of [α-^{32}P]-ATP (3000 Ci/mmol, 10 mCi/ml). In vitro transcription reactions were incubated at 37°C for 2 h followed by DNase treatment and purification using RNA Clean and Concentrator columns (Zymo Research). Full-length tRNA transcripts were verified on a 15% Polyacrylamide-urea gel stained with SYBR Gold nucleic

acid stain (Thermo Fisher). Before conducting enzymatic assays, all tRNA substrates were refolded by thermal denaturation at 95°C for 2 min in buffer containing a final concentration 5 mM TRIS pH 7.5 and 0.16 mM EDTA, quick chilling on ice for 2 min and refolding at 37°C in the presence of Hepes pH 7.5, $MgCl_2$, and NaCl.

For adenosine deaminase assays, ~150 ng of refolded tRNA substrate was incubated with either skin fibroblast extract or Strep-purified ADAT3. Reactions were incubated at 37°C for 30min—1 h and RNA was purified using RNA Clean and Concentrator columns. The tRNA was eluted in 10 µL of water and was subjected to nuclease P1 digestion overnight in total volume of 13 µL and 0.125 units of P1 in 250 mM Ammonium Acetate pH 5.35. Half of the P1-nuclease treated samples were spotted on POLYGRAM polyester Cellulose MN 300 plates (Macherey Nagel) run in solvent B (0.1 M sodium phosphate buffer pH 6.8:NH_4 sulfate:n-propanol (100:60:2 [v:w:v]). Phosphorimaging was conducted on a Bio-Rad Personal Molecular Imager followed by analysis using NIH ImageJ software.

Microscopy

Procedure was previously described (Ramos et al. 2019). Hela cells were plated at 2.5×10^5 cells on a six-well plate. Cells were transfected 1 d after plating with a 1.25–5 µg of DNA using Lipofectamine 3000. Cells were imaged 24 h post-transfection on an EVOS fluorescence microscopy imaging system (ThermoFisher) quantification. For DNA staining, cells were washed twice with PBS and then incubated for 30 min at 37°C with PBS containing 10% FBS and 1 µM of Hoechst and then imaged. For localization quantification, five images were taken of each well and the number of GFP-positive cells were counted in each of the five frames.

Ethics statement and approvals

Ethical approval for whole-exome sequencing (WES) was received from the Uppsala Ethical Review Board and informed written consent was obtained from the parents.

Whole-exome sequencing

Exome enrichment was performed using SureSelect (Agilent) version 4 following the manufacturer's protocol and samples were sequenced on Illumina HiSeq Sequencer. The sequencing was performed to achieve at least 30× coverage of the captured regions.

Sequence reads were mapped to human reference genome Hg19 as previously described (Halvardson et al. 2016). Analysis of the data was performed to identify disease-causing variants under recessive and de novo dominant models. Identified variants were verified by Sanger sequencing using standard protocols, and subsequently classified according to the American College of Medical Genetics and Genomics (ACMG) guidelines (Richards et al. 2015). Patients' data have been submitted to DECIPHER. (https://decipher.sanger.ac.uk/).

SUPPLEMENTAL MATERIAL

Supplemental material is available for this article.

ACKNOWLEDGMENTS

We are grateful to the participating family for their cooperation. Sequencing was performed using the SciLifeLab National Genomics Infrastructure at Uppsala Genome Center and the Uppsala SNP & Seq Facility. Computational analyses were performed on resources provided by SNIC through Uppsala Multidisciplinary Center for Advanced Computational Science (UPPMAX). We thank members of the Fu laboratory for helpful discussions on the manuscript. This work was supported by National Science Foundation CAREER award 1552126 to D.F. and the Sävstaholm Society to ACT. The funders had no role in study design, data collection and analysis, decision to publish, or preparation of the manuscript.

Author contributions: J.R., M.P., J.H., F.H., E.K., B.P., R.B., S.M.K., L.F., and A.T. collected the data. J.R., L.F., A.T., and D.F wrote the manuscript. J.R., L.F., A.T., and D.F. contributed to experimental design.

Received May 13, 2020; accepted July 20, 2020.

REFERENCES

Alazami AM, Hijazi H, Al-Dosari MS, Shaheen R, Hashem A, Aldahmesh MA, Mohamed JY, Kentab A, Salih MA, Awaji A, et al. 2013. Mutation in ADAT3, encoding adenosine deaminase acting on transfer RNA, causes intellectual disability and strabismus. *J Med Genet* **50:** 425–430. doi:10.1136/jmedgenet-2012-101378

Angelova MT, Dimitrova DG, Dinges N, Lence T, Worpenberg L, Carre C, Roignant JY. 2018. The emerging field of epitranscriptomics in neurodevelopmental and neuronal disorders. *Front Bioeng Biotechnol* **6:** 46. doi:10.3389/fbioe.2018.00046

Bhaumik S, Alexander R. 2020. *Oxford textbook of the psychiatry of intellectual disability*. Oxford University Press.

Bornelov S, Selmi T, Flad S, Dietmann S, Frye M. 2019. Codon usage optimization in pluripotent embryonic stem cells. *Genome Biol* **20:** 119. doi:10.1186/s13059-019-1726-z

Dewe JM, Fuller BL, Lentini JM, Kellner SM, Fu D. 2017. TRMT1-catalyzed tRNA modifications are required for redox homeostasis to ensure proper cellular proliferation and oxidative stress survival. *Mol Cell Biol* **37:** e00214-17. doi:10.1128/MCB.00214-17

El-Hattab AW, Saleh MA, Hashem A, Al-Owain M, Asmari AA, Rabei H, Abdelraouf H, Hashem M, Alazami AM, Patel N, et al. 2016. ADAT3-related intellectual disability: further delineation of the phenotype. *Am J Med Genet A* **170A:** 1142–1147. doi:10.1002/ajmg.a.37578

Elias Y, Huang RH. 2005. Biochemical and structural studies of A-to-I editing by tRNA:A34 deaminases at the wobble position of transfer RNA. *Biochemistry* **44:** 12057–12065. doi:10.1021/bi050499f

Gerber AP, Keller W. 1999. An adenosine deaminase that generates inosine at the wobble position of tRNAs. *Science* **286:** 1146–1149. doi:10.1126/science.286.5442.1146

Grosjean H, Keith G, Droogmans L. 2004. Detection and quantification of modified nucleotides in RNA using thin-layer chromatography. *Methods Mol Biol* **265:** 357–391. doi:10.1385/1-59259-775-0:357

Guy MP, Phizicky EM. 2014. Two-subunit enzymes involved in eukaryotic post-transcriptional tRNA modification. *RNA Biol* **11:** 1608–1618. doi:10.1080/15476286.2015.1008360

Halvardson J, Zhao JJ, Zaghlool A, Wentzel C, Georgii-Hemming P, Mansson E, Ederth Savmarker H, Brandberg G, Soussi Zander C, Thuresson AC, et al. 2016. Mutations in HECW2 are associated with intellectual disability and epilepsy. *J Med Genet* **53:** 697–704. doi:10.1136/jmedgenet-2016-103814

Heiss M, Reichle VF, Kellner S. 2017. Observing the fate of tRNA and its modifications by nucleic acid isotope labeling mass spectrometry: NAIL-MS. *RNA Biol* **14:** 1260–1268. doi:10.1080/15476286.2017.1325063

Kawahara Y. 2012. Quantification of adenosine-to-inosine editing of microRNAs using a conventional method. *Nat Protoc* **7:** 1426–1437. doi:10.1038/nprot.2012.073

Kim J, Malashkevich V, Roday S, Lisbin M, Schramm VL, Almo SC. 2006. Structural and kinetic characterization of *Escherichia coli* TadA, the wobble-specific tRNA deaminase. *Biochemistry* **45:** 6407–6416. doi:10.1021/bi0522394

Motorin Y, Muller S, Behm-Ansmant I, Branlant C. 2007. Identification of modified residues in RNAs by reverse transcription-based methods. *Methods Enzymol* **425:** 21–53. doi:10.1016/S0076-6879(07)25002-5

Patel DR, Apple R, Kanungo S, Akkal A. 2018. Intellectual disability: definitions, evaluation and principles of treatment. *Pediatric Medicine* **1:** 11. doi:10.21037/pm.2018.12.02

Pereira M, Francisco S, Varanda AS, Santos M, Santos MAS, Soares AR. 2018. Impact of tRNA modifications and tRNA-modifying enzymes on proteostasis and human disease. *Int J Mol Sci* **19:** 3738. doi:10.3390/ijms19123738

Rafels-Ybern A, Attolini CS, Ribas de Pouplana L. 2015. Distribution of ADAT-dependent codons in the human transcriptome. *Int J Mol Sci* **16:** 17303–17314. doi:10.3390/ijms160817303

Rafels-Ybern A, Torres AG, Grau-Bove X, Ruiz-Trillo I, Ribas de Pouplana L. 2017. Codon adaptation to tRNAs with inosine modification at position 34 is widespread among Eukaryotes and present in two Bacterial phyla. *RNA Biol* **15:** 500–507. doi:10.1080/15476286.2017.1358348

Rafels-Ybern A, Torres AG, Camacho N, Herencia-Ropero A, Roura Frigole H, Wulff TF, Raboteg M, Bordons A, Grau-Bove X, Ruiz-Trillo I, et al. 2019. The expansion of inosine at the Wobble position of tRNAs, and its role in the evolution of proteomes. *Mol Biol Evol* **36:** 650–662. doi:10.1093/molbev/msy245

Ragone FL, Spears JL, Wohlgamuth-Benedum JM, Kreel N, Papavasiliou FN, Alfonzo JD. 2011. The C-terminal end of the *Trypanosoma brucei* editing deaminase plays a critical role in tRNA binding. *RNA* **17:** 1296–1306. doi:10.1261/rna.2748211

Ramos J, Fu D. 2019. The emerging impact of tRNA modifications in the brain and nervous system. *Biochim Biophys Acta Gene Regul Mech* **1862:** 412–428. doi:10.1016/j.bbagrm.2018.11.007

Ramos J, Han L, Li Y, Hagelskamp F, Kellner SM, Alkuraya FS, Phizicky EM, Fu D. 2019. Formation of tRNA Wobble inosine in humans is disrupted by a millennia-old mutation causing intellectual disability. *Mol Cell Biol* **39:** e00203-19. doi:10.1128/MCB.00203-19

Richards S, Aziz N, Bale S, Bick D, Das S, Gastier-Foster J, Grody WW, Hegde M, Lyon E, Spector E, et al. 2015. Standards and guidelines for the interpretation of sequence variants: a joint consensus recommendation of the American College of Medical Genetics and Genomics and the Association for Molecular Pathology. *Genet Med* **17:** 405–424. doi:10.1038/gim.2015.30

Salehi Chaleshtori AR, Miyake N, Ahmadvand M, Bashti O, Matsumoto N, Noruzinia M. 2018. A novel 8-bp duplication in ADAT3 causes mild intellectual disability. *Hum Genome Var* **5:** 7. doi:10.1038/s41439-018-0007-9

Schmidt TG, Batz L, Bonet L, Carl U, Holzapfel G, Kiem K, Matulewicz K, Niermeier D, Schuchardt I, Stanar K. 2013. Development of the Twin-Strep-tag(R) and its application for purification of recombinant proteins from cell culture supernatants. *Protein Expr Purif* **92:** 54–61. doi:10.1016/j.pep.2013.08.021

Sharkia R, Zalan A, Jabareen-Masri A, Zahalka H, Mahajnah M. 2019. A new case confirming and expanding the phenotype spectrum of ADAT3-related intellectual disability syndrome. *Eur J Med Genet* **62:** 103549. doi:10.1016/j.ejmg.2018.10.001

Spears JL, Rubio MA, Gaston KW, Wywial E, Strikoudis A, Bujnicki JM, Papavasiliou FN, Alfonzo JD. 2011. A single zinc ion is sufficient for an active *Trypanosoma brucei* tRNA editing deaminase. *J Biol Chem* **286:** 20366–20374. doi:10.1074/jbc.M111.243568

Thomas E, Lewis AM, Yang Y, Chanprasert S, Potocki L, Scott DA. 2019. Novel missense variants in ADAT3 as a cause of syndromic intellectual disability. *J Pediatr Genet* **8:** 244–251. doi:10.1055/s-0039-1693151

Torres AG, Batlle E, Ribas de Pouplana L. 2014. Role of tRNA modifications in human diseases. *Trends Mol Med* **20:** 306–314. doi:10.1016/j.molmed.2014.01.008

Torres AG, Pineyro D, Rodriguez-Escriba M, Camacho N, Reina O, Saint-Leger A, Filonava L, Batlle E, Ribas de Pouplana L. 2015. Inosine modifications in human tRNAs are incorporated at the precursor tRNA level. *Nucleic Acids Res* **43:** 5145–5157. doi:10.1093/nar/gkv277

Torres AG, Wulff TF, Rodriguez-Escriba M, Camacho N, Ribas de Pouplana L. 2018. Detection of inosine on transfer RNAs without a reverse transcription reaction. *Biochemistry* **57:** 5641–5647. doi:10.1021/acs.biochem.8b00718

Tsutsumi S, Sugiura R, Ma Y, Tokuoka H, Ohta K, Ohte R, Noma A, Suzuki T, Kuno T. 2007. Wobble inosine tRNA modification is essential to cell cycle progression in G(1)/S and G(2)/M transitions in fission yeast. *J Biol Chem* **282:** 33459–33465. doi:10.1074/jbc.M706869200

Tuorto F, Parlato R. 2019. rRNA and tRNA bridges to neuronal homeostasis in health and disease. *J Mol Biol* **431:** 1763–1779. doi:10.1016/j.jmb.2019.03.004

Unger FM, Takemura S. 1973. A comparison between inosine- and guanosine-containing anticodons in ribosome-free codon-anticodon binding. *Biochem Biophys Res Commun* **52:** 1141–1147. doi:10.1016/0006-291X(73)90619-0

Wolf J, Gerber AP, Keller W. 2002. tadA, an essential tRNA-specific adenosine deaminase from *Escherichia coli*. *EMBO J* **21:** 3841–3851. doi:10.1093/emboj/cdf362

Wulff TF, Arguello RJ, Molina Jordan M, Roura Frigole H, Hauquier G, Filonava L, Camacho N, Gatti E, Pierre P, Ribas de Pouplana L, et al. 2017. Detection of a subset of posttranscriptional transfer RNA modifications in vivo with a restriction fragment length polymorphism-based method. *Biochemistry* **56:** 4029–4038. doi:10.1021/acs.biochem.7b00324

Zhou W, Karcher D, Bock R. 2014. Identification of enzymes for adenosine-to-inosine editing and discovery of cytidine-to-uridine editing in nucleus-encoded transfer RNAs of *Arabidopsis*. *Plant Physiol* **166:** 1985–1997. doi:10.1104/pp.114.250498

Identification and rescue of a tRNA wobble inosine deficiency causing intellectual disability disorder

Jillian Ramos, Melissa Proven, Jonatan Halvardson, et al.

RNA 2020 26: 1654-1666 originally published online August 6, 2020
Access the most recent version at doi:10.1261/rna.076380.120

3.2 Oligonukleotid-MS als Methode zur Sequenzaufklärung von RNA

Gemeinsamer Prolog

Um den Inosingehalt in der tRNA nicht nur quantitativ per isotopenmarkierter Nukleosid-Massenspektrometrie zu bestimmen, sondern auch die genaue Position innerhalb der tRNA zu verifizieren, braucht es eine LC-MS/MS-Methode, die Oligonukleotide analysieren kann. Diese Methode sollte ionenpaarreagenzfrei sein, um eine breite Anwendung auf verschiedenen Massenspektrometern ohne Kontamination zu gewährleisten. Nach der erfolgreichen Etablierung der geeigneten Methode für Oligonukleotide von bis zu einer Länge von 10-meren, die z.B. durch einen Endonukleaseverdau mit RNase T1 entstehen, wurde *in vitro* transkribierte $tRNA^{Val}_{AAC}$ zu 50 % sequenzverifiziert. Ferner wurde das *in vitro* deaminierte Inosin an der Position 34 der $tRNA^{Val}_{AAC}$ bestätigt. Mittels isotopenmarkierter *in vitro* tRNA konnte die Deaminierungsrate auch per Oligonukleotid-MS bestimmt und die generierten Nukleosid-MS-Daten bestätigt werden. Demodifizierungs- genauer Demethylierungsprozesse an Oligonukleotiden wurden ebenso wie Modifikationen in nativer tRNA sequenzspezifisch nachgewiesen. Die Oligo-MS-Methode wurde sowohl auf einem niedrigauflösenden (QQQ) als auch auf einem hochauflösenden Massenspektrometer (Orbitrap) angewendet (*Nucleic Acids Res*., **2020**). Die detaillierten Einzelschritte, sowie generelle aber auch praktische Hinweise, die bei der Etablierung einer solchen Methode zu beachten sind, sind zusätzlich in einem Buchkapitel beschrieben (*Methods in Enzymology*, **2021**).

„Broadly applicable oligonucleotide mass spectrometry for the analysis of RNA writers and erasers *in vitro*", **F. Hagelskamp[#]**, K. Borland[#], J. Ramos, A. G. Hendrick, D. Fu, S. Kellner, *Nucleic Acids Res*., **2020**, Apr 17; 48 (7): e41.

([#] geteilte Erstautorenschaft)

Autorenbeitrag: Die Entwicklung und Etablierung der Oligo-MS-Methode erfolgte durch Stefanie Kellner und mich. Alle genannten Experimente und QQQ-Messungen sowie dazugehörige Datenanalysen wurden von mir durchgeführt. Kayla Borland generierte und wertete die HRMS-Daten aus. Jilian Ramos und Dragony Fu spendeten uns den aufgereinigten humanen Proteinkomplex ADAT2/3. Alan G. Hendrick stellte uns das AlkB Protein zur Verfügung. Die Ausarbeitung des Manuskripts erfolgte in Zusammenarbeit von Stefanie Kellner, Kayla Borland und mir.

„Analysis of the epitranscriptome with ion-pairing reagent free oligonucleotide mass spectrometry", **F. Hagelskamp**, S. Kellner, *Methods in Enzymology*, **2021**, 658, RNA Modification Enzymes (7).

Autorenbeitrag: Die beschriebenen Methoden wurden von mir entwickelt, optimiert und etabliert. Alle Experimente und Daten wurden von mir durchgeführt und ausgewertet. Die Ausarbeitung des Manuskripts wurde von Stefanie Kellner und mir in Zusammenarbeit erledigt.

Published online 21 February 2020

Nucleic Acids Research, 2020, Vol. 48, No. 7 ***e41***
doi: 10.1093/nar/gkaa091

Broadly applicable oligonucleotide mass spectrometry for the analysis of RNA writers and erasers *in vitro*

Felix Hagelskamp[1,†], Kayla Borland[1,†], Jillian Ramos[2], Alan G. Hendrick[3], Dragony Fu[2] and Stefanie Kellner[1,*]

[1]Department of Chemistry, Ludwig Maximilians University Munich, Butenandtstrasse 5-13, 81377 Munich, Germany, [2]Department of Biology, Center for RNA Biology, University of Rochester, Rochester, NY 14627, USA and [3]STORM Therapeutics, Moneta Building, Babraham Research Campus, Cambridge CB22 3AT UK

Received July 29, 2019; Revised January 23, 2020; Editorial Decision February 3, 2020; Accepted February 06, 2020

ABSTRACT

RNAs are post-transcriptionally modified by dedicated writer or eraser enzymes that add or remove specific modifications, respectively. Mass spectrometry (MS) of RNA is a useful tool to study the modification state of an oligonucleotide (ON) in a sensitive manner. Here, we developed an ion-pairing reagent free chromatography for positive ion detection of ONs by low- and high-resolution MS, which does not interfere with other types of small compound analyses done on the same instrument. We apply ON-MS to determine the ONs from an RNase T1 digest of *in vitro* transcribed tRNA, which are purified after ribozyme-fusion transcription by automated size exclusion chromatography. The thus produced $tRNA^{Val}_{AAC}$ is substrate of the human tRNA ADAT2/3 enzyme and we confirm the deamination of adenosine to inosine and the formation of $tRNA^{Val}_{IAC}$ *in vitro* by ON-MS. Furthermore, low resolution ON-MS is used to monitor the demethylation of ONs containing 1-methyladenosine by bacterial AlkB *in vitro*. The power of high-resolution ON-MS is demonstrated by the detection and mapping of modified ONs from native total tRNA digested with RNase T1. Overall, we present an oligonucleotide MS method which is broadly applicable to monitor *in vitro* RNA (de-)modification processes and native RNA.

INTRODUCTION

Ribonucleic acids (RNA) contain a vast variety of chemical modifications, which derive from the four canonical nucleosides adenosine, guanosine, uridine and cytidine. Modifications are introduced by dedicated enzymes, sometimes referred to as RNA writers. In analogy, RNA erasers exist, which demethylate adenosine in messenger RNA (mRNA) (1,2) or transfer RNA (tRNA) (3,4). Many RNA modifying enzymes add methyl groups to either the nucleobase or the ribose. For example, tRNA methyltransferase 1 (TRMT1) is responsible for the dimethylation of guanosine to 2,2-dimethylguanosine in tRNA ($m^{22}G$) (5) and methyltransferase like proteins 3/14 (METTL3/METTL14) methylate position 6 of adenosine and the epitranscriptomic mark m^6A forms in mRNA. In addition to RNA modification by methylation, the conversion of adenosine to inosine by deaminases such as the adenosine deaminase tRNA specific enzyme 2/3 (ADAT2/3) has been reported (6). Interestingly, many neurological diseases are connected with mutations in RNA modifying enzymes such as TRMT1 (5) and ADAT2/3 (7). In addition to the active decoration of RNA with modifications, the removal by active demethylation is also possible. Demethylation of m^6A and its ribose methylated variant m^6Am has been reported in human mRNA (1,2). Bacterial RNAs, including tRNA and rRNA, are also methylated, however there are no reports of active demethylation of enzymatically methylated sites. In many bacteria, the methylation of adenosine at position N1 (1-methyladenosine, m^1A) is not found in DNA or tRNA. However, alkylation stress can lead to direct m^1A formation in DNA and RNA. Due to methylating agents, which chemically methylate nucleic acids, bacteria have the ability for active demethylation. This m^1A is removed by the alpha-ketoglutarate-dependent dioxygenase AlkB (8). In human tRNAs, m^1A is found in 42% of all tRNAs at position 58. m^1A58 has been reported to be substrate to the human homologues of AlkB, namely ALKBH1 (3) and ALKBH3 (9).

The detection of modified moieties in RNA is possible by chemical means (10), by sequencing (11) and mass spectrometry (MS) (12). Even with the ever-rising number of sequencing techniques, which detect modified nucleosides in whole transcriptomes, MS remains the key technique for characterization of modified nucleosides. RNA MS analytics can be subdivided into three major principles. The first relies on complete enzymatic digestion of the RNA into

*To whom correspondence should be addressed. Tel: +49 089 2180 77724; Email: stkech@cup.lmu.de
†The authors wish it to be known that, in their opinion, the first two authors should be regarded as Joint First Authors.

the nucleoside building block and is highly sensitive with lower limits of detection (LLOD) in the fmol and amol range (nucleoside-MS). This technique is commonly used for detection (12), quantification (13) or discovery (14,15) of modified nucleosides. The second uses enzymes, which only partially digest the RNA and smaller oligonucleotides (ON) emerge (in this manuscript referred to as ON-MS). In the case of ON-MS, some of the sequence context surrounding a modified nucleoside is preserved and the technique is used to place modified nucleosides in known and unknown RNA sequences. Here, the pioneering work of the McCloskey (16,17), Limbach (18) and Suzuki (19) lab have largely contributed to the establishment of ON-MS. Disadvantages of this bottom-up approach are the loss of (most) sequence information, congestion of peaks in a small mass range, which mess up spectra, as well as the detection loss of low-abundant-modified RNAs by domination of their unmodified counterparts (20–22). The third principle of MS-based RNA analytics is the analysis of full-length RNAs (top-down-MS) at sophisticated mass spectrometers which has been pioneered by the Breuker lab (23–26). Top-down-MS of RNA is suited for many types of modification and it reveals the sample heterogeneity. It provides a high sequence coverage and information without a time-consuming digestion step. The disadvantage of top-down approaches is the need for RNA shorter ∼60 nts and the available dissociation steps in the MS field are low-efficiency processes. Another challenge is the underdevelopment of back-end bioinformatic tools. Nevertheless, quantitation of modified nucleobases has been also shown by top-down-MS (27). Both bottom-up- and top-down-MS approaches utilize MS/MS analysis and the underlying RNA dissociation reactions have been reviewed (28). From the perspective of instrumentation, high-resolution mass spectrometers are ideally suited for the MS and MS/MS analysis of RNA and its fragments. Instruments, such as time-of-flight, iontrap or orbitrap MS, deliver the necessary resolution to determine the charge state of the ONs and they allow sequence prediction based on their accuracy. Low resolution instruments, such as triple quadrupole MS, are not commonly applied for oligonucleotide MS analysis as they lack the resolution to distinguish similar ONs and to clearly determine the charge state of an ionized ON.

In contrast to top-down-MS, bottom-up-MS relies on the chromatographic separation of the ONs to solve the problem of congested MS spectra. The liquid chromatography is achieved by using an RP-18-based column and an ion-pairing reagent such as triethyl-ammonium-acetate (TEAA), which separates the oligonucleotides by their length. The eluting oligonucleotides are then analyzed in negative ionization mode by a high-resolution mass spectrometer and sequenced according to their fragmentation pattern (29,30) or modification footprints (31). With TEAA dependent flow chromatography (32), it is now possible to analyze 2–5 ng of purified tRNA isoacceptors (∼80–200 fmol pure tRNA) and determine the sequence and modification status of these tRNAs (33). Due to the common use of organic bases as ion-pairing reagents for ON separation and thus negative ionization, oligonucleotide MS is mostly used in labs with liquid chromatography coupled mass spectrometry (LC-MS) instruments dedicated for ON analysis. For other labs, the limitation of using ion-pairing reagents is the difficulty of their removal from the instrument. Residual ion-pairing reagents stay on the LC system and interfere with other types of chromatography and in addition they reduce the sensitivity of the mass spectrometer. To overcome this problem ion-pairing reagent free chromatography can be used on a reverse phase (RP) column (34). Here, the retention behavior of oligonucleotides is unexplored. Another alternative is chromatography on a hydrophilic interaction liquid chromatography (HILIC) column which will allow separation in a similar fashion to ion-pairing chromatography (35). Both methods are reported in combination with negative ionization mode MS detection and are thus not applicable for labs with mass spectrometers that preferably operate in positive ionization mode. Recently, a method was presented which used positive ionization detection of oligonucleotides after ion-pairing chromatography (36). Thus, laboratories have currently the option of doing classical ON-MS (ion-pairing reagent chromatography in negative ionization mode), ion-pairing reagent free ON-MS in negative mode or ion-pairing chromatography in positive mode. Thus, there is currently no method available which overcomes both limitations for a broad application of ON-MS.

A general challenge for MS-based modification analysis is its non-quantitative nature. For quantification, the signal intensity of an analyte must correlate with its concentration or amount. In MS, the signal intensity depends of course on the amount of analyte, but in addition on a multitude of other parameters such as salt load, ionization properties of the analyte, instrument parameters and so on. These detection fluctuations make quantification by MS a challenging task, which can only be done by using stable isotope labeled internal standards (SILIS) of the analyte of interest. For nucleoside-MS, this problem has been overcome by synthetic (37) or biosynthetic (13,38) preparation of stable isotope labeled nucleosides. For ON-MS, biosynthetic approaches have been reported (39,40). Another elegant way to solve the problem was presented by the Limbach lab (41). They performed the enzymatic digest of the unknown RNA in the presence of $H_2{}^{18}O$, which results in oxygen-18 incorporation into the oligonucleotide 3′-phosphate. As a third option, *in vitro* transcribed RNA is prepared in the presence of stable isotope-labeled nucleoside triphosphates (NTP) that is then used as an internal standard (42,43).

Although ON-MS has become a powerful tool for analysis of RNA modifications within their sequence context, it is not commonly applied. Due to the benefits of ON-MS, we developed a TEAA free chromatography, which separates the ONs not by length, but by chemical composition of the sequence. In this manuscript, we describe the development and separation principle of the method using synthetic ONs. Detection is achieved by low-resolution and high-resolution MS in positive ionization mode. We present MS/MS data for the analyzed ONs and determine the LLOD in various detection modes. We describe the automated purification of unlabeled and stable isotope labeled *in vitro* transcripts of $tRNA^{Val}_{AAC}$ and $tRNA^{Ser}_{UGA}$ by ribozyme fusion transcription. These *in vitro* transcripts and native tRNA from HEK cells are analyzed by our ON-MS method. To verify correct folding of the produced tR-

NAs, we use the adenosine-to-inosine deaminating enzyme ADAT2/3 on $tRNA^{Val}_{AAC}$. Inosine formation is observed by both nucleoside-MS and ON-MS. Importantly, these experiments are done on the same day using the same instrument which highlights the compatibility of our ON-MS method with sensitive small compound analysis. Furthermore, we use the developed ON-MS method to monitor the demethylation of short oligonucleotides containing 1-methyladenosine by bacterial AlkB *in vitro*.

Overall, we provide a method for automated purification of RNA transcripts and a broadly applicable ON-MS method for instruments commonly used for other types of small compound analysis, especially nucleoside analysis.

MATERIALS AND METHODS

Salts, reagents and nucleosides

All salts, solvents and reagents were obtained from Sigma Aldrich (Munich, Germany) at molecular biology grade unless stated otherwise. All solutions and buffers were made with water from a Millipore device (Milli-Q, Merck, Darmstadt, Germany). Nucleosides: adenosine (A), cytidine (C), guanosine (G) and uridine (U) were purchased from Sigma Aldrich. 1-methyladenosine (m^1A) and inosine (I) were purchased from Carbosynth (Newbury, UK).

Oligonucleotides

All oligonucleotides were delivered in a stock concentration of 100 μM in water and are listed in Supplementary Table S1.

AlkB in vitro assay

An aliquot of bacterial AlkB protein (Peak Proteins, Cheshire, UK) was thawed on ice. Every assay was performed in a volume of 50 μl with a final concentration of 50 mM TRIS HCl pH 7.5, 15 mM KCl, 2 mM L-ascorbate, 300 μM α-ketoglutarate, 300 μM Fe(II) $(NH_4)_2(SO_4)_2 \times 6H_2O$. L-ascorbate, α-ketoglutarate and diammonium iron (II) sulfate hexahydrate stock solutions were made afresh. A total of 10 μM of the synthetic RNA oligonucleotide was incubated with 1 μM AlkB enzyme. All assays were incubated at 37°C for 1 h and immediately stopped afterward by filtering through a molecular weight cut-off filter (VWR, Partnumber: 516-0229) for oligonucleotides or RNA precipitation for tRNA *in vitro* transcripts, respectively.

tRNA digestion for nucleoside mass spectrometry

Up to 1 μg RNA in 30 μl aqueous digestion mix were digested to single nucleosides by using 0.2 u Alkaline Phosphatase, 0.02 u Phosphodiesterase I (VWR, Radnor, PA, USA) and 0.2 u Benzonase in 5 mM TRIS (pH 8.0) and 1 mM $MgCl_2$. Furthermore, 0.5 μg tetrahydrouridine (Merck, Darmstadt, Germany), 1 μM butylated hydroxytoluene and 0.1 μg pentostatine were added. The mixture was incubated with the RNA for 2 h at 37°C and filtered through 96-well filterplates (AcroPrep™ Advance 350 10 K Omega™, PALL Corporation, New York, USA) at 4°C for 30 min at 3000 × *g*, or through single tubes (VWR, Partnumber: 516-0229) at room temperature for 7 min at 5000 × *g*. The filtrate was mixed with 1/10 Vol. of 10× yeast SILIS (stable isotope labeled internal standard) (38) for absolute quantification.

Nucleoside mass spectrometry

For nucleoside-MS measurements, a liquid chromatography unit (1290 Infinity II, Agilent Technologies, Waldbronn, Germany) equipped with a diode-array detector (DAD, Agilent Technologies) was used that was interfaced with a triple quadrupole mass spectrometer (G6470A, Agilent Technologies) via an electrospray ionization (ESI) source (Jet Stream, Agilent Technologies). For separation of nucleosides, a Synergi Fusion-RP column (Phenomenex®, Torrance, California, USA; Synergi® 2.5 μm Fusion-RP 100 Å, 150 × 2.0 mm) at 35°C and a flow rate of 0.35 ml/min were used. The eluents were 5 mM NH_4OAc, brought to pH 5.3 with glacial acetic acid (buffer A), and pure acetonitrile (buffer B). The gradient started at 100% A for 1 min, followed by an increase of solvent B to 10% over 5 min. From 5 to 7 min, solvent B was increased to 40% and was maintained for 1 min before returning to 100% solvent A in 0.5 min and a 2.5 min re-equilibration period. The QQQ mass spectrometer was operated in dynamic multiple reaction monitoring (dMRM) mode between 1.1 min and 9 min with a cell accelerator voltage of 5 eV. Operating parameters: positive-ion mode, skimmer voltage of 15 V, cell accelerator voltage of 5 V, N_2 gas temperature of 230°C and N_2 gas flow of 6 l/min, sheath gas (N_2) temperature of 400°C with a flow of 12 l/min, capillary voltage of 2500 V, nozzle voltage of 0 V and nebulizer at 40 psi. The detailed mass spectrometric parameters for each nucleoside are given in Supplementary Table S2.

Calibration for nucleoside mass spctrometry

For calibration, synthetic nucleosides Cytidine, Uridine, Guanosine, Adenosine, 1-methyladenosine (m^1A) and Inosine (I) were weighed and dissolved in water to a stock concentration of 1–10 mM. Calibration solutions ranging from 0.15 to 500 pmol for each canonical nucleoside and from 0.15 to 500 fmol for each modified nucleoside were prepared by serial dilution (1:10). The calibration solutions were mixed with 1/10 Vol. of 10× yeast SILIS and analyzed by nucleoside-MS. Data were analyzed using Agilent's Quantitative or Qualitative Software. The absolute amount determined for m^1A and I was normalized to the amount of injected RNA as determined by the absolute abundance of all four canonical nucleosides (38).

Mammalian cells

HEK 293T and HeLa ACC 57 cells (DSMZ, Braunschweig, Germany) were cultured in Dulbecco's Modified Eagle Medium (DMEM). DMEM medium was prepared by dissolving 8.4 g DMEM powder D5030 in 1 l pure water. Before sterile filtration, carbonate and phenol red were added to a final concentration of 3.7 g/l $NaHCO_3$ and 0.0159 g/l phenol red. Stocks of glucose (225 g/l) and L-glutamine

(15 g/l) were prepared and sterile filtered. These solutions were added to the DMEM medium before usage to a final concentration of 4.5 g/l glucose, 0.584 g/l L-glutamine and 10% fetal calf serum (FCS). The methionine concentration was 0.15 g/l in the final media. For splitting, the cells were treated with TrypLE Express (Gibco, Carlsbad, CA, USA). The cells were incubated and cultivated at 10% CO_2 atmosphere.

RNA isolation

HEK and HeLa cells were harvested directly in cell culture flasks using 1 ml TRI-Reagent® per 25 cm^2. Isolation was performed according to the manufacturer's protocol with chloroform (Roth, Karlsruhe, Germany). The RNA was finally dissolved in 30 μl water.

PCR

All polymerase chain reactions (PCR) were performed in a total volume of 50 μl with a final concentration of 1-fold Phusion Buffer HF (New England Biolabs, Ipswich, MA, USA) and 0.8 μM forward and reverse primer. The sequence of templates and primers are given in Supplementary Table S1. Additionally, 1 μl dNTPs, 0.5 μl Phusion polymerase and 100 ng of the desired DNA template were added. All samples were amplified with the same PCR program: 95°C for 2 min, 95°C for 30 s for 20 amplification cycles, 57°C for 30 s for 20 times and 68°C for 1 min for 20 times. At the end of the program, the PCR reaction was incubated at 68°C for 1 min and was cooled down to 4°C. Every PCR reaction was performed twice and pooled afterward for the T7 *in vitro* transcription.

T7 *in vitro* transcription

The total volume of the T7 *in vitro* transcription was 200 μl. A total of 100 μl PCR product were added to T7 buffer mix and T7 enzyme (TranscriptAid T7 High Yield Transcription Kit, Thermo Fisher Scientific, Waltham, MA, USA) and 1.6 μl of each rNTP (^{14}N-rNTPs were provided by the kit, ^{15}N-rNTPs were purchased by Silantes, Munich, Germany, Partnumber.: 121306100). The mixture was incubated for 2 h at 37°C and 600 rpm. After 2 h incubation, the sample was treated with 2 μl T7 enzyme mix and 5 μl 50 mM $MgCl_2$ and incubated for additional 2 h. After another 2 h incubation, the sample was treated again with 2 μl T7 enzyme mix and 5 μl 50 mM $MgCl_2$ and incubated for additional 2 h to improve the yield of the transcription. In total, the transcription was finished after 6 h. DNA template was removed by addition of 4 μl DNase 1, which is provided in the kit, 1 h at 37°C. In the next step, $MgCl_2$ was added with a final concentration of 5 mM and the sample was incubated at 60°C for 1 h to auto-catalytically cleave the precursor *in vitro* transcript into its target tRNA. Prior to RNA precipitation, the sample was centrifuged at 5000 × *g* for 5 min at room temperature to remove the insoluble pyrophosphate of the transcription reaction. The supernatant was precipitated by addition of 0.1 Vol. of 5 M ammonium acetate and 2.5 Vol. of ice-cold ethanol (100%) followed by overnight incubation at −20°C. The RNA was pelleted by centrifugation (12 000 × *g*, 40 min, 4°C), washed with 70% ethanol and resuspended in 30 μl water.

Size exclusion chromatography (SEC)

For purification of tRNA from total RNA or purification of tRNA *in vitro* transcripts from precursor products, size exclusion chromatography (SEC) was used on an Agilent 1100 HPLC system (Degasser, G1279A; Quad Pump, G1311A; ALS, G1313A; COLCOM, G1316A; VWD, G1314A; Analyt FC, G1364C). For method development, three columns with 7.8 × 300 mm, 2.7 μm particle size from Agilent (Waldbronn, Germany) were tested. The SEC-3 (Partnumber: 5190-2511 reported by Dedon lab (44)), the AdvanceBio 300 Å (Partnumber: 1180-5301) and the AdvanceBio 130 Å (Partnumber: 1180-5350).

The column temperature was set to 40°C for native tRNA purification using the Advance Bio 300 Å and 60°C for *in vitro* transcript purification using the AdvanceBio 130 Å. For elution, a 1 ml/min isocratic flow of 0.1 M ammonium acetate was used. Eluting RNA was detected at 254 nm with a diode array detector. The eluted RNA was collected by a fraction collector and the eluent was evaporated (GeneVac, EZ-2 PLUS, Ipswich, UK) to a volume of ∼50 μl before ethanol precipitation. The purified RNA was dissolved in 30 μl water for further enzymatic assays or MS analysis.

Handling guide for SEC columns

For prolongation of the column lifetime, it is essential to avoid sudden pressure changes. Thus we recommend to run a conditioning method, which slowly increases the flow rate from 0 ml/min to 1 ml/min within 20 min. For tRNA purification from total RNA, a column temperature of 40°C is sufficient. For purification of *in vitro* transcripts, 60°C yielded better separation results. Note: Column lifetime is shortened at 60°C and thus long exposures to high temperatures should be avoided. After use, the column was stored in 0.05% NaN_3.

RNA concentration and quality measurements

The RNA concentration was determined with an Implen Nanophotometer NP 80 (Munich, Germany). For quality control of SEC purified *in vitro* transcripts, the Agilent 2100 Bioanalyzer (Small RNA analysis chip, Partnumber: 5067-1548, Agilent, Waldbronn, Germany) was used.

Isoacceptor purification

The procedure was adapted from Hauenschild *et al.* (45). For tRNA isoacceptor purification, pre-purified total tRNA was used. The sequence of the biotinylated 2′-deoxyoligonucleotide probes is listed in Supplementary Table S1.

Purification of ADAT2/3

Open Reading Frame sequences encoding for human ADAT2 and ADAT3 were cloned into the petDuet plasmid. ADAT2 was cloned into Multiple Cloning Site (MCS)

1 which allows fusion with a HIS tag. ADAT3 was cloned into MCS2. BL21DE3 RIPL *Escherichia coli* cells (Agilent) were transformed with the above plasmid. Starter culture was grown to an O.D of 0.1–0.5, and inoculated into a larger culture to an O.D of 0.05 and cells were induced with Isopropyl-β-D-thiogalactoside (IPTG) at an O.D. of 0.6–0.8. After induction, *E. coli* were grown at 20°C for 15 h. Cells were harvested and lysed by sonication in a buffer containing 20 mM TrisHCl pH 7.6, 5% glycerol, 0.1% Triton, 1 mM Dithiothreitol (DTT), 0.1 mM (Phenylmethylsulfonylfluorid) PMSF, 500 mM NaCl, 25 mM imidazole. Cell lysates were oscillated with HisPur Colbalt Resin (Thermo Scientific # 89964) at 4°C for 2 h. Beads were washed 3× with buffer containing 20 mM TrisHCl pH 7.6, 5% Glycerol, 0.1% Triton, 1 mM DTT, 0.1 mM PMSF, 300 mM NaCl and 25 mM imidazole. Elution of protein was carried out with above buffer containing 300 mM imidazole. Elution buffer was exchanged to buffer containing 20 mM TRIS, 5% Glycerol, 0.1% Triton, 150 mM NaCl and 1 mM DTT. Expression and purification was verified by sodium dodecyl sulphate-PAGE (polyacrylamide gel electrophoresis) followed by western blotting. Quantification of purified protein was carried out by Coomassie with BSA size standards. Final concentration of ADAT2/3 was ∼8 ng/μl.

ADAT2/3 assay

An aliquot of ADAT2/3 protein was thawed on ice. A total of 6 μl tRNA substrate (115 ng/μl) were incubated in 6 μl water and 6 μl melting mix. The melting mix buffer was prepared with 30 mM TRIS pH 7.5 and 1 mM ethylenediaminetetraacetic acid. To denature the tRNA, the mix was heated to 95°C for 2 min and immediately placed on ice for 3 min for tRNA folding. In the next step, 3 μl folding mix was added and incubated for 20 min at 37°C. The folding mix buffer was prepared with final concentrations of 333 mM HEPES pH 7.5, 20 mM $MgCl_2$ and 333 mM NaCl. A total of 9 μl of ADAT2/3 was added to obtain a total reaction volume of 30 μl and incubated for 1 h at 37°C and immediately stopped afterward by RNA precipitation with 300 μl $LiClO_4$ in acetone (2%). After incubation at room temperature for 5 min, the sample was centrifuged at 5000 × *g* for 5 min. The supernatant was discarded and the tRNA pellet was solved in 20 μl milliQ water for further analysis.

tRNA digestion for oligonucleotide mass spectrometry

RNase T1 was diluted to a 10 U/μl solution by mixing 2 μl of the RNase T1 stock (186 U/μl, Sigma-Aldrich, Munich, Germany) with 35.2 μl TRIS pH 7.5 (25 mM). The diluted RNase T1 should be stored at 4°C. Up to 1 μg RNA was digested with RNase T1 at 37°C for 1 h in a total volume of 50 μl with final concentrations of 25 mM TRIS pH 7.5, 100 mM NaCl and 1 U/μl RNase T1 and 0.2 u/μl Alkaline Phosphatase. The digested samples were filtered through a molecular weight 10 kDa cut-off filter (VWR, Dreieich, Germany, Partnumber: 516-0229) and analyzed by MS.

Oligonucleotide mass spectrometry

For oligonucleotide MS measurements, the instrument described in the nucleoside-MS section was used. For separation of oligonucleotides, a Synergi Fusion-RP column (Phenomenex®, Torrance, CA, USA; Synergi® 2.5 μm Fusion-RP 100 Å, 150 × 2.0 mm) at 35°C and a flow rate of 0.35 ml/min were used. The eluents were 10 mM NH_4OAc (pH 7.0) (buffer A) and pure acetonitrile (buffer B) (Carl-Roth, Karlsruhe, Germany; LC-MS grade, purity ≥95.95). The gradient started at 100% buffer A, followed by an increase of B to 5% over 10 min. From 10 to 12 min, buffer B was increased to 50% and was maintained for 1 min before returning to 100% buffer A and a 4 min re-equilibration period. For source optimization experiments a shorter gradient was used starting at 100% buffer A, increased to 2% buffer A over 1 min, increased to 10% A by 4 min, then to 50% A by 5 min, held at 50% A for 0.5 min then returned to 100% A. The same re-equilibration period as the previous method was used. The QQQ mass spectrometer was operated in full scan (MS2Scan), between 500–1000 m/z with a fragmentor voltage of 100 V and a cell accelerator voltage of 5 V in positive ionization mode. For determination of CID spectra, collision energies of 5–40 eV were used and the instrument operated in Product Ion Scan mode. Mass transition of ONs were used in a targeted MRM method. Data were analyzed using Agilent's Qualitative Analysis Software.

High-resolution mass spectra of oligonucleotide ions were recorded by a Thermo Finnigan LTQ Orbitrap XL with a heated electrospray ionization (HESI) source was operated in positive ionization mode with a capillary voltage of −10 V and temperature of 310°C. The spray voltage to 3.3 kV, and the atmospheric pressure chemical ionization (APCI) temperature was set to 135°C. Sheath, auxiliary and sweep gases were set to the following respectively 5, 35 and 7 arbitrary units. MS1 specta were collected from 200 to 1000 *m/z* and data-dependent acquisition (DDA) set to acquire MS2 spectra of the top three most abundant ions. Data acquisition and analysis was completed on the Thermo Xcalibur software platform.

RESULTS

Exploring the applicability of a TEAA-free chromatography for oligonucleotide mass spectrometry

In a first step, we wanted to find a TEAA (triethylammoniumacetate) and other ion-pairing reagents free chromatography for separation of oligonucleotides which might be compatible with commonly used mass spectrometers and small compound analysis. A literature search, to avoid ion-pairing reagents, revealed a method from 1994, where an RP-18 column was used for separation of tRNA isoacceptors (46). Here, the elution was achieved by a gradient of simple ammonium acetate and acetonitrile, which is comparable to the separation procedure of nucleosides (38). Inspired by this early work, we tested the separation of synthetic oligonucleotides (ON) on our nucleoside column (Phenomenex, Fusion-RP) using a 10 mM ammonium acetate buffer and acetonitrile for elution. Due to the negatively charged phosphate backbone of RNA, we did not expect good retention on a hydrophobic RP-18 column. However, due to the special column material of the tested column, we observed excellent retention for the tested ONs. As the UV chromatogram (λ260 nm) in Figure 1A shows, the tested 8-mer

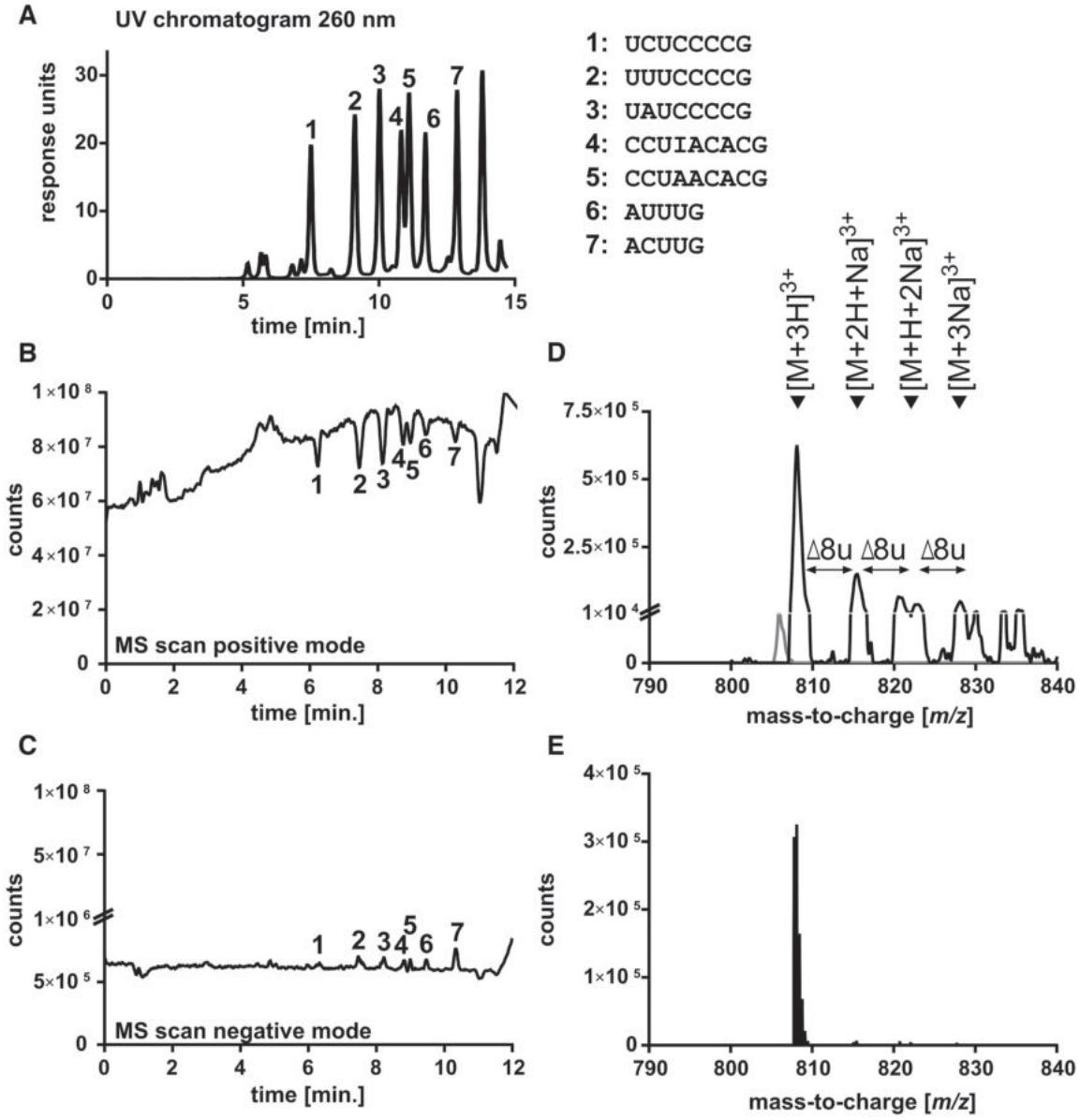

Figure 1. Separation and detection of synthetic oligonucleotides (ON) by MS. (**A**) UV chromatogram (λ 260 nm) of various ONs (20 pmol injection) separated by our ion-pairing reagent free chromatography. (**B**) Detection of the ONs from (A) by MS using positive ionization. (**C**) Detection of the ONs from (A) by MS using negative ionization. (**D**) Mass spectrum of the first eluting ON from (A) in positive ion mode (black) and negative ion mode (gray) on a low-resolution triple quadrupole instrument. The charge state is determined by the pattern of sodium charges in the spectrum. (**E**) Mass spectrum of the first eluting ON from (A) in positive ion mode (black) on a high resolution Orbitrap instrument.

ONs elute first, followed by 9-mer ONs and 5-mer ONs. To understand which properties of the ONs influence the retention behavior, we used ONs, which only differ in one nucleobase in their sequence. As shown in Figure 1A, the cytidine containing 8-mer elutes first, while the exchange to a uridine leads to better retention. The permutated 8-mer with adenosine is retained most on the column. In the 5-mer, we observe a better retention of the cytidine containing ON compared to its U containing permutation. In case of the 9-mer ONs, the deamination of one adenosine into inosine leads to reduced retention. In these sequence contexts, we clearly see a dependence of the retention behavior on the chemistry of the present nucleobases and not on the length of the ON. From our data, we conclude that the retention behavior of ONs in our TEAA-free system depends on two factors: the distribution of nucleobases and the sequence. We observe no rules which allow prediction of ON elution.

In a next step, we connected our developed chromatographic system with our low resolution triple quadrupole (QQQ) mass spectrometer. We tuned the instrument in both negative and positive ionization mode using the tune mix supplied by the manufacturer and determined the optimal source parameters for sensitive detection of ON 13

(CCUAACACG) (Supplementary Figure S1). With these parameters, we scanned for the eluting ONs in a mass range of m/z 500–1000 in positive and negative ionization mode. We received MS signals of all tested ONs below 10 nt in both positive and negative ionization mode (Figure 1B/C). Our instrument is commonly operated in positive ionization mode, and thus it was no surprise to find a substantially higher sensitivity in positive ionization mode. We attribute this observation to the fact that the instrument is only operated in positive ion mode with the respective buffers for ideal protonation in the ESI source. Thus, the ionization efficiency in negative ion mode is reduced. On other instruments, the sensitivity is higher in negative mode compared to positive mode (47). We recommend assessment of the most sensitive ionization mode on every mass spectrometer by running a mixture of short synthetic ONs. The addition of the modifier 1,1,1,3,3,3-Hexafluor-2-propanol (HFIP) did not improve the detection in positive or negative ion mode. Due to the common use of our instrument in positive ion mode and the higher sensitivity, we decided to use the positive ionization mode for further analyses. We used the mongo-oligo mass calculator tool (https://mods.rna.albany.edu/masspec/Mongo-Oligo) to compare our experimental signals with the predicted signals. For the tested ONs, we observed the predicted m/z signals, commonly of the +2 charge state for 5 mers, +3 charge for 8 mers and +4 charge for 10 mers (Supplementary Figure S2). The charge state of an ON is commonly calculated with the natural abundance of carbon-13 on high-resolution instruments. The difference between the ^{12}C-m/z value and the ^{13}C-m/z value is ∼1 in a +1 charge state, ∼0.5 in a +2 charge state, ∼0.3 in a +3 charge state, etc. On a low-resolution instrument, such as the used QQQ MS, the natural isotope abundance is not resolved and cannot be used to predict the charge state. As an alternative, the difference between the (multi-) protonated ion and the sodium charged ion can be used. In a +1 charge state, the difference is 22 units, in a +2 charge state it is 11 units (charged by one protonation and one sodium cation), in a +3 charge state it is ∼7 units (two protons and one sodium cation), etc. Our mass spectrum for the C-permutated 8-mer ONs revealed a main signal at m/z 808.1 (protonated species) and a m/z 816 for the Na^+-charge and thus we conclude a +3 charge state of this ON (see Figure 1D). For the 8-mer ONs, other charge states are of minor abundance (see full mass spectra in Supplementary Figure S3).

In addition to the analyses of ONs by low resolution MS, we wanted to test the compatibility of our method with a high resolution mass spectrometer. The instrument was optimized with the 9-mer ON 13 and the optimal parameters were chosen according to the results given in Supplementary Figure S1. As shown in Figure 1E and Supplementary Figure S2, all tested ONs were detectable by high-resolution MS in positive ionization mode. On this instrument Na^+ adducts were of minor abundance and protonated species dominated the MS spectra.

MS of oligonucleotides is commonly used to determine the sequence and location of modified nucleosides (26,48). For this purpose, fragmentation of the ONs by collision-induced-dissociation (CID) is a useful tool and the behavior of ONs in positive and negative ionization mode is well described (47). On the low resolution QQQ instrument, we analyzed ON 13 and ramped CID energies from 0 to 30 eV. The recorded product ion scans are displayed in Figure 2A. With increasing collision energy, the signal of the precursor ion decreases, while multiple new signals appear in the spectra. At higher collision energies, the most prominent product ions in positive ionization mode are protonated nucleobase fragment ions. At energies around 15–20 eV, c and y ions become apparent (Figure 2B). Due to the low resolution of a QQQ instrument, the charge state of these c- and y-ions cannot be determined and thus QQQ MS is not suitable for *de novo* sequencing. The signal to fragment matching in Figure 2B and for other ONs in Supplementary Figure S4 was only possible due to the known sequence of the ON and the use of the Mongo oligonucleotide tool (https://mods.rna.albany.edu/masspec/Mongo-Oligo). CID analysis on the high resolution MS produced more c- and y- fragment ions of known charge states and thus *de novo* sequencing is theoretically possible (Supplementary Figure S5).

Low resolution instruments such as our used QQQ mass spectrometer are commonly used for the sensitive detection and quantification of small compounds. In our hands, the LLOD and lower limits of quantification (LLOQ) of modified nucleosides is in the single digit fmol range or even amol range (38). For ON analysis, we injected dilutions of ON 13 and ON 14 and found LLODs/LLOQs of 200 fmol in MS2Scan mode, 800 fmol in MS/MS mode and 800 fmol in Product Ion (PI) Scan mode for sequence determination purposes (Figure 2C). For isolated tRNA isoacceptors, the lowest sensitivity was achieved with a TEAA dependent nano-LC setup (33). With nano-LC, 2–5 ng tRNA (∼80–200 fmol) are sufficient for analysis which is comparable to our results.

Although the sensitivity towards ONs is lower compared to small molecule analysis, it is sufficient to analyze ONs derived from synthesis, *in vitro* experiments or potentially even native RNAs.

Preparation of *in vitro* transcribed tRNA by SEC

To expand the field of application, we wanted to use our method on partial RNA digests of full-length *in vitro* transcripts and also native RNAs. Thus, we decided to produce two human tRNAs by ribozyme-fusion *in vitro* transcription and analyze the transcripts after RNase T1 digestion by ON-MS. After transcription, the cleaved transcript is commonly purified by PAGE and the ribozyme and the full-length transcript are removed (49). However, PAGE purified RNA always contains small amounts of polyacrylamide, which potentially interacts with later MS. Thus, we adapted a previously described method based upon size exclusion chromatography (SEC, SEC-3 column) that is rapid, automatable and produces clean RNA (44). We have found the AdvanceBio SEC column to be more robust and thus recommend this column for tRNA purification from total RNA. We supply a detailed handling guide to prolong column lifetime to several hundred injections in the materials and methods section. A comparative profile of an RNA ladder (1000 nts to 50 nts) loaded onto these two 300 Å columns is shown in Figure 3A and B. Especially at the used

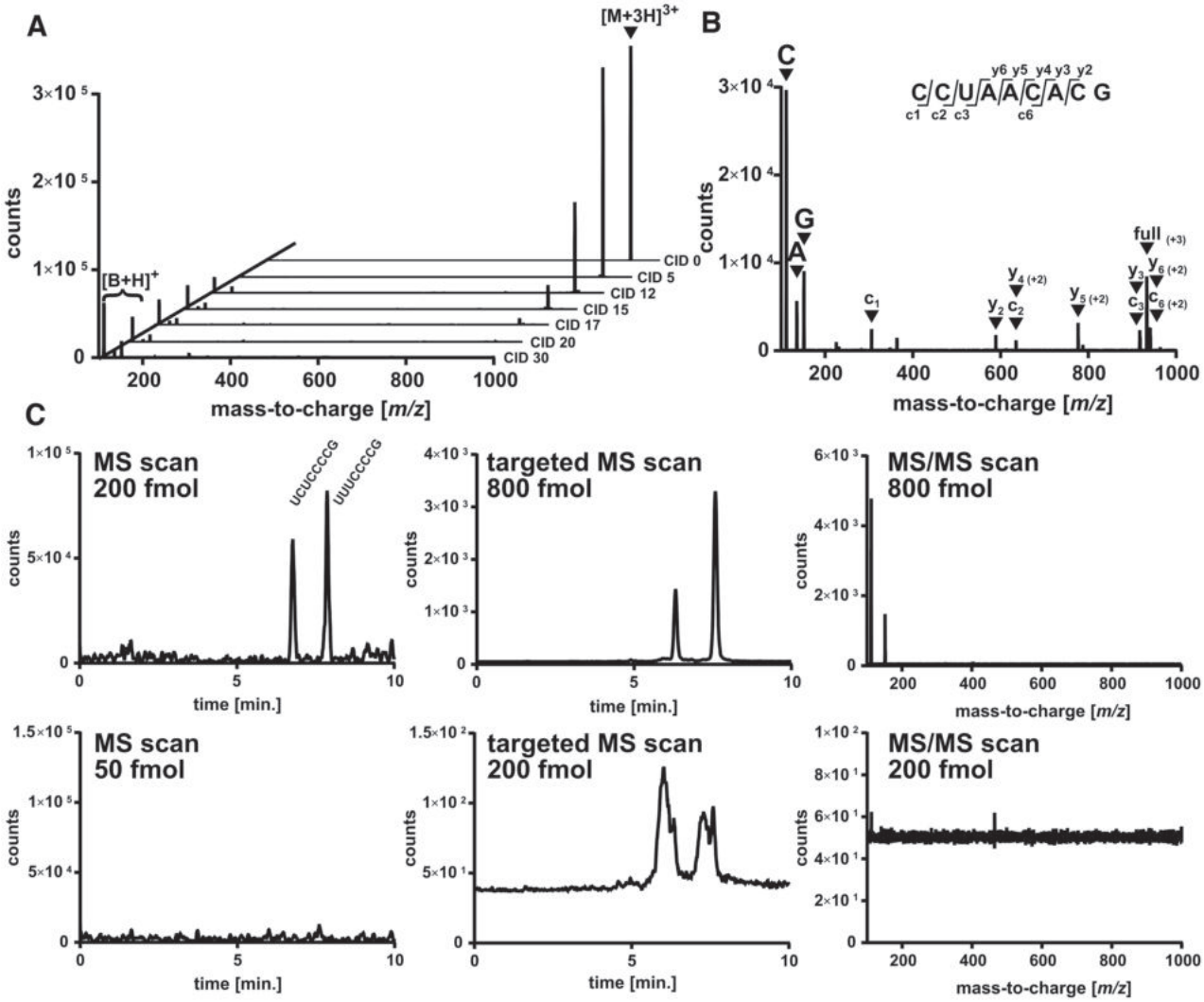

Figure 2. Collision-induced dissociation (CID) and sensitivity of oligonucleotides on a low resolution triple quadrupole mass spectrometer (30 pmol injection). (**A**) MS/MS spectra of the 8-mer CCUAACACG at various collision energies (CID 0–30 eV). The emergence of base fragments is indicated with $[B+H]^+$. (**B**) MS/MS spectrum of CCUAACACG at a CID energy of 15 eV. The resulting fragments are assigned to the known sequence by using (https://mods.rna.albany.edu/masspec/Mongo-Oligo). Base fragments are abbreviated with C—cytosine, A—adenine and G—guanine. (**C**) LLOD for the ONs U(U/C)UCCCCG in MS scan mode (left), targeted MS mode (middle) of the mass transition 808.1→112 and 808.5→112 and MS/MS scan mode using the precursor m/z 808.1 and 808.5. The upper graphs are above the LLOD, the lower graphs are just below the LLOD.

column temperature of 60°C, both columns nicely separate the 50 and 80 nts marker from the longer RNAs >150 nts. As expected, native tRNA elutes at the same time as the 80 nts marker, which indicates that secondary structures play no role in the separation of RNAs. Thus, these columns are ideal for separation of large RNAs such as ribosomal RNA (rRNA) and mRNA from the smaller tRNAs. The AdvanceBio column is also available with a 130 Å pore size. We tested the separation efficiency of this column with the ladder and as it is to be expected, the large RNA markers can no longer be separated due to reduced interaction with the smaller pores (Figure 3C). The 130 Å column is less suitable for the separation of total RNA. However, it has a potential for the separation of RNAs smaller 80 nts, *e.g.* tRNA and tRNA-derived fragments (tRF or tiRNA) (Supplementary Figure S6).

For the sake of column preservation, we tested the chromatographic resolution at lower temperatures. We find sufficient separation of the small 80 nts from the larger RNAs (>150 nts) at 40°C (Supplementary Figure S7). We have applied the AdvanceBio 300 Å SEC column at 40°C in several studies for the purification of tRNA from total RNA (5,50–51). The purification was always reliable and thus we recommend this column with the developed parameters for tRNA purification.

For the purification of tRNA from ribozyme-fusion *in vitro* transcription, both 300 Å and 130 Å pore size columns have been tested. $tRNA^{Ser}_{UGA}$ is an 85 nts long tRNA and fused with the ribozyme fusion transcript is 135 nts in length. The fusion transcript auto-catalytically cleaves itself into the 85 nts long tRNA and the 40 nts long ribozyme. As shown in Figure 3D, the tRNA peak is separated from

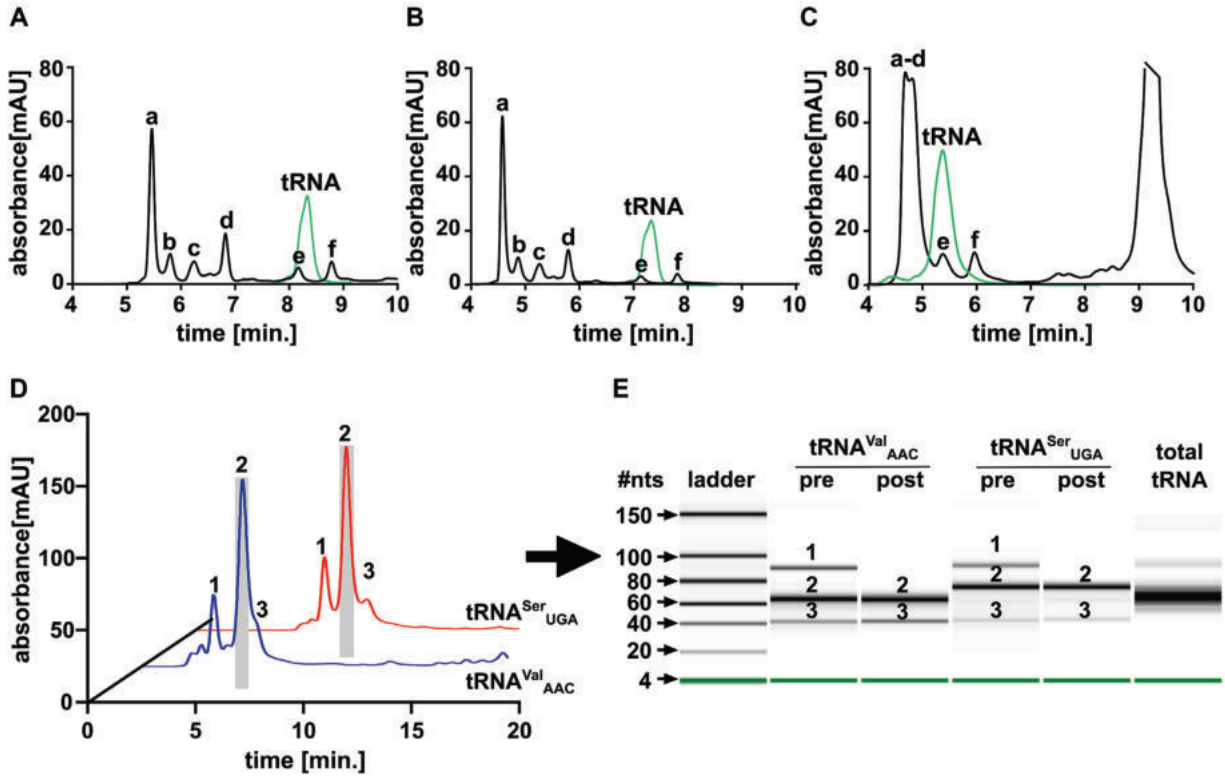

Figure 3. SEC of RNA for automated purification **(A)-(C)** Separation of an RNA ladder (black) of a: 1000 nts, b: 500 nts, c: 300nts, d: 150 nts, e: 80 nts and f: 50 nts. For comparison, the elution of total tRNA is shown in green. **(A)** SEC-3, 300 Å **(B)** AdvanceBio SEC 300 Å **(C)** AdvanceBio SEC 130 Å **(D)** Purification of T7 *in vitro* transcribed $tRNA^{Val}_{AAC}$ (blue) and $tRNA^{Ser}_{UGA}$ (red) on a 130 Å column at 60°C. Peak 1: tRNA-ribozyme fusion product, Peak 2: tRNA, Peak 3: ribozyme; **(E)** Quality control of the T7 transcription mix before purification (pre) and after SEC separation (post) for $tRNA^{Val}_{AAC}$ and $tRNA^{Ser}_{UGA}$ on an automated gel-electrophoresis system. 1: tRNA-ribozyme fusion product, 2: tRNA, 3: ribozyme

the full-length transcript, while the cleaved ribozyme partly co-elutes with the tRNA (130 Å column at 60°C). We collected the tRNA peak and analyzed the fraction by high-resolution automated electrophoresis (Bioanalyzer). Here, we find that some of the ribozyme (40 nts) is still detectable in the tRNA fraction but the full-length transcript (135 nts) is completely removed (Figure 3E). If necessary, the collection of the tRNA peak is possible in a smaller time window or second purification round and thereby the ribozyme can be completely removed (Supplementary Figure S8). After successful purification of the comparably long $tRNA^{Ser}$, we were curious whether purification of a tRNA with short variable loop is possible by our automated system. For this purpose, we prepared a fusion-transcript of $tRNA^{Val}_{AAC}$. The full-length transcript is 124 nts long, the tRNA itself 76 nts and the ribozyme again 40 nts. For this tRNA, the size difference between tRNA and the ribozyme is only 36 nts. As a rule of thumb, SEC separation of biomolecules is possible as long as they differ in size by a factor of two. This prerequisite is not met in case of $tRNA^{Val}$ and as expected, the separation of the produced tRNA and the ribozyme is not possible (Figure 3D, blue chromatogram). The ribozyme co-elutes as a shoulder and subsequently, more ribozyme can be found in the purified tRNA transcript (Figure 3E). Similar to the presented solution for $tRNA^{Ser}$, a reduced collection time window can help to remove the remaining ribozyme if complete removal of the ribozyme is necessary for subsequent experiments.

Overall, SEC purification of ribozyme-fusion transcribed tRNAs is an alternative to purification by PAGE. The complete transcription mix can be loaded onto the SEC column without pre-purification and within 20 min the pure tRNA fraction is received in a volume of 500–1000 μl in 0.1 M ammonium acetate. Concentration of the tRNA product is possible by subsequent solvent evaporation and/or ethanol precipitation.

Analysis of RNase T1 treated tRNA by oligonucleotide mass spectrometry

With the tRNA transcripts in hand, we were ready to test our LC-MS method by injecting a partial digest of the produced tRNAs. For this purpose, 1 μg of each transcript was incubated with RNase T1. The enzyme was removed by molecular weight cut-off filtration and 200 ng (~8 pmol) of the resulting ON mixture were injected onto the LC-QQQ set-up in scanning mode. As expected from our experiments with synthetic ONs, we observe separation of the RNase T1 derived ON mixture as seen for the total ion chromatogram shown in Figure 4A ($tRNA^{Val}_{AAC}$) and 4b ($tRNA^{Ser}_{UGA}$). The color-coded tRNA sequences are shown in Supplementary Figure S9. For $tRNA^{Val}_{AAC}$, we prepared transcripts containing stable isotope labeled nucleotides $^{15}N_3$-cytidine or $^{15}N_5$-guanosine. The fragments of the unlabeled and labeled transcripts elute at the same retention time. The low resolution mass spectra of the eluting peaks allowed the as-

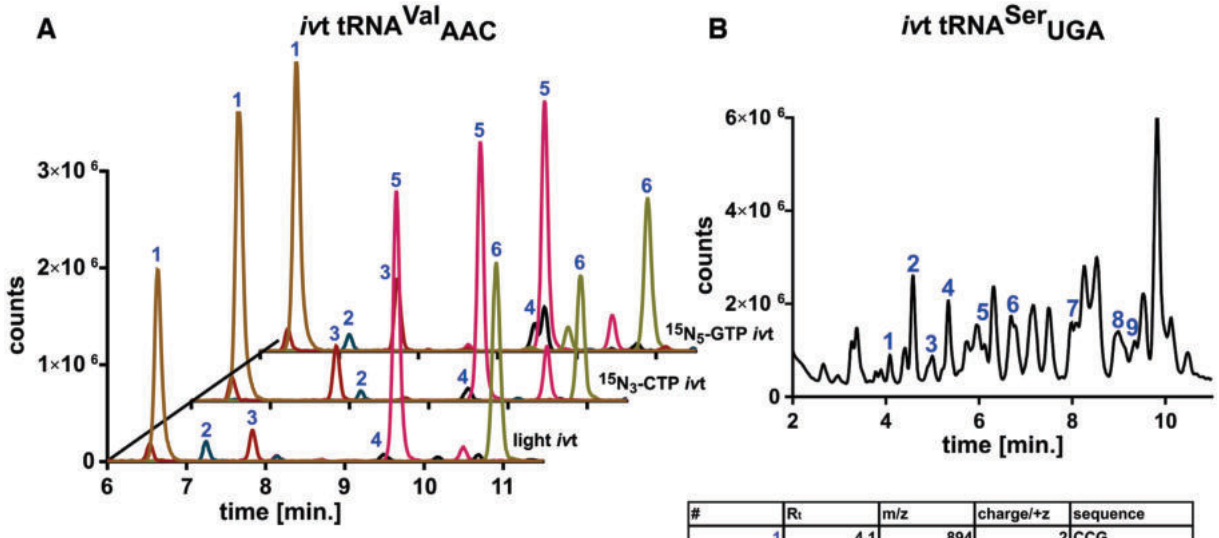

#	Rt	charge/+z	light *ivt* m/z	^{15}N-CTP *ivt* m/z	^{15}N-GTP *ivt* m/z	sequence
1	6.5	1	590	590	595	UG
2	7.2	2	906	909	908	UCCCUG
3	7.8	2	601	603	604	UUCG
4	9.5	3	933	937	935	CCUAACACG
5	9.6	1	919	919	924	UAG
6	10.9	3	834	837	834	AAACACCA

#	Rt	m/z	charge/+z	sequence
1	4.1	894	2	CCG
2	4.6	589	1	CG
3	5	895	1	UCG
4	5.3	590	1	UG
5	6.1	601	2	UUCG
6	6.7	808	3	UUUCCCCG
7	8.1	919	1	UAG
8	9	919	1	AUG
9	9.4	777	2	UUAAG

Figure 4. MS chromatograms of *in vitro* transcribed (IVT) tRNAs after RNase T1 digestion. (**A**) Extracted ion chromatograms of tRNA$^{Val}_{AAC}$ IVT without stable isotopes (light ivt), with $^{15}N_3$-Cytidine or $^{15}N_5$-Guanosine. The sequences of the numbered peaks were determined by low resolution MS. The retention time (R_t), charge state and m/z values for the unlabeled and stable isotope labeled sequences are given in the table. (**B**) Total ion chromatogram of tRNA$^{Ser}_{UGA}$ IVT. The sequences of the numbered peaks were determined by low-resolution MS and are listed below the chromatogram.

signment of the ON sequences, which are derived from various sequences of the tRNA. As expected, we observe differences in the m/z value due to the stable isotopes in the ^{15}N containing fragments compared to the unlabeled fragments (Figure 4A). Thus, our method is capable of separating RNase T1 derived tRNA digests. In this context, we observed a low MS abundance of the 9 mer fragment (#4) compared to the 8 mer fragment (#6) from tRNA^{Val}. This is explained by the different amount of acetonitrile (ACN) at these retention times. While the 9-mer elutes at around 4.5% ACN, the 8-mer elutes later and with ∼ 25% ACN. With higher amounts of ACN, the ionization efficiency is increased and thus later eluting compounds have a higher signal intensity. When the gradient is eliminated by direct injection of ONs or elution at isocratic ACN conditions (Supplementary Figure S2), the abundance of all injected synthetic ONs is comparable and thus we conclude that the ionization efficiency is not majorly impacted by the composition of canonical nucleosides.

RNA and especially tRNA are heavily post-transcriptionally modified. To study the applicability of our method to native RNA, we treated total tRNA from HEK cell culture with RNase T1, separated the resulting fragments with our chromatographic method and analyzed the effluent by high-resolution MS. Here, the mass resolving power of the Orbitrap instrument is necessary to confirm the sequence and modification status of the observed tRNA derived ONs. With this approach, we could identify several modified ONs from total tRNA. The corresponding chromatograms and MS/MS spectra are shown in Figure 5.

ADAT2/3 deaminates tRNA$^{Val}_{AAC}$ at position 34 *in vitro*

Since tRNA modifying enzymes depend on a correctly folded tRNA substrate for their activity, we tested whether the SEC purified IVTs fold into the expected tRNA shape and are thus usable in *in vitro* modification assays. For these assays, we used human ADAT2/3 enzyme, which has been shown to catalyze the deamination of wobble adenosine at position 34 of *in vitro* transcribed tRNA$^{Val}_{AAC}$ to inosine (52). We incubated tRNA$^{Val}_{AAC}$ with purified ADAT2/3 expecting deamination of A34 to I34. The presumably deaminated tRNA was digested by RNase T1 and we screened for the tRNA sequence covering position 34, namely CCUAACACG and CCUIACACG (see Figure 6A). Surprisingly, we only found the unmodified sequence CCUAACACG and not the inosine containing sequence (Figure 6B). Due to this unexpected result, we digested an aliquot of the ADAT2/3 treated tRNA to nucleosides and switched to quantitative nucleoside analysis. While no inosine was detected in the untreated tRNA by nucleoside MS, we could detect an 8.0% conversion of adenosine to inosine per tRNA molecule in the ADAT2/3 modified transcript (Figure 6F). From this finding we conclude that our SEC puri-

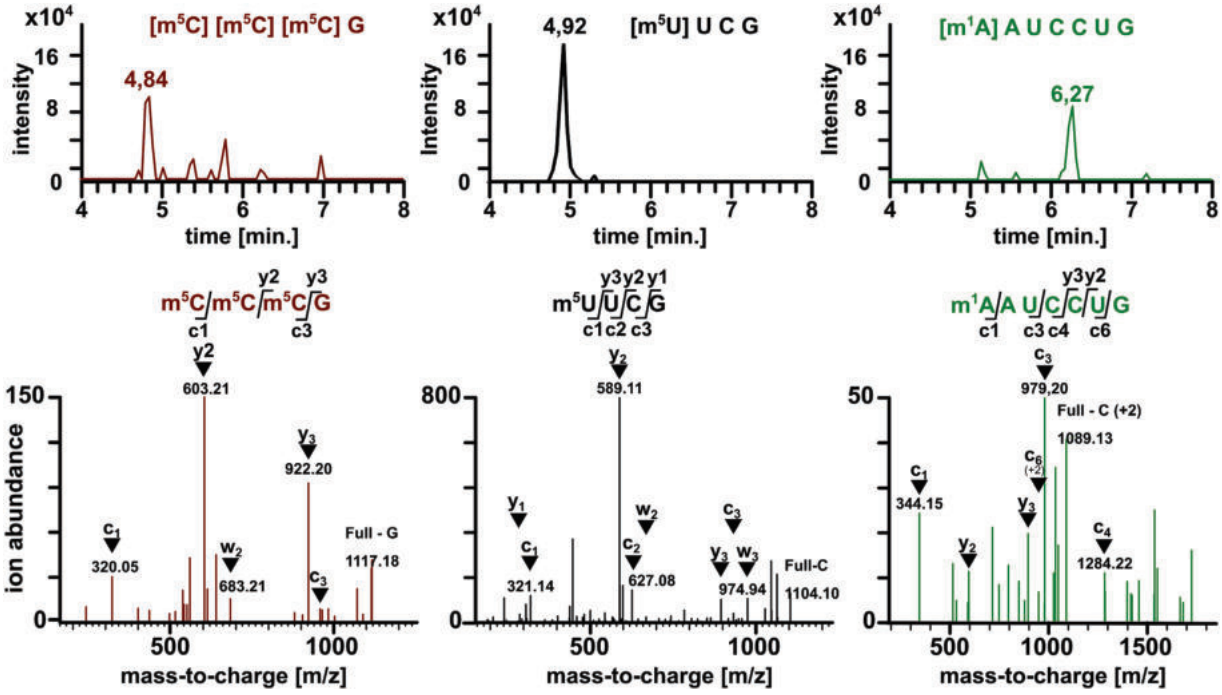

Figure 5. Extracted ion chromatograms and MS/MS spectra of modified RNA fragments from HEK 293 cell total tRNA digested with RNase T1. Spectra were recorded on a high-resolution Orbitrap instrument at CID energies of 35 eV. Fragments were assigned using (https://mods.rna.albany.edu/masspec/Mongo-Oligo) calculations from known modified tRNA sequences (acquired from modomics database).

fied tRNA folds correctly and is thus recognized as a substrate by the tRNA modifying enzyme ADAT2/3.

Intrigued by the absence of the inosine modified ON in the Oligo-MS analysis and with the goal to assign the location of the A-to-I editing in $tRNA^{Val}_{AAC}$, we utilized the synthetic 9-mer ONs presented in Figure 1A. These ONs represent the sequences expected from an RNase T1 digestion of $tRNA^{Val}_{AAC}$ (unmodified: CCUAACACG and modified: CCUIACACG). RNase T1 is a commonly used endoribonuclease, which specifically cleaves RNA after guanosine moieties. Guanosine and adenosine differ at position 6 and position 2 of their purine structures. Inosine and guanosine are identical at position 6 but differ at position 2. Due to the high chemical similarity of inosine and guanosine, we wondered whether RNase T1 is capable of inosine recognition and subsequent cleavage. A literature search revealed that the detection of inosine by sequencing is commonly done utilizing RNase T1 (53,54). In MS-based RNA modification studies, this knowledge is not yet widespread. To test the impact of RNase T1 on I containing RNA in MS, we incubated the A and I containing ONs with RNase T1 and analyzed the resulting mixture. For CCUAACACG, we observe one prominent peak which corresponds to the full-length ON and a second peak (less than 30%), corresponding to the 3′cleavage product ACACG (Supplementary Figure S11). In contrast, full-length CCUIACACG, is barely detectable after RNase T1 treatment. Instead, two new peaks are found (Supplementary Figures S10 and 11). One corresponds to the 3′ fragment ACACG and the other to the inosine containing 5′ cleavage product CCUI (Supplementary Figure S10). From our observation it is now clear, that RNase T1 cleaves both guanosine and inosine containing RNA sequences which impacts bottom-up oligonucleotide mass sepctrometry. Based upon our results, the substrate preference of RNase T1 can now be summarized as G > I > A.

In case of $tRNA^{Val}_{AAC}$, RNase T1 will then result in an additional cleavage after I34 (Supplementary Figure S12). We re-analyzed ADAT2/3 treated and untreated tRNA by oligonucleotide MS and screened for the newly identified ONs. We detected the CCUI fragment in unlabeled and ^{15}N-Cytidine-labeled tRNA digests after ADAT2/3 treatment, which indicates the A-to-I conversion of position 34 of the tRNA. Due to the similar mass of the CCUI and the CCUA fragment (1 Da), the result must be confirmed in the +1 charge state on a low resolution instrument or by high resolution MS. Analysis of the sample on the Orbitrap instrument revealed indeed formation of CCUI and thus confirms our findings from low resolution MS (Supplementary Figure S13). For quantification of the deamination reaction, we used the synthetic ON CCUIACACG and prepared an external calibration with its RNase T1 digest and re-analayzed the samples on the QQQ MS. We detected 7.6% inosine formation using this external calibration method (Figure 6C and D). Mass spectrometric quantification is ideally done using stable isotope labeled internal standards. Here, we used our $^{15}N_3$-cytidine labeled transcript of $tRNA^{Val}$ as the substrate and the unlabeled synthetic ON as the internal standard. With this method, we find a 6.2% conversion of A34 to I34 (Figure 6E). This result is 1.3-fold lower compared to our accurate nucleoside-MS method (Figure 6F), which is acceptable for most potential applications of our method. Our data suggests that our method is capable of absolute quantification, but fur-

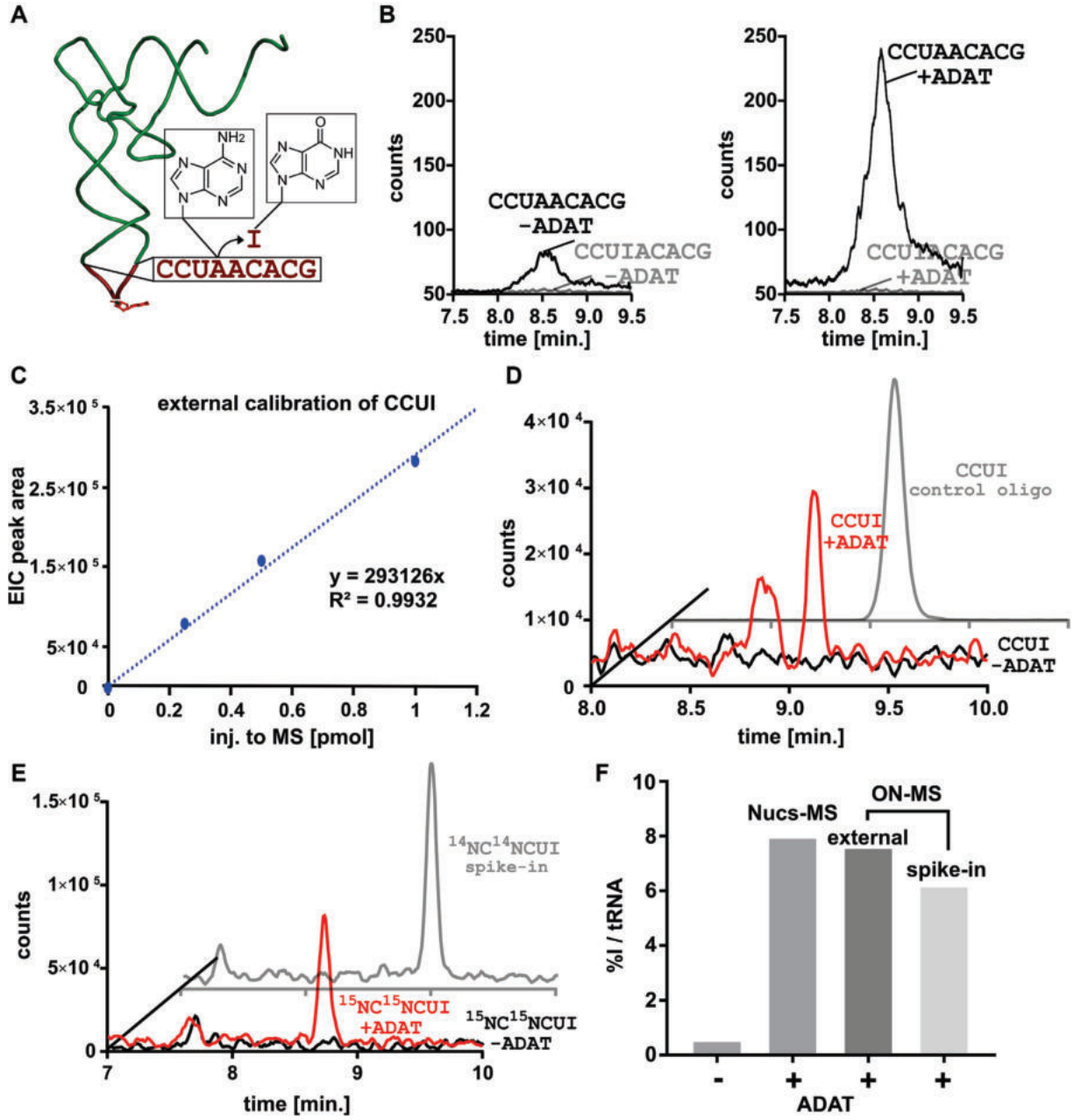

Figure 6. *In vitro* modification of $tRNA^{Val}_{AAC}$ by ADAT2/3. (**A**) 3D structure of $tRNA^{Val}_{AAC}$ in green. In red, the RNase T1 fragment of the ADAT2/3 target site is shown. (**B**) RNase T1 digest of untreated (left) and ADAT2/3 treated (right) $tRNA^{Val}_{AAC}$. In black, the signal for the resulting A-containing ON is shown and in gray, the signal of the I-containing ON. (**C**) Calibration curve of the CCUI fragment for external calibration quantification by low-resolution oligonucleotide MS. (**D**) Extracted ion chromatograms of RNase T1 digested $tRNA^{Val}_{AAC}$ before (black) and after (red) ADAT2/3 treatment. In gray the synthetic CCUI oligo is shown as a retention time control. (**E**) Extracted ion chromatograms of RNase T1 digested $^{15}N_3$-cytidine-labeled $tRNA^{Val}_{AAC}$ before (black) and after (red) ADAT2/3 treatment. In gray the signal of the spiked in synthetic CCUI oligo is shown. (**F**) Quantification of ADAT2/3 treated tRNA reveals the abundance of inosine per tRNA (%I / tRNA). Quantification was achieved by isotope dilution MS of a complete nucleoside digest (Nucs-MS), by external calibration and by isotope standard spike-in for oligonucleotide MS.

ther studies using internal standards as suggested by (39–43) must be performed to determine the accuracy and precision for a given biological context.

The activity of AlkB is sequence dependent

Another context which benefits from ON-MS on a low resolution MS, is *in vitro* modification/demodification experiments. Here, we applied our method to the analysis of 1-methyladenosine (m^1A)-modified ONs to study the demethylation by AlkB (8). With the goal to study the substrate specificity of AlkB by ON-MS, we designed three m^1A-containing ONs. In human tRNA, m^1A is commonly found at position 58. Sequence overlay of 13 random human tRNAs revealed the weight matrix of the nucleobases surrounding m^1A58 in human tRNAs (Supplementary Figure S14). The first ON (UUCG(m^1A)UUC), was designed to match this sequence surrounding m^1A58 from human tRNAs and is thus referred to as ON-human. The second ON reflects a mutated version of the ON-human, where three preserved bases are exchanged (ON-mutated, UAGG(m^1A)UUG). The last ON, ON-ribo, reflects the sequence surrounding the only possible m^1A site of *E. coli* 16S rRNA; (CGUC(m^1A)CAC). This site is found to be methylated in bacteria resistant to certain antibiotics (55). With this experiment, we wanted to evaluate the activity of AlkB toward these three ONs and whether a sequence dependence is observable.

All three ONs were incubated with 10 μM AlkB. The subsequent ON-MS analysis revealed the formation of demethylated ONs as shown in Figure 7A–C. The demethylated ONs elute at a later retention time compared to the respective m^1A modified ONs on our TEAA-free chromatography due to the lost positive charge of m^1A. For ON-human and ON-ribo, we observe only trace formation of the demethylated ON (Figure 7A/C). In contrast, we observed more demethylated ON for ON-mutated. At first glance, our observation indicates that the m^1A site of *E. coli* rRNA, and the ON with the sequence of eukaryotic tRNA m^1A58 are less suitable substrates to AlkB compared to the completely unnatural substrate, ON-mutated. However, without the use of stable isotope labeled internal standards, MS is non-quantitative and the data may not be interpreted in such a way.

To provide a quantitative method, we digested the AlkB treated and untreated ONs to nucleosides and performed nucleoside-MS with our established stable isotope dilution MS (38). For this purpose, we equilibrated the system for 1 h by flushing the instrument with our aqueous nucleoside-MS buffer and performed our quantitative nucleoside experiments. Before AlkB treatment, we find 0.23 m^1A per ON-human, 0.12 m^1A per ON-mutated and 0.19 m^1A per ON-ribo. At a low AlkB concentration (1 μM), we observe 9.8% demethylation for the ON-human ($P = 0.0067$). The ON-mutated shows 12.9% demethylation ($P < 0.0001$) and the ON-ribo 18.6% demethylation ($P < 0.0001$). The absolute quantification data is in stark contrast to the non-quantitative results observed by the oligonucleotide MS. Intriguingly, AlkB seems to prefer the only potential m^1A site found in bacteria, namely m^1A1408 of the 16 S rRNA. Our observation is confirmed by incubation of the same ONs

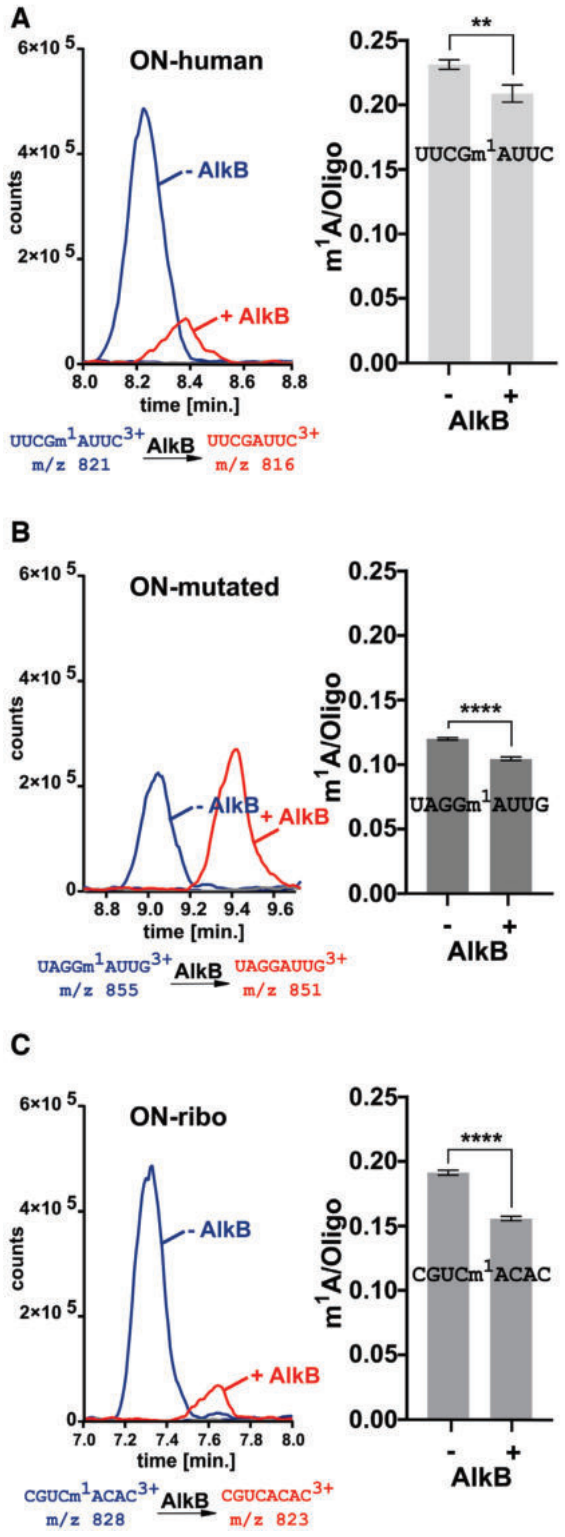

Figure 7. *in vitro* AlkB assay with different m^1A containing oligonucleotides (ON) (**A**–**C**) left: ON-MS of m^1A containing ONs after incubation with 10 μM AlkB and their assigned m/z values, charge states and sequences. (A–C) right: amount of m^1A per ON determined by isotope dilution MS of fully digested ONs with and without 1 μM AlkB treatment; bars represent the mean, error bars the standard deviation, $n = 3$ biological replicates, a two-tailed, unpaired students t-test was performed (ON-human: $P = 0.0067$; ON-mutated: $P < 0.0001$; ON-ribo: $P < 0.0001$).

Table 1. Advantages and Limitations of TEAA-free and other commonly used ON-MS methods

	TEAA-based ON-MS	TEAA free low-resolution MS	TEAA free high-resolution MS
Analysis of native RNA			
• Known sequence	yes	yes	yes
• Unknown sequence	yes	no	yes
Analysis of synthetic ONs	yes	yes	yes
Analysis of ONs longer 10 nts	no	no	no
Compatibility with small compound analyses	no	yes	yes
LC and MS contamination	yes	no	no
2D analysis (57)	yes	no	no
Sensitivity	Lower compared to nucleoside MS	Lower compared to nucleoside MS	Lower compared to nucleoside MS
Quantitative accuracy and precision	(39–43)	Not fully determined	Not fully determined

with higher amounts of AlkB (10 μM, Supplementary Figure S15).

DISCUSSION

In this manuscript we present a method for the separation of oligonucleotides and subsequent detection by oligonucleotide MS (ON-MS). While methods for ON-MS have been available for several years, key hurdles toward their broader application were the use of ion-pairing reagents such as TEAA and negative ionization. We have overcome these hurdles by successfully using a modified RP-18 column with a simple ammonium acetate buffer in combination with acetonitrile. These are common solvents for LC-MS instruments, which do not contaminate the system or interfere with subsequent analysis of other compounds. The broad applicability is demonstrated by our analyses of synthetic ONs, RNase T1 digestion derived RNA fragments of *in vitro* transcripts and native tRNA on both low and high-resolution mass spectrometers. A higher resolving power is required to distinguish mass differences of oligonucleotides, their sequence and modification content. A key challenge is that the nucleotide bases uridine and cytidine (and adenosine and inosine) have a mass difference of only 1 Da, which is already the resolution limit of the QQQ MS. For the analysis of unknown sequences, the mass accuracy and resolving power of the mass spectrometer must therefore be sufficient to resolve this difference (56). A second benefit of high resolution MS, is the determination of charge states even in MS/MS experiments which allows sequence determination and localization of modified nucleosides as demonstrated in Figure 5.

Nevertheless, low resolution MS instruments are valuable for the analysis of oligonucleotides of known sequence which have been prepared for e.g. *in vitro* analysis of RNA modifying (Figure 6) or demethylating enzymes (Figure 7).

A single sample run is <15 min and ONs below 10 nt are separated according to their chemistry, but the elution order is not predictable. Thus 2D analysis of sequences as shown by the Szostak lab is not possible with our method (57). In our hands, switching from ON-MS to sensitive nucleoside-MS is possible within 60 min to allow system and column equilibration. A comparison of our TEAA free and the common ON-MS method is given in Table 1.

For the analysis of RNA modifying enzymes, the preparation and use of *in vitro* transcribed RNA is highly useful. In this manuscript, we use ribozyme-fusion transcription of a 76 nts long tRNA and an 85 nts long tRNA. Instead of laborious PAGE purification, we use automated SEC. With nucleoside-MS (Figure 6F), we show that the thus purified tRNA is recognized and converted by ADAT2/3, which demonstrates the correct folding of the tRNA. With the goal to determine the position of A-I conversion, the produced tRNAs are digested by RNase T1 and the resulting fragments are separated by our TEAA-free chromatography. It is noteworthy that our chromatography allows the separation of ONs where only one oxygen is replaced with an amino group. The RNase T1 derived fragments are assigned by the detected m/z values in positive ionization mode by low resolution MS (Figures 4 and 6). For such *in vitro* experiments, there is no immediate need for high-resolution MS as the resulting fragments and MS/MS products can be predicted and resolved by low resolution MS. In case of the studied A-I conversion, the target fragment differs in only 1 Da, which can be resolved by low-resolution MS in the +1 charge state, but not in higher charge states. In such cases, the use of high-resolution instruments might become necessary for confirmation (Supplementary Figure S13).

We observe efficient cleavage after inosine by RNase T1 in the A-I converted tRNA and synthetic ONs as expected from approaches to sequence inosine containing RNA (53,54). This substrate diversity of RNase T1 is not commonly described in the bottom-up-MS literature but due to the high abundance of inosine in tRNA (6) and mRNA (58) it should be kept in mind when using RNase T1.

Altogether, we present various MS-based approaches for the bottom-up analysis of RNA which are easily transferrable to laboratories which avoided ON-MS in the past due to the problems introduced by ion-pairing reagents and negative ion mode. We demonstrate that switching from ON-MS to small compound analysis and back is possible after a brief equilibration procedure (Figures 6 and 7). With this, ON-MS can be routinely used on any LC-MS system to study RNA modifications in their sequence context.

DATA AVAILABILITY

https://mods.rna.albany.edu/masspec/Mongo-Oligo, http://modomics.genesilico.pl/.

SUPPLEMENTARY DATA

Supplementary Data are available at NAR Online.

ACKNOWLEDGEMENTS

S.K. is grateful to Agilent Technologies (Waldbronn, Germany) for providing test columns during method development. F.H. and S.K. thank Thomas Carell and his group for instrument time and scientific discussion.

FUNDING

Deutsche Forschungsgemeinschaft [CIPSMwoman, KE1943/3-1, KE1943/4-1 to S.K.]; National Science Foundation CAREER Award [1552126 to J.R, D.F.]. Funding for open access charge: Deutsche Forschungsgemeinschaft.

Conflict of interest statement. None declared.

REFERENCES

1. Jia,G., Fu,Y., Zhao,X., Dai,Q., Zheng,G., Yang,Y., Yi,C., Lindahl,T., Pan,T., Yang,Y.G. *et al.* (2011) N6-methyladenosine in nuclear RNA is a major substrate of the obesity-associated FTO. *Nat. Chem. Biol.*, **7**, 885–887.
2. Zheng,G., Dahl,J.A., Niu,Y., Fedorcsak,P., Huang,C.M., Li,C.J., Vagbo,C.B., Shi,Y., Wang,W.L., Song,S.H. *et al.* (2013) ALKBH5 is a mammalian RNA demethylase that impacts RNA metabolism and mouse fertility. *Mol. Cell*, **49**, 18–29.
3. Liu,F., Clark,W., Luo,G., Wang,X., Fu,Y., Wei,J., Wang,X., Hao,Z., Dai,Q., Zheng,G. *et al.* (2016) ALKBH1-Mediated tRNA demethylation regulates translation. *Cell*, **167**, 816–828.
4. Wei,J., Liu,F., Lu,Z., Fei,Q., Ai,Y., He,P.C., Shi,H., Cui,X., Su,R., Klungland,A. *et al.* (2018) Differential m(6)A, m(6)Am, and m(1)A demethylation mediated by FTO in the cell nucleus and cytoplasm. *Mol. Cell*, **71**, 973–985.
5. Dewe,J.M., Fuller,B.L., Lentini,J.M., Kellner,S.M. and Fu,D. (2017) TRMT1-Catalyzed tRNA modifications are required for redox homeostasis to ensure proper cellular proliferation and oxidative stress survival. *Mol. Cell Biol.*, **37**, e00214-17.
6. Gerber,A.P. and Keller,W. (1999) An adenosine deaminase that generates inosine at the wobble position of tRNAs. *Science*, **286**, 1146–1149.
7. Ramos,J., Han,L., Li,Y., Hagelskamp,F., Kellner,S.M., Alkuraya,F.S., Phizicky,E.M. and Fu,D. (2019) Formation of tRNA wobble inosine in humans is disrupted by a millennia-old mutation causing intellectual disability. *Mol. Cell Biol.*, **39**, e00203–19.
8. Ougland,R., Zhang,C.M., Liiv,A., Johansen,R.F., Seeberg,E., Hou,Y.M., Remme,J. and Falnes,P.O. (2004) AlkB restores the biological function of mRNA and tRNA inactivated by chemical methylation. *Mol. Cell*, **16**, 107–116.
9. Ueda,Y., Ooshio,I., Fusamae,Y., Kitae,K., Kawaguchi,M., Jingushi,K., Hase,H., Harada,K., Hirata,K. and Tsujikawa,K. (2017) AlkB homolog 3-mediated tRNA demethylation promotes protein synthesis in cancer cells. *Sci. Rep.*, **7**, doi:10.1038/srep42271.
10. Heiss,M. and Kellner,S. (2017) Detection of nucleic acid modifications by chemical reagents. *RNA Biol.*, **14**, 1166–1174.
11. Motorin,Y. and Helm,M. (2019) Methods for RNA modification mapping using deep sequencing: Established and new emerging technologies. *Genes (Basel)*, **10**, 35.
12. Takeda,N., Pomerantz,S.C. and McCloskey,J.A. (1991) Detection of ribose-methylated nucleotides in enzymatic hydrolysates of RNA by thermospray liquid chromatography-mass spectrometry. *J. Chromatogr.*, **562**, 225–235.
13. Kellner,S., Ochel,A., Thuring,K., Spenkuch,F., Neumann,J., Sharma,S., Entian,K.D., Schneider,D. and Helm,M. (2014) Absolute and relative quantification of RNA modifications via biosynthetic isotopomers. *Nucleic Acids Res.*, **42**, e142.
14. Kellner,S., Neumann,J., Rosenkranz,D., Lebedeva,S., Ketting,R.F., Zischler,H., Schneider,D. and Helm,M. (2014) Profiling of RNA modifications by multiplexed stable isotope labelling. *Chem. Commun. (Camb.)*, **50**, 3516–3518.
15. Dal Magro,C., Keller,P., Kotter,A., Werner,S., Duarte,V., Marchand,V., Ignarski,M., Freiwald,A., Muller,R.U., Dieterich,C. *et al.* (2018) A vastly increased chemical variety of RNA modifications containing a thioacetal structure. *Angew. Chem. Int. Ed. Engl.*, **57**, 7893–7897.
16. Limbach,P.A., Crain,P.F. and McCloskey,J.A. (1995) Molecular mass measurement of intact ribonucleic acids via electrospray ionization quadrupole mass spectrometry. *J. Am. Soc. Mass Spectrom.*, **6**, 27–39.
17. Guymon,R., Pomerantz,S.C., Crain,P.F. and McCloskey,J.A. (2006) Influence of phylogeny on posttranscriptional modification of rRNA in thermophilic prokaryotes: the complete modification map of 16S rRNA of Thermus thermophilus. *Biochemistry*, **45**, 4888–4899.
18. Hossain,M. and Limbach,P.A. (2009) Multiple endonucleases improve MALDI-MS signature digestion product detection of bacterial transfer RNAs. *Anal. Bioanal. Chem.*, **394**, 1125–1135.
19. Ikeuchi,Y., Kimura,S., Numata,T., Nakamura,D., Yokogawa,T., Ogata,T., Wada,T., Suzuki,T. and Suzuki,T. (2010) Agmatine-conjugated cytidine in a tRNA anticodon is essential for AUA decoding in archaea. *Nat. Chem. Biol.*, **6**, 277–282.
20. Meng,Z. and Limbach,P.A. (2005) Shotgun sequencing small oligonucleotides by nozzle-skimmer dissociation and electrospray ionization mass spectrometry. *Eur. J. Mass Spectrom. (Chichester)*, **11**, 221–229.
21. Hossain,M. and Limbach,P.A. (2007) Mass spectrometry-based detection of transfer RNAs by their signature endonuclease digestion products. *RNA*, **13**, 295–303.
22. Taucher,M., Ganisl,B. and Breuker,K. (2011) Identification, localization, and relative quantitation of pseudouridine in RNA by tandem mass spectrometry of hydrolysis products. *Int. J. Mass Spectrom.*, **304**, 91–97.
23. Taucher,M., Rieder,U. and Breuker,K. (2010) Minimizing base loss and internal fragmentation in collisionally activated dissociation of multiply deprotonated RNA. *J. Am. Soc. Mass Spectrom.*, **21**, 278–285.
24. Huang,T.Y., Liu,J. and McLuckey,S.A. (2010) Top-down tandem mass spectrometry of tRNA via ion trap collision-induced dissociation. *J. Am. Soc. Mass Spectrom.*, **21**, 890–898.
25. Taucher,M. and Breuker,K. (2010) Top-down mass spectrometry for sequencing of larger (up to 61 nt) RNA by CAD and EDD. *J. Am. Soc. Mass Spectrom.*, **21**, 918–929.
26. Taucher,M. and Breuker,K. (2012) Characterization of modified RNA by top-down mass spectrometry. *Angew. Chem. Int. Ed. Engl.*, **51**, 11289–11292.
27. Glasner,H., Riml,C., Micura,R. and Breuker,K. (2017) Label-free, direct localization and relative quantitation of the RNA nucleobase methylations m6A, m5C, m3U, and m5U by top-down mass spectrometry. *Nucleic Acids Res.*, **45**, 8014–8025.
28. Schurch,S. (2016) Characterization of nucleic acids by tandem mass spectrometry—the second decade (2004-2013): From DNA to RNA and modified sequences. *Mass Spectrom. Rev.*, **35**, 483–523.
29. Juhasz,P., Roskey,M.T., Smirnov,I.P., Haff,L.A., Vestal,M.L. and Martin,S.A. (1996) Applications of delayed extraction matrix-assisted laser desorption ionization time-of-flight mass spectrometry to oligonucleotide analysis. *Anal. Chem.*, **68**, 941–946.
30. Chou,C.W., Limbach,P.A. and Cole,R.B. (2002) Fragmentation pathway studies of oligonucleotides in matrix-assisted laser desorption/ionization mass spectrometry by charge tagging and H/D exchange. *J. Am. Soc. Mass Spectrom.*, **13**, 1407–1417.
31. Farand,J. and Beverly,M. (2008) Sequence confirmation of modified oligonucleotides using chemical degradation, electrospray ionization, time-of-flight, and tandem mass spectrometry. *Anal. Chem.*, **80**, 7414–7421.
32. Suzuki,T., Ikeuchi,Y., Noma,A., Suzuki,T. and Sakaguchi,Y. (2007) Mass spectrometric identification and characterization of RNA-modifying enzymes. *Methods Enzymol.*, **425**, 211–229.
33. Suzuki,T. and Suzuki,T. (2014) A complete landscape of post-transcriptional modifications in mammalian mitochondrial tRNAs. *Nucleic Acids Res.*, **42**, 7346–7357.

34. Popova,A.M. and Williamson,J.R. (2014) Quantitative analysis of rRNA modifications using stable isotope labeling and mass spectrometry. *J. Am. Chem. Soc.*, **136**, 2058–2069.
35. Lobue,P.A., Jora,M., Addepalli,B. and Limbach,P.A. (2019) Oligonucleotide analysis by hydrophilic interaction liquid chromatography-mass spectrometry in the absence of ion-pair reagents. *J. Chromatogr. A*, **1595**, 39–48.
36. Weng,G., Sun,B., Liu,Z., Wang,F. and Pan,Y. (2019) Analysis of oligonucleotides by ion-pair reversed-phase liquid chromatography coupled with positive mode electrospray ionization mass spectrometry. *Anal. Bioanal. Chem.*, **411**, 4167–4173.
37. Bruckl,T., Globisch,D., Wagner,M., Muller,M. and Carell,T. (2009) Parallel isotope-based quantification of modified tRNA nucleosides. *Angew. Chem. Int. Ed. Engl.*, **48**, 7932–7934.
38. Borland,K., Diesend,J., Ito-Kureha,T., Heissmeyer,V., Hammann,C., Buck,A.H., Michalakis,S. and Kellner,S. (2019) Production and application of stable Isotope-Labeled internal standards for RNA modification analysis. *Genes (Basel)*, **10**, 26.
39. Waghmare,S.P. and Dickman,M.J. (2011) Characterization and quantification of RNA post-transcriptional modifications using stable isotope labeling of RNA in conjunction with mass spectrometry analysis. *Anal. Chem.*, **83**, 4894–4901.
40. Kung,A.W., Kilby,P.M., Portwood,D.E. and Dickman,M.J. (2018) Quantification of dsRNA using stable isotope labeling dilution liquid chromatography/mass spectrometry. *Rapid Commun. Mass Spectrom.*, **32**, 590–596.
41. Li,S. and Limbach,P.A. (2012) Method for comparative analysis of ribonucleic acids using isotope labeling and mass spectrometry. *Anal. Chem.*, **84**, 8607–8613.
42. Paulines,M.J. and Limbach,P.A. (2017) Stable isotope labeling for improved comparative analysis of RNA digests by mass spectrometry. *J. Am. Soc. Mass Spectrom.*, **28**, 551–561.
43. Taoka,M., Nobe,Y., Hori,M., Takeuchi,A., Masaki,S., Yamauchi,Y., Nakayama,H., Takahashi,N. and Isobe,T. (2015) A mass spectrometry-based method for comprehensive quantitative determination of post-transcriptional RNA modifications: the complete chemical structure of Schizosaccharomyces pombe ribosomal RNAs. *Nucleic Acids Res.*, **43**, e115.
44. Chionh,Y.H., Ho,C.H., Pruksakorn,D., Ramesh Babu,I., Ng,C.S., Hia,F., McBee,M.E., Su,D., Pang,Y.L., Gu,C. *et al.* (2013) A multidimensional platform for the purification of non-coding RNA species. *Nucleic Acids Res.*, **41**, e168.
45. Hauenschild,R., Tserovski,L., Schmid,K., Thuring,K., Winz,M.L., Sharma,S., Entian,K.D., Wacheul,L., Lafontaine,D.L., Anderson,J. *et al.* (2015) The reverse transcription signature of N-1-methyladenosine in RNA-Seq is sequence dependent. *Nucleic Acids Res.*, **43**, 9950–9964.
46. Kanduc,D. (1994) Fractionation of rat liver tRNA by reversed-phase high performance liquid chromatography: isolation of Iso-tRNAs(Pro). *Prep. Biochem.*, **24**, 167–174.
47. Riml,C., Glasner,H., Rodgers,M.T., Micura,R. and Breuker,K. (2015) On the mechanism of RNA phosphodiester backbone cleavage in the absence of solvent. *Nucleic Acids Res.*, **43**, 5171–5181.
48. Gaston,K.W. and Limbach,P.A. (2014) The identification and characterization of non-coding and coding RNAs and their modified nucleosides by mass spectrometry. *RNA Biol.*, **11**, 1568–1585.
49. Wyatt,J.R., Chastain,M. and Puglisi,J.D. (1991) Synthesis and purification of large amounts of RNA oligonucleotides. *Biotechniques*, **11**, 764–769.
50. Heiss,M., Reichle,V.F. and Kellner,S. (2017) Observing the fate of tRNA and its modifications by nucleic acid isotope labeling mass spectrometry: NAIL-MS. *RNA Biol.*, **14**, 1260–1268.
51. Reichle,V.F., Weber,V. and Kellner,S. (2018) NAIL-MS in E. coli determines the source and fate of methylation in tRNA. *Chembiochem*, **19**, 2575–2583.
52. Torres,A.G., Pineyro,D., Rodriguez-Escriba,M., Camacho,N., Reina,O., Saint-Leger,A., Filonava,L., Batlle,E. and Ribas de Pouplana,L. (2015) Inosine modifications in human tRNAs are incorporated at the precursor tRNA level. *Nucleic Acids Res.*, **43**, 5145–5157.
53. Cattenoz,P.B., Taft,R.J., Westhof,E. and Mattick,J.S. (2013) Transcriptome-wide identification of A >I RNA editing sites by inosine specific cleavage. *RNA*, **19**, 257–270.
54. Morse,D.P. and Bass,B.L. (1997) Detection of inosine in messenger RNA by inosine-specific cleavage. *Biochemistry*, **36**, 8429–8434.
55. Macmaster,R., Zelinskaya,N., Savic,M., Rankin,C.R. and Conn,G.L. (2010) Structural insights into the function of aminoglycoside-resistance A1408 16S rRNA methyltransferases from antibiotic-producing and human pathogenic bacteria. *Nucleic Acids Res.*, **38**, 7791–7799.
56. Thomas,B. and Akoulitchev,A.V. (2006) Mass spectrometry of RNA. *Trends Biochem. Sci.*, **31**, 173–181.
57. Bjorkbom,A., Lelyveld,V.S., Zhang,S., Zhang,W., Tam,C.P., Blain,J.C. and Szostak,J.W. (2015) Bidirectional direct sequencing of noncanonical RNA by Two-Dimensional analysis of mass chromatograms. *J. Am. Chem. Soc.*, **137**, 14430–14438.
58. Paul,M.S. and Bass,B.L. (1998) Inosine exists in mRNA at tissue-specific levels and is most abundant in brain mRNA. *EMBO J.*, **17**, 1120–1127.

Analysis of the epitranscriptome with ion-pairing reagent free oligonucleotide mass spectrometry

Felix Hagelskamp and Stefanie Kellner*
Goethe-University Frankfurt, Institute of Pharmaceutical Chemistry, Frankfurt, Germany
*Corresponding author: e-mail address: kellner@pharmchem.uni-frankfurt.de

Contents

Abstract

RNA modifications gain growing attention as a new frontier in the life sciences but with the rise of RNA vaccines also in biomedical drug development. Impeccable characterization of RNA modifications within their sequence context remains an analytical challenge. Oligonucleotide mass spectrometry (ON-MS), an approach similar to bottom-up proteome analysis, is capable of defining a short 5–15 nucleotide sequence context of an RNA modification while delivering information on the chemical character of the modified nucleotide.

Methods in Enzymology
ISSN 0076-6879
https://doi.org/10.1016/bs.mie.2021.06.024

Commonly, ON-MS requires the use of ion pairing reagents for ON separation which is not compatible with most other MS-based applications and only few laboratories run dedicated MS instruments for the task.

Here, we present an ON-MS technique which is independent of ion pairing reagents and can be used on any available mass spectrometer without risking its sensitivity for other analytes. In this chapter, we describe the experiments necessary for ON-MS method development, ON-MS application to native and synthetic RNAs and finally a guideline for data analysis.

1. Introduction

Ribonucleic acid (RNA) executes important functions in translation or gene regulation and needs an expanded set of nucleosides to allow this functionality. For these tasks, RNA is chemically modified by specific enzymes at defined positions. To investigate the effect and function of RNA modifications, mass spectrometry (MS) is a commonly accepted choice.

Depending on the RNA digestion prior to MS, two major principles of MS analysis are distinguished.

For nucleoside-MS, a complete enzymatic digestion of RNA to the nucleoside level is usually performed with endonucleases, phosphodiesterases and phosphatases, such as benzonase, snake venom phosphodiesterase and calf-intestinal phosphatase (CIP) (Crain, 1990) (see Fig. 1A). Nucleoside-MS can give information on the chemical structure of modifications at unbelievable low abundance, but nucleoside analysis has several disadvantages that should be noted. Due to the complete loss of sequence information, the location of a modified nucleoside is unknown and therefore contamination with other RNA obscures quantitative results by, *e.g.*, dilution with differently modified RNA. Another obstacle is the creation of artifacts through the digestion protocol (Jora et al., 2021).

In the bottom-up approach, a single RNA or mixture of RNA sequences is digested into oligonucleotides (ON), resolved by chromatography and then analyzed by tandem mass spectrometry (MS/MS). This approach was first introduced to the scientific community by McCloskey and co-workers (Kowalak, Pomerantz, Crain, & McCloskey, 1993). In general, RNA is enzymatically digested using site-specific ribonucleases (RNases), which are specific to certain nucleotides such as RNase T1 (guanosine-specific) (Donis-Keller, Maxam, & Gilbert, 1977), cusavitin

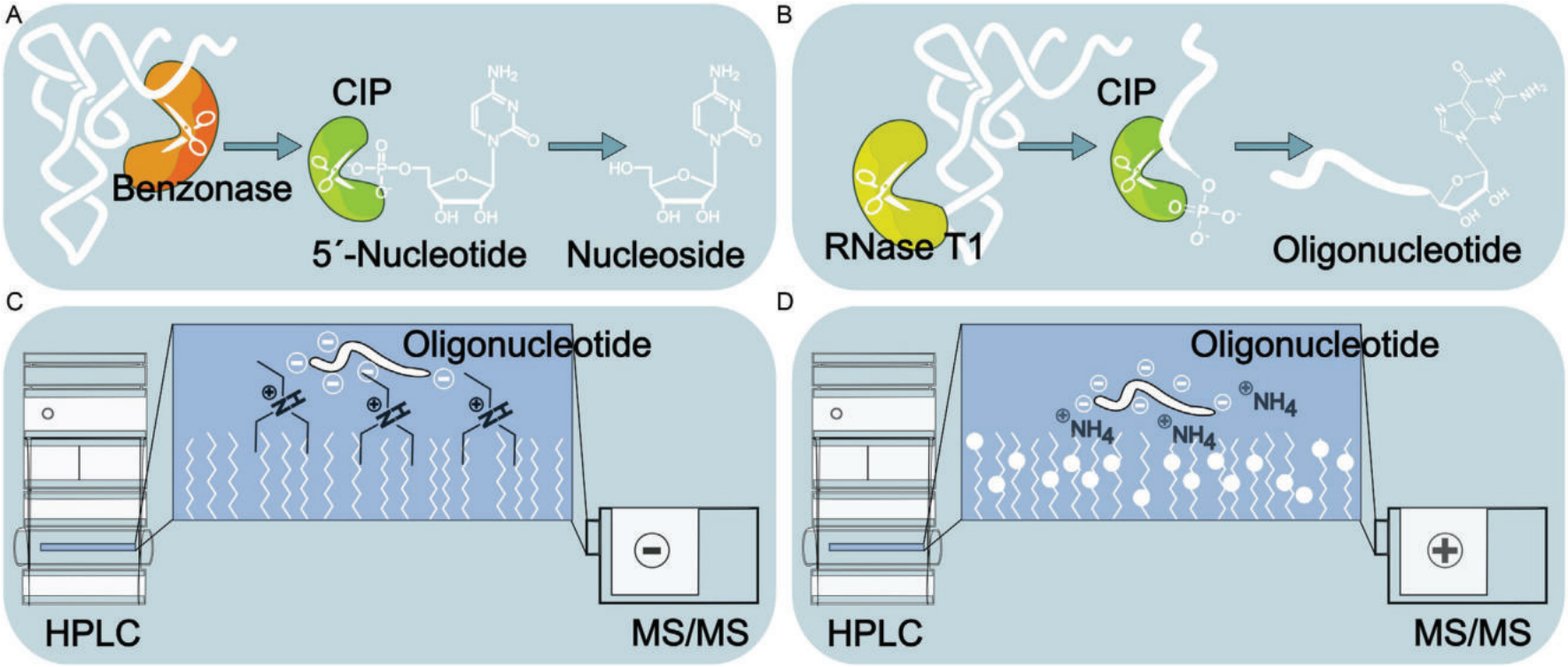

Fig. 1 Different types of RNA-MS analytics. (A) In a nucleoside-MS measurement, nucleases, *e.g.*, benzonase, hydrolyze RNA to single 5′-nucleotides which can be dephosphorylated by the help of phosphatases, *e.g.*, CIP, to nucleosides. (B) In the oligonucleotide-MS (ON-MS) setup, selective endonucleases, *e.g.*, RNase T1, cleave the RNA at specific sites. (C) Oligonucleotides (ON) of different length are commonly separated by ion-pairing chromatography. Here, a C18 reverse-phase column with triethylammonium modifier is shown. ONs are detected by negative ionization mass spectrometry. (D) Modified C18 phases in combination with ammonium acetate buffers allow for sensitive detection of ONs in positive ionization mode.

(cytidine-specific) (Addepalli, Venus, Thakur, & Limbach, 2017) or MC1 (uridine-specific) (Addepalli, Lesner, & Limbach, 2015). They produce sequence-specific ONs from 5mer to 15mer in length that can be dephosphorylated by CIP to yield less complex MS-data (Fig. 1B). Recently, combined approaches with two or more RNases acting on the RNA have been published and an increased sequence coverage up to 85% has been reported for *E. coli* 23S rRNA and 75% for total tRNA (Thakur, Estevez, Lobue, Limbach, & Addepalli, 2020).

Due to the relatively high hydrophilicity by the multiple negatively charged phosphate backbone, ON chromatography uses ion-pairing reagents as mobile phase modifiers to improve the retention, sensitivity and ionization in MS analysis (IP-LC, Fig. 1C; Note: sensitivity is only increased in negative ionization mode) (Biba, Foley, & Welch, 2017; Li, El Zahar, Saad, van der Hage, & Bartlett, 2018). Common ion pairing reagents comprise triethylammonium acetate (TEAA) and hexafluoroisopropanol (HFIP). After separation of ONs, detection is facilitated by high resolution mass spectrometers in negative ionization mode. Although ON-MS is a powerful technique for epitranscriptome analysis, it has two major drawbacks: first, ion-pairing reagents cause ion suppression, which is minimized when operating the MS negative mode. Second, the modifiers contaminate the mass spectrometer, especially for positive ionization mode as commonly used for bottom-up proteomics. The thus necessary use of dedicated MS instruments limits the number of research groups interested in ON-MS due to the tremendous costs and lower versatility of dedicated mass spectrometers.

Our ON-MS approach overcomes these problems with ion-pairing reagent free chromatography and MS compatible conditions, *e.g.*, aqueous ammonium acetate buffers and acetonitrile (Fig. 1D). With our system, we obtain satisfying chromatographic resolution to separate complex biological samples while running the MS in positive ionization mode. With our method, ON-MS can be used on most LC-MS set-ups. As an example, we monitor enzymatic reactions such as single base demethylations in a sequence dependent fashion (Hagelskamp et al., 2020).

2. Materials

Prepare all solutions and buffers in ultrapure type I water. All steps starting from RNA isolation should be performed with RNase free equipment. For LC-MS/MS analysis, salts and reagents of LC-MS grade must be used.

2.1 Cell culture

- HEK 293 and HeLa ACC 57 cells (DSMZ, Braunschweig, Germany)
- Dulbecco's Modified Eagle Media (DMEM) powder D5030 (Sigma-Aldrich, Munich, Germany)
- non-dialyzed FBS (Biowest, Nuaillé, France)
- phenol red powder P3532 (Sigma-Aldrich, Munich, Germany)
- growth medium: DMEM D5030, 10% non-dialyzed FBS, 4.5 g/L glucose, 3.7 g/L $NaHCO_3$, 0.584 g/L L-glutamine, 0.15 g/L L-methionine, 0.0159 g/L phenol red
- single-use vacuum filter 99950 (TPP, Trasadingen, Switzerland)
- Heracell Vios 160i CO_2 incubator (Thermo Fisher Scientific, San Jose, CA, USA)

2.2 RNA isolation

- TRI reagent (Sigma-Aldrich, Munich, Germany)
- Chloroform (Carl Roth, Karlsruhe, Germany)

2.3 RNA purification

- HPLC system for SEC: any isocratic system with UV detection, *e.g.*, Agilent 1100
- SEC columns: for tRNA; AdvanceBio SEC 300 Å, 2.7 μm, 7.8 × 300 mm and for purification of *in vitro* transcribed tRNA; AdvanceBio SEC 130 Å, 2.7 μm, 7.8 × 300 mm (Agilent, Waldbronn, Germany)
- SEC buffer: 0.1 M NH_4OAc (7.7 g/L)
- Implen Nanophotometer NP 80 (Implen, Munich, Germany)

2.4 PCR and *in vitro* transcription

- Phusion High-Fidelity DNA polymerase with Phusion Buffer HF (New England Biolabs, Ipswich, MA, USA)
- Deoxynucleotide (dNTP) solution mix (New England Biolabs, Ipswich, MA, USA)
- TranscriptAid T7 High Yield Transcription kit (Thermo Fisher Scientific, Waltham, MA, USA)
- Set of 4 ^{15}N-labeled rNTPs lithium salt solution (Silantes, Munich, Germany)
- Labcycler Basic (SensoQuest, Göttingen, Germany)
- Shaking incubator TS Basic (CellMedia, Elsteraue, Germany)
- DNase I (RNase-free) (New England Biolabs, Ipswich, MA, USA)

2.5 AlkB *in vitro* assay

- Bacterial AlkB protein (Peak Proteins, Cheshire, UK)
- *in vitro* assay buffers: TRIS HCl, KCl, L-ascorbate, α-ketoglutarate, $MgCl_2$, $Fe(II)(NH_4)_2(SO_4)_2 \times 6\ H_2O$ (see **Note 1**)

2.6 Primers, oligonucleotides and templates

All used primers, oligonucleotides and DNA templates are listed in Table 1.

2.7 Digestion

- Ribonuclease T1 (Sigma-Aldrich, Munich, Germany),
- Molecular weight 10 kDa cut-off filter (VWR, Driesch, Germany),
- CIP (P0114–10KU, Sigma-Aldrich, Munich, Germany),
- NaCl, TRIS HCl (Sigma-Aldrich, Munich, Germany).

2.8 LC-MS

- High resolution LC-MS: *e.g.*, Dionex Ultimate 3000 HPLC system coupled with LTQ Orbitrap XL equipped with a heated electrospray ionization (HESI) source (Thermo Finnigan, San Jose, USA)
- High sensitivity LC-MS/MS: *e.g.*, Agilent 1290 Infinity II with diode array detector (DAD) and G6470A triple quadrupole, electrospray ionization (ESI-MS) (Agilent, Waldbronn, Germany)
- Chromatography: Phenomenex®, Synergi Fusion-RP 100 Å, 2.5 μm, 150 × 2.0 mm column (Phenomenex, Torrance, USA)
- LC-MS buffer A for nucleoside-MS: 5 mM NH_4OAc, pH 5.3. (0.3854 g NH_4OAc, 65 μL glacial acetic acid, bring to a final volume of 1 L in ultrapure water).
- LC-MS buffer A for ON-MS: 10 mM NH_4OAc, pH 7 (0.7708 g NH_4OAc, bring to a final volume of 1 L in ultrapure water).
- LC-MS vials with 200 μL volume capacity (VWR, Radnor, USA)

3. Methods

3.1 General workflow of an oligonucleotide (ON)-MS experiment

An ON-MS experiment can be divided into several categories. The variety of RNA substrates ranges from native RNA to synthetic ONs or *in vitro* transcribed RNA. ONs smaller than 10 nucleotides can be directly measured to study, *e.g.*, RNA-acting enzymes, while longer RNAs require

Table 1 All DNA and RNA oligonucleotides were delivered in a stock concentration of 100 μM in water and are listed in the table below.

ON	Type	Name	Sequence (5′ → 3′)	Manufacturer
ON 1	DNA	Primer with T7 promoter sequence	CGC GCG AAG CTT AAT ACG ACT CAC TAT A	IBA (Göttingen, Germany)
ON 2	DNA	tRNA Ser UGA primer	TGG CGT AGT CGG C	IBA
ON 3	DNA	tRNA Val AAC primer	TGG TGT TTC CGC CTG	IBA
ON 4	DNA	T7 template tRNA Ser UGA	TGG CGT AGT CGG CAG GAT TCG AAC CTG CGC GGG GAG ACC CCA ATG GAT TTC AAG TCC ATC GCC TTA ACC ACT CGG CCA CGA CTA CGA CGG TAC CGG GTA CCG TTT CGT CCT CAC GGA CTC ATC AGG TAG TCG TGT CTC CCT ATA GTG AGT CGT ATT	IBA
ON 5	DNA	T7 template tRNA Val AAC	TGG TGT TTC CGC CTG GTT TTG ATC CAG GGA CCT TTC GCG TGT TAG GCG AAC GTG ATA ACC ACT ACA CTA CGG AAA CGA CGG TAC CGG GTA CCG TTT CGT CCT CAC GGA CTC ATC AGG TTT CCG TAT CTC CCT ATA GTG AGT CGT ATT	IBA
ON 6	RNA	5-mer	ACU UG	IBA
ON 7	RNA	8-mer	UUU CCC CG	IBA
ON 8	RNA	10-mer	AAA UCC AUU G	IBA
ON 9	RNA	8mer m^1A oligo	UUC Gm^1AU UC	IBA
ON 10	RNA	8mer m^1A oligo	UAG Gm^1AU UG	IBA
ON 11	RNA	8mer m^1A oligo	CGU Cm^1AC AC	IBA

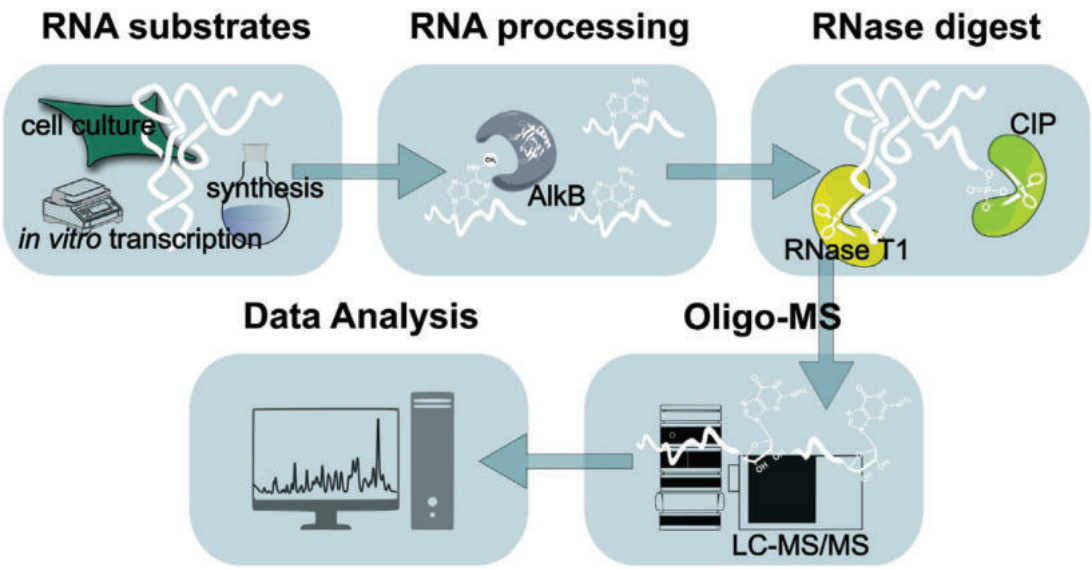

Fig. 2 General workflow of an ON-MS experiment. RNA from either mammalian cell culture, *in vitro* transcription or chemical synthesis serve as substrates for enzymatic assays or size exclusion chromatography. To obtain ONs in a length suitable for mass spectrometry, the RNA is hydrolyzed with specific enzymes such as RNase T1 and CIP (calf-intestinal phosphatase).

endonuclease treatment prior to ON-MS. *In silico* endonuclease fragmentation, MS1 and MS2 spectra prediction is possible using Mongo Oligo (freeware provided by the KU Leuven, Belgium) or RNAModMapper (Yu, Lobue, Cao, & Limbach, 2017) (see Fig. 2).

3.1.1 Considerations for biological samples (RNA substrates)

If a modification site is to be mapped in an ON, enough starting material and high modification density is required. For our low resolution QQQ system, we need 200 ng of sequence-defined ONs per analysis or 10 µg of purified total tRNA for tRNA isoacceptor purification and subsequent ON-MS analysis. For method development, commercially available ONs with defined length and sequence and known modification sites are a convenient starting point. For native tRNA analysis, pooling of multiple cell culture flasks with high seeding areas might be required to obtain sufficient material.

Subsequent quantification of ONs is possible if a stable isotope labeled internal standard (SILIS) is available. Native SILIS RNA can be produced in bacteria, yeast (Borland et al., 2019) or cell culture (Heiss, Hagelskamp, Marchand, Motorin, & Kellner, 2021) by feeding stable isotope labeled nutrients. Another option is *in vitro* transcription in the presence of ^{15}N- or ^{13}C-GTP. SILIS-RNA and SILIS-ONs are added to the samples of interest prior to endonuclease treatment and MS analysis.

3.1.2 Considerations for RNA digestion

Choosing the correct digestion strategy is crucial: RNase T1 cuts at the 3′ end of every guanosine moiety, but also after modified residues such as 2-methylguanosine or inosine. If the modification status of an RNA sample is unclear, modified residues might lead to more fragments than expected. Guanosine-rich sequences result in smaller ONs which are more difficult to analyze with our chromatography optimized for 5–10 mer long ONs. Other unselective RNases might generate oligonucleotides too short when they cut the RNA more often. Phosphatases which remove 5′ or 3′ phosphates are recommended, as they simplify MS spectra and MS/MS fragmentation patterns.

3.1.3 Considerations for mass spectrometry

ON-MS is currently not suitable for *de novo* sequencing of RNA. Thus, the sequence of the RNA of interest must be known prior to ON-MS. If only little starting material, *e.g.*, less than 200 ng of purified RNA is available, nucleoside-MS with a sensitive triple quadrupole MS is advised to determine the chemical nature of the modified RNA. If sufficient sample material is available, and the sequence of the purified RNA is known, ON-MS is a powerful tool for site-specific analysis of RNA modifications. Targeted MS/MS approaches with generation of collision-induced dissociated fragments reveal and confirm the surrounding sequence and should be preferred over single stage MS analysis. High-resolution MS analysis is advised for experiments which involve RNA modifications with minor mass deviation from the canonical nucleotides, *e.g.*, inosine.

3.2 RNA substrates

This ion-pairing reagent-free ON-MS approach requires RNA input material derived from different origins, which can be divided into three different classes (cell culture, *in vitro* transcription, chemical synthesis, each described below):

3.2.1 Cell culture

1. HEK 293 T and HeLa ACC 57 cells are cultured in Dulbecco's Modified Eagle Medium (DMEM) supplemented with sodium hydrogencarbonate, phenol red, glucose, L-glutamine and fetal calf serum (see Table 2) in an incubator with 10% CO_2 atmosphere
2. To passage the mammalian cells cultured in T25 flasks, after aspiration of the growth medium 5 mL of PBS is added

Table 2 Pipetting scheme for 1 L of normal growth medium (before use, the medium is sterile filtered through a disposable vacuum filter).

Compound	Stock concentration	Weight
DMEM powder		8.4 g
$NaHCO_3$		3.7 g
L-glutamine	15 g/L	0.584 g
Phenol red		0.0159 g
Glucose	225 g/L	4.5 g
FCS		100 mL
Ultrapure water		ad 1 L

3. Gently shake the flask, aspirate again to remove remaining dead, non-adherent cells
4. If RNA should be isolated, continue with RNA Isolation (Section 3.3.1). If cells should be maintained and splitted, incubate the culture with 1 mL TrypLE Express Trypsin solution at 37 °C for not longer than 30 s (HEK 293 T) and 2 min (HeLa ACC 57) to yield detached cells
5. Add the desired amount of pre-warmed medium, mix thoroughly without generation of air bubbles and transfer 1 mL into a falcon
6. Centrifuge with 1300 × *g* at room temperature for 3 min
7. Aspirate the supernatant, resuspend the cell pellet in 5 mL growth medium and transfer it into a new T25 flask

3.2.2 T7 in vitro *transcribed RNA as substrate or internal standard*

First, a polymerase chain reaction (PCR) is used to produce a DNA template of the tRNA of interest in an appropriate amount. The components of the PCR are as follows: a primer with the T7 promoter sequence, a DNA template of the entire tRNA sequence with an elongation that will later represent a neat T7 polymerase binding, transcription start site and the hammerhead ribozyme and a PCR primer for the other end of the fusion product (see Fig. 3).

1. In two different PCR tubes (2 reactions), Phusion buffer HF 5 ×, ON 1, 3 and 5 for $tRNA^{Val}_{AAC}$ or ON 1, 2, 4 for $tRNA^{Ser}_{UGA}$, ultrapure water, dNTP-mix and Phusion polymerase are combined (see Table 3).
2. After addition of the Phusion polymerase as last compound, it is essential to mix the whole solution by pipetting up and down with a suitable pipet and immediately move on with the following step.

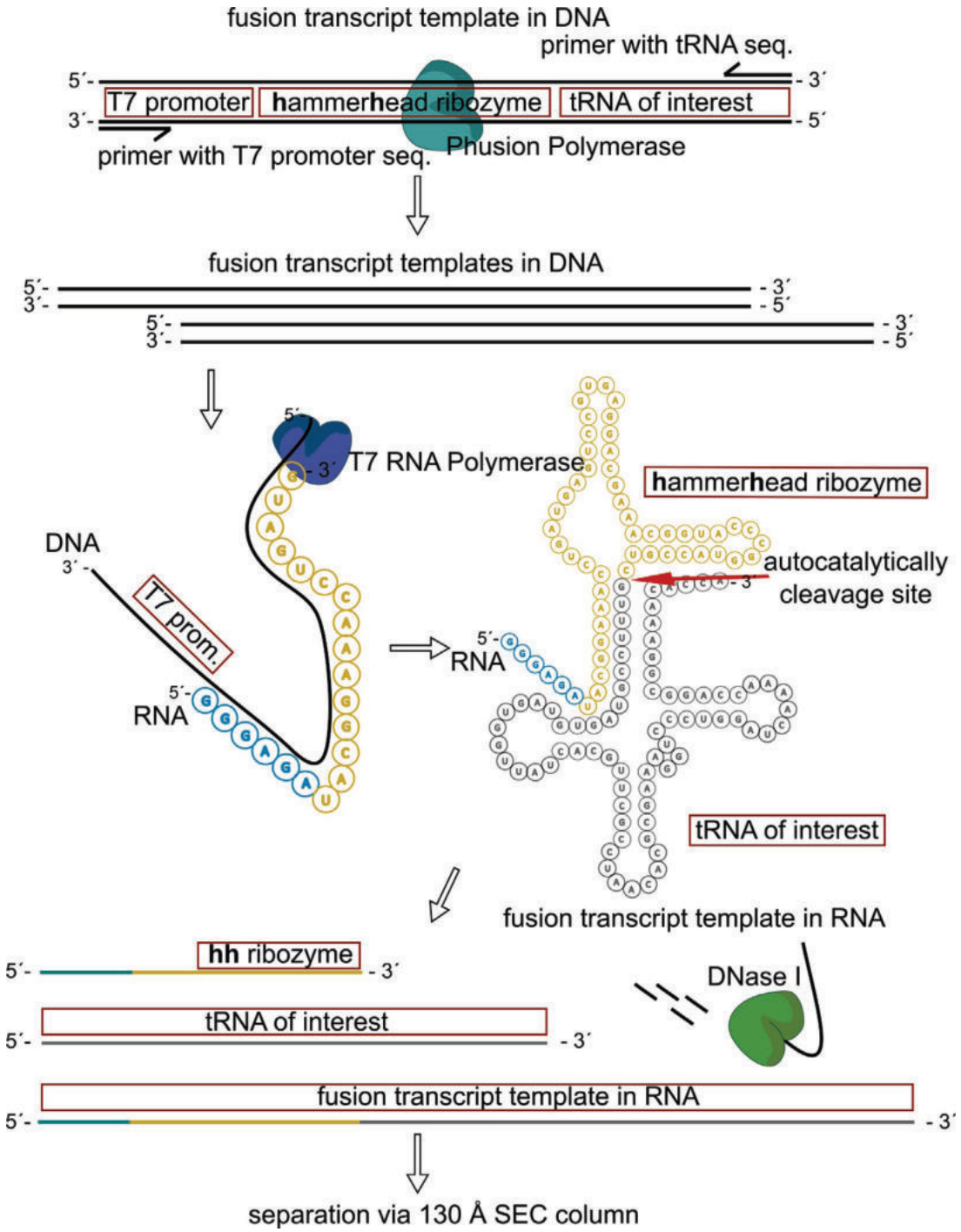

Fig. 3 *In vitro* transcription of a tRNA of interest. First, the DNA template with its encoded sequence regions for the T7 promoter region (T7 prom), hammerhead ribozyme (hh) and the tRNA sequence is amplified by PCR. In a next step, RNA is generated with T7 RNA Polymerase, autocatalytically cleaved and the DNA is digested by DNase I. The created RNA is purified by a SEC 130 Å column.

3. Place both PCR tubes in the LabCycler and run the in Table 4 described program.
4. Combine the contents from both PCR tubes (2 reactions).

Next, process the PCR reaction mixture with T7 *in vitro* transcription kit. If one or more canonical nucleosides should carry a stable isotope label,

Table 3 Pipetting scheme for PCR reaction mixture (50 µL ≡ 1 reaction).

Compound	Stock concentration	Volume
Phusion Buffer HF	5 ×	10 µL
primer with prom.(ON 1)	4 µM	12 µL
tRNA PCR primer(ON 2,3)	4 µM	12 µL
tRNA template(ON4,5)	0.1 µg/µL	1 µL
Phusion Polymerase		1 µL
dNTP mix		1 µL
Ultrapure water		fill up to 50 µL

Table 4 PCR program for *in vitro* transcribed tRNA with two reactions

Temperature	Time	Cycles
92 °C	2 min	1
92 °C	15 s	30
47 °C	20 s	30
72 °C	30 s	30 back to 92 °C step (row 2)
72 °C	10 min	1
4 °C (see Note 2)	Infinity	1

Thermocycler parameters: lid 96 °C, preheating pressure 30 N and block temperature preheating 25 °C.

unlabeled rNTPs should be exchanged by labeled rNTPs at this step. Each of the four rNTP can be exchanged separately (Fig. 4).

5. Combine in a microtube, T7 transcription buffer 10 ×, magnesium chloride, ultrapure water, all four canonical rNTPs as ^{15}N or ^{14}N variant and T7 enzyme mix (see Table 5) (see **Note 3**).
6. Place the mix for 2 h at 37 °C and 300 rpm in a shaking incubator.
7. After 2 h of incubation, add 1.5 µL enzyme mix and 5 µL of 50 mM $MgCl_2$ (as a cofactor for a functional polymerase). A slight blur indicates a pyrophosphate precipitate which is a good indicator that the transcription works (see **Note 4**).
8. Perform the in step 7 described procedure two more times. In total, the T7 transcription requires at least 8 h.
9. Centrifuge the 8 h incubated *in vitro* transcription mix at room temperature with a low-speed bench-top centrifuge to obtain a pyrophosphate pellet.

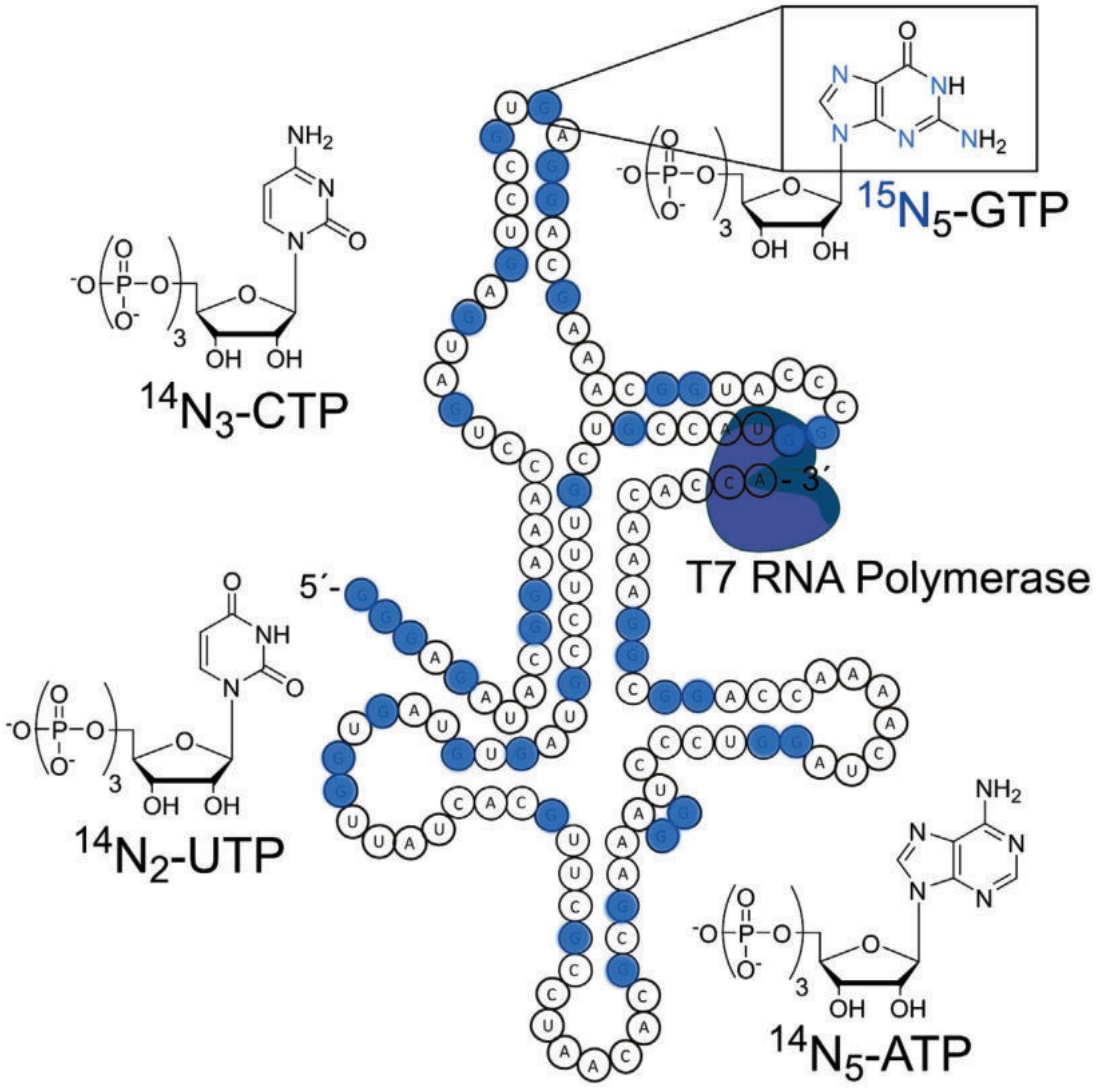

Fig. 4 *In vitro* transcription with stable isotope labeled GTP. The generated tRNA carries $^{15}N_5$ labeled guanosine and ^{14}N variants for all three other canonicals.

Table 5 Pipetting scheme for the T7 reaction mixture (200 µL ≡ 2 reactions).

Compound	Stock concentration	Volume
T7 transcription buffer	10 ×	10 µL
$MgCl_2$	50 mM	3 µL
T7 enzyme mix		3.2 µL
rNTPs (4 ×)		1.6 µL each (4 ×)
PCR product (2 reactions)		100 µL
ultrapure water		fill up to 200 µL

10. Transfer the supernatant into a new microtube and pipet 4 µL of DNase I into the mixture and incubate at 37 °C for 1 h.
11. In a last step, the DNase I treated transcript is mixed with 20 µL 5 M NH_4OAc and 500 µL 100% ice-cold ethanol and stored over night or for at least 12 h in the −20 °C freezer.
12. Centrifuge the over-night precipitated *in vitro* transcript at 4 °C and 12,000 × *g* for 60 min.
13. Discard the supernatant and resuspend the pellet in 30 µL ultrapure water.
14. This elongated fusion-tRNA transcript (precursor) needs to cleave autocatalytically itself into its target tRNA and the 5′-elongation (see **Note 5**). To ensure cleavage, the RNA is incubated for 1 h at 60 °C in the presence of 5 µL 50 mM $MgCl_2$. A reaction control is realized by size exclusion chromatography (SEC, *e.g.*, 130 Å column, see Section 3.3.2 SEC separation for native tRNA and *IV*T).
15. Continue to read on in Section 3.3.2

3.2.3 Synthetic oligonucleotides

To establish ON-MS, it is necessary to develop a suitable chromatography that allows optimal separation of a variety of ONs of different lengths and compositions. Synthetic ONs ranging from 5mers to 8mers to 10mers are commercially available and can be used. Ideally, the sequence corresponds to RNA fragments generated through endonuclease treatment of the target RNA (*e.g.*, T1 digest fragments of $tRNA^{Ser}_{UGA}$: ON 6 (ACUUG); ON 7 (UUUCCCCG); ON 8 (AAAUCCAUUG)).

3.3 Processing of RNA

The processing of RNA in this subsection begins with RNA isolation of native RNA from mammalian cells (see Section 3.3.1). In Section 3.3.2, we describe the method of SEC to separate different RNA species or to purify *in vitro* transcription reactions.

In addition to separating RNAs, we extend the processing of RNA toward enzymatic *in vitro* demethylation or modification assays (see Section 3.3.3).

3.3.1 RNA isolation for native RNA

1. After aspirating PBS (see step 3, Section 3.2.1) cells are directly harvested and lysed in culture flasks using TRI Reagent. We suggest using 1 mL per 8×10^6 cells (≙ confluent T25 flask of HEK293).

Thoroughly pipette up and down and transfer the cell suspension into a 1.5 mL tube (see **Note 6**).

2. Vortex for 20 s then incubate for 5 min at room temperature (see **Notes 7/8**).
3. Add $\frac{1}{5}$ of the volume used for cell lysis of chloroform (*e.g.*, 200 µL chloroform to 1 mL cell suspension in TRI Reagent) and mix thoroughly until the whole suspension becomes uniformly opaque
4. Leave the mixture at room temperature for 5 min and centrifuge for 10 min at 10,000 × *g* at 4 °C
5. Transfer the aqueous phase (upper, clear) into a new 1.5 mL tube and add an equal volume of isopropanol (*e.g.*, ∼ 500 µL isopropanol per 1 mL TRI).
6. Mix thoroughly and precipitate RNA over night at −20 °C (see **Note 9**).
7. For pelleting, centrifuge RNA at 4 °C at 12,000 × *g* for 60 min. Implement a wash step with 70% ethanol
8. Resuspend pellet in 30 µL ultrapure water. Resuspended RNA can be stored at −20 °C for several years (see **Note 10**).

3.3.2 SEC separation for native tRNA and in vitro *transcribed tRNA*

1. For purification of tRNA and bulk rRNA, size exclusion chromatography (SEC) on a HPLC system is employed using SEC buffer as the mobile phase (Chionh et al., 2013). An AdvanceBio SEC 300 Å, 2.7 µm, 7.8 × 300 mm column allows fast separation of tRNA from rRNAs using an isocratic elution at 1 mL/min with a column temperature of 40 °C (Hagelskamp et al., 2020). After equilibration of the column for at least 30 min, up to 100 µg of total RNA can be injected. The large rRNA subunits co-elute from 4.0 to 5.0 min and the pure total tRNA elutes from 6.7 to 7.7 min as shown in Fig. 5 (see **Note 11**).
2. For purification of *in vitro* transcribed tRNA an AdvanceBio SEC 130 Å, 2.7 µm, 7.8 × 300 mm column is used. The run is done at 60 °C in 22 min and with a flow rate of 0.5 mL/min., the other parameters are not changed. Uncleaved fusion product elutes first at minute 9.7, then the target tRNA at minute 10.5 to minute 11.0 (collected), followed by hammerhead ribozyme and finally single unincorporated rNTPs as shown in Fig. 5.

   To increase the lifetime of both in step 1 and 2 described SEC columns, a slow flow rate ramping at instrument start and stop should be performed (see **Note 12**).

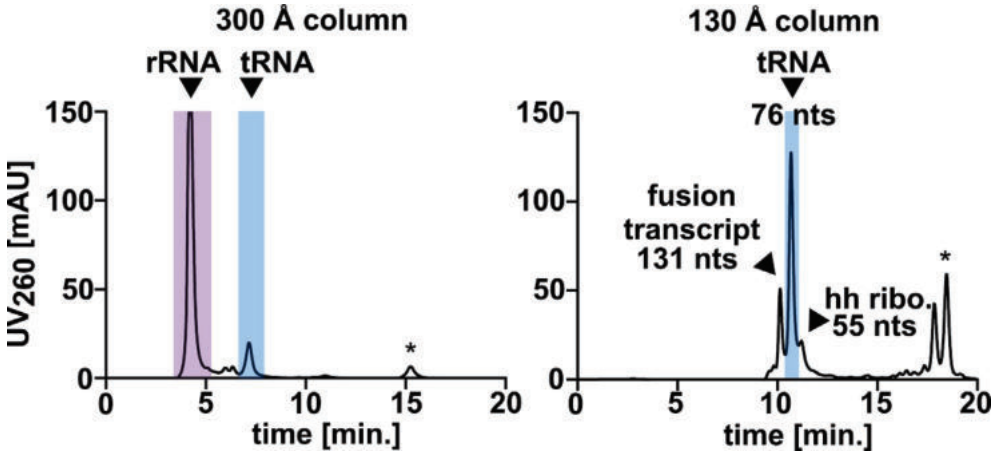

Fig. 5 Size exclusion chromatograms of two columns with different pore size. On the left side, extracted total RNA from cell culture is purified and separated into the ribosomal RNA fraction and the transfer RNA fraction. The right chromatogram shows the separation of *in vitro* transcribed tRNA from oligonucleotides with a shorter length on a column with smaller pore size. (Length fusion transcript: 131 nts, tRNA: 76 nts and hh ribozyme: 55 nts).

3. Collect the desired fractions and concentrate them to ~50 µL using a lyophilizer or vacuum concentrator (see **Note 13**).
4. Add $\frac{1}{10}$ of the volume of 5 M NH_4OAc, then add 2.5 × of the volume ice-cold 100% ethanol (see **Note 14**). Precipitate and resuspend RNA as described in step 7 in Section 3.3.1.

3.3.3 *RNA* in vitro *demethylation with AlkB*

1. An aliquot of bacterial AlkB protein is thawed on ice
2. Aqueous α-ketoglutarate, L-ascorbate and iron (II) salt solutions are made as fresh as possible and used immediately after resuspension in ultrapure water (see **Note 1**).
3. A master mix with all required salts and buffers is produced (see pipetting scheme in Table 6) and aliquoted in every reaction microtube
4. All assays are incubated for 1 h at 37 °C and 300 rpm in a shaking heat block
5. For quenching of the AlkB demethylation reaction, the reaction mixture is filtered through a 10 kDa cut-off filter (for nucleosides up to ONs with a length of a 10mer or by EtOH precipitation (as described in step 7 in Section 3.3.1)) for longer oligonucleotides, *e.g.*, tRNA

Table 6 Pipetting scheme for an *in vitro* AlkB assay.

Compound	Stock concentration	Volume
m^1A-oligonucleotide (ON9,10,11)	100 µM	5 µL
KCl	100 mM	7.5 µL
TRIS HCl pH 7.5	1 M	2.5 µL
L-ascorbate	20 mM	5 µL
α-Ketoglutarate	10 mM	1.5 µL
$Fe(II)(NH_4)_2(SO_4)_2 \times 6\ H_2O$	10 mM	1.5 µL
AlkB	39.1 µM	1.3 µL
Ultrapure water		fill up to 50 µL

Table 7 Pipetting scheme for RNase T1 digest for up to 2 µg of RNA.

Compound	Stock concentration	Volume
RNase T1	10 U/µL	5 µL
NaCl	300 mM	15 µL
TRIS HCl pH 7.5	125 mM	10 µL
CIP	10 U/µL	1 µL
RNA		x µL
ultrapure water		fill up to 50 µL

3.4 RNase T1 digest for ON-MS

1. RNase T1 is diluted to a 10 U/µL solution by mixing 2 µL of the RNase T1 stock (in this case with a concentration 186 U/µL) with 35.2 µL of 25 mM TRIS pH 7.5 buffer solution
2. 2 µg of the synthesized *in vitro* transcript (see Section 3.2.2) is digested with RNase T1, TRIS pH 7.5, NaCl, CIP (detailed recipe see in Table 7).
3. Add up to 50 µL with ultrapure water and transfer the sample to a heat block for 1 h at 37 °C
4. Stop the digest by filtering through a 10 kDa molecular weight cut-off filter and continue with MS analysis

3.5 Low- and high-resolution mass spectrometry

The RNase T1-derived oligonucleotide fragments as well as the internal standard fragments from stable isotope labeled *in vitro* transcripts are assigned by low resolution MS (*e.g.*, QQQ-MS). For such *in vitro* experiments, there is no need for high-resolution MS as the resulting fragments can be predicted and resolved by low resolution MS. In the case of A-to-I edited ONs, whose mass difference is only 1 Da in the +1 charge state, we recommend using high-resolution MS (orbitrap-MS) (see **Note 15**). Modified and low abundant fragments resulting from digestion of HEK293 tRNA with RNase T1 are another reason for using high resolution mass spectrometry to confirm sequence and modification status in complex biological mixtures.

3.5.1 Low-resolution QQQ for oligonucleotide mass spectrometry

Because of the ion-pairing reagent-free chromatography, the analysis of nucleosides and oligonucleotides is possible on the same instrument. In our experience, it is possible to switch from ON-MS to nucleoside MS within 60 min to allow the system and column to equilibrate (see **Note 16**).

1. Chromatographic separation of the analytes is achieved by high performance liquid chromatography (HPLC). The separation is accomplished using a Synergi Fusion-RP 100 Å 2.5 μm, 150 × 2.0 mm column from Phenomenex with a gradient elution
2. For separation of nucleosides or ONs on HPLC, we recommend the following parameters:

column temperature 35 °C, flow rate 0.35 mL/min, buffer A 5 mM NH_4OAc pH 5.3 for nucleoside MS and 10 mM NH_4OAc pH 7.0 for ON-MS, buffer B is 100% acetonitrile. The separation potential of nucleosides and oligonucleotides in the chromatography and the respective acetonitrile gradient are shown in Fig. 6.

3. The liquid chromatography runs with the following gradient (Table 8):

3.5.2 Comparison of chromatographic set-up for nucleoside-MS and ON-MS

Simple biological mixtures from, *e.g.*, *in vitro* transcription (Fig. 7) or synthetic ONs (Fig. 8) can be measured by low resolution QQQ-MS. As shown in Fig. 7, unlabeled and stable isotope labeled tRNA *IV*Ts produce sequence specific ONs during endonuclease treatment which can be detected by untargeted MS scanning analysis of targeted MS/MS analysis. A sequence coverage of 49% is possible with a single endonuclease for the shown $tRNA^{Val}_{AAC}$.

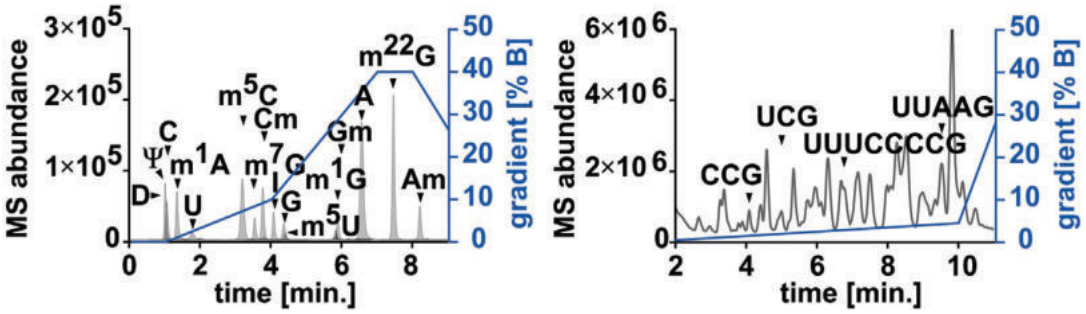

Fig. 6 MS chromatograms of a nucleoside MS (left) and oligonucleotide MS (right) run. All modified and canonical nucleosides (overlayed MRM chromatograms, grey) or all RNase T1 derived oligonucleotides (total ion chromatogram with assigned sequence masses, grey) are separated on a reverse phase column with ammonium acetate buffer. In blue the ratio of acetonitrile during gradient elution is plotted.

Table 8 HPLC gradient for nucleoside MS and ON-MS.

Time	Organic solvent (B) for nucleoside MS = pure acetonitrile	Time	Organic solvent (B) for oligonucl. MS = pure acetonitrile
0 min–1 min	0%	**0 min–10 min**	Increasing to 5%
1–4 min	Increasing to 10%	**10–12 min**	Increasing to 50%
4–7 min	Increasing to 40%	**12–13 min**	50%
7–8 min	40%	**13–13.5 min**	Decreasing to 0%
8–11 min	0%	**13.5–18 min**	0%

ON-MS is ideally suited to study the sequence context of RNA demethylation processes. *E.g.*, an 8mer minimal substrate with a 1-methyladenosine modification is incubated with the bacterial demethylase AlkB. The demethylated ONs elute later due to the lost positive charge of the adenine base. Furthermore, the methylated and unmethylated ON can be distinguished using mass spectrometry. In this context, substrate specificity of RNA writers and erasers can be studied.

3.5.3 High-resolution orbitrap for ON-MS

To detect assigned modified RNase T1 fragments in complex biological mixtures, it is important to use high resolution mass spectrometry. Fragmentation and generation of c- and y-ions are essential to determine modification status (see **Note 17**) (Fig. 9).

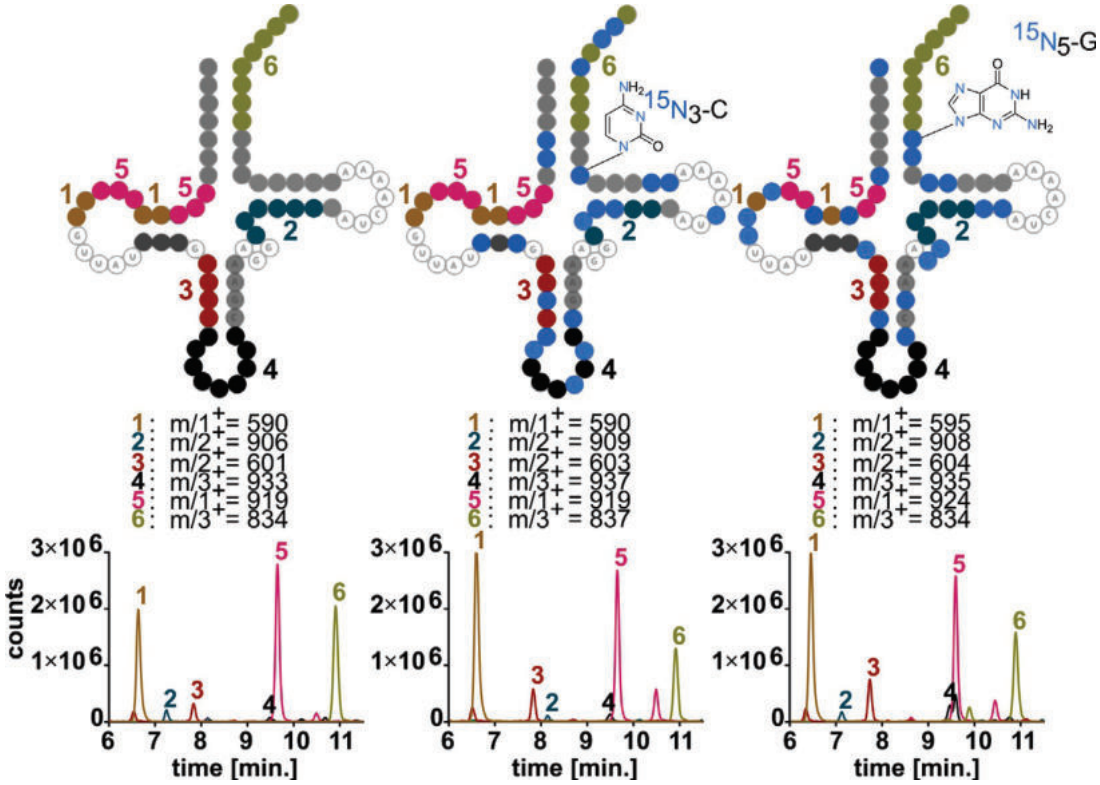

Fig. 7 Low-resolution MS chromatograms of differently stable isotope labeled *in vitro* transcribed $tRNA^{Val}_{AAC}$. On the top, the 2D tRNA structure is depicted with color-coded and numbered T1 fragments that were detected in the respective MS chromatogram (bottom, overlayed and colored extracted ion chromatograms). Marked in blue are the ^{15}N-incorporated nucleosides, middle structure shows $^{15}N_3$-Cytidine variant, right tRNA structure shows the $^{15}N_5$-Guanosine variant. All fragment numbers (1–6) with their *m/z* values are listed under the respective tRNA structure variants. They elute—as all isotopologues—with the same retention time (shown on the bottom, colored overlayed EICs).

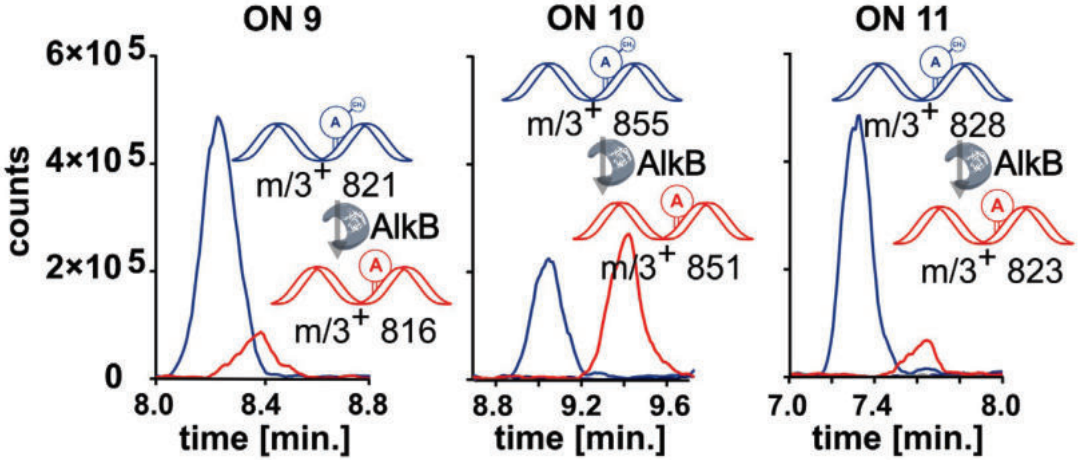

Fig. 8 Low-resolution MS chromatograms of 1-methyladenosine-containing 8mer oligonucleotides. The extracted ion chromatograms of all modified (marked in blue) and unmodified (marked in red, after AlkB treatment) ONs are shown from left (ON 9: UUCGm^1AUUC) to center (ON 10: UAGGm^1AUUG) to right (ON 11: CGUCm^1ACAC).

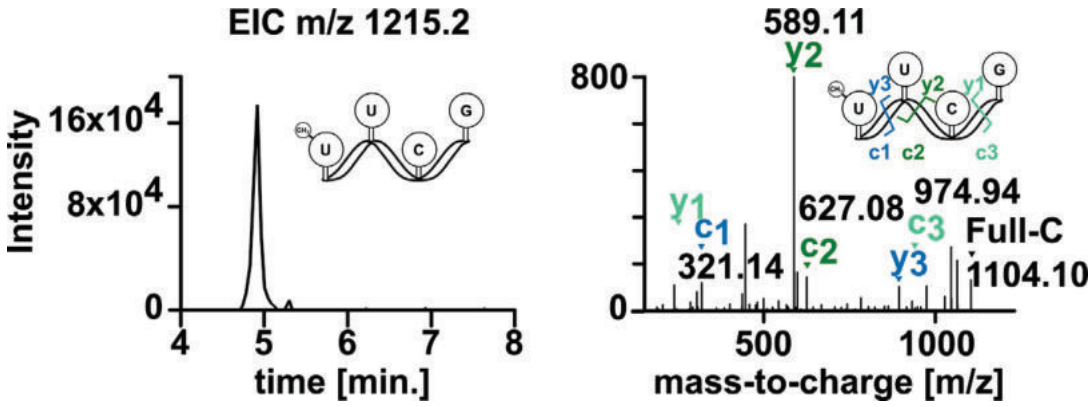

Fig. 9 High-resolution MS chromatogram and corresponding MS spectra of m^5UUCG oligonucleotide from HEK293 cell total tRNA fraction. On the left side, the extracted ion chromatogram shows a retention time of 4.92 min for the m^5UUCG fragment, on the right the MS/MS spectrum is depicted with the assigned c- and y-ions.

3.6 Data analysis

3.6.1 Agilent's Qualsoftware

We analyze data with the qualitative MassHunter Software from Agilent.

3.6.2 In silico *tools and data analysis*

MongoOligo (http://rna.rega.kuleuven.be/masspec/mongo.htm) is a free online software for calculation of, *e.g.*, RNase T1 digestion products, exact/monoisotopic masses, electrospray ion series and predicted MS/MS peaks of any ON. The resulting computational m/z values serve as a basic for comparing experimental MS spectra to those computational values to identify oligonucleotides. The workflow of data analysis using MongoOligo is shown in Fig. 10. RNA ModMapper (Lobue, Yu, Jora, Abernathy, & Limbach, 2019) is an alternative tool, which is provided as a download software from the Limbach lab. Another alternative is Ariadne which additionally allows prediction of stable isotope labeled ON-MS spectra and database search for RNA identification (https://ariadne.riken.jp/index.html) (Nakayama et al., 2009). The most recent addition to support ON-MS spectra usage is NASE, a computational platform for high-throughput analysis of RNA sequences and modifications similar to bottom-up proteomics search engines (Wein et al., 2020).

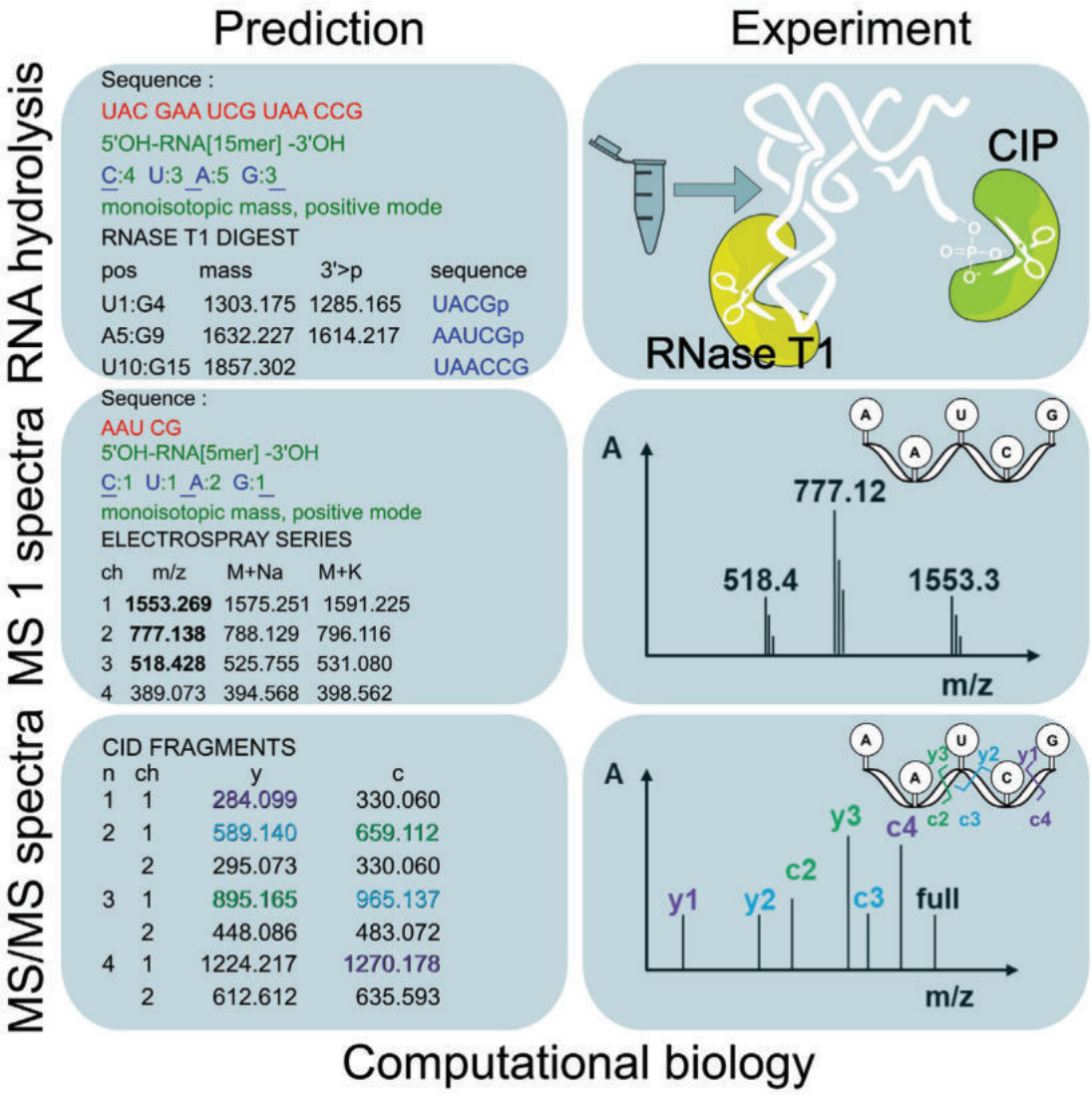

Fig. 10 Workflow of data analysis. ON-MS experiments require a comparison of predicted (*in silico*) and experimental data. On the left side, MongoOligo software (Mongo Oligo Mass Calculator v2.06 (kuleuven.be) (Mongo Oligo Mass Calculator v2.06 (kuleuven.be) is used to predict ONs arising after RNase T1 treatment, their MS spectra and MS/MS spectra. On the right side, the corresponding experimental work such as RNase T1/CIP digest, recorded MS1 and MS/MS spectra of the AAUCG fragment is shown. Through manual or computational comparison of experimental and *in silico* data, ON-MS experiments can be analyzed.

4. Notes

1. Aqueous α-ketoglutarate, L-ascorbate and iron (II) salt solutions must be prepared fresh as possible, right before use to circumvent unwanted oxidation or degradation processes that decrease the enzymatic activity in the assay

2. The last step of the PCR at 4 °C should be as short as possible, stopped after the device is at 4 °C and the samples placed on ice for the following steps
3. ^{13}C labeled rNTPs (from Silantes, Munich, Germany) are an alternative to the ^{15}N labeled rNTPs. Deuterated rNTPS should be avoided as H/D exchange is not always suitable for SILIS based quantification
4. The precipitate consists of magnesium pyrophosphate. Therefore, magnesium needs to be re-supplemented to keep the T7 polymerase functional. Later on, magnesium ions are also required for autocatalytic cleavage of the hammerhead
5. Most of the autocatalytic cleavage occurs during the 8 h of transcription. But sufficient amount of magnesium ions and higher temperature (60 °C instead of 37 °C) ensures correct folding of hh motif and quantitative cleavage of fusion transcript
6. TRIzol is toxic, corrosive, environmental- and health-hazardous, so handle with care! Direct TRIzol or trypsinization harvest of the mammalian cells lead to changes in native RNA modification pattern and must be considered
7. Lysed cells can be stored at −20 °C up to 1 month
8. The harvesting procedure might differ for other cell types, *e.g.*, for yeast
9. Precipitation for 1 h is possible but may result in lower quantities. The use of a − 80 °C freezer might be considered for very short precipitation times
10. From our experience, thiolated nucleosides and especially wobble uridines are susceptible to degradation upon long term storage
11. Retention times might shift depending on the operating life of the column. Always inject a test sample for proper evaluation of retention times
12. To increase the lifetime of both in step 1 and 2 described SEC columns, a slow flow rate ramping at instrument start and stop should be performed
13. Take care that the RNA is not concentrated to dryness as this might lead to degradation of the RNA or to insolubility
14. Alternatively, co-precipitants (*e.g.*, 1 μL of GlycoBlue™, Thermo Fisher Scientific, Darmstadt, Germany) can be added to each sample to facilitate RNA precipitation and simplify washing steps
15. We recommend using high-resolution MS (Orbitrap-MS or TOF-MS) as it is beneficial over low-resolution MS (QQQ-MS) regarding the analysis of modified RNAs or the exact determination of multiple c- and y-fragment ions in native RNA

16. Exchange of the aqueous ammonium acetate buffer and the equilibration of the column with the new buffer last approx. 60 min. An ionization mode change of the mass spectrometer is not needed
17. Nomenclature of fragment ions was introduced by McLuckey, Van Berkel, and Glish (1992): c-ions: charge remains at 5′ end, y-ions: charge remains at 3′ end

Acknowledgments

This work was funded through the Deutsche Forschungsgemeinschaft (KE1943/4-1—SPP1784 and Project-ID 325871075—SFB 1309). We thank Prof. Thomas Carell, the Department of Chemistry and LMU Munich for continuous support. A special thank you to Dr. Kayla Borland for sharing her know-how in oligonucleotide MS with us.

References

Addepalli, B., Lesner, N. P., & Limbach, P. A. (2015). Detection of RNA nucleoside modifications with the uridine-specific ribonuclease MC1 from Momordica charantia. *RNA*, *21*(10), 1746–1756. https://doi.org/10.1261/rna.052472.115.

Addepalli, B., Venus, S., Thakur, P., & Limbach, P. A. (2017). Novel ribonuclease activity of cusativin from Cucumis sativus for mapping nucleoside modifications in RNA. *Analytical and Bioanalytical Chemistry*, *409*(24), 5645–5654. https://doi.org/10.1007/s00216-017-0500-x.

Biba, M., Foley, J. P., & Welch, C. J. (2017). Chapter 6—Liquid chromatographic separation of oligonucleotides. In S. Fanali, P. R. Haddad, C. F. Poole, & M.-L. Riekkola (Eds.), Liquid chromatography, 2nd ed. (pp. 159–182). Elsevier.

Borland, K., Diesend, J., Ito-Kureha, T., Heissmeyer, V., Hammann, C., Buck, A. H., et al. (2019). Production and application of stable isotope-labeled internal standards for RNA modification analysis. *Genes (Basel)*, *10*(1). https://doi.org/10.3390/genes10010026.

Chionh, Y. H., Ho, C. H., Pruksakorn, D., Ramesh Babu, I., Ng, C. S., Hia, F., et al. (2013). A multidimensional platform for the purification of non-coding RNA species. *Nucleic Acids Research*, *41*(17), e168. https://doi.org/10.1093/nar/gkt668.

Crain, P. F. (1990). Preparation and enzymatic hydrolysis of DNA and RNA for mass spectrometry. *Methods in Enzymology*, *193*, 782–790. https://doi.org/10.1016/0076-6879(90)93450-y.

Donis-Keller, H., Maxam, A. M., & Gilbert, W. (1977). Mapping adenines, guanines, and pyrimidines in RNA. *Nucleic Acids Research*, *4*(8), 2527–2538. https://doi.org/10.1093/nar/4.8.2527.

Hagelskamp, F., Borland, K., Ramos, J., Hendrick, A. G., Fu, D., & Kellner, S. (2020). Broadly applicable oligonucleotide mass spectrometry for the analysis of RNA writers and erasers in vitro. *Nucleic Acids Research*, *48*(7), e41. https://doi.org/10.1093/nar/gkaa091.

Heiss, M., Hagelskamp, F., Marchand, V., Motorin, Y., & Kellner, S. (2021). Cell culture NAIL-MS allows insight into human tRNA and rRNA modification dynamics in vivo. *Nature Communications*, *12*(1), 389. https://doi.org/10.1038/s41467-020-20576-4.

Jora, M., Borland, K., Abernathy, S., Zhao, R., Kelley, M., Kellner, S., et al. (2021). Chemical amination/imination of carbonothiolated nucleosides during RNA hydrolysis. *Angewandte Chemie (International Ed. in English)*, *60*(8), 3961–3966. https://doi.org/10.1002/anie.202010793.

Kowalak, J. A., Pomerantz, S. C., Crain, P. F., & McCloskey, J. A. (1993). A novel method for the determination of post-transcriptional modification in RNA by mass spectrometry. *Nucleic Acids Research*, *21*(19), 4577–4585. https://doi.org/10.1093/nar/21.19.4577.

Li, N., El Zahar, N. M., Saad, J. G., van der Hage, E. R. E., & Bartlett, M. G. (2018). Alkylamine ion-pairing reagents and the chromatographic separation of oligonucleotides. *Journal of Chromatography. A*, *1580*, 110–119. https://doi.org/10.1016/j.chroma.2018.10.040.

Lobue, P. A., Yu, N., Jora, M., Abernathy, S., & Limbach, P. A. (2019). Improved application of RNAModMapper—An RNA modification mapping software tool—For analysis of liquid chromatography tandem mass spectrometry (LC-MS/MS) data. *Methods*, *156*, 128–138. https://doi.org/10.1016/j.ymeth.2018.10.012.

McLuckey, S. A., Van Berkel, G. J., & Glish, G. L. (1992). Tandem mass spectrometry of small, multiply charged oligonucleotides. *Journal of the American Society for Mass Spectrometry*, *3*(1), 60–70. https://doi.org/10.1016/1044-0305(92)85019-G.

Nakayama, H., Akiyama, M., Taoka, M., Yamauchi, Y., Nobe, Y., Ishikawa, H., et al. (2009). Ariadne: A database search engine for identification and chemical analysis of RNA using tandem mass spectrometry data. *Nucleic Acids Research*, *37*(6), e47. https://doi.org/10.1093/nar/gkp099.

Thakur, P., Estevez, M., Lobue, P. A., Limbach, P. A., & Addepalli, B. (2020). Improved RNA modification mapping of cellular non-coding RNAs using C- and U-specific RNases. *Analyst*, *145*(3), 816–827. https://doi.org/10.1039/c9an02111f.

Wein, S., Andrews, B., Sachsenberg, T., Santos-Rosa, H., Kohlbacher, O., Kouzarides, T., et al. (2020). A computational platform for high-throughput analysis of RNA sequences and modifications by mass spectrometry. *Nature Communications*, *11*(1), 926. https://doi.org/10.1038/s41467-020-14665-7.

Yu, N., Lobue, P. A., Cao, X., & Limbach, P. A. (2017). RNAModMapper: RNA modification mapping software for analysis of liquid chromatography tandem mass spectrometry data. *Analytical Chemistry*, *89*(20), 10744–10752. https://doi.org/10.1021/acs.analchem.7b01780.

3.3 Eraser-Enzyme *in vitro*

3.3.1 Wahl der Parameter des AlkBH *in vitro*-Experiments

in vitro-Optimierung der Enzymkonzentration

Um die für eine *in vitro* Demethylierung von RNA-Modifikationen benötigte Menge an AlkBH-Enzym zu bestimmen, wurden jeweils die gleiche Menge an RNA-Substrat, in diesem Fall humane 28S rRNA, 18S rRNA und tRNA mit unterschiedlichen Konzentrationen an AlkBH1, AlkBH3 und AlkBH7 inkubiert. Zunächst wurde die absolute Menge der RNA-Modifikationen, die literaturbekannte Demethylierungsziele von AlkBH1 sind[125] [124] [123], bestimmt. Beispielhaft zeigt die Abbildung **3.1 A** dies für die Modifikation m^1A in verschiedenen RNA-Spezies. Während AlkBH1 in 28S rRNA das m^1A-Substrat bei 1 µM in 2 Stunden demethyliert, kann das Enzym in der 18S rRNA in der gleichen Zeit keine Demethylierung durchführen. Hier ist zu erwähnen, dass weniger natives m^1A in 18S rRNA im Vergleich zu tRNA und 28S rRNA vorhanden ist. Somit ist bei gleichbleibender Katalysegeschwindigkeit des Enzyms weniger Substrat in der kleinen eukaryotischen ribosomalen Untereinheit vorhanden. In tRNA kann das m^1A ebenfalls durch AlkBH1 demethyliert werden und es ist festzustellen, dass eine höhere Enzymkonzentration von 5 µM zu einer stärker ausgeprägten Demethylierung führt. Die Geschwindigkeit der Demethylierung von tRNAs ist bei 5 µM AlkBH1-Enzym linear zur Substratkonzentration, da noch nicht alle Bindungsstellen im aktiven Zentrum des AlkBH1 besetzt sind.

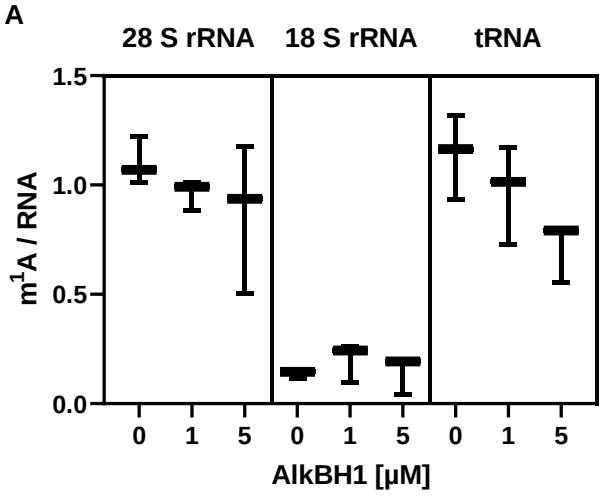

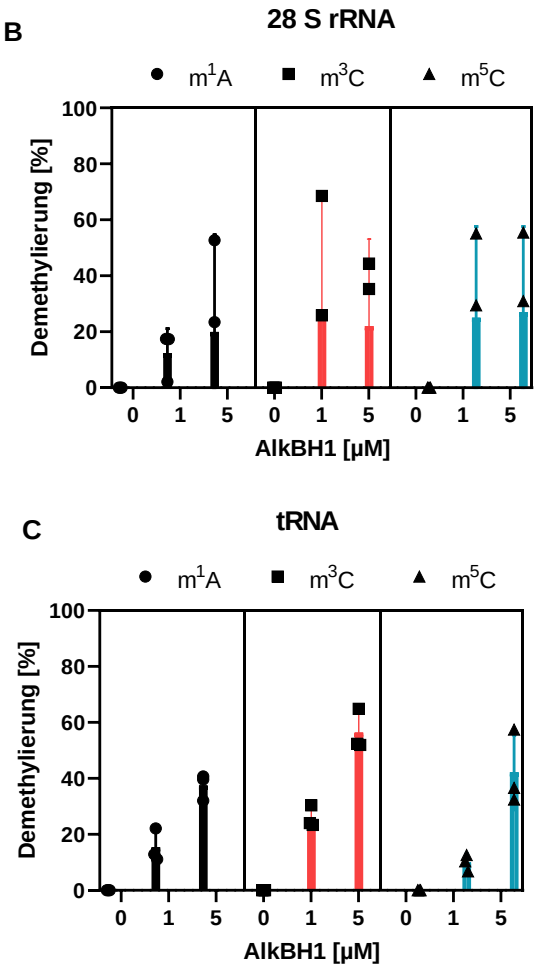

Abbildung 3.1: Auswirkungen unterschiedlicher AlkBH1 Enzymkonzentration auf RNA-Modifikationen. Graph **A** zeigt den absoluten m^1A-Gehalt in 28S rRNA, 18S rRNA und tRNA nach einem *in vitro*-Experiment mit AlkBH1 in Konzentrationen bis zu 5 µM und ebengenannten RNA-Spezies an. In **B** ist die Auswirkung auf weitere RNA-Modifikationen in tRNA, wie m^3C und m^5C, in Prozent Demethylierung dargestellt. Graph **C** zeigt die Demethylierungsraten in 28S rRNA. Alle Werte sind Mittelwerte aus n=3 biologischen Replikaten und die Fehlerbalken repräsentieren die Standardabweichung.

Um eine Priorisierung des AlkBH1-Enzyms auf unterschiedliche RNA-Modifikationen genauer zu analysieren, wurden in Abbildung **3.1 B** und **3.1 C** Demethylierungsraten in Prozent nach folgender Formel angegeben, wobei Mod. für alle drei näher analysierten Modifikationen steht:

$$Demethylierung\ [\%] = 100 - \frac{Mod.in\ AlkBH1\ Probe\ [pmol]}{Mod.in\ 0\ \mu M\ AlkBH1\ Probe\ [pmol]} * 100$$

Hierbei fällt auf, dass m^3C in Anwesenheit von 5 µM Enzym zu ungefähr 60 % in tRNA und 30 % in 28S rRNA demethyliert und somit gegebenüber m^5C und m^1A bevorzugt wird. Der Trend, dass mehr Enzym zu größerer Demethylierung führt, wird weiterhin

bestätigt. Somit ist die Maximalkatalysegeschwindigkeit von AlkBH1 noch nicht erreicht, beziehungsweise die Substratsättigung noch nicht eingetreten. Aus Gründen der Praktibilität beim Pipettieren des *in vitro*-Ansatzes wurde im Folgenden jedoch eine Konzentration von 1 µM AlkBH1 gewählt.

Für die anderen AlkB Homologen, welche in dieser Arbeit besprochen werden, wurde anfangs ebenfalls eine Enzymkonzentrationsreihe mit gleichbleibender Menge RNA und konstanter Inkubationszeit von 2 Stunden gemessen. In Abbildung **3.2 A** sind Enyzmkonzentrationen von 0 µM – 1,5 µM AlkBH3 und ihre Auswirkungen auf m^1A, m^3C und m^5C zu sehen. m^5C ist unter den genannten Bedingungen (2 Stunden, 37 °C) kein Demethylierungsziel von AlkBH3 in tRNA in diesem Konzentrationsbereich, während m^3C hingegen mit 1 µM Enzym zu 40 % demethyliert wird. Somit kann daraus geschlossen werden, dass AlkBH3 eine höhere Affinität zu m^3C besitzt als AlkBH1 (vgl. 30 % bei 1 µM und konstanter Zeit) und es leichter demethylieren kann. Des Weiteren ist auffällig, dass die Steigerung der Konzentration auf 1,5 µM bei AlkBH3 nicht mehr zu einer Zunahme der Demethylierungsaktivität führt, d.h. dass alle RNA-Substrate bereits an Enzyme gebunden wurden und eine Enzymsättigung vorliegt. Es wurde sich deshalb für kommende *in vitro*-Versuche auf 1 µM festgelegt.

Als Letztes sollte das Demethylierungspotenzial von AlkBH7 untersucht werden. Dieses ist für seine Aktivität gegenüber Proteinen, bekannt[207]. Zhang et al. haben AlkBH7 als m^1A- und $m^{22}G$-Demethylase in mitochondrialer pre-tRNA identifiziert, konnten aber keine weiteren mitochrondrialen oder cytosolischen RNA-Ziele finden [141]. Wie Abbildung **3.2 B** zeigt, wird mit steigender Konzentration eine Demethylierung aller drei beobachteten Modifikationen erreicht. Es ist darauf hinzuweisen, dass dieser Demethylierungsgrad durch physiologisch irrelevante Konzentrationen, wie 30 µM, erreicht wurde.

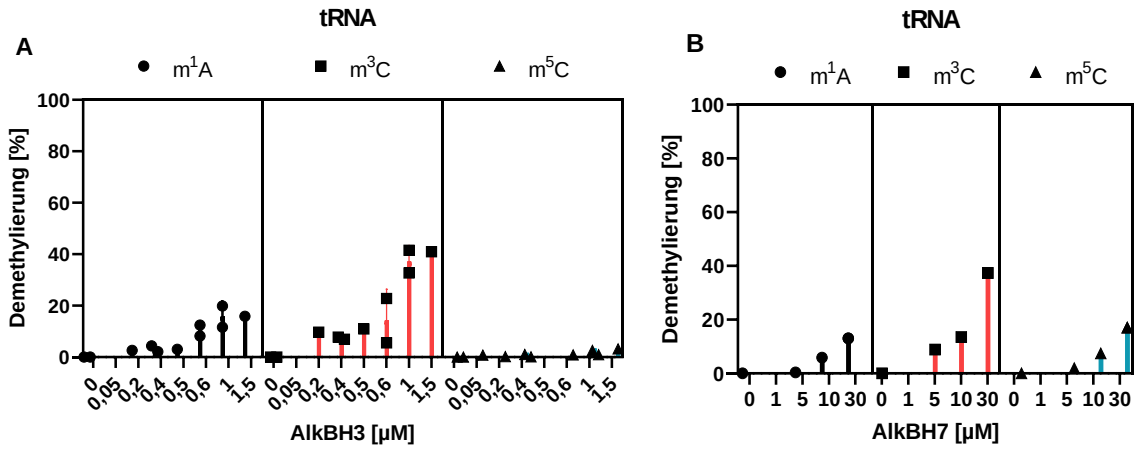

Abbildung 3.2: Weitere AlkBH-Enzymkonzentrationsoptimierungen. Graph **A** zeigt die Demethylierungsraten von m^1A, m^3C und m^5C in tRNA in Prozent mit AlkBH3 Enzym in Konzentrationen bis zu 1,5 µM. In **B** wird die Demethylierung der gleichen Modifikationen mittels AlkBH7 (0-30 µM) gezeigt. Die Messwerte geben den Mittelwert aus n=2 biologischen Replikaten wieder.

Deshalb wurden die weiteren *in vitro*-Enzymexperimente mit 10 µM durchgeführt, bei denen eine Demethylierung aller drei Modifikationen größer als 5 % nach 2 Stunden erreicht werden kann.

Zusammenfassend lässt sich sagen, dass mit jedem der 3 AlkB Homologen eine Demethylierung von tRNA Ziel-Modifikationen erreicht werden kann, wenn mehr Enzym eingesetzt wird. Die Enzymkonzentration sollte jedoch hinsichtlich der physiologischen Relevanz und Praktikabilität festgelegt werden.

in vitro-Optimierung der Inkubationszeit und der Pufferkomposition

Nachdem die Menge an eingesetzten AlkBH-Enzym im vorherigen Kapitel angepasst wurde, soll der Einfluss der Inkubationszeit bei 37 °C sowie die Konzentrationen der Puffer- und Salze, die für die Demethylaseaktivität entscheidend sind, getestet werden. Hierfür wurden die einzelnen Reaktionsgefäßansätze bis zu 150 Minuten bei 37 °C inkubiert und durch Zugabe des 10-fachen Volumens an Lithiumperchlorat in Aceton bei Raumtemperatur und anschließender Zentrifugation gefällt. Abbildung **3.3** zeigt für den Demethylierungsgrad durch AlkBH3 der drei RNA-Modifikationen m^1A, m^3C und m^5C in Abhängigkeit der Zeit. Eine Inkubationszeit von mindestens 120 Minuten wird benötigt, um bei den drei untersuchten Modifikationen ein Maximum der Demethylierung zu erreichen. Eine längere Inkubationszeit ändert den Level an RNA-Modifkationen nicht, da die Einstellung eines Enzym-Substrat-Gleichgewichtes bereits stattgefunden hat.

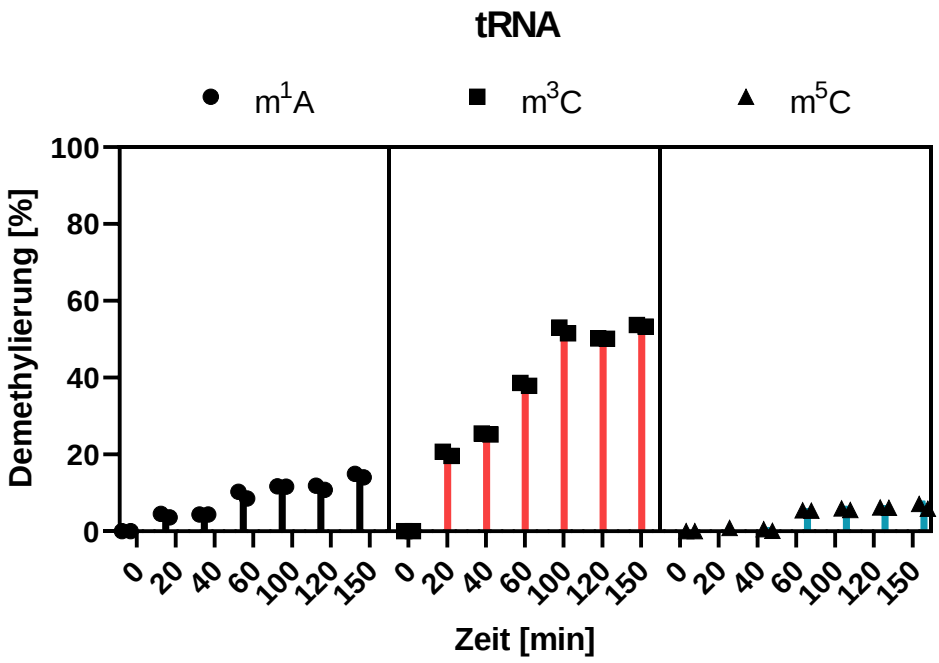

Abbildung 3.3: Auswirkungen der *in vitro* Inkubationszeit mit AlkBH3 auf RNA-Modifikationen. Der Graph zeigt den Demethlylierungsgrad von m^1A, m^3C und m^5C in tRNA nach einem *in vitro*-Experiment mit 1 µM AlkBH3. Die Proben wurden zwischen 0 und 150 Minuten lang inkubiert und durch Lithiumperchloratfällung der RNA die Inkubation gestoppt. Alle Werte sind Mittelwerte aus n=2 biologischen Replikaten und die Fehlerbalken repräsentieren die Standardabweichung.

Entscheidend für die Aktivität eines Enzymes sind neben dem jeweiligen RNA-Substrat die Temperatur, die Ionenstärke, aber auch der pH-Wert der Reaktionslösung. Nachdem eine Reaktion um den physiologischen pH-Wert 7,4 wünschenswert ist, wurden die zwei Puffersysteme TRIS und HEPES, beide pH 7,5 verglichen. Wie in Abbildung **3.4 A** zu erkennen, führt der HEPES-Puffer zu einer besseren Aktivität des AlkBH3 an tRNA, welches durch einen höheren Demethylierungsgrad, insbesondere von m^3C, auffällt. Dieses kann mit der besseren Pufferkapazität des HEPES gegenüber TRIS bei diesem pH erklärt werden. So liegt der pK_a von HEPES bei 7,5, TRIS hingegen bei 8,1. Je näher der pH der Reaktionslösung am pK_a des Salzes liegt, desto größer ist die Pufferwirkung. Des Weiteren hält HEPES den pH-Wert der Reaktionslösung bei Temperaturänderung konstanter als TRIS.

Da AlkBH-Enzyme allgemein für die Katalyse ein Metall-Ion Fe^{2+} als Cofaktor im aktiven Zentrum besitzen müssen, sollte auch die Konzentration an Fe^{2+} bei der *in vitro* Reaktion optimiert werden. In Abbildung **3.4 B** ist zu sehen, dass eine Konzentration von 300 µM Fe^{2+}-Salz m^3C in tRNA zu 40 % und m^1A zu 20 % demethyliert. Alle aktiven Zentren sind damit mit Fe^{2+}-Ionen ausgestattet und die Enzymaktivität ist maximal.

Auch ist auffällig, dass mehr Fe^{2+}-Ionen (600 µM oder 1 mM) nicht zu einer gesteigerten Enzymaktivität führen, sondern diese sogar verringern, was in der steigenden Ionenstärke begründet ist, die auf das Enzym inhibitorisch wirkt.

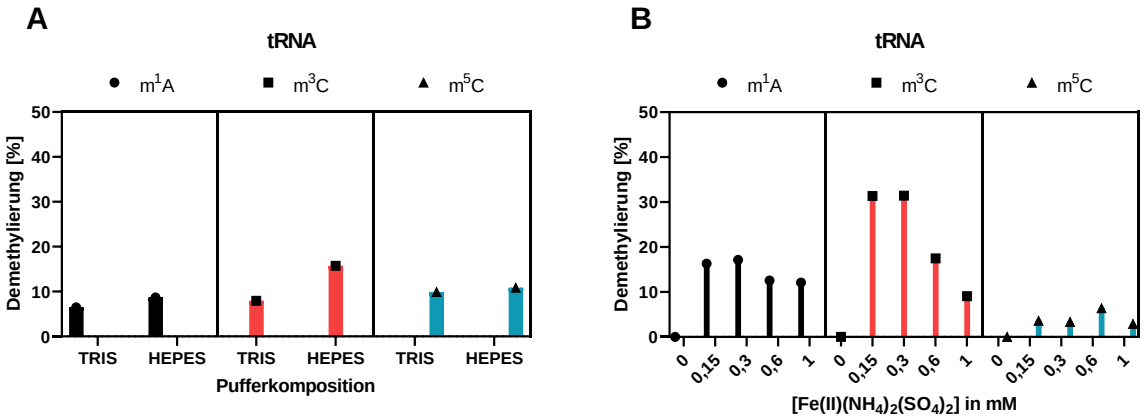

Abbildung 3.4: Auswirkungen unterschiedlicher Pufferkomponenten und ihrer Konzentration auf RNA-Modifikationen. Graph **A** zeigt den Unterschied in der Demethylierungsaktivität von AlkBH3 auf m^1A, m^3C und m^5C in tRNA durch Zugabe von entweder 50 mM TRIS pH 7,5 oder 50 mM HEPES pH 7,5. In **B** ist die Auswirkung der Eisen(II)-Salz-Konzentration, welche von 0 bis 1 mM variiert, auf m^1A, m^3C und m^5C in tRNA m^5C, in Prozent Demethylierung dargestellt. Es wurde hierbei HEPES-Puffer verwendet.

Neben den für die Enzymaktivität essentiellen Cofaktoren, Fe^{2+}, Mg^{2+}, α-Ketoglutarat und L-Ascorbat sollte der Einfluss des Salzgehaltes auf die Demethylierungsreaktion überprüft werden. Die Hauptbestandteile des Puffers und größte Beeinflusser des Salzgehaltes sind Kaliumchlorid (KCl) und HEPES. Diese wurden jeweils in variierenden Konzentrationen zur Reaktion hinzugefügt. Abbildung **3.5** zeigt die Demethylierung von m^1A, m^3C und m^5C in tRNA in Abhängigkeit der Salzkonzentration von HEPES und KCl. Die meiste Aktivität von AlkBH3 ist in 50 mM HEPES pH 7,5 und 15 mM KCl zu beobachten. Deshalb wurde sich auf diese Pufferbedingung für alle zukünftigen *in vitro*-Experimente festgelegt. Eine Steigerung der Salzkonzentration bis zu 100 mM HEPES pH 7,5 und 200 mM KCl führt zu einer Abnahme der Aktivität und sollte daher vermieden werden.

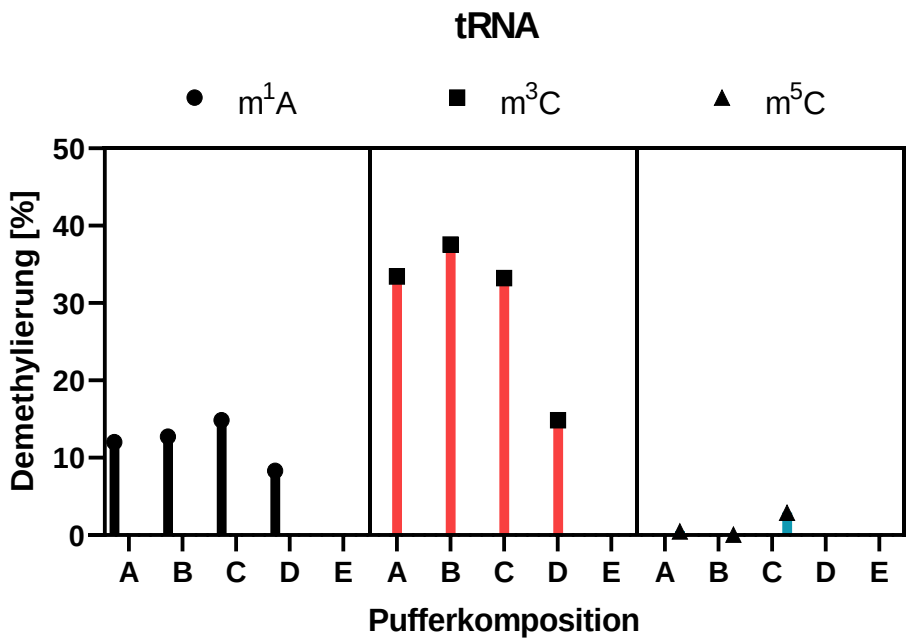

Abbildung 3.5: Auswirkungen weiterer Puffer- und Salzkonzentrationen. Der Graph zeigt den Unterschied in der Demethylierungsaktivität von AlkBH3 auf m^1A, m^3C und m^5C in tRNA durch Zugabe der Pufferkompositionen A bis E an. Hierbei handelt es sich bei Komposition A um 10 mM HEPES pH 7,5 und 10 mM KCl, bei B um 50 mM HEPES pH 7,5 und 15 mM KCl, bei C um 25 mM HEPES pH 7,5 und 50 mM KCl, bei D um 50 mM HEPES pH 7,5 und 100 mM KCl und bei E um 100 mM HEPES pH 7,5 und 200 mM KCl.

Zur Feststellung der Demethylierungsrate wird LC-MS/MS von einem RNA-Totalverdau gemacht. Um einen Einfluss der RNA Hydrolysebedingungen auf das Ergebnis auszuschließen, wurden drei unterschiedliche Verdaubedingungen getestet. Ein unzureichender Nukleaseverdau könnte z.B. in der Bildung von AlkBH-Enzym-Substratkomplexen begründet sein. Hierbei würden demethylierte RNAs am AlkBH-Enzym gebunden, durch ihre Unerreichbarkeit nicht hydrolysiert, bei der abschließenden Größenausschlussfiltration (engl. *molecular weight cut-off*) von Nukleosiden im Filter verbleiben und nicht per MS detektiert. Zunächst wurde in Abbildung **3.6 A** die etablierte Verdaumethode von 2 Stunden bei 37 °C mit einer Neuen von 22 Stunden bei 22 °C verglichen. Durch die längere Inkubationszeit mit Benzonase kann zwar mehr m^3C und Cytidin in den AlkBH3-Enzymproben detektiert werden, jedoch nimmt die Anzahl an m^3C und Cytidin in den Negativ-Kontrollen ab. Die Stoffmenge in den Negativ-Kontrollen ist für eine Berechnung des Demethylierungslevels aber auch entscheidend.

Somit lässt sich sagen, dass die durch die längere Inkubationszeit besser verdauten RNAs in den Enzym-Proben auch dazu führen, dass mehr RNA in den Negativkontrollen ungewollt degradiert und nicht mehr mittels Massenspektrometrie gemessen werden kann. In einem weiteren Versuch wurde die etablierte Methode mit Verdaubedingung C verglichen. In der tRNA sorgte die 20 Stunden längere Inkubation bei 37 °C in allen drei analysierten RNA-Modifikationen (m^1A, m^3C und m^5C) und Cytidin für mehr Degradierung von tRNA in den Negativ-Kontrollen (vgl. Abbildung **3.6 B**). Aufgrund dieser gegenläufigen Effekte wurde für weitere Experimente an dem etablierten Verdauprotokoll festgehalten.

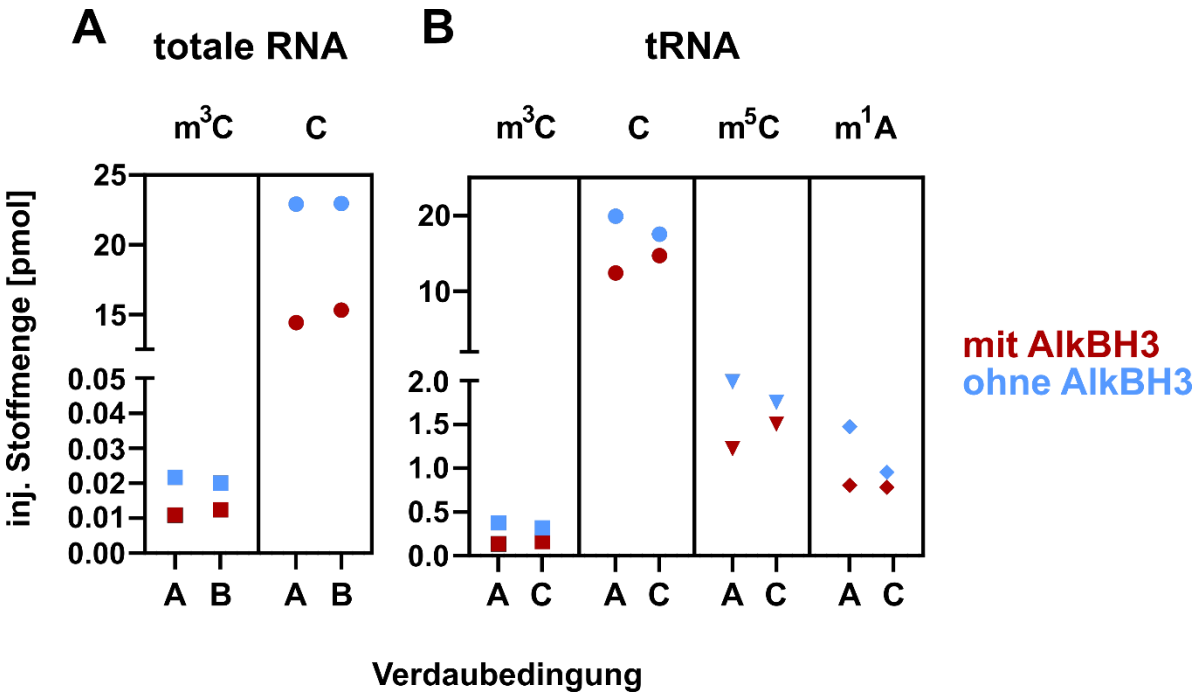

Abbildung 3.6: Auswirkungen verschiedener Verdaubedingungen auf RNA-Modifikationen. Graph **A** zeigt die detektierten Stoffmengen in pmol von m^3C und C. Es wurde 250 ng totale RNA für nach Inkubation mit AlkBH3 Enzym (rote Datenpunkte) oder ohne Enzym (Negativkontrolle = blaue Datenpunkte) unter Bedingung A für 2 Stunden bei 37 °C oder unter Bedingung B für 22 Stunden bei 22 °C mit Benzonase verdaut. In **B** sind die Stoffmengen für m^3C und C und zwei weiterer RNA-Modifikationen, m^5C und m^1A, gezeigt. Abweichend zu Graph **A** wurde tRNA als Substrat eingesetzt und Verdaubedingung A (siehe oben) mit einer weiteren Bedingung C (22 Stunden bei 37 °C) verglichen.

Abschließend wurden folgende optimierten Bedingungen für weitere *in vitro* Experimente mit AlkBH-Enzymen festgesetzt, da unter diesen eine jeweils höhere Aktivität des Enzyms zu beobachten war:

120 Minuten Inkubationszeit mit AlkBH-Enzym; 300 µM Fe^{2+}; 50 mM HEPES pH 7,5 und 15 mM KCl mit abschließenden Benzonaseverdau in 2 Stunden bei 37 °C.

3.3.2 *in vitro*-Methylierung von tRNA durch Methylmethansulfonat (MMS)

Um festzustellen, ob die AlkBH-Demethylasen zwischen endogenen, nativ vorkommenden tRNA-Modifikationen und Methylierungsschäden differenzieren, musste zunächst ein Methylierungsreagenz, in diesem Fall MMS, die tRNA schädigen. MMS wurde in verschiedenen Konzentrationen bis zu 500 mM zur tRNA gegeben und in Abbildung **3.7** die Methylierungseffizienz gegen die Konzentration an MMS aufgetragen. Je mehr MMS im Reaktionsgefäß vorliegt, desto höher werden die absoluten Level aller drei analysierten Modifikationen in tRNA. Da die tRNA durch anschließende RNA-Fällung vom Methylierungsreagenz separiert werden kann, wird der nachfolgende AlkBH-Inkubationsschritt nicht beeinflusst.

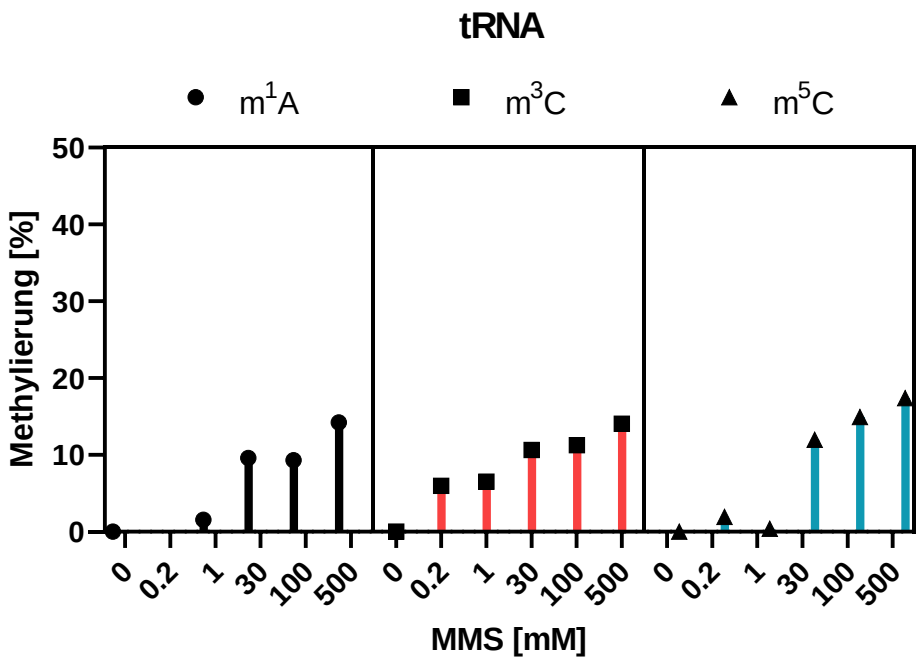

Abbildung 3.7: Methylierung von tRNA mit Methylierungsreagenz MMS. Der Graph zeigt den Unterschied in der Methylierungsaktivität des Methylmethansulfonats (MMS) auf m^1A, m^3C und m^5C in tRNA durch Zugabe verschiedener Konzentrationen an. Es wurden 250 ng tRNA mit 0 – 500 mM MMS für eine Stunde bei 37 °C inkubiert.

Für die im Kapitel 3.3.4 beschriebenen *in vitro*-Experimente wurde eine MMS-Konzentration von 500 mM gewählt, um eine nennenswerte Methylierung der tRNA zu erreichen. Das entspricht einem 2,5 Mio.-fachen Überschuss gegenüber dem tRNA-Substrat.

3.3.3 *in vitro*-Inhibierung von AlkBH-Enzymen durch 2-Hydroxyglutarat (2-HG)

AlkBH-Demethylasen können durch 2-HG in ihrer Aktivität inhibiert werden[208] [209]. Das 2-HG wirkt aufgrund seiner strukturellen Ähnlichkeit zu α-Ketoglutarat (vgl. Abbildung **3.8**) als kompetitiver Inhibitor im aktiven Fe^{2+}-Zentrum der AlkBH-Enzymfamilie. Mutationen in dem Enzym Isocitratdehydrogenase (IDH), die z.B. in Patienten mit akuter myeloischer Leukämie vorkommen, sorgen für die Akkumulation einer bis zu 45-mal höheren Konzentration an 2-HG im Vergleich zu α-Ketoglutarat[210] [211].

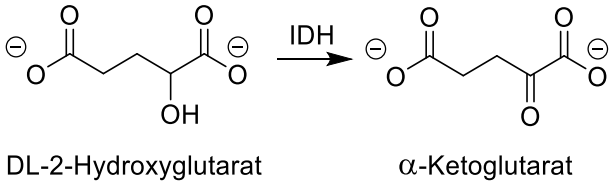

Abbildung 3.8: IDH-katalysierte Reaktion von DL-2-Hydroxyglutarat (2-HG) zu α-Ketoglutarat.

Um ein detailliertes Konzentrations- zu Inhibitionsgeschehen des AlkBH3-Enzyms zu beobachten, wurde *in vitro* AlkBH3 mit nativer tRNA und variierenden 2-HG Konzentrationen versetzt. Abbildung **3.9** zeigt, dass mit steigender Inhibitorkonzentration bis zu 13,5 mM 2-HG die Aktivität des AlkBH3 komplett zum Erliegen kommt.

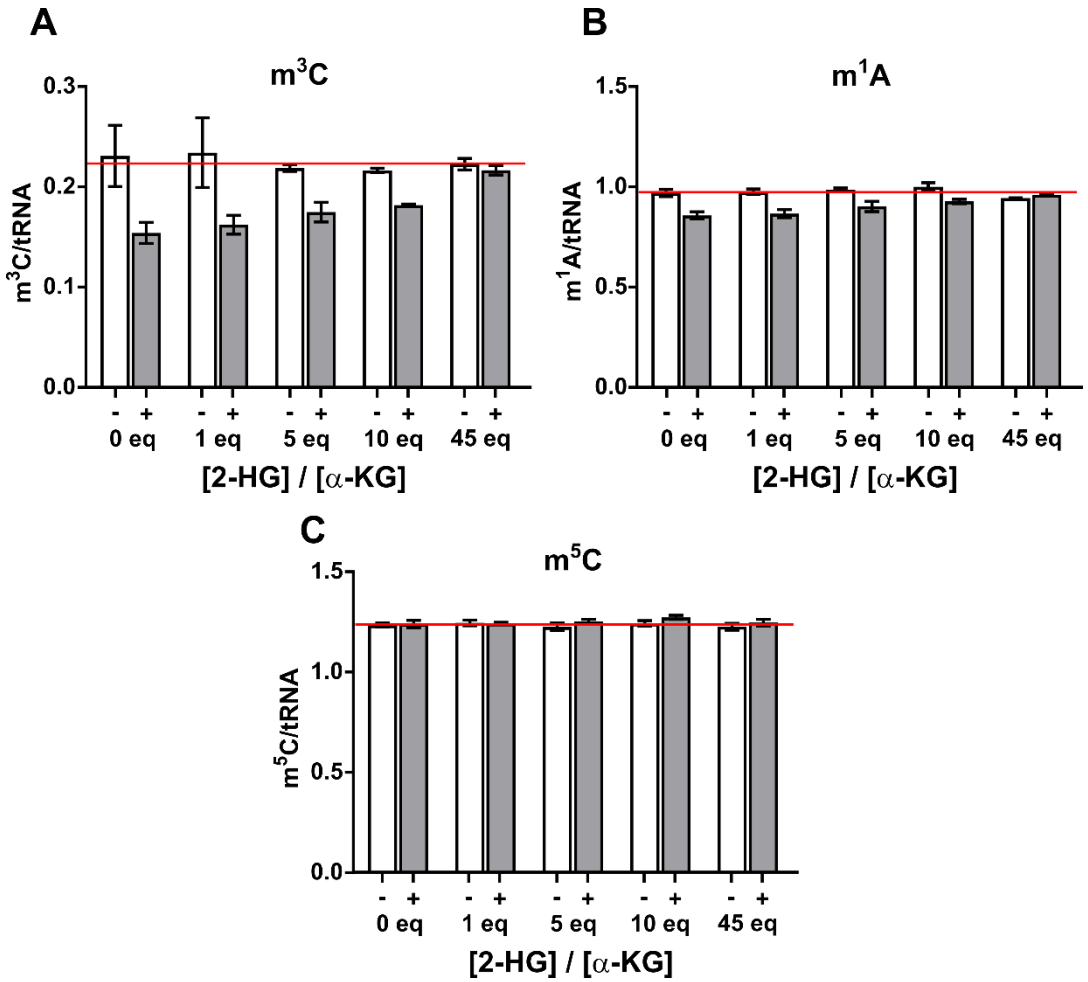

Abbildung 3.9: Inhibierung von AlkBH3 durch Zugabe von 2-Hydroxyglutarat (2-HG). Der Graph **A** zeigt den Unterschied im absoluten Level von m^3C, m^1A und m^5C in tRNA durch Zugabe von 2-HG. Die Äquivalente (eq) des 2-HG beziehen sich auf die in dem *in vitro* Experiment eingesetzte Menge an α-Ketoglutarat (300 µM). Die rote Linie markiert das Modifikationslevel, welches ohne Einsatz des AlkBH3 Enzyms, vorliegt. Diese Enzym-Negativkontrollen sind als weiß gefüllte Balken abgebildet. Graphen **B** und **C** zeigen die Effekte des 2-Hydroxyglutarats auf die Modifikationen m^1A und m^5C. Alle Werte sind Mittelwerte aus n=3 biologischen Replikaten und die Fehlerbalken repräsentieren die Standardabweichung.

Zusammenfassend lässt sich eine Auswirkung auf die untersuchten RNA-Modifikationen in tRNA mit steigender Konzentration des Inhibitors 2-HG im *in vitro*-AlkBH3 Experiment erkennen. Vor allem die Demethylierungssubstrate m^3C und m^1A werden durch das 2-HG inhibierte AlkBH3-Enzym nicht mehr in 2 Stunden demodifiziert. Die AlkBH3-Katalysegeschwindigkeit wurde durch 2-HG vermindert, indem 2-HG den Anteil der Enzymmoleküle mit gebundenem Substrat verringert.

3.3.4 *In vitro*-Demethylierung von RNA durch AlkBHs

Nachdem in Kapitel 3.3.1 und 3.3.2 Optimierungen für das *in vitro*-Experiments durchgeführt wurden, wurden in diesem Kapitel *in vitro* transkribierte tRNA oder native tRNA optional mit MMS versetzt und danach mit einem der drei AlkBH-Enzyme, AlkBH1, AlkBH3 oder AlkBH7 inkubiert.

Zusätzlich wurde native 28S und 18S rRNA als Substrat für AlkBH3 verwendet, um die Effekte von AlkBH3 *in vitro* auf ribosomale RNA zu analysieren.

in vitro-Demethylierung von tRNA durch AlkBH1

Um die Auswirkungen von MMS auf tRNA ohne native Modifikationen zu betrachten, wurde auf *in vitro* transkribierte $tRNA^{Val}_{AAC}$ als RNA-Substrat zurückgegriffen. Bei der *in vitro* Transkription können sequenz-spezifische RNAs von der T7-RNA-Polymerase durch definierte Verknüpfung der vier kanonischen Nukleotid-Triphosphate synthetisiert werden. Diese RNAs enthalten somit keine RNA-Modifikationen. Erst durch Zugabe von MMS können diese RNA-Modifikationen als Methylierungsschäden auftreten. Betrachtet man die absoluten Level folgender fünf RNA-Modifikationen in *in vitro* transkribierter tRNA (IVT), m^5C, m^3C, m^7G, m^1A und m^1G, fällt auf, dass nur m^7G erhöht ist im Vergleich zur MMS-Negativkontrolle (Abbildung **3.10**). Dieses Ergebnis ist in Übereinstimmung mit den von Reichle *et al*. erhobenen Daten[205]. m^7G ist die RNA-Modifikation, die unter Methylierungsstress als Hauptschaden entsteht. Nach Inkubation mit AlkBH1 wird das durch MMS entstandene m^7G zu 32 % demethyliert, sodass 0,6 m^7G-Moleküle pro IVT per LC-MS/MS gemessen wurden. Sowohl das IVT als auch das AlkBH1-Enzym sind nicht mit nativer RNA kontaminiert, da keine RNA-Modifikationen ohne MMS-Zugabe zu detektieren sind.

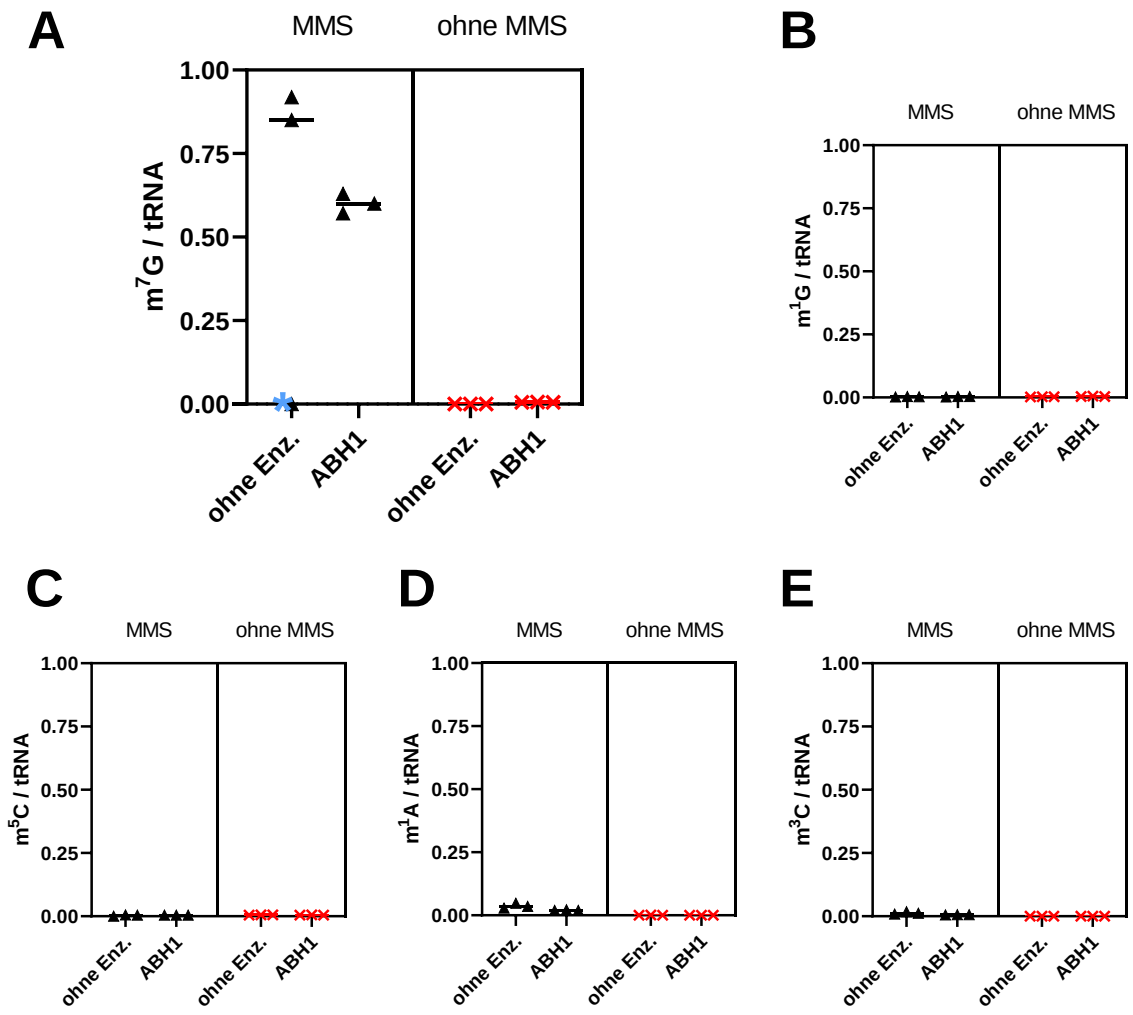

Abbildung 3.10: Demethylierung von *in vitro* transkribierter tRNA$^{Val}_{AAC}$ durch AlkBH1 mit und ohne MMS. Der Graph **A** zeigt den absoluten Level von m^{7}G in *in vitro* transkribierter tRNA$^{Val}_{AAC}$ mit MMS in schwarz und ohne MMS in Rot. Der blaue Stern markiert einen Ausreißer, der nicht in die statistischen Berechnungen miteinbezogen wurde. Die Graphen **B** bis **E** zeigen die Level der anderen RNA-Modifikationen. Alle Werte stammen von n=3 biologischen Replikaten.

Um die Auswirkungen von AlkBH1 auf native Substrate zu analysieren, wurde anschließend aus HEK 293 Zellen aufgereinigte tRNA verwendet. In Abbildung **3.11** sind die absoluten Level der fünf beobachteten RNA-Modifikationen dargestellt. Wie bei den Experimenten mit IVT fällt auf, dass m^{7}G (Abbildung **3.11 D**) als Hauptschaden unter MMS-Stress entsteht und des Weiteren der Gehalt an m^{1}A und m^{3}C signifikant erhöht ist. Keine signifikanten Unterschiede weisen, wie erwartet, die Modifikationen m^{5}C und m^{1}G auf. Das AlkBH1-Enzym demethyliert m^{5}C, m^{3}C, m^{1}A, m^{7}G und m^{1}G signifikant zu jeweils 32 %, 37 %, 33 %, 28 % und 33 %. Nach MMS-Stress werden 42 % m^{5}C, 41 % m^{3}C, 41 % m^{1}A, 54 % m^{7}G und 42 % m^{1}G demethyliert.

Somit repariert AlkBH1 eine Reihe nativer RNA-Modifikationen und zufällig eingebrachte Methylierungen, welche durch MMS entstanden sind.

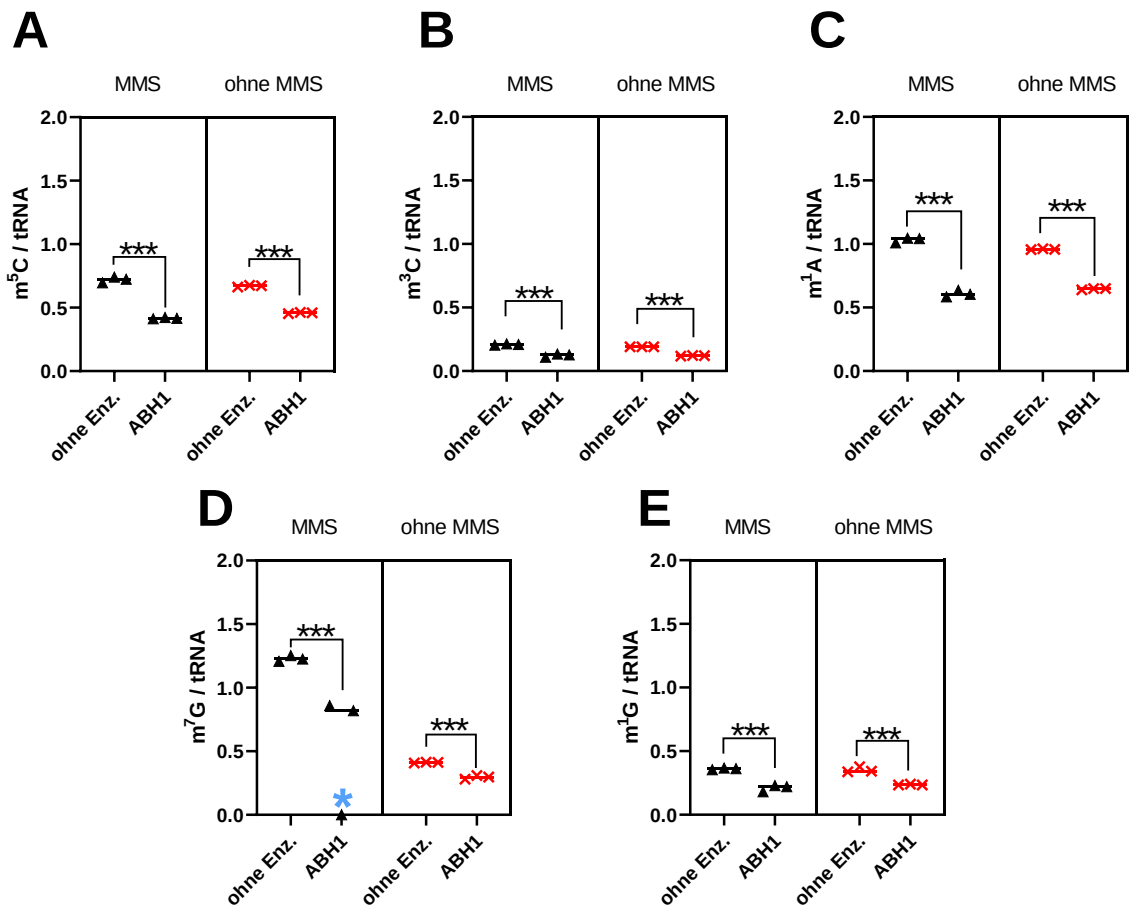

Abbildung 3.11: Demethylierung von nativer tRNA durch AlkBH1 mit und ohne MMS. Der Graph **A** zeigt den absoluten Level von m^5C in nativer tRNA mit MMS in schwarz und ohne MMS in Rot. Die Graphen **B** (m^3C), **C** (m^1A), **D** (m^7G) und **E** (m^1G) zeigen die Level der anderen RNA-Modifikationen. Der blaue Stern in Graph **D** markiert einen Ausreißer, der nicht in die statistischen Berechnungen miteinbezogen wurde. Alle Werte stammen von n=3 biologischen Replikaten. Die Zweiweg-Varianzanalyse bestimmt die p-Werte, welche grafisch eingetragen sind (p<0,001 = ***).

in vitro-Demethylierung von tRNA durch AlkBH3

Um Unterschiede zwischen den verschiedenen AlkB-Homologen zu erkennen, wurde das Enzym AlkBH3 in der gleichen Konzentration wie AlkBH1 eingesetzt (1 µM). Alle weiteren Parameter wurden identisch gewählt. Wie in Abbildung **3.12** zu sehen, schafft AlkBH3 es im Gegensatz zu AlkBH1 nicht, das unter MMS-Stress entstandene m^7G in dem *in vitro* Transkript zu demethylieren. Alle weiteren analysierten RNA-Modifikationen wurden nicht durch MMS-Stress gebildet.

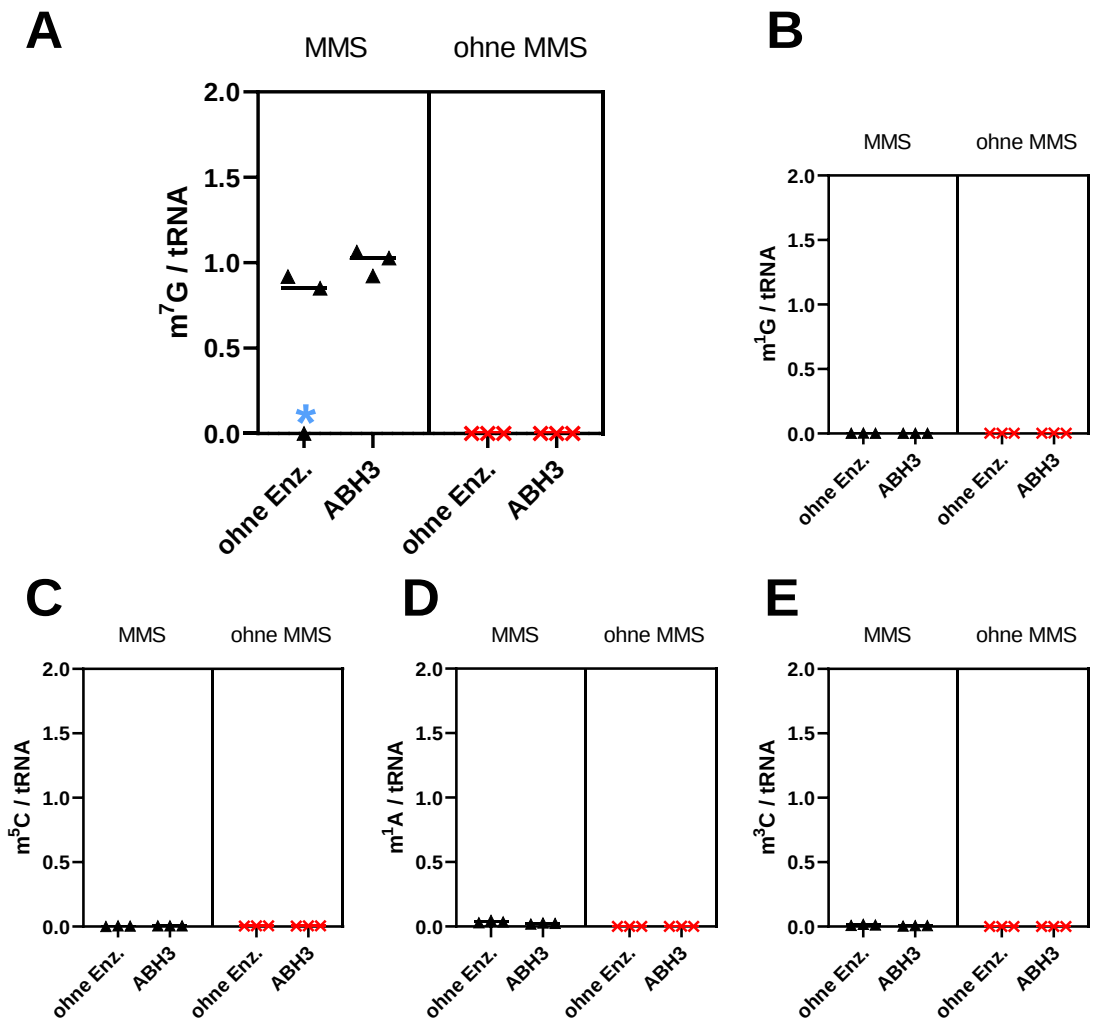

Abbildung 3.12: Demethylierung von *in vitro* transkribierter tRNA$^{Val}_{AAC}$ durch AlkBH3 mit und ohne MMS. Der Graph **A** zeigt den absoluten Level von m^{7}G in *in vitro* transkribierter tRNA$^{Val}_{AAC}$ mit MMS in schwarz und ohne MMS in Rot. Die Graphen **B** bis **E** zeigen die Level der anderen RNA-Modifikationen. Der blaue Stern in Graph **A** markiert einen Ausreißer, der nicht in die statistischen Berechnungen miteinbezogen wurde. Alle Werte stammen von n=3 biologischen Replikaten.

In nativer tRNA werden die Level von m^{3}C und m^{1}A durch AlkBH3 beeinflusst (Abbildung **3.13**). Dies ist in Übereinstimmung mit der Literatur[133] [132]. Sie werden signifikant zu 31 % (m^{3}C) und 9 % (m^{1}A) demethyliert. Unter vorherigem MMS-Stress sogar zu 51 % (m^{3}C) und 43 % (m^{1}A).

Natives m^{5}C, m^{7}G und m^{1}G ist auch wie MMS-methyliertes m^{7}G kein Substrat für das AlkBH3-Enzym in diesem Experiment.

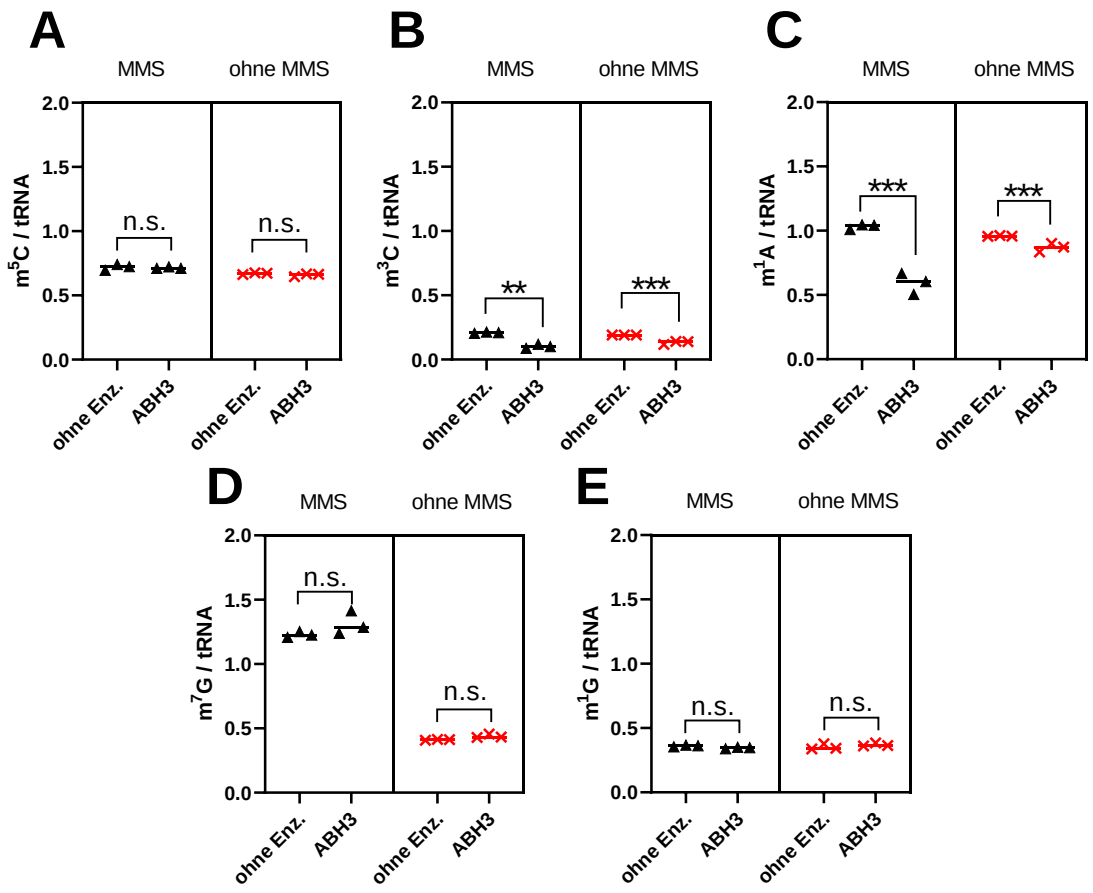

Abbildung 3.13: Demethylierung von nativer tRNA durch AlkBH3 mit und ohne MMS. Der Graph **A** zeigt den absoluten Level von m^5C in nativer tRNA mit MMS in schwarz und ohne MMS in Rot. Die Graphen **B** (m^3C), **C** (m^1A), **D** (m^7G) und **E** (m^1G) zeigen die Level der anderen RNA-Modifikationen. Alle Werte stammen von n=3 biologischen Replikaten. Die Zweiweg-Varianzanalyse bestimmt die p-Werte, welche grafisch eingetragen sind (n.s. = nicht signifikant; p<0,01 = **; p<0,001 = ***).

in vitro-Demethylierung von tRNA durch AlkBH7

AlkBH7 wurde in einer Konzentration von 10 µM den Reaktionsgefäßen zugesetzt. Demethylierungseffekte auf die *in vitro* transkribierte tRNA sind wie bei AlkBH3 nicht zu beobachten (vgl. Abbildung **3.14 A**).

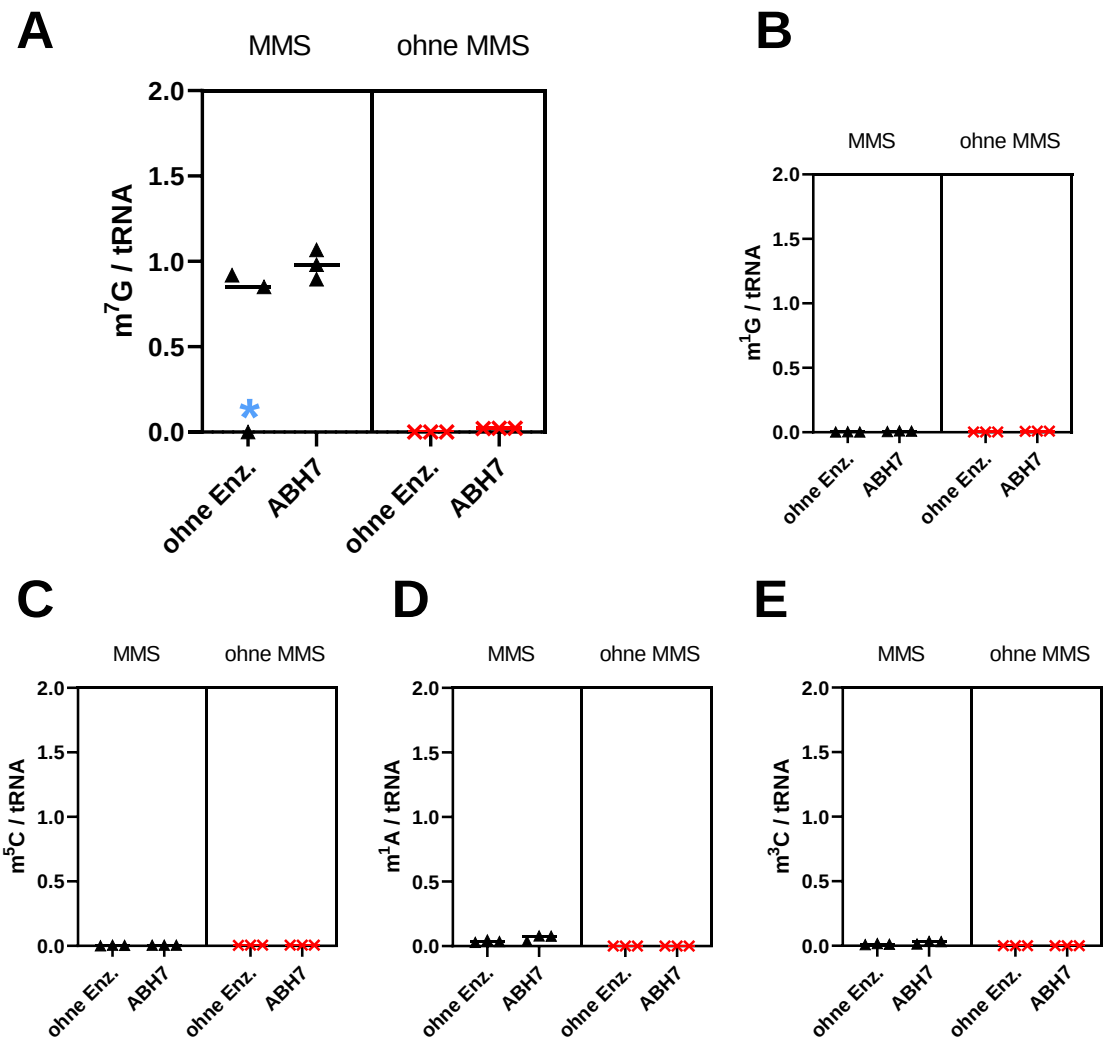

Abbildung 3.14: Demethylierung von *in vitro* transkribierter tRNA$^{Val}_{AAC}$ durch AlkBH7 mit und ohne MMS. Der Graph **A** zeigt den absoluten Level von m^{7}G in *in vitro* transkribierter tRNA$^{Val}_{AAC}$ mit MMS in schwarz und ohne MMS in Rot. Die Graphen **B** bis **E** zeigen die Level der anderen RNA-Modifikationen. Der blaue Stern markiert einen Ausreißer, der nicht in die statistischen Berechnungen miteinbezogen wurde. Alle Werte stammen von n=3 biologischen Replikaten.

Durch die größere Konzentration kann AlkBH7 natives m^{5}C, m^{3}C und m^{1}A in tRNA zu 14 %, 18 % und 15 % in 2 Stunden demethylieren. MMS-methylierte Substrate werden zu 20 % (m^{5}C), 17 % (m^{3}C), 19 % (m^{1}A) und 19 % (m^{1}G) signifikant durch AlkBH7 demethyliert (siehe Abbildung **3.15**).

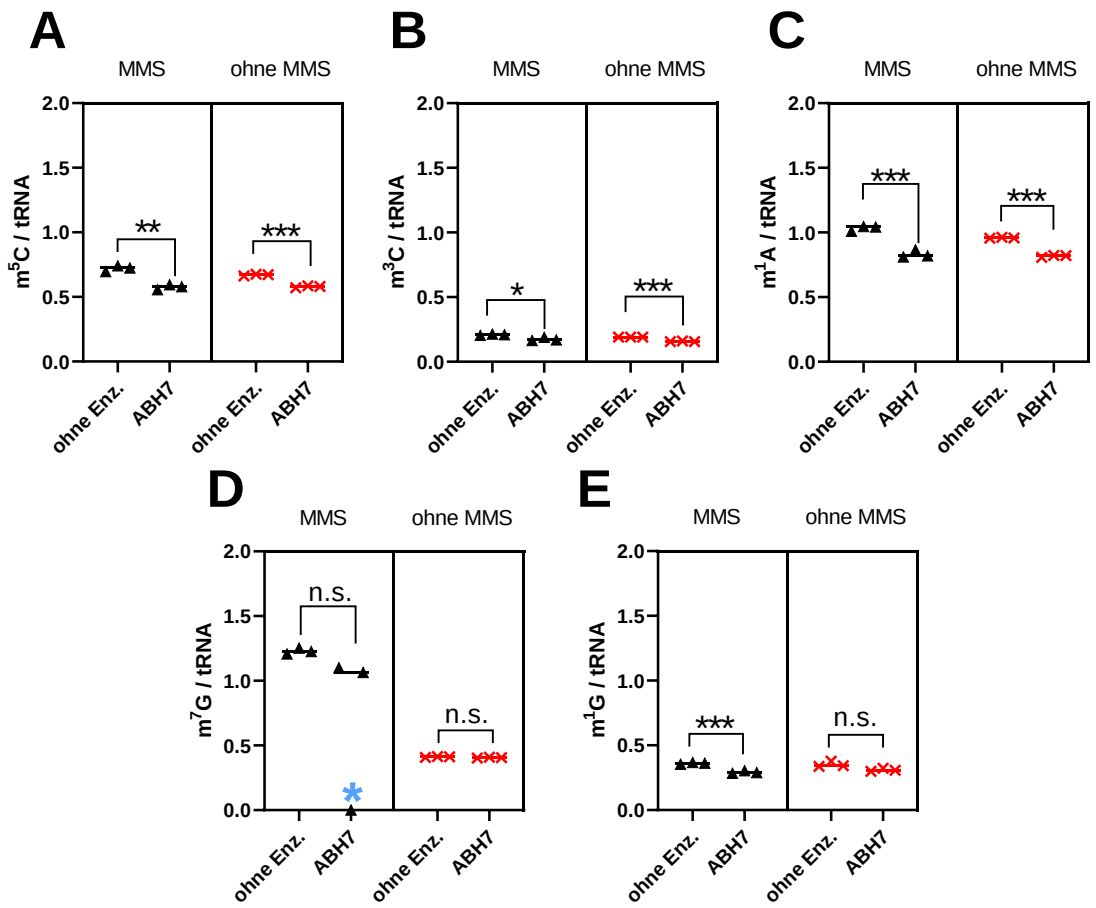

Abbildung 3.15: Demethylierung von nativer tRNA durch AlkBH7 mit und ohne MMS. Der Graph **A** zeigt den absoluten Level von m^5C in nativer tRNA mit MMS in schwarz und ohne MMS in Rot. Die Graphen **B** (m^3C), **C** (m^1A), **D** (m^7G) und **E** (m^1G) zeigen die Level der anderen RNA-Modifikationen. Der blaue Stern markiert einen Ausreißer, der nicht in die statistischen Berechnungen miteinbezogen wurde. Alle Werte stammen von n=3 biologischen Replikaten. Die Zweiweg-Varianzanalyse bestimmt die p-Werte, welche grafisch eingetragen sind (n.s. = nicht signifikant; $p<0,05$ = *; $p<0,01$ = **; $p<0,001$ = ***).

Das Kapitel 3.3.4 ist in folgender Abbildung **3.16** als Heatmap zusammenfassend grafisch dargestellt. AlkBH1 besitzt *in vitro* viele Substrate in der tRNA und kann auch positionsunabhänig demethylieren, was durch die vorherige Zugabe von MMS zur Reaktion bestätigt wurde. AlkBH3 agiert, wie in der Literatur bekannt, an m^1A und m^3C und besitzt keine weiteren RNA-Modifikationen als Substrate. AlkBH7 hingegen kann drei RNA-Modifikationen in tRNA *in vitro* demethylieren. Dies ist bisher noch nicht literaturbekannt, kann aber auch in der physiologisch sehr großen Menge an Enzym begründet liegen.

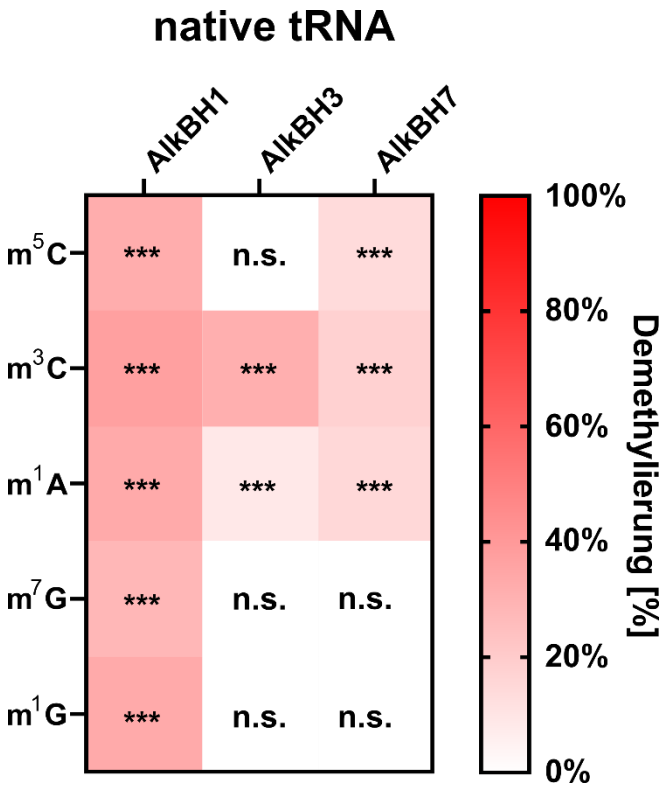

Abbildung 3.16: Zusammenfassung der Demethylierung von nativer tRNA durch AlkBH-Homologe *in vitro*. Die Heatmap zeigt die Demethylierungsraten in Prozent in nativer tRNA ohne MMS-Stress von m^5C, m^3C, m^1A, m^7G und m^1G. Die p-Werte sind grafisch in den jeweiligen Feldern der Heatmap eingetragen (n.s. = nicht signifikant = weißes Feld = $p>0,05$; $p<0,001$ = ***).

in vitro-Demethylierung von rRNA durch AlkBH3

Um die Demethylierungsaktivität von AlkBH3 abschließend an größeren, kompakteren Biomolekülen zu testen, wurden die beiden großen eukaryotischen, ribosomalen Untereinheiten 28S rRNA und 18S rRNA *in vitro* mit Enzym inkubiert. 1 µM Enzym ist in der Lage, wie in Abbildung **3.17 C** zu sehen, m^1A zu 42 % zu demethylieren. Hierbei handelt sich höchstwahrscheinlich um das literaturbekannte m^1A_{1322}[212]. Alle weiteren RNA-Modifikationen sind kein Substrat für AlkBH3 und werden auch nach MMS-Stress nicht repariert. Auch der Hauptschaden m^7G wird nicht signifikant beseitigt.

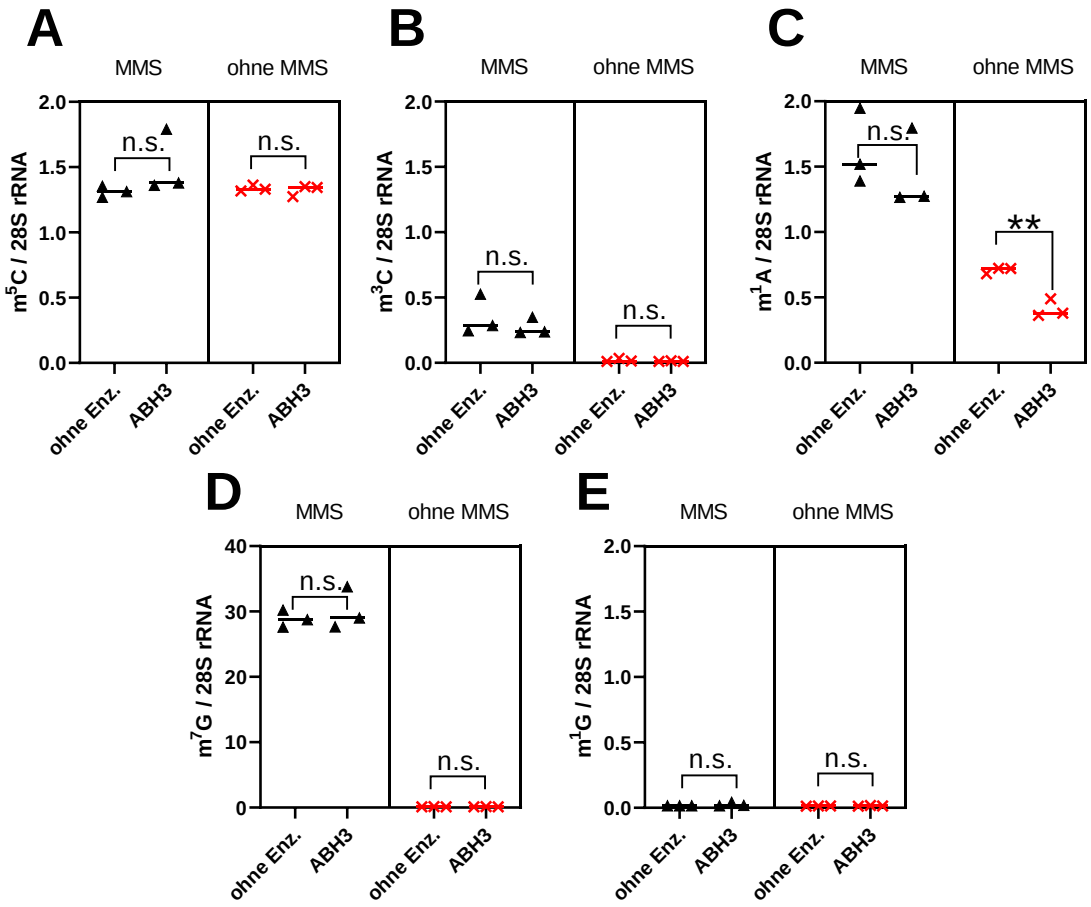

Abbildung 3.17: Demethylierung von nativer 28S rRNA durch AlkBH3 mit und ohne MMS. Der Graph **A** zeigt den absoluten Level von m^5C in nativer tRNA mit MMS in schwarz und ohne MMS in Rot. Die Graphen **B** (m^3C), **C** (m^1A), **D** (m^7G) und **E** (m^1G) zeigen die Level der anderen RNA-Modifikationen. Alle Werte stammen von n=3 biologischen Replikaten. Die Zweiweg-Varianzanalyse bestimmt die p-Werte, welche grafisch eingetragen sind (n.s. = nicht signifikant; p<0,01 = **).

In 18S rRNA ist m^1A nur noch substöchiometrisch zu detektieren und ist somit kein Demethylierungssubstrat mehr. Substöchiometrisches Vorkommen einer RNA-Modifikation wird durch ein absolutes Level < 0,05 Modifikationen/RNA-Molekül definiert, d.h. wenn nur maximal 5 % aller RNA-Makromoleküle diese bestimmte Modifikation tragen. In Abbildung **3.18** veranschaulicht, dass alle anderen beobachteten RNA-Modifikationslevels in 18S rRNA von AlkBH3 weiterhin unbeeinflusst sind.

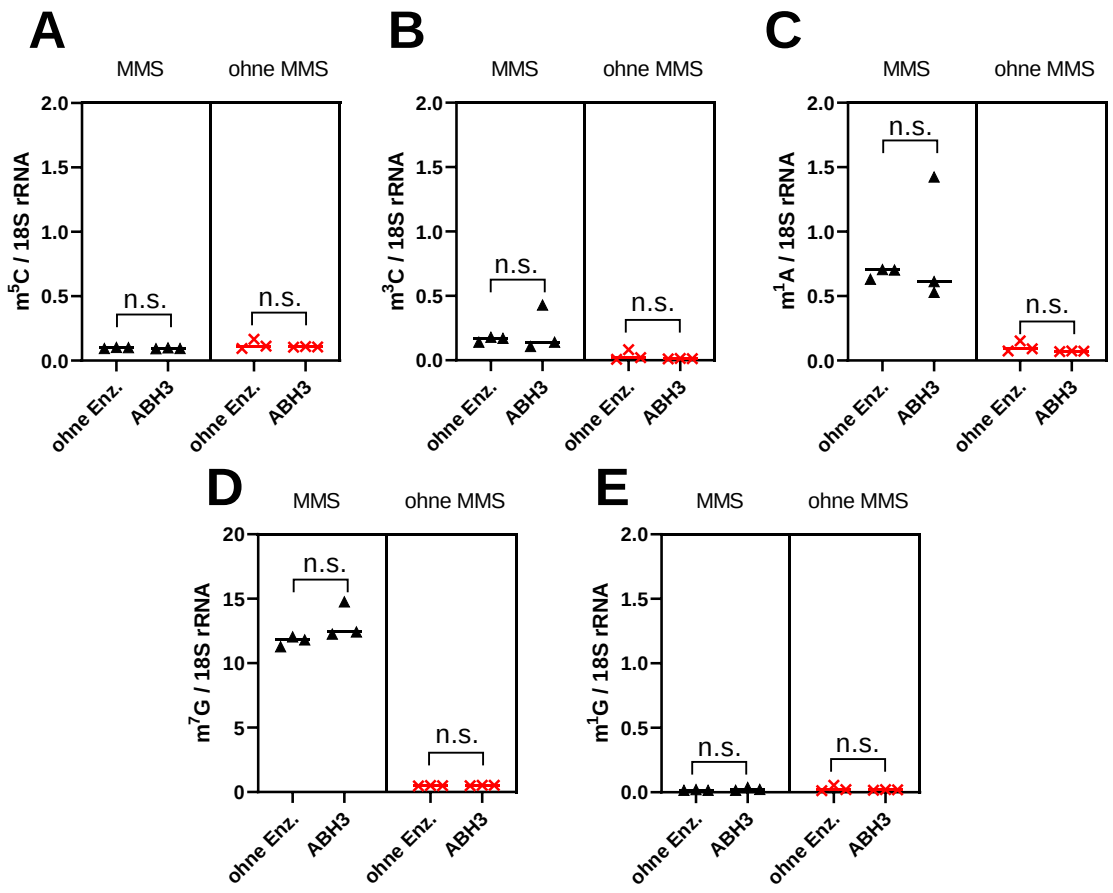

Abbildung 3.18: Demethylierung von nativer 18S rRNA durch AlkBH3 mit und ohne MMS. Der Graph **A** zeigt den absoluten Level von m^5C in nativer tRNA mit MMS in schwarz und ohne MMS in Rot. Die Graphen **B** (m^3C), **C** (m^1A), **D** (m^7G) und **E** (m^1G) zeigen die Level der anderen RNA-Modifikationen. Alle Werte stammen von n=3 biologischen Replikaten. Die Zweiweg-Varianzanalyse bestimmt die p-Werte, welche grafisch eingetragen sind (n.s. = nicht signifikant).

3.4 Eraser-Enzyme *in vivo*

3.4.1 Einfluss von Glucose auf AlkBH1 und RNA-Modifikationen *in vivo*

Um die von Liu et al.[120] postulierte tRNA-Demethylierung von der Modifikation m^1A_{58} durch AlkBH1 nachzuvollziehen und weitergehend die Glucoseabhängigkeit zu testen, wurden eukaryotische HEK 293- und HeLa-Zellen unter Glucosestressbedingungen kultiviert und das RNA-Modifikationsprofil von isolierten tRNA-Isoakzeptoren, $tRNA^{His}_{GUG}$ und $tRNA^{Gly}_{GCC}$ analysiert.

Hierfür wurden zunächst 24h vor Glucosestressbeginn 800.000 HEK 293-Zellen pro T25-Zellkulturflasche in DMEM-Medium ausgesät. Die Inkubation unter vier verschiedenen Mediumbedingungen dauerte 8h. Hierbei wurde - abweichend von Liu *et al*. - zwischen Serumstress (2 % im Gegensatz zu 10 % FBS) und Glucosestress ($1\frac{g}{L}$ anstelle von $4{,}5\frac{g}{L}$) differenziert. Nach RNA-Isolierung und Größenausschlusschromatographie wurden jeweils 500 ng der erhaltenen tRNA-Fraktion zur Separierung von einzelnen tRNA-Isoakzeptoren mittels Oligohybridisierung eingesetzt. Die erhaltenen Isoakzeptoren wurden mit Hilfe der Endonuklease Benzonase zu Nukleosiden verdaut und durch Zugabe des SILIS aus *S. cerevisiae* das m^1A/G %-Level quantifiziert. Die oberen beiden Graphen der Abbildung **3.19** zeigen den m^1A-Gehalt in Histidin- und einer Glycin-codierenden tRNA aus HEK 293-Zellen unter den vier genannten Nährmediumbedingungen. Allgemein lässt sich sagen, dass der Histidin-tRNA-Isoakzeptor mehr m^1A als $tRNA^{Gly}_{GCC}$ enthält. Allerdings haben die 8h Serum- und Glucosemangelproben von keiner der beiden tRNAs einen Einfluss auf die Menge an m^1A. Diese Beobachtung steht im Wiederspruch zu Liu *et al*., welche signifikant weniger m^1A/G% in den beiden erwähnten tRNA-Isoakzeptoren in den Nahrungsmangelproben gemessen haben. Um eine mögliche Zelllinienspezifität der Glucoseabhängigkeit zu erkennen, wurden zusätzlich HeLa-Zellen kultiviert und mit Ernährungsmangel gestresst. Es fällt in dem unteren Graph in Abbildung **3.19** auf, dass das Modifikationsniveau insgesamt niedriger als in HEK 293-Zellen ist, was mit dem Niveau von Liu *et al*. übereinstimmt. Es konnten jedoch auch in HeLa-Zellen keine signifikanten m^1A-Unterschiede in $tRNA^{Gly}_{GCC}$ in Abhängigkeit von der Glucose- oder Serumverfügbarkeit detektiert werden.

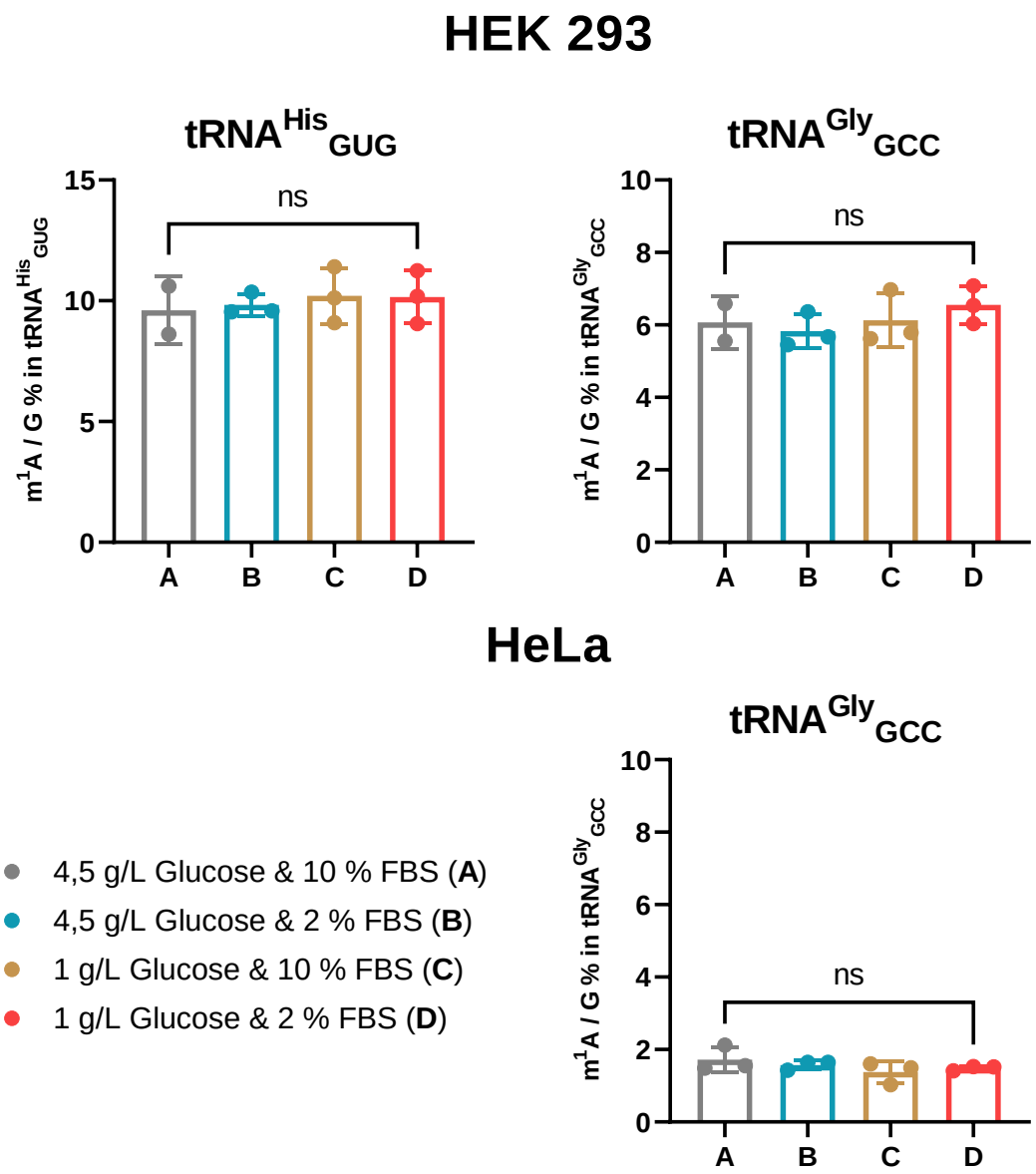

Abbildung 3.19: Quantifizierung des m^{1}A/G%-Gehalts in tRNA$^{Gly}_{GCC}$ und tRNA$^{His}_{GUG}$ aus eukaryotischen Zellen unter Nahrungsmangel. Die Graphen zeigen das m^{1}A-Niveau in zwei spezifischen tRNA-Isoakzeptoren nach einem *in vivo*-Mediuminkubatiosexperiment. Die variablen Komponenten des DMEM-Mediums, Glucose und FBS, sind in einzelnen farblich markierten Balken dargestellt. Die Legende befindet sich links unten. Alle Werte sind Mittelwerte aus n=3 biologischen Replikaten und die Fehlerbalken repräsentieren die Standardabweichung. Es wurden ungepaarte Student´s-t-Tests zur Ermittlung der Signifikanz durchgeführt. Hierbei wurden die bei Liu et al. verwendeten Bedingungen (4,5 g/L Glucose & 10 % FBS vs. 1 g/L Glucose & 2 % FBS) miteinander verglichen (ns = nicht signifikant).

Zusammenfassend lässt sich sagen, dass weder Serum- noch Glucosestress einen Einfluss auf die Demethylierungsaktivität von AlkBH1 *in vivo* auf m^1A in tRNA haben. Die Experimentparameter, die Oligohybridisierungssequenzen sowie die Art der Quantifizierung über $m^1A/G\%$ wurden nach Liu *et al*. gewählt. Zwei Zelllinien wurden getestet, jedoch ergibt sich weder für HEK 293 noch für HeLa eine Glucoseabhängigkeit der AlkBH1-Aktivität. Die Ergebnisse von Liu *et al*. sind nicht reproduzierbar. Die Ursache hierfür könnte in den verwendeten immortalisierten Zelllinien liegen, die von unterschiedlichen Herstellern bezogen wurden. Ihr unbegrenztes Teilungsverhalten fördert Aberrationen im Modifikationsniveau, sodass Artefakte in einzelnen kultivierten Zelllinien entstehen können.

Um eine detailliertere Betrachtung der AlkBH1-Aktivität *in vivo* zu erreichen, wird in dem Kapitel 3.4.3 ein Knockdown des AlkBH1-Proteins etabliert und mehrere RNA-Modifikationen absolut quantifiziert.

Des Weiteren soll mittels NAIL-MS die Dynamik der m^1A-Modifikation genauer untersucht werden. In einem isotopenmarkierten Pulse-Chase-Experiment kann die Herkunft des m^1As definiert und die Methylierungsdynamik des AlkBH1-Knockdowns erforscht werden.

3.4.2 NAIL-MS als Methode zur Erfassung der Dynamik von RNA-Modifikationen

Um ein NAIL-MS-Experiment (kurz für engl.: ***n****ucleic* ***a****cid* ***i****sotope* ***l****abeling coupled* ***m****ass* ***s****pectrometry*) durchführen zu können, ist es essentiell stabile isotopenmarkierte Nukleosidvorläufer metabolisch in die RNA einzubauen. Somit kann eine Diskriminierung zwischen originaler RNA aus alten Nukleosiden und neu transkribierter RNA aus isotopenmarkierten Nukleosiden in einem NAIL-MS-Experiment stattfinden. Mit Zugabe von isotopenmarkiertem CD_3-Methionin, welches in NAIL-MS-Medium vorhanden sein kann, ist es z.B. möglich zwischen Demodifizierungsprozessen durch Demethylasen, Degradierung von modifizierter RNA und Verdünnungseffekten durch Transkription neuer RNAs zu unterscheiden.

Gemeinsamer Prolog

Um diese Dynamiken der RNA-Modifikationen in eukaryotischen Zellen zu analysieren, muss zunächst aufgrund der Komplexität des Zellkulturmediums eine

Isotopenmarkierungsstrategie überlegt werden, mit der eine einheitliche und vollständige Markierung der RNA-Nukleoside möglich ist. Dies wurde durch Supplementierung mit den Metaboliten $^{13}C_5$, $^{15}N_2$-Uridin, $^{15}N_5$-Adenin und CD_3-Methionin in verschiedenen eukaryotischen Zellkultursystemen erreicht (*Nat. Comm*., **2021**). Eine detailliertere Beschreibung der Methodik von NAIL-MS sowie die Anwendung in weiteren Modellorganismen, wie *E. coli* und *S. cerevisiae*, wurde in einer weiteren Publikation gegeben (*Methods*, **2019**). Im folgenden Kapitel wurde durch ein zusätzliches Experiment die Dynamik auf die Demethylierungssubstrate von einigen AlkBH-Enyzmen, m^3C und m^1A, erforscht.

„Cell culture NAIL-MS allows insight into human tRNA and rRNA modification dynamics *in vivo*", M. Heiß, **F. Hagelskamp**, V. Marchand, Y. Motorin, S. Kellner, *Nat. Comm*., **2021**, 12 (1); 389.

Autorenbeitrag: Die Auswahl der verwendeten isotopenmarkierten Metabolite wurde von mir zusammen mit Matthias Heiß getroffen. Die Etablierung dieser Isotopenmarkierungsstrategie in HeLa-Zellen erfolgte durch mich. Die Sequenzierung der RNA wurde von Virginie Marchand und Yuri Motorin ausgeführt und die Sequenzierungsdaten ausgewertet. Alle weiteren Experimente wurden von Matthias Heiß durchgeführt. Die Ausarbeitung des Manuskripts wurde von Stefanie Kellner, Matthias Heiß und mir in Zusammenarbeit erledigt.

„Surpassing limits of static RNA modification analysis with dynamic NAIL-MS", V. F. Reichle, S. Kaiser, M. Heiß, **F. Hagelskamp**, K. Borland, S. Kellner; *Methods (San Diego, Calif.)*, **2019**, 156: 91-101.

Autorenbeitrag: Die Etablierung der NAIL-MS-Isotopenmarkierungsstrategie in Zellkultur erfolgte durch mich in Zusammenarbeit mit Matthias Heiß. Alle weiteren *in vivo* Experimente in Zellkultur und Hefe wurden von Matthias Heiß durchgeführt. Die Daten zu bakterieller RNA wurden von Valentin Reichle generiert. Steffen Kaiser erhob die Daten für einen komparativen NAIL-MS Ansatz. Die Ausarbeitung des Manuskripts erfolgte durch intensive Zusammenarbeit aller Autorinnen und Autoren.

nature COMMUNICATIONS

ARTICLE

https://doi.org/10.1038/s41467-020-20576-4 OPEN

Cell culture NAIL-MS allows insight into human tRNA and rRNA modification dynamics in vivo

Matthias Heiss[1], Felix Hagelskamp[1], Virginie Marchand[2], Yuri Motorin[2] & Stefanie Kellner[1,3]✉

Recently, studies about RNA modification dynamics in human RNAs are among the most controversially discussed. As a main reason, we identified the unavailability of a technique which allows the investigation of the temporal processing of RNA transcripts. Here, we present nucleic acid isotope labeling coupled mass spectrometry (NAIL-MS) for efficient, monoisotopic stable isotope labeling in both RNA and DNA in standard cell culture. We design pulse chase experiments and study the temporal placement of modified nucleosides in $tRNA^{Phe}$ and 18S rRNA. In existing RNAs, we observe a time-dependent constant loss of modified nucleosides which is masked by post-transcriptional methylation mechanisms and thus undetectable without NAIL-MS. During alkylation stress, NAIL-MS reveals an adaptation of tRNA modifications in new transcripts but not existing ones. Overall, we present a fast and reliable stable isotope labeling strategy which allows in-depth study of RNA modification dynamics in human cell culture.

[1] Department of Chemistry, Ludwig-Maximilians-University Munich, Butenandtstr. 5-13, 81377 Munich, Germany. [2] Université de Lorraine, CNRS, Inserm, UMS2008/US40 IBSLor and UMR7365 IMoPA, F-54000 Nancy, France. [3] Institute of Pharmaceutical Chemistry, Goethe-University Frankfurt, Max-von-Laue-Str, 9, 60438 Frankfurt, Germany. ✉email: stefanie.kellner@cup.uni-muenchen.de

Most RNAs studied to date were found to be covalently modified by dedicated enzymes in a site-specific manner. In addition to the placement of RNA modifications by RNA writer enzymes, their direct removal through e.g., demethylation by RNA erasers was reported. In human cells, the α-ketoglutarate dependent dioxygenases ALKBH5 and/or FTO were found to catalyze the demethylation of e.g., (2′-O-methyl-) N6-methyladenosine ($m^6A(m)$) in mRNA[1,2] and thus influence, e.g., the stability and translational function of mRNA[1,3–8].

For human tRNAs, a similar relationship of RNA writers and erasers was observed. E.g., ALKBH1 demethylates 1-methyladenosine (m^1A) and appears to be responsive to glucose starvation in some cell lines[9]. Considering the half-life of mammalian tRNAs (~100 h[10]), a fast adaptation by removal of modified residues appears beneficial to react to changes in the cellular environment[11]. Unfortunately, it is currently not possible to analyze the speed of both modification and demethylation reactions inside human cells. Thus, it is not possible to study the impact of external stimuli and stress on human RNA modification kinetics and processing of mature RNA.

tRNA is the most extensive and chemically diverse modified RNA with ~10–15% of all nucleosides being modified[12]. Recent studies showed that certain modified nucleosides in specific tRNAs are only partially modified[13,14] and that tRNA modification abundance differs among tissues[15,16]. This would allow for an adaptation of translation by tRNA modification as recently suggested[17]. While the speed of tRNA amino acid charging[18] and tRNA transcription and half-live are known[10], the speed of modification processes is difficult to study. For example, $tRNA^{Phe}$ is heavily post-transcriptionally modified and in addition one of the best studied RNAs[19–21]. By using stable isotope labeled $tRNA^{Phe}$ substrate and cellular extracts, the modification dynamics and hierarchy was recently solved in *S. cerevisiae* using NMR spectroscopy[22]. Under the influence of chemical stress, *S. cerevisiae* was reported to adapt its abundance of tRNA modifications and thus influence its translation and the term stress induced tRNA reprogramming was coined[11,23]. Similar evidence has been observed in other organisms, including mammals[24]. In this context, the question remains by which mechanism and how fast tRNA modifications respond to external stimuli.

In contrast to tRNA, 18S rRNA is mainly modified by methylation of ribose and altogether only 2.05% nucleosides are modified. While tRNA modifications are easily accessible for potential RNA erasers, rRNA modifications are placed in the functional regions of the ribosome[25]. Although modified sites in rRNA have been reported to regulate translation initiation by promoting the recognition of different mRNA subsets[26], their inaccessibility in mature ribosomes makes them a difficult target for RNA erasers.

Current studies of RNA modifications are limited to either mass spectrometric analysis[16] or sequencing[27,28]. Both techniques provide information on the modification status at the time point of sample harvest and give no details on the mechanisms of RNA modification adaptation. To overcome this limitation, we have recently developed NAIL-MS (nucleic acid isotope labeling coupled mass spectrometry) in bacteria[29,30] and yeast[31], which reveals the dynamics of RNA modification processes. The technique is based on metabolic stable isotope labeling of RNA using simple nutrients with e.g., carbon-13, nitrogen-15, or sulfur-34. By combining differentially labeled media in a pulse chase set-up, we recently succeeded to observe tRNA demethylation through AlkB in *E. coli* in vivo. Currently, NAIL-MS studies are not available for human cell lines as a monoisotopic labeling of all four canonical nucleosides is highly complex.

Here, we report a fast and reliable method for monoisotopic stable isotope labeling in both RNA and DNA (>95% within 7 days) in common human cell lines and growth media. We apply the cell culture NAIL-MS method and reveal the dynamics of human tRNA and 18S rRNA modifications in depths unreachable by any other tool for RNA modification analysis. Furthermore, we resolve the mechanism of stress induced tRNA modification reprogramming in the presence of methylation stress. With cell culture NAIL-MS it is finally possible to study the speed of both modification and demethylation reactions inside human cells. Thus, it will be possible to study the impact of external stimuli and stress on human RNA modification kinetics and processing of mature RNA.

Results

Absolute quantification of human $tRNA^{Phe}$ modifications. $tRNA^{Phe}$ is heavily post-transcriptionally modified and in addition one of the best studied RNAs[19–22]. Thus, it is an ideal model to study the temporal dynamics of its modifications. In a first step, we purified $tRNA^{Phe}_{GAA}$ from HEK 293 cells using a complementary DNA probe[13]. We used our established isotope dilution LC-MS/MS analysis for absolute quantification of modified nucleosides and plotted the modification profile in Fig. 1[16]. For pseudouridine (Ψ), dihydrouridine (D), 2,2-dimethylguanosine (m^2_2G), and 2′-O-methylguanosine (Gm) our experimental data matches the expected values and we see full modification[32]. The abundance of 1-methyladenosine (m^1A position 14 and 58), 7-methylguanosine (m^7G), 5-methyluridine (m^5U or rT), and 2′-O-methylcytidine (Cm) is lower compared to the literature, presumably due to partial modification of the respective sites. Partial modification has been suggested to play a role in stress induced reprogramming of tRNA modifications[17]. The abundance of 5-methylcytidine (m^5C) is slightly higher than expected and can be explained by the additional methylation of C48 by NSUN2[33].

Although 1-methylguanosine (m^1G) is not reported in $tRNA^{Phe}_{GAA}$, we found around 0.3 m^1G per tRNA. This observation can be explained by the fact that m^1G is a precursor during the biosynthesis of wybutosine (yW), a hypermodified nucleoside reported at position 37 of $tRNA^{Phe}_{GAA}$[34,35]. Due to the unavailability of a synthetic standard, yW could not be quantified in this study. In addition, we also quantified the abundance of other modified nucleosides (Table S1). We found around 0.3 6-methyladenosine (m^6A) per tRNA, potentially caused by intracellular Dimroth rearrangement of m^1A[36]. In addition, we found 0.063 inosine (I) and 0.026 1-methylinosine (m^1I) per $tRNA^{Phe}$. These are most likely artefacts from spontaneous A and m^1A deamination. All other modified nucleosides were found with an abundance of less than 1.6% (e.g., 0.016 N^6-threonylcarbamoyladenosine (t^6A) per tRNA) which indicates a high purity of isolated $tRNA^{Phe}$. Northern Blot analysis and deep sequencing of purified $tRNA^{Phe}_{GAA}$ sample indicated that this tRNA represents >90% with only minor contaminations by other tRNAs and rRNA (Figs. S1a and S2).

Overall, the detected quantities of modified nucleosides from purified $tRNA^{Phe}_{GAA}$ are in accordance with the reported values and thus it is a suitable model to study the temporal placement of modified nucleosides.

Stable isotope labeling of RNA in human cell culture. For this purpose, a method is needed which allows the discrimination of mature RNA from new transcripts. NAIL-MS (nucleic acid isotope labeling coupled mass spectrometry) relies on the metabolic incorporation of stable isotope labeled nutrients into RNA and allows the distinction of original RNA and new RNA within a pulse chase experiment. With this tool, we studied the temporal placement of modified nucleosides in *S. cerevisiae* total tRNA[31]

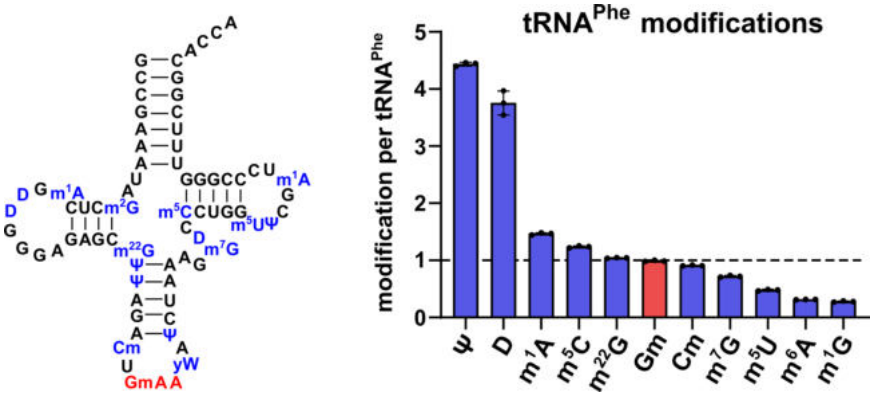

Fig. 1 Absolute quantification of human tRNA$^{Phe}_{GAA}$ modifications. The tRNA cloverleaf on the left shows the expected sequence of human tRNA$^{Phe}_{GAA}$ including reported modifications[32]. Right: Absolute quantification of purified tRNA$^{Phe}_{GAA}$ from HEK 293 cells done by LC-MS/MS. All experiments are from $n = 3$ biol. replicates. Bars reflect the mean and error bars reflect standard deviation.

and the demethylation during tRNA repair in *E. coli*[37]. Both organisms are rather simple and can be grown in minimal media with controlled availability of stable isotope labeled nutrients.

In contrast, human cell culture medium is highly complex and requires the addition of fetal bovine serum (FBS). FBS is a natural product of undefined composition and variable concentration of metabolites. Thus, a complete and monoisotopic labeling of nucleosides and even nucleobases for a pulse chase NAIL-MS assay is challenging.

From our experience, the target isotopologue of a nucleoside must be at least 3 u heavier compared to the naturally occurring nucleoside to avoid false positive results by the detection of the natural carbon-13 signals.

De novo synthesis of nucleosides utilizes several amino acids such as glutamine or aspartic acid (Fig. S3A, B)[38]. Hence, we supplemented the growth media with stable isotope labeled glutamine. After 5 days (2 passages), we observed the expected stable isotope labeling of RNA (Fig. S3C). Cytidine, guanosine and adenosine got a mass increase of +2 whereas uridine just increased by +1. Due to the overlap with naturally occurring (^{13}C)-isotopologues, this mass increase was not sufficient for our planned experiments.

As recently described, it is possible to use glucose-free growth medium and supplement with $^{13}C_6$-glucose[37]. The feeding with $^{13}C_6$-glucose leads to the formation of nucleosides with a variable number of ^{13}C-atoms per nucleoside (Fig. S3C). During method development, we utilized the non-monoisotopic nature of $^{13}C_6$-glucose labeling to test the incorporation efficiency of various unlabeled metabolites. Addition of aspartate and pyruvate did not allow the envisioned monoisotopic labeling (Fig. S4). The addition of the nucleobases adenine and uracil resulted in ribose labeled purines but undefined labeled pyrimidines. This indicates a direct usage of adenine from the medium which is then enzymatically connected with $^{13}C_5$-ribose followed by further processing to guanosine and the respective triphosphates (Fig. S3B). RNA supplemented with the nucleosides adenosine and uridine showed undefined labeled purines and only unlabeled pyrimidines (Fig. S5). This indicates that uridine is taken up by the cells and immediately utilized for cytidine and RNA synthesis (Fig. S3A). In summary, our data indicates that the addition of adenine and uridine blocks de novo purine and pyrimidine synthesis (Fig. S3A, B) and $^{13}C_6$-glucose medium is not necessary for our labeling strategy (Fig. S5). Concentration optimization of both compounds revealed that final concentrations of 0.1 mM adenine and 0.2 mM uridine in the $^{13}C_6$-glucose medium are needed to suppress signals from de novo synthesized nucleosides (Fig. S6).

Hence, we used $^{15}N_5$-adenine and $^{13}C_5$,$^{15}N_2$-uridine (Fig. 2a) in medium with unlabeled glucose. The high-resolution mass spectra of the resulting RNA nucleosides showed the desired labeling for >95% of all canonical nucleosides after 7 days (Fig. 2b). A +7 mass increase is observed for cytidine and uridine and a +5 and +4 mass increase for adenosine and guanosine, respectively. By using dialyzed FBS, the signal of unlabeled adenosine could be further reduced in comparison to normal FBS (Fig. S7). Similarly, DNA nucleosides become stable isotope labeled (Fig. S8).

With these metabolites, a pulse chase NAIL-MS study is possible in human cell culture. To this end, we achieve excellent labeling in HEK 293, HAP and HeLa cell lines using supplemented DMEM, RPMI or IMDM medium (Fig. S9).

In mouse embryonic stem cells (mESC), the addition of $^{15}N_5$-adenine and $^{13}C_5$,$^{15}N_2$-uridine leads to non-monoisotopic labeling. Here, the labeling efficiency is improved from 35 to 70% by the usage of dialyzed FBS (Fig. S10).

In HEK 293 cells, the signals of new tRNA transcripts became detectable and quantifiable after 120 min of labeling (Figs. S11/S12).

Most modified nucleosides in RNA carry one or more methylations. To follow the fate of these methylated nucleosides in the context of RNA maturation and methylation damage response, we used CD_3-labeled methionine. Methionine is the precursor amino acid of S-adenosylmethionine (SAM) which in turn is cofactor of most RNA methyltransferases. In the presence of CD_3-methionine, most methylated nucleosides get a mass increase of +3 and can thus be distinguished from nucleosides modified in the presence of unlabeled methionine. High resolution mass spectra of fully labeled m^5C, m^7G, and m^1A are exemplarily shown in Fig. 2c. In order to achieve complete labeling of methyl-groups, methionine depleted medium has to be used. We chose DMEM D0422 (from Sigma-Aldrich, Munich, Germany) which lacks glutamine, cystine and methionine (Fig. S13). Neither cell shape nor growth speed were influenced by the labeling and both were comparable to standard DMEM (e.g., D6546, from Sigma-Aldrich) (Fig. S14).

The combination of nucleoside and methyl-group labeling allows the design of elegant pulse chase studies to follow the fate of RNA in human cells.

Validation of human cell culture NAIL-MS. After finding a suitable way for monoisotopic labeling of RNA in human cells, we wanted to rule out the possibility of the labeling itself impacting the abundance of RNA modifications. For this purpose, cells were grown in labeled or unlabeled media for 7 days. Both media

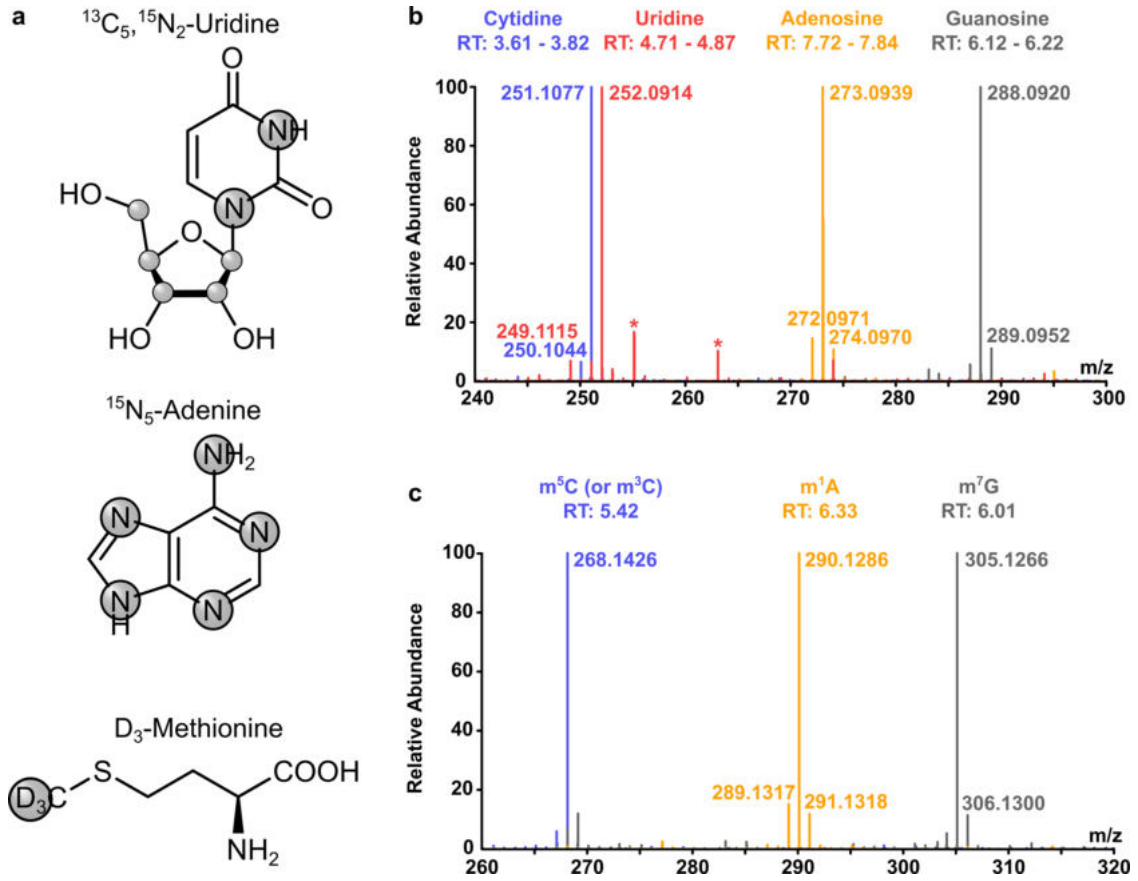

Fig. 2 High resolution mass spectra of stable isotope labeled nucleosides from cell culture. a Labeling of compounds used for stable isotope labeling in cell culture. Grey circles indicate the positions of isotopes (^{13}C, ^{15}N, or $^{2}H/D$). **b** Merged high resolution mass spectra of the 4 canonical nucleosides of total tRNA after labeling of HEK 293 cells with shown compounds for 7 days. Background signals are marked with asterisks. **c** Merged high resolution mass spectra of three exemplary modifications (m^5C, m^7G, and m^1A) in total tRNA after stable isotope labeling of HEK 293 cells for 7 days.

contained adenine, uridine and methionine as either unlabeled or labeled nutrients. Cells were harvested with TRI reagent and split into two aliquots. One aliquot (2/3 Vol) was used for immediate RNA isolation and purification, while the remaining aliquot of the labeled and unlabeled cells were mixed and RNA was co-isolated and co-purified (Figs. 3a and S15). The total tRNA was enzymatically digested to nucleosides and their abundance determined by isotope dilution mass spectrometry[16]. In the aliquot from unlabeled samples, only unlabeled nucleosides were detectable, while the aliquot of the labeled cells showed mainly signals (>98%) for labeled nucleosides. As expected from the mixed sample, we detected unlabeled and labeled isotopologues of all canonicals in similar amounts (Fig. 3b). Next, we quantified the abundance of modified nucleosides. For normalization, unlabeled modifications were referenced to unlabeled canonicals and labeled modifications were referenced to labeled canonicals. The calculated quantities of modified nucleosides present in $tRNA^{Phe}$ (according to Fig. 1) are plotted for the unlabeled against labeled tRNA in Fig. 3c. This validation revealed that the quantities of modified nucleosides are independent of the media and that the labeling procedure itself does not interfere with the isotope dilution MS quantification. This finding is in accordance with our northern blot data, where we observe no change in $tRNA^{Phe}$ abundance in dependence of the labeling medium (Fig. S1b). The deviation from the expected values (dotted diagonal line) is the error of this NAIL-MS experiment and the limitation to detect differences in a biological setup (also see Fig. S16). E.g., In total tRNA, 2′-O-methyluridine (Um) has the largest error as its abundance deviates 1.6 fold in labeled and unlabeled media.

The promising results from the validation experiments allowed the design of pulse chase experiments. Such experiments start with cells seeded in medium-I which, upon experiment initiation, is exchanged to medium-II with different isotopically labeled nutrients. The concept is shown in Fig. 3d. To rule out possible differences in the results in dependence of the starting medium, we designed a brief validation experiment. In the forward experiment, cells are seeded in unlabeled medium and switched to labeled medium while the reverse experiment starts in labeled medium (after a 7 day labeling period) before switching to unlabeled.

For analysis of modified nucleoside quantities, we harvested the cells and extracted total tRNA after switching to medium-II (time points 0, 6, 24, and 48 h). To assess the suitability of the method for temporal placement of modified nucleosides into the total tRNA, we focused on the abundance of new modified nucleosides in the newly transcribed tRNA. For direct comparison, the ratio of found (6, 24, 48 h–new transcripts) and expected (0 h–original transcripts) modified nucleoside quantity was formed and plotted over time. As expected, we observed the incorporation of modified nucleosides into the new tRNA after medium exchange. While the timing of the tRNA modification process was comparable in the reverse and forward experiment, the start values were obscured in the reverse experiment due to low, but detectable signals of unlabeled nucleosides. For this and economic considerations, we decided to perform forward pulse chase

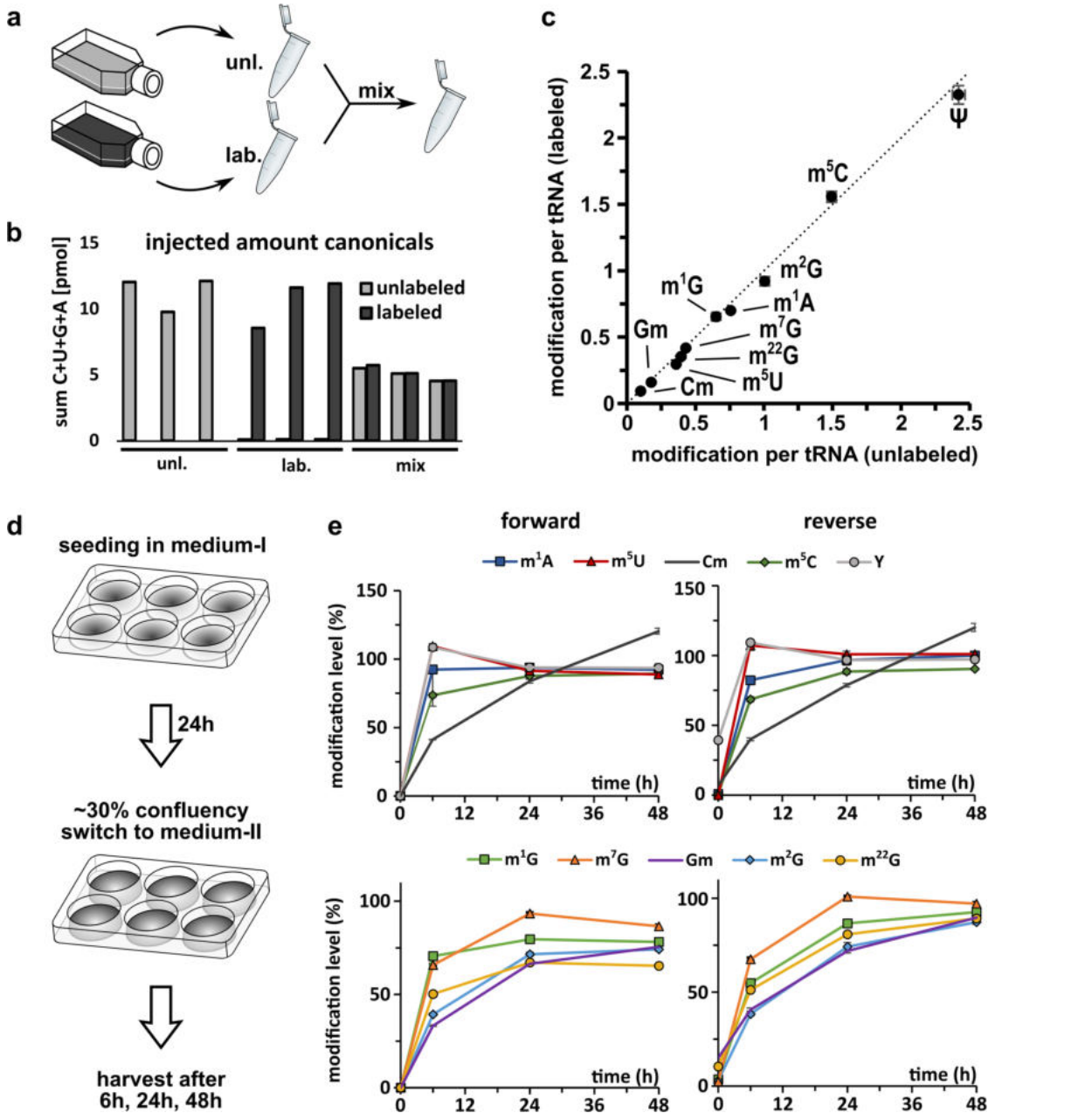

Fig. 3 Validation of cell culture NAIL-MS. a Cells were grown in unlabeled or fully labeled media for 7 days. Upon harvesting one aliquot was mixed prior to processing (mix). Total tRNA was purified and all samples were analyzed by LC-MS/MS. **b** Summed amount of canonical nucleosides (C + U + G + A) detected by LC-MS/MS for unlabeled and labeled isotopologues. The bars show single replicates of three unlabeled, three labeled and three mixed aliquots. **c** Abundance of labeled modifications plotted against the abundance of unlabeled modifications in the mix samples. The dotted line indicates the location of the expected values as a visual guide. **d** Experimental setup of time course study to investigate temporal placement of RNA modifications. The experiment was done forward (start with unlabeled, change to labeled medium) and reverse (vice versa). **e** Results of time course study. Plotted on the *y*-axis is the abundance of modification in new transcripts normalized to the abundance before experiment initiation (T = 0). Note: In the reverse experiment, minor signals of unlabeled nucleosides are present at T = 0 and thus the starting value is sometimes larger than 0%. All experiments were done with purified total tRNA and are from $n = 3$ biol. replicates. Symbols reflect the mean and error bars reflect standard deviation.

experiments in the future to avoid the excessive use of labeled medium.

Temporal placement of modified nucleosides in RNA. From a biological perspective, we observed that most modified nucleosides reach their final abundance (100% compared to the starting point) within 48 h (Fig. 3e). Some modified nucleosides, such as m^1A, m^5C, Ψ, and m^5U, are already >90% after 6 h which indicates a fast incorporation after transcription. These modified nucleosides are located in the structure-stabilizing positions of the tRNA's D-loops and TΨC-loops and thus a fast and reliable modification is to be expected[39]. m^7G is also involved in structure stabilization[40] and yet, this methylation is placed rather slowly in total tRNA. Other modified nucleosides such as Cm, Gm, and the base-methylated G derivatives (m^1G, m^2G, and $m^{22}G$) are incorporated more slowly and the final modification density is not reached within 48 h.

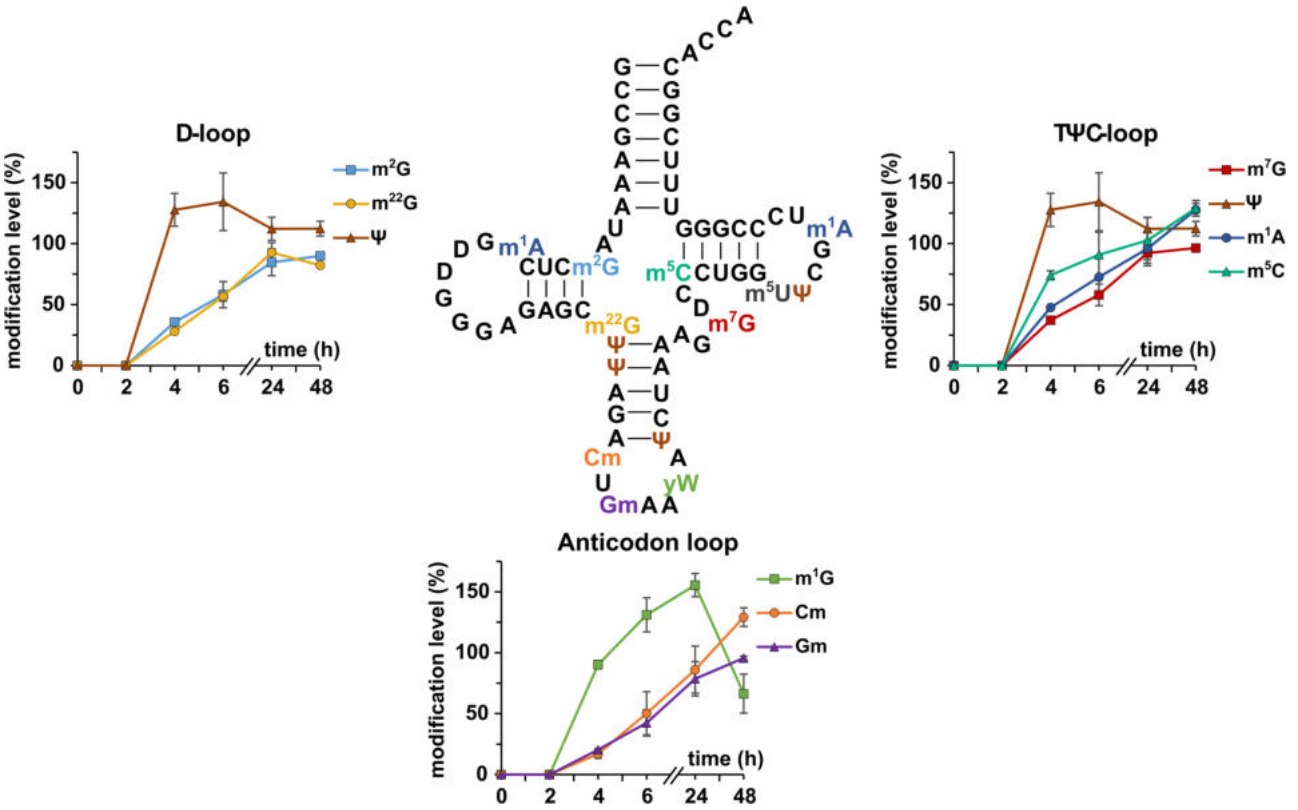

Fig. 4 Temporal placement of modified nucleosides in tRNA$^{Phe}_{GAA}$. Cells were grown in unlabeled DMEM D0422 (supplemented with unlabeled uridine and adenine) for 7 days. At T = 0 the medium was exchanged to DMEM D0422 supplemented with labeled uridine and adenine. Cells were harvested after set time points. tRNA^{Phe} was purified and analyzed by LC-MS/MS. Modifications are plotted next to their location in the D-, TΨC- or anticodon loop. Plotted on the *y*-axis is the abundance of modification in new transcripts normalized to the respective nucleoside originating from unlabeled medium before experiment initiation (T = 0). The experiment was done in $n = 3$ biol. replicates for time points 2, 4, and 48 h and in $n = 6$ biol. replicates for time points 0, 6, and 24 h. Symbols reflect the mean and error bars reflect standard deviation.

While the modified nucleosides of total tRNA are placed by various enzymes at various positions, we were interested to observe the modification process of defined enzymes in a defined substrate. For this purpose, we performed a pulse chase experiment and purified tRNA$^{Phe}_{GAA}$ after 0, 2, 4, 6, 24, and 48 h. The abundance of modified nucleosides in new tRNA transcripts is shown in Fig. 4. We observe an immediate high abundance of Ψ, which argues towards an immediate isomerization of e.g., U55 to Ψ55 as observed in yeast[22]. In fact, we observe 1.5-fold more Ψ in the early lifetime of tRNA$^{Phe}_{GAA}$ as is expected from mature tRNA$^{Phe}_{GAA}$ (Fig. 1). At these early time points, the abundance of new tRNA$^{Phe}_{GAA}$ transcripts is low and thus the MS signal intensity is close to the lower limit of quantification (LLOQ). Uridine and its modifications have a low ionization efficiency and thus a higher LLOQ compared to other modified nucleosides. Thus, biological interpretation of Ψ and m^{5}U (Fig. S17) quantities must be conducted carefully. D is not included in this analysis, due to its artificial addition to the samples through the deaminase inhibitor tetrahydrouridine (which was omitted for analysis in Fig. 1 and thus allowed quantification of D). While m^{7}G is the next modified nucleoside placed in yeast tRNA^{Phe}, our data hints towards a fast incorporation of m^{5}C followed by m^{1}A and finally m^{7}G. Here, the dynamic placement of modifications in the TΨC-loop seems to be slightly different between yeast and human. The slow incorporation of m^{2}G in the D-stem is in accordance with the reports from yeast. In the anticodon-loop (ac-loop), we observe a rather slow formation of Gm and Cm. These modified nucleosides are not involved in structure stabilization but codon-anticodon binding[41,42] and protein translation. Our data implies that structure stabilization by modified nucleosides is a key necessity and must thus happen early on, while ac-loop modifications are not immediately needed and are potentially placed on-demand. One exception is the formation of wybutosine (yW). Its precursor modification m^{1}G is immediately incorporated into tRNA^{Phe} before its abundance drops at later time points, presumably due to its further processing into yW.

Dynamics of tRNA and 18S rRNA modifications. With the design of our pulse chase NAIL-MS assay, we can observe RNA maturation processes by quantifying the abundance of modified nucleosides in new transcripts. In addition, we can follow the fate of original RNA (unlabeled nucleosides in forward experiment) and observe methylation or demethylation events.

In Fig. 5a, we plotted the abundance of exemplary modified nucleosides from original total tRNA, which were present before medium exchange. Other modified nucleosides are shown in Fig. S18. Similar to our initial observations in *S. cerevisiae*[31], we observed a constant loss of modified nucleosides from original tRNAs. In the common, unlabeled analysis of modified nucleosides, the decrease in modification density from original tRNA is not visible as it is masked by the addition of new methyl marks to original tRNAs at early time points (post-methylation) and by quickly modified new transcripts at later time points (ratio original/new transcripts in Figs. S18/19). Here, the post-methylation reaction is captured by the CD_3-methionine added in the chase phase (medium-II) and is termed "methyl" in Fig. 5a.

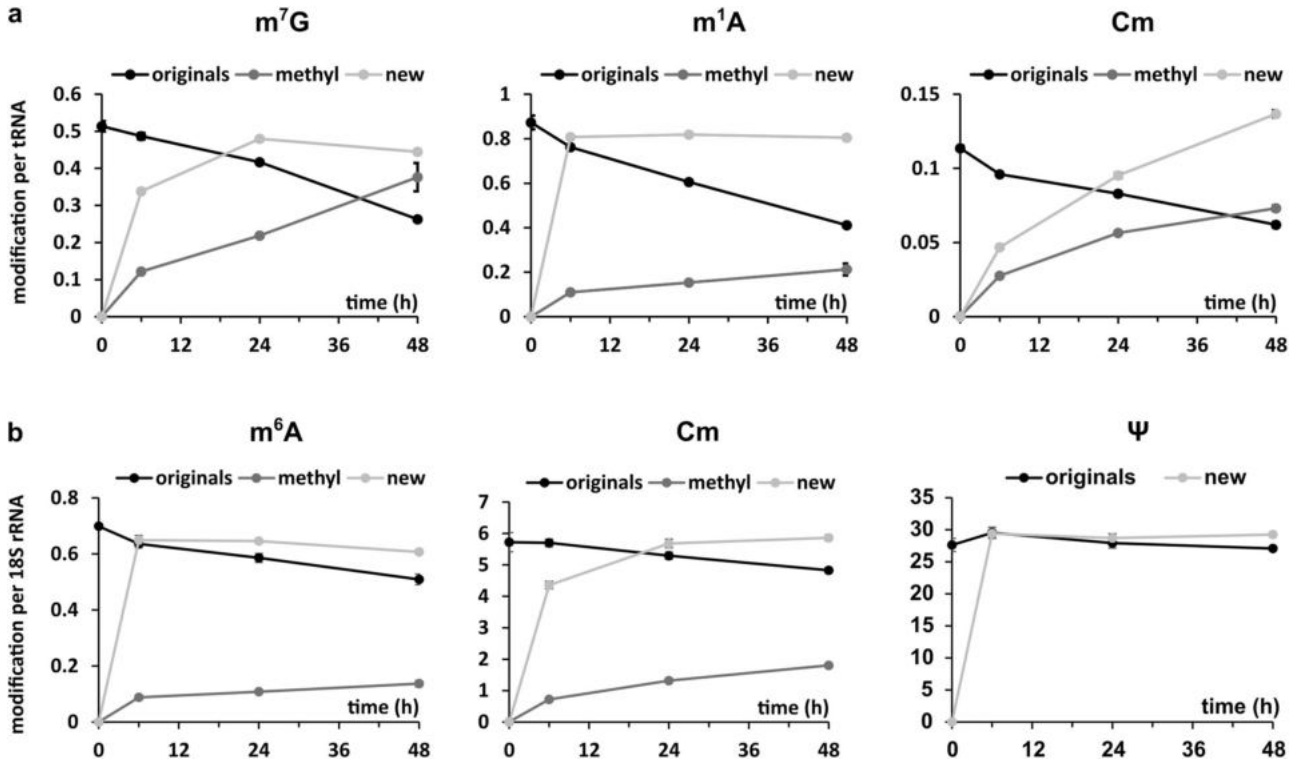

Fig. 5 Dynamics of modified nucleosides in total tRNA and 18S rRNA. a Results for total tRNA. **b** Results for 18S rRNA. Original nucleosides (originals, black line) existed before experiment initiation. Post-methylated nucleosides (methyl, dark grey line) are modifications arising from the methylation of original RNA after experiment initiation. New nucleosides (new, light grey line) show the incorporation of modification into new transcripts. Data points reflect the mean and standard deviations of $n = 3$ biol. replicates.

Intriguingly, the extent of post-methylation depends on the modified nucleoside. For m^7G and Cm, it is more pronounced compared to m^1A. Interestingly, many modified nucleosides which are placed almost immediately after transcription, show low amounts of post-methylation while those with a delayed incorporation showed substantial post-methylation.

Similar to tRNA, ribosomal RNA nucleosides are modified, mainly at locations close to the functional region of the ribosome[25]. From yeast studies, it is known that most ribose rRNA modifications are inserted immediately or even co-transcriptionally[43]. For Ψ and other base modifications, the time point of placement during rRNA maturation is yet unknown. In a forward pulse-chase experiment, we have isolated 18S rRNA and quantified the abundance of the original and new modified nucleosides. As expected from yeast, ribose methylations appear early on in new 18S rRNA transcripts. Intriguingly, m^6A and Ψ are inserted as fast or even faster. This indicates an immediate placement after transcription which is in agreement with their inaccessibility at later stages of ribosome biogenesis (Fig. S19).

Impact of methylation stress on tRNA modification processes. We have recently applied NAIL-MS to profile bacterial tRNA damage by methylating agents[29] and described the repair mechanisms in vivo[37]. With the goal to study the stress response in human cells, we determined the effect of methyl methanesulfonate (MMS) on growth of HEK 293 cells (Fig. S20). In these experiments, we observed a strong influence of trypsinization on cell survival, which we avoided in later experiments.

Until now, it was not possible to study the extent of m^1A and m^7G damage formation in human RNA due to the presence of enzymatically placed m^1A and m^7G. With our cell culture labeling scheme, we succeeded to implement a methylome discrimination assay and determine the absolute abundance of these major RNA damages. For this purpose, cells were grown in CD_3-methionine supplemented medium for 7 days before addition of 1 mM MMS. While enzymatically placed methylations are CD_3-labeled, MMS damaged sites are CH_3-labeled and thus easily distinguishable from the enzymatic sites by mass spectrometry. To enable the tracing of the damaged tRNAs without interference of new transcripts, we included a switch to fully labeled media ($^{13}C/^{15}N$-nucleoside body + CD_3) for labeling of new transcripts. The timeline and concept is given in Fig. 6a. Samples of MMS and MOCK treated cells were taken before and after 1 h of MMS exposure and up to 6 h after removal of MMS, where cells were left to recover from MMS treatment.

From these samples, we purified $tRNA^{Phe}_{GAA}$ and quantified the abundance of canonical and modified nucleosides. By comparison of canonical nucleosides, we could observe a higher ratio of new transcripts over original transcripts in the unstressed samples compared to the stressed samples (Fig. S21). This is to be expected as stressed cells stop growing and thus less transcription and translation are taking place. In addition, the prolonged abundance of original tRNA suggests that methylation stress does not lead to extensive degradation of tRNAs.

The quantification of methylated nucleosides derived from direct MMS methylation indeed showed formation of the known damage products m^7G and potentially m^1A. In comparison to the natural abundance of these modified nucleosides (~0.5 m^7G and 1 m^1A per $tRNA^{Phe}_{GAA}$), the damage accounts for less than 1% of these methylated nucleosides (Fig. 6b). In other words, only 1 out of around 200 tRNA molecules gets an additional m^7G by MMS damage. For m^1A the damage is found in 1 out of 1000 tRNAs (0.1%). No other reported MMS damage products were detected in human $tRNA^{Phe}$.

While RNA methylation damage repair was observed in *E. coli*, using a similar NAIL-MS approach, no demethylation was

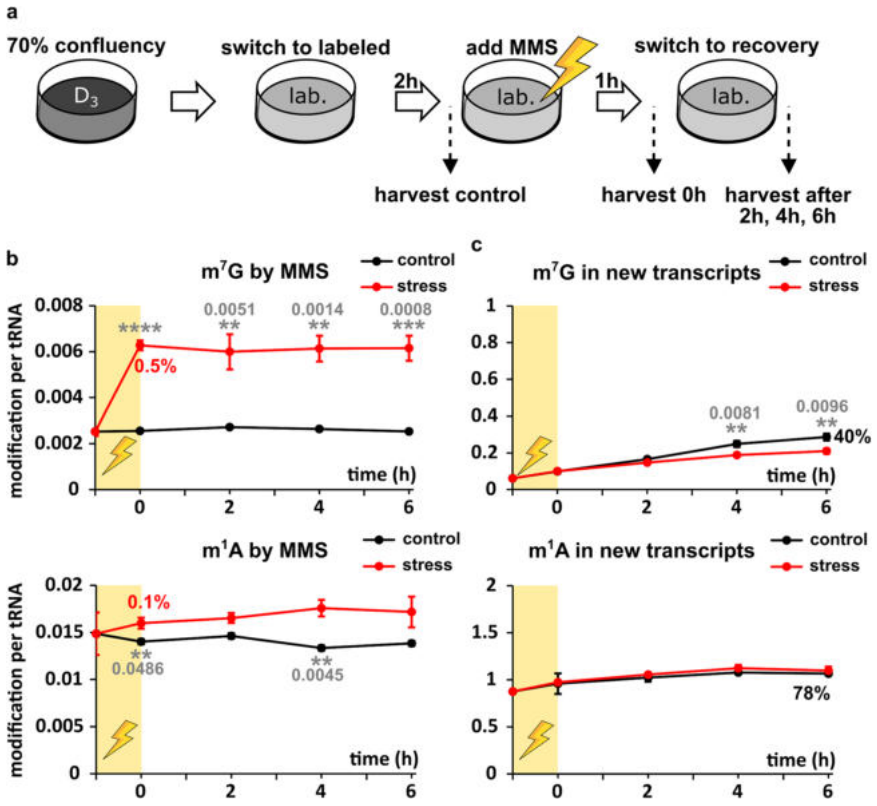

Fig. 6 Effect of methylation stress on tRNA modifications. a 70% confluent CD_3-methionine labeled cells were incubated with fully labeled media for 2 h before the LD_{50} dose of methyl methanesulfonate (MMS, yellow shaded area) was added. Control samples were treated the same, substituting the MMS stock solution with PBS. After 1 h the stress (or control) media was replaced by fresh labeled media. After set time points, cells were harvested and $tRNA^{Phe}_{GAA}$ was purified and subjected to LC-MS/MS analysis. **b** Unlabeled modifications were referenced to unlabeled canonicals to calculate the amount of modifications arising from direct methylation damage by MMS. Red numbers at time point 0 give the percentage of damaged nucleoside referenced to the naturally occurring amount of the respective modification (amount of original modification before experiment initiation). **c** Labeled modifications were referenced to labeled canonicals to calculate the amount of modification in new tRNA transcripts. The numbers at time point 6 give the percentage of modification amount in the control sample referenced to the naturally occurring amount of the respective modification. All experiments are from $n = 3$ biol. replicates. Symbols reflect the mean and error bars reflect standard deviation. *P*-values from student t-test (equal distribution, two-sided): $^*p < 0.05$, $^{**}p < 0.01$, $^{***}p < 0.001$, and $^{****}p < 0.0001$. Where reasonable, exact *P*-values are given as grey numbers in the figure.

detectable in the human cell line. Even 6 h after removal of the methylating agent, the abundance of non-enzymatically methylated m^7G and m^1A stayed unchanged in the original transcripts. This observation indicates that human cells either have a highly expressed and fast acting RNA demethylase for RNA damage repair or no RNA demethylase at all. Also, the abundance of damaged nucleosides could be below a threshold limit to trigger damage repair in human cells.

We next asked the question, whether human cells react to methylation stress by adaptation of tRNA modifications. This adaptation can be mechanistically achieved by addition or removal of modified nucleosides to original tRNAs, by delayed modification of new tRNAs or a combination of both. For methylation stress, we did not see a difference in modified nucleoside abundance in original tRNA compared to the unstressed control (Fig. S22). (Note: In this NAIL-MS study, the supplemented methionine was CD_3-labeled in both the pulse and the chase phase. Thus, it is not possible to observe the decrease of enzymatically placed modifications in original tRNA over time as shown in Fig. 5).

Finally, we studied the abundance of modified nucleosides in new tRNA transcripts in dependence of stress. For methylated guanosine derivatives (m^7G, m^1G, m^2G, and $m^{22}G$), we observed a slightly reduced, but statistically significant (e.g., m^7G $p_{6h} = 0.0096$) incorporation into $tRNA^{Phe}_{GAA}$ under stress compared to the control samples (Figs. 6c and S22). For Cm and Gm, we observed a higher abundance under stressed conditions while m^1A or m^5C were comparable. Our results imply that human cells (i) adapt their tRNA modifications to methylation stress by differentially modifying new transcripts and (ii) consider tRNA modification as a highly important process and thus continue even during stress exposure.

Discussion

Current analyses of the epitranscriptome are limited to snapshot moments and cannot truly follow dynamic processes inside cells. While NAIL-MS allows the observation of RNA modification adaptation processes[37,44] it was not possible to apply the technique in human cell culture due to the complexity of culture medium. $^{13}C_6$-glucose is a reasonable and economic option for stable isotope labeling (28 € per 50 mL medium)[45] but it suffers from the formation of multiple isotopologues which complicates its application especially when additional feeding with CD_3-methionine is required. In such studies, the signals of partially ^{13}C-labeled nucleosides and CD_3-methylated nucleosides can overlap and quantification becomes impossible. In contrast, supplementation of various media with $^{15}N_5$-adenine and $^{13}C_5$,$^{15}N_2$-uridine results in monoisotopic labeling with no overlap with naturally occurring ^{13}C-isotopologues or artificially CD_3-methylated nucleosides (305 € per 50 mL medium). Thus, a

broad applicability and even quantification by isotope dilution mass spectrometry is possible. While we observe best results with dialyzed FBS, it is also possible to use regular FBS instead if it is preferable to the cells. If the nucleoside of interest is a G or A derivative, $^{13}C_6$-glucose labeling can be combined with supplementation of unlabeled adenine. This approach is less costly and produces monoisotopically labeled A and G derivatives with a $^{13}C_5$-ribose moiety (Figs. S5 and S6).

An important consideration for any NAIL-MS study is the constant supplementation with adenine and uridine, even when unlabeled medium is used to prevent activation of de novo synthesis pathways. Independently of the chosen nucleic acid labeling scheme, we strongly recommend validation experiments as shown in Fig. 3c. Such an experiment is crucial to later judge the statistical significance of e.g., pulse chase studies. For example, our validation experiment indicates that a less than 1.6 fold change in Um would not be biologically significant (Fig. S16). In such a case we recommend the direct comparison to a control sample (such as those in Fig. 6) to judge the accuracy of the received NAIL-MS data.

Furthermore, we suggest careful interpretation of new transcript data at early time points of pulse chase experiments. As described for Ψ and m^5U (Fig. S17), it is possible that some modified nucleosides are early on too close to the lower limit of quantification (LLOQ) in new transcripts and thus the received quantities must be interpreted carefully.

We have studied the temporal placement of modified nucleosides in $tRNA^{Phe}$ as a model. Our data implies that structure stabilization by modified nucleosides is a key necessity and must thus happen early on, while anticodon-loop modifications are not immediately needed and are potentially placed on-demand. One exception is the formation of wybutosine (yW). Its precursor modification m^1G is immediately incorporated into $tRNA^{Phe}$ before its abundance drops at later time points, presumably due to its further processing into yW. By NMR spectroscopy in combination with stable isotope labeling, Barraud et al. recently observed an inhibition of $m^{22}G$ formation by m^2G[22]. In our hands, $m^{22}G$ is placed into $tRNA^{Phe}$ as fast as is m^2G, but as both modifications are incorporated slowly it is possible that $m^{22}G$ is placed in a non-m^2G modified sub-population. This question might be approached by combining NAIL with oligonucleotide MS.

With NAIL-MS we are not limited to RNA modification studies in new transcripts. In addition, we can follow the fate of RNA modifications in mature transcripts. In human cells, we observe a constant loss of modified nucleosides from tRNAs, similar to our initial report in *S. cerevisiae*[31]. The extent of the decrease is similar for all modified nucleosides in tRNA (~50% lower within 48 h) including non-methylated modifications, which argues towards a preferential degradation of modified tRNA. In 18S rRNA, we see a similar loss of modified nucleosides from original transcripts which is with ~20% within 48 h less pronounced as in tRNA. The ~2-fold longer half-life of rRNA compared to tRNA[46] supports our hypothesis of preferred degradation of modified RNA which is most likely connected to the life time of RNA.

The constant loss of pre-existing modifications from original RNA is masked in the early time points of the experiment by observable post-transcriptional methylation of original RNA. For many modified nucleosides, the extent of post-methylation of existing transcripts is connected to the extent of modification in new transcripts (Figs. S18 and S19). Some modified nucleosides such as m^7G, m^3U, m^3C, mcm^5s^2U and Um show no correlation between post-methylation and new methylation abundance. Except m^7G, all these modified nucleosides are placed in or close to the anticodon-loop which indicates that the modification extent at these positions reflects rather demand than maturation. Another hypothesis for the post-methylation arises from reports on tRNA demethylation. For m^1A and m^3C, demethylation by members of the ALKBH family has been proposed[9,47,48]. Such a demethylated site might be target to re-methylation and this process would lead to the formation of post-methylated nucleosides. While the common analysis of tRNA modifications by sequencing and quantitative mass spectrometry provides a static view on the substrates of ALKBH enzymes, future NAIL-MS experiments will shed light onto the dynamic performance of these enzymes in vivo.

Such a detailed analysis is especially important for understanding the processes behind stress induced adaptation of tRNA modifications. To this end, we have studied the impact of methylation stress on tRNA modifications. Even at a harsh dose of MMS (1 mM), we observe only 1 damage derived m^1A and 5 m^7G per 1000 tRNAs. Other damage products were not observed. Intriguingly, these damages do not seem to be repaired in human cells.

In our hands, methylation stress has no impact on the abundance of modified nucleosides in tRNA present during the stress exposure. In contrast, the abundance of some modified nucleosides is slightly, but significantly changed in new transcripts. This indicates that cells regulate their tRNA modifications on the level of new transcripts and not existing transcripts. Overall modification processes of tRNA are not stalled during stress recovery which indicates that properly modified tRNAs are of high importance to the cell.

NAIL-MS is a powerful technique which depends, as common to state-of-the-art mass spectrometry of modified nucleosides, on a complete enzymatic digest to the nucleoside building block. Thus, all sequence context surrounding modified nucleosides is lost and the technique relies strongly on the purity of the sample. This is especially important for mRNA[49]. If reliable mRNA purification is possible, the true dynamics of m^6A and other mRNA modifications becomes finally available through NAIL-MS.

Methods

Salts, reagents, media, and nucleosides. All salts, reagents and media were obtained from Sigma-Aldrich (Munich, Germany) at molecular biology grade unless stated otherwise. The isotopically labeled compounds $^{13}C_5$,$^{15}N_2$-Uridine (Ribose-$^{13}C_5$, 98%; $^{15}N_2$, 96–98%) and $^{15}N_5$-Adenine ($^{15}N_5$, 98%) were obtained from Cambridge Isotope Laboratories (Tewksbury, MA, USA). Unlabeled glutamine, isotopically labeled L-glutamine-amide-^{15}N (98 atom% ^{15}N), L-aspartic-^{15}N acid (98 atom% ^{15}N) and (D_3)-L-methionine (98 atom% D) were obtained from Sigma-Aldrich. Isotopically labeled $^{13}C_6$-glucose (≥99 atom% ^{13}C) was obtained from Eurisotope (Saarbruecken, Germany). All solutions and buffers were made with water from a Sartorious arium® pro ultrapure water system (Goettingen, Germany). The nucleosides adenosine (A), cytidine (C), guanosine (G) and uridine (U), were obtained from Sigma-Aldrich. 1-Methyladenosine (m^1A), N3-methylcytidine (m^3C), N6-methyladenosine (m^6A), 7-methylguanosine (m^7G), 5-methylcytidine (m^5C), 5-methyluridine (m^5U), 2′-O-methylcytidine (Cm), 2′-O-methylguanosine (Gm), 1-methylguanosine (m^1G), N2-methylguanosine (m^2G), 2-dimethylguanosine ($m^{22}G$), pseudouridine (Ψ), inosine (I), 2′-O-methyluridine (Um), 2′-O-methyladenosine (Am), and 5-methoxycarbonylmethyl-2-thiouridine (mcm^5s^2U) were obtained from Carbosynth (Newbury, UK). Dihydrouridine (D) was obtained from Apollo Scientific (Stockport, UK). N6-threonylcarbamoyladenosine (t^6A) was obtained from TRC (North York, Canada). N3-methyluridine (m^3U) and N6-isopentenyladenosine (i^6A) were generous gifts from the Dedon lab. 5-carbamoylmethyl-2-thiouridine (ncm^5s^2U) was a generous gift from the Helm lab. 1-Methylinosine (m^1I) was a generous gift from STORM Therapeutics LTD (Cambridge, UK).

Cell culture. All cell culture media and supplements were obtained from Sigma-Aldrich (Munich, Germany) unless stated otherwise. Standard Basal medium for HEK 293 culture was DMEM D6546 high glucose supplemented with 10% FBS and 0.584 g/L L-glutamine. Cells were split 1:7 using standard procedures every 2–3 days to counter overgrowth. Cells cultured in DMEM medium were kept at 10% CO_2 for proper pH adjustment. For all experiments where labeling of nucleosides was involved DMEM D0422 without methionine and cystine was used. DMEM D0422 was supplemented with 10% dialyzed FBS (Biowest, Nuaillé, France), 0.584 g/L L-glutamine, 0.063 g/L cystine (stock concentration 78.75 g/L dissolved in 1 M HCl), 0.03 g/L methionine, 0.05 g/L uridine, and 0.015 g/L adenine. Uridine, adenine and methionine were either added as unlabeled or labeled compounds depending on the desired labeling. HeLa cells were cultured and labeled using the same media.

For Labeling in RPMI R0883, dialyzed FBS, glutamine, methionine, uridine, and adenine were added in the same concentrations as for DMEM D0422.

HAP1 cells were either labeled using DMEM D0422 as described above or IMDM I3390 where FBS, glutamine, uridine, adenine and methionine were added in the same concentrations as used for DMEM D0422 medium. Cells grown in RPMI or IMDM medium were kept at 5% CO_2 for proper pH adjustment.

Mouse embryonic stem cells (mESC) were cultured as recently reported[50]. Isotopically labeled compounds were added as described for regular cell culture labeling.

For biological replicates one culture was split into several flask at least 24 h prior to experiment initiation.

Cell lysis and RNA purification. Cells were directly harvested on cell culture dishes using 1 mL TRI reagent for T25 flasks or 0.5 mL TRI reagent for smaller dishes. The total RNA was isolated according to the supplier's manual with chloroform (Roth, Karlsruhe, Germany). tRNA and 18S rRNA were purified by size exclusion chromatography (AdvanceBio SEC 300 Å, 2.7 µm, 7.8 × 300 mm for tRNA and BioSEC 1000 Å, 2.7 µm, 7.8 × 300 mm for 18S rRNA, Agilent Technologies) according to published procedures[31,51]. The RNA was resuspended in water (35 µL).

Isoacceptor purification. The procedure was adapted from Hauenschild et al.[13]. For $tRNA^{Phe}_{GAA}$ purification, a mixture of 1 µg SEC-purified total tRNA and 100 pmol complementary oligonucleotide was heated to 90 °C for 3 min in a total volume of 100 µL 5× SSC buffer (0.75 M NaCl, 75 mM trisodiumcitrate pH 7) and subsequently incubated for 10 min at 65 °C. The sequence of the biotinylated 2′-deoxyoligonucleotide is 5′–(Biotin) AAATGGTGCCGAAACCCGGGATCGA ACCAGGGT–3′ (Sigma Aldrich, Munich, Germany). For each sample, 25 µL Magnetic Dynabeads® MyOne™ Streptavidin T1 (Thermo Fisher Scientific, Darmstadt, Germany) were primed three times in Binding and Wash buffer (5 mM Tris-HCl pH 7.5, 0.5 mM EDTA, 1 M NaCl) and once in 5× SSC buffer. An aliquot of 25 µL magnetic beads in 5× SSC buffer was added to the prepared mixture of tRNA and oligonucleotide and incubated for 30 min at room temperature. Beads were then washed once with 1× SSC buffer and three times with 0.1× SSC buffer before elution of purified $tRNA^{Phe}_{GAA}$ in 20 µL Milli-Q water at 75 °C for 3 min.

Northern blot analysis. Isolated RNA samples and control oligonucleotides (in vitro synthesized $tRNA^{Ser}_{UGA}$, tRNA fragment $Glycin_{GCC}$) were separated by implementing a 12% TBE-urea PAGE in 1× TBE buffer (Roth, Karlsruhe, Germany). Samples were denatured at 90 °C for 1 min, directly loaded on the gel and run at 275 V for 40 min. The RNA was then transferred onto a Hybond-N + nylonmembrane (GE Healthcare, Chicago, US) at 375 mA, 4 °C in 1× TBE buffer for 2 h and subsequently crosslinked twice with UV light at the energy of 120 mJ/cm^2. The membrane was incubated in hybridization buffer (5x Denhardt's solution, 1% SDS, 6.6× SSPE) for 30 min before 100 pmol of the respective probe was added. Fluorescent probes (3′ and 5′ Cyanine-3 modified, from Sigma-Aldrich, Munich, Germany) were designed to overlap with ~30 nt of the target RNA using the same sequence for $tRNA^{Phe}$ as used for isoacceptor purification. The sequence of all probes used can be found in Table S2. Hybridization was performed overnight at 37 °C in a shaking incubator. After two wash steps in 2× SSPE, 0.5% SDS for 10 min at room temperature the membrane was imaged at an Amersham Imager 680. Stripping was done by pouring boiling 0.1× SSPE buffer onto the membrane and incubation for 5 min. To get rid of remaining signal completely this procedure was repeated 10 times before reprobing.

Sequencing. Analysis of $tRNA^{Phe}_{GAA}$ purity by deep sequencing was performed by mild RNA fragmentation under strong alkaline conditions (5 min, 96 °C, pH 9.2). Resulting fragments were 3′-dephosphorylated by Antarctic phosphatase (New England Biolabs, Frankfurt, Germany) and 5′-phosphorylated by PNK/ATP treatment[52]. Library preparation was done using NEBNext® Multiplex Small RNA Library Prep Set for Illumina (NEB) according to the manufacturer's instructions. Quality of the library preparation was assessed by HS DNA chip on Bioanalyzer 2100 (Agilent). Sequencing was done using HiSeq1000 in single-read SR50 mode. Resulting raw reads (~10 mln/sample) were trimmed by trimmomatic v.032 to remove the adapted sequence and aligned using bowtie2 to the reference containing human rRNA sequences and non-redundant subset of human tRNAs. Over 90% of the reads was mapped by this approach, demonstrating that contamination by other cellular RNAs remains minor.

tRNA digestion for mass spectrometry. Total tRNA (300 ng) in aqueous digestion mix (30 µL) was digested to single nucleosides by using 2 U alkaline phosphatase, 0.2 U phosphodiesterase I (VWR, Radnor, Pennsylvania, USA), and 2 U benzonase in Tris (pH 8, 5 mM) and $MgCl_2$ (1 mM) containing buffer. Furthermore, 0.5 µg tetrahydrouridine (Merck, Darmstadt, Germany), 1 µM butylated hydroxytoluene, and 0.1 µg pentostatin were added to avoid deamination and oxidation of the nucleosides. When quantification of dihydrouridine was intended tetrahydrouridine was omitted. After incubation for 2 h at 37 °C, 20 µL of LC-MS buffer A (QQQ) was added to the mixture and then filtered through 96-well filter plates (AcroPrep Advance 350 10 K Omega, PALL Corporation, New York, USA) at 3000 × *g* and 4 °C for 30 min. A stable isotope labeled internal standard (SILIS) was produced in *S. cerevisiae* using ^{13}C and ^{15}N rich growth medium (Silantes, Munich, Germany, Product# 111601402) following recently described procedures[16,31]. 1/10 Vol. of SILIS was added to each filtrate before analysis by QQQ mass spectrometry. For each sample 10 µL were injected (~60 ng of sample tRNA).

High resolution mass spectrometry. The ribonucleosides were separated using a Dionex Ultimate 3000 HPLC system with a Synergi, 2.5 µm Fusion-RP, 100 Å, 100 × 2 mm column (Phenomenex®, Torrance, California, USA). Mobile phase A was 10 mM ammonium formate and mobile phase B was 80% acetonitrile containing 2 mM ammonium formate. Gradient elution started with 0% B and increased to 12% B after 10 min and to 80% after 12 min. After 4 min elution at 80% B and subsequently regeneration of starting conditions to 100% A after 5 min, the column was equilibrated at 100% A for 8 min. The flow rate was 0.2 mL/min and the column temperature 30 °C. High-resolution mass spectra were recorded by a ThermoFinnigan LTQ Orbitrap XL operated in positive ionization mode. The parameters of the mass spectrometer were tuned with a freshly mixed solution of uridine (10 µM). Capillary voltage was set to 20 V and capillary temperature to 300 °C. Sheath gas and sweep gas flow rate was set to 0, and auxiliary gas flow rate to 35. Source voltage was set to 4.0 kV and tube lens to 75 V.

QQQ mass spectrometry. For quantitative mass spectrometry an Agilent 1290 Infinity II equipped with a diode-array detector (DAD) combined with an Agilent Technologies G6470A Triple Quad system and electrospray ionization (ESI-MS, Agilent Jetstream) was used. Operating parameters: positive-ion mode, skimmer voltage of 15 V, cell accelerator voltage of 5 V, N_2 gas temperature of 230 °C and N_2 gas flow of 6 L/min, sheath gas (N_2) temperature of 400 °C with a flow of 12 L/min, capillary voltage of 2500 V, nozzle voltage of 0 V, and nebulizer at 40 psi. The instrument was operated in dynamic MRM mode (Table S3).

For separation a Synergi, 2.5 µm Fusion-RP, 100 Å, 100 × 2 mm column (Phenomenex®, Torrance, California, USA) at 35 °C and a flow rate of 0.35 mL/min was used in combination with a binary mobile phase of 5 mM NH_4OAc aqueous buffer A, brought to pH 5.3 with glacial acetic acid (65 µL/L), and an organic buffer B of pure acetonitrile (Roth, Ultra LC-MS grade, purity ≥99.98). The gradient started at 100% solvent A for 1 min, followed by an increase to 10% solvent B over 4 min. From 5 to 7 min, solvent B was increased to 40% and maintained for 1 min before returning to 100% solvent A in 0.5 min and a 2.5 min re-equilibration period.

Calibration. For calibration, synthetic nucleosides were weighed and dissolved in water to a stock concentration of 1–10 mM. The calibration solutions ranged from 0.025 to 100 pmol for each canonical nucleoside and from 0.00125 pmol to 5 pmol for each modified nucleoside. Each calibration was spiked with 10% SILIS. The sample data were analyzed by the quantitative and qualitative MassHunter Software from Agilent. The areas of the MRM signals were integrated for each modification. The values of integrated MS signals from target nucleosides were set into relation to the respective MS signals of the respective isotope labeled SILIS nucleosides after Eq. (1) to receive the nucleoside isotope factor (NIF):

$$\mathrm{NIF}_{\mathrm{nucleoside}} = \frac{\mathrm{signal\ area}_{\mathrm{nucleoside}}}{\mathrm{signal\ area}_{\mathrm{respective\ SILIS}}} \quad (1)$$

Results from Eq. (1) were plotted against the expected molar amount of nucleosides and regression curves were plotted through the data points. The slopes represent the respective relative response factors for the nucleosides (rRFN) and enable an absolute quantification. The principle is described in more detail in our published protocol[16]. The plotting of these calibration curves is done automatically by the quantitative MassHunter Software and should be checked manually for linearity.

Data analysis. Molar amounts of nucleosides in samples were calculated after Eq. (2) using the signal areas of target compounds and SILIS in the samples and the respective rRFN, determined by calibration measurements. This step is done automatically by the quantitative MassHunter Software.

$$n_{\mathrm{sample\ nucleoside}} = \frac{\mathrm{signal\ area}_{\mathrm{sample\ nucleoside}}}{\mathrm{rRFN}_{\mathrm{nucleoside}} \bullet \mathrm{signal\ area}_{\mathrm{respective\ SILIS}}} \quad (2)$$

To make different samples quantitatively comparable, the molar amount of each modified nucleoside was normalized by the molar amount of injected RNA to receive the number of modifications per RNA. Therefore, the calculated amounts of injected canonicals were divided by their expected occurrence in the respective RNAs and averaged afterwards (see Eq. (3) for tRNA). The numbers for each canonical nucleoside were either taken from the sequence of 18S rRNA, $tRNA^{Phe}$ (reported modifications subtracted)[32], or determined empirically for total tRNA analyses.

$$n_{\mathrm{tRNA}} = \frac{\frac{n_C}{\#C} + \frac{n_U}{\#U} + \frac{n_G}{\#G} + \frac{n_A}{\#A}}{4} \quad (3)$$

In the case of NAIL-MS experiments, the different isotopologues were referenced to their respective labeled canonicals, so that original (unlabeled) modifications were referenced to original tRNA molecules and new (labeled) modifications were referenced to new tRNA molecules (see Eqs. (4) and (5)).

Table S4 gives a summary of the calculations exemplarily for m^7G.

$$\#\mathrm{mod/tRNA(original)} = \frac{n_{\mathrm{sample\ nucleoside}}(\mathrm{unlabeled})}{n_{\mathrm{tRNA}}(\mathrm{unlabeled})} \quad (4)$$

$$\#\mathrm{mod/tRNA(new)} = \frac{n_{\mathrm{sample\ nucleoside}}(\mathrm{labeled})}{n_{\mathrm{tRNA}}(\mathrm{labeled})} \quad (5)$$

Statistics. All experiments were performed at least 3 times (biological replicates) to allow student t-test analysis. *P*-values of student t-test (unpaired, two-tailed, equal distribution) were calculated using Excel.

Reporting summary. Further information on research design is available in the Nature Research Reporting Summary linked to this article.

Data availability

Sequencing data are available under accession PRJEB41141 at ENA database. The data supporting the findings of this study are available from the corresponding authors upon reasonable request. Source data are provided with this paper.

Received: 22 April 2020; Accepted: 4 December 2020;
Published online: 15 January 2021

References

1. Mauer, J. et al. Reversible methylation of m(6)Am in the 5′ cap controls mRNA stability. *Nature* **541**, 371–375 (2017).
2. Zheng, G. et al. ALKBH5 is a mammalian RNA demethylase that impacts RNA metabolism and mouse fertility. *Mol. Cell* **49**, 18–29 (2013).
3. Jia, G. et al. N6-methyladenosine in nuclear RNA is a major substrate of the obesity-associated FTO. *Nat. Chem. Biol.* **7**, 885–887 (2011).
4. Tang, C. et al. ALKBH5-dependent m6A demethylation controls splicing and stability of long 3′-UTR mRNAs in male germ cells. *Proc. Natl Acad. Sci. USA* **115**, E325–E333 (2018).
5. Wei, J. et al. Differential m(6)A, m(6)Am, and m(1)A demethylation mediated by FTO in the cell nucleus and cytoplasm. *Mol. Cell* **71**, 973–985 e975 (2018).
6. Mauer, J. & Jaffrey, S. R. FTO, m(6) Am, and the hypothesis of reversible epitranscriptomic mRNA modifications. *FEBS Lett.* **592**, 2012–2022 (2018).
7. Zhou, J. et al. N(6)-methyladenosine guides mRNA alternative translation during integrated stress response. *Mol. Cell* **69**, 636–647 e637 (2018).
8. Zhang, X. et al. Structural insights into FTO's catalytic mechanism for the demethylation of multiple RNA substrates. *Proc. Natl Acad. Sci. USA* **116**, 2919–2924 (2019).
9. Liu, F. et al. ALKBH1-mediated tRNA demethylation regulates translation. *Cell* **167**, 816–828 e816 (2016).
10. Gattoni, R., Keohavong, P. & Stevenin, J. Splicing of the E2A premessenger RNA of adenovirus serotype 2. Multiple pathways in spite of excision of the entire large intron. *J. Mol. Biol.* **187**, 379–397 (1986).
11. Chan, C. T. et al. A quantitative systems approach reveals dynamic control of tRNA modifications during cellular stress. *PLoS Genet.* **6**, e1001247 (2010).
12. Carell, T. et al. Structure and function of noncanonical nucleobases. *Angew. Chem. Int. Ed. Engl.* **51**, 7110–7131 (2012).
13. Hauenschild, R. et al. The reverse transcription signature of N-1-methyladenosine in RNA-Seq is sequence dependent. *Nucleic Acids Res.* **43**, 9950–9964 (2015).
14. Clark, W. C., Evans, M. E., Dominissini, D., Zheng, G. & Pan, T. tRNA base methylation identification and quantification via high-throughput sequencing. *RNA* **22**, 1771–1784 (2016).
15. Brandmayr, C. et al. Isotope-based analysis of modified tRNA nucleosides correlates modification density with translational efficiency. *Angew. Chem. Int. Ed. Engl.* **51**, 11162–11165 (2012).
16. Borland K. et al. Production and application of stable isotope-labeled internal standards for RNA modification analysis. *Genes* **10**, 26 (2019).
17. Pan, T. Modifications and functional genomics of human transfer RNA. *Cell Res.* **28**, 395–404 (2018).
18. Dittmar, K. A., Sorensen, M. A., Elf, J., Ehrenberg, M. & Pan, T. Selective charging of tRNA isoacceptors induced by amino-acid starvation. *EMBO Rep.* **6**, 151–157 (2005).
19. Klug, A., Ladner, J. & Robertus, J. D. The structural geometry of co-ordinated base changes in transfer RNA. *J. Mol. Biol.* **89**, 511–516 (1974).
20. Kim, S. H. et al. Three-dimensional tertiary structure of yeast phenylalanine transfer RNA. *Science* **185**, 435–440 (1974).
21. Shi, H. & Moore, P. B. The crystal structure of yeast phenylalanine tRNA at 1.93 A resolution: a classic structure revisited. *RNA* **6**, 1091–1105 (2000).
22. Barraud, P. et al. Time-resolved NMR monitoring of tRNA maturation. *Nat. Commun.* **10**, 3373 (2019).
23. Chan, C., Pham, P., Dedon, P. C. & Begley, T. J. Lifestyle modifications: coordinating the tRNA epitranscriptome with codon bias to adapt translation during stress responses. *Genome Biol.* **19**, 228 (2018).
24. Deng, W. et al. Trm9-catalyzed tRNA modifications regulate global protein expression by codon-biased translation. *PLoS Genet.* **11**, e1005706 (2015).
25. Sloan, K. E. et al. Tuning the ribosome: the influence of rRNA modification on eukaryotic ribosome biogenesis and function. *RNA Biol.* **14**, 1138–1152 (2017).
26. Yoon, A. et al. Impaired control of IRES-mediated translation in X-linked dyskeratosis congenita. *Science* **312**, 902–906 (2006).
27. Helm, M. & Motorin, Y. Detecting RNA modifications in the epitranscriptome: predict and validate. *Nat. Rev. Genet.* **18**, 275–291 (2017).
28. Motorin, Y. & Helm, M. Methods for RNA modification mapping using deep sequencing: established and new emerging technologies. *Genes* **10**, 35 (2019).
29. Reichle, V. F., Weber, V. & Kellner, S. NAIL-MS in *E. coli* determines the source and fate of methylation in tRNA. *Chembiochem* **19**, 2575–2583 (2018).
30. Reichle, V. F., Petrov, D. P., Weber, V., Jung, K. & Kellner, S. NAIL-MS reveals the repair of 2-methylthiocytidine by AlkB in *E. coli*. *Nat. Commun.* **10**, 5600 (2019).
31. Heiss, M., Reichle, V. F. & Kellner, S. Observing the fate of tRNA and its modifications by nucleic acid isotope labeling mass spectrometry: NAIL-MS. *RNA Biol.* **14**, 1260–1268 (2017).
32. Boccaletto, P. et al. MODOMICS: a database of RNA modification pathways. 2017 update. *Nucleic Acids Res.* **46**, D303–D307 (2018).
33. Tuorto, F. et al. RNA cytosine methylation by Dnmt2 and NSun2 promotes tRNA stability and protein synthesis. *Nat. Struct. Mol. Biol.* **19**, 900–905 (2012).
34. Blobstein, S. H., Grunberger, D., Weinstein, I. B. & Nakanishi, K. Isolation and structure determination of the fluorescent base from bovine liver phenylalanine transfer ribonucleic acid. *Biochemistry* **12**, 188–193 (1973).
35. Perche-Letuvee, P., Molle, T., Forouhar, F., Mulliez, E. & Atta, M. Wybutosine biosynthesis: structural and mechanistic overview. *RNA Biol.* **11**, 1508–1518 (2014).
36. Macon, J. B. & Wolfenden, R. 1-Methyladenosine. Dimroth rearrangement and reversible reduction. *Biochemistry* **7**, 3453–3458 (1968).
37. Reichle, V. F. et al. Surpassing limits of static RNA modification analysis with dynamic NAIL-MS. *Methods* **156**, 91–101 (2019).
38. Jensen, K. F., Dandanell, G., Hove-Jensen, B. & WillemoEs, M. Nucleotides, nucleosides, and nucleobases. *EcoSal Plus* **3**, 3.6.2 (2008).
39. Motorin, Y. & Helm, M. tRNA stabilization by modified nucleotides. *Biochemistry* **49**, 4934–4944 (2010).
40. Kim, S. H. et al. The general structure of transfer RNA molecules. *Proc. Natl Acad. Sci. USA* **71**, 4970–4974 (1974).
41. Ashraf, S. S. et al. Role of modified nucleosides of yeast tRNA(Phe) in ribosomal binding. *Cell Biochem. Biophys.* **33**, 241–252 (2000).
42. Han, L., Guy, M. P., Kon, Y. & Phizicky, E. M. Lack of 2′-O-methylation in the tRNA anticodon loop of two phylogenetically distant yeast species activates the general amino acid control pathway. *PLoS Genet.* **14**, e1007288 (2018).
43. Kos, M. & Tollervey, D. Yeast pre-rRNA processing and modification occur cotranscriptionally. *Mol. Cell* **37**, 809–820 (2010).
44. Heiss, M. & Reichle, V. F. & Kellner S. Observing the fate of tRNA and its modifications by nucleic acid isotope labeling mass spectrometry: NAIL-MS. *RNA Biol.* **14**, 1–9 (2017).
45. Reichle, V. F. et al. Surpassing limits of static RNA modification analysis with dynamic NAIL-MS. *Methods* **156**, 91–101 (2018).
46. Miller, B. G. The biological half-lives of ribosomal and transfer RNA in the mouse uterus. *J. Endocrinol.* **59**, 81–85 (1973).
47. Chen, Z. et al. Transfer RNA demethylase ALKBH3 promotes cancer progression via induction of tRNA-derived small RNAs. *Nucleic Acids Res.* **47**, 2533–2545 (2019).
48. Ueda, Y. et al. AlkB homolog 3-mediated tRNA demethylation promotes protein synthesis in cancer cells. *Sci. Rep.* **7**, 42271 (2017).
49. Legrand, C. et al. Statistically robust methylation calling for whole-transcriptome bisulfite sequencing reveals distinct methylation patterns for mouse RNAs. *Genome Res.* **27**, 1589–1596 (2017).
50. Rahimoff, R. et al. 5-Formyl- and 5-carboxydeoxycytidines do not cause accumulation of harmful repair intermediates in stem cells. *J. Am. Chem. Soc.* **139**, 10359–10364 (2017).
51. Chionh, Y. H. et al. A multidimensional platform for the purification of non-coding RNA species. *Nucleic Acids Res.* **41**, e168 (2013).
52. Galvanin, A. et al. Diversity and heterogeneity of extracellular RNA in human plasma. *Biochimie* **164**, 22–36 (2019).

Acknowledgements

This study was funded through the Deutsche Forschungsgemeinschaft (KE1943/3-1). M.H., F.H., and S.K. thank Angie Kirchner, Thomas Carell and his group for instrument time (high-resolution mass spectrometer) and advice.

Author contributions

M.H. and S.K. planned the experiments and wrote the manuscript. M.H., V.M., and F.H. conducted the experiments. M.H., Y.M., and S.K. performed data analysis.

Funding

Open Access funding enabled and organized by Projekt DEAL.

Competing interests

The authors declare no competing interests.

Additional information

Supplementary information is available for this paper at https://doi.org/10.1038/s41467-020-20576-4.

Correspondence and requests for materials should be addressed to S.K.

Peer review information *Nature Communications* thanks Guifang Jia and the other, anonymous, reviewer(s) for their contribution to the peer review of this work.

Methods 156 (2019) 91–101

Contents lists available at ScienceDirect

Methods

journal homepage: www.elsevier.com/locate/ymeth

Surpassing limits of static RNA modification analysis with dynamic NAIL-MS

Valentin F. Reichle, Steffen Kaiser, Matthias Heiss, Felix Hagelskamp, Kayla Borland, Stefanie Kellner*

LMU Munich, Faculty of Chemistry and Pharmacy, Department of Organic Chemistry, Butenandtstr. 5, 81377 Munich, Germany

ARTICLE INFO

Keywords:
Epitranscriptome
tRNA modification
LC-MS/MS
Nucleic acid isotope labeling coupled mass spectrometry (NAIL-MS)
tRNA damage repair
Demethylation

ABSTRACT

Ribonucleic acids (RNA) are extensively modified. These modifications are quantified by mass spectrometry (LC-MS/MS) to determine the abundance of a modification under certain conditions or in various genetic backgrounds. With LC-MS/MS the steady state of modifications is determined, and thus we only have a static view of the dynamics of RNA modifications. With nucleic acid isotope labeling coupled mass spectrometry (NAIL-MS) we overcome this limitation and get access to the dynamics of RNA modifications. We describe labeling techniques for *E. coli*, *S. cerevisiae* and human cell culture and the current instrumental limitations. We present the power of NAIL-MS but we also outline validation experiments, which are necessary for correct data interpretation.

As an example, we apply NAIL-MS to study the demethylation of adenine and cytidine, which are methylated by the damaging agent methyl-methanesulfonate in *E. coli*. With NAIL-MS we exclude the concurrent processes for removal of RNA methylation, namely RNA degradation, turnover and dilution. We use our tool to study the speed and efficiency of 1-methyladenosine and 3-methylcytidine demethylation.

We further outline current limitations of NAIL-MS but also potential future uses for *e.g.* relative quantification of tRNA isoacceptor abundances.

1. Introduction

1.1. State-of-the-art quantification of modified nucleosides

Ribonucleic acids (RNA) are key players in the central dogma of molecular biology. Messenger RNA (mRNA), ribosomal RNA (rRNA) and transfer RNA (tRNA) participate in protein synthesis, while the group of non-coding RNAs (ncRNAs) are crucial for many processes, including gene regulation as interfering RNAs (miRNAs) and guide RNAs. As RNAs fulfill many important and diverse functions, more than 4 building blocks are needed. Therefore, a large chemical diversity of ribonucleoside modifications can be found [1]. The chemical alterations of the canonical RNA nucleosides are comprised of simple methylations, isomerization, thiolation or even addition of complex groups like amino acids. Modifications that occur on the base are usually indicated by a small letter (*e.g.* m- for methylation or s- for thiolation) before calling the base (C, U, G or A). The position on the base is inserted as superscript between the short abbreviation and the base; *e.g.* 5-methylcytidine is abbreviated as m^5C. Some modifications, like the hypermodification queuosine, are abbreviated with their own capital letter, *e.g.* Q. Specific enzymes insert RNA modifications post-transcriptionally.

Studies of modified RNA rely on sensitive detection of modified nucleosides, which is commonly done with triple quadrupole mass spectrometry (described in various reviews [2–4]). The principle and workflow of such analyses is shown in Fig. 1**a**. After purification of the RNA of interest (here tRNA), the RNA is enzymatically digested into nucleosides and ideally an internal standard is added. The sample is injected on the LC-MS/MS system where the nucleosides are separated chromatographically and their mass transitions are monitored in the mass spectrometer. Using calibration curves, the absolute quantity of each nucleoside can be calculated and the number of modification per tRNA can be plotted.

1.2. Nucleic acid isotope labeling (NAIL)

Key to the quantification of nucleosides by mass spectrometry is the availability of the synthetic nucleoside in weighable quantities (or a known extinction coefficient) and an internal standard. The internal standard is ideally an isotopomer of the nucleoside of interest. While the natural nucleoside contains regular isotopes like hydrogen (H) carbon-12 (^{12}C), nitrogen-14 (^{14}N) its isotopomer will contain one or more heavy isotopes like deuterium (D), carbon-13 (^{13}C) or nitrogen-15 (^{15}N). The isotopomer is therefore heavier than the natural nucleoside

* Corresponding author.
E-mail address: stefanie.kellner@cup.lmu.de (S. Kellner).

https://doi.org/10.1016/j.ymeth.2018.10.025
Received 1 August 2018; Received in revised form 25 October 2018; Accepted 31 October 2018
Available online 03 November 2018

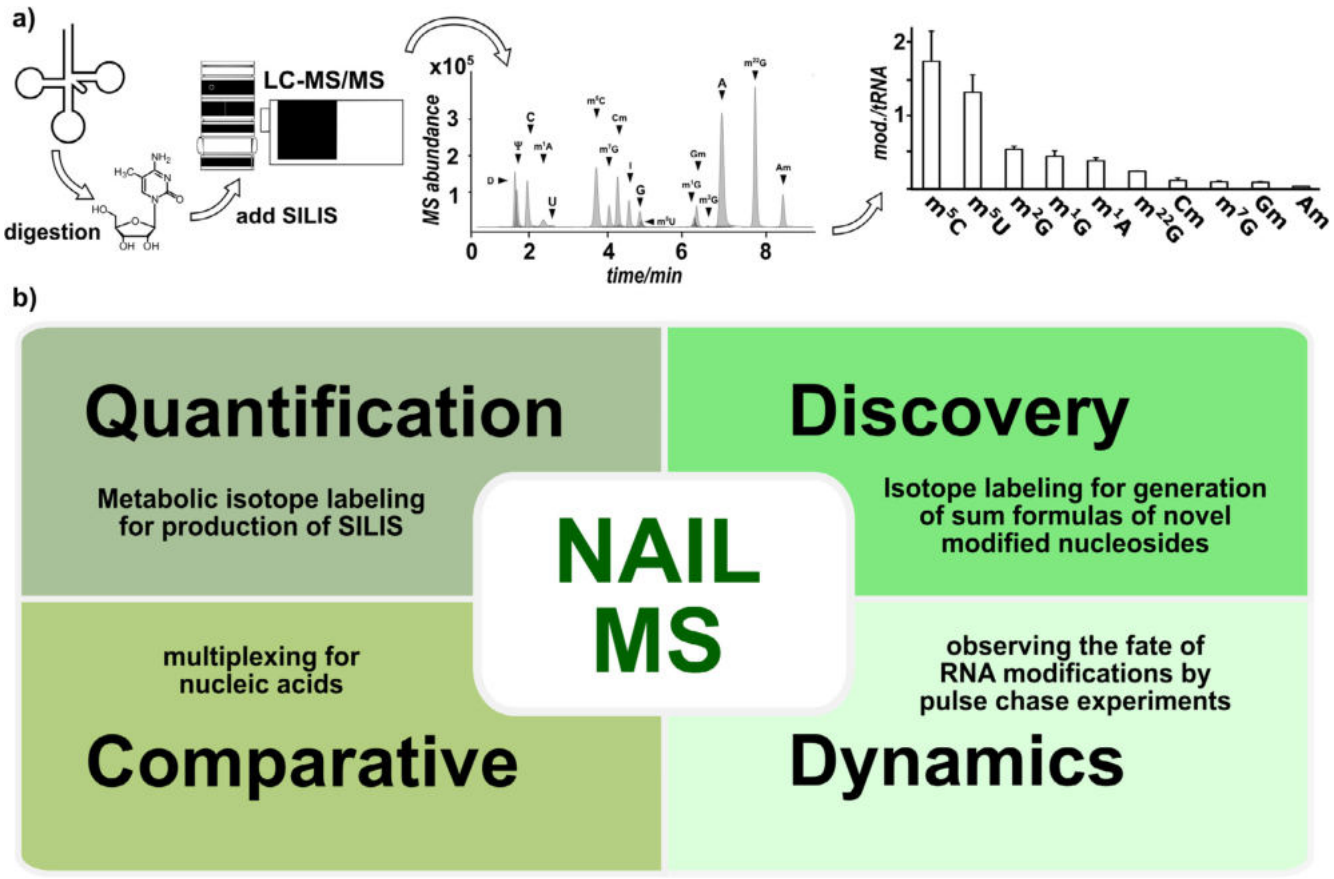

Fig. 1. a General workflow for quantification of modified nucleosides. The RNA is isolated and digested to the nucleoside building blocks (here, 5-methylcytidine). The stable isotope label internal standard (SILIS) is added and the sample is subjected to LC-MS/MS analysis. After chromatographic separation, the nucleosides are detected in the mass spectrometer and the abundance can be calculated and plotted. **b** Current and potential uses of NAIL-MS (nucleic acid isotope labeling coupled mass spectrometry).

and it can be used as an internal standard in mass spectrometry. Such internal standards are referred to as stable isotope labeled internal standards (SILIS) and the technique as isotope dilution mass spectrometry. The generation of these isotopomers can be done either synthetically [5–7] or biosynthetically by metabolic labeling in bacteria, yeast or algae [8–10].

Metabolic labeling relies on the incorporation of heavy isotopes from heavy-labeled growth media into the RNA. The heavy labeled RNA is isolated and processed for preparation of a SILIS for quantification. The usage of SILIS reduces the detection fluctuations of the mass spectrometer and thus reliable quantitative data becomes available to study RNA modifications.

However, nucleic acid isotope labeling (NAIL) should not be limited to quantification purposes. One can envision the use in a variety of experiments, which are or will become valuable tools in the research of modified nucleosides. Fig. 1**b** reviews the current usage of NAIL and potential future uses in RNA modification analysis. In addition to the usage of NAIL in **quantification**, its use to facilitate the **discovery** of novel modified nucleosides is widespread. Here, isotope labeling has become a key tool for sum formula generation and is highly helpful for structure prediction and verification [11–14].

1.2.1. Comparative NAIL

One of the caveats in the area of RNA modification research is the lack of key technologies comparable to those boosting protein research [15,16]. In the field of proteomics, a variety of mass spectrometry tools have emerged and allowed scientists to study proteins and their networks in more detail. Many of these tools focus on the comparison of proteomes (all proteins within a cell) in the context of stress studies or functional analyses by, *e.g.* multiplexing. Multiplexing allows the direct comparison of samples by mixing them within a single tube and performing a single analysis. They can be distinguished by mass spectrometry either by a chemical labeling step prior to mixing or by metabolic isotope labeling during sample generation. Especially metabolic isotope labeling has the advantage of overcoming purification biases. Additionally, mass spectrometric detection fluctuations are of no consequence. Metabolic isotope labeled proteomics (SILAC-Proteomics [17]) allows a direct comparison of proteomes within a single measurement with high accuracy. In principle, SILAC-like multiplexing is possible by NAIL, and we see a significant potential in such a SILAC-like approach in RNA modification research. We refer to this technique as **comparative NAIL**, which is also a useful tool for validation of dynamic NAIL-MS experiments.

1.2.2. Dynamic NAIL

While epigenetics is an intensively studied area, the analogue process in RNA, termed epitranscriptomics, is far less studied. This is mainly caused by our limited number of tools to study the dynamics of RNA modifications and, in addition, the complex process of finding biological consequences to RNA modifications. DNA is the storage of the genetic code. Therefore, modifications of DNA must be removed by an enzymatic process, which leaves the DNA sequence untouched and the DNA intact. Otherwise, mutations would occur and harm the organism. While it should be possible for the cell to use similar removal mechanisms in RNA, RNA has a second option for removal of an unwanted modification – the whole RNA itself is degraded and an unmodified new RNA is transcribed. The potential competition between these two processes makes it difficult to study the dynamics of RNA

modifications. Although many studies described that mRNA is enzymatically demodified, the mechanisms are still reviewed skeptically [18]. These doubts arise from the used techniques for *in vivo* analysis of the demodification process. In these studies, quantitative mass spectrometry of RNA modifications was used to observe an active demodification *in vivo* [19]. However, the absolute number of a modification within an RNA does not reflect the origin of the modification. A decrease in modification density can be explained by enzymatic demodification processes but also by increased degradation of modified RNA or even by increased transcription of unmodified RNA. *Vice versa*, an increase in modification density can be explained by additional modification events in the original RNA or by increased degradation of non-modified RNAs.

Current analyses of nucleic acid modifications are limited in respect to their blindness towards the underlying mechanisms, which lead to changes of modification content. NAIL-MS expands our current analytical toolbox and overcomes limitations by providing insight into the dynamics of nucleic acid modifications.

1.3. Nucleic acid isotope labeling as a tool to observe nucleic acid modification dynamics

From the natural RNA modifications known to date (~160), 70 contain a methylation of the base or the ribose [1]. These methylations are enzymatically incorporated at defined positions of the RNA. Especially m^6A in mRNA has gained major interest since this is the first RNA modification, which is incorporated by a methyltransferase (writer) and can be removed by demethylation *via* FTO or AlkBH5 (erasers).

In yeast, it was found that tRNA modifications are highly dynamic during cellular stress and are used by the cell for efficient stress survival by changing the translational speed of stress response proteins [20]. Although the dynamic nature of tRNA modifications is crucial to cell survival, it remains unclear how the cell achieves the adaptation of the modification profile. Additionally, cells are facing various stressors that can actively methylate the RNA such as methyl-methanesulfonate (MMS). Such methylations are randomly distributed across the accessible sites in RNA. *In vitro* tests showed that methylation of positions 1 of adenine and 3 of cytosine are quickly repaired by AlkB in *E. coli* [21].

Only one study showed the repair of m^1A by AlkB *in vivo*. This early pulse-chase study, based on radioactively labeled adenine, showed removal of m^1A from MMS damaged RNA by AlkB *in vivo*. Other studies that report demethylation processes in RNA did not present clear *in vivo* evidence of demethylation due to the limitations of static LC-MS/MS quantification.

Our first steps to overcome this limitation was in 2017, when we utilized non-radioactive isotope labeling of DNA to observe damage and repair of a DNA modification in bacteria. The combination of different labeling media allowed the creation of a pulse-chase experiment, which was used to observe repair of phosphorothioates in bacterial DNA [22]. The principle is shown in Fig. 2**a**. The bacteria were pre-cultured in heavy labeled media resulting in complete heavy labeling of the DNA nucleosides. In the heavy media, the bacteria were exposed to hypochlorous acid and the DNA present at this moment was damaged. After the exposure the bacteria were placed into unlabeled media and replication produced unlabeled DNA. By this approach it was possible to distinguish DNA present during the exposure from DNA synthesized after the exposure by mass spectrometry. Thus, we could see the loss of original phosphorothioates upon reaction with the chemical *in vivo* and the subsequent repair by the phosphorothiolating dnd enzymes. In the same year, we adapted the approach to RNA modification analysis in yeast [9]. As shown in Fig. 2**b**, we followed the modification density of tRNA in dependence of the growth phase and we identified the underlying mechanisms for several modified nucleosides (here 7-methylguanosine, m^7G, is shown). With NAIL-MS we can assess RNA turnover, RNA biosynthesis and dilution effects and determine the modification content of RNAs in response to *e.g.* growth or stress.

With LC-MS/MS the steady state of modifications is determined and thus is limited to a static view on dynamic RNA modification processes. Here, we present nucleic acid isotope labeling coupled mass spectrometry (NAIL-MS) which overcomes these current limitations and allows dynamic analysis of RNA modifications. We describe labeling techniques for *E. coli*, *S. cerevisiae* and human cell culture and the current instrumental limitations and recommended validation experiments.

We apply NAIL-MS to study the repair of adenine and cytidine, which are methylated by the damaging agent MMS in *E. coli*. With NAIL-MS, we exclude the concurrent processes for removal of RNA methylation, namely RNA degradation, turnover and dilution. The power of NAIL-MS is demonstrated by showing the kinetics of demethylation of damage-derived 1-methyladenosine and 3-methylcytidine in *E. coli in vivo*. We further outline current limitations of NAIL-MS but also potential future uses for *e.g.* relative quantification of RNA abundances.

2. Material and methods

2.1. Salts, reagents, isotopes and nucleosides

All salts were obtained from Sigma Aldrich (Munich, Germany) at molecular biology grade unless stated otherwise. Isotopically labeled compounds: ^{15}N-NH_4Cl (≥98% atom) and L-methionine-methyl-D_3 (98% atom) from Sigma-Aldrich. $^{13}C_6$-glucose (≥99% atom) and $Na_2{}^{34}SO_4$ (≥99.1% atom) from Eurisotop (Saarbruecken, Germany). 1,3-$^{15}N_2$-uracil (98% atom) from Cambridge Isotope Laboratories (Tewksbury, MA, USA). All solutions and buffers were made with water from a Millipore device (Milli-Q, Merck). Nucleosides: adenosine (A), cytidine (C), guanosine (G), uridine (U) and N2-methylguanosine (m^2G) from Sigma Aldrich. 1-Methyladenosine (m^1A), 2-methyladenosine (m^2A), N3-methylcytidine (m^3C), N6-methyladenosine (m^6A), 7-methylguanosine (m^7G), 5-methylcytidine (m^5C), 5-methyluridine (m^5U), 2′-O-methylcytidine (Cm), 2′-O-methylguanosine (Gm), 1-methylguanosine (m^1G) and 3-methyluridine (m^3U) from Carbosynth (Newbury, UK).

2.2. Specific laboratory equipment

Injection vial for HPLC and LC-MS: 0.3 mL PP Snap Ring Micro Vial, 32 × 11.6 mm, transparent, VWR (Radnor, PA, USA), Cat. No. 548-0120.

Injection vial cap: 11 mm Snap Ring Cap, tr., natural rubber/TEF, 60°, 1.0 mm, VWR (Radnor, PA, USA), Cat. No. 548-0014.

Fraction Collector glass vial: 1.5 mL Screw vial, 32 × 11.6 mm clear, VWR (Radnor, PA, USA), Cat. No. VWRI548-0018.

Glass vial cap: 8 mm PP-Screw cap black hole, VWR (Radnor, PA, USA), Cat. No. VWRI548-3322.

Culture tube: Centrifuge tube 50, TPP (Trasadingen, Switzerland), Product No.91050

2.3. Experimental settings

2.3.1. Metabolic isotope labeling

2.3.1.1. Bacteria. For each experiment a single colony from an LB agar plate with *E. coli* BW25113 was picked and used for culture inoculation.

We used minimal media M9 with and without the indicated isotopes for all bacterial cultures.

Unlabeled 10× M9 stock solution: mix 68 g/L Na_2HPO_4, 30 g/L KH_2PO_4, 2.5 g/L NaCl and 10 g/L NH_4Cl and autoclave. Store at room temperature.

Nitrogen-15-labeled 10x M9 stock solution: mix 68 g/L Na_2HPO_4, 30 g/L KH_2PO_4, 2.5 g/L NaCl and (!) **10 g/L ^{15}N-NH_4Cl** (!) and autoclave. Store at room temperature.

Other stock solutions: $MgCl_2$ (0.1 M), $CaCl_2$ (0.1 M), Na_2SO_4 (0.1 M) and 20 w/w% glucose (or $^{13}C_6$-glucose) are prepared by sterile

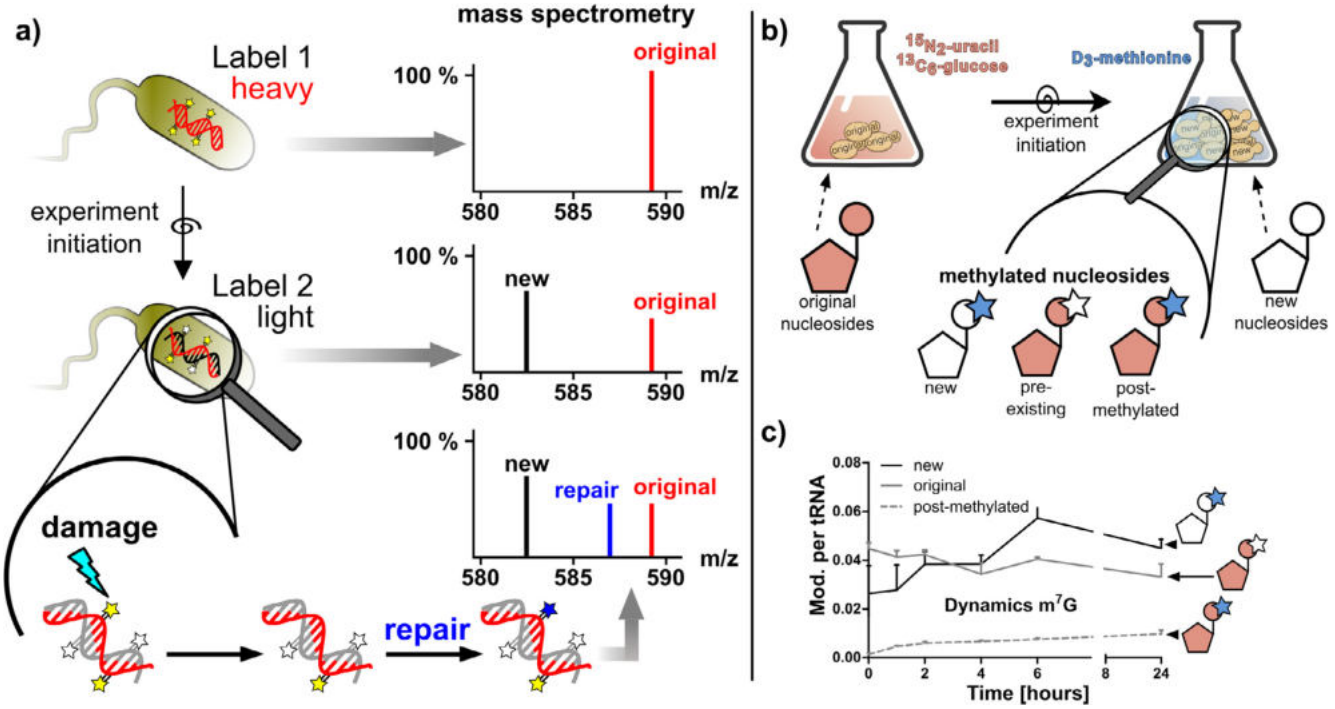

Fig. 2. a Principle of a NAIL-MS assay, which allows the observation of DNA modification damage repair *in vivo*. The bacteria are cultured in heavy isotope containing media, and therefore the DNA is heavy labeled, as observed by mass spectrometry. After exposure to the damage, the media is exchanged to a light media and newly replicated DNA is light labeled. The repair of original, but damaged DNA is observed by the formation of an intermediately labeled species in the mass spectrometer. (Adapted from [22].) **b** Principle of a dynamic NAIL-MS assay of tRNA in *S. cerevisiae* and the dynamics of 7-methylguanosine (m^7G) in tRNAs after experiment initiation. The drop in pre-existing m^7G is masked by an increase of post-methylated m^7G added to the pre-existing tRNAs (from [9]).

filtration.

For an unlabeled 5 mL pre-culture (or 50 mL exposure culture, respectively) mix 500 µL (5 mL) 10x M9 stock solution with 100 µL (1 mL) glucose, 100 µL (1 mL) $MgCl_2$, 100 µL (1 mL) Na_2SO_4 and 5 µL (50 µL) $CaCl_2$.

For ^{13}C-labeled cultures, $^{13}C_6$-glucose was used.

For ^{15}N-labeled cultures, the ^{15}N-10x M9 stock solution was used.

For CD_3-labeling, 200 µL of L-methionine-methyl-D_3 (stock 5 g/L) were added to 5 mL of culture volume.

2.3.1.2. Yeast. A single colony of a *S. cerevisiae* BY4741 YPD agar plate was picked and used for inoculation of 5 mL YNB media. 10x YNB (Carl Roth GmbH, Karlsruhe, Germany) was prepared according to manufacturer's manual. 1x YNB media was supplemented with the following metabolites to a final concentration of: 10 g/L glucose, 0.02 g/L uracil, 0.02 g/L methionine, 0.02 g/L arginine, 0.1 g/L aspartic acid, 0.1 g/L glutamine, 0.02 g/L histidine, 0.06 g/L leucine, 0.03 g/L lysine, 0.05 g/L phenylalanine, 0.4 g/L serine, 0.2 g/L threonine, 0.04 g/L tryptophan, 0.03 g/L tyrosine and 0.15 g/L valine (only L-amino acids were used). Depending on the desired labeling, $^{13}C_6$-glucose and L-methionine-methyl-D_3 were used instead of the unlabeled compounds.

2.3.1.3. Mammalian cells. HEK 293 T cells were cultured in Dulbeccós Modified Eagle Media (DMEM) or RPMI 1640 media (Gibco, Carlsbad, CA, USA). DMEM media was prepared by dissolving 8.4 g DMEM powder D5030 (Sigma Aldrich) in 1 L milli-Q water. Before sterile filtration, carbonate and phenol red were added to a final concentration of 3.7 g/L $NaHCO_3$ and 0.0159 g/L phenol red. Stocks of glucose (200 g/L) and L-glutamine (15 g/L) were prepared and sterile filtered. These were added to the DMEM media before usage to a final concentration of 2 g/L glucose, 0.584 g/L L-glutamine and 10% dialyzed fetal calf serum (Sigma Aldrich, Product No. F0392-500ML). The methionine concentration was 0.15 g/L in the final media. Depending on the desired labeling either $^{13}C_6$-glucose and L-methionine-methyl-D_3 or their unlabeled isotopomers were used. The cells were incubated at 10% CO_2 atmosphere and cultivated in the labeled media for at least 2 days (5 days for complete labeling). For splitting, the cells were treated with TrypLE Express (Gibco, Carlsbad, CA, USA).

2.3.2. RNA isolation and tRNA purification

Bacteria cultures were centrifuged at 1200 × *g* for 5 min, yeast cultures at 3500 × *g* for 5 min. The supernatant was discarded and the cell pellet was suspended in 1 mL TRI-Reagent® (Sigma-Aldrich) per 5 mL culture, respectively. Yeast cells were additionally vortexed for 5 min using acid-washed Glass beads (Sigma-Aldrich) equivalent to ~200 µL. HEK cells were harvested directly in cell culture dishes/flasks using 1 mL TRI-Reagent® per 25 cm^2. After transfer into an Eppendorf tube and incubation at room temperature for 5 min, 200 µL of chloroform (≥ 99% purity, Roth) were added to 1 mL of the TRI-Reagent® solution of each organism and the mixture was vortexed for at least 10 s. The biphasic solution was allowed to settle at room temperature for 5 min and centrifuged at room temperature for 20 min at 10,000 × *g*. The clear upper phase (~500 µL) was transferred into a new vial, 500 µL of isopropanol (Roth, Karlsruhe, Germany) were added and the solution was mixed thoroughly. The mixture was stored at -20 °C overnight. The precipitated total RNA was pelleted by centrifugation for 40 min at 12,000 × *g* and 4 °C. The RNA pellet was washed two times with 100–200 µL 70% EtOH and finally dissolved in 30 µL water.

For purification of tRNA from total RNA size exclusion chromatography (SEC) [23] was used on an Agilent 1100 HPLC system (Degasser, G1279A; Quat Pump, G1311A; ALS, G1313A; COLCOM, G1316A; VWD, G1314A; Analyt FC, G1364C) with an AdvanceBio column, 300 Å pore size, 2.7 µm particle size, 7.8 × 300 mm (Agilent, Waldbronn, Germany). For elution, a 1 mL/min isocratic flow of 0.1 M ammonium acetate was used. Eluting RNA was detected at 254 nm with a diode array detector. Under these conditions, tRNA elutes at a retention time

between 7 and 8 min. The 1 mL tRNA fraction was collected and evaporated (GeneVac, EZ-2 PLUS, Ipswich, UK) to a volume of ~100 µL before precipitation by addition of 0.1 vol of 5 M ammonium acetate and 2.5 vol of ice-cold ethanol (100%). (!) Ammonium acetate is the precipitation method of choice if mass spectrometric analysis is desired. Sodium ions interfere with mass spectrometric detection of nucleosides and should be avoided if possible (!) After rigorous mixing, the tRNA was allowed to precipitate at −20 °C overnight. The tRNA was pelleted by centrifugation (12,000*g*, 40 min, 4 °C), washed with 70% ethanol and resuspended in 30 µL water.

2.3.3. Pulse-Chase NAIL-MS

A single *E. coli* colony was picked and grown in 5 mL unlabeled M9 media overnight (37 °C, shaking at 250 rpm). From this pre-culture, a second overnight culture was prepared by inoculating 50 mL unlabeled media with the complete 5 mL pre-culture. On the next day, these bacteria were added to 120 mL of unlabeled M9 media to a final OD of 1.0. After 60 min of growth at 37 °C and 250 rpm, the first 7 mL aliquot was taken for RNA isolation. The remaining culture was equally split in 2 Erlenmeyer flasks (100 mL glass size) of 56.5 mL each. One was exposed to 95.7 µL MMS (99% purity), the other to the same amount of water (MOCK) and gently stirred before both cultures were left to grow for 60 min at 37 °C with shaking at 250 rpm. After 60 min exposure, an aliquot of 7 mL was drawn from each culture and the RNA was isolated. The remaining bacteria were centrifuged (1200 × *g*, 5 min) and the MMS/MOCK containing supernatants were discarded. The bacteria pellets were washed with 5 mL $^{15}N/CD_3$-methionine labeled M9 media and each suspended in 50 mL fresh $^{15}N/CD_3$-methionine M9 media. For recovery, the bacteria were grown at 37 °C, 250 rpm and after 1, 2, 3, 4 and 10 h 7 mL aliquots were drawn for RNA isolation.

2.3.4. tRNA digestion for mass spectrometry

100 ng tRNA in 30 µL aqueous digestion mix were digested to single nucleosides by using Alkaline Phosphatase (0.2 U, Sigma-Aldrich, Munich, Germany), Phosphodiesterase I (0.02 U, VWR, Radnor, Pennsylvania, USA) and Benzonase (0.2 U Sigma-Aldrich, Munich, Germany) in Tris (5 mM, pH 8.0) and $MgCl_2$ (1 mM) containing buffer. Furthermore, tetrahydrouridine (THU, 0.5 µg from Merck), butylated hydroxytoluene (BHT, 1 µM, Sigma-Aldrich, Munich, Germany) and Pentostatin (0.1 µg, Sigma-Aldrich, Munich, Germany) were added to avoid deamination and oxidation of nucleosides [2]. All mentioned concentrations/amounts are final concentrations/amounts used in a 30 µL final digestion volume. The mixture was incubated with the RNA for 2 h at 37 °C and filtered through 96 well filterplates (AcroPrep ™Advance 350 10 K Omega™, PALL Corporation, New York, USA) at 4 °C for 30 min at 3000 × *g*, or through single tubes (VWR, 10 kDa MWCO) at room temperature for 7 min at 5000 × *g*. The filtrate was mixed with *E. coli* SILIS 10:1 (stable isotope labeled internal standard [8]) and measured with the triple quadrupole mass spectrometer.

2.4. LC-MS instruments and methods

2.4.1. Triple quadrupole instrument

For quantification an Agilent 1290 Infinity II equipped with a DAD combined with an Agilent Technologies G6470A Triple Quad system and electro-spray ionization (ESI-MS, Agilent Jetstream) was used. Optimized operating parameters: positive ion mode, skimmer voltage 15 V, Cell Accelerator Voltage 5 V, N_2 gas temperature 230 °C and N_2 gas flow 6 L/min, sheath gas (N_2) temperature 400 °C with a flow of 12 L/min, Capillary Voltage of 2500 V, Nozzle Voltage of 0 V and the Nebulizer at 40 psi. The instrument was operated in dynamic MRM mode and the individual mass spectrometric parameters for the nucleosides are given in Supplementary Tables S2 and S3. Mobile phase A was 5 mM NH_4OAc (≥99%, HiPerSolv CHROMANORM®, VWR), brought to pH = 5.3 with glacial acetic acid (≥99%, HiPerSolv CHROMANORM®, VWR). Mobile phase B was pure acetonitrile (Roth, LC-MS grade, purity ≥99.95). A Kinetex EVO column (Phenomenex®, Torrance, California, USA; Kinetex® 1.7 µm EVO C18 100 Å, 150 × 2.1 mm) at a temperature of 35 °C with an eluent flow rate of 0.35 mL/min was used. The gradient started at 100% solvent A, followed by an increase to 10% solvent B over 10 min. From 10 to 15 min solvent B was increased to 45% and maintained for 3 min before returning to 100% solvent A and a 3 min re-equilibration period. Alternatively, a Synergi Fusion-RP column (Phenomenex®, Torrance, California, USA; Synergi® 2.5 µm Fusion-RP 100 Å, 150 × 2.0 mm) at 35 °C and a flow rate of 0.35 mL/min was used for yeast and mammalian cell analysis. Gradient elution started with 100% A for 1 min, increased to 10% B after 5 min, and to 40% after 7 min. The column was flushed with 40% B for 1 min. After regeneration of starting condition for 0.5 min the column was re-equilibrated at 100% A for 3 additional minutes.

2.4.2. High-resolution mass spectrometry

The ribonucleosides were separated using a Dionex Ultimate 3000 HPLC system on an Interchim Uptisphere120-3HDO C18 or an RP-18 column (Synergi, 2.5 µm Fusion-RP C18 100 Å, 100 × 2 mm; Phenomenex®, Torrance, California, USA). Mobile phase A was 2 mM ammonium acetate and mobile phase B was 80% acetonitrile containing 2 mM ammonium acetate. Gradient elution started with 0% B and increased to 12% B after 10 min and to 80% after 12 min. After 4 min elution at 80% B and subsequently regeneration of starting conditions to 100% A after 5 min, the column was equilibrated at 100% A for 8 min. The flow rate was 0.2 mL/min and the column temperature 30 °C. High-resolution mass spectra of precursor and product ions were recorded by a ThermoFinnigan LTQ Orbitrap XL. The parameters of the mass spectrometer were tuned with a freshly mixed solution of adenosine (5 µM). The parameters were sheath gas flow rate, 5 arb; auxiliary gas flow rate, 35 arb; sweep gas flow rate, 0 arb; spray voltage, 5.0 kV; capillary temperature, 200 °C; capillary voltage, 20 V, tube lens 65 V.

2.5. Calibration and equations

For calibration, synthetic nucleosides were weighed and dissolved to a stock concentration of 1–10 mM. Calibration solutions ranging from 0.15 pmol to 500 pmol for each canonical nucleoside and from 0.15 fmol to 500 fmol for each modified nucleoside were prepared in water. The calibration solutions were mixed with the *E. coli* SILIS and analyzed with the appropriate method. The value of each integrated peak area of the nucleoside was divided through the respective SILIS area. The linear regression for each nucleoside's normalized signal/concentration plot gives the relative response factor for nucleosides (rRFN) [8]. The sample data were analyzed by the Quantitative and Qualitative MassHunter Software from Agilent. The areas of the nucleoside signals were integrated for each modification and their isotope derivatives. The area was divided through the respective SILIS area and divided through the rRFN value from the respective calibration to receive the absolute amount of the modification or canonical. Finally, the absolute amounts of the modifications were referenced to the absolute amounts of the precursor canonical. In case of the validation and dynamic NAIL-MS experiment the different isotopomers were referenced to their respective labeled canonicals, so that original modifications are referenced to original canonicals and new modifications were referenced to new canonicals. See the following equations for m^1A as an example:

	m^1A (fmol)	A (fmol)	Normalization
Original Here: unlabeled	$\frac{area\ m1A\ (unlabeled)}{RFN\ m1A \times area\ m1A\ (SILIS)}$	$\frac{area\ A\ (unlabeled)}{RFN\ A \times area\ A\ (SILIS)}$	$\frac{m1A\ (original)}{A\ (original)}$

New	$\frac{area\ m1A\ (labeled)}{RFN\ m1A \times area\ m1A\ (SILIS)}$	$\frac{area\ A\ (labeled)}{RFN\ A \times area\ A\ (SILIS)}$	$\frac{m1A\ (new)}{A\ (new)}$
Here: labeled			

2.6. Other instruments

Orbital Shaker-Incubator ES-20 (BioSan, Riga, Latvia); Rotina 380 R centrifuge (Hettich, Tuttlingen, Germany); Centrifuge 5427 R (Eppendorf, Hamburg, Germany); Perfect Spin 24 R refrigerated micro centrifuge (PeQlab/VWR, Erlangen, Germany); Vortexer (Heathrow Scientific, IL, USA), Product Code: 120212; Nanophotometer N60 Touch (Implen, Munich, Germany), T60966; Speedvac EZ-2^{PLUS} (GeneVac, Ipswich, UK).

3. Important considerations for NAIL-MS studies

As the term NAIL-MS states, there are two key features for setting up such studies. The first is defined isotope labeling of the nucleic acid (NAIL) and the second is the availability of a mass spectrometer (MS). In addition, we recommend rigorous validation of NAIL-MS studies, which will be discussed in detail.

3.1. Labeling techniques

Before starting a NAIL-MS experiment, a labeling technique must be established, which leads to a defined labeling of the nucleic acid. Microorganisms like *E. coli* [8] and *S. cerevisiae* [9] are effortlessly labeled in minimal media or complete media (*e.g.* from Silantes, Munich, Germany). In addition, algae like *Chlamydomonas reinhardtii* or worms such as *Caenorhabditis elegans* can be labeled [10,24]. Fig. 3**a** shows the mass spectra of digested tRNA from an *E. coli* culture in minimal media M9 using $^{13}C_6$-glucose as the carbon source (left) or using CD_3-methionine (right). By feeding $^{13}C_6$-glucose overnight, 83% of carbon atoms in the tRNA are ^{13}C labeled in the exemplary nucleoside guanosine (G). Thus a mass increase of +10 is observed for G compared to unlabeled G (and ~17% of a +9 species). Most enzymatic methylation reactions require S-adenosyl methionine (SAM) as the methyl donor. After the methylation, the resulting S-adenosyl homocysteine is recharged with a methyl group by methionine. Feeding organisms CD_3-methionine leads to the formation of CD_3-SAM and transfer of heavy methyl marks onto nucleic acids [25,26]. This is also observed for 7-methylguanosine (m^7G) from CD_3-methionine supplemented bacterial cultures, which has a mass increase of +3 compared to unlabeled m^7G (note: the +4 is the natural ^{13}C isotope peak of m^7G). We recently shared this labeling technique, which helped Dal Magro et al. to determine the structure of a novel RNA modification in bacteria, namely $msms^2i^6A$ [11].

For purines in *S. cerevisiae*, we mainly observe a +6 mass increase upon culturing in $^{13}C_6$-glucose media overnight and a +3 for m^7G in CD_3-methionine media (Fig. 3**b**). It is noteworthy that both labeling techniques do not lead to a single defined isotopomer. Further validation is necessary to assess the impact of multiple isotopomer formation (see chapter on validation). In addition to the presented $^{13}C_6$-glucose and CD_3-methionine labeling, it is possible to use $^{15}NH_4Cl$ or $^{34}Na_2SO_4$ [22] in *E. coli* or $^{15}N_2$-uracil in yeast for further labeling options. It is also possible to combine the carbon, nitrogen, sulfur and methyl sources into a single media.

While yeast is already less efficiently labeled in minimal media compared to *E. coli* (compare Fig. 3**a** and **b**), labeling in human cell culture is even more difficult. We have tested HEK 293 T and Hela cell lines in both DMEM and RPMI media using $^{13}C_6$-glucose and CD_3-methionine. While labeling of methyl groups with CD_3-methionine is similarly successful in HEK cells (Fig. 3**c**) as it is in yeast cells, $^{13}C_6$-glucose labeling is less promising. We observed for all nucleosides a variety of formed isotopomers, which were found to be independent of the used serum. Culturing for a longer time did not increase labeling efficiency. Fig. 3**c** shows the guanosine signal from tRNA of a 5 day-labeled HEK culture in the presence of 2 g/l $^{13}C_6$-glucose. Here, a mass shift of +5, +6, +7 and +8 is observed for G. The +5 reflects a guanosine with a $^{13}C_5$-labeled ribose but unlabeled base. The +6 to +8 labeled peaks reflect guanosine isotopomers with $^{13}C_5$-labeled ribose and $^{13}C_X$-labeled base. Such a labeling technique is not suitable for comparative NAIL-MS studies (but potentially for dynamic NAIL-MS). $^{13}C_6$-glucose appears not to be the metabolite of choice for successful NAIL-MS experiments in cell culture systems. The determination of a metabolite or even a mixture of metabolites, which can be used to achieve a defined labeling in cell culture, is the major bottleneck in establishing NAIL-MS in cell culture.

When choosing a labeling technique for comparative or pulse-chase NAIL-MS, the abundance of natural isotopes, especially ^{13}C (1.1% rel. abundance) has to be considered. Pyrimidines and purines have 9 and 10 Carbon atoms, respectively. Statistically, ~10% of all nucleosides carry one ^{13}C atom (m/z +1), 1% carry two ^{13}C atoms (m/z +2) and 0.1% carry three ^{13}C atoms (m/z +3). We recommend labeling techniques, which increase the mass by at least 3 Dalton to avoid the detection of the natural ^{13}C-isotopomers of the nucleosides.

The preparation of isotopically labeled media requires the acquisition of isotopically labeled compounds, which are more expensive than the unlabeled compound. We have summarized the cost of 1 Liter NAIL-MS media in an overview in Table 1. Per NAIL-MS experiment around 20–50 mL heavy labeled media is necessary. The least expensive isotope labeling is achieved in bacteria (76 €/L) and cell culture (290 €/L), but here the labeling efficiency is quite low. Yeast minimal media (945 €/L) labeling is affordable, but yeast complete media (2025 €/L) is the most expensive and therefore solely recommended for the production of internal standards.

3.2. Mass spectrometry

For the detection of modified nucleosides, sensitive triple quadrupole instruments are used. The first quadrupole filters for the nucleosides' m/z values (*e.g.* m/z 298 for m^7G). In the collision cell (historically second quadrupole), the nucleoside is fragmented into nucleobase and ribose and the charge remains on the nucleobase. The third quadrupole filters for the nucleobases' m/z values (*e.g.* m/z 166 for m^7G). The detection of product ions from defined precursor ions is called a mass transition. For m^7G, the mass transition is 298 → 166. Commonly, 20–30 modified nucleosides are analyzed in a single run. This is achieved by fast switching from one nucleoside's mass transition to the next (around every 5–10 ms). If ions from the previous nucleoside remain in the mass spectrometer, although the instrument selects for the next nucleoside, false positive signals can be observed. Especially for co-eluting isotopomers with small differences in mass transitions, carry-over in the collision cell falsifies the detected quantities of the compounds. Linear collision cells with hexapoles and octopoles have high carry-over tendencies and should be validated for usability for NAIL-MS methods. The desired method can be tested by injection of single-labeled samples, which should only produce signals for the isotopomers from the used label. Signals from other isotopomer mass transitions are considered artefacts and the method is not usable for NAIL-MS studies. The carry-over error can be reduced by programming only 1–2 nucleosides into the method or by using time-gated selection of mass transitions. The new generation of QQQ instruments use faster collision cells (curved or T-wave), which have less to no carry-over. Note: Carry-over is rarely a problem in common nucleoside quantification as most nucleosides are chromatographically separated and thus do not disturb each other in the mass spectrometer.

3.3. Validation of NAIL-MS experiments

Insufficient labeling and a slow mass spectrometry can result in false positive results or misinterpretation. Thus, NAIL-MS experiments must

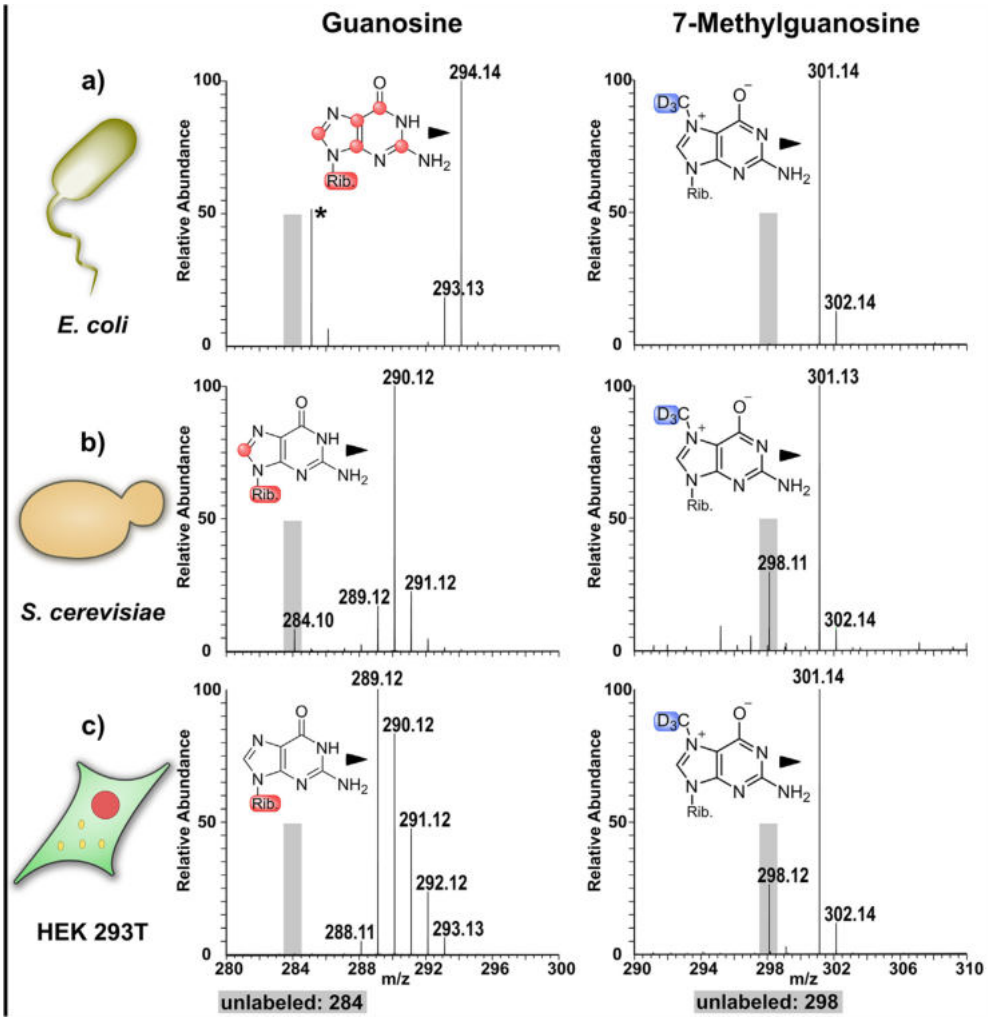

Fig. 3. High resolution mass spectra from ^{13}C labeled guanosine and CD_3-labeled 7-methylguanosine in *E. coli* (a), *S. cerevisiae* (b) and HEK 293 T (c). The grey bars in the spectra point out the expected *m/z* value of the unlabeled compounds. *Coeluting compound.

Table 1
Costs of NAIL-MS suitable media per Liter media in €uro.

Used isotope	CD_3	^{13}C	^{15}N	^{34}S
Bacteria (*E. coli*)	17	360	76	510
Yeast minimal	45	945	/	/
Yeast complete	1125	2025	/	/
Human cell culture	123	290	/	/

be carefully validated before they can be used for biological questions. The first step in validation should be to determine the labeling efficiency. As previously mentioned, it is crucial that the labeling leads to only one labeled isotopomer (*e.g.* 95% *m/z* of +5) and not several (*e.g.* 37% *m/z* +5, 31% *m/z* +6 and 18% *m/z* +7 as seen for guanosine in Fig. 3**c**). We recommend testing each labeling strategy by scanning the nucleoside mass range (*e.g. m/z* 240–400) and validate the abundance of all nucleoside isotopomers. If more than one isotopomer is formed under one labeling condition, we recommend optimization of the labeling technique. Sometimes low purity of the isotopically labeled metabolites/salts can also result in labeling inefficiency. In these cases, materials from other suppliers with higher isotope purity should be tested.

For validation of multiplexing and dynamic NAIL-MS we further recommend a control multiplexing experiment as shown in Fig. 4**a**. The media of choice is prepared in the unlabeled and isotopically labeled variant.

At this step it is crucial that both media are identical except for the isotope composition. Small differences in media composition already influence the abundance of modified nucleosides and the validation result. Thus, we recommend parallel preparation of the media using labeled and unlabeled stock solutions (!).

The two media are inoculated with the same number of cells and grown in parallel under identical conditions. After the appropriate amount of time (*e.g.* overnight for *E. coli*, 24 h for yeast and 5 days for HEK cells), the cells are harvested in *e.g.* TRI® reagent and mixed in a single container. From now on all processing steps are performed in parallel to avoid purification biases. From the isolated total RNA, the RNA of interest (*e.g.* tRNA) is isolated and prepared for LC-MS/MS by enzymatic digestion. The sample contains labeled and unlabeled nucleosides, and the amount of each modified nucleoside can be determined, normalized and plotted. Fig. 4**b** shows a successful validation of an *E. coli* $^{13}C_6$-glucose labeling procedure. Here, the quantities of most modified nucleosides from total tRNA are identical in labeled and unlabeled media.

The abundance of D (dihydrouridine) is in general higher in the ^{12}C samples compared to the ^{13}C samples. This is explained by contaminating ^{12}C-dihydrouridine from the used deaminase inhibitor tetrahydrouridine. Other uridine and cytidine derivatives showed a comparable modification profile in the ^{12}C and ^{13}C tRNA. A more than 1.1 fold difference in modification density is observed for m^2A. The

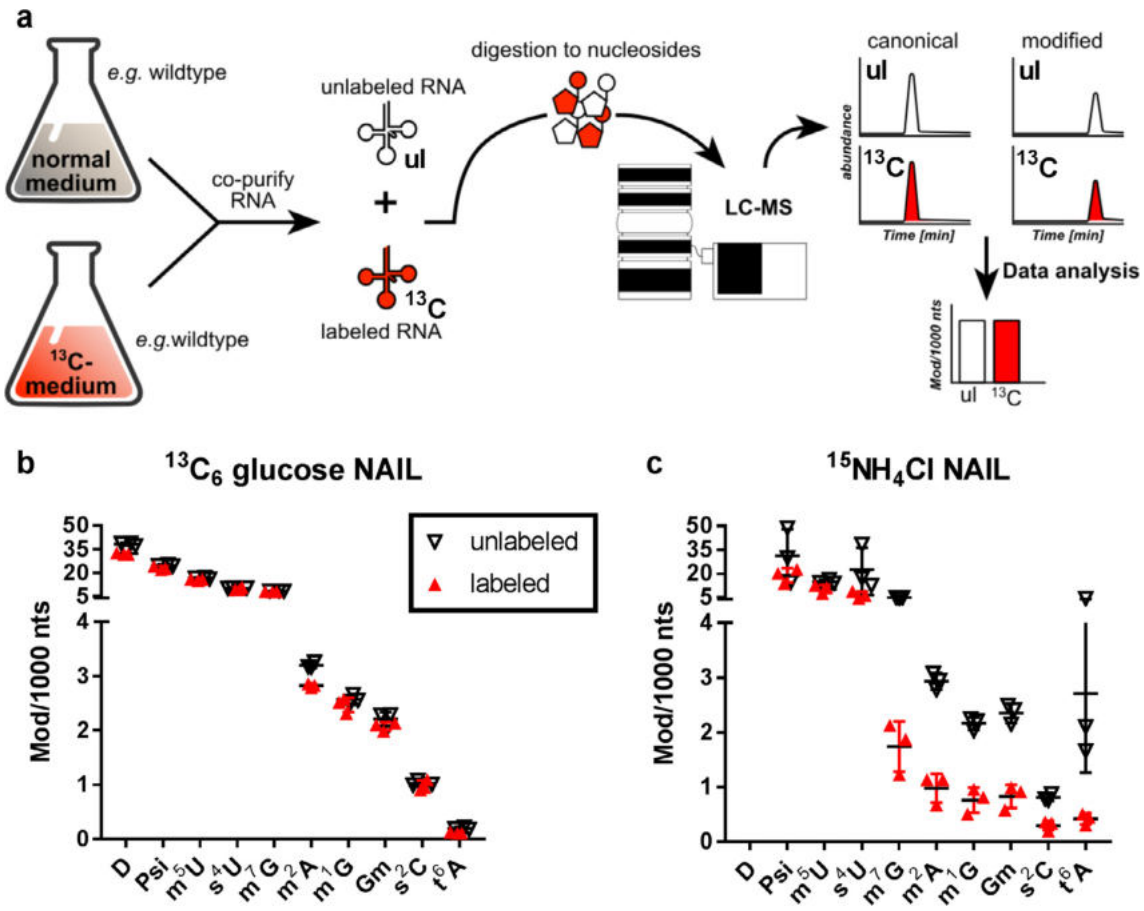

Fig. 4. a The principle of comparative NAIL-MS for validation of labeling. **b** and **c** *E. coli* comparative NAIL validation from a ^{13}C labeled culture mixed with an unlabeled culture (b) and a ^{15}N-labeled culture mixed with an unlabeled culture (c). y-axis labeling: Mod. per 1000 nts (Modification per 1000 nucleotides). Results from labeled RNA are marked in red, from unlabeled in black. (data represents 3 biol. replicates and error bars reflect the standard deviation.) (For interpretation of the references to color in this figure legend, the reader is referred to the web version of this article.)

observed fold difference between labeled and unlabeled tRNA is defined as the limit of precision in comparative NAIL-MS experiments and should be given in a table for any NAIL-MS study (Supplementary Table S1). The $^{13}C_6$-glucose labeling can be used for comparative NAIL studies of organisms with varying genetic background or under various growth conditions. It is also very useful if samples from complex purification procedures are compared as co-purification eliminates potential purification biases. It is also suitable for pulse-chase NAIL-MS studies, which focus on both the original RNA modification content and the new transcript modification content.

Fig. 4**c** shows the validation of a ^{15}N labeling technique in *E. coli*, which is less successful. Here, we observe lower modification content in the ^{15}N labeled bacterial tRNA compared to the unlabeled tRNA. The limit of precision of this validation experiment is larger as shown in Supplementary Table S1. ^{15}N labeling is more error prone compared to ^{13}C labeling in *E. coli* due to the media preparation. M9 media requires the preparation of a M9 salt stock, which also contains the $^{15}NH_4Cl$ salt for ^{15}N labeling. This M9 stock mix has a limited shelf life, and upon aging of the M9 stock mix the modification content in bacteria changes. Thus, ^{15}N labeling can be only used for comparative NAIL when both unlabeled and labeled M9 stock mix are freshly prepared and ideally in parallel. For pulse-chase NAIL-MS ^{15}N labeling is acceptable if, for example, the labeling is only used to distinguish original RNA from newly transcribed RNA. In these studies, modification profiles cannot be compared, but changes in the RNA modification profile of *e.g.* original RNA can be studied and effects of transcription can be excluded.

4. Results

4.1. Observing the repair of methylation damage in E. coli tRNA by pulse-chase NAIL-MS

We recently applied NAIL-MS to discriminate the origin of methylated RNA nucleosides in *E. coli* treated with the methylating agent MMS. We observed direct methylation of all canonical nucleosides and 7-methylguanosine, 1-methyladenosine, 6-methyladenosine, 3-methylcytidine and 3-methyluridine as the main damage products. In a dynamic NAIL-MS assay we followed the fate of these damage products and we observed demethylation of 1-methyladenosin and 3-methylcytidine after 24 h [27]. Here, we want to present the assay in more detail and we performed a NAIL-MS time-course experiment, which allows the determination of the demethylation kinetics. An assay to observe the repair of methylated RNA nucleosides is possible by NAIL-MS under the following conditions: A) A "backbone" labeling technique is needed, which allows discrimination of the damaged RNA from newly transcribed RNA. B) Availability of a labeling technique, which additionally distinguishes the damaged modification from the natural modification (here CD_3-methyl groups) [27]. C) The "damage" label and "backbone" label must be sufficiently resolvable in the mass spectrometer, *i.e.* if the "damage" label is +3, the "backbone label" cannot be +3 but should be ideally larger than +5. D) An internal standard must be available which is clearly distinguishable from all potential heavy isotope combinations from the biological assay.

In this study, we used 15-Nitrogen for the "backbone" labeling which results in a labeling of +5 for purines, +3 for cytidine and +2

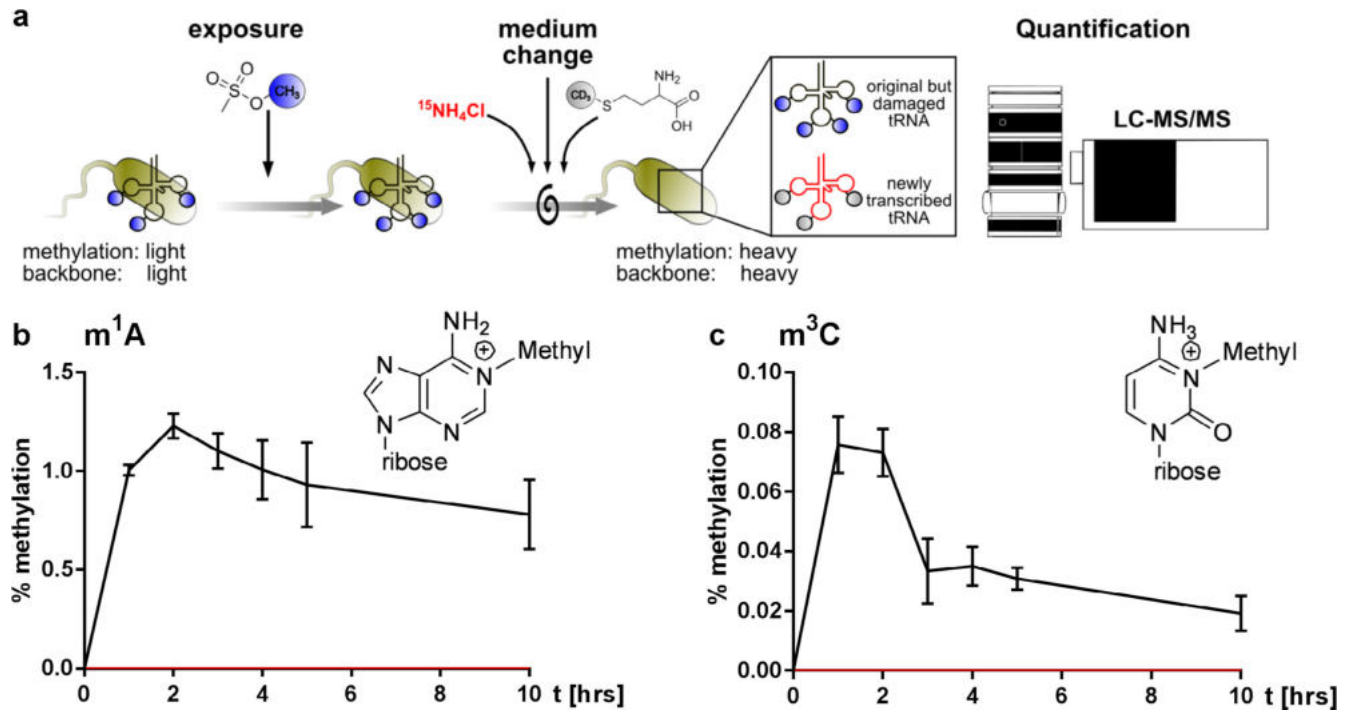

Fig. 5. a Concept of a pulse-chase NAIL-MS assay to distinguish the modified nucleosides from damaged tRNAs and newly transcribed tRNAs. (Adapted from [27].) **b** and **c** Pulse-chase NAIL-MS assay for 1-methyladenosine (**b**, m^{1}A) and 3-methylcytidine (**c**, m^{3}C). Color code: Black: damaged tRNAs. Red: newly trtranscribed tRNAs (Error bars represent the standard error of 3 biological replicates.)

Table 2
Mass transitions of 1-methyladenosine isotopomers in pulse-chase NAIL-MS for RNA repair observation.

Compound Group	Compound Name	Precursor Ion	Product Ion	Ret Time (min)
Unlabeled (original)	A	268	136	5.7
	m^{1}A	282	150	1.7
^{15}N and ^{13}C labeled (internal standard)	A SILIS	283	146	5.7
	m^{1}A SILIS	298	161	1.7
CD_3 labeled (post-methylated)	m^{1}A CD_3	285	153	1.7
^{15}N labeled (new)	A ^{15}N	273	141	5.7
^{15}N and CD_3 labeled (new)	m^{1}A ^{15}N_CD_3	290	158	1.7

for uridine. As the "damage/methylation" label we used CD_3-methionine (+3). The assay was set up as outlined in Fig. 5**a** and samples were drawn every hour after removal of the MMS. The bacteria are grown in unlabeled M9 media and exposed to the LD_{50} dose of MMS (Supplementary Fig. S1). The original RNA as well as all methylated nucleosides were unlabeled ($m/z \pm 0$). After 60 min, the MMS is removed by media exchange. The new media contains only ^{15}N as the nitrogen source and CD_3-methionine. Newly transcribed RNA is now labeled with ^{15}N (m/z +5, +3 or +2) and methylated nucleosides have an additional +3 label (m/z is thus +8, +6 or +5). Original tRNA, which is enzymatically methylated after media exchange receives a +3 label from the CD_3-methionine (m/z is thus +3). Using mass spectrometry, the tRNA exposed to the MMS and the newly transcribed tRNA can be clearly distinguished and the abundance of modified nucleosides in the original tRNA can be quantified. An exemplary list for the mass transitions of all m^{1}A isotopomers is given in Table 2 and for the other nucleosides in Supplementary Table S3. Here, and in the recently published study [27], we solely focused on the fate of the damaged tRNA from unlabeled bacteria culture. In such a case, the validation of NAIL-MS can be omitted, as the modification profile of the new transcripts is not of interest.

In *E. coli*, the quantities of the usually unnatural nucleosides m^{1}A and m^{3}C peak after 2 h with around 1% damaged adenosines (Fig. 5**b**) and only 0.08% damaged cytidines (Fig. 5**c**) in tRNA. The abundance of m^{1}A is slowly decreasing in the damaged tRNA over the 10 h recovery period. Two potential scenarios can explain this: The first scenario is degradation of m^{1}A-damaged tRNAs. The sequence of each tRNA contains at least 10 adenines in *E. coli* [1]. 1% of all adenosine methylation damage thus translates to a statistical abundance of m^{1}A in 1 out of 10 tRNAs. Thus 10% of the total tRNA pool needs to be degraded for removal of m^{1}A. If m^{1}A-targeted tRNA degradation was the cause, a faster tRNA dilution rate in comparison to unstressed *E. coli* would be observable. However, we observe the opposite (Supplementary Fig. S2b). The original tRNA pool from MMS stressed bacteria is less quickly diluted by newly transcribed tRNA in comparison to the unstressed bacteria. Thus, we consider the scenario of m^{1}A-targeted tRNA degradation as unlikely.

The second scenario is the proposed repair by demethylation. We see this hypothesis as proven, since we did not observe increased degradation of the original, damaged tRNA pool. Therefore, the only cause for the decrease in m^{1}A abundance is active demethylation of m^{1}A (potentially by AlkB [28]).

With our NAIL-MS assay, we can also follow the speed of m^{3}C repair by demethylation *in vivo*. The repair is even quicker (Fig. 5**c**), which is most likely caused by the comparably low abundance of m^{3}C sites in the tRNAs.

5. Discussion and outlook

LC-MS/MS is the method of choice for quantification of modified nucleosides. However, it is currently limited and only provides data on the quantities of modified nucleosides in an RNA but not about the dynamic changes and the underlying mechanisms. These limitations can be overcome by using nucleic acid isotope labeling coupled mass spectrometry (NAIL-MS). We present currently used approaches of isotope labeling in microorganisms such as *E. coli* and *S. cerevisiae*. Furthermore, we demonstrate the difficulties of adapting these methods

to human cell culture. In our hands, cell culture labeling by addition of $^{13}C_6$-glucose is not sufficient to allow successful application of comparative NAIL-MS experiments. However, for dynamic pulse-chase experiments where *e.g.* only the original RNA is the focus of the analysis, the labeling should allow sufficient resolution to distinguish the original RNA from new transcripts. Thus, we foresee a wide usage of cell culture labeling by addition of $^{13}C_6$-glucose in dynamic NAIL-MS experiments to answer current questions regarding open questions in the field such as: Is the change in the epitranscriptome due to a complete renewal of the transcriptome? Are modifications added to the existing transcriptome to confront *e.g.* stress? And are modifications removed actively *in vivo*? Due to the many isotopomers formed for each nucleoside and its respective modifications, we also foresee that massive validation is necessary to answer these questions by $^{13}C_6$-glucose in dynamic NAIL-MS. Ideally, other metabolites, *e.g.* precursors of nucleoside biosynthesis are found which lead to single isotopomer formation in cell culture. Thus, the usage of comparative NAIL and more elegant pulse-chase experiments would become possible in cell culture.

Regarding comparative NAIL-MS, we also foresee a unique opportunity towards determination of changes in RNA abundance as a consequence of stress or the loss of an RNA modification. Instead of quantifying the abundance of modified nucleosides, it should be possible to focus on the quantities of canonical nucleosides instead. As Fig. 6 shows, the total RNA from a comparative NAIL experiment is analyzed and the ratio of canonical nucleosides from labeled and unlabeled total RNA is determined. The ratio from the total RNA is later used for normalization and set to 100%. From the total RNA mixture, the RNA of interest, here isoacceptor tRNAs, can be purified [29]. The quantities of canonical nucleosides from an isoacceptor tRNA can be determined and subsequently the ratio of labeled and unlabeled is formed. In a control experiment, the abundance of all tRNA isoacceptors is expected to be identical in the unlabeled and labeled samples. The ratio of the pure isoacceptor tRNA can be compared to the total RNA ratio and plotted in %. Indeed, we observe in our $^{13}C_6$-glucose validation experiments from *E. coli* (Fig. 6) the same ratio of labeled and unlabeled canonical nucleosides for total RNA and several purified tRNA isoacceptors.

In a comparative NAIL experiment, it should be possible to detect changes in *e.g.* tRNA isoacceptor abundances because of stress or genetic manipulation of an RNA writer. By mixing an unlabeled control sample with a labeled, but *e.g.* stressed sample, the potential changes of tRNA isoacceptor abundance should be detectable. We expect that the ratio of canonical nucleosides would be different in total RNA and the purified tRNA isoacceptor and thus the impact of the stress on the relative abundance of the tRNA isoacceptor should be revealed. If our assumption is correct, we see a broad usability of comparative NAIL-MS to determine relative abundances of RNAs.

As an example, we show the repair kinetics of 1-methyladenosine (m^1A) and 3-methylcytidine (m^3C) in bacterial tRNA after exposure to MMS *in vivo*. We find that m^1A is slowly removed from original tRNA over the timeframe of observation. This is in accordance with previous work done with radioisotope labeling [28]. In contrast to the published work, we used *E. coli* without previous induction of AlkB which is reflected in the rather slow repair of m^1A observed in our NAIL-MS study. Similarly, we can observe the removal of m^3C from the bacterial tRNA which appears to happen a lot faster. The reason can be the relatively low abundance of m^3C damage compared to m^1A damage. It is also possible that m^3C is the better substrate for the tRNA demethylase.

In this study, we found around 1% of all adenines in tRNA are methylated by the methylating agent MMS after one hour of exposure to the LD_{50} dose. From a chemical point of view, the N1 position of adenine can be considered a good nucleophile which is easily methylated by an electrophile such as MMS. Therefore, we wonder how strongly the N1 position of adenine interacts with natural electrophiles such as S-adenosyl methionine (SAM). SAM is the natural methylating agent of the cell, and the methylation reaction of nucleic acids usually depends on an enzyme which activates the nucleoside first. However, chemically, the N1 position of adenosine is already a good nucleophile, and it should be possible, that some methylation occurs by reaction with SAM inside the cell, especially in those environments, which are rich in SAM and those RNAs that have one or more non base-paired adenosines. Considering the current dispute on the distribution of m^1A in mRNA [30–32], we wonder if some of the 0.02% m^1A (per A) [33] in mRNA is due to non-enzymatic methylation by SAM. In eukaryotic mRNA, the 5′ end is methylated (m^7G of the mRNA cap) and thus the 5′ end and its adenosines are always exposed to high amounts of SAM. Statistically, a sub-stoichiometric methylation of these adenosines is possible and should be taken into account during data interpretation. Of course, the origin of the 5′ UTR methylation, enzymatic or chemical, does not play a major role upon determining the function of the methylated adenosine.

With nucleic acid isotope labeling coupled mass spectrometry (NAIL-MS) we overcome current limitations and assess the dynamics of RNA modifications. We show the repair of m^1A and m^3C *in vivo* by discriminating the concurrent processes for removal of RNA methylation, namely RNA degradation, turnover and dilution. Dynamic NAIL-MS and comparative NAIL-MS are powerful tools which finally allow the observation of dynamic processes of RNA and its modifications.

Acknowledgements

The Kellner lab thanks Thomas Carell and his group for instrument

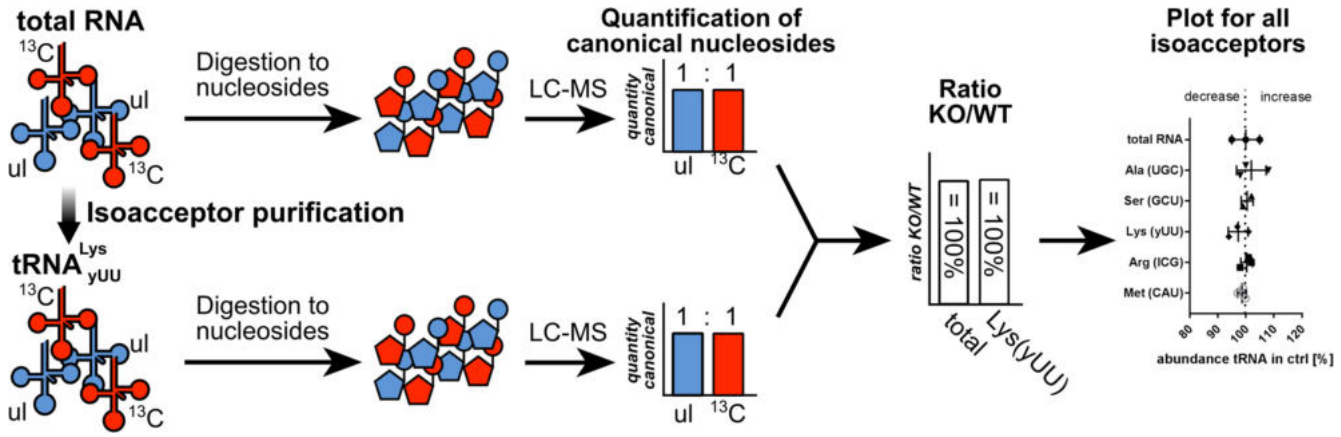

Fig. 6. Concept of relative tRNA isoacceptor abundance determination by NAIL-MS. The ratio of co-purified total RNA from unlabeled (ul) and ^{13}C labeled cells is 1:1 in this example. From the same RNA sample, a tRNA isoacceptor is purified by oligonucleotide hybridization. After digestion the ratio of the canonical nucleosides is determined and compared to the ratio from total RNA. The resulting data of each isoacceptor tRNA is plotted for all isoacceptors (n = 3).

time (high-resolution mass spectrometer) and valuable discussion. The bacteria projects are funded by the Fonds der Chemischen Industrie, Frankfurt, Germany (FCI) and the DFG (CIPSM and SFB 1309). Yeast work was funded by the SPP 1784 of the DFG and the cell culture work by the Emmy Noether program of the DFG. VFR is funded by the FCI.

Appendix A. Supplementary data

Supplementary data to this article can be found online at https://doi.org/10.1016/j.ymeth.2018.10.025.

References

[1] P. Boccaletto, et al., MODOMICS: a database of RNA modification pathways. 2017 update, Nucleic Acids Res. 46 (D1) (2018) D303–D307.
[2] W.M. Cai, et al., A platform for discovery and quantification of modified ribonucleosides in RNA: application to stress-induced reprogramming of tRNA modifications, Methods Enzymol. 560 (2015) 29–71.
[3] K. Thuring, et al., Analysis of RNA modifications by liquid chromatography-tandem mass spectrometry, Methods 107 (2016) 48–56.
[4] C. Wetzel, P.A. Limbach, Mass spectrometry of modified RNAs: recent developments, Analyst 141 (1) (2016) 16–23.
[5] C. Brandmayr, et al., Isotope-based analysis of modified tRNA nucleosides correlates modification density with translational efficiency, Angew. Chem. Int. Ed. Engl. 51 (44) (2012) 11162–11165.
[6] T. Bruckl, et al., Parallel isotope-based quantification of modified tRNA nucleosides, Angew. Chem. Int. Ed. Engl. 48 (42) (2009) 7932–7934.
[7] D. Pearson, et al., LC-MS based quantification of 2'-ribosylated nucleosides Ar(p) and Gr(p) in tRNA, Chem. Commun. (Camb.) 47 (18) (2011) 5196–5198.
[8] S. Kellner, et al., Absolute and relative quantification of RNA modifications via biosynthetic isotopomers, Nucleic Acids Res. 42 (18) (2014) e142.
[9] M. Heiss, V.F. Reichle, S. Kellner, Observing the fate of tRNA and its modifications by nucleic acid isotope labeling mass spectrometry: NAIL-MS, RNA Biol. 14 (9) (2017) 1260–1268.
[10] L.P. Sarin, et al., Nano LC-MS using capillary columns enables accurate quantification of modified ribonucleosides at low femtomol levels, RNA 24 (10) (2018) 1403–1417.
[11] C. Dal Magro, et al., A vastly increased chemical variety of RNA modifications containing a thioacetal structure, Angew. Chem. Int. Ed. Engl. 57 (26) (2018) 7893–7897.
[12] J.J. Thiaville, et al., Novel genomic island modifies DNA with 7-deazaguanine derivatives, Proc. Natl. Acad. Sci. U.S.A. 113 (11) (2016) E1452–E1459.
[13] C.E. Dumelin, et al., Discovery and biological characterization of geranylated RNA in bacteria, Nat. Chem. Biol. 8 (11) (2012) 913–919.
[14] S. Kellner, et al., Profiling of RNA modifications by multiplexed stable isotope labelling, Chem. Commun. (Camb.) 50 (26) (2014) 3516–3518.
[15] N.L. Anderson, N.G. Anderson, Proteome and proteomics: new technologies, new concepts, and new words, Electrophoresis 19 (11) (1998) 1853–1861.
[16] R. Apweiler, et al., Approaching clinical proteomics: current state and future fields of application in cellular proteomics, Cytometry A 75 (10) (2009) 816–832.
[17] S.E. Ong, et al., Stable isotope labeling by amino acids in cell culture, SILAC, as a simple and accurate approach to expression proteomics, Mol. Cell. Proteomics 1 (5) (2002) 376–386.
[18] N.A. Rosa-Mercado, J.B. Withers, J.A. Steitz, Settling the m(6)A debate: methylation of mature mRNA is not dynamic but accelerates turnover, Genes Dev. 31 (10) (2017) 957–958.
[19] K.D. Meyer, S.R. Jaffrey, The dynamic epitranscriptome: N6-methyladenosine and gene expression control, Nat. Rev. Mol. Cell Biol. 15 (5) (2014) 313–326.
[20] C.T. Chan, et al., A quantitative systems approach reveals dynamic control of tRNA modifications during cellular stress, PLoS Genet. 6 (12) (2010) e1001247.
[21] P.A. Aas, et al., Human and bacterial oxidative demethylases repair alkylation damage in both RNA and DNA, Nature 421 (6925) (2003) 859–863.
[22] S. Kellner, et al., Oxidation of phosphorothioate DNA modifications leads to lethal genomic instability, Nat. Chem. Biol. 13 (8) (2017) 888–894.
[23] Y.H. Chionh, et al., A multidimensional platform for the purification of non-coding RNA species, Nucleic Acids Res. 41 (17) (2013) e168.
[24] P. van Delft, et al., The profile and dynamics of RNA modifications in animals, ChemBioChem 18 (11) (2017) 979–984.
[25] T. Pfaffeneder, et al., Tet oxidizes thymine to 5-hydroxymethyluracil in mouse embryonic stem cell DNA, Nat. Chem. Biol. 10 (7) (2014) 574–581.
[26] M. Bachman, et al., 5-Hydroxymethylcytosine is a predominantly stable DNA modification, Nat. Chem. 6 (12) (2014) 1049–1055.
[27] V.F. Reichle, V. Weber, S. Kellner, NAIL-MS in *E. coli* determines the source and fate of methylation in tRNA, ChemBioChem (2018).
[28] R. Ougland, et al., AlkB restores the biological function of mRNA and tRNA inactivated by chemical methylation, Mol. Cell 16 (1) (2004) 107–116.
[29] R. Hauenschild, et al., The reverse transcription signature of N-1-methyladenosine in RNA-Seq is sequence dependent, Nucleic Acids Res. 43 (20) (2015) 9950–9964.
[30] S. Schwartz, m(1)A within cytoplasmic mRNAs at single nucleotide resolution: a reconciled transcriptome-wide map, RNA 24 (11) (2018) 1427–1436.
[31] X. Xiong, X. Li, C. Yi, N(1)-methyladenosine methylome in messenger RNA and non-coding RNA, Curr. Opin. Chem. Biol. 45 (2018) 179–186.
[32] X. Li, et al., Base-resolution mapping reveals distinct m(1)A methylome in nuclear- and mitochondrial-encoded transcripts, Mol. Cell 68 (5) (2017) 993–1005.e9.
[33] X. Li, et al., Transcriptome-wide mapping reveals reversible and dynamic N(1)-methyladenosine methylome, Nat. Chem. Biol. 12 (5) (2016) 311–316.

Um das Verhalten von m^3C und m^1A, welche Demethylierungsziele der AlkBH-Enzymfamilie sind, in einem NAIL-MS-Experiment zu analysieren, wurden HEK 293-Zellen an Tag 0 aus unmarkiertem Medium in stabilem isotopenmarkierten NAIL-MS-Medium passagiert (siehe Abbildung **3.20**). An Tag 3 wurde eine Passagierung mit anschließender RNA-Isolation eines Teils des Zellpellets durchgeführt. An Tag 6 wurde erneut passagiert, aber noch zwei weitere Tage kultiviert, bevor ein aus einem Teil der Zellen RNA isoliert wurde (8 Tage).

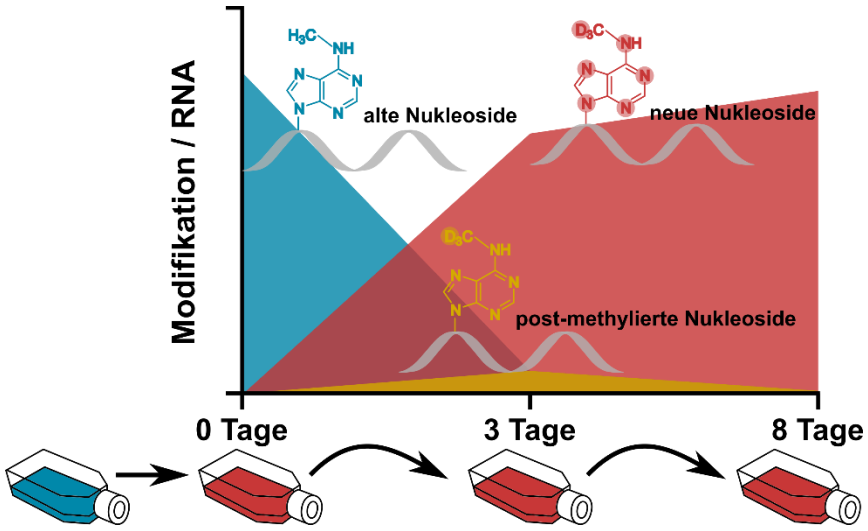

Abbildung 3.20: Schema der Isotopenmarkierung einer beliebigen RNA-Modifikation in eukaryotischen Zellen. Der Graph zeigt den Einbau neuer, isotopenmarkierter RNA-Nukleoside oder Methylgruppen an bestehenden RNA-Nukleosiden mit der Zeit. Es wurde unmarkiertes Medium an Tag 0 gegen stabiles, isotopenmarkiertes NAIL-MS-Medium getauscht und zweimal (an Tag 3 und Tag 6) passagiert.

In Abbildung **3.21 A** ist zu sehen, dass nach 3 Tagen Inkubation in markiertem Medium 67 % der alten, unmarkierten m^3C-Nukleoside und nach 8 Tagen nur noch < 1 % vorhanden sind. Dies ist durch den Abbau alter tRNA-Transkripte, sowie der Verdünnung durch zweimaliges Passagieren zu erklären. Der gegenläufige Effekt beschreibt die Zunahme von neuen, markierten m^3C-Nukleosiden mit der Zeit, da alle neu transkribierten tRNAs aus den Nährstoffen und Nukleosidvorläufern des NAIL-MS-Mediums biosynthetisiert werden. Zusammenfassend mit Abbildung **3.21 B** kann festgestellt werden, dass die endogenen tRNA-Modifikationslevel konstant sind. So trägt am Anfang des Experiments jede tRNA 1,0 unmarkiertes m^1A und nach 8 Tagen 1,0 isotopenmarkiertes m^1A. Bei dem Experiment werden nicht nur neue Nukleoside in die tRNA eingebaut, sondern auch alte, bereits inkorporierte Nukleoside nach dem Wechsel auf NAIL-MS-Medium mit CD_3-Methylgruppen versehen. Abbildung **3.21 C**

zeigt, dass nach 3 Tagen ein Maximum für die post-methylierten Spezies erreicht ist und nach 8 Tagen keine CD_3-markierten, alten RNA-Modifikationen detektiert werden können. Durch die Degradation der tRNA mit der Zeit werden somit in bis zu 8 Tagen neben den alten Nukleosiden auch die post-methylieren Nukleoside in der tRNA abgebaut.

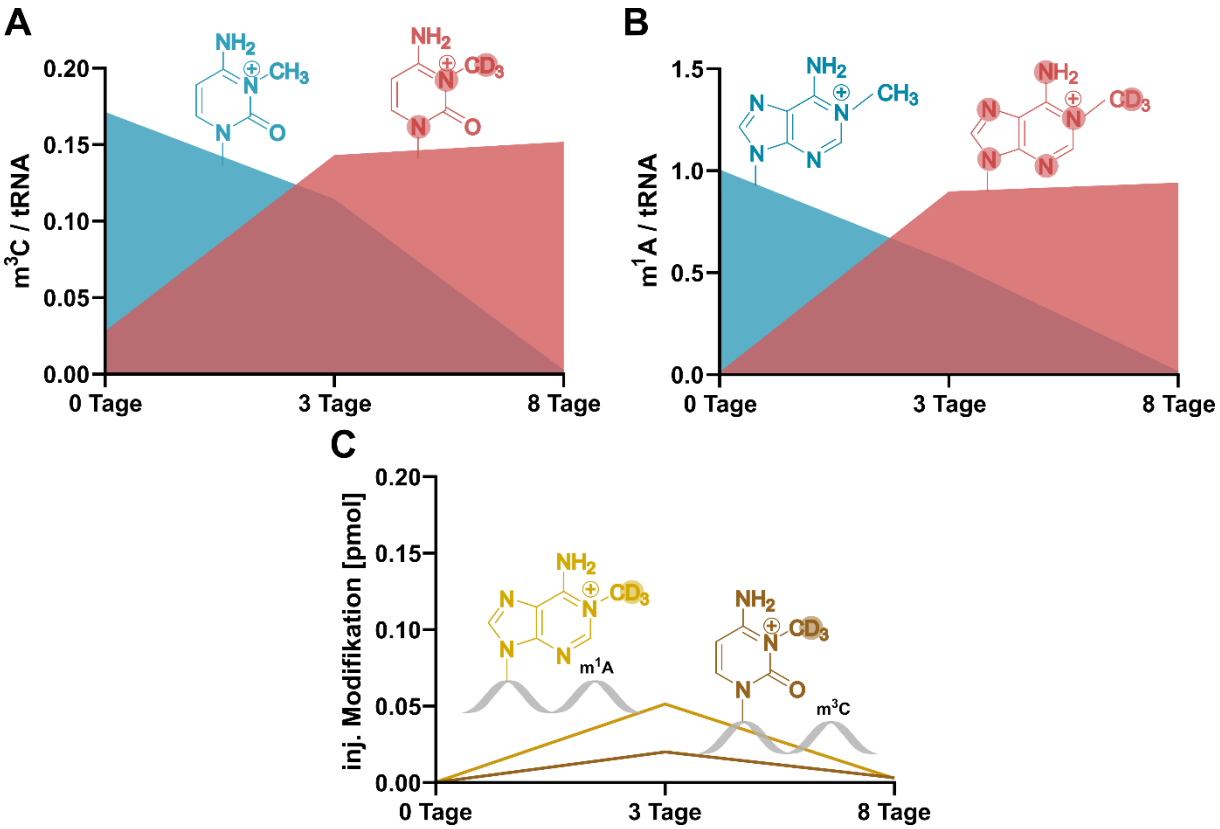

Abbildung 3.21: Isotopenmarkierung von RNA-Modifikationen mit der Zeit nach Wechsel auf NAIL-MS-Medium. Der Graph **A** zeigt das Vorkommen der unterschiedlich markierten (neu, rot) oder unmarkierten (alt, blau) m^3C-Nukleoside in tRNA vom Zeitpunkt des Mediumwechsels bis zu 8 Tagen nach dem Wechsel. Graph **B** stellt dies für m^1A-Nukleoside dar. In **C** ist die Häufigkeit der post-methylierten Spezies von m^1A (gelb) und m^3C (braun) abgebildet. Hierbei wurde die injizierte Menge in pmol verwendet und auf eine Referenzierung zu alter oder neuer tRNA verzichtet.

Mit dem in *Nat. Comm.* publizierten NAIL-MS-Medium wurde nach diesem Isotopeneinbauexperiment mit Fokus auf die RNA-Demethylierungsziele von AlkBH-Enzymen *in vivo*, m^3C und m^1A, weitergearbeitet.

3.4.3 Einfluss des Knockdown von AlkBH1 *in vivo* auf RNA-Modifikationen

Ziel des Knockdown des AlkBH1-Proteins *in vivo* war es, RNA-Modifikationen zu identifizieren, die unterschiedlich häufig in den Knockdown-Proben im Gegensatz zu den Transfektionskontrollen vorkommen. Ein signifikanter Anstieg einer Modifikation in einer Knockdown-Probe bedeutet, dass diese wahrscheinlich ein Substrat für AlkBH1 ist. Neben der *in vivo*-Bestätigung vorheriger *in vitro*-Substrate von AlkBH1 sollte auch eine mögliche Kompensation des Knockdown durch andere Demethylasen untersucht werden.

Durch ein Pulse-Chase-NAIL-MS-Experiment, welches in Abbildung **3.22** genauer skizziert ist, wurden HEK 293 Zellen in unmarkiertem Medium ausgesät, mit siRNA gegen AlkBH1 mRNA transfiziert, dann inkubiert, um einen Knockdown des AlkBH1 auf Transkript- und Proteinebene zu erreichen und schließlich nach Inkubation mit isotopenmarkiertem NAIL-MS-Medium für 0 oder 8 Stunden geerntet.

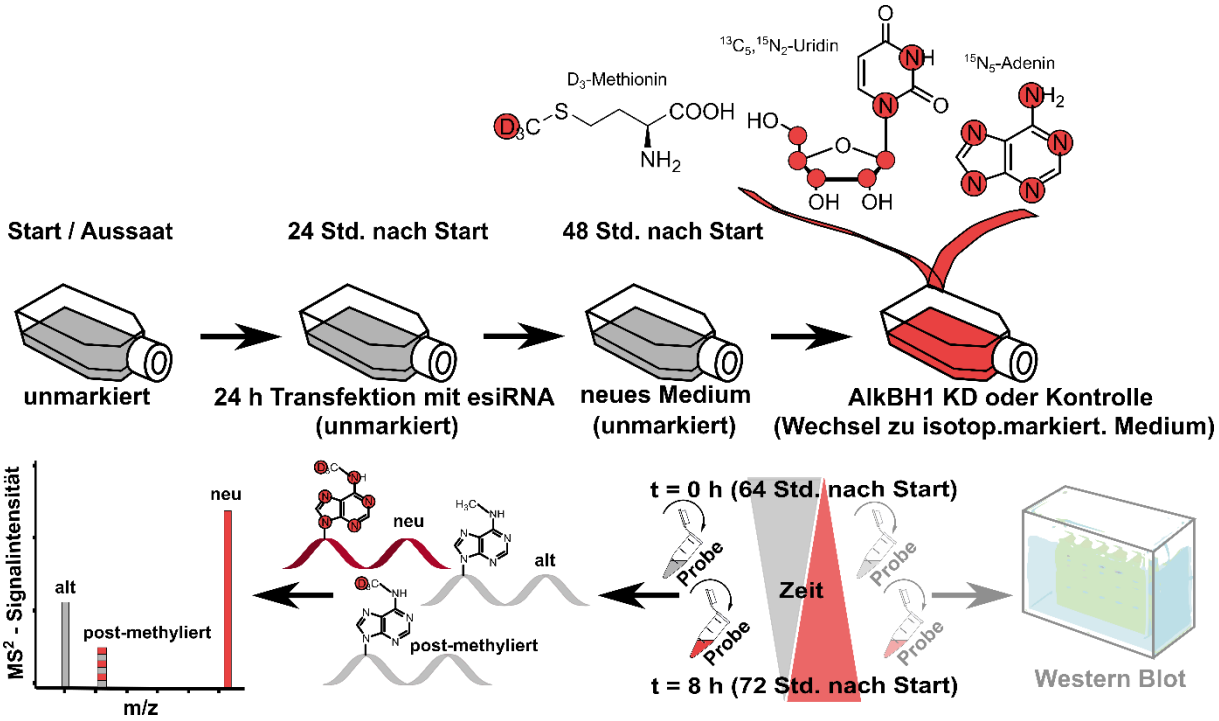

Abbildung 3.22: Schematischer Aufbau des AlkBH1-KD Pulse-Chase-NAIL-MS-Experiments. HEK 293 Zellen werden in unmarkiertem NAIL-MS-Medium (grau) kultiviert und nach Transfektion mit esiRNA für einen AlkBH1-Knockdown in stabilem isotopenmarkierten Medium (rot) bis zu 8 Stunden wachsen gelassen. Mittels Massenspektrometrie kann die Herkunft der einzelnen Nukleoside zu den jeweiligen Zeitpunkten nachvollzogen werden. Ein Teil der Zellen wird für die Überprüfung der Knockdown-Effizienz per Western-Blot benötigt (ausgegraut, aufgrund der Präparation und Analyse durch *M. Sc. Paria Asadi Atoi*).

Nach 8 Stunden in stabilem isotopenmarkierten NAIL-MS-Medium besteht die RNA der HEK 293-Zellen aus drei verschiedenen Nukleosidspezies, den Unmarkierten, Alten, den Isotopenmarkierten, Neuen und den Post-Methylierten. Diese können aufgrund ihrer unterschiedlichen Masse im Massenspektrometer getrennt detektiert werden.

Um den Knockdown des AlkBH1-Proteins zu verifizieren, wurden von *M. Sc. Paria Asadi Atoi* Zellproben genommen und mit Hilfe eines Western Blots analysiert. Nach 8 Stunden (72 Stunden nach Aussaat) wurden 58 % des AlkBH1 in der Knockdown-Probe im Vergleich zur zeitgleich entnommenen Transfektionskontrolle detektiert, was einem 42 % Knockdown von AlkBH1 entspricht (siehe Abbildung **3.23**).

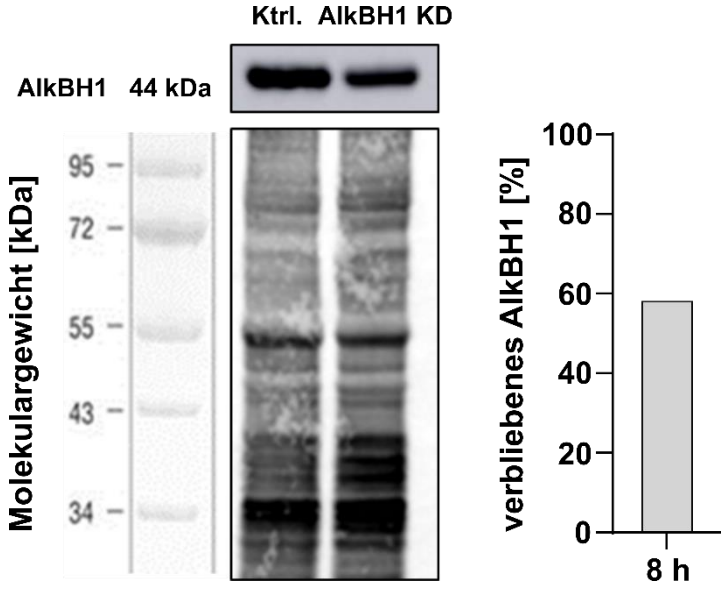

Abbildung 3.23: Western Blot des AlkBH1-KD Pulse-Chase-NAIL-MS-Experiments von *M. Sc. Paria Asadi Atoi*. Das Protein-Lysat der zwei entnommenen 8h-Proben wurde mit Hilfe eines „Invitrogen No-Stain™ Protein labeling reagent“ (Prod.Nr.: A44717, ThermoFisher Scientific, Waltham, MA, USA) angefärbt, aus den Intensitäten der Banden mit dem Programm „ImageJ“ die Effizienz des Knockdowns im Vergleich zur Transfektionskontrolle berechnet und im rechten Balkendiagramm dargestellt.

Um nun die Effekte eines AlkBH1-Knockdowns auf RNA-Modifikationen detaillierter zu betrachten, wurde zu den zwei Zeitpunkten isolierte Gesamt-RNA durch Größenausschlusschromatographie in 28S rRNA, 18S rRNA und eine totale tRNA-Fraktion separiert. Eine Aufreinigung in $tRNA^{His}_{GUG}$ und $tRNA^{Gly}_{GCC}$ war aufgrund der geringen Probenmenge bei diesem NAIL-MS-Experiment nicht möglich. In jeder RNA-Spezies wurden die Level der fünf RNA-Modifikationen m^1A, m^3C, m^5C, m^7G und m^6A absolut quantifiziert. In Abbildung **3.24** ist zu sehen, dass weder bei m^1A noch bei m^3C

ein signifikanter Unterschied zwischen Knockdown von AlkBH1 und der Kontrolle besteht. Dies ist in allen drei beobachteten RNA-Spezies und auch in den neu entstandenen RNAs der Fall.

Durch den Wechsel in stabiles isotopenmarkiertes NAIL-MS-Medium nach AlkBH1-Gen-Stilllegung zeigt der Gehalt an neu, markierter RNA nur die RNA-Modifikationen, die nach dem Knockdown von der Zelle produziert wurden. Für m^1A in 28S rRNA ist zu sehen, dass die in den 8 Stunden neu transkribierten großen, ribosomalen Untereinheiten die gleiche Modifikationsdichte, wie die alten 28S rRNAs besitzen. Die m^1A-Modifikation wird somit sehr früh, potentiell co-transkriptional oder spätestens innerhalb von 8 Stunden nach Synthese an der rRNA platziert. Beim Vergleich von alten, unmarkierten Nukleosiden bei Mediumwechsel und nach 8 Stunden Inkubation fällt auf, dass in der tRNA nach Inkubation weniger m^1A vorhanden ist. Diese Beobachtung wurde bereits in meiner Arbeit mit Matthias Heiß beschrieben[213]. Dadurch, dass tRNAs im Gegensatz zu rRNAs eine kürzere Halbwertszeit besitzen, werden in 8 Stunden mehr alte tRNAs abgebaut. m^3C kommt in den analysierten rRNAs nur substöchiometrisch vor und in neu synthetisierter tRNA wird es, wie m^1A, im Knockdown sowie in der Kontrolle auf gleichem Niveau eingebaut.

Die in der Literatur beschriebenen und in den vorherigen *in vitro*-Experimenten (Kapitel 3.3.4) mit AlkBH1 gefundenen Demethylierungssubstrate konnten mit dem NAIL-MS-Experiment nicht als *in vivo* AlkBH1-Ziele bestätigt werden.

Dies kann daran liegen, dass die RNA-Isolationsmethode cytosolische nicht von mitochrondrialer RNA trennen kann und somit durch den größeren Anteil an cytosolischer RNA mitochondriale AlkBH1-Effekte nicht zu detektieren sind. Zum anderen könnten weitere, nicht definierte RNA-Demethylasen den Knockdown von AlkBH1 kompensieren und so die ursprünglichen Mengen der beobachteten RNA-Modifikationen wiederherstellen.

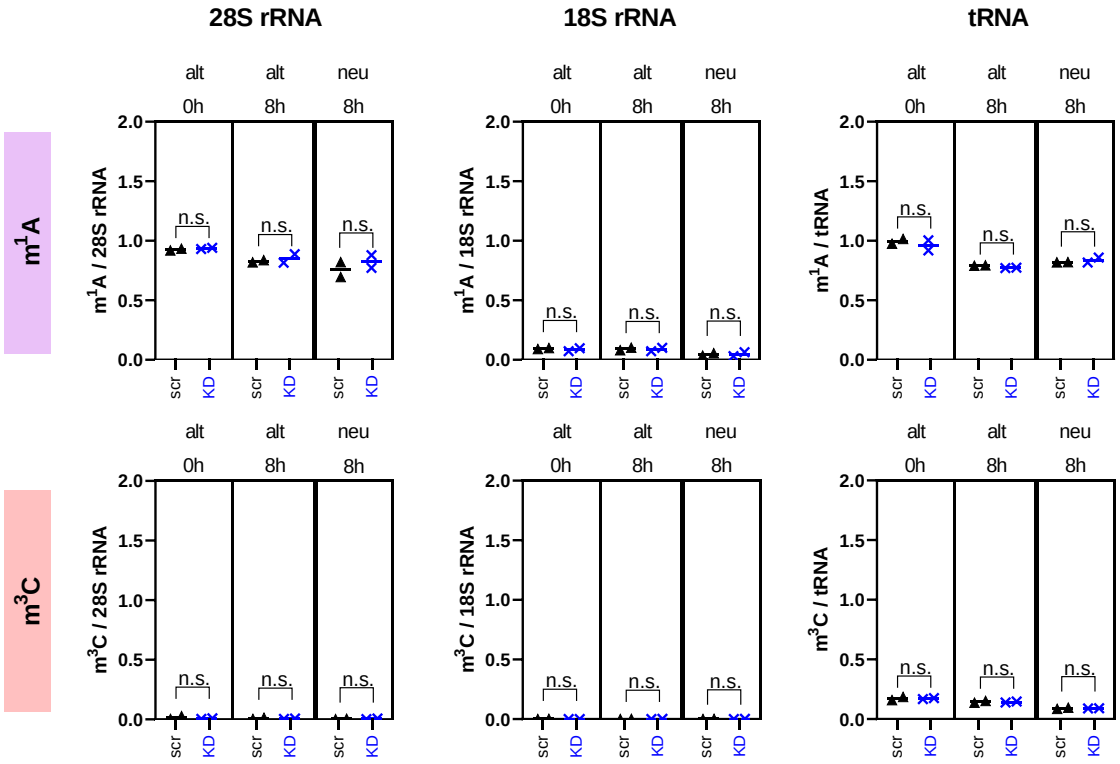

Abbildung 3.24: Quantifizierung der RNA-Modifikationen m^1A und m^3C im Pulse-Chase-NAIL-MS-Experiment nach AlkBH1 Knockdown. Die Boxplots zeigen die absoluten Werte für m^1A (erste Reihe) und m^3C (zweite Reihe) pro jeweiligem RNA-Molekül (linke Spalte: 28S rRNA; mittlere Spalte: 18S rRNA; rechte Spalte: tRNA). Jeder Boxplot unterteilt sich in drei Spalten, wobei links die alten, unmarkierten Nukleoside vor dem Mediumwechsel (t = 0h, 64 Std. nach Aussaat), in der Mitte die alten, unmarkierten Nukleoside nach Inkubation mit stabilem isotopenmarkierten Medium (t = 8h, 72 Std. nach Aussaat) und rechts die neuen, markierten Nukleoside nach 8 Stunden Inkubation abgebildet werden. Zu jedem Zeitpunkt wurde RNA sowohl aus AlkBH1-Knockdownproben (KD, blau) als auch aus den Transfektionskontrollen (scr: engl. für scramble control, schwarz) isoliert. Alle Werte stammen von n=2 biologischen Replikaten. Die Zweiweg-Varianzanalyse bestimmt die Signifikanz, welche über den Datenpunkten eingetragen ist (n.s. = nicht signifikant).

Drei weitere RNA-Modifikationen sind in Abbildung **3.25** dargestellt. Weder m^6A, noch m^5C oder m^7G werden in den AlkBH1-Knockdown-Proben weniger demethyliert. Bei m^5C in tRNA fällt auf, dass nach 8 Stunden Inkubation in stabilem isotopenmarkierten Medium weniger neues m^5C vorhanden ist, als vor Mediumwechsel Altes. Durch post-transkriptional agierende Methyltranferasen (m^5C-Writer-Enzyme) wird sukzessive neu synthetisierte tRNA methyliert, wobei mehr Zeit als die 8 Stunden Inkubation benötigt wird.

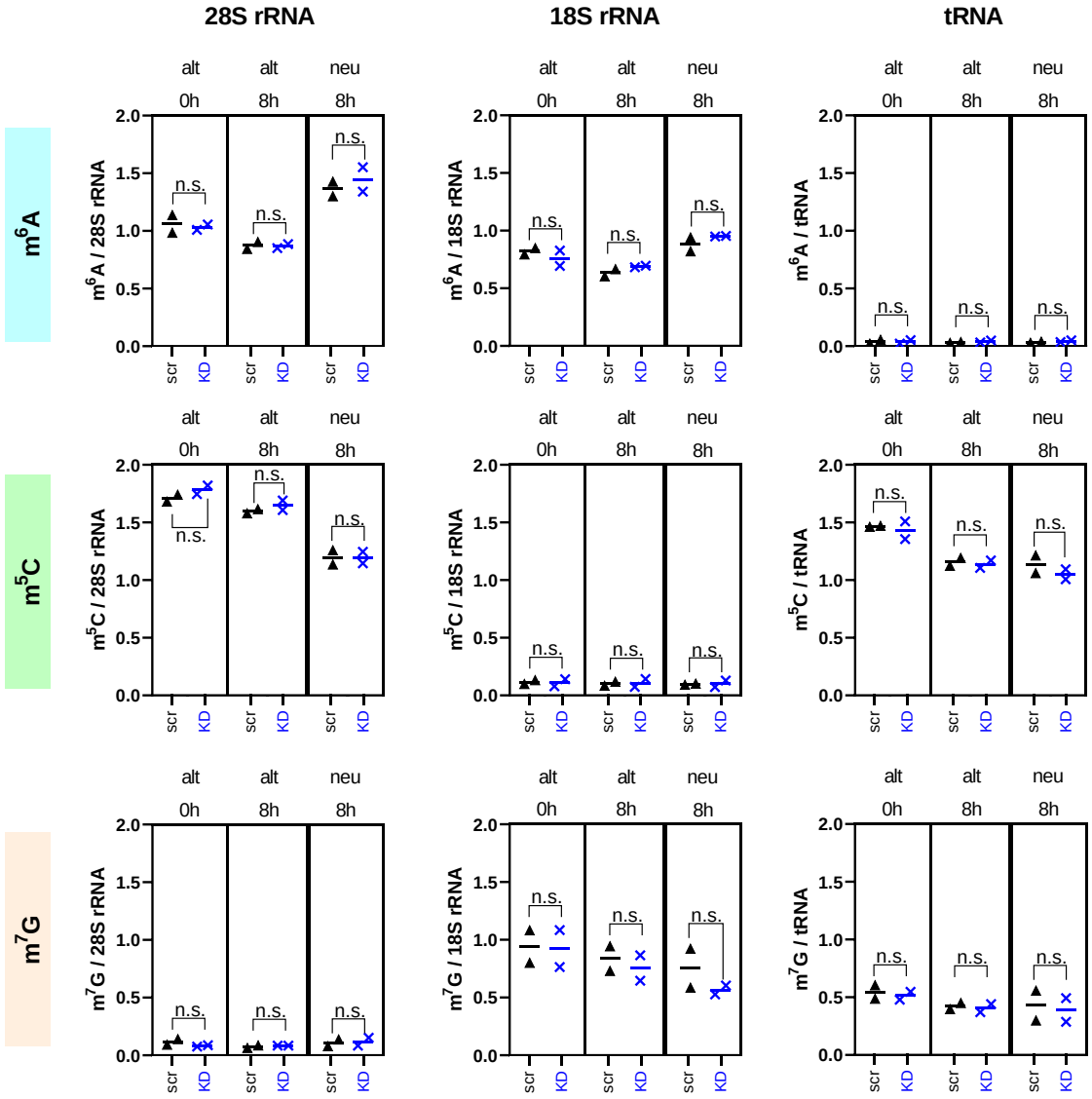

Abbildung 3.25: Quantifizierung der RNA-Modifikationen m^6A, m^5C und m^7G im Pulse-Chase-NAIL-MS-Experiment nach AlkBH1 Knockdown. Die Boxplots zeigen die absoluten Werte für m^6A (erste Reihe), m^5C (zweite Reihe) und m^7G (dritte Reihe) pro jeweiligem RNA-Molekül (linke Spalte: 28S rRNA; mittlere Spalte: 18S rRNA; rechte Spalte: tRNA). Jeder Boxplot unterteilt sich in drei Spalten, wobei links die alten, unmarkierten Nukleoside vor dem Mediumwechsel (t = 0h, 64 Std. nach Aussaat), in der Mitte die alten, unmarkierten Nukleoside nach Inkubation mit stabilem isotopenmarkierten Medium (t = 8h, 72 Std. nach Aussaat) und rechts die neuen, markierten Nukleoside nach 8 Stunden Inkubation abgebildet werden. Zu jedem Zeitpunkt wurde RNA sowohl aus AlkBH1-Knockdownproben (KD, blau) als auch aus den Transfektionskontrollen (scr: engl. für scramble control, schwarz) isoliert. Alle Werte stammen von n=2 biologischen Replikaten. Die Zweiweg-Varianzanalyse bestimmt die Signifikanz, welche über den Datenpunkten eingetragen ist (n.s. = nicht signifikant).

Neben den neuen und alten Nukleosiden kommen nach 8 Stunden Inkubation auch noch post-methylierte Nukleoside in RNAs vor. Sie entstehen, wenn vor dem Mediumwechsel synthetisierte RNAs innerhalb der 8 Stunden Inkubation durch

Methyltransferasen, welche das neu zur Verfügung gestellte CD_3-Methionin nutzen, methyliert werden. Wie in Abbildung **3.26** zu sehen ist, wird meistens ein kleiner Teil der RNAs post-methyliert. Eine ausgeprägtere Post-Methylierung lässt auf ein post-transkriptionalen Einbau der jeweiligen Modifikation oder einen längeren Maturierungsprozess der RNA-Spezies schließen. Post-Methylierung findet in einem Zeitfenster nach dem Wechsel des Mediums bis zur vollständigen Degradation alter RNAs oder ihrer weitgehenden Verdünnung durch Passagieren der Zellen statt.

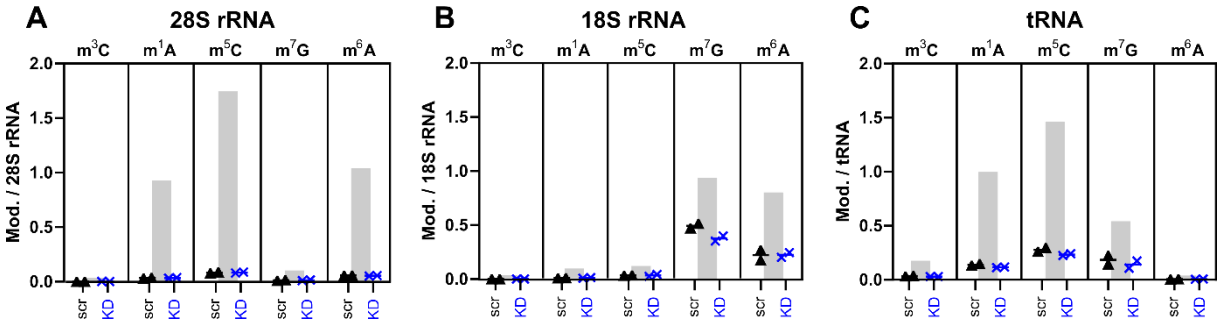

Abbildung 3.26: Quantifizierung der Postmethylierung von RNA-Modifikationen im Pulse-Chase-NAIL-MS-Experiment nach AlkBH1 Knockdown. Der Graph **A** zeigt das Vorkommen der postmethylierten Nukleoside nach 8 Stunden Inkubation in isotopenmarkiertem NAIL-MS-Medium in 28S rRNA. Es wurde RNA sowohl aus AlkBH1-Knockdownproben (KD, blau) als auch aus den Transfektionskontrollen (scr: engl. für scramble control, schwarz) isoliert. Alle Werte stammen von n=2 biologischen Replikaten. Die endogenen Level in der 28S rRNA sind als graue Balken dargestellt (alte, unmarkierte Nukleoside vor Mediumwechsel). **B** und **C** zeigen die Postmethylierung nach 8 Stunden in 18S rRNA und tRNA.

Zusammenfassend lässt sich kein Unterschied in der Häufigkeit der fünf RNA-Modifikationen in den AlkBH1-Knockdown-Proben im Gegensatz zu den Transfektionskontrollen erkennen. Zum einen kann die Kompensation von AlkBH1 *in vivo* durch andere Demethylasen oder durch weiterhin aktives AlkBH1 nicht ausgeschlossen werden, da ein stärkerer Knockdown oder ein kompletter Knockout von AlkBH1 durch die esiRNA Gen-Stilllegung nicht möglich war. Zum anderen können denkbare mitochondriale Demethylierungen von AlkBH1 aufgrund der kleinen Menge im Vergleich zu cytosolischer RNA nicht detektiert worden sein.

3.4.4 Einfluss des Knockdown von AlkBH3 *in vivo* auf RNA-Modifikationen

Neben dem *in vivo* Protein-Knockdown von AlkBH1 sollte mit AlkBH3 ein weiterer Eraser in einem Knockdownexperiment untersucht werden. Es sollte erforscht werden, ob RNA-Substrate, wie m^1A und m^3C, in AlkBH3 Knockdown-Proben häufiger vorkommen als in den jeweiligen Kontrollen. Dieses gibt indirekt Aufschluss über mögliche RNA-Modifikationen, die von AlkBH3 im Cytosol demethyliert werden.

Für das bereits für AlkBH1 angewendete Pulse-Chase-NAIL-MS-Experiment wurden HEK 293 Zellen in unmarkiertem Medium ausgesät, diesmal mit esiRNA gegen AlkBH3 transfiziert, dann inkubiert, um einen Knockdown des AlkBH3 auf Transkript- und Proteinebene zu erreichen und schließlich nach Inkubation mit isotopenmarkiertem NAIL-MS-Medium für 0 oder 8 Stunden geerntet.

Um den Grad des Knockdown von AlkBH3-Protein zu bestimmen, wurden von *M. Sc. Paria Asadi Atoi* erneut Zellproben genommen und mit einem Western Blot analysiert. In den AlkBH3 Knockdown-Proben wurde im Vergleich zu den zeitgleich entnommenen Transfektionskontrollen keine Bande mehr für AlkBH3 detektiert. Dies entspricht einer Knockdown-Effizienz von 100 % (siehe Abbildung **3.27**). Allerdings scheint allgemein die Menge an AlkBH3 in ungestressten Zellen sehr gering zu sein, da nur eine sehr schwache Bande für das Protein erkennbar ist. Daher ist es möglich, dass nach esiRNA Knockdown eine kleine, nicht detektierbare Menge an AlkBH3 in den Zellen vorlag.

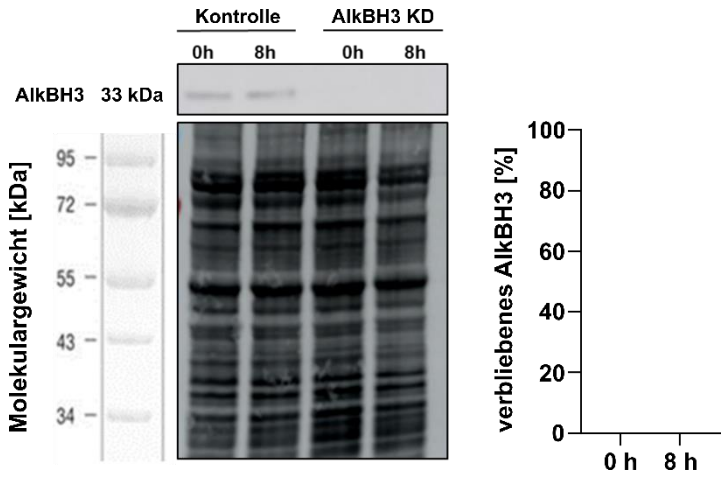

Abbildung 3.27: Western Blot des AlkBH3-KD Pulse-Chase-NAIL-MS-Experiments von *M. Sc. Paria Asadi Atoi*. Das Protein-Lysat der vier entnommenen Proben wurde per Elektrophorese aufgetrennt und später angefärbt. Aus den Intensitäten der Banden wurde die Effizienz des Knockdowns im Vergleich zur Transfektionskontrolle berechnet und im rechten Balkendiagramm dargestellt.

Nach Aufreinigung dreier RNA-Spezies (28S rRNA, 18S rRNA und tRNA), Verdau zu Nukleosiden und MS-Analyse kann - wie in Abbildung **3.28** zu sehen – kein Unterschied der Modifikationen m^1A und m^3C festgestellt werden. m^1A und m^3C entstehen in den neu transkribierten RNA innerhalb der 8 Stunden Inkubation durch Methylierung (co-transkriptional) in dem gleichen Ausmaß, wie zuvor aus unmarkierten Nukleosiden transkribierte RNAs ihr Modifikationslevel erhalten.

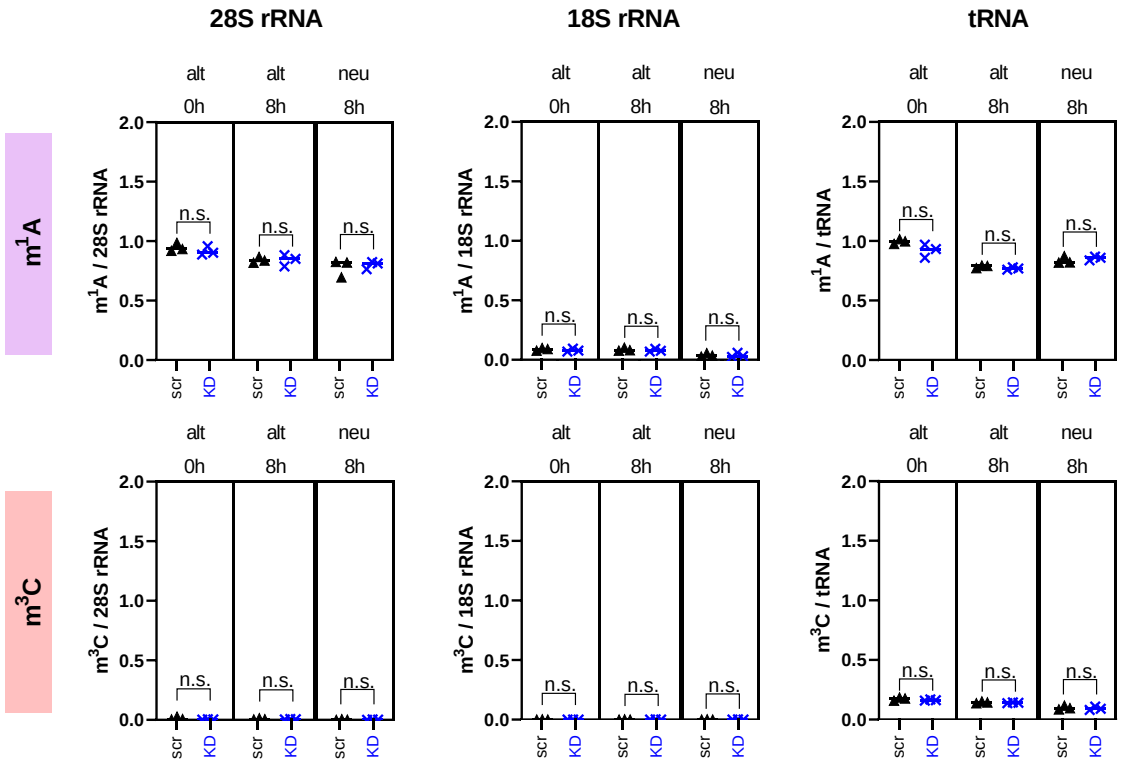

Abbildung 3.28: Quantifizierung der RNA-Modifikationen m^1A und m^3C im Pulse-Chase-NAIL-MS-Experiment nach AlkBH3 Knockdown. Die Boxplots zeigen die absoluten Werte für m^1A (erste Reihe) und m^3C (zweite Reihe) pro jeweiligem RNA-Molekül (linke Spalte: 28S rRNA; mittlere Spalte: 18S rRNA; rechte Spalte: tRNA). Jeder Boxplot unterteilt sich in drei Spalten, wobei links die alten, unmarkierten Nukleoside vor dem Mediumwechsel (t = 0h, 64 Std. nach Aussaat), in der Mitte die alten, unmarkierten Nukleoside nach Inkubation mit stabilem isotopenmarkierten Medium (t = 8h, 72 Std. nach Aussaat) und rechts die neuen, markierten Nukleoside nach 8 Stunden Inkubation abgebildet werden. Zu jedem Zeitpunkt wurde RNA sowohl aus AlkBH3-Knockdownproben (KD, blau) als auch aus den Transfektionskontrollen (scr: engl. für scramble control, schwarz) isoliert. Alle Werte stammen von n=3 biologischen Replikaten. Die Zweiweg-Varianzanalyse bestimmt die Signifikanz, welche über den Datenpunkten eingetragen ist (n.s. = nicht signifikant).

Betrachtet man weitere RNA-Modifikationsniveaus in Abbildung **3.29** fällt auf, dass der *in vivo* AlkBH3-Knockdown keine Auswirkungen auf m^6A, m^5C und m^7G besitzt. m^5C

wird in 28S rRNA und tRNA post-transkriptional methyliert, da die Niveaus der neu,8h-Proben noch nicht das der alt,0h-Proben erreicht haben.

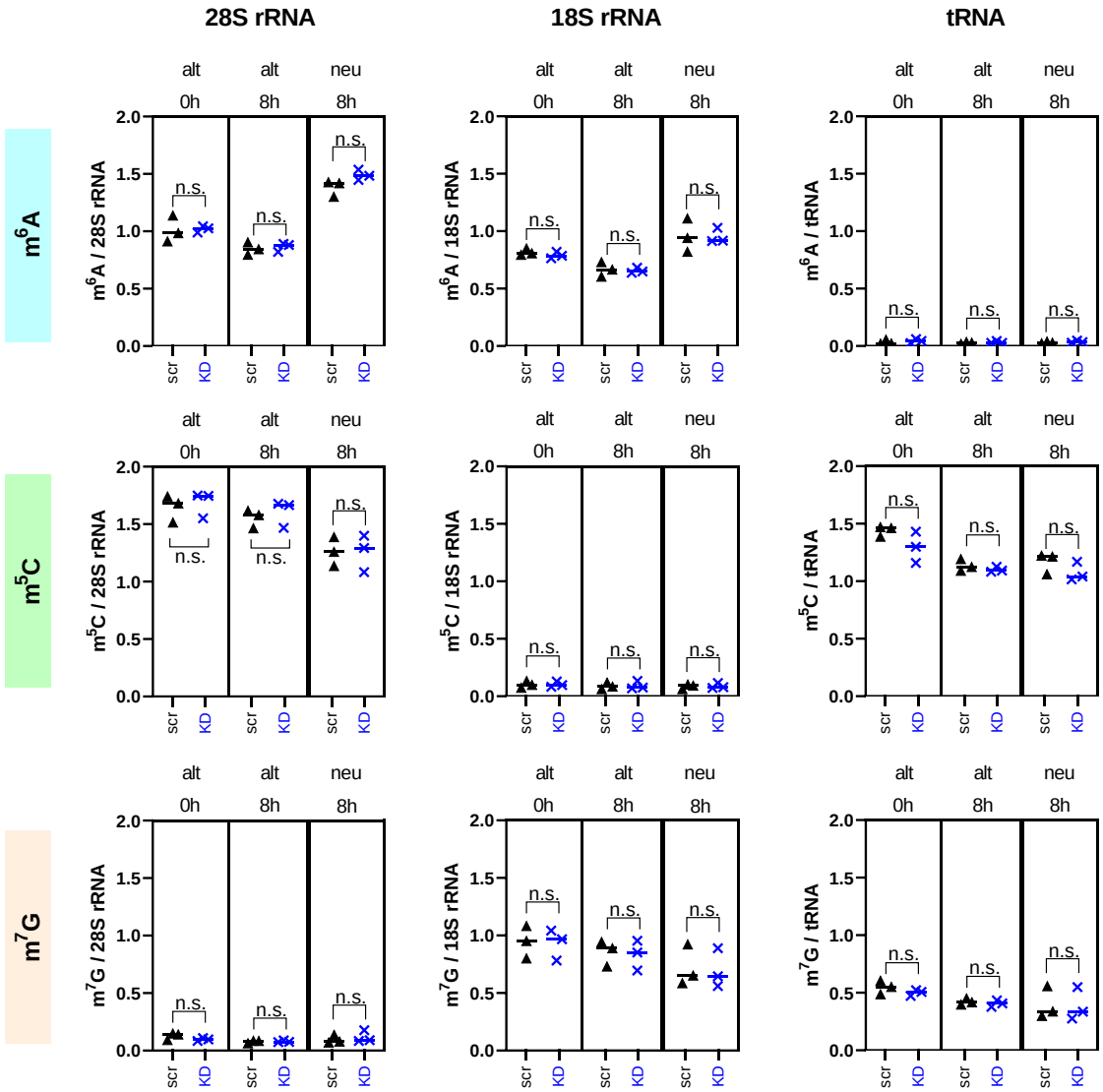

Abbildung 3.29: Quantifizierung der RNA-Modifikationen m^6A, m^5C und m^7G im Pulse-Chase-NAIL-MS-Experiment nach AlkBH3 Knockdown. Die Boxplots zeigen die absoluten Werte für m^6A (erste Reihe), m^5C (zweite Reihe) und m^7G (dritte Reihe) pro jeweiligem RNA-Molekül (linke Spalte: 28S rRNA; mittlere Spalte: 18S rRNA; rechte Spalte: tRNA). Jeder Boxplot unterteilt sich in drei Spalten, wobei links die alten, unmarkierten Nukleoside vor dem Mediumwechsel (t = 0h, 64 Std. nach Aussaat), in der Mitte die alten, unmarkierten Nukleoside nach Inkubation mit stabilem isotopenmarkierten Medium (t = 8h, 72 Std. nach Aussaat) und rechts die neuen, markierten Nukleoside nach 8 Stunden Inkubation abgebildet werden. Zu jedem Zeitpunkt wurde RNA sowohl aus AlkBH3-Knockdownproben (KD, blau) als auch aus den Transfektionskontrollen (scr: engl. für scramble control, schwarz) isoliert. Alle Werte stammen von n=3 biologischen Replikaten. Die Zweiweg-Varianzanalyse bestimmt die Signifikanz, welche über den Datenpunkten eingetragen ist (n.s. = nicht signifikant).

Durch post-transkriptionale Methylierung entstandene RNA-Modifikationen können durch ihre spezielle Isotopenmarkierung im Verlauf des NAIL-MS-Experiments als solche erkannt werden. In nachfolgender Abbildung **3.30** sind diese im Verhältnis zum endogenen Level der jeweiligen Modifikation (graue Balken) gezeigt. m^5C in tRNA und 28S rRNA ist das am meisten post-methylierte Substrat. Circa 0,3 m^5C pro existierendem RNA-Molekül wurden in den 8 Stunden methyliert.

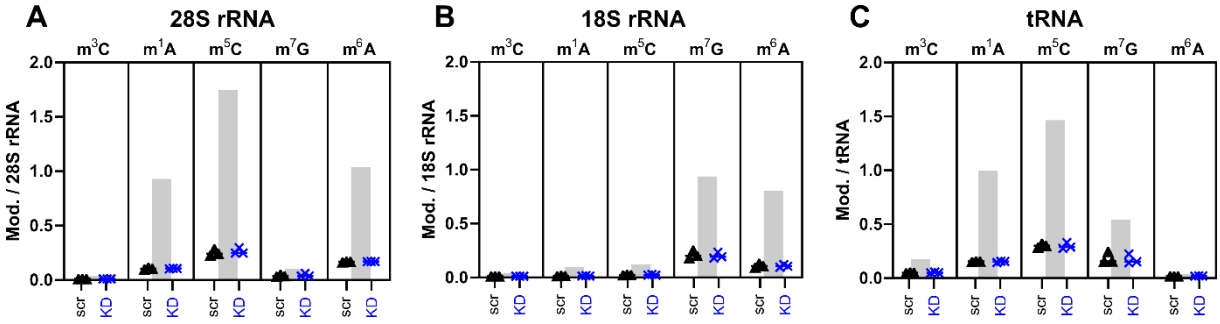

Abbildung 3.30: Quantifizierung der Postmethylierung von RNA-Modifikationen im Pulse-Chase-NAIL-MS-Experiment nach AlkBH3 Knockdown. Der Graph **A** zeigt das Vorkommen der postmethylierten Nukleoside nach 8 Stunden Inkubation in isotopenmarkiertem NAIL-MS-Medium in 28S rRNA. Es wurde RNA sowohl aus AlkBH3-Knockdownproben (KD, blau) als auch aus den Transfektionskontrollen (scr: engl. für scramble control, schwarz) isoliert. Alle Werte stammen von n=3 biologischen Replikaten. Die endogenen Level der Modifikationen in der 28S rRNA sind als graue Balken dargestellt (alte, unmarkierte Nukleoside vor Mediumwechsel). **B** und **C** zeigen die Postmethylierung nach 8 Stunden in 18S rRNA und tRNA.

Ähnlich zu dem AlkBH1-Knockdown zeigt auch der AlkBH3-Knockdown keinen Effekt auf die Niveaus ausgewählter RNA-Modifikationen. *In vitro* Substrate, wie m^1A in 28S rRNA, des AlkBH3-Enzyms sind in diesem *in vivo* Experiment entweder keine Ziele mehr oder werden durch andere, nicht definierte Demethylasen kompensatorisch auf dem gleichen Niveau gehalten.

3.4.5 Einfluss des Knockdown von AlkBH5 *in vivo* auf RNA-Modifikationen

Ein weiteres NAIL-MS-Experiment sollte die Auswirkungen von AlkBH5 auf die Modifikationen innerhalb der RNA klären. AlkBH5 soll laut Literatur m^6A in mRNA demethylieren[135]. Während *Dr. Kayla Borland* die mRNA des Pulse-Chase-NAIL-MS-Experiments isolierte und analysierte, sollten die Effekte eines AlkBH5-Knockdowns auf m^6A in rRNAs und tRNA untersucht werden. Um ein mögliches regulatorisches

Netzwerk an Modifikationen, die durch AlkBH5 beeinflusst werden, zu entdecken, wurden weitere acht abundante RNA-Modifikationen analysiert.

Durch das Design des NAIL-MS-Experiments ist es zudem möglich, den Abbau sowie die Synthese der verschiedenen RNA-Spezies und RNA-Nukleoside zeitlich zu verfolgen und so mögliche kinetische Differenzen zwischen Knockdown- und Kontrollprobe zu entdecken.

Der experimentelle Aufbau in Abbildung **3.31** *in vivo* unterschied sich nur marginal von denen für AlkBH1 (s. Abbildung **3.22**) oder AlkBH3. Es wurde stattdessen AlkBH5 mission esiRNA eingesetzt, sowie zusätzlich zur rRNA und tRNA noch mRNA isoliert.

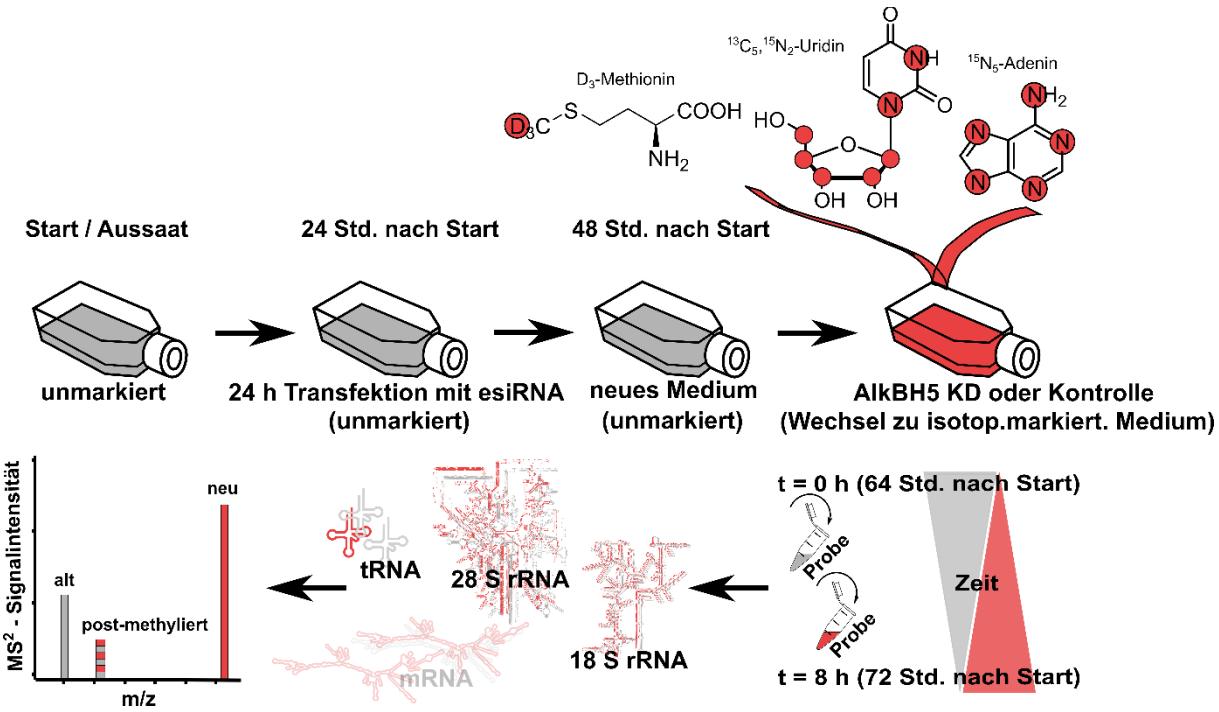

Abbildung 3.31: Schematischer Aufbau des AlkBH5-KD Pulse-Chase-NAIL-MS-Experiments. HEK 293 Zellen werden in unmarkiertem NAIL-MS-Medium (grau) kultiviert und nach Transfektion mit esiRNA für einen AlkBH5-Knockdown in stabilem isotopenmarkierten Medium (rot) bis zu 8 Stunden wachsen gelassen. Die RNA-Spezies werden per Größenausschlusschromatografie oder Oligohybridisierung (mRNA, ausgegraut aufgrund der Präparation und Analyse durch *Dr. Kayla Borland*) separiert. Mittels Massenspektrometrie kann die Herkunft der einzelnen Nukleoside nachvollzogen werden.

Der erfolgreiche Knockdown von AlkBH5 auf Proteinebene wurde von *M. Sc. Paria Asadi Atoi* mit Western Blot bestätigt. Drei biologische Replikate (insgesamt 6 Protein-Lysat-Proben) des 8h-Zeitpunktes wurden analysiert. Abbildung **3.32** zeigt 56 % verbliebenes AlkBH5-Protein in den KD-Proben. Ein 44 % Knockdown wurde somit erreicht.

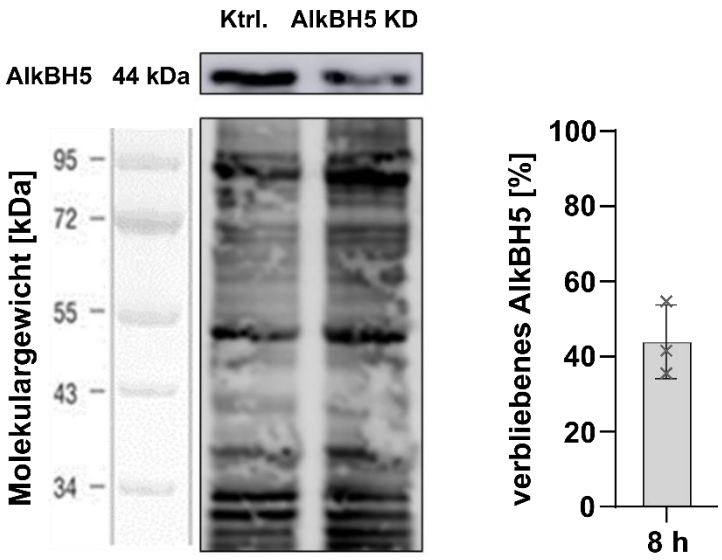

Abbildung 3.32: Western Blot des AlkBH5-KD Pulse-Chase-NAIL-MS-Experiments von *M. Sc. Paria Asadi Atoi*. Das Protein-Lysat der sechs entnommenen 8h-Proben wurde per Elektrophorese aufgetrennt und später angefärbt (hier sind nur zwei exemplarische Banden gezeigt). Aus den Intensitäten der Banden wurde die Effizienz des Knockdowns im Vergleich zur Transfektionskontrolle berechnet und im rechten Balkendiagramm dargestellt. Die Daten stammen von n=3 biologischen Replikaten.

Vergleicht man die unmarkierten RNA-Nukleoside nach der Transfektion, aber vor dem Wechsel in isotopenmarkiertes Medium, erkennt man keinen Unterschied im Modifikationsniveau. Dieses gilt für 8 RNA-Modifikationen in 3 RNA-Spezies (Abbildung **3.33**).

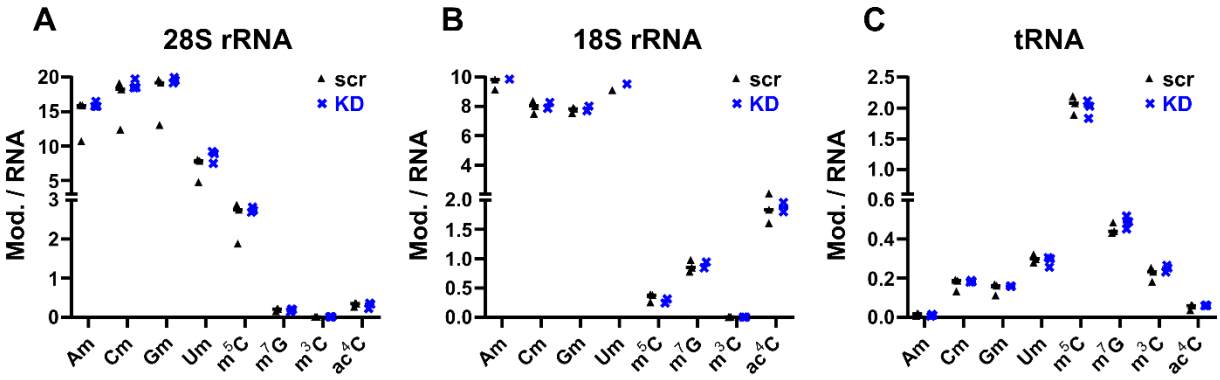

Abbildung 3.33: Quantifizierung der unmarkierten RNA-Modifikationen im Pulse-Chase-NAIL-MS-Experiment nach AlkBH5 Knockdown. Die Graphen zeigen die absoluten Werte für 8 RNA-Modifikationen pro jeweiligem RNA-Molekül (**A**: 28S rRNA; **B**: 18S rRNA; **C**: tRNA). Es wurde RNA sowohl aus AlkBH5-Knockdownproben (KD, blau) als auch aus den Transfektionskontrollen (scr: engl. für scramble control, schwarz) isoliert. Alle Werte stammen von n=3 biologischen Replikaten.

Nach Mediumwechsel wurden neu-synthetisierte RNA-Moleküle aus isotopenmarkierten Nukleosiden hergestellt und das Verhältnis der unmarkierten Nukleoside durch alle Nukleoside kann als Maß dafür stehen, wie schnell bereits existierende RNA-Moleküle degradiert wurden. Guanosin wurde als kanonisches Nukleosid für die in Abbildung **3.34** dargestellten Degradations- oder Umsatzraten gewählt.

Hierbei fällt auf, dass zum Zeitpunkt des Mediumwechsels bereits existierende mRNA schneller abgebaut wurde als die anderen RNA-Spezies. Dieses lässt sich mit der kürzeren Halbwertszeit von mRNA gegenüber z.B. tRNA erklären[214]. Nach 8 Stunden sind nur noch 70 % der unmarkierten mRNAs vorhanden. 28S rRNA, 18S rRNA und tRNA besitzen längere Halbwertszeiten und nur circa 10 % der Moleküle wurden degradiert, somit nicht mehr isoliert und per Massenspektrometrie detektiert.

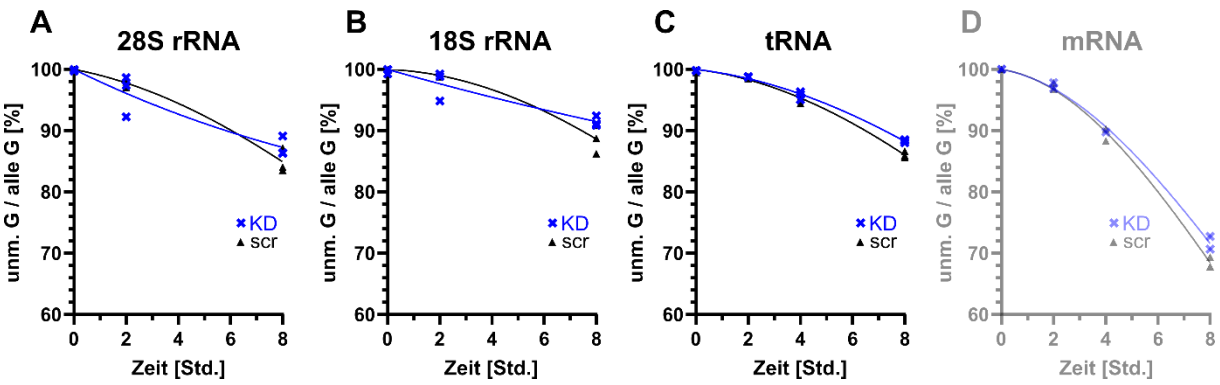

Abbildung 3.34: Umsatzraten verschiedener RNA-Spezies während des Pulse-Chase-NAIL-MS-Experiment nach AlkBH5 Knockdown. Der Graph **A** zeigt die Umsatzrate der 28S rRNA. Die Guanosine wurden aus AlkBH5-Knockdownproben (KD, blau) und aus den Transfektionskontrollen (scr: engl. für scramble control, schwarz) isoliert. Alle Werte stammen von n=3 biologischen Replikaten. Die Umsatzraten von 18S rRNA, tRNA und mRNA (ausgegraut aufgrund der Präparation und Analyse durch *Dr. Kayla Borland*) sind in den Graphen **B** – **D** abgebildet.

Nach der Betrachtung der Kinetik von RNA-Spezies in Abbildung **3.34** zeigt die Kinetik der m^6A-Nukleoside in Abbildung **3.35** eine statische Modifikationsdichte im Verlauf des NAIL-MS-Experiments. Während m^6A in tRNA nicht zu detektieren ist, wurde es in beide rRNA-Spezies (28S und 18S) co-transkriptional oder innerhalb der maximalen 8 Stunden in isotopenmarkiertem Medium inkorporiert. Die AlkBH5-Knockdownproben unterscheiden sich hinsichtlich ihrer m^6A-Abundanz nicht von den Transfektions-/scramble-Kontrollen.

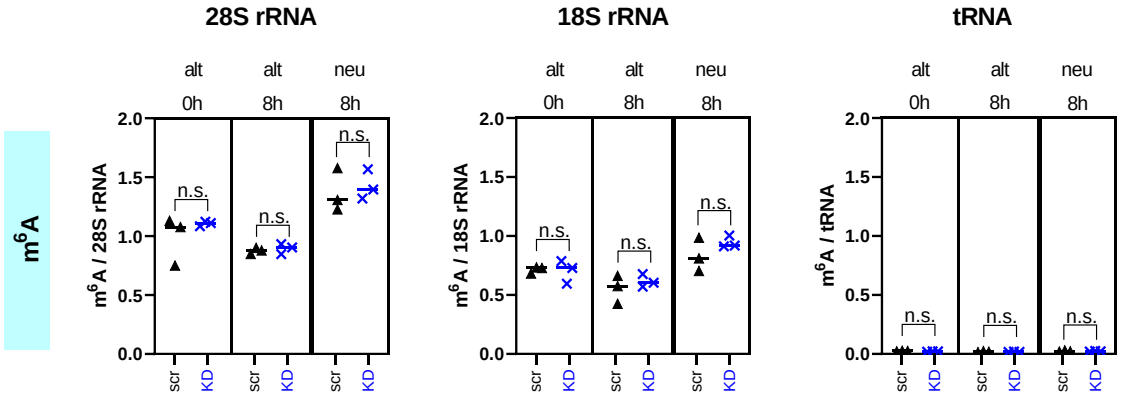

Abbildung 3.35: Quantifizierung der RNA-Modifikation m^{6}A im Pulse-Chase-NAIL-MS-Experiment nach AlkBH5 Knockdown. Die Boxplots zeigen die absoluten Werte für m^{6}A pro jeweiligem RNA-Molekül (linke Spalte: 28S rRNA; mittlere Spalte: 18S rRNA; rechte Spalte: tRNA). Jeder Boxplot unterteilt sich in drei Spalten, wobei links die alten, unmarkierten Nukleoside vor dem Mediumwechsel (t = 0h, 64 Std. nach Aussaat), in der Mitte die alten, unmarkierten Nukleoside nach Inkubation mit stabilem isotopenmarkierten Medium (t = 8h, 72 Std. nach Aussaat) und rechts die neuen, markierten Nukleoside nach 8 Stunden Inkubation abgebildet werden. Zu jedem Zeitpunkt wurde RNA sowohl aus AlkBH5-Knockdownproben (KD, blau) als auch aus den Transfektionskontrollen (scr: engl. für scramble control, schwarz) isoliert. Alle Werte stammen von n=3 biologischen Replikaten. Die Zweiweg-Varianzanalyse bestimmt die Signifikanz, welche über den Datenpunkten eingetragen ist (n.s. = nicht signifikant).

Um weitere mögliche Substrate von AlkBH5 festzustellen, wurden weitere abundante RNA-Modifikationen in tRNA und rRNA analysiert (Abbildung **3.36**). Weder m^{3}C noch m^{5}C oder m^{7}G besitzen signifikant, abweichende Level in den AlkBH5-Knockdown-Proben. In keiner der drei beobachteten RNA-Spezies ist die Synthese der RNA sowie die Methylierung eingeschränkt. Einzig neues isotopenmarkiertes m^{5}C in tRNA konnte nach 8 Stunden Inkubation nicht vollständig zu der alten Modifikationsdichte methyliert werden. Dies könnte mit post-transkriptional arbeitenden m^{5}C-Methyltransferasen erklärt werden, die einige Zeit benötigen, um den Modifikationsstatus in neuen RNA-Transkripten wiederherzustellen.

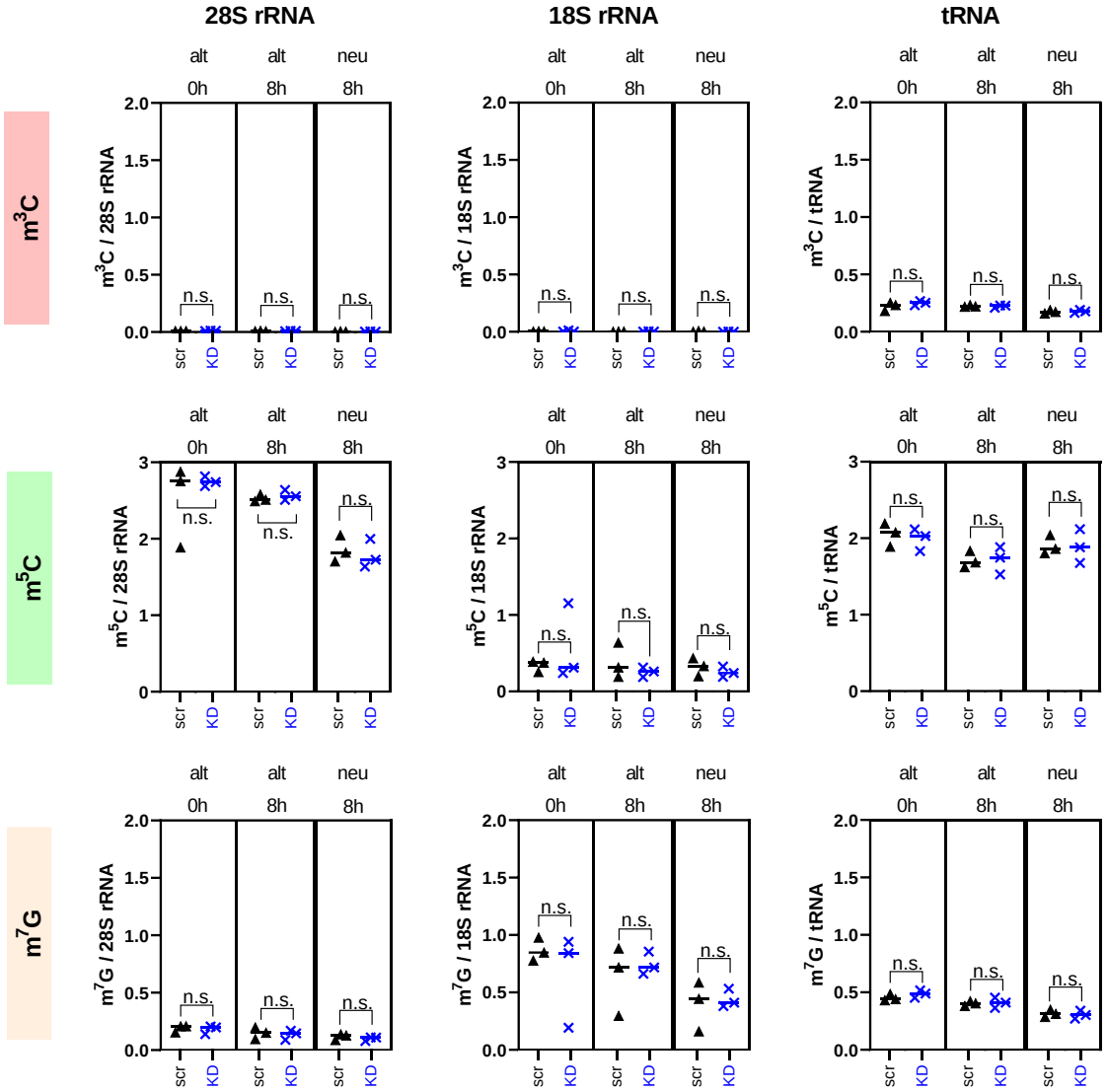

Abbildung 3.36: Quantifizierung der RNA-Modifikationen m^3C, m^5C und m^7G im Pulse-Chase-NAIL-MS-Experiment nach AlkBH5 Knockdown. Die Boxplots zeigen die absoluten Werte für m^3C (erste Reihe), m^5C (zweite Reihe) und m^7G (dritte Reihe) pro jeweiligem RNA-Molekül (linke Spalte: 28S rRNA; mittlere Spalte: 18S rRNA; rechte Spalte: tRNA). Jeder Boxplot unterteilt sich in drei Spalten, wobei links die alten, unmarkierten Nukleoside vor dem Mediumwechsel (t = 0h, 64 Std. nach Aussaat), in der Mitte die alten, unmarkierten Nukleoside nach Inkubation mit stabilem isotopenmarkierten Medium (t = 8h, 72 Std. nach Aussaat) und rechts die neuen, markierten Nukleoside nach 8 Stunden Inkubation abgebildet werden. Zu jedem Zeitpunkt wurde RNA sowohl aus AlkBH5-Knockdownproben (KD, blau) als auch aus den Transfektionskontrollen (scr: engl. für scramble control, schwarz) isoliert. Alle Werte stammen von n=3 biologischen Replikaten. Die Zweiweg-Varianzanalyse bestimmt die Signifikanz, welche über den Datenpunkten eingetragen ist (n.s. = nicht signifikant).

Diese post-transkriptionalen Prozesse können durch ihre spezielle Isotopenmarkierung, die sie an RNA-Modifikationen hinterlassen genauer betrachtet werden (siehe Abbildung **3.37**). Unmarkierte kanonische Nukleoside wurden nach

Wechsel in NAIL-MS-Medium durch Methyltransferasen mit CD_3-Methylgruppen des CD_3-Methionins versehen. Sie unterscheiden sich von co-transkriptional prozessierten RNA-Modifikationen, die aus stabilen isotopenmarkierten Basen- und/oder Zuckerpuckern und CD_3-Methylgruppen aufgebaut wurden.

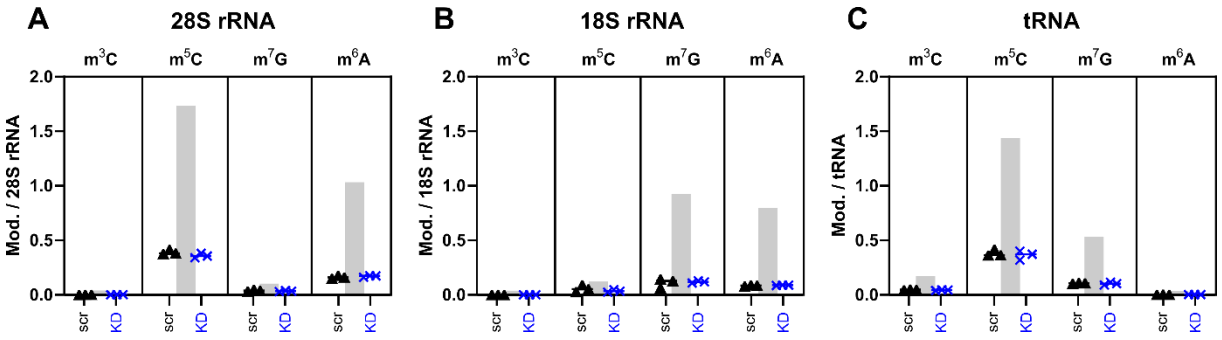

Abbildung 3.37: Quantifizierung der Postmethylierung von RNA-Modifikationen im Pulse-Chase-NAIL-MS-Experiment nach AlkBH5 Knockdown. Der Graph **A** zeigt das Vorkommen der postmethylierten Nukleoside nach 8 Stunden Inkubation in isotopenmarkiertem NAIL-MS-Medium in 28S rRNA. Es wurde RNA sowohl aus AlkBH5-Knockdownproben (KD, blau) als auch aus den Transfektionskontrollen (scr: engl. für scramble control, schwarz) isoliert. Alle Werte stammen von n=3 biologischen Replikaten. Die endogenen Level in der 28S rRNA sind als graue Balken dargestellt (alte, unmarkierte Nukleoside vor Mediumwechsel). **B** und **C** zeigen die Postmethylierung nach 8 Stunden in 18S rRNA und tRNA.

Ungefähr 15 % der zum 8 Stunden-Zeitpunkt vorkommenden m^5Cs in 28S rRNA und tRNA, sowie m^6As in 28S rRNA sind postmethyliert.

Der AlkBH5-*in vivo*-KD in diesem Kapitel besitzt keinen Einfluss auf die Modifikationsdichte von m^6A, m^3C, m^5C und m^7G. Die substanzielle Postmethylierung von m^5C ist durch post-transkriptional arbeitende Enzyme begründbar, doch die Postmethylierung von z.B. m^6A bedarf weiterer Experimente, da die Generierung von m^6A co-transkriptional geschieht und deswegen nur isotopenmarkiertes m^6A und unmarkiertes m^6A, aber kein postmethyliertes m^6A in den Proben vorkommen sollte.

3.4.6 Einfluss von Actinomycin D auf RNA-Modifikationen *in vivo*

Nachdem die Post-Methylierung von Cytidin zu m^5C durch post-transkriptional agierende Methyltransferasen erklärt werden kann, wird z.B. m^6A co-transkriptional im Nucleus generiert. Die AlkBH5-NAIL-MS-Daten weisen auf einen Anteil an postmethyliertem m^6A hin, welches mit der Biologie des m^6A nicht vereinbar wäre.

Um die Postmethylierung innerhalb des NAIL-MS-Experiments genauer zu charakterisieren und transkriptionelle Effekte auszuschließen, soll mit Actinomycin D

(AcmD) ein RNA-Polymerasen-Inhibitor getestet werden. Der Grad der Inhibierung wurde in diesem Kapitel an der Entstehung neuer RNA-Transkripte bzw. Nukleoside gemessen. Um eine mögliche Inhibierung von Acm D auf Writer-Enzyme oder allgemein Proteinebene zu erforschen, wurden durch *M. Sc. Gregor Ammann* weitere hier nicht beschriebene SILAC-Experimente und Proteom-Massenspektrometrie durchgeführt.

Zunächst wurde die Konzentration an AcmD bestimmt, mit der die Inhibition der Transkription von RNAs gelingt. Hierbei musste auch sichergestellt werden, dass die Inhibierung innerhalb der 8 Stunden des NAIL-MS-Pulse-Chase-Experiments andauert. Wie in Abbildung **3.38** zu sehen, wurden HEK 293-Zellen zum Zeitpunkt des Mediumwechsels in stabiles isotopenmarkiertes Medium mit Acm D versetzt. Nach 2 und 8 Stunden wurden die Zellen geerntet, die RNA isoliert und nach Spezies separiert, verdaut und per LC-MS/MS analysiert.

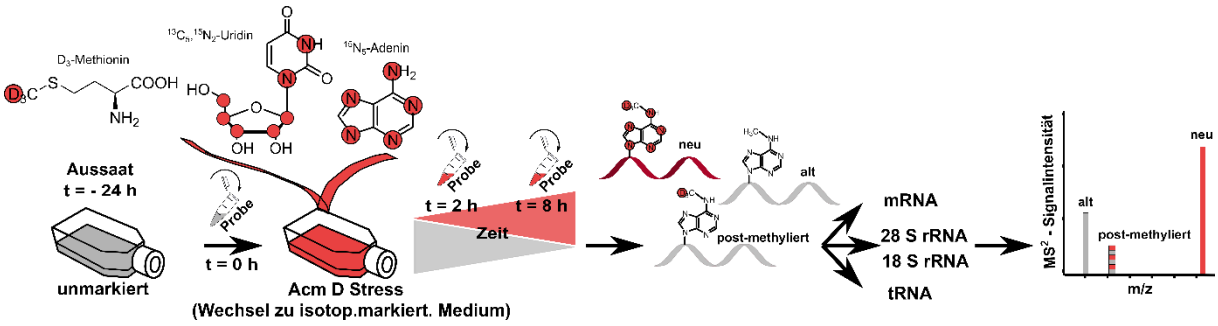

Abbildung 3.38: Schematischer Aufbau des Actinomycin D Pulse-Chase-NAIL-MS-Experiments. HEK 293 Zellen werden in unmarkiertem NAIL-MS-Medium (grau) kultiviert, bei dem Wechsel in stabiles isotopenmarkiertes Medium (rot) mit Actinomycin D (Acm D) versetzt und bis zu 8 Stunden wachsen gelassen. Die RNA-Spezies werden per Größenausschlusschromatografie oder Oligohybridisierung (mRNA) separiert. Mittels Massenspektrometrie kann die Herkunft der einzelnen Nukleoside nachvollzogen werden.

Die Inhibierung der RNA-Polymerasen und die damit verringerte Einbau von neuen Nukleosiden in RNA kann aus den LC-MS/MS-Daten für Adenosin wie folgt berechnet werden:

$$neue\ Transkripte\ [\%] = \frac{isotop.mark.A\ [pmol]}{isotop.mark.A\ [pmol] + unmarkiert\ A\ [pmol]} * 100$$

Während unter Normalbedingungen nach 2 Stunden 4 % und nach 8 Stunden 20 – 30 % aller rRNAs und tRNAs aus neuen Nukleosiden synthetisiert wurden, sinkt die Transkriptionsrate bei Einsatz von 1 µg/mL Acm D auf 0,5 % für tRNA nach 2 Stunden

und nach 8 Stunden auf 1,1 %. rRNA wird stärker inhibiert und nur 0,1 % neue rRNAs entstehen nach 2 und 8 Stunden. Mit steigender Konzentration inhibiert Acm D die Neusynthese von RNAs (siehe Abbildung **3.39**). Bei Dosen größer als 1 µg/mL Acm D verformen sich die HEK-Zellen zunächst rundlich und sterben mit der Zeit ab, was durch die Ablösung der Zellen vom Boden der Zellkulturflasche beobachtet wurde.

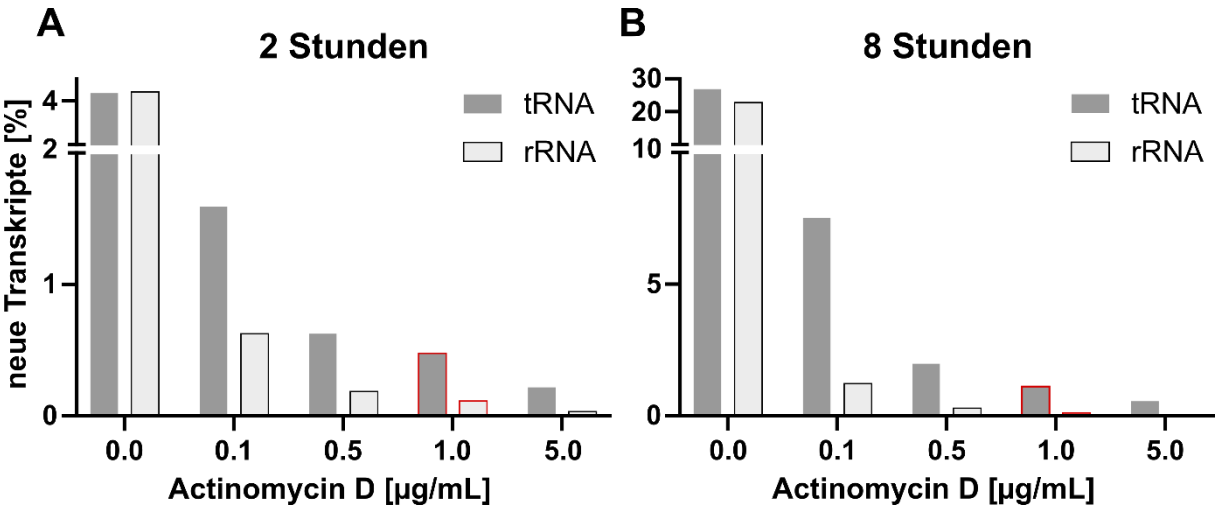

Abbildung 3.39: Entstehung neuer RNA-Transkripte mit Actinomycin D im Pulse-Chase-NAIL-MS-Experiment. Der Graph **A** zeigt das Vorkommen neuer Nukleoside nach 2 Stunden Inkubation mit varierenden Konzentrationen an Acm D in isotopenmarkiertem NAIL-MS-Medium in totaler rRNA und tRNA. Graph **B** zeigt dieses Vorkommen nach 8 Stunden Inkubation mit Acm D. Rot umrandet ist die Konzentration, mit der in den weiteren Versuchen gearbeitet wurde.

Nachdem die Konzentration an Acm D festgelegt auf 1 µg/mL war, wurden mit einem biologischen Triplikat die Auswirkungen auf alle bisher analysierten RNA-Spezies erforscht (Abbildung **3.40**). Zunächst fällt auf, dass alle beobachteten RNA-Spezies unter Acm D nur stark verringert synthetisiert werden. Die Daten, die die Negativkontrollen repräsentieren, sind in Übereinstimmung mit den biologischen Halbwertszeiten. Da mRNA eine Halbwertszeit von 7 Stunden hat[215], wurden in 8 Stunden 60 % aller mRNA neu transkribiert, um eine konstante Anzahl an mRNAs innerhalb der Zelle zu gewährleisten. Es wurden 25 % tRNAs und 15 % rRNA in 8 Stunden neu synthetisiert.

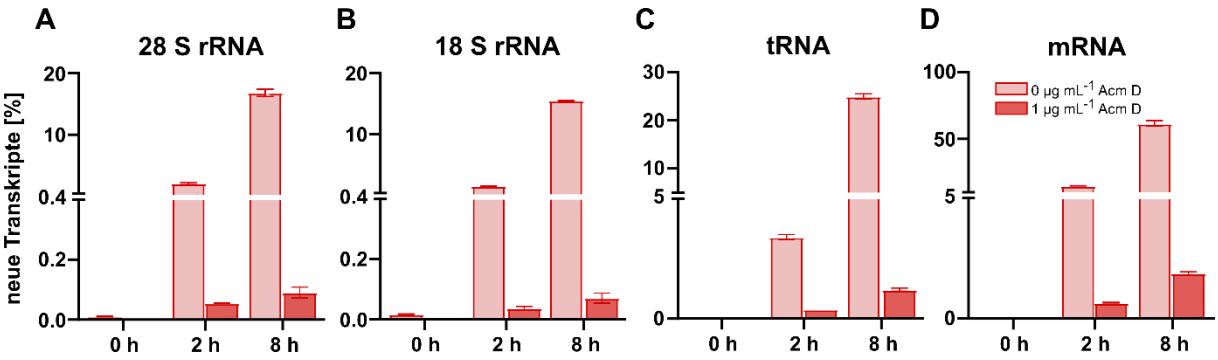

Abbildung 3.40: Transkription verschiedener RNA-Spezies unter Acm D-Stress. Graph **A** bildet das Vorkommen stabiler isotopenmarkierter Nukleoside nach 2 und 8 Stunden Inkubation in NAIL-MS-Medium in 28S rRNA ab. Die blassrosa Balken gehören zu den Acm D-Negativkontrollen, während die roten Balken die 1 µg mL^{-1} Acm D repräsentieren. Alle Werte stammen von n=3 biologischen Replikaten. **B** - **D** zeigen die Anzahl neuer Transkripte in 18S rRNA, tRNA und mRNA.

Um die Inhibition durch Acm D für jede RNA-Spezies zu verdeutlichen, wurde die verbliebene Biosyntheserate nach folgender Rechnung bestimmt:

$$verbliebene\ Biosynthese\ [\%] = \frac{neue\ Transkripte\ in\ AcmD\ Proben\ [\%]}{neue\ Transkripte\ in\ Negativkontrollen\ [\%]} * 100$$

In Abbildung **3.41 A** ist zu sehen, dass die HEK 293-Zelle unter 1 µg/mL Acm D noch 4,8 % tRNAs im Vergleich zu Normalbedingungen herstellt. 3 % mRNAs werden synthetisiert und die Transkription von rRNAs wird nahezu komplett inhibiert, sodass 0,5 % der rRNAs entstehen. Diese RNA-Spezies abhängige Inhibierung durch Acm D wurde durch Perry *et al.* beschrieben[61] und ist schematisch in Abbildung **3.41 B** dargestellt. Zur Hemmung der für die Synthese der 45S rRNA zuständigen RNA-Polymerase I wird eine geringere Konzentrationen an Acm D benötigt als für die mRNA zuständige RNA-Polymerase II und für die tRNA zuständige RNA-Polymerase III.

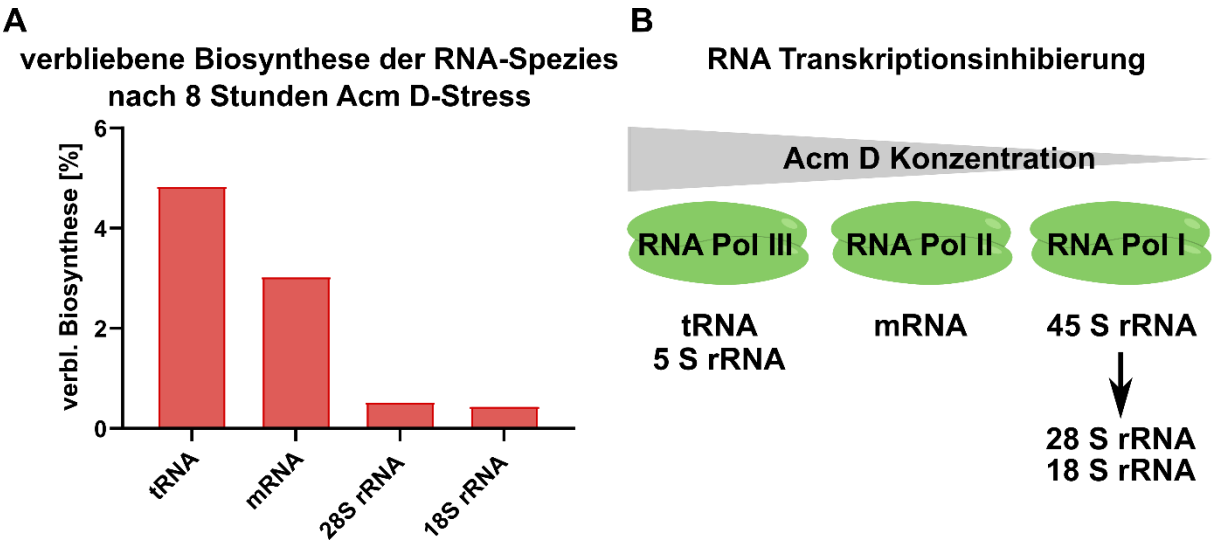

Abbildung 3.41: Inhibierung der Transkription durch Acm D. Die verbliebene Biosynthese der RNA-Spezies ist in Graph **A** abgebildet. Schema **B** stellt die Konzentrationsabhängigkeit des Acm D und die Wirkung auf die RNA-Transkription dar.

Nachdem eine Inhibierung der RNA-Synthese mit Actinomycin D stattgefunden hat, wurde im Folgenden genauer auf die RNA-Modifikationen eingegangen. So zeigt Abbildung **3.42** alle in dem NAIL-MS-Experiment vorkommenden m^6A-Isotopologe in totaler RNA zu verschiedenen Zeitpunkten.

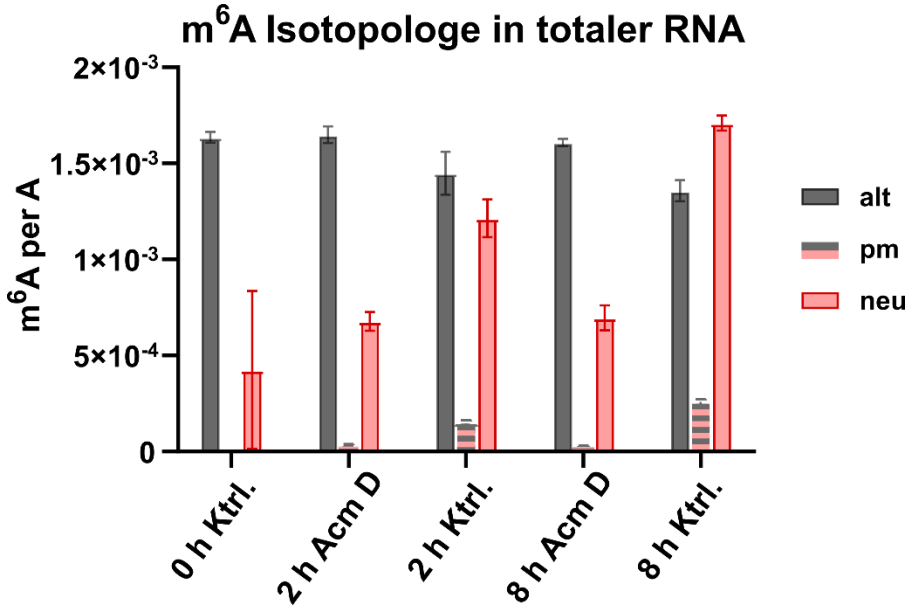

Abbildung 3.42: Vorkommen verschiedener m^6A-Isotopologe mit 1 µg mL^{-1} Acm D im Pulse-Chase-NAIL-MS-Experiment. Graue Balken symbolisieren alte, unmarkierte m^6A-Nukleoside, grau-rosa gestreifte Balken repräsentieren pm (postmethylierte) m^6As und rosa Balken neu, stabile, isotopenmarkierte m^6As. Alle Werte stammen aus von n=2 biologischen Replikaten. Die Balken sind Mittelwerte und die Fehlerbalken bilden die Standardabweichung ab.

Es fällt auf, dass mit 1 µg/mL Actinomycin D nicht nur weniger neue m^6As in RNA eingebaut, sondern auch weniger Adenosine nachträglich zu m^6As methyliert wurden. Diese Abhängigkeit der Transkription und Postmethylierung kann entweder damit begründet werden, dass neben der Inhibition von RNA-Polymerasen auch Writer-Enzyme von Acm D inhibiert wurden oder dass im Moment des Mediumwechsels ein vorliegendes Reservoir an alten Nukleosiden / RNAs mit neuen Nukleosiden vermischt oder umgebaut wurde und sich eine Hybrid-RNA aus unterschiedlichen Isotopologen bildet.

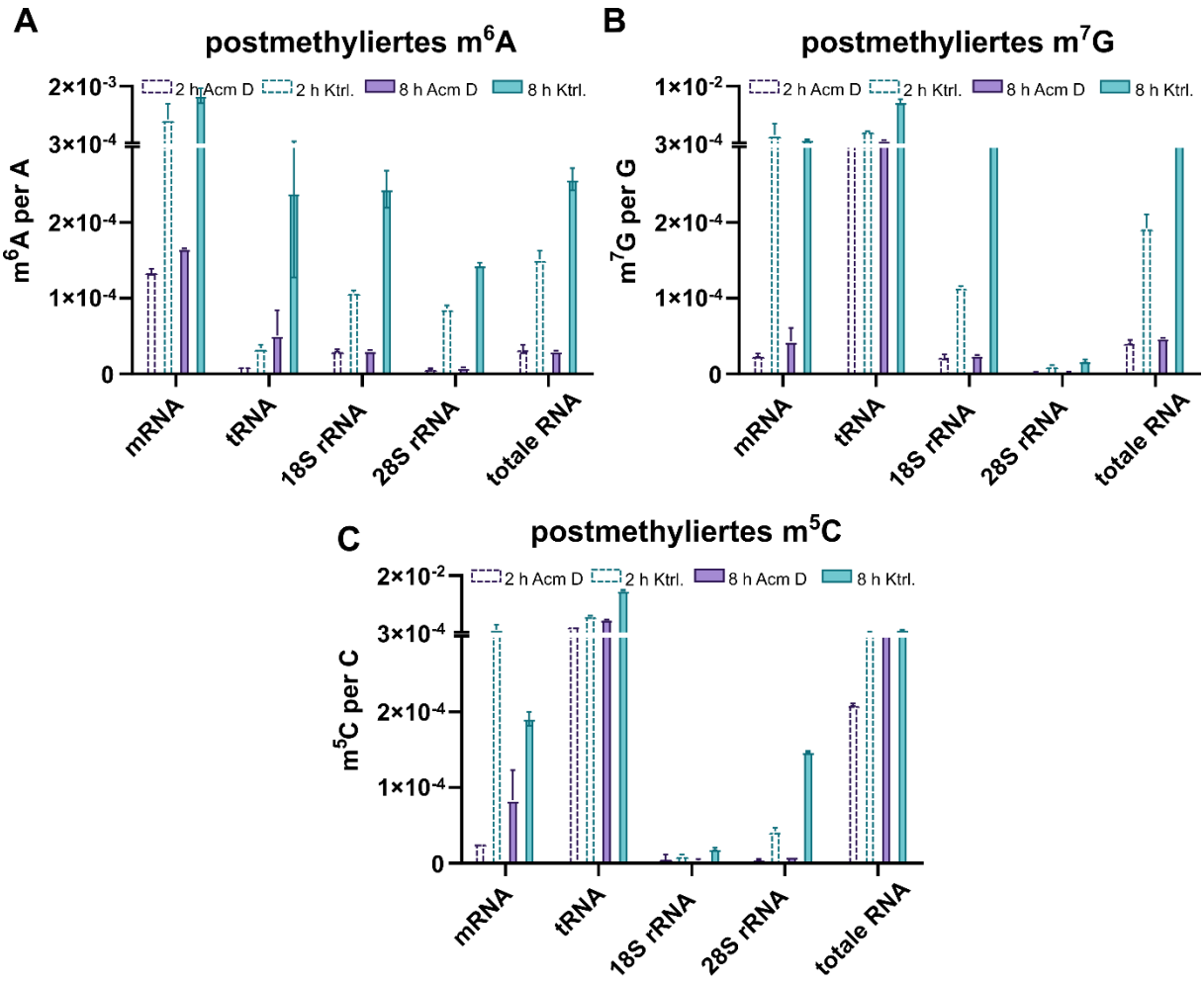

Abbildung 3.43: Quantifizierung der Postmethylierung von RNA-Modifikationen im Pulse-Chase-NAIL-MS-Experiment nach Actinomycin D-Stress. A zeigt das Vorkommen der postmethylierten m^6A-Nukleoside nach 2 oder 8 Stunden Inkubation mit oder ohne 1 µg mL^{-1} Acm D in isotopenmarkiertem NAIL-MS-Medium. Alle Werte stammen von n=2 biologischen Replikaten. **B** und **C** zeigen die Postmethylierung von m^7G und m^5C. Die Postmethylierung wurde in Modifikation pro zugehörigen kanonischen Nukleosid angegeben.

Der Abbildung **3.43** ist zu entnehmen, dass neben der Postmethylierung von m^6A auch die von m^7G und m^5C in verschiedenen RNA-Spezies mit Acm D reduziert ist. Dieser

globale Effekt von Acm D auf mehrere RNA-Modifikationen in diversen RNA-Spezies legt die Vermutung nahe, dass die beobachtete „post-transkriptionelle“ Methylierung vermutlich eine Momentaufnahme von neu-transkribierten Hybrid-Spezies darstellen.

SILAC-Experimente und Proteom-MS sind nötig, um zu erforschen, ob Acm D zusätzlich zu seiner Wirkung auf RNA-Transkription eine Inhibierung von Proteinen, wie z.B. Writer-Enzymen, verursacht.

Die Postmethylierung von RNA-Modifikationen tritt in NAIL-MS-Pulse-Chase-Experimenten nach dem Wechsel in stabiles, isotopenmarkiertes Medium auf. Die hier gezeigten Daten weisen darauf hin, dass die Postmethylierung in Wahrheit eine temporale Limitierung der NAIL-MS-Methode aufzeigt, da sie in den Chase-Phasen bis zu 8 Stunden substantiell vorkommt. Wie in Abbildung **3.21** gezeigt, erreichen die postmethylierten Isotopologe ihr Maximum nach 3 Tagen Inkubation und sind nach 8 Tagen nicht mehr zu detektieren, da zu diesem Zeitpunkt bereits durch Verdünnung und Degradation alter RNA-Transkripte oder aus alten Nukleosiden zusammengesetzten Hybrid-RNAs stattgefunden hat.

4. Ausblick

Es konnte die Etablierung der Technik NAIL-MS durch den Einsatz von isotopenmarkiertem Adenin, Uridin, optional Methionin und dialysiertem FBS als Zusatz im Nährmedium in humaner Zellkultur erfolgreich abgeschlossen werden. Trotz leichter synthetischer Verunreinigungen des Uridins konnte die Isotopenmarkierungsstrategie dazu beitragen, die Synthese, den Abbau, die Inkorporation und Reparatur von RNA-Spezies und RNA-Modifikationen zeitlich zu verfolgen. So war es möglich, auf RNA-Modifikationsebene zwischen co- und post-transkriptionalen Prozessen zu differenzieren.

Konkret konnten verschiedene literaturbekannte RNA-Demethylierungsziele von AlkBH-Enzymen *in vitro* bestätigt und die RNA-Modifikationslevel in isolierten, nativen RNA-Spezies (z.B. 28S rRNA, 18S rRNA, tRNA) absolut quantifiziert werden. *In vivo* konnte in keiner analysierten RNA-Spezies eine aktive Demethylierung von RNA-Modifikationen durch AlkBH-Enzyme beobachtet werden. Dieses Ergebnis steht im Widerspruch zu den bisherigen bekannten RNA-Demodifizierungsstudien mit AlkBH-Enzymen, die jedoch zur Detektion auf statischen MS-Methoden basieren. Um den in dieser Arbeit vorgestellten NAIL-MS-Ansatz, der bei der Zuordnung der Herkunft von RNA-Modifikationen den anderen Ansätzen bereits überlegen ist, auch vor dem Hintergrund vielfältiger biologischer Prozesse zu erweitern, ist ein Hinzuziehen weiterer orthogonaler Enzym-Knockdown oder Knockout-Strategien, sowie eine Unterteilung in mitochondriale und cytosolische RNA-Substrate sinnvoll.

Bei der Anwendung von NAIL-MS im Kontext der AlkBH-Enzyme wurde eine temporale Limitierung der Methode gefunden. So konnten post-methylierte RNA-Modifikationen, wie das teilweise isotopenmarkierte m^6A, in definierten Zeiten nach dem Mediumwechsel detektiert werden. Diese Beobachtung ist nicht mit der Biologie der Modifikation, die co-transkriptional inkorporiert wird, vereinbar. Zur Trennung von Transkriptionsprozessen und Methylierungen durch RNA-modifizierende Enzyme wurde Transkriptionsinhibitor Acm D eingesetzt. Die Post-Methylierung mehrerer RNA-Modifikation unter AcmD verringerte sich. Diese Erkenntnis warf zwei weitere Fragen auf: Zum einen muss eine zeitgleiche Analyse der Proteoms stattfinden, um zu klären, ob auch Writer-Enzyme von der Inhibierung betroffen sind. Eine Kombination von SILAC und NAIL-MS-Experiment ist in Zukunft fähig, diese Frage zu beantworten und wird bereits erprobt. Zum anderen könnten Hybrid-RNAs aus alten und neuen

Nukleosiden nach dem Mediumwechsel temporär entstehen. Oligonukleotid-MS kann hierbei das mögliche Recycling von einzelnen Nukleotidbausteinen in einem Strang beweisen.

Die Entwicklung einer kompatiblen Oligonukleotid-LC-MS-Methode war Teil dieser Arbeit und mit Hilfe einer ionenpaarreagenzfreien Chromatographie ist es gelungen, die Deaminaseaktivität von ADAT2/3, welches Inosin an Position 34 von einigen tRNA-Isoakzeptoren generiert, *in vitro* sequenziell und quantitativ zu bestimmen. Mit dem Hinzuziehen eines hochaufgelösten Massenspektrometers konnten zudem mehrere native tRNA-Modifikationen in ihrem Sequenzkontext bestätigt werden. Um die Anwendungsgebiete von dieser breit-einsetzbaren Oligonukleotid-LC-MS-Methode zu erweitern, ist es ratsam, in Zukunft neben dem Verdau durch die RNase T1 weitere spezifische Endonukleasen einzusetzen (siehe Abbildung **1.12**). Diese steigern die Sequenzabdeckung und die erleichtern so die umfassende Detektion weiterer RNA-Modifikationen. So wären beispielweise die Detektionen unterschiedlicher Modifikationen aus humanem Zelllysat möglich. Es würde zudem eine Methode entwickelt werden können, die sich bestens zur Qualitätskontrolle von RNA-basierten Medikamenten und Impfstoffen eignet. Dieses ist gerade im Kontext der neu-entwickelten Coronaimpfstoffe von großer Aktualität und wissenschaftlicher Relevanz.

5. Material und Methoden

Die im Folgenden beschriebenen Materialien und Vorgehensweisen beziehen sich auf die unveröffentlichten Ergebnisse. Protokolle zu Materialien und Methoden der veröffentlichten Ergebnisse finden sich direkt in den Publikationen unter der Sektion „Materials and Methods“. Lediglich interne Hinweise oder detailliertere Beschreibungen zur Durchführung der bereits in den Publikationen beschriebenen Verfahren werden in diesem Abschnitt ergänzt.

5.1 Materialien

Chemikalien und Nukleoside

Alle Salze und Chemikalien wurden, sofern nicht anders angegeben, von Sigma-Aldrich (München, Deutschland) in molekular-biologischer Qualität erworben. Zellkulturmedien sowie PBS und Trypsin wurden ebenfalls von Sigma-Aldrich erhalten. Nicht-dialysiertes und dialysiertes FBS wurden von BioWest SAS (Nuaillé, Frankreich) bezogen. Die isotopenmarkierten Verbindungen $^{13}C_5$,$^{15}N_2$-Uridin (Ribose-$^{13}C_5$, 98%; $^{15}N_2$, 96–98%) und $^{15}N_5$-Adenin ($^{15}N_5$, 98%) wurden von Cambridge Isotope Laboratories (Tewksbury, MA, USA) erworben. (D_3)-L-Methionin (98 Atom-% D) wurde von Sigma-Aldrich bezogen. Lösungsmittel in LC-MS Qualität (Acetonitril, Isopropanol, Methanol) wurden von der Firma Roth (Karlsruhe, Deutschland) erworben. Lösungsmittel in HPLC Qualität wurden von VWR (Darmstadt, Deutschland) bezogen. Alle Lösungen und Puffer wurden mit Wasser aus einer Sartorious arium® Pro Reinstwasseranlage (Göttingen, Deutschland) hergestellt. Die Nukleoside Adenosin, Cytidin, Guanosin und Uridin wurden von Sigma-Aldrich erworben. Dihydrouridin (D) wurde von Apollo Scientific (Stockport, UK) erworben. N6-Threonylcarbamoyladenosin (t^6A) wurde von TRC (North York, Kanada) erworben. 2-Methylguanosin (m^2G) wurde von ChemScene LLC (Monmouth Junction, NJ, USA) erworben. N3-Methyluridin (m^3U), N6-Isopentenyladenosin (i^6A) und 2-Methyladenosin (m^2A) waren großzügige Geschenke des Dedon-Labors. 5-carbamoylmethyl-2-thiouridine (ncm^5s^2U) war ein großzügiges Geschenk des Helm-Labors. 1-Methylinosin (m^1I) war ein großzügiges Geschenk von STORM Therapeutics LTD (Cambridge, UK). Alle weiteren RNA-Nukleoside wurden von Carbosynth (Newbury, UK) erworben. Für alle hier nicht ausgewiesenen Materialien wird die Herkunft im jeweiligen Kapitel angegeben.

Geräte

Tabelle 5.1: Geräteliste

Gerät	detailierte Bezeichnung
CO_2-Inkubator	Thermo Scientific Heracell™ VIOS 160i CO_2-Inkubator mit Edelstahlkammer
Sicherheitswerkbank	Thermo Scientific Safe 2020
automatischer Zellzähler	Invitrogen Countess® II automated cell counter
Mikroskop	Zeiss Axiovert 200
Wasserbad	Memmert WNB22
Ultratiefkühlbox	FRYKA Tiefkühlbox B 35-85 F210101
HPLC	Agilent 1100 HPLC System
LC-MS/MS	Agilent 1260 Infinity II LC System Agilent 6470A Triple Quadrupole mit Jet Stream ESI-Quelle
HRMS	Thermo Scientific Dionex Ultimate 3000 LC System Thermo Scientific LTQ Orbitrap XL mit HESI-Quelle
SpeedVac	Genevac EZ-2 Plus Evaporating System
Nanophotometer	Implen NanoPhotometer® N60
Bioanalyzer	Agilent 2100 Bioanalyzer
Thermocycler	SensoQuest Labcycler
Thermoschüttler	CellMedia TS basic
Zentrifugen	Eppendorf 5417R / Hettich Rotina 380 R

Zelllinien und Enzyme

Tabelle 5.2: Liste der verwendeten Zelllinien und Enzyme

Enzyme / Zelltypen	Details
ADAT 2/3	Großzügiges Geschenk des Fu-Labors
Bakterielles AlkB	Peak Proteins, Cheshire, UK (Großzügiges Geschenk von STORM Therapeutics LTD)
AlkBH1	Großzügiges Geschenk von *M. Sc. Olga Hofmeister* und des Schneider-Labors
AlkBH3	abcam ab105620 (Cambridge, UK)
AlkBH7-Wildtyp	Großzügiges Geschenk des Schneider-Labors
AlkBH7-R191Q Mutante	Großzügiges Geschenk des Schneider-Labors
HEK 293 Zellen	DSMZ, Braunschweig, Deutschland
HeLa ACC 57 Zellen	DSMZ, Braunschweig, Deutschland

Stocklösungen und Medien für Zellkultur

- „Grund-Medium“: 44 mL DMEM D6546, 5 mL FBS (nicht dialysiert ODER dialysiert), 1 mL L-Glutamin (50×)
- „unmarkiertes NAIL-MS-Medium“: 42,4 mL DMEM D0422, 5 mL dialysiertes FBS, 1 mL L-Glutamin (50×), 1 mL Adenin (50×), 500 µL Uridin (100×), 100 µL L-Methionin (500×), 40 µL Cystin (1250×)
- „stabiles isotopenmarkiertes NAIL-MS-Medium“: 42,4 mL DMEM D0422, 5 mL dialysiertes FBS, 1 mL L-Glutamin (50×), 1 mL $^{15}N_5$-Adenin (50×), 500 µL $^{13}C_5$,$^{15}N_2$-Uridin (100×), 100 µL (D_3)-L-Methionin (500×), 40 µL Cystin (1250×)
- „Trypsin-Stopp-Medium“ *: 45 mL DMEM D6546 ODER DMEM D4022, 5 mL FBS (nicht dialysiert ODER dialysiert)
- „Auftau-Medium“: 39 mL DMEM D6545, 10 mL FBS (nicht dialysiert), 1 mL L-Glutamin (50×)
- „Kryokonservierungs-Medium“ (2×): 8 mL FBS (nicht dialysiert), 2 mL DMSO

* Trypsin-Stopp-Medium dient der Desaktivierung der Proteaseaktivität des Trypsins bei der Passagierung von Zellen und wurde aus dem zum jeweiligen Experiment passenden Medium und FBS hergestellt.

Tabelle 5.3: Herstellung der Stocklösungen für die Verwendung in der Zellkultur. Aliquots von Glutamin, Uridin und FBS wurden bei –20 °C gelagert. Alle weiteren Stocklösungen wurden bei 4 °C gelagert. Einwaagen sind für die jeweilige Konzentration der unmarkierten Komponenten angegeben. Bei Verwendung der isotopenmarkierten Komponenten wurde die Einwaage entsprechend angepasst. Alle Stocklösungen wurden nach der Herstellung steril filtriert und gegebenenfalls aliquotiert. Die nötige Verdünnung in Zellkulturmedium ist in Klammern angegeben.

Stocklösung		Rezept
200 mM	Glutamin (50×)	292 mg in 10 mL MilliQ-Wasser
325 mM	Cystin (1250×)	157 mg in ~ 1 M HCl (1 mL HCl konz. + 11 mL MilliQ-Wasser
100 mM	Methionin (500×)	153 mg in 10 mL MilliQ-Wasser
5 mM	Adenin (50×)	6,8 mg in 10 mL MilliQ-Wasser
20 mM	Uridin (100×)	24,4 mg in 5 mL MilliQ-Wasser

SEC-Puffer

In eine saubere 1 L Labor Gewindeflasche wurden 7,7 g NH_4OAc (molekularbiologische Qualität) gegeben und mit 1000 mL hochreinem Wasser aufgefüllt, sodass eine 100 mM Lösung vorlag.

20× SSC Puffer

Zu einer 2 mL einer 1,5 M Trinatriumcitrat-Lösung (pH 7,0) wurden 1,75 g NaCl zugegeben. Es wurde mit reinem Wasser auf ein Gesamtvolumen von 10 mL aufgefüllt. Endkonzentrationen: Trinatriumcitrat-Lösung (300 mM), NaCl (3 M). Andere Konzentrationen des SSC Puffers wurden durch entsprechende Verdünnung des 20× SSC Puffer mit MilliQ-Wasser hergestellt.

1× B&W Puffer

584 mg NaCl wurden mit 38,5 µL einer 1M EDTA Lösung und 50 µL einer 1 M Tris-HCl Lösung (pH 7,5) vereint. Dieses Gemisch wurde mit hochreinem Wasser auf ein Gesamtvolumen von 10 mL gebracht. Endkonzentrationen: NaCl (1 M), EDTA (0,5 mM), Tris-HCl (5 mM).

3× tRNA Denaturierungspuffer

300 µL einer 1M Tris-HCl Lösung (pH 7,5) wurden mit 40 µL einer 0,25 M EDTA Lösung vereint. Dieses Gemisch wurde mit hochreinem Wasser auf ein Gesamtvolumen von 10 mL gebracht. Endkonzentrationen: Tris-HCl (30 mM), EDTA (1 mM).

7× tRNA Faltungspuffer

3,33 mL einer 1M HEPES Lösung (pH 7,5) wurden mit 200 µL einer 1M $MgCl_2$ Lösung und 666 µL einer 5 M NaCl Lösung vereint. Dieses Gemisch wurde mit hochreinem Wasser auf ein Gesamtvolumen von 10 mL gebracht. Endkonzentrationen: HEPES (333 mM), NaCl (333 mM), $MgCl_2$ (20 mM).

AlkB und AlkBH-Lagerungspuffer

Um die Aktivität des AlkB und AlkBH-Enyzme zu erhalten, wurden für die jeweiligen Homologe optimierte Puffer hergestellt, in welchen die Enzyme gelagert, verdünnt und für Experimente eingesetzt wurden:

- AlkB Lagerungspuffer (50 mL): Endkonzentrationen: 20 mM Tris-HCl (pH 8,0), 5 % Glycerin (v/v), 2 mM DTT, 200 mM NaCl.
- AlkBH1 Lagerungspuffer (50 mL): Endkonzentrationen: 20 mM Tris-HCl (pH 7,5), 10 % Glycerin (v/v), 250 mM NaCl.
- AlkBH3 Lagerungspuffer (50 mL): Endkonzentrationen: 20 mM Tris-HCl (pH 8,0), 10 % Glycerin (v/v), 2 mM DTT, 100 mM NaCl.
- AlkBH7 Lagerungspuffer (50 mL): Endkonzentrationen: 25 mM Tris-HCl (pH 8,0), 10 % Glycerin (v/v), 2 mM DTT, 150 mM NaCl.

LC-MS/QQQ (Nukleosid-MS) Puffer

In eine saubere 1 L Labor Gewindeflasche wurden 0,385 g NH_4OAc (LC-MS Qualität, ≥ 99%, VWR), gegeben und mit 1000 mL hochreinem Wasser aufgefüllt (Endkonzentration 5 mM). Zur Einstellung des korrekten pH-Werts (5,3) wurden 65 µL Essigsäure (HiPerSolv CHROMANORM for LC/MS, Essigsäure 99%, VWR Chemicals) zugegeben.

LC-MS/HRMS (Oligo-MS) Puffer

In eine saubere 1 L Labor Gewindeflasche wurden 0,771 g NH_4OAc (LC-MS Qualität, ≥ 99%, VWR), gegeben und mit 1000 mL hochreinem Wasser aufgefüllt (Endkonzentration 10 mM, pH 7).

5.2 Zellkulturmethoden

Zellen wurden in wasserdampfgesättigter Atmosphäre unter 10% CO_2 bei 37 °C kultiviert. Medien und Lösungen wurden vor Benutzung in einem Wasserbad auf 37 °C erwärmt. Für Passagierungen von Zellen wurde die Konfluenz über mikroskopische Betrachtung bestimmt.

Kryokonservierung und Revitalisierung von Zelllinien

Für die Kryokonservierung von HEK 293 Zellen wurde diese in 2× T75 Zellkulturflaschen kultiviert und anschließend trypsiniert (3 mL Trypsin pro Flasche). Jeweils 12 mL Standard-Medium wurde zugegeben, die Zellen resuspendiert und die Konzentration bestimmt. Zellen wurden zentrifugiert (130× g, 3 min) und in der entsprechenden Menge Standard-Medium resuspendiert um eine Konzentration von $4×10^6$ Zellen/mL zu erhalten. Die gleiche Menge 2× Kryokonservierungsmedium wurde vorsichtig zugegeben um eine finale Konzentration von $2×10^6$ Zellen/mL zu erhalten. Je 1 mL der Zellsuspension wurde in Kryoröhrchen überführt und über Nacht bei –70 °C in einem mit Isopropanol gefüllten Gefrierbehälter (Thermo Scientific™ Mr. Frosty™) gelagert. Die Zellen wurden am nächsten Tag in einen Flüssigstickstoff-Tank überführt.

Für die Revitalisierung von Zellen wurde 1 mL gefrorene Zellsuspension durch Schwenken des Probengefäßes im Wasserbad bei 37 °C schnellstmöglich aufgetaut. Diese wurde vorsichtig in 5 mL vorgewärmtes Auftau-Medium überführt und anschließend zentrifugiert (130× g, 3 min). Das Zellpellet wurde in Auftau-Medium resuspendiert und in einer T25 Zellkulturflasche kultiviert. Für eine weitere, folgende Passagierung wurde ebenfalls Auftau-Medium verwendet.

Passagierung von Zellen

Die an der T25-Zellkulturflasche adhärenten Zellen wurden vorsichtig mit 5 mL PBS gespült, um einerseits abgestorbene Zellen loszuwerden und andererseits

inhibierende Einflüsse von Serumbestandteilen auf die Trypsin-Aktivität zu verhindern. Anschließend wurden die Zellen für 2 min in 1 mL Trypsin bei 37 °C inkubiert. Mit 4,5–7 mL Trypsin-Stopp-Medium (je nach gewünschter Passagierung) wurde die Zellsuspension homogenisiert und anschließend 1 mL davon zentrifugiert (130× g, 3 min). Das Zellpellet wurde in 5 mL frischem Medium resuspendiert und in einer neuen T25 Zellkulturflasche kultiviert. Es wurde stets eine Subkultivierung bei einer Konfluenz von ~ 80% angestrebt. Passagierungen wurden in der Regel dreimal wöchentlich durchgeführt.

Zellexperimente

Für die Aussaat von Zellen für Isotopenmarkierungs- oder Protein-Knockdown-Experimenten oder Stressexperimenten (NAIL-MS AlkBH *in vivo*-Knockdown, Actinomycininkubation) wurde die Zelldichte mithilfe des automatischen Zellzählers oder mittels einer Fuchs-Rosenthal-Zählkammer bestimmt. Nach einer Kultivierungsphase von mindestens 24 h wurde der jeweilige Mediumwechsel durchgeführt, die Transfektionsmixtur oder Actinomycin D (Art.-Nr.: A1410-2MG, Sigma-Aldrich, München, Deutschland) zugegeben. Auf einen PBS-Spülschritt wurde, falls nicht anders vermerkt, verzichtet. Falls aufgrund des experimentellen Designs ein erneuter Mediumwechsel nötig war, wurde dieser analog durchgeführt. Dabei wurde stets darauf geachtet, das ursprüngliche Medium restlos abzunehmen.

Knockdown von AlkBH Enzymen *in vivo*

Für den Knockdown von AlkBH1 (Art.-Nr.: EHU135521-50µg, Sigma Aldrich, München, Deutschland) oder AlkBH3 (Art.-Nr.: EHU06458-50µg, Sigma Aldrich, München, Deutschland) oder AlkBH5 (Art.-Nr.: EHU021751-50µg, Sigma Aldrich, München, Deutschland) und einer Kontrolle (Art.-Nr.: EHUFLUC-50µg, Sigma Aldrich, München, Deutschland) wurden die dazugehörigen „Mission esiRNAs“ erworben. Des Weiteren wurde Transfektionsreagenz (Art.-Nr.: 114-07, Polyplus Transfection, Illkirch, Frankreich) erworben. Zuerst wurden 0,7 Mio. HEK 293 Zellen pro T25 Zellkulturflasche, welche 5 mL „unmarkiertes NAIL-MS“ Medium enthielt, ausgesät. 24 Stunden später (30% Konfluenz) wurde 250 µL Transfektionsmix gemäß Tabelle **5.4** hergestellt. Es wurde die esiRNA mit jetPrime Puffer vermischt, für 10 sek. gevortext, bevor das jetPrime Reagenz hinzugegeben, 1 sek. gevortext und für 10 min. inkubiert wurde. Anschließend wurde der Mix zu den Zellen pipettiert, wobei darauf geachtet

wurde, dass dieser nur tröpfchenweise, gut verteilt und unter sanftem Schwenken in die Zellkulturflasche gegeben wurde.

Tabelle 5.4: Transfektionsmix für den Knockdown von AlkBH-Enzymen *in vivo*. Hierbei handelt es sich um ein Rezept für die Transfektion einer T25 Zellkulturflasche. Im folgenden NAIL-MS Experiment wurden zwei Flaschen mit derselben esiRNA transfiziert. Um Pipettierfehler zu vermeiden, wurde deshalb jeder Transfektionsmix mit dem 2,2-fachen Volumen angesetzt.

Komponente	Stammkonzentration	Volumen
jetPrime™ Puffer		227,5 µL
jetPrime™ Reagenz		10 µL
esiRNA	200 ng μL^{-1}	12,5 µL

Nach einer Transfektionsinkubationszeit von 24 Stunden wurde das alte Medium entfernt und ohne PBS Pufferwaschschritt neues, auf 37 °C vorgewärmtes „unmarkiertes NAIL-MS“ Medium zu den Zellen gegeben. 16 Stunden danach wurde dieses Medium entfernt, ein 5 mL PBS-Pufferwaschschritt durchgeführt und ein T25 pro Knockdown-Ansatz mit 1 mL TRI Reagent® geerntet und zur Isolation der Gesamt-RNA in ein Eppendorf Mikroreaktionsgefäß überführt. Die übriggebliebene Zellkulturflasche wurde nach dem Waschschritt mit 5 mL neuem „stabilen isotopenmarkierten NAIL-MS“ Medium inkubiert. Nach 8 Stunden wurden auch diese Zellkulturflaschen ohne weiteren Waschschritt mittels TRI Reagent® zur Isolation der Gesamt-RNA vorbereitet. Sollte neben der RNA-Analytik auch die Effizienz des Knockdowns auf Protein-Ebene per Western Blot bestätigt werden, mussten die Zellen nach Abnahme des Mediums nicht direkt mit TRI Reagent®, sondern mit 1 mL Trypsin versetzt werden. Nach einer Inkubationszeit von 2 min. wurde die Zellsuspension in 1 mL „Trypsin-Stopp“ Medium aufgenommen und bei 2000× g und Raumtemperatur für 2 min. in zwei Mikroreaktionsgefäßen zentrifugiert. Nach dem Absaugen des Mediums wurde ein Zellpellet bei –80 °C zur weiteren Western-Blot-Analyse (durch *M. Sc. Paria Asadi Atoi*) tiefgefroren und das andere in 1 mL TRI Reagent® aufgenommen.

Actinomycin D Stressexperiment

Für das Transkriptionsinhibitionsexperiment wurden zunächst in einer 6-Well-Platte pro Platte 0,8 Mio. HEK 293 Zellen in 2 mL „unmarkiertem NAIL-MS“ Medium ausgesät. 24 Stunden nach Aussaat (60 % Konfluenz) wurden zeitgleich mit dem Mediumwechsel zu „stabilem isotopenmarkierten NAIL-MS“ Medium verschiedene

Konzentrationen an Actinomycin D (Art.-Nr.: A1410-2MG, Sigma Aldrich, München, Deutschland) oder DMSO als Kontrolle in die Zellgefäße gegeben. Die Inkubation in dem „stabilen isotopenmarkierten NAIL-MS“ Medium dauerte zwischen 2–24 Stunden und wurde mit der Abnahme des Mediums, eines PBS-Waschschrittes und der Aufnahme der Zellen in 500 µL TRI Reagent® abgeschlossen.

5.3 Biochemische Methoden

Isolation der Gesamt-RNA

Für die Extraktion von RNA wurden die Zellen nach Absaugen des Mediums direkt in TRI Reagent® aufgenommen (1 mL pro 25 cm^2). Die Zellsuspension wurde 15 Sekunden gevortext und 5 min bei Raumtemperatur inkubiert. Pro 1 mL TRI Reagent® wurden 200 µL Chloroform hinzugegeben und 20 Sekunden gevortext, bis eine einheitlich trübe Mischung entstand. Nach 15 min wurde die Mischung zur vollständigen Phasentrennung 15 min bei 12.000× g und 4 °C zentrifugiert. Die obere, wässrige Phase wurde in ein neues Mikroreaktionsgefäß überführt und mit dem identischen Volumen an Isopropanol vermischt. Nach Fällung der RNA bei –20 °C über Nacht wurde die Lösung bei 12.000× g und 4 °C für mindestens 60 Minuten zentrifugiert. Der Überstand wurde abgenommen, das Pellet vorsichtig mit 70% Ethanol gewaschen und erneut zentrifugiert (12.000× g, 4 °C, 5–10 min). Nach sorgfältiger Abnahme des Ethanols wurde das RNA-Pellet in ~ 30 µL hochreinem Wasser resuspendiert.

RNA Aufreinigung per Größenausschlusschromatographie

Für die Aufreinigung von tRNA und Gesamt-rRNA wurde Größenausschlusschromatographie (SEC) verwendet. Als mobile Phase diente SEC-Puffer. Eine AdvanceBio SEC 300 Å 2,7 µm, 7,8 × 300 mm Säule ermöglichte die Trennung von tRNA von Gesamt-rRNA unter Verwendung einer isokratischen Elution bei 1 mL/min und einer Säulentemperatur von 40 °C. Nach Äquilibrieren der Säule für mindestens 30 Minuten wurde bis zu 100 µg der Gesamt-RNA injiziert. Die großen rRNA-Untereinheiten eluieren von 3,5–4,8 min und die tRNA von 6,9–7-9 min. Diese Zeiten wurden mit ansteigendem Alter der Säule geringfügig angepasst.

Für die Aufreinigung von 18S rRNA und 28S rRNA wurde eine AdvanceBio SEC 1000 Å 2,7 µm, 7,8 × 300 mm Säule verwendet. Sonstige Parameter sind die gleichen wie zuvor. 28S rRNA eluiert von 5,0–7,2 min und 18S rRNA von 7,5–8,5 min.

Für die kombinierte Aufreinigung von totaler RNA in sowohl tRNA als auch 28S und 18S rRNA wurde die AdvanceBio SEC 1000 Å Säule mittels eines Kapillarenverbindungsstücks nach der AdvanceBio SEC 300 Å Säule in den Säulenofen der Agilent HPLC 1100 Anlage eingebaut. Sonstige Parameter sind die gleichen wie zuvor, nur die Laufzeit der Methode wurde auf 31 Minuten verlängert. 28S rRNA eluiert von 11,1–12,1 min, 18S rRNA von 12,5–13,5 min und tRNA von 18,5–19,5 min. Mit Hilfe der „Tandem“-SEC wurde die Ausbeute an 28S und 18S rRNA gesteigert, da zusätzliche SpeedVac- und Resuspendierungsschritte wegfallen.

Für die Aufreinigung *in vitro* transkribierter tRNA wurde eine AdvanceBio SEC 130 Å 2,7 µm, 7,8 × 300 mm Säule verwendet. Die Trennung erfolgte bei einer Säulentemperatur von 60 °C unter Verwendung einer isokratischen Elution bei 0,5 mL/min in 22 min. Nicht gespaltenes Fusionstranskript eluiert von 9,5–9,7 min und die gewünschte tRNA je nach Nukleotidlänge von 10,5–11,0 min.

Die gewünschten Fraktionen wurden gesammelt und mit einer SpeedVac auf 30–50 µL aufkonzentriert. Das 2,5-fache Volumen an 100 % Ethanol und 1 µL GlycoBlue™ (Thermo Fisher, Waltham, MA, USA) wurden zugegeben. Nach Fällung der RNA bei –20 °C über Nacht wurde die Lösung bei 12.000× g und 4 °C für mindestens 60 Minuten zentrifugiert. Der Überstand wurde abgenommen, das Pellet vorsichtig mit 70% Ethanol gewaschen und erneut zentrifugiert (12.000× g, 4 °C, 5–10 min). Nach sorgfältiger Abnahme des Ethanols wurde das RNA-Pellet in ~ 30 µL hochreinem Wasser resuspendiert.

RNA Aufreinigung über Oligonukleotid-Hybridisierung

Isolation von tRNA-Isoakzeptoren

Die Aufreinigung spezifischer RNA-Moleküle erfolgte über Oligonukleotid(ON)-Hybridisierung. Ein angepasstes Protokoll von Hauenschild *et al.*[216] wurde verwendet. Ein 30–40 Nukleotide langes, zur Sequenz der Ziel-RNA revers komplementäres Oligonukleotid, an das über einen kurzen, optionalen AAA-Adapter ein Biotin-Tag angehängt wurde, wurde für jedes aufzureinigende tRNA-Molekül entworfen. Die

Sequenzen können Tabelle **5.5** entnommen werden. Pro aufzureinigende Probe wurden 25 µL Dynabeads™ Streptavidin (T1 oder C1) in einem Mikroreaktionsgefäß vorgelegt. Über eine magnetische Halterung werden die Dynabeads™ am Gefäßrand konzentriert und die klare Lösung kann abpipettiert werden. Die Dynabeads™ wurden so anschließend 3-mal mit je 25 µL pro Ansatz 1× B&W Puffer gewaschen und zusätzlich einmal mit 25 µL 5× SSC Puffer pro Ansatz.

Tabelle 5.5: Oligonukleotide zur Aufreinigung von tRNA-Molekülen. Die Identität gibt das aufzureinigende RNA-Molekül an. Alle verwendeten Oligonukleotid-Stammlösungen besitzen eine Konzentration von 100 µM. *Interne Kennnummer in der Oligonukleotid-Datenbank des AK Kellner (Stand 2021)

Identität	Kenn-Nr.*	Sequenz (5‘ – 3‘)
$tRNA^{Gly}_{GCC}$	SK05	[Btn]TGCATTGGCCGGGAATCGAACCCGGGGCCTC
$tRNA^{His}_{GUG}$	SK06	[Btn]TGCCGTCACTCGGATTCGAACCGAGGTTGCTG
$tRNA^{Lys}_{yUU}$	SK07	[Btn]CCAACGTGGGGCTCGAACCCACGACCCT
$tRNA^{Ser}_{UGA}$	SK22	[Btn]AAATTTCAAGTCCATCGCCTTAACCACTCGGCCACGACTAC

Es wurde 1 µL Biotin-DNA-Oligonukleotid (100 µM) in ein Mikroreaktionsgefäß vorgelegt. 0,5–1 µg in hochreinem Wasser gelöste RNA wurde zugegeben. Für die Aufreinigung von tRNA Isoakzeptoren wurde die totale tRNA-Fraktion der SEC verwendet. Nach der Zugabe von 25 µL 20× SSC Puffer wurde das Gesamtvolumen durch Auffüllen mit hochreinem Wasser auf 100 µL erhöht. Das Gemisch wurde zur Denaturierung der RNA für 3 min bei 90 °C erhitzt und danach direkt in einen Heizblock bei 65 °C überführt und dort 10 min inkubiert. Nach anschließendem Abkühlen auf Raumtemperatur (~ 5 min) wurde jedem Ansatz 25 µL äquilibrierte Dynabeads™ in 5× SSC Puffer zugegeben (T1 oder C1). Der Ansatz wurde 30–60 min bei 25 °C bei 600 rpm inkubiert. Nicht hybridisierte RNA wurde durch Abnehmen des Überstandes unter Verwendung der magnetischen Halterung entfernt. Die Dynabeads™ wurden einmal mit 50 µL 1× SSC Puffer gewaschen, 3-mal mit 25 µL 0,1× SSC Puffer und anschließend in 20 µL MilliQ-Wasser angelöst. Nach Inkubation bei 75 °C für 3 min wurde die von den Dynabeads™ getrennte RNA-haltige Lösung in ein frisches Mikroreaktionsgefäß überführt. Bis zur weiteren Verarbeitung wurde die RNA bei – 20 °C gelagert.

Isolation von mRNA

Die Aufreinigung von mRNA erfolgte aus Gesamt-RNA mittels Oligonukleotid(ON)-Hybridisierung. Es wurde das Set „Dynabeads mRNA Purification“(Art.-Nr.: 61006, ThermoFisher Scientific, Waltham, MA, USA) verwendet, um mit einem 25 Nukleotide langen, zur Sequenz des PolyA-Schwanzes revers komplementären Oligonukleotids, welches an einem magnetischen Dynabead™ immobilisiert wurde, mRNA zu isolieren. Alle Komponenten des Sets wurden während des Versuchs auf Eis gelagert. Pro aufzureinigende Probe wurden 75 µg Gesamt-RNA angelöst in 100 µL hochreinem Wasser verwendet. Die Probe wurde 2 min. bei 65 °C und 500 rpm inkubiert, um die Sekundärstruktur zu zerbrechen. Die Probe wurde bis zur weiteren Prozessierung auf Eis gelagert. Es wurden 200 µL der Dynabeads™ Suspension pro Probe vorlegt und mit Hilfe einer magnetischen Halterung Dynabeads™ von Pufferlösung durch Abpipettieren getrennt. Die Dynabeads™ wurden in 100 µL Bindungspuffer (Endkonzentration: 20 mM Tris-HCl pH 7,5, 1M LiCl und 2 mM EDTA) resuspendiert. Dieser Vorgang des Waschens wurde einmal wiederholt, bevor zu den 100 µL Bindungspuffer/ Dynabead™ Suspension 100 µL Probe gegeben wurde. Es wurde durch Vortexen gemischt und bei 25 °C und 600 rpm 5 min. inkubiert. Zum Abnehmen des Überstandes wurde das Reaktionsgefäß wieder in die magnetische Halterung überführt und nach einer Equilibrierungszeit von 1 min. die klare Lösung abpipettiert. Die Dynabeads™ wurden anschließend in 200 µL Waschpuffer (Endkonzentration: 10 mM Tris-HCl pH 7,5, 150 mM LiCl und 1 mM EDTA) resuspendiert. Dieser Prozess des Waschens wurde ein weiteres Mal wiederholt und der Waschpuffer entfernt, bevor die Dynabeads™ in 20 µL Elutionspuffer (Endkonzentration: 10 mM Tris-HCl pH 7,5) resuspendiert wurden. Zum Abschmelzen der Probe von den Dynabeads™ wurde das Reaktionsgefäß für 2 min. bei 65 °C erhitzt. Nach sofortigem Transfer zur magnetischen Halterung und kurzer Äquilibrierungszeit wurden die Poly(A)-Schwanz aufgereinigten RNAs in der Lösung abpipettiert.

Um mögliche ribosomale RNA Verunreinigungen zu entfernen, wurde die Probe mit Hilfe des RiboMinus™ Eukaryote Kit v2 (Art.-Nr.: A15020, ThermoFisher Scientific, Waltham, MA, USA) aufgereinigt. Nachdem der in dem Kit befindliche Hybridisierungpuffer (2×) in einem Heizblock auf 50 °C erwärmt wurde, wurde gemäß **Tabelle 5.6** der Hybridisierungsansatz pipettiert, wobei das gesamte eluierte Volumen (20 µL) aus dem „Dynabeads mRNA Purification“ Experiment eingesetzt wurde.

Tabelle 5.6: Hybridisierungsansatz für Aufreinigung von mRNA.

Komponente	Stammlösung	Volumen
Hybridisierungspuffer	2x	50 µL
RiboMinus Probe Mix v2 Oligo Module v2		4 µL
PolyA-RNA		20 µL
MilliQ-Wasser		zu 100 µL

Nach Vortexen wurde dieser Mix für 10 min. bei 70 °C in einem Heizblock inkubiert. Nach dieser Inkubationszeit wurde die Probe sofort in einen weiteren bereitstehenden Heizblock mit einer Temperatur von 37 °C für 20 min. transferiert. Während dieser Zeit wurden pro Probe 500 µL RiboMinus™ Magnetic Beads equilibriert. Hierbei wurden die Beads in ein Eppendorf Reaktiongefäß überführt, an einer magnetischen Halterung ausgerichtet, der Überstand abgenommen und mit 500 µL hochreinem Wasser gewaschen. Nachdem die Beads ein weiteres Mal mit 500 µL Wasser gewaschen wurden, wurden 200 µL (1×) Hybridisierungpuffer hinzupipettiert. Anschließend wurden die Beads für mindestens 5 min. auf 37 °C erwärmt. Durch Vereinigen von Beads (200 µL) und RNA-Probe (100 µL) wurde die Hybridisierung der PolyA-Schwanz aufgereinigten RNA gestartet und für 5 min. bei 37 °C inkubiert. Nach einer Equilibrierungszeit von 1 min. an der magnetischen Halterung wurde der Überstand (300 µL), welcher keine ribosomale RNA mehr enthält, abpipettiert und in ein neues Reaktionsgefäß überführt. Die Lösung wurde an der SpeedVac auf 100 µL eingeengt und mit 1 µL GlycoBlue™ (Thermo Fisher, Waltham, MA, USA), 10 µL 5 M NH_4OAc und 250 µL 100 % eiskaltem Ethanol über Nacht bei –20 °C gefällt. Nachdem die Lösung bei 12.000× g und 4 °C für mindestens 60 Minuten zentrifugiert wurde, wurde das RNA-Pellet in 20 µL hochreinem Wasser resuspendiert.

Oligonukleotide

Tabelle 5.7: RNA-Oligonukleotide für die massenspektrometrische Methodenentwicklung. Die in der nachfolgenden Tabelle gelisteten Oligonukleotide wurden von IBA (Göttingen, Deutschland) erworben. In dem Oligonukleotid enthaltene RNA-Modifikationen (bspw. Inosin und N1-Methyladenosin) sind in der Sequenz rot markiert. Alle verwendeten Oligonukleotid-Stammlösungen besitzen eine Konzentration von 100 µM. *Interne Kennnummer in der Oligonukleotid-Datenbank des AK Kellner (Stand 2021)

Kenn-Nr.*	Länge	Sequenz (5‘ – 3‘)
SK13	5	ACUUG
SK14	8	UUUCCCCG
SK15	8	UCUCCCCG
SK16	10	AAAUCCAUUG
SK17	20	GUAGUCGUGGCCGAGUGGUU
SK18	30	GUAGUCGUGGCCGAGUGGUUAAGGCGAUGG
SK19	40	GUAGUCGUGGCCGAGUGGUUAAGGCGAUGGACUU GAAAUC
SK47	8	UAUCCCCG
SK48	5	AUUUG
SK60	9	CCUAACACG
SK61	9	CCU**I**ACACG
SK72	8	UUCG**m^{1}A**UUC
SK73	8	UAGG**m^{1}A**UUG
SK74	8	CGUC**m^{1}A**CAC

Tabelle 5.8: DNA-Oligonukleotide für die in vitro Transkription von tRNA-Molekülen. Die in der nachfolgenden Tabelle gelisteten Oligonukleotide wurden von IBA (Göttingen, Deutschland) erworben. Alle verwendeten Oligonukleotid-Stammlösungen besitzen eine Konzentration von 100 µM. *Interne Kennnummer in der Oligonukleotid-Datenbank des AK Kellner (Stand 2021)

Kenn-Nr.*	Länge	Sequenz (5‘ – 3‘)
SK09	156	TGGCGTAGTCGGCAGGATTCGAACCTGCGCGGGGA GACCCCAATGGATTTCAAGTCCATCGCCTTAACCAC TCGGCCACGACTACGACGGTACCGGGTACCGTTTC GTCCTCACGGACTCATCAGGTAGTCGTGTCTCCCTA TAGTGAGTCGTATT
SK10	28	CGCGCGAAGCTTAATACGACTCACTATA
SK11	13	TGGCGTAGTCGGC
SK59	15	TGGTGTTTCCGCCTG
SK80	147	TGGTGTTTCCGCCTGGTTTTGATCCAGGGACCTTTC GCGTGTTAGGCGAACGTGATAACCACTACACTACGG AAACGACGGTACCGGGTACCGTTTCGTCCTCACGGA CTCATCAGGTTTCCGTATCTCCCTATAGTGAGTCGTA TT

in vitro Transkription

Mit Hilfe der *in vitro* Transkription wurden definierte tRNA-Moleküle in µg-Maßstab synthetisiert. Hierbei wurde zuerst eine Polymerase-Kettenreaktion (*engl.* polymerase chain reaction, PCR) durchgeführt, um ausreichend DNA-Templat zu generieren. Die Komponenten der PCR sind Folgende: Für bspw. $tRNA^{Val}_{AAC}$ wurden ein Primer mit T7 Promoter-Sequenz (SK10), ein zur spezifischen tRNA revers komplementärer Primer (SK59) und ein DNA-Templat (SK80) benötigt. Analog wurden für die *in vitro* Transkription von $tRNA^{Ser}_{UGA}$ die Oligonukleotide (SK10, SK11, SK09) der Tabelle **5.8** verwendet. Die Komponenten wurden gemäß Tabelle **5.9** pipettiert.

Tabelle 5.9: Herstellung des PCR-Mix für die *in vitro* Transkription. Beispielhaft für $tRNA^{Ser}_{UGA}$ ist in der folgenden Tabelle ein PCR-Pipettierschema gezeigt. Es wurde das Set mit Polymerase und HF

Puffer (Art.-Nr.: M0531S, New England Biolabs, Ipswich, MA, USA) und dNTP-Mix (Art.-Nr.: N0447S, New England Biolabs, Ipswich, MA, USA) erworben.

Komponente	Stammlösung	Volumen
Phusion HF Puffer	5x	10 µL
SK10	4 µM	12 µL
SK11	4 µM	12 µL
SK09	0.1 µg/µL	1 µL
Phusion Polymerase		1 µL
dNTP Mix		1 µL
MilliQ-Wasser		zu 50 µL

Nachdem die Polymerase als Letztes zu dem Ansatz PCR-Reaktionsgefäß hinzupipettiert wurde, wurde durch Auf- und Abpipettieren gründlich gemischt. Das Gefäß wurde sofort in einen Thermocycler überführt und folgendes Programm gemäß Tabelle **5.10** gestartet.

Tabelle 5.10: Protokoll des PCR-Programms für die *in vitro* Transkription. Es wurden folgende Geräteparameter eingestellt: Deckeltemperatur 96 °C, Vorwärmedruck 30 N und vorwärmende Blocktemperatur 25 °C. Nach Durchlaufens des vierten Schrittes wurde erneut Schritt 2 ausgeführt. Dieses wurde dreißigmal wiederholt ehe zu Schritt 5 übergegangen wurde. Nach Beendigung des fünften Schrittes wurde die Probe auf 4 °C gekühlt. Hierbei wurde darauf geachtet, dass die Probe sobald sie diese Temperatur erreicht hat, entnommen und das Programm beendet wurde.

Schritt	Temperatur	Zeit	Wiederholungen
1	92 °C	2 min.	1
2	92 °C	15 sek.	30
3	47 °C	20 sek.	30
4	72 °C	30 sek.	30
5	72 °C	10 min.	1
6	4 °C	variabel	1

Es wurden zwei identische PCR-Ansätze aus den jeweiligen PCR-Gefäßen in ein Eppendorf Microreaktionsgefäß transferiert. Um die T7 in vitro Transkription zu starten, wurden folgende Komponenten aus Tabelle **5.11** dem Reaktionsgefäß zugesetzt.

Tabelle 5.11: T7 *in vitro* Transkription. Es wurden das Set T7 Transcript Aid HighYield (Art.-Nr.: K0441, ThermoFisher Scientific, Waltham, MA, USA) und stabile isotopenmarkierte Ribonukleintriphosphate (rNTPs) (Art.-Nr.: 121306100, Silantes, München, Deutschland) erworben.

Komponente	Stammlösung	Volumen
T7 Transkriptionspuffer	10x	10 µL
$MgCl_2$	50 mM	3 µL
T7 Polymerase		3,2 µL
rNTPs (4x)		jeweils 1,6 µL

PCR Produkt		100 µL
MilliQ-Wasser		zu 200 µL

Das Set T7 Transcript Aid HighYield enthält neben der T7 Polymerase und dem dazugehörigen Transkriptionspuffer auch einzelne Reaktionsgefäße mit CTP, UTP, GTP und ATP. Je nachdem ob ein stabiles isotopenmarkiertes *in vitro* Transkript gewünscht wurde, wurden rNTPs von ThermoFisher Scientific oder Silantes verwendet. Für die *in vitro* Transkription wurde das Mikroreaktionsgefäß in einem Heizblock bei 37 °C und 300 rpm für 2 Stunden inkubiert. Danach wurden weitere 1,5 µL T7 Polymerase und 5 µL 50 mM $MgCl_2$ hinzupipettiert. Bei erfolgreicher Transkription kann eine leichte Trübung der Lösung durch ausgefallenes Pyrophosphat beobachtet werden. Anschließend wurde für 2 weitere Stunden bei den oben genannten Parametern inkubiert. Nach erneuter Zugabe der gleichen Mengen an T7 Polymerase und $MgCl_2$ wurde für 2 Stunden inkubiert. Die *in vitro* Transkription dauerte mindestens 8 Stunden und wurde durch Zentrifugieren des überschüssigen Pyrophosphates und Zugabe von 4 µL DNase I (Art.-Nr.: M0303S, New England Biolabs, Ipswich, MA, USA) zum Überstand beendet. Der DNase I Verdau des DNA-Templates wurde bei 37 °C und 300 rpm in einer Stunde durchgeführt. In einem letzten Schritt wurde die in vitro transkribierte RNA mittels Ethanolfällung über Nacht bei –20 °C gefällt. Das 2,5-fache Volumen an 100 % Ethanol (500 µL) wurde zusammen mit 20 µL 5M NH_4OAc zur Lösung gegeben. Nachdem die Lösung bei 12.000× g und 4 °C für mindestens 60 Minuten zentrifugiert wurde, wurde das RNA-Pellet in ~ 100 µL hochreinem Wasser resuspendiert.

ADAT2/3 Inkubationsexperiment

Mit dem vom Fu-Labor präparierten humanen ADAT2/3-Protein wurde ein *in vitro*-Inkubationsexperiment mit tRNA durchgeführt. Hierzu wurde das Protein langsam auf Eis aufgetaut. In einem Reaktionsgefäß wurden währenddessen 6 µL (115 ng/µL) tRNA mit 6 µL hochreinem Wasser und 6 µL 3× tRNA-Denaturierungspuffer gemischt. Zur Denaturierung der tRNA wurde das Gemisch für 2 Minuten auf 95 °C erhitzt und anschließend unverzüglich für 3 Minuten auf Eis gelagert. Danach wurden 3 µL des 7× tRNA-Faltungspuffers hinzugefügt und für 20 Minuten bei 37 °C inkubiert. 9 µL des ADAT2/3-Proteins mit einer Konzentration von 8 ng/µL wurden zur vorbereiteten tRNA pipettiert und für 1 Stunde bei 37 °C inkubiert. Die Reaktion wurde durch Zugabe von

10-fachem Volumen an 2 % Lithiumperchlorat in Aceton (300 µL) gestoppt und nach Inkubation bei Raumtemperatur für 5 Minuten und Zentrifugation für 5 Minuten bei 5.000× g wurde die tRNA gefällt. Nach Abnahme des Überstandes wurde die im Reaktionsgefäß verbliebene tRNA in 20 µL hochreinem Wasser angelöst.

AlkBH Inkubationsexperiment

Die unterschiedlichen humanen Homologe des AlkB-Proteins, die im Abschnitt „Zelllinien und Enzyme“ aufgeführt sind, wurden - wenn nötig – immer mit ihrem AlkBH-Lagerungspuffer verdünnt. Die finalen Konzentrationen der Salze in einem Mikroreaktionsgefäß sind: 50 mM HEPES pH 7,5, 15 mM KCl, 2 mM L-Ascorbat, 2 mM $MgCl_2$, 300 µM α-Ketoglutarat und 300 µM $Fe(II)(NH_4)_2(SO_4)_2$. Dafür wurden folgende wässrige Stocklösungen in 10 mL oder 50 mL-Zentrifugenröhrchen angesetzt: 1 M HEPES pH 7,5, 100 mM KCl, 20 mM L-Ascorbat, 20 mM $MgCl_2$, 10 mM α-Ketoglutarat und 10 mM $Fe(II)(NH_4)_2(SO_4)_2$. Hierbei wurde insbesondere bei den Lösungen des L-Ascorbats, des α-Ketoglutarats und des Fe(II)-Salzes darauf geachtet, dass diese kurz vor Experimentstart hergestellt wurden. Wenn möglich, wurde für die in dem jeweiligen Inkubationsexperiment konzentrationskonstante Salzlösungen ein Master-Mix pipettiert. Nach Zugabe des AlkBH-Enzyms und des RNA-Substrats wurde der 50 µL fassende Reaktionsansatz per Auf- und Abpipettieren vermischt und in einem Heizblock für 2 Stunden bei 37 °C inkubiert. Das Stoppen der Inkubation sowie die Fällung der RNA wurde erreicht, indem das 10-fache Volumen an 2 % Lithiumperchlorat-Lösung in Aceton (500 µL) dem Ansatz hinzugefügt wurde. Nach Inkubation bei Raumtemperatur für 5 Minuten und Zentrifugation für 5 Minuten bei 5.000× g wurde die RNA gefällt. Nach Abnahme des Überstandes wurde die im Reaktionsgefäß verbliebene RNA in 20 µL hochreinem Wasser angelöst. Anschließend wurde die RNA mit der Endonuklease Benzonase verdaut. Das Prozedere ist im Abschnitt „Verdau für Nukleosid-Analytik“ genau beschrieben.

RNA-Konzentrationsbestimmung

Die RNA-Ausbeuten wurden mit Hilfe eines Nanophotometers bestimmt. Dazu wurde die gefällte RNA in hochreinem Wasser resuspendiert und 1,5 µL zur Konzentrationsbestimmung verwendet.

Bioanalyzer-Messungen

Nach Vorbereitung der jeweiligen Agilent RNA Chips (6000 Pico RNA Chip für mRNA oder Small RNA Chips für *in vitro* transkribierte tRNA) gemäß den entsprechenden Anleitungen wurden jeweils 1 µL der entsprechend verdünnten Proben auf den jeweiligen Chip aufgetragen und mit dem Agilent 2100 Bioanalyzer und den vorinstallierten Methoden „Eukaryote Total RNA Pico Series II.xsy“ bzw. „Small RNA Series II.xsy“ gemessen.

Verdau für Nukleosid-Analytik

Ein Verdau Master-Mix kann gemäß Tabelle **5.12** für die entsprechende Anzahl an Proben hergestellt werden. $MgCl_2$ und Tris sind Bestandteile des Puffersystems. Benzonase und SPD (*engl.* snake venom phosphodiesterase) sind Nukleasen und CIP (*engl.* calf intestine phosphatase) die Phosphatase. Pentostatin und THU (Tetrahydrouridin) schützen die Nukleoside vor Desaminierung und BHT (Butylhydroxytoluol) wirkt als Antioxidans. Für den hier gezeigten Master-Mix müssen 20 µL Probe mit 10 µL Master-Mix verdaut werden. Bei abweichenden Volumina wurde die Menge an $MgCl_2$ und TRIS entsprechend angepasst. Alle weiteren Angaben beziehen sich auf den Verdau von 4 µg RNA und müssen/können nur bei einer Erhöhung/Verringerung der RNA-Menge angepasst werden. Nach Verdau für 2 h bei 37 °C wurden alle Proben mit halben Volumen an LC-MS Puffer verdünnt (bspw. 30 µL Verdau + 15 µL LC-MS Puffer). Mit jeder Probe wurde 1 µL SILIS (10×) co-injiziert (bspw. 9 µL Probe + 1 µL SILIS). Der Verdau von maximal 3 µg RNA SILIS wurde nach einem 10 µg RNA-Protokoll durchgeführt, optional mit dem 0,1× fachen Volumen an Theophyllin (100 µM) und LC-MS/QQQ-Puffer versetzt. Hierbei wurde die hinzugebende Menge an Puffer so gewählt, dass eine Zielkonzentration von 20 ng/µL RNA erreicht wurde.

Tabelle 5.12: Beispielhafter Master-Mix für den Verdau von RNA. Der gezeigte Master-Mix bezieht sich auf den Verdau von 20 µL Probe mit 10 µL Master-Mix. Bis zu 4 µg RNA werden innerhalb von 2 h bei 37 °C zu Nukleosiden verdaut.

Komponente	Stammlösung		Zielkonzentration	1x	50x
$MgCl_2$	10 mM	→	1 mM	3 µL	150 µL
TRIS pH = 8	50 mM	→	5 mM	3 µL	150 µL
Benzonase	1 U/µL	→	0,8 U	0,8 µL	40 µL
CIP (Alk.Phos.)	1 U/µL	→	0,8 U	0,8 µL	40 µL
SPD (PDE1)	0,1 U/µL	→	0,08 U	0,8 µL	40 µL
Pentostatin	1 mg/mL	→	0,4 µg	0,4 µL	20 µL
THU	5 mg/mL	→	2 µg	0,4 µL	20 µL
BHT	10 mM	→	4 µM	0,4 µL	20 µL
H_2O				0,4 µL	20 µL

Verdau für Oligonukleotid-Analytik

RNase T1 wurde auf 10 U/µL verdünnt, indem 2 µl der RNase T1 Stammlösung (186 U/µl, Sigma-Aldrich, München, Deutschland) mit 35,2 µl TRIS pH 7,5 (25 mM) gemischt wurden (verdünnte RNase T1 wurde bei 4 °C gelagert und maximal einen Monat lang verwendet). 2 µg RNA wurden mit RNase T1 bei 37 °C für 1 h in einem Gesamtvolumen von 40 µl mit Endkonzentrationen von 10 mM TRIS pH 7,5, 0,5 mM $MgCl_2$, 1 U/µl RNase T1 und 0,02 U/µl CIP verdaut. Die verdauten Proben wurden durch einen Cut-Off-Filter mit einem Molekulargewicht von 10 kDa (VWR, Dreieich, Deutschland) filtriert.

5.4 Analytik

QQQ Methoden

Die Trennung der Nukleoside erfolgte über eine Synergi Fusion-RP-Säule (Synergi® 2,5 µm Fusion-RP 100 Å, 150 × 2,0 mm, Phenomenex®, Torrance, CA, USA). Als Puffer wurden LC-MS/QQQ Puffer (Puffer A) und pures Acetonitril (Puffer B) verwendet. Der Gradient beginnt mit 100% Puffer A für 1 min, gefolgt von einem Anstieg auf 10% Puffer B über eine Dauer von 4 min. Puffer B wird dann über 2 min auf 40% erhöht und für 1 min beibehalten bevor über eine Dauer von 0,5 min wieder

auf 100% Puffer A gewechselt und die Säule für 2,5 min re-equilibriert wird. Die Gesamtzeit beträgt 11 min und die Flussrate 0,35 mL/min bei einer Säulentemperatur von 35 °C.

Für die Ionisierung der Nukleoside wurde eine ESI Quelle verwendet (ESI-MS, Agilent Jetstream). Die Gastemperatur (N_2) lag bei 230 °C mit einer Flussrate von 6 L/min. Die Sheath-Gastemperatur lag bei 400 °C mit einer Flussrate von 12 L/min. Die Kapillarspannung (capillary voltage) lag bei 2500 V, die Skimmer-Spannung bei 15 V, die Düsenspannung (nozzle voltage) bei 0 V und der Vernebelungsdruck (nebulizer pressure) bei 40 Psi. Die Zellbeschleunigungsspannung (cell accelerator voltage) lag bei 5 V. Alle Methoden wurden im DMRM- und positiven Ionenmodus durchgeführt. Die Fragmentorspannung und die Kollisionsenergie wurden für jedes Nukleosid spezifisch optimiert. Optimierte Parameter befinden sich zusammen mit den Retentionszeiten und den Massenübergängen unmarkierter und isotopenmarkierter RNA-Nukleoside im Abschnitt „Nukleosid-MS-Parameter“. Die MS1-Auflösung wurde auf „Wide“, die MS2-Auflösung auf „Unit“ gesetzt und der SILIS-Übergang jeweils direkt als interner Standard markiert.

Kalibrierung

Zur Kalibrierung wurden synthetische Nukleoside eingewogen und in Wasser auf eine Stammkonzentration von 1–10 mM gelöst. Die Kalibrierlösungen reichten von 0,0125 pmol bis 100 pmol für jedes kanonische Nukleosid und von 0,00625 pmol bis 5 pmol für jedes modifizierte Nukleosid. Die Konzentrationen von Ψ und D reichten von 0,00625 pmol bis 20 pmol. Analog zu den Proben wurde mit jeder Kalibrierung 1 µL SILIS (10×) co-injiziert. Die Kalibriergerade und die entsprechende Auswertung der Proben wurden mit Hilfe des Tabellenprogramms Excel sowie über die qualitative MassHunter Software von Agilent durchgeführt. Das Prinzip der Quantifizierung mithilfe eines SILIS wird in Borland *et al*.[203] beschrieben.

Normalisierung / Berechnung pro RNA-Molekül

Um verschiedene Proben quantitativ vergleichbar zu machen, wurde die molare Menge jedes modifizierten Nukleosids auf die molare Menge der Summe der injizierten kanonischen Nukleoside referenziert. Bei bekannter Sequenz des RNA-Moleküls (bspw. tRNA-Isoakzeptoren oder ribosomaler RNA) wurde auf die Menge an RNA-

Molekülen (n_{RNA}) normiert, um die Anzahl der Modifikationen pro RNA-Molekül zu erhalten. Dazu wurden die berechneten Mengen der injizierten kanonischen Nukleoside (bspw. n_C) gemäß nachfolgender Gleichung durch ihre zu erwartende Menge (#) im jeweiligen RNA-Molekül dividiert und anschließend gemittelt. Die Zahlen für jedes kanonische Nukleosid (#) wurden aus der Sequenz der RNA-Moleküle entnommen.

$$n_{RNA} = \frac{\frac{n_C}{\#C} + \frac{n_U}{\#U} + \frac{n_G}{\#G} + \frac{n_A}{\#A}}{4}$$

Im Falle der NAIL-MS Experimente wurden die verschiedenen Isotopologe auf ihre entsprechend markierten kanonischen Nukleoside referenziert, so dass ursprüngliche (unmarkierte) und postmethylierte Modifikationen auf die ursprünglichen RNA-Moleküle und neue (isotopenmarkierte) Modifikationen auf neue RNA-Moleküle referenziert wurden.

HRMS von Oligonukleotiden

Die Trennung der Oligonukleotide erfolgte über eine Synergi Fusion-RP-Säule (Synergi® 2,5 µm Fusion-RP 100 Å, 150 × 2,0 mm, Phenomenex®, Torrance, CA, USA). Als Puffer wurden LC-MS/HRMS Puffer (Puffer A) und pures Acetonitril (Puffer B) verwendet. Der Gradient beginnt bei 0% Puffer B und steigt bis 10 min auf 5% Puffer B und anschließend bis 12 min auf 50% Puffer B an. Nach 1 min bei 50% Puffer B wurde über eine Dauer von 1 min zu 100% Puffer A umgespült. Die Säule wurde für 4 min bei 100% A re-equilibriert. Die Gesamtzeit beträgt 18 min und die Flussrate 0,35 mL/min bei einer Säulentemperatur von 35 °C.

Hochauflösende Massenspektren der Oligonukleotid-Ionen wurden mit einem Thermo Finnigan LTQ Orbitrap XL mit einer beheizten Elektrospray-Ionisationsquelle (HESI) aufgenommen, die im positiven Ionisationsmodus mit einer Kapillarspannung von -10 V und einer Temperatur von 310 °C betrieben wurde. Die Sprühspannung wurde auf 3,3 kV und die Temperatur für die chemische Ionisation bei Atmosphärendruck (APCI) auf 135 °C eingestellt. Sheath-, Auxiliary- und Sweep-Gase wurden auf 5, 35 und 7 „arbitrary Units“ eingestellt. MS1-Spektren wurden von 400 bis 2000 m/z aufgenommen und die datenabhängige Erfassung (DDA) wurde so eingestellt, dass MS2-Spektren der beiden häufigsten Ionen mit einer Vorläufer-Ionenliste von 636,1, 646,4, 742,5, 756,2, 953,7, 969,2, 1113,2 und 1133,7 erfasst wurden. Die MS2-

Fragmentierung verwendete CID mit einer normalisierten Kollisionsenergie von 35. Die Datenerfassung und -analyse erfolgte mit der Softwareplattform Thermo Xcalibur.

Nukleosid-MS-Parameter

Für die MRM-Methoden wurden folgende, in Tabelle **5.13** gezeigte Parameter der einzelnen Nukleoside festgelegt. Die Retentionszeit (R_t) wurde geringfügig vor jeder MS-Messung angepasst, da der Zustand, sowie die Anzahl der bereits durchgeführten Injektionen das Elutionsverhalten der Nukleoside verändern kann.

Tabelle 5.13: Nukleosid-Chromatographie- und Quellparameter.

Compound Gruppe	Compound Name	Vorläufer Ion	Produkt Ion	R_t (Min.)	ΔR_t (Min.)	Fragmentor	Kollisions Energie
A	A	268,1	136,0	5,3	1	200	20
A	A lab	273,0	141,0	5,3	1	200	20
A SILIS	A SILIS	283,0	146,0	5,3	1	200	20
ac^4C	ac^4C	286,1	154,0	5	1	85	9
ac^4C	ac^4C lab	293,0	156,0	5	1	85	9
ac^4C SILIS	ac^4C SILIS	300,0	163,0	5	1	85	9
Am	Am	282,1	136,0	6	1	130	17
Am	Am D3	285,0	136,0	6	1	130	17
Am	Am lab	287,0	141,0	6	1	130	17
Am	Am lab D3	290,0	141,0	6	1	130	17
Am SILIS	Am SILIS	298,0	146,0	6	1	130	17
C	C	244,1	112,0	2,1	1	200	20
C	C lab	251,0	114,0	2,1	1	200	20
C SILIS	C SILIS	256,0	119,0	2,1	1	200	20
Cm	Cm	258,1	112,0	4,1	1	180	9
Cm	Cm D3	261,0	112,0	4,1	1	180	9
Cm	Cm lab	265,0	114,0	4,1	1	180	9
Cm	Cm lab D3	268,0	114,0	4,1	1	180	9
Cm SILIS	Cm SILIS	271,0	119,0	4,1	1	180	9
D	D	247,1	115,0	1,6	1	70	5
D	D lab	254,0	117,0	1,6	1	70	5
D SILIS	D SILIS	258,0	121,0	1,6	1	70	5
G	G	284,1	152,0	4,3	1	200	20
G	G lab	288,0	156,0	4,3	1	200	20
G SILIS	G SILIS	299,0	162,0	4,3	1	200	20
Gm	Gm	298,1	152,0	5	1	100	9
Gm	Gm D3	301,0	152,0	5	1	100	9
Gm	Gm lab	302,0	156,0	5	1	100	9
Gm	Gm lab D3	305,0	156,0	5	1	100	9
Gm SILIS	Gm SILIS	314,0	162,0	5	1	100	9

I	I	269,1	137,0	4,1	1	100	10
I	I lab	273,0	141,0	4,1	1	100	10
I SILIS	I SILIS	283,0	146,0	4,1	1	100	10
m^1A	m^1A	282,1	150,0	2,2	1,5	150	25
m^1A	m^1A D3	285,0	153,0	2,2	1,5	150	25
m^1A	m^1A lab	287,0	155,0	2,2	1,5	150	25
m^1A	m^1A lab D3	290,0	158,0	2,2	1,5	150	25
m^1A SILIS	m^1A SILIS	298,0	161,0	2,2	1,5	150	25
m^1G	m^1G	298,1	166,0	4,9	0,5	105	13
m^1G	m^1G D3	301,0	169,0	4,9	0,5	105	13
m^1G	m^1G lab	302,0	170,0	4,9	0,5	105	13
m^1G	m^1G lab D3	305,0	173,0	4,9	0,5	105	13
m^1G SILIS	m^1G SILIS	314,0	177,0	4,9	0,5	105	13
$m^{22}G$	$m^{22}G$	312,1	180,0	5,7	1	105	13
$m^{22}G$	$m^{22}G$ D3	318,0	186,0	5,7	1	105	13
$m^{22}G$	$m^{22}G$ lab	316,0	184,0	5,7	1	105	13
$m^{22}G$	$m^{22}G$ lab D3	322,0	190,0	5,7	1	105	13
$m^{22}G$ SILIS	$m^{22}G$ SILIS	329,0	192,0	5,7	1	105	13
m^2G	m^2G	298,1	166,0	5,1	0,5	95	17
m^2G	m^2G D3	301,0	169,0	5,1	0,5	95	17
m^2G	m^2G lab	302,0	170,0	5,1	0,5	95	17
m^2G	m^2G lab D3	305,0	173,0	5,1	0,5	95	17
m^2G SILIS	m^2G SILIS	314,0	177,0	5,1	0,5	95	17
m^3C	m^3C	258,1	126,0	2	1,5	88	14
m^3C	m^3C D3	261,0	129,0	2	1,5	88	14
m^3C	m^3C lab	265,0	128,0	2	1,5	88	14
m^3C	m^3C lab D3	268,0	131,0	2	1,5	88	14
m^3C SILIS	m^3C SILIS	271,0	134,0	2	1,5	88	14
m^3U	m^3U	259,1	127,0	4,8	0,6	75	9
m^3U	m^3U D3	262,0	130,0	4,8	0,6	75	9
m^3U	m^3U lab	266,0	129,0	4,8	0,6	75	9
m^3U	m^3U lab D3	269,0	132,0	4,8	0,6	75	9
m^5C	m^5C	258,1	126,0	3,8	1	185	13
m^5C	m^5C D3	261,0	129,0	3,8	1	185	13
m^5C	m^5C lab	265,0	128,0	3,8	1	185	13
m^5C	m^5C lab D3	268,0	131,0	3,8	1	185	13
m^5C SILIS	m^5C SILIS	271,0	134,0	3,8	1	185	13
m^5U	m^5U	259,1	127,0	4,4	1	95	9
m^5U	m^5U D3	262,0	130,0	4,4	1	95	9
m^5U	m^5U lab	266,0	129,0	4,4	1	95	9
m^5U	m^5U lab D3	269,0	132,0	4,4	1	95	9
m^5U SILIS	m^5U SILIS	271,0	134,0	4,4	1	95	9

m^{6}A	m^{6}A	282,1	150,0	6,5	1	125	17
m^{6}A	m^{6}A D3	285,0	153,0	6,5	1	125	17
m^{6}A	m^{6}A lab	287,0	155,0	6,5	1	125	17
m^{6}A	m^{6}A lab D3	290,0	158,0	6,5	1	125	17
m^{6}A SILIS	m^{6}A SILIS	298,0	161,0	6,5	1	125	17
m^{7}G	m^{7}G	298,1	166,0	3,5	1,5	100	13
m^{7}G	m^{7}G D3	301,0	169,0	3,5	1,5	100	13
m^{7}G	m^{7}G lab	302,0	170,0	3,5	1,5	100	13
m^{7}G	m^{7}G lab D3	305,0	173,0	3,5	1,5	100	13
m^{7}G SILIS	m^{7}G SILIS	314,0	177,0	3,5	1,5	100	13
mcm^{5}s^{2}U	mcm^{5}s^{2}U	333,1	201,0	6,2	1	92	8
mcm^{5}s^{2}U	mcm^{5}s^{2}U D3	336,1	204,0	6,2	1	92	8
mcm^{5}s^{2}U	mcm^{5}s^{2}U lab	340,1	203,0	6,2	1	92	8
mcm^{5}s^{2}U	mcm^{5}s^{2}U lab D3	343,1	206,0	6,2	1	92	8
mcm^{5}s^{2}U SILIS	mcm^{5}s^{2}U SILIS	347,1	210,0	6,2	1	92	8
U	U	245,1	113,0	3	1	95	5
U	U lab	252,0	115,0	3	1	95	5
U SILIS	U SILIS	256,0	119,0	3	1	95	5
Um	Um	259,2	113,0	4,6	1	96	8
Um	Um D3	262,2	113,0	4,6	1	96	8
Um	Um lab	266,2	115,0	4,6	1	96	8
Um	Um lab D3	269,2	115,0	4,6	1	96	8
Um SILIS	Um SILIS	271,1	119,0	4,6	1	96	8
Y	Y	245,1	209,0	1,7	1	90	5
Y	Y lab	252,0	216,0	1,7	1	90	5
Y SILIS	Y SILIS	256,0	220,0	1,7	1	90	5

6. Abbildungsverzeichnis

7. Tabellenverzeichnis

8. Referenzen

1. Alazami, A.M., et al., *Mutation in ADAT3, encoding adenosine deaminase acting on transfer RNA, causes intellectual disability and strabismus.* J Med Genet, 2013. **50**(7): p. 425-30.
2. Martinez, F.J., et al., *Whole exome sequencing identifies a splicing mutation in NSUN2 as a cause of a Dubowitz-like syndrome.* J Med Genet, 2012. **49**(6): p. 380-5.
3. Watson, J.D. and F.H. Crick, *Molecular structure of nucleic acids; a structure for deoxyribose nucleic acid.* Nature, 1953. **171**(4356): p. 737-8.
4. Crick, F., *Central dogma of molecular biology.* Nature, 1970. **227**(5258): p. 561-3.
5. Brenner, S., F. Jacob, and M. Meselson, *An unstable intermediate carrying information from genes to ribosomes for protein synthesis.* Nature, 1961. **190**: p. 576-581.
6. Rich, A. and U.L. RajBhandary, *Transfer RNA: molecular structure, sequence, and properties.* Annu Rev Biochem, 1976. **45**: p. 805-60.
7. Baer, B.W. and R.D. Kornberg, *The protein responsible for the repeating structure of cytoplasmic poly(A)-ribonucleoprotein.* J Cell Biol, 1983. **96**(3): p. 717-21.
8. Yehudai-Resheff, S., M. Hirsh, and G. Schuster, *Polynucleotide phosphorylase functions as both an exonuclease and a poly(A) polymerase in spinach chloroplasts.* Mol Cell Biol, 2001. **21**(16): p. 5408-16.
9. Roeder, R.G. and W.J. Rutter, *Multiple forms of DNA-dependent RNA polymerase in eukaryotic organisms.* Nature, 1969. **224**(5216): p. 234-7.
10. Marshall, E., *Biomedicine. Move provokes bruising fight over U.K. biomedical institute.* Science, 2005. **307**(5710): p. 652.
11. Wierzbicki, A.T., J.R. Haag, and C.S. Pikaard, *Noncoding transcription by RNA polymerase Pol IVb/Pol V mediates transcriptional silencing of overlapping and adjacent genes.* Cell, 2008. **135**(4): p. 635-48.
12. Burgess, R.R., et al., *Factor stimulating transcription by RNA polymerase.* Nature, 1969. **221**(5175): p. 43-6.
13. Kuhn, C.D., et al., *Functional architecture of RNA polymerase I.* Cell, 2007. **131**(7): p. 1260-72.
14. Engel, C., et al., *Structural Basis of RNA Polymerase I Transcription Initiation.* Cell, 2017. **169**(1): p. 120-131 e22.
15. Cramer, P., D.A. Bushnell, and R.D. Kornberg, *Structural basis of transcription: RNA polymerase II at 2.8 angstrom resolution.* Science, 2001. **292**(5523): p. 1863-76.
16. Jasiak, A.J., et al., *Structural biology of RNA polymerase III: subcomplex C17/25 X-ray structure and 11 subunit enzyme model.* Mol Cell, 2006. **23**(1): p. 71-81.
17. Werner, F. and D. Grohmann, *Evolution of multisubunit RNA polymerases in the three domains of life.* Nat Rev Microbiol, 2011. **9**(2): p. 85-98.
18. Segall, J., T. Matsui, and R.G. Roeder, *Multiple factors are required for the accurate transcription of purified genes by RNA polymerase III.* J Biol Chem, 1980. **255**(24): p. 11986-91.
19. Matsui, T., et al., *Multiple factors required for accurate initiation of transcription by purified RNA polymerase II.* J Biol Chem, 1980. **255**(24): p. 11992-6.
20. Mishima, Y., et al., *Fractionation and reconstitution of factors required for accurate transcription of mammalian ribosomal RNA genes: identification of a species-dependent initiation factor.* Nucleic Acids Res, 1982. **10**(21): p. 6659-70.
21. Roeder, R.G. and W.J. Rutter, *Specific nucleolar and nucleoplasmic RNA polymerases.* Proc Natl Acad Sci U S A, 1970. **65**(3): p. 675-82.
22. Miller, O.L., Jr. and B.R. Beatty, *Visualization of nucleolar genes.* Science, 1969. **164**(3882): p. 955-7.

23. Warner, J.R., *The economics of ribosome biosynthesis in yeast.* Trends Biochem Sci, 1999. **24**(11): p. 437-40.

24. Lifton, R.P., et al., *The organization of the histone genes in Drosophila melanogaster: functional and evolutionary implications.* Cold Spring Harb Symp Quant Biol, 1978. **42 Pt 2**: p. 1047-51.

25. Learned, R.M., S. Cordes, and R. Tjian, *Purification and characterization of a transcription factor that confers promoter specificity to human RNA polymerase I.* Mol Cell Biol, 1985. **5**(6): p. 1358-69.

26. Clos, J., D. Buttgereit, and I. Grummt, *A purified transcription factor (TIF-IB) binds to essential sequences of the mouse rDNA promoter.* Proc Natl Acad Sci U S A, 1986. **83**(3): p. 604-8.

27. Evers, R. and I. Grummt, *Molecular coevolution of mammalian ribosomal gene terminator sequences and the transcription termination factor TTF-I.* Proc Natl Acad Sci U S A, 1995. **92**(13): p. 5827-31.

28. Swaffer, M.P., et al., *RNA polymerase II dynamics and mRNA stability feedback determine mRNA scaling with cell size.* bioRxiv, 2021: p. 2021.09.20.461005.

29. Buratowski, S., et al., *Five intermediate complexes in transcription initiation by RNA polymerase II.* Cell, 1989. **56**(4): p. 549-61.

30. Van Dyke, M.W., R.G. Roeder, and M. Sawadogo, *Physical analysis of transcription preinitiation complex assembly on a class II gene promoter.* Science, 1988. **241**(4871): p. 1335-8.

31. Kelleher, R.J., 3rd, P.M. Flanagan, and R.D. Kornberg, *A novel mediator between activator proteins and the RNA polymerase II transcription apparatus.* Cell, 1990. **61**(7): p. 1209-15.

32. Westover, K.D., D.A. Bushnell, and R.D. Kornberg, *Structural basis of transcription: separation of RNA from DNA by RNA polymerase II.* Science, 2004. **303**(5660): p. 1014-6.

33. Brueckner, F. and P. Cramer, *Structural basis of transcription inhibition by alpha-amanitin and implications for RNA polymerase II translocation.* Nat Struct Mol Biol, 2008. **15**(8): p. 811-8.

34. Gregersen, L.H., R. Mitter, and J.Q. Svejstrup, *Using TTchem-seq for profiling nascent transcription and measuring transcript elongation.* Nat Protoc, 2020. **15**(2): p. 604-627.

35. Schwalb, B., et al., *TT-seq maps the human transient transcriptome.* Science, 2016. **352**(6290): p. 1225-8.

36. Shatkin, A.J., *Methylated messenger RNA synthesis in vitro by purified reovirus.* Proc Natl Acad Sci U S A, 1974. **71**(8): p. 3204-7.

37. Berget, S.M., et al., *Spliced segments at the 5' termini of adenovirus-2 late mRNA: a role for heterogeneous nuclear RNA in mammalian cells.* Cold Spring Harb Symp Quant Biol, 1978. **42 Pt 1**: p. 523-9.

38. Darnell, J.E., et al., *Polyadenylic acid sequences: role in conversion of nuclear RNA into messenger RNA.* Science, 1971. **174**(4008): p. 507-10.

39. Geiduschek, E.P. and G.A. Kassavetis, *The RNA polymerase III transcription apparatus.* J Mol Biol, 2001. **310**(1): p. 1-26.

40. Robertson, H.D., S. Altman, and J.D. Smith, *Purification and properties of a specific Escherichia coli ribonuclease which cleaves a tyrosine transfer ribonucleic acid presursor.* J Biol Chem, 1972. **247**(16): p. 5243-51.

41. Maraia, R.J. and T.N. Lamichhane, *3' processing of eukaryotic precursor tRNAs.* Wiley Interdiscip Rev RNA, 2011. **2**(3): p. 362-75.

42. Sprinzl, M. and F. Cramer, *The -C-C-A end of tRNA and its role in protein biosynthesis.* Prog Nucleic Acid Res Mol Biol, 1979. **22**: p. 1-69.

43. Paushkin, S.V., et al., *Identification of a human endonuclease complex reveals a link between tRNA splicing and pre-mRNA 3' end formation.* Cell, 2004. **117**(3): p. 311-21.

44. Oettel, S., et al., *Human transcription factors IIIC2 , IIIC1 and a novel component IIIC0 fulfil different aspects of DNA binding to various pol III genes.* Nucleic Acids Res, 1997. **25**(12): p. 2440-7.

45. Kedinger, C., et al., *Alpha-amanitin: a specific inhibitor of one of two DNA-pendent RNA polymerase activities from calf thymus.* Biochem Biophys Res Commun, 1970. **38**(1): p. 165-71.

46. Lindell, T.J., et al., *Specific inhibition of nuclear RNA polymerase II by alpha-amanitin.* Science, 1970. **170**(3956): p. 447-9.

47. Bushnell, D.A., P. Cramer, and R.D. Kornberg, *Structural basis of transcription: alpha-amanitin-RNA polymerase II cocrystal at 2.8 A resolution.* Proc Natl Acad Sci U S A, 2002. **99**(3): p. 1218-22.

48. Rudd, M.D. and D.S. Luse, *Amanitin greatly reduces the rate of transcription by RNA polymerase II ternary complexes but fails to inhibit some transcript cleavage modes.* J Biol Chem, 1996. **271**(35): p. 21549-58.

49. Hartmann, G., et al., *The specific inhibition of the DNA-directed RNA synthesis by rifamycin.* Biochim Biophys Acta, 1967. **145**(3): p. 843-4.

50. Campbell, E.A., et al., *Structural mechanism for rifampicin inhibition of bacterial rna polymerase.* Cell, 2001. **104**(6): p. 901-12.

51. McClure, W.R. and C.L. Cech, *On the mechanism of rifampicin inhibition of RNA synthesis.* J Biol Chem, 1978. **253**(24): p. 8949-56.

52. Rottman, F. and A.J. Guarino, *The Inhibition of Phosphoribosyl-Pyrophosphate Amidotransferase Activity by Cordycepin Monophosphate.* Biochim Biophys Acta, 1964. **89**: p. 465-72.

53. Horowitz, B., B.A. Goldfinger, and J. Marmur, *Effect of cordycepin triphosphate on the nuclear DNA-dependent RNA polymerases and poly(A) polymerase from the yeast, Saccharomyces cerevisiae.* Arch Biochem Biophys, 1976. **172**(1): p. 143-8.

54. Holbein, S., et al., *Cordycepin interferes with 3' end formation in yeast independently of its potential to terminate RNA chain elongation.* RNA, 2009. **15**(5): p. 837-49.

55. Hill, D.L. and L.L. Bennett, Jr., *Purification and properties of 5-phosphoribosyl pyrophosphate amidotransferase from adenocarcinoma 755 cells.* Biochemistry, 1969. **8**(1): p. 122-30.

56. Christie, N.T., et al., *6-Thioguanine-induced DNA damage as a determinant of cytotoxicity in cultured Chinese hamster ovary cells.* Cancer Res, 1984. **44**(9): p. 3665-71.

57. Bailey, S.A., D.E. Graves, and R. Rill, *Binding of actinomycin D to the T(G)nT motif of double-stranded DNA: determination of the guanine requirement in nonclassical, non-GpC binding sites.* Biochemistry, 1994. **33**(38): p. 11493-500.

58. Lo, Y.S., et al., *The structural basis of actinomycin D-binding induces nucleotide flipping out, a sharp bend and a left-handed twist in CGG triplet repeats.* Nucleic Acids Res, 2013. **41**(7): p. 4284-94.

59. Trask, D.K. and M.T. Muller, *Stabilization of type I topoisomerase-DNA covalent complexes by actinomycin D.* Proc Natl Acad Sci U S A, 1988. **85**(5): p. 1417-21.

60. Sobell, H.M., *Actinomycin and DNA transcription.* Proc Natl Acad Sci U S A, 1985. **82**(16): p. 5328-31.

61. Perry, R.P. and D.E. Kelley, *Inhibition of RNA synthesis by actinomycin D: characteristic dose-response of different RNA species.* J Cell Physiol, 1970. **76**(2): p. 127-39.

62. Boccaletto, P., et al., *MODOMICS: a database of RNA modification pathways. 2017 update.* Nucleic Acids Res, 2018. **46**(D1): p. D303-D307.

63. Cohn, W.E. and E. Volkin, *Nucleoside-5'-Phosphates from Ribonucleic Acid.* Nature, 1951. **167**(4247): p. 483-484.

64. Huang, L., et al., *A conserved aspartate of tRNA pseudouridine synthase is essential for activity and a probable nucleophilic catalyst.* Biochemistry, 1998. **37**(1): p. 344-51.

65. Juhling, F., et al., *tRNAdb 2009: compilation of tRNA sequences and tRNA genes.* Nucleic Acids Res, 2009. **37**(Database issue): p. D159-62.

66. Miller, N. and P. Cerutti, *Structure of the photohydration products of cytidine and uridine.* Proc Natl Acad Sci U S A, 1968. **59**(1): p. 34-8.

67. de Jager, T.L., A.E. Cockrell, and S.S. Du Plessis, *Ultraviolet Light Induced Generation of Reactive Oxygen Species.* Adv Exp Med Biol, 2017. **996**: p. 15-23.

68. Liu, M., et al., *The role of oxidative stress in influenza virus infection.* Microbes Infect, 2017. **19**(12): p. 580-586.

69. Hamilton, J.T., et al., *Chloride methylation by plant pectin: an efficient environmentally significant process.* Science, 2003. **301**(5630): p. 206-9.

70. Hecht, S.S., *DNA adduct formation from tobacco-specific N-nitrosamines.* Mutat Res, 1999. **424**(1-2): p. 127-42.

71. Daiber, A., et al., *Oxidative stress and inflammation contribute to traffic noise-induced vascular and cerebral dysfunction via uncoupling of nitric oxide synthases.* Redox Biol, 2020. **34**: p. 101506.

72. Hsu, G.W., et al., *Error-prone replication of oxidatively damaged DNA by a high-fidelity DNA polymerase.* Nature, 2004. **431**(7005): p. 217-21.

73. Simms, C.L., et al., *An active role for the ribosome in determining the fate of oxidized mRNA.* Cell Rep, 2014. **9**(4): p. 1256-64.

74. Tremblay, S., et al., *2'-Deoxycytidine glycols, a missing link in the free radical-mediated oxidation of DNA.* J Biol Chem, 1999. **274**(30): p. 20833-8.

75. Zahn, K.E., et al., *The miscoding potential of 5-hydroxycytosine arises due to template instability in the replicative polymerase active site.* Biochemistry, 2011. **50**(47): p. 10350-8.

76. Yan, L.L. and H.S. Zaher, *How do cells cope with RNA damage and its consequences?* J Biol Chem, 2019. **294**(41): p. 15158-15171.

77. Ezaz-Nikpay, K. and G.L. Verdine, *The effects of N7-methylguanine on duplex DNA structure.* Chem Biol, 1994. **1**(4): p. 235-40.

78. Rusyn, I., et al., *Effects of ethylene oxide and ethylene inhalation on DNA adducts, apurinic/apyrimidinic sites and expression of base excision DNA repair genes in rat brain, spleen, and liver.* DNA Repair (Amst), 2005. **4**(10): p. 1099-110.

79. Wang, X., et al., *Structural basis of N(6)-adenosine methylation by the METTL3-METTL14 complex.* Nature, 2016. **534**(7608): p. 575-8.

80. Liu, J., et al., *A METTL3-METTL14 complex mediates mammalian nuclear RNA N6-adenosine methylation.* Nat Chem Biol, 2014. **10**(2): p. 93-5.

81. Ping, X.L., et al., *Mammalian WTAP is a regulatory subunit of the RNA N6-methyladenosine methyltransferase.* Cell Res, 2014. **24**(2): p. 177-89.

82. Schwartz, S., et al., *Perturbation of m6A writers reveals two distinct classes of mRNA methylation at internal and 5' sites.* Cell Rep, 2014. **8**(1): p. 284-96.

83. Csepany, T., et al., *Sequence specificity of mRNA N6-adenosine methyltransferase.* J Biol Chem, 1990. **265**(33): p. 20117-22.

84. Liu, N., et al., *N(6)-methyladenosine-dependent RNA structural switches regulate RNA-protein interactions.* Nature, 2015. **518**(7540): p. 560-4.

85. Dominissini, D., et al., *Topology of the human and mouse m6A RNA methylomes revealed by m6A-seq.* Nature, 2012. **485**(7397): p. 201-6.

86. Camper, S.A., et al., *Effect of undermethylation on mRNA cytoplasmic appearance and half-life.* Mol Cell Biol, 1984. **4**(3): p. 538-43.

87. Lin, S., et al., *The m(6)A Methyltransferase METTL3 Promotes Translation in Human Cancer Cells.* Mol Cell, 2016. **62**(3): p. 335-345.

88. Finkel, D. and Y. Groner, *Methylations of adenosine residues (m6A) in pre-mRNA are important for formation of late simian virus 40 mRNAs.* Virology, 1983. **131**(2): p. 409-25.

89. Xiang, Y., et al., *RNA m(6)A methylation regulates the ultraviolet-induced DNA damage response.* Nature, 2017. **543**(7646): p. 573-576.

90. Wang, Y., et al., *N6-methyladenosine modification destabilizes developmental regulators in embryonic stem cells.* Nat Cell Biol, 2014. **16**(2): p. 191-8.

91. Barbieri, I., et al., *Promoter-bound METTL3 maintains myeloid leukaemia by m(6)A-dependent translation control.* Nature, 2017. **552**(7683): p. 126-131.

92. Xu, L., et al., *Three distinct 3-methylcytidine (m(3)C) methyltransferases modify tRNA and mRNA in mice and humans.* J Biol Chem, 2017. **292**(35): p. 14695-14703.

93. Mao, X.L., et al., *Mutually exclusive substrate selection strategy by human m3C RNA transferases METTL2A and METTL6.* Nucleic Acids Res, 2021. **49**(14): p. 8309-8323.

94. Ignatova, V.V., et al., *METTL6 is a tRNA m(3)C methyltransferase that regulates pluripotency and tumor cell growth.* Sci Adv, 2020. **6**(35): p. eaaz4551.

95. Gatza, M.L., et al., *An integrated genomics approach identifies drivers of proliferation in luminal-subtype human breast cancer.* Nat Genet, 2014. **46**(10): p. 1051-9.

96. Tan, X.L., et al., *Genetic variation predicting cisplatin cytotoxicity associated with overall survival in lung cancer patients receiving platinum-based chemotherapy.* Clin Cancer Res, 2011. **17**(17): p. 5801-11.

97. Steinberg, S. and R. Cedergren, *A correlation between N2-dimethylguanosine presence and alternate tRNA conformers.* RNA, 1995. **1**(9): p. 886-91.

98. Dewe, J.M., et al., *TRMT1-Catalyzed tRNA Modifications Are Required for Redox Homeostasis To Ensure Proper Cellular Proliferation and Oxidative Stress Survival.* Mol Cell Biol, 2017. **37**(21).

99. Davarniya, B., et al., *The Role of a Novel TRMT1 Gene Mutation and Rare GRM1 Gene Defect in Intellectual Disability in Two Azeri Families.* PLoS One, 2015. **10**(8): p. e0129631.

100. Blaesius, K., et al., *Mutations in the tRNA methyltransferase 1 gene TRMT1 cause congenital microcephaly, isolated inferior vermian hypoplasia and cystic leukomalacia in addition to intellectual disability.* Am J Med Genet A, 2018. **176**(11): p. 2517-2521.

101. Zhang, K., et al., *An intellectual disability-associated missense variant in TRMT1 impairs tRNA modification and reconstitution of enzymatic activity.* Hum Mutat, 2020. **41**(3): p. 600-607.

102. Suzuki, T., *The expanding world of tRNA modifications and their disease relevance.* Nat Rev Mol Cell Biol, 2021. **22**(6): p. 375-392.

103. Sprinzl, M., et al., *Compilation of tRNA sequences and sequences of tRNA genes.* Nucleic Acids Res, 1998. **26**(1): p. 148-53.

104. Novoa, E.M., et al., *A role for tRNA modifications in genome structure and codon usage.* Cell, 2012. **149**(1): p. 202-13.

105. Crick, F.H., *Codon--anticodon pairing: the wobble hypothesis.* J Mol Biol, 1966. **19**(2): p. 548-55.

106. Gerber, A.P. and W. Keller, *An adenosine deaminase that generates inosine at the wobble position of tRNAs.* Science, 1999. **286**(5442): p. 1146-9.

107. Ramos-Morales, E., et al., *The structure of the mouse ADAT2/ADAT3 complex reveals the molecular basis for mammalian tRNA wobble adenosine-to-inosine deamination.* Nucleic Acids Res, 2021. **49**(11): p. 6529-6548.

108. Torres, A.G., et al., *Inosine modifications in human tRNAs are incorporated at the precursor tRNA level.* Nucleic Acids Res, 2015. **43**(10): p. 5145-57.

109. Kataoka, H., Y. Yamamoto, and M. Sekiguchi, *A new gene (alkB) of Escherichia coli that controls sensitivity to methyl methane sulfonate.* J Bacteriol, 1983. **153**(3): p. 1301-7.

110. Chen, B.J., P. Carroll, and L. Samson, *The Escherichia coli AlkB protein protects human cells against alkylation-induced toxicity.* J Bacteriol, 1994. **176**(20): p. 6255-61.

111. Aravind, L. and E.V. Koonin, *The DNA-repair protein AlkB, EGL-9, and leprecan define new families of 2-oxoglutarate- and iron-dependent dioxygenases.* Genome Biol, 2001. **2**(3): p. RESEARCH0007.

112. Welford, R.W., et al., *Incorporation of oxygen into the succinate co-product of iron(II) and 2-oxoglutarate dependent oxygenases from bacteria, plants and humans.* FEBS Lett, 2005. **579**(23): p. 5170-4.

113. Sundheim, O., et al., *Human ABH3 structure and key residues for oxidative demethylation to reverse DNA/RNA damage.* EMBO J, 2006. **25**(14): p. 3389-97.

114. Trewick, S.C., et al., *Oxidative demethylation by Escherichia coli AlkB directly reverts DNA base damage.* Nature, 2002. **419**(6903): p. 174-8.

115. Falnes, P.O., R.F. Johansen, and E. Seeberg, *AlkB-mediated oxidative demethylation reverses DNA damage in Escherichia coli.* Nature, 2002. **419**(6903): p. 178-82.

116. Duncan, T., et al., *Reversal of DNA alkylation damage by two human dioxygenases.* Proc Natl Acad Sci U S A, 2002. **99**(26): p. 16660-5.

117. Aas, P.A., et al., *Human and bacterial oxidative demethylases repair alkylation damage in both RNA and DNA.* Nature, 2003. **421**(6925): p. 859-63.

118. Ma, C.J., et al., *AlkB Homologue 1 Demethylates N(3)-Methylcytidine in mRNA of Mammals.* ACS Chem Biol, 2019. **14**(7): p. 1418-1425.

119. Wu, T.P., et al., *DNA methylation on N(6)-adenine in mammalian embryonic stem cells.* Nature, 2016. **532**(7599): p. 329-33.

120. Liu, F., et al., *ALKBH1-Mediated tRNA Demethylation Regulates Translation.* Cell, 2016. **167**(3): p. 816-828 e16.

121. Muller, T.A., et al., *Characterization of human AlkB homolog 1 produced in mammalian cells and demonstration of mitochondrial dysfunction in ALKBH1-deficient cells.* Biochem Biophys Res Commun, 2018. **495**(1): p. 98-103.

122. Kawarada, L., et al., *ALKBH1 is an RNA dioxygenase responsible for cytoplasmic and mitochondrial tRNA modifications.* Nucleic Acids Res, 2017. **45**(12): p. 7401-7415.

123. Haag, S., et al., *NSUN3 and ABH1 modify the wobble position of mt-tRNAMet to expand codon recognition in mitochondrial translation.* EMBO J, 2016. **35**(19): p. 2104-2119.

124. Rashad, S., et al., *The stress specific impact of ALKBH1 on tRNA cleavage and tiRNA generation.* RNA Biol, 2020. **17**(8): p. 1092-1103.

125. Westbye, M.P., et al., *Human AlkB homolog 1 is a mitochondrial protein that demethylates 3-methylcytosine in DNA and RNA.* J Biol Chem, 2008. **283**(36): p. 25046-56.

126. Zhang, M., et al., *Mammalian ALKBH1 serves as an N(6)-mA demethylase of unpairing DNA.* Cell Res, 2020. **30**(3): p. 197-210.

127. Ougland, R., et al., *AlkB restores the biological function of mRNA and tRNA inactivated by chemical methylation.* Mol Cell, 2004. **16**(1): p. 107-16.

128. Li, X., et al., *Transcriptome-wide mapping reveals reversible and dynamic N(1)-methyladenosine methylome.* Nat Chem Biol, 2016. **12**(5): p. 311-6.

129. You, C., et al., *Roles of Aag, Alkbh2, and Alkbh3 in the Repair of Carboxymethylated and Ethylated Thymidine Lesions.* ACS Chem Biol, 2016. **11**(5): p. 1332-8.

130. Dango, S., et al., *DNA unwinding by ASCC3 helicase is coupled to ALKBH3-dependent DNA alkylation repair and cancer cell proliferation.* Mol Cell, 2011. **44**(3): p. 373-84.

131. Wollen, K.L., et al., *ALKBH3 partner ASCC3 mediates P-body formation and selective clearance of MMS-induced 1-methyladenosine and 3-methylcytosine from mRNA.* J Transl Med, 2021. **19**(1): p. 287.

132. Ueda, Y., et al., *AlkB homolog 3-mediated tRNA demethylation promotes protein synthesis in cancer cells.* Sci Rep, 2017. **7**: p. 42271.

133. Chen, Z., et al., *Transfer RNA demethylase ALKBH3 promotes cancer progression via induction of tRNA-derived small RNAs.* Nucleic Acids Res, 2019. **47**(5): p. 2533-2545.

134. Bian, K., et al., *DNA repair enzymes ALKBH2, ALKBH3, and AlkB oxidize 5-methylcytosine to 5-hydroxymethylcytosine, 5-formylcytosine and 5-carboxylcytosine in vitro.* Nucleic Acids Res, 2019. **47**(11): p. 5522-5529.

135. Zheng, G., et al., *ALKBH5 is a mammalian RNA demethylase that impacts RNA metabolism and mouse fertility.* Mol Cell, 2013. **49**(1): p. 18-29.

136. Xu, C., et al., *Structures of human ALKBH5 demethylase reveal a unique binding mode for specific single-stranded N6-methyladenosine RNA demethylation.* J Biol Chem, 2014. **289**(25): p. 17299-311.

137. Tang, C., et al., *ALKBH5-dependent m6A demethylation controls splicing and stability of long 3'-UTR mRNAs in male germ cells.* Proc Natl Acad Sci U S A, 2018. **115**(2): p. E325-E333.

138. Ensfelder, T.T., et al., *ALKBH5-induced demethylation of mono- and dimethylated adenosine.* Chem Commun (Camb), 2018. **54**(62): p. 8591-8593.

139. E, A.A., C. He, and A. Klungland, *ALKBHs-facilitated RNA modifications and de-modifications.* DNA Repair (Amst), 2016. **44**: p. 87-91.

140. Wang, G., et al., *The atomic resolution structure of human AlkB homolog 7 (ALKBH7), a key protein for programmed necrosis and fat metabolism.* J Biol Chem, 2014. **289**(40): p. 27924-36.

141. Zhang, L.S., et al., *ALKBH7-mediated demethylation regulates mitochondrial polycistronic RNA processing.* Nat Cell Biol, 2021. **23**(7): p. 684-691.

142. Vagbo, C.B., et al., *Methylation damage to RNA induced in vivo in Escherichia coli is repaired by endogenous AlkB as part of the adaptive response.* DNA Repair (Amst), 2013. **12**(3): p. 188-95.

143. Reichle, V.F., et al., *NAIL-MS reveals the repair of 2-methylthiocytidine by AlkB in E. coli.* Nat Commun, 2019. **10**(1): p. 5600.

144. Cozen, A.E., et al., *ARM-seq: AlkB-facilitated RNA methylation sequencing reveals a complex landscape of modified tRNA fragments.* Nat Methods, 2015. **12**(9): p. 879-84.

145. Falnes, P.O., *Repair of 3-methylthymine and 1-methylguanine lesions by bacterial and human AlkB proteins.* Nucleic Acids Res, 2004. **32**(21): p. 6260-7.

146. Liu, F., et al., *ALKBH1-Mediated tRNA Demethylation Regulates Translation.* Cell, 2016. **167**(7): p. 1897.

147. Lee, D.H., et al., *Repair of methylation damage in DNA and RNA by mammalian AlkB homologues.* J Biol Chem, 2005. **280**(47): p. 39448-59.

148. Stanley, J. and S. Vassilenko, *A different approach to RNA sequencing.* Nature, 1978. **274**(5666): p. 87-9.

149. Donis-Keller, H., A.M. Maxam, and W. Gilbert, *Mapping adenines, guanines, and pyrimidines in RNA.* Nucleic Acids Res, 1977. **4**(8): p. 2527-38.

150. Maden, B.E., *Mapping 2'-O-methyl groups in ribosomal RNA.* Methods, 2001. **25**(3): p. 374-82.

151. Ryvkin, P., et al., *HAMR: high-throughput annotation of modified ribonucleotides.* RNA, 2013. **19**(12): p. 1684-92.

152. Behm-Ansmant, I., M. Helm, and Y. Motorin, *Use of specific chemical reagents for detection of modified nucleotides in RNA.* J Nucleic Acids, 2011. **2011**: p. 408053.

153. Bakin, A. and J. Ofengand, *Four newly located pseudouridylate residues in Escherichia coli 23S ribosomal RNA are all at the peptidyltransferase center: analysis by the application of a new sequencing technique.* Biochemistry, 1993. **32**(37): p. 9754-62.

154. Sakurai, M., et al., *Inosine cyanoethylation identifies A-to-I RNA editing sites in the human transcriptome.* Nat Chem Biol, 2010. **6**(10): p. 733-40.

155. Okada, S., et al., *Transcriptome-wide identification of A-to-I RNA editing sites using ICE-seq.* Methods, 2019. **156**: p. 66-78.

156. Kan, L.S., et al., *NMR study on the methyl and methylene proton resonances of tRNA Phe yeast.* Biochem Biophys Res Commun, 1974. **59**(1): p. 22-9.

157. Agris, P.F., H. Sierzputowska-Gracz, and C. Smith, *Transfer RNA contains sites of localized positive charge: carbon NMR studies of [13C]methyl-enriched Escherichia coli and yeast tRNAPhe.* Biochemistry, 1986. **25**(18): p. 5126-31.

158. Kumar, R.K. and D.R. Davis, *Synthesis and studies on the effect of 2-thiouridine and 4-thiouridine on sugar conformation and RNA duplex stability.* Nucleic Acids Res, 1997. **25**(6): p. 1272-80.

159. Vermeulen, A., S.A. McCallum, and A. Pardi, *Comparison of the global structure and dynamics of native and unmodified tRNAval.* Biochemistry, 2005. **44**(16): p. 6024-33.

160. Barraud, P., et al., *Time-resolved NMR monitoring of tRNA maturation.* Nat Commun, 2019. **10**(1): p. 3373.

161. Karas, M. and F. Hillenkamp, *Laser desorption ionization of proteins with molecular masses exceeding 10,000 daltons.* Anal Chem, 1988. **60**(20): p. 2299-301.

162. Fenn, J.B., et al., *Electrospray ionization for mass spectrometry of large biomolecules.* Science, 1989. **246**(4926): p. 64-71.

163. Kirpekar, F., et al., *Matrix assisted laser desorption/ionization mass spectrometry of enzymatically synthesized RNA up to 150 kDa.* Nucleic Acids Res, 1994. **22**(19): p. 3866-70.

164. Nordhoff, E., et al., *Comparison of IR- and UV-matrix-assisted laser desorption/ionization mass spectrometry of oligodeoxynucleotides.* Nucleic Acids Res, 1994. **22**(13): p. 2460-5.

165. Gehrke, C.W. and K.C. Kuo, *Ribonucleoside analysis by reversed-phase high-performance liquid chromatography.* J Chromatogr, 1989. **471**: p. 3-36.

166. Pomerantz, S.C. and J.A. McCloskey, *Analysis of RNA hydrolyzates by liquid chromatography-mass spectrometry.* Methods Enzymol, 1990. **193**: p. 796-824.

167. Nordhoff, E., F. Kirpekar, and P. Roepstorff, *Mass spectrometry of nucleic acids.* Mass Spectrom Rev, 1996. **15**(2): p. 67-138.

168. Barker, S.A., et al., *Intermediates in the photosynthetic cycle.* Biochim Biophys Acta, 1956. **21**(2): p. 376-7.

169. Ong, S.E., et al., *Stable isotope labeling by amino acids in cell culture, SILAC, as a simple and accurate approach to expression proteomics.* Mol Cell Proteomics, 2002. **1**(5): p. 376-86.

170. Ong, S.E., I. Kratchmarova, and M. Mann, *Properties of 13C-substituted arginine in stable isotope labeling by amino acids in cell culture (SILAC).* J Proteome Res, 2003. **2**(2): p. 173-81.

171. Schiesser, S., et al., *Mechanism and stem-cell activity of 5-carboxycytosine decarboxylation determined by isotope tracing.* Angew Chem Int Ed Engl, 2012. **51**(26): p. 6516-20.

172. Li, S. and P.A. Limbach, *Method for comparative analysis of ribonucleic acids using isotope labeling and mass spectrometry.* Anal Chem, 2012. **84**(20): p. 8607-13.

173. Paulines, M.J. and P.A. Limbach, *Stable Isotope Labeling for Improved Comparative Analysis of RNA Digests by Mass Spectrometry.* J Am Soc Mass Spectrom, 2017. **28**(3): p. 551-561.

174. Waghmare, S.P. and M.J. Dickman, *Characterization and quantification of RNA post-transcriptional modifications using stable isotope labeling of RNA in conjunction with mass spectrometry analysis.* Anal Chem, 2011. **83**(12): p. 4894-901.

175. Popova, A.M. and J.R. Williamson, *Quantitative analysis of rRNA modifications using stable isotope labeling and mass spectrometry.* J Am Chem Soc, 2014. **136**(5): p. 2058-69.

176. Taoka, M., et al., *A mass spectrometry-based method for comprehensive quantitative determination of post-transcriptional RNA modifications: the complete chemical structure of Schizosaccharomyces pombe ribosomal RNAs.* Nucleic Acids Res, 2015. **43**(18): p. e115.

177. Brandmayr, C., et al., *Isotope-based analysis of modified tRNA nucleosides correlates modification density with translational efficiency.* Angew Chem Int Ed Engl, 2012. **51**(44): p. 11162-5.

178. Wang, J., et al., *Quantifying the RNA cap epitranscriptome reveals novel caps in cellular and viral RNA.* Nucleic Acids Res, 2019. **47**(20): p. e130.

179. Kellner, S., et al., *Absolute and relative quantification of RNA modifications via biosynthetic isotopomers.* Nucleic Acids Res, 2014. **42**(18): p. e142.

180. Heiss, M., V.F. Reichle, and S. Kellner, *Observing the fate of tRNA and its modifications by nucleic acid isotope labeling mass spectrometry: NAIL-MS.* RNA Biol, 2017. **14**(9): p. 1260-1268.

181. McLuckey, S.A., G.J. Van Berkel, and G.L. Glish, *Tandem mass spectrometry of small, multiply charged oligonucleotides.* J Am Soc Mass Spectrom, 1992. **3**(1): p. 60-70.

182. Limbach, P.A., P.F. Crain, and J.A. McCloskey, *Characterization of oligonucleotides and nucleic acids by mass spectrometry.* Curr Opin Biotechnol, 1995. **6**(1): p. 96-102.

183. Taucher, M. and K. Breuker, *Top-down mass spectrometry for sequencing of larger (up to 61 nt) RNA by CAD and EDD.* J Am Soc Mass Spectrom, 2010. **21**(6): p. 918-29.

184. Taucher, M. and K. Breuker, *Characterization of modified RNA by top-down mass spectrometry.* Angew Chem Int Ed Engl, 2012. **51**(45): p. 11289-92.

185. Calderisi, G., H. Glasner, and K. Breuker, *Radical Transfer Dissociation for De Novo Characterization of Modified Ribonucleic Acids by Mass Spectrometry.* Angew Chem Int Ed Engl, 2020. **59**(11): p. 4309-4313.

186. Kowalak, J.A., et al., *A novel method for the determination of post-transcriptional modification in RNA by mass spectrometry.* Nucleic Acids Res, 1993. **21**(19): p. 4577-85.

187. Thakur, P., et al., *Improved RNA modification mapping of cellular non-coding RNAs using C- and U-specific RNases.* Analyst, 2020. **145**(3): p. 816-827.

188. Lobue, P.A., et al., *Improved application of RNAModMapper - An RNA modification mapping software tool - For analysis of liquid chromatography tandem mass spectrometry (LC-MS/MS) data.* Methods, 2019. **156**: p. 128-138.

189. Wein, S., et al., *A computational platform for high-throughput analysis of RNA sequences and modifications by mass spectrometry.* Nat Commun, 2020. **11**(1): p. 926.

190. Yamaki, Y., et al., *Direct Determination of Pseudouridine in RNA by Mass Spectrometry Coupled with Stable Isotope Labeling.* Anal Chem, 2020. **92**(16): p. 11349-11356.

191. Jiang, T., et al., *Oligonucleotide Sequence Mapping of Large Therapeutic mRNAs via Parallel Ribonuclease Digestions and LC-MS/MS.* Anal Chem, 2019. **91**(13): p. 8500-8506.

192. Yu, N., et al., *tRNA Modification Profiles and Codon-Decoding Strategies in Methanocaldococcus jannaschii.* J Bacteriol, 2019. **201**(9).

193. Li, F., et al., *Multiple heart-cutting mixed-mode chromatography-reversed-phase 2D-liquid chromatography method for separation and mass spectrometric characterization of synthetic oligonucleotides.* J Chromatogr A, 2020. **1625**: p. 461338.

194. Li, F. and M. Lammerhofer, *Impurity profiling of siRNA by two-dimensional liquid chromatography-mass spectrometry with quinine carbamate anion-exchanger and ion-pair reversed-phase chromatography.* J Chromatogr A, 2021. **1643**: p. 462065.

195. Apffel, A., et al., *Analysis of Oligonucleotides by HPLC-Electrospray Ionization Mass Spectrometry.* Anal Chem, 1997. **69**(7): p. 1320-5.

196. Li, N., et al., *Alkylamine ion-pairing reagents and the chromatographic separation of oligonucleotides.* J Chromatogr A, 2018. **1580**: p. 110-119.

197. McGinnis, A.C., E.C. Grubb, and M.G. Bartlett, *Systematic optimization of ion-pairing agents and hexafluoroisopropanol for enhanced electrospray ionization mass spectrometry of oligonucleotides.* Rapid Commun Mass Spectrom, 2013. **27**(23): p. 2655-64.

198. Lobue, P.A., et al., *Oligonucleotide analysis by hydrophilic interaction liquid chromatography-mass spectrometry in the absence of ion-pair reagents.* J Chromatogr A, 2019. **1595**: p. 39-48.

199. Crain, P.F., *Preparation and enzymatic hydrolysis of DNA and RNA for mass spectrometry.* Methods Enzymol, 1990. **193**: p. 782-90.

200. Jora, M., et al., *Chemical Amination/Imination of Carbonothiolated Nucleosides During RNA Hydrolysis.* Angew Chem Int Ed Engl, 2021. **60**(8): p. 3961-3966.

201. Kaiser, S., et al., *Strategies to Avoid Artifacts in Mass Spectrometry-Based Epitranscriptome Analyses.* Angew Chem Int Ed Engl, 2021.

202. Zhang, L.S., et al., *Transcriptome-wide Mapping of Internal N(7)-Methylguanosine Methylome in Mammalian mRNA.* Mol Cell, 2019. **74**(6): p. 1304-1316 e8.

203. Borland, K., et al., *Production and Application of Stable Isotope-Labeled Internal Standards for RNA Modification Analysis.* Genes (Basel), 2019. **10**(1).

204. Reichle, V.F., et al., *Surpassing limits of static RNA modification analysis with dynamic NAIL-MS.* Methods, 2019. **156**: p. 91-101.

205. Reichle, V.F., V. Weber, and S. Kellner, *NAIL-MS in E. coli Determines the Source and Fate of Methylation in tRNA.* Chembiochem, 2018. **19**(24): p. 2575-2583.

206. Yoluc, Y., E. van de Logt, and S. Kellner-Kaiser, *The Stress-Dependent Dynamics of Saccharomyces cerevisiae tRNA and rRNA Modification Profiles.* Genes (Basel), 2021. **12**(9).

207. Fu, D., J.J. Jordan, and L.D. Samson, *Human ALKBH7 is required for alkylation and oxidation-induced programmed necrosis.* Genes Dev, 2013. **27**(10): p. 1089-100.

208. Xu, W., et al., *Oncometabolite 2-hydroxyglutarate is a competitive inhibitor of alpha-ketoglutarate-dependent dioxygenases.* Cancer Cell, 2011. **19**(1): p. 17-30.

209. Elkashef, S.M., et al., *IDH Mutation, Competitive Inhibition of FTO, and RNA Methylation.* Cancer Cell, 2017. **31**(5): p. 619-620.

210. Gross, S., et al., *Cancer-associated metabolite 2-hydroxyglutarate accumulates in acute myelogenous leukemia with isocitrate dehydrogenase 1 and 2 mutations.* J Exp Med, 2010. **207**(2): p. 339-44.

211. Chen, F., et al., *Oncometabolites d- and l-2-Hydroxyglutarate Inhibit the AlkB Family DNA Repair Enzymes under Physiological Conditions.* Chem Res Toxicol, 2017. **30**(4): p. 1102-1110.

212. Sharma, S., et al., *A single N(1)-methyladenosine on the large ribosomal subunit rRNA impacts locally its structure and the translation of key metabolic enzymes.* Sci Rep, 2018. **8**(1): p. 11904.

213. Heiss, M., et al., *Cell culture NAIL-MS allows insight into human tRNA and rRNA modification dynamics in vivo.* Nat Commun, 2021. **12**(1): p. 389.

214. Schwanhausser, B., et al., *Corrigendum: Global quantification of mammalian gene expression control.* Nature, 2013. **495**(7439): p. 126-7.

215. Sharova, L.V., et al., *Database for mRNA half-life of 19 977 genes obtained by DNA microarray analysis of pluripotent and differentiating mouse embryonic stem cells.* DNA Res, 2009. **16**(1): p. 45-58.

216. Hauenschild, R., et al., *The reverse transcription signature of N-1-methyladenosine in RNA-Seq is sequence dependent.* Nucleic Acids Res, 2015. **43**(20): p. 9950-64.